Die approbierte Originalversion dieser Dissertation ist in der Hauptbibliothek der Technischen Universität Wien aufgestellt und zugänglich.
http://www.ub.tuwien.ac.at

The approved original version of this thesis is available at the main library of the Vienna University of Technology.
http://www.ub.tuwien.ac.at/eng

DISSERTATION

Evaluation of dual fluidized bed biomass gasification plants generating electricity, valuable gases, and district heat

---

ausgeführt zum Zwecke der Erlangung des akademischen Grades eines
Doktors der technischen Wissenschaften (Dr. techn.)
eingereicht an der TU Wien,
Fakultät für Maschinenwesen und Betriebswissenschaften
von

Michael Kraussler

Mat.Nr.: 0825858

unter der Leitung von
Univ. Prof. Dipl.-Ing. Dr. techn. Hermann Hofbauer
Institut für Verfahrenstechnik, Umwelttechnik und
und Technische Biowissenschaften, E166

begutachtet von

Prof. Jürgen Karl
Friedrich-Alexander-Universität
Erlangen-Nürnberg
Lehrstuhl für
Energieverfahrenstechnik
Fürther Straße 244f
D-90429 Nürnberg

Prof. Markus Lehner
Montanuniversität
Leoben
Lehrstuhl für
Verfahrenstechnik des
industriellen Umweltschutzes
Franz-Josef-Straße 18
A-8700 Leoben

Diese Arbeit wurde von der Österreichischen Forschungsförderungsgesellschaft im Rahmen des COMET Programms mit der Fördernummer 844605 unterstützt.

Ich nehme zur Kenntnis, dass ich zur Drucklegung meiner Arbeit unter der Bezeichnung Dissertation nur mit Bewilligung der Prüfungskommission berechtigt bin.

Eidesstattliche Erklärung

Ich erkläre an Eides statt, dass die vorliegende Arbeit nach den anerkannten Grundsätzen für wissenschaftliche Abhandlungen von mir selbstständig erstellt wurde. Alle verwendeten Hilfsmittel, insbesondere die zugrunde gelegte Literatur, sind in dieser Arbeit genannt und aufgelistet. Die aus den Quellen wörtlich entnommenen Stellen, sind als solche kenntlich gemacht.

Das Thema dieser Arbeit wurde von mir bisher weder im In- noch Ausland einer Beurteilerin/einem Beurteiler zur Begutachtung in irgendeiner Form als Prüfungsarbeit vorgelegt. Diese Arbeit stimmt mit der von den Begutachtern beurteilten Arbeit überein.

Wien, Februar, 2018

Danksagung

An erster Stelle möchte ich mich bei Univ. Prof. Hermann Hofbauer dafür bedanken, dass er mir die Chance gegeben hat, unter seiner Anleitung diese Dissertation zu erstellen.

Anschließend möchte ich mich bei Dr. Walter Haslinger bedanken, der mir die Anstellung bei Bioenergy2020+ ermöglicht hat. Eine fixe Anstellung zu haben, während man an seiner Dissertation arbeitet, ist keine Selbstverständlichkeit.

In weiterer Folge danke ich meiner Familie - meiner Mutter Hannelore, meinem Vater Erich und meinem Bruder Robert - ohne deren Unterstützung mein Studium und in weiterer Folge diese Arbeit nicht möglich gewesen wäre. Ihr habt mich zu dem gemacht, was ich heute bin und dafür bin ich euch unendlich dankbar.

Ganz besonders danke ich auch meiner Freundin, Christine. Deine Unterstützung und aufheiternde Art haben mich täglich motiviert und dafür gesorgt, dass ich mich jeden Tag auf zu Hause gefreut habe.

Zum Schluss möchte ich mich noch bei allen ehemaligen und aktuellen Kollegen bei Bioenergy2020+ und der TU Wien, Studenten und Projektpartner bedanken, die mich im Laufe meiner Dissertation begleitet und unterstützt haben. Alle Namen an dieser Stelle aufzuzählen würde den Umfang dieser Arbeit sprengen und dafür sorgen, dass ich jemanden vergesse, wodurch ich ein schlechtes Gewissen hätte. Ihr alle habt mir dabei geholfen, mich zu motivieren und für ein Arbeitsklima gesorgt, sodass ich mich jeden Tag auf die Arbeit freuen konnte.

Abstract

Global warming led to the Paris agreement which was signed by the majority of all countries in order to reduce the CO_2 emission to keep the global temperature increase below 1.5 °C. Therefore, a shift towards renewable energy carriers is necessary. Renewable energy carriers already have a high share in Austria's electricity sector. More than 70 % of the electricity demand is met by renewable sources. However, the industrial sector and the transportation sector highly depend on fossil energy carriers. In contrast, biomass, especially solid biomass like wood chips, has still a high utilization potential for different processes in Austria. In order to use this potential and to reduce the CO_2 emissions, dual fluidized bed biomass steam gasification with its high efficiency and product flexibility can be employed. Therefore, different processes for the production of electricity, valuable gases (hydrogen, synthetic natural gas, and a gas mixture composed of hydrogen and methane), and district heat were investigated in this thesis. The techno-economic feasibility of the investigated processes was evaluated as well as its most significant influencing parameters.

Therefore, a robust and reliable data basis derived from commercial gasification plant data, experimental work carried out as part of this thesis, and an extensive literature review was used. With this data basis, mass and energy balances of the investigated processes were calculated. Subsequently, pinch analyses were carried out in order to prove the technical feasibility of the process layouts before the techno-economic assessments for fuel capacities of 10, 50, and 100 MW were evaluated.

The results show that governmental support and subsidies are necessary for an economically feasible operation of the investigated processes. The most significant influencing parameters of the economic feasibility are the production efficiency, the annual operating hours, the investment costs, and the feedstock price.

Kurzfassung

Im Zuge des Klimagipfels in Paris haben sich die unterzeichnenden Länder dazu verpflichtet ihre CO_2 Emissionen zu verringern, um die globale Erwärmung auf 1.5 °C zu beschränken. Um dieses Ziel zu erreichen, ist der vermehrte Einsatz von erneuerbaren Energieträgern erforderlich. Erneuerbare Energieträger spielen bereits heute eine wichtige Rolle in Österreichs Stromsektor. Über 70 % des Elektrizitätsbedarfs werden mittels erneuerbaren Energien erzeugt. Im Gegensatz dazu sind der Transportsektor und die Industrie sehr stark von fossilen Energieträgern abhängig. Biomasse, besonders feste Biomasse wie Hackschnitzel, besitzt noch großes Potential für verschiedene Anwendungen und kann einen Beitrag zur Reduktion der CO_2 Emissionen leisten. Um dieses Potential zu nutzen, bietet sich die Zweibett-Wirbelschicht-Dampfvergasung an. Diese bietet hohe Effizienz und Flexibilität hinsichtlich der Produkte. Aus diesem Grund werden in dieser Arbeit verschiedene Prozesse zur Erzeugung von Elektrizität, hochwertigen Gasen (Wasserstoff, synthetisches Erdgas und eine Gasmischung bestehend aus Wasserstoff und Methan) und Fernwärme untersucht. In weiterer Folge wurde die techno-ökonomische Machbarkeit sowie deren wichtigsten Einflussgrößen ermittelt.

Ausgangspunkt für die Berechnungen war eine belastbare Datenbasis bestehend aus Daten kommerzieller Vergasungsanlagen, Experimenten, die im Laufe dieser Arbeit entstanden sind, und einer umfangreichen Literaturstudie. Mit diesen Daten wurden Massen - und Energiebilanzen der untersuchten Prozesse berechnet. Um die technische Machbarkeit zu untersuchen, wurde die Wärmeintegration der Prozesse untersucht, bevor die techno-ökonomische Machbarkeit für Anlagen mit Brennstoffwärmeleistungen von 10, 50, und 100 MW evaluiert wurde.

Die Ergebnisse zeigen, dass gezielte Fördermaßnahmen notwendig sind, damit die untersuchten Prozesse wirtschaftlich betrieben werden können. Den größten Einfluss auf die Wirtschaftlichkeit hat der energetische Wirkungsgrad vor den jährlichen Betriebsstunden, den Investitionskosten und dem Holzpreis.

Contents

1 Introduction 8

1.1 Motivation . . . 8

1.1.1 Austrian energy statistics . . . 9

1.1.2 Development of energy prices . . . 12

1.2 State of the art processes . . . 14

1.2.1 Combined heat and power . . . 14

1.2.2 Hydrogen production . . . 16

1.2.3 Synthetic natural gas . . . 17

1.2.4 Simultaneous hydrogen and methane production . . . 18

1.3 Aim of the work . . . 18

2 Materials and methods 22

2.1 Employed unit operations . . . 23

2.1.1 Dual fluidized bed gasification of biomass . . . 23

2.1.2 Water gas shift unit . . . 30

2.1.3 Tar scrubber . . . 31

2.1.4 Amine scrubber . . . 32

2.1.5 Methanation and prior gas cleaning . . . 35

2.1.6 Pressure swing adsorption . . . 39

2.1.7 Gas engines . . . 40

2.2 Calculation of the mass and energy balances . . . 41

2.3 Pinch analysis and heat integration . . . 43

2.4 Techno-economic assessment . . . 44

2.4.1 Investment costs . . . 44

2.4.2 Production costs . . . 45

2.4.3 Assessment . . . 46

3 Results and discussion 49

3.1 Experimental investigation of a water gas shift unit . . . 49

3.2 Techno-economic assessment . . . 54

3.2.1 Process A: Combined heat and power . . . 55

3.2.2 Process B: Hydrogen and district heat . . . 68

3.2.3 Process C: Synthetic natural gas and district heat . . . 82
3.2.4 Process D: Hydrogen and methane 96

4 Comparison of the investigated processes 107
4.1 10 MW plants 108
4.2 50 MW plants 110
4.3 100 MW plants 111
4.4 Sensitivity comparison 111

5 Conclusion and outlook 115

A Simulation stream data 149
A.1 Process A: Combined heat and power 149
A.2 Process B: Hydrogen and district heat 152
A.3 Process C: Synthetic natural gas and district heat 155
A.4 Process D: Hydrogen and methane 160

B Publications 164

1 Introduction

This thesis investigates the techno-economic feasibility of biomass gasification-based processes for the generation of

- combined heat and power (CHP),
- H_2 and district heat,
- synthetic natural gas (SNG) and district heat, and
- a gas mixture mainly composed of H_2 and CH_4 referred to HNG

for Austria in 2017. In addition, the most significant parameters influencing the techno-economic feasibility of the processes are investigated. Therefore, this section gives some background information about the Austrian energy market. Furthermore, the price development over the last years of wood, natural gas, and electricity is covered. Consequently, the state of the art of biomass-based CHP, H_2, SNG, and HNG concepts is briefly given.

1.1 Motivation

In December 2015, 195 member states of the United Nations Framework Convention on Climate Change (UNFCCC) negotiated the so called Paris agreement in order to reduce the impact of the climate change through [1]

- holding the increase in the global average temperature well below 2 °C above pre-industrial levels and to pursue effort to limit the temperature increase to 1.5 °C above pre-industrial levels, recognizing that this would significantly reduce the risks and impacts of climate change.
- increasing the ability to adapt to the adverse impacts of climate change and foster climate change resilience and low greenhouse gas emissions development, in a manner that does not threaten food production.
- making finance flows consistent with a pathway towards low greenhouse gas emissions and climate-resilient development.

By December 2016, 192 states and the European Union have signed the agreement. Each country has to set measures in order to reach the above mentioned targets of the agreement [2]. This agreement should force the signing countries to reduce their CO_2 emissions and to support the use of renewable energy carriers. In addition, this agreement offers the possibility to reduce the import dependence from fossil fuels and could add economic value to the countries. For example, in 2013 Austria imported energy worth about 14.8 billion EUR. Therefrom, about 9.7 billion EUR for oil, 3.3 billion EUR for gas, 1.1 billion EUR for electricity, and about 0.7 billion EUR for coal [3]. Hence, in Austria there is significant potential to shift economic value into the own market by using biomass-based processes and other renewable energy sources.

1.1.1 Austrian energy statistics

Historically, renewable energy carriers have had a significant share of Austria's primary energy production. However, Austria is also dependent on the import of fossil energy carriers like oil, natural gas, and coal. Figure 1 shows the distribution of the energy production in Austria in 2015.

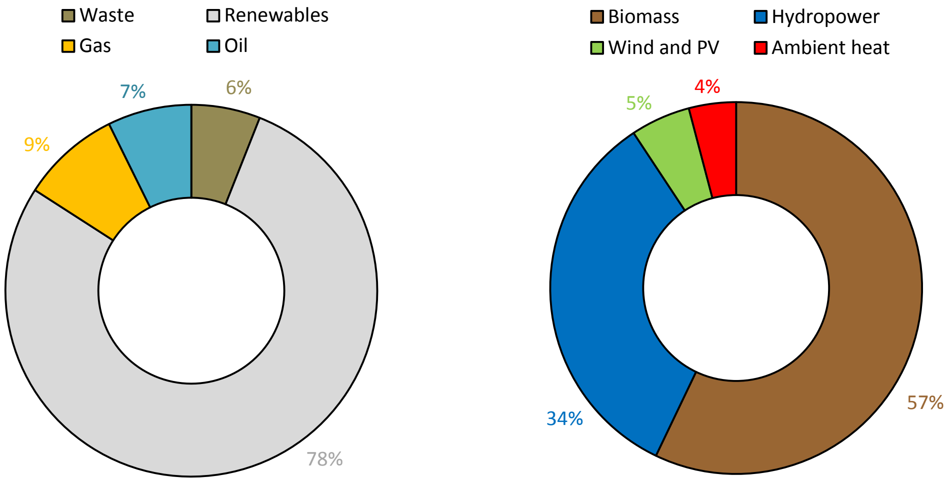

Figure 1: Distribution of the total primary energy production (left) and the primary energy production of renewables (right) in Austria in 2015 [4].

The primary energy production of 508 PJ was mainly covered by renewable energy carriers like hydro, wind, solar, and ambient heat. From these 78 % of the primary energy production, 57 % were covered by biogenous energy carriers, for example, fire wood, pellets, wood chips, bio fuels, waste lye of pulp and paper industry, biogas, or sewage sludge. These biogenous energy carriers were mainly used for heating [4].

Figure 2 shows the distribution of the electricity and district heat generation in Austria in 2015.

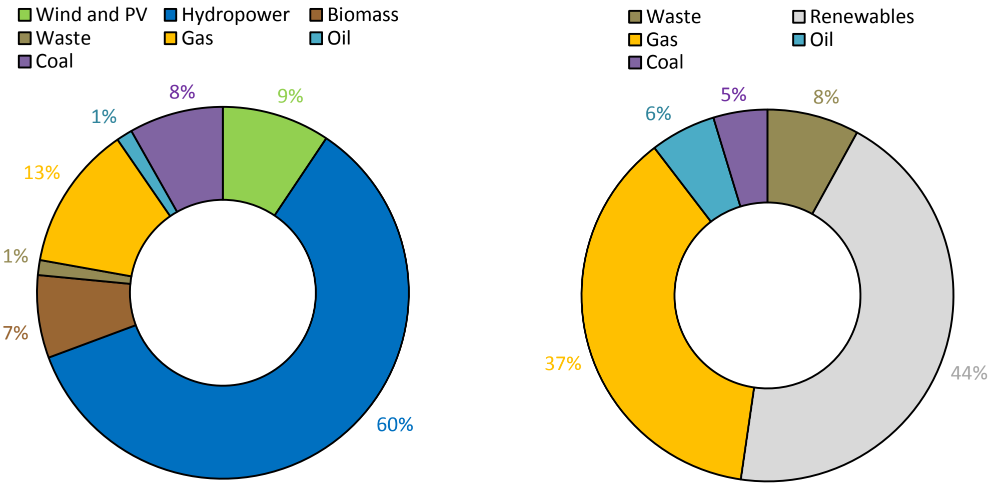

Figure 2: Distribution of the electricity generation (left) and district heat generation (right) in Austria in 2015 [4].

In 2015, 222 PJ of electricity were generated in Austria. The electricity was mainly produced by hydropower followed by natural gas, wind and photovoltaic, and coal. About 7 % of the electricity generation was generated by biomass, mainly by combined heat and power (CHP) plants [4]. The overall district heat consumption in Austria was 84 PJ in 2015. Renewable energy carriers generated most of the demanded district heat, mainly by combustion of solid biomass [4].

Figure 3 shows the gross domestic consumption and the energetic end use in Austria in 2015.

The gross domestic consumption in 2015 was about 1409 PJ. Oil based products had the highest share followed by renewable energy carries and

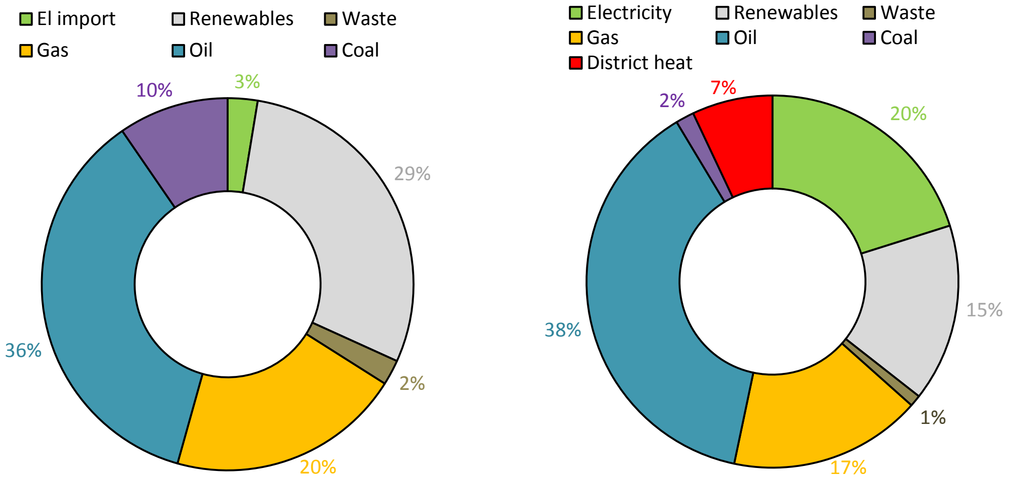

Figure 3: Gross domestic consumption (left) and energetic end use (right) in Austria in 2015 [4].

natural gas. Wood-based biomass had the highest share (about 63 %) of the gross domestic consumption of the biogenous energy carriers [4]. The energetic end use in Austria was about 1087 PJ in 2015. Again, the highest share was oil followed by electricity. The natural gas was mainly demanded by industrial processes and household heating. The share of the renewables was mainly caused by household heating with biomass [4].

In general, renewable energy carriers have already a high share in Austria's energy system compared to other EU states. However, oil and natural gas have an equally high share taking the gross domestic consumption and the energetic end use into account. Therefore, in order to effectively reduce the CO_2 emissions, measures should be applied aiming to substitute oil and natural gas in the Austrian energy system.

The domestic biomass resources in Austria are already extensively used [5]. Nevertheless, according to Biermayr et al. [6], the utilization of biomass-based household heating systems decreased over the past year. Consequently, in order to maximize the economic and ecologic efficiency of the bioenergy sector, the focus should shift towards the most efficient applications [7]. In addition, Lichtscheidl et al. [8] and Ehrig et al. [9] see that biomass, especially solid biomass like wood chips, has still a high potential in Austria, especially within the background of increasing utilization of electricity for household heating [6]. Therefore, biomass-based process concepts which offer a high fuel utilization rate should be employed in order to generate higher value products like electricity and valuable gases. Hence, heat from biomass should be mainly produced as by product of the processes.

1.1.2 Development of energy prices

Overall, energy prices in Austria increased over the past years [3]. Figure 4 shows the consumer price index of overall energy, fire wood, electricity, district heat, and natural gas from 2000 to 2015.

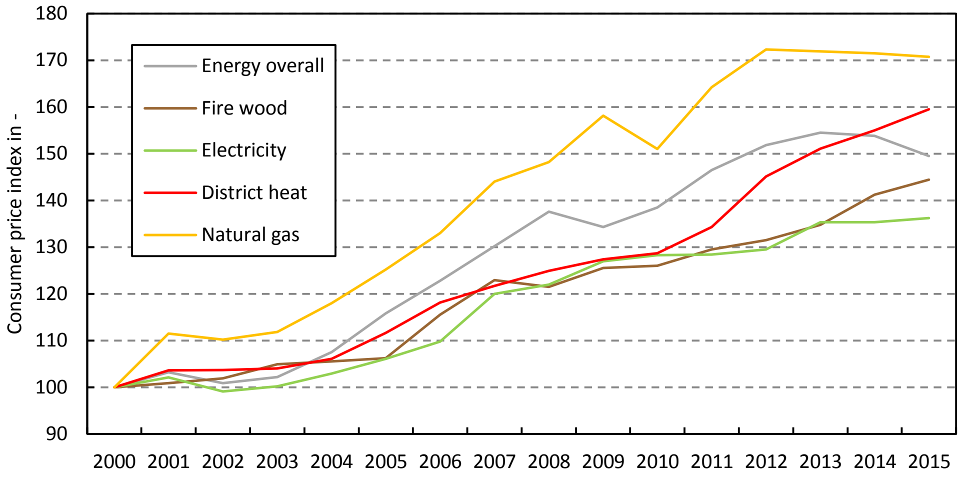

Figure 4: Consumer price index of different energy carriers in Austria from 2000 to 2015 [4].

The prices of all indicated energy carriers increased since the year 2000. In addition, there is a significant increase of the fire wood prices between 2005 and 2007. Wood chips are used in several district heating plants as well as in biomass-based CHP plants. In 2004, several new plants were started up in Austria which led to an increasing demand of wood chips. Therefore, between 2005 and 2007, the wood chip prices (dry basis) increased from about 70 $\mathrm{EUR} \cdot \mathrm{t}^{-1}$ to about 75 $\mathrm{EUR} \cdot \mathrm{t}^{-1}$. Furthermore, in 2012 the price reached about 90 $\mathrm{EUR} \cdot \mathrm{t}^{-1}$ resulting in an increase of 29 % since 2005 [10].

Figure 5 shows the profiles of the industry prices of electricity and natural gas from 2005 to 2015.

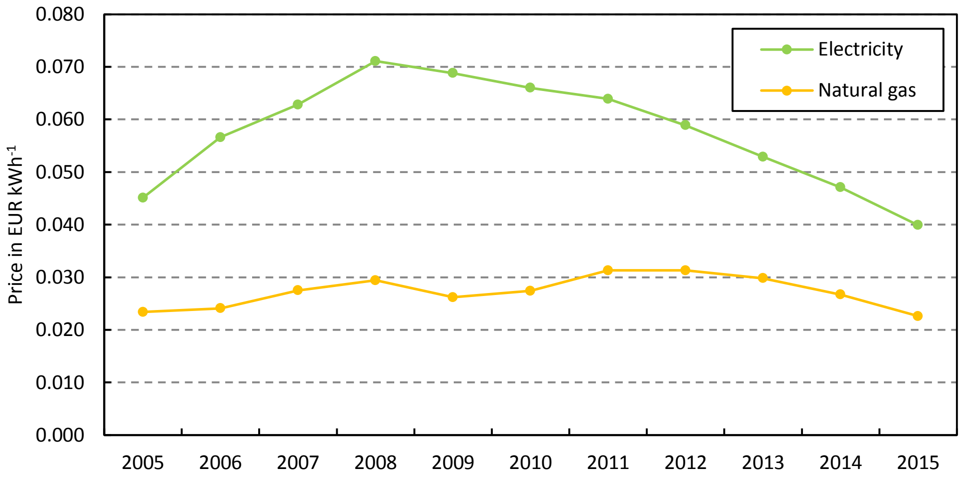

Figure 5: Development of industry prices for electricity and natural gas in Austria from 2005 to 2015 (excl. taxes and other charges) [11, 12].

It can be seen that the electricity price had a maximum at the beginning of the financial crisis in 2008. However, the natural gas price stayed on the same level.

Figure 6 shows the price development of electricity, natural gas, and wood chips in Austria for end users in the private sector from 2011 to 2017.

The price levels stayed at a consistent level over the last years. In addition, it can be seen that the wood chip prices are significantly lower than the prices for electricity and natural gas. This shows the potential of a higher share of biomass-based energy carriers in the Austrian energy system, which would also add economic value to the country. Nevertheless, because of the comparably high demand of wood chips in Austria, the wood chip prices for end users in the private sector increased by 158 % since 2005. However, biomass is still one of the most important energy carriers in Austria and its demand is further increasing [6].

In conclusion, a reduction of CO_2 emissions is necessary in order to achieve the targets of the Paris agreement. Austria already has a significant share of renewables in the electricity and district heat production. In contrast, the

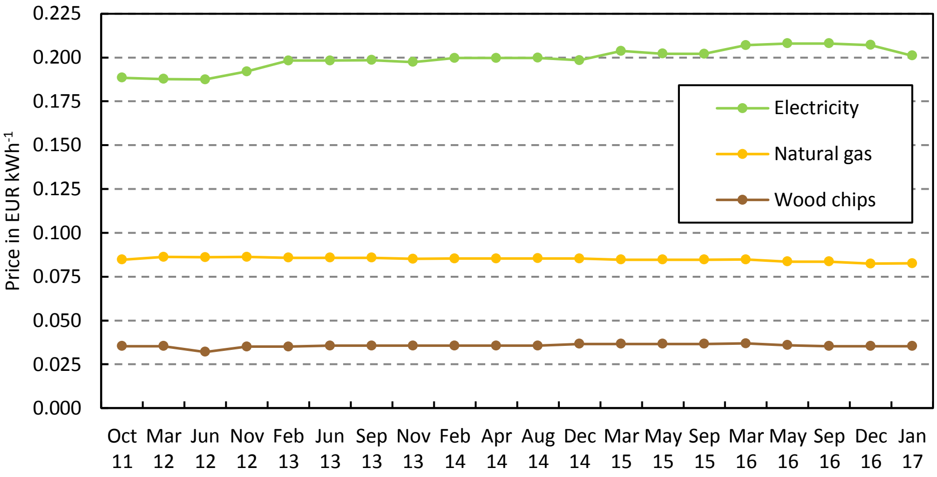

Figure 6: End-user prices of electricity, natural gas, and wood chips for the private sector in Austria from 2011 to 2017 [13].

industrial sector and the transportation sector mainly use fossil fuels in order to cover their energy demand. Especially, the industrial sector could lower its CO_2 emissions by using biomass-derived products, for example $BioH_2$, BioSNG, or BioHNG. However, the low electricity and natural gas prices are a hard-economic competition for biomass-based concepts.

1.2 State of the art processes

This section gives a brief introduction of the current state of the art of biomass-based CHP plants, production of H_2, as well as processes for SNG and HNG production.

1.2.1 Combined heat and power

CHP plants are technologically proven and reliable with a history of more than 100 years. In a CHP system, excess heat, which can be as much as 60 to 80 % of the total primary energy in combustion-based electricity generation by operating a Clausius-Rankine process, is used for different purposes. Typically, CHP is defined as the combined production of electrical (or mechanical) and useful thermal energy from the same primary energy source [14].

In order to reach a significant reduction of CO_2 emissions, the Austrian government introduced feed-in tariffs for renewable electricity in dependence of the capacity of the plants (compare Figure 7).

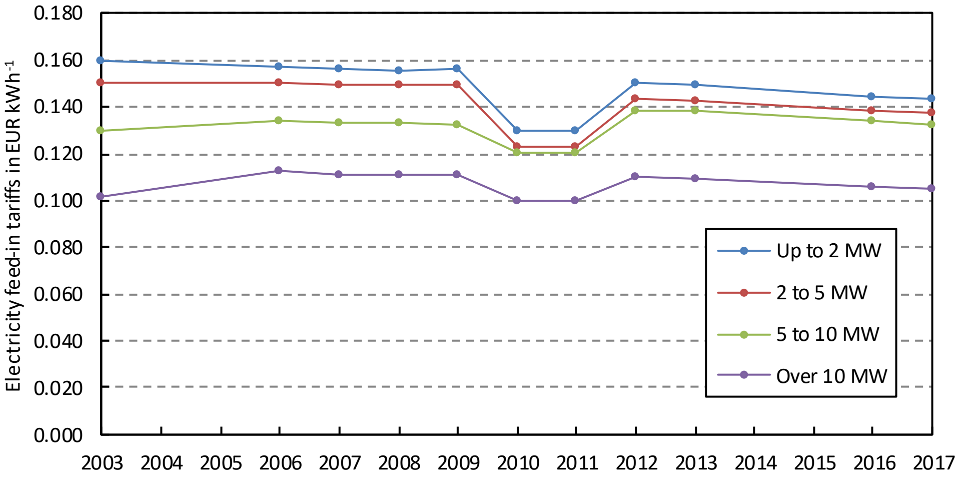

Figure 7: Overview of Austrian electricity feed-in tariffs for CHP plants using solid biomass as feedstock in $\mathrm{EUR} \cdot \mathrm{kWh}^{-1}$ from 2003 to 2017 [15, 16, 17].

The feed-in tariffs for newly erected CHP plants generating renewable electricity from solid biomass steadily decreased over the past years. Nevertheless, the feed-in tariffs led to a significant increase of the number of CHP plants in Austria. Those plants were mainly based on anaerobic digestion with subsequent combustion of biogas in a gas engine or Rankine cycle plants using lignocellulose biomass as feedstock. In 2017, the installed capacity of biomass-based electricity generation in Austria is 473.8 MW, which equals about 2.2 % of the overall installed capacity for electricity generation [18].

In addition, the CHP plants in Güssing, Oberwart, and Villach, employing the dual fluidized bed (DFB) biomass steam gasification technology which will be decribed in the more detailed in Section 2.1.1, were erected in Austria. Furthermore, several other DFB plants were built in other countries not only producing CHP but also serving a different purpose like BioSNG production (GoBiGas project) [19, 20].

1.2.2 Hydrogen production

Hydrogen is an important resource for a wide range of applications in the chemical industry [21]. Steam reforming of natural gas and other processes with fossil fuels as feedstock produce more than 95 % of the hydrogen which is needed in industry [22]. These large-scale steam reformer plants mainly cover the H_2 demand of refineries and ammonia plants and can reach efficiencies (H_2 output to natural gas input) of up to 85 % [23]. However, other industries, like glass, food, metal, and petrochemicals also need H_2 but in significantly smaller amounts. Consequently, small-scale natural gas steam reformer plants have been established throughout these markets because in most cases on-site supply of H_2 offers better economy if compared to delivery by trucks [24]. Nevertheless, steam reforming of natural gas or other fossil feedstock causes significant CO_2 emissions. Figure 8 shows a simplified flowchart of a typical steam reforming process for H_2 production.

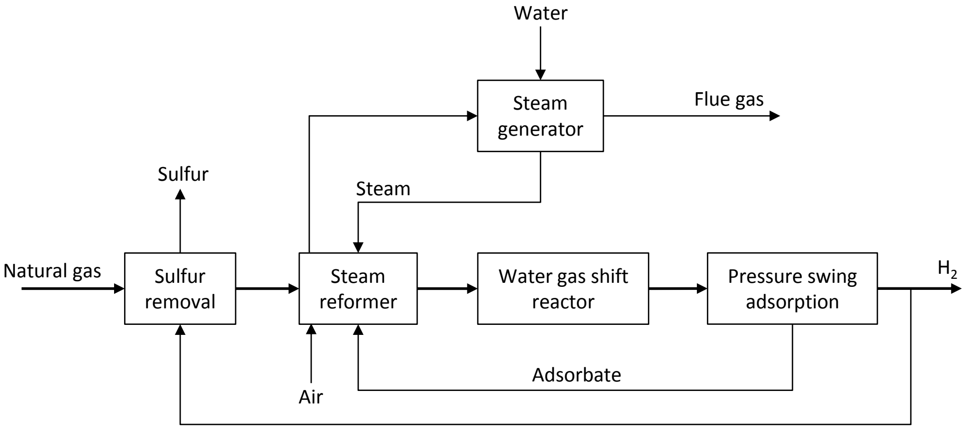

Figure 8: Simplfied flowchart of a natural gas steam reforming process for H_2 production based on [25].

Natural gas is desulfurized with a partial flow of generated H_2 and subsequently fed into the steam reformer where product gas, mainly composed of H_2, CO, CO_2, and CH_4, is generated. The product gas is fed into a water gas shift (WGS) reactor in order to lower the CO content and to increase the H_2 content. Finally, CO, CO_2, and CH_4 are separated in a pressure swing adsorption unit. The steam reformer is heated by the combustion of the adsorbate and the flue gas is used to generate steam for the steam reformer.

Another way of producing H_2 is electrolysis of water. Especially alkaline water electrolysis (AEL) is a well-established and commercially used technology for production of H_2. It is mainly used to generate small-scale H_2 supplies on-site [26, 27]. If powered by renewable electricity, the generated H_2 is CO_2-neutral. In addition, the proton exchange membrane (PEM) water electrolysis becomes also interesting for H_2 production, especially within the background of fluctuating renewable power sources like wind turbines and photovoltaic because of their good partial load behavior [26].

1.2.3 Synthetic natural gas

Today, the generation of SNG via the thermochemical route by gasification is mainly carried out with lignite as feedstock. The first commercial SNG production plant was the Great Plains Synfuels Plant in North Dakota, USA, employing lignite gasification [28]. Furthermore, China is also planning the erection of several lignite coal-based SNG production plants in the next years. However, these plants have to be watched critically regarding its CO_2 emissions and their general environmental impact [29]. In contrast, the GoBiGas plant in Gothenburg, Sweden, is a DFB biomass steam gasification technology-based BioSNG plant which is in demonstration and generates SNG from biomass [30]. Furthermore, a BioSNG pilot plant employing fluidized bed methanation was extensively investigated at the site of the commercial DFB CHP plant in Güssing, Austria [31, 32].

Upgrading of biogas to biomethane is commonly utilized to produce SNG for injecting into the grid. In this process, the most crucial operation is a separation of CO_2 from biogas, which is carried out by unit operations like absorption, adsorption, or gas permeation (membranes). Although the upgrading of biogas can be beneficial, its market is still small [33].

Nevertheless, biogas upgrading and BioSNG production based on the thermochemical route via gasification must not necessarily be competitive technologies as different feedstock for the processes can be used. The injection regulations for both technologies are defined in the standard EN 16723-1:2016.

1.2.4 Simultaneous hydrogen and methane production

Gas mixtures composed of H_2 and CH_4, sometimes referred to as hythane [34] and referred to as HNG in this thesis, were extensively investigated for usage in internal combustion engines in order to supplement compressed natural gas as car fuel, for example in Larsen and Wallace [35], Ortenzi et al. [36], and Sierens and Rosseel [37]. Verhelst and Wallner [38] report, that due to the similarity of the Wobbe index of H_2 and CH_4, a gas mixture composed of those components could be used as fuel, for example, for cars, for gas boilers, or for industrial applications and, therefore can supplement fossil CH_4 in natural gas grids. The Wobbe index (according to DIN 51857 "Gaseous fuels and other gases - Calculation of calorific value, density, relative density and Wobbe index of pure gases and gas mixture") describes the flow of energy through a given throttle at a given pressure in the gas grid [39]. However, another important factor, which has to be considered, is material compatibility because of the higher H_2 content [40].

First experiments for the production of BioHNG based on DFB biomass steam gasification were carried out at the site of the commercial DFB plant in Oberwart. Product gas was processed in a WGS unit and in a pressure swing adsorption (PSA) unit. Based on the achieved Wobbe index, the generated BioHNG gas mixture could have been used as natural gas substitute in industrial applications. The achieved energetic BioHNG to biomass efficiency was about 40 %.

1.3 Aim of the work

As described in the previous section, a reduction of the CO_2 emissions is necessary in order to achieve the targets of the Paris agreement. Especially, Austria is very depended on the import of carbon-based energy carriers like oil or natural gas. These fossil energy carriers are mainly used in the transportation sector (oil), for electricity and heat generation (natural gas), and for the industry (oil and natural gas). A part of the natural gas is also used for H_2 generation. However, Austria has also a very long history in using biomass as energy carrier [6]. In addition, Austria has still potential in the use of solid biomass feedstock for different processes. Therefore, this thesis investigates different biomass-based processes employing the DFB steam gasification technology as it enables CHP generation, BioH_2 and district heat production, production of BioSNG and district heat, and the production of a gas mixture consisting of H_2 and CH_4 which is referred to as BioHNG as possible future CO_2 neutral supplement for natural gas. In addition, there are also liquid synfuels discussed as future replacement of fossil fuels. However, those are not further discussed in this thesis.

Table 1 and Figure 9 give an overview about the investigated processes.

Table 1: Overview about the investigated processes.

Processes	Electricity	BioH_2	BioSNG	BioHNG	District heat
A	•				•
B		•			•
C			•		•
D				•	

All investigated processes are based on the DFB steam gasification of wood chips. Subsequently, the generated product gas is converted in four different processes configurations. Process A is a CHP process aiming at the production of electricity and district heat via combustion of the generated product gas in a gas engine. Process B aims at the generation of BioH_2 with a purity higher than 99.9 % and district heat. In this process, the product gas is fed into a WGS reactor, where CO is converted into additional H_2. Subsequently, most of the tar is removed in a RME scrubber before the gas is fed into an amine scrubber for CO_2 removal. Finally, a PSA unit separates H_2 from the other gas components. Process C generates BioSNG, which could be injected into the natural gas grid as well as district heat. In this process, tar is removed in a RME scrubber. The cleaned product gas is subsequently fed into a WGS unit and into a series of methanation reactors to generate CH_4 from H_2 and CO. Finally, the CO_2 is separated by an amine scrubber. Process D aims at the production of a gas mixture composed of H_2

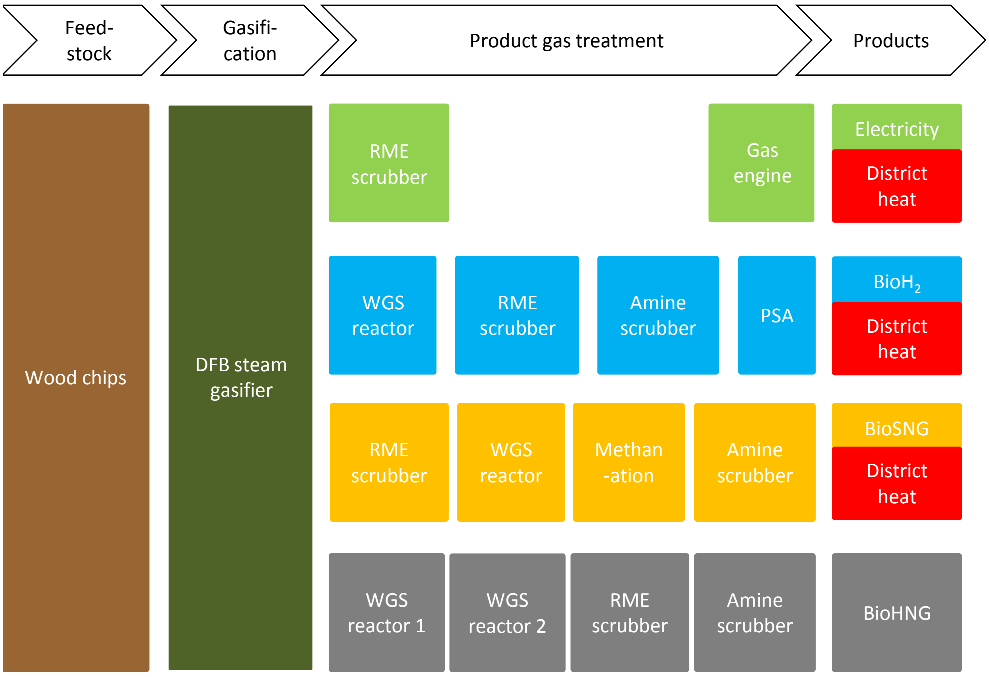
Feed-stock
Gasifi-cation
Product gas treatment
Products
Wood chips
DFB steam gasifier
RME scrubber
Gas engine
Electricity
District heat
WGS reactor
RME scrubber
Amine scrubber
PSA
BioH2
District heat
RME scrubber
WGS reactor
Methan-ation
Amine scrubber
BioSNG
District heat
WGS reactor 1
WGS reactor 2
RME scrubber
Amine scrubber
BioHNG

Figure 9: Graphical overview about the investigated processes.

and CH_4 as possible natural gas substitute for industrial processes, referred to as BioHNG. In this route, which is less complex than the BioSNG route, the product gas is fed into two WGS units in series to reduce the CO content and to increase the H_2 content. Subsequently, tar is removed in a RME scrubber before the gas is fed into an amine scrubber to remove the CO_2.

As the WGS unit plays a major role in processes B, C, and D, it was extensively investigated with real product gas extracted from the commercial DFB gasification plant in Oberwart (Papers 1 to 5). Based on these results and among other data from commercial DFB plants and literature, a techno-economic assessment of the presented processes is carried out considering plant capacities of 10, 50, and 100 MW gasifier fuel power in Austria in the base year 2017. Therefore, the following questions should be answered:

- What are technically feasible operating conditions for a WGS unit processing product gas from DFB biomass steam gasification plants?

- What are economically feasible selling prices for electricity, BioH_2, BioSNG, BioHNG for different plant capacities in Austria in 2017 and
- which parameters have the most significant influence on the techno-economic feasibility of the investigated processes?
- Furthermore, how can those parameters be influenced and improved?

2 Materials and methods

This chapter introduces the approach which was used for carrying out the techno-economic assessment of the investigated processes (see Figure 10). Aim of this specific approach is to have a reliable and robust data basis.

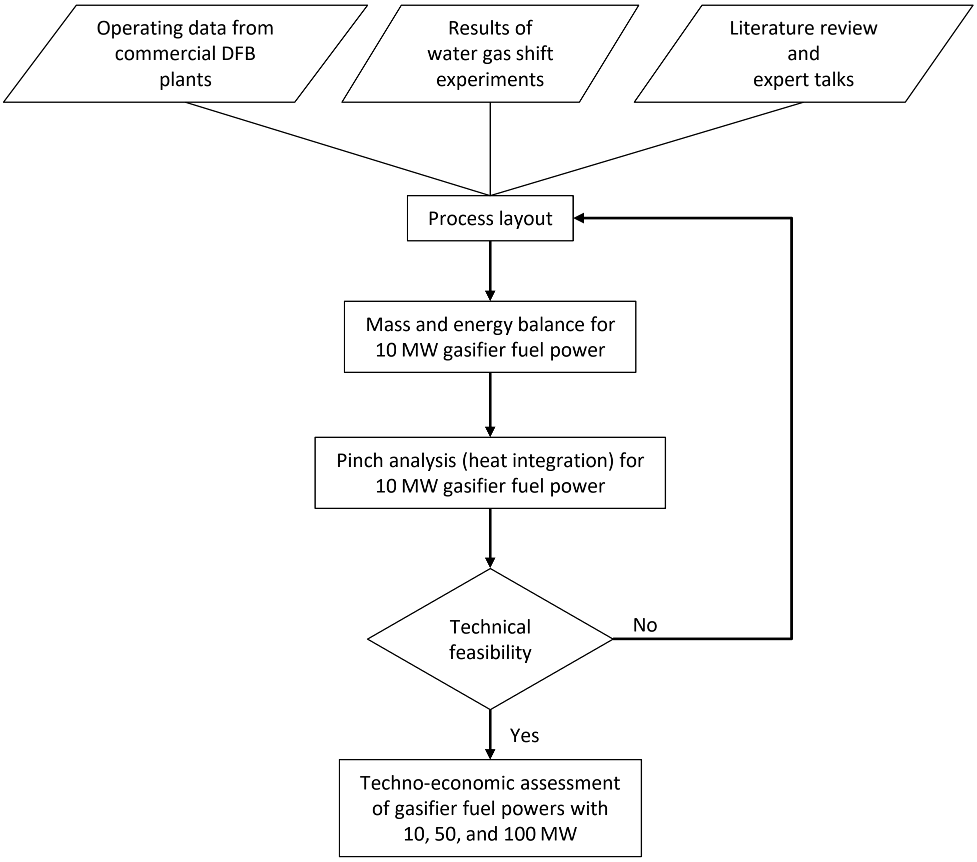
Operating data from commercial DFB plants
Results of water gas shift experiments
Literature review and expert talks
Process layout
Mass and energy balance for 10 MW gasifier fuel power
Pinch analysis (heat integration) for 10 MW gasifier fuel power
Technical feasibility
No
Yes
Techno-economic assessment of gasifier fuel powers with 10, 50, and 100 MW

Figure 10: Approach for the evaluation of the investigated processes.

Based on commercial DFB plant data, experimental results of a WGS unit (Paper 1 to 5), literature review, expert talks, and experiences, mass and energy balances were calculated for each investigated process with a gasifier fuel power of 10 MW. Subsequently, a pinch analysis was performed in order to assess the technical feasibility of the processes. If the technical feasibility was given, the techno-economic assessment was carried out for 10, 50, and 100 MW gasifier fuel power using in principle the same process layout. In the following, an overview about the employed main unit operations is given. Subsequently, the approach for the calculation of the mass and energy balances and the approach for the techno-economic assessment is introduced.

2.1 Employed unit operations

This chapter gives an overview of the state of the art of the main unit operations which were used for the investigated processes. The data are based on literature study, experimental work carried out within this thesis, as well as on plant data from commercial DFB CHP plants.

2.1.1 Dual fluidized bed gasification of biomass

Gasification is the thermal conversion of a carbonaceous solid fuel into a product gas in the presence of a specific gasification fluid. Depending on the used gasification agent, two gasification approaches can be identified: autothermal and allothermal gasification. In general, gasification is comprised of several steps:

(a) evaporation of moisture at temperatures up to 150 °C,

(b) pyrolysis, therefore release of volatiles (H_2, CO, CO_2, CH_4, tar, etc.) between 200 and 650 °C,

(c) reactions of volatiles in the gas phase between 700 and 1000 °C, and

(d) heterogeneous reactions of char between 700 and 1000 °C [21, 41].

During the gasification process, mainly the following homogeneous and heterogeneous reactions take place (compare Kaltschmitt et al. [41]). Based on these equations, the following gasification agents can be identified: O_2, H_2O, CO_2, and H_2.

Homogeneous gasification reactions

$$CO + H_2O \rightleftharpoons H_2 + CO_2 \qquad \Delta H_{298} = -41.2\ \mathrm{kJ \cdot mol^{-1}} \tag{1}$$

$$CH_4 + H_2O \rightleftharpoons 3H_2 + CO \qquad \Delta H_{298} = +206.2\ \mathrm{kJ \cdot mol^{-1}} \tag{2}$$

$$CO + \frac{1}{2}O_2 \rightleftharpoons CO_2 \qquad \Delta H_{298} = -282.9\ \mathrm{kJ \cdot mol^{-1}} \tag{3}$$

$$H_2 + \frac{1}{2}O_2 \rightleftharpoons H_2O \qquad \Delta H_{298} = -241.8\ \mathrm{kJ \cdot mol^{-1}} \tag{4}$$

$$CH_4 + CO_2 \rightleftharpoons 2H_2 + 2CO \qquad \Delta H_{298} = +247.3\ \mathrm{kJ \cdot mol^{-1}} \tag{5}$$

$$CH_4 + 2O_2 \rightleftharpoons 2H_2O + CO_2 \qquad \Delta H_{298} = -808.2\ \mathrm{kJ \cdot mol^{-1}} \tag{6}$$

Heterogeneous gasification reactions

$$C + O_2 \rightleftharpoons CO_2 \qquad \Delta H_{298} = -393.4\ \mathrm{kJ \cdot mol^{-1}} \tag{7}$$

$$C + \frac{1}{2}O_2 \rightleftharpoons CO \qquad \Delta H_{298} = -110.5\ \mathrm{kJ \cdot mol^{-1}} \tag{8}$$

$$C + H_2O \rightleftharpoons H_2 + CO \qquad \Delta H_{298} = +131.3\ \mathrm{kJ \cdot mol^{-1}} \tag{9}$$

$$C + CO_2 \rightleftharpoons 2CO \qquad \Delta H_{298} = +172.4\ \mathrm{kJ \cdot mol^{-1}} \tag{10}$$

$$C + 2H_2 \rightleftharpoons CH_4 \qquad \Delta H_{298} = -74.9\ \mathrm{kJ \cdot mol^{-1}} \tag{11}$$

In general, for autothermal gasification, either air, pure O_2, or a mixture of O_2 and steam can be used. Therefore, the heat for the endothermal gasification reactions is supplied by partial combustion of the fuel. In case of allothermal gasification, steam or CO_2 or a combination of both is used as gasification agent. In order to supply the heat for the endothermic gasification reactions, either a heat pipe heat exchanger or a circulating bed material, as it is employed in the DFB process, can be used.

A special type of the fluidized bed gasifier is the already mentioned DFB gasifier which enables allothermal gasification using steam as gasification agent. The heat is supplied by a circulating bed material. Figure 11 shows the principle of the DFB process which is described in detail in [41].

The fuel is fed into the gasification reactor where it reacts with steam into a product gas mainly consisting of H_2, CO, CO_2, CH_4, and steam. The heat for the endothermic gasification reactions is supplied by the circulating

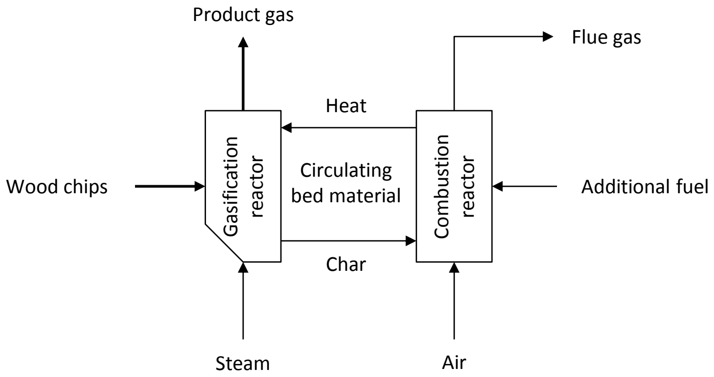

Figure 11: Principle of the DFB gasification process.

bed material olivine, which shows catalytic activity regarding gasification reactions and tar reduction [42, 43]. After releasing the sensible heat in the gasification reactor, the olivine is transported into the combustion reactor where biomass char, a partial flow of the used tar scrubbing fluid, and a partial flow of product gas is burnt in order to heat up the olivine.

Table 2 gives an overview of plant data from the commercial DFB biomass gasification plants in Güssing and Oberwart which are operated as CHP plants. The Oberwart data are derived from two different measurement campaigns, one took place in 2012 [44] and one took place in 2016 [45]. Between those campaigns, several improvements were implemented.

Table 3 shows the typical product gas composition of the DFB biomass steam gasification process with wood chips as fuel and olivine as circulating bed material.

The product gas has a high H_2 content and a suitable H_2 to CO ratio for several synthesis reactions, for example methanation, Fischer-Tropsch synthesis, and mixed alcohols synthesis [47]. Furthermore, the CH_4 content accounts for about one third of the lower heating value of the product gas. N_2 is used as inertization fluid for the commercial CHP plants in order to overlay the fuel feeding system and blowers. Therefore, the product gas

Table 2: Input streams of commercial DFB CHP plants.

	Güssing [46]	Oberwart [44]	Oberwart [45]	Units
Input streams				
Gasifier fuel power	7.80	8.40	8.37	MW
Wood chips (wet basis)	2065	2783	2603	$kg \cdot h^{-1}$
ω_{H_2O} before dryer	20 %	35.9 %	32.0 %	$kg \cdot kg^{-1}$
ω_{H_2O} after dryer	20 %	26.4 %	16.8 %	$kg \cdot kg^{-1}$
Electricity (consumption)	200	420	214	kW
Fresh RME	17	6	20	$kg \cdot h^{-1}$
N_2	75	75	33	$m^3 \cdot h^{-1}$
CaO	10	5	10	$kg \cdot h^{-1}$
Fresh olivine	40	20	20	$kg \cdot h^{-1}$
Output streams				
Ash	178	78	48	$kg \cdot h^{-1}$

Table 3: Typical dry product gas composition of the DFB gasification process with olivine as bed material [41].

	Values	Units
H_2	35 % to 40 %	$m^3 \cdot m^{-3}$
CO	22 % to 25 %	$m^3 \cdot m^{-3}$
CO_2	20 % to 25 %	$m^3 \cdot m^{-3}$
CH_4	9 % to 11 %	$m^3 \cdot m^{-3}$
N_2	< 1 %	$m^3 \cdot m^{-3}$
LHV	12 to 14	$MJ \cdot m^{-3}$

contains a volumetric N_2 content of about 1.9 %. Known from experience and experimental test runs at the commercial DFB plant in Güssing, without N_2 as inertization fluid, the volumetric N_2 content in the product gas would be about 0.5 % (mainly leakage from the combustion reactor to the gasification reactor).

Based on the data in Table 2, a reference gasification plant was simulated with the simulation software IPSEpro (compare Benedikt [48]) in order to acquire detailed mass and energy balances which were the basis for the techno-economic assessment of the different investigated processes.

Table 4 shows a typical fuel analysis of wood chips, fresh RME, tar, and char which were used for the simulation of the DFB reference plant.

Table 4: Analysis of the wood chips, fresh RME, tar, and char used for the simulation of the DFB gasifier. All values on water-free basis [48].

	Wood chips	Fresh RME	Tar	Char	Units
Ash	0.98 %	0.00 %	0.00	0.00	$kg \cdot kg^{-1}$
C	49.35 %	93.00 %	94.00	84.80	$kg \cdot kg^{-1}$
H	6.03 %	5.00 %	6.00	3.20	$kg \cdot kg^{-1}$
O*	43.45 %	2.00 %	0.00	12.00	$kg \cdot kg^{-1}$
N	0.17 %	0.00 %	0.00	0.00	$kg \cdot kg^{-1}$
S	0.013 %	0.00 %	0.00	0.00	$kg \cdot kg^{-1}$
Cl	0.005 %	0.00 %	0.00	0.00	$kg \cdot kg^{-1}$
LHV	18.17	36.87	38.49	31.25	$MJ \cdot kg^{-1}$

*O was calculated by difference.

Table 5 shows the operating data of the 10 MW DFB reference gasification plant.

The GCMS tar content before the rapeseed methyl ester (RME) scrubber was 5 $g \cdot m^{-3}$ dry product gas and after the RME scrubber 1.5 $g \cdot m^{-3}$ dry product gas. The benzene, toluene, ethylbenzene, and toluene (BTEX) content was not considered in the simulation. However, based on experiments and operating experiences of the commercial DFB plants, the BTEX content is usually three to five times higher than the content of other tar components (compare Bardolf [49]). In addition, it was assumed that the RME scrubber removes all gravimetric tar.

Figure 12 shows a Sankey diagram of the reference gasifier indicating the LHV-based chemical energy and the heat streams.

Table 5: Key data of the reference DFB gasification plant [48]. N_2 was used as inertization fluid for the CHP process whereas CO_2 was used for the other processes. The volumetric flow rate is given at STP.

	Reference	Units
Input streams		
Gasifier fuel power	10	MW
Wood chips (before dryer)	3417	$kg \cdot h^{-1}$
ω_{H_2O} before dryer	40 %	$kg \cdot kg^{-1}$
ω_{H_2O} after dryer	20 %	$kg \cdot kg^{-1}$
Electricity (consumption)	350	kW
Fresh RME	20	$kg \cdot h^{-1}$
N_2 or CO_2	40	$m^3 \cdot h^{-1}$
CaO	5	$kg \cdot h^{-1}$
Fresh olivine	20	$kg \cdot h^{-1}$
Output streams		
Ash	45	$kg \cdot h^{-1}$

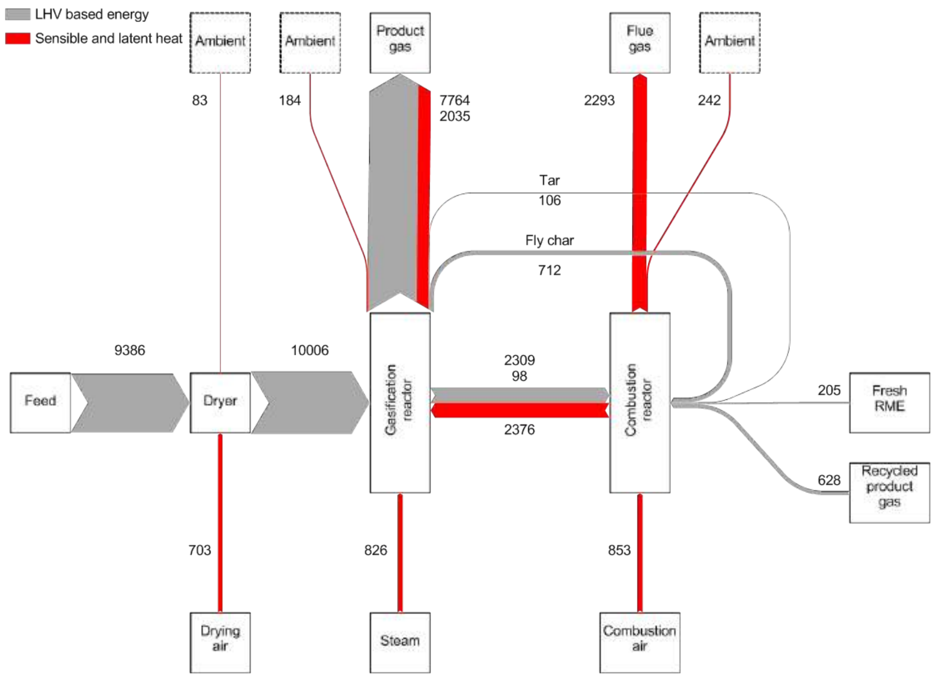
LHV based energy
Sensible and latent heat
Ambient
Ambient
Product gas
Flue gas
Ambient
83
184
7764
2035
2293
242
Tar
106
Fly char
712
9386
10006
Feed
Dryer
Gasification reactor
2309
98
2376
Combustion reactor
205
Fresh RME
628
Recycled product gas
703
826
853
Drying air
Steam
Combustion air

Figure 12: 10 MW reference DFB gasifier Sankey diagram. All streams are given in kW.

In the dryer, the gravimetric water content of the wood chips is reduced from about 40 % to 20 % which leads to an increase of the LHV-based chemical energy to about 10 MW. Fly char is separated by a product gas filter and subsequently fed into the combustion reactor where it serves as fuel. Tar, which is contained in the product gas is partially removed by the RME scrubber and steadily fed into the combustion reactor together with the used RME. Beside the fly char, tar, RME, and additional fuel in form of recycled product gas is fed into the combustion reactor. The overall heat losses of the gasification process are about 509 kW at 10 MW gasifier fuel power.

Figure 13 shows the annual operating hours of the CHP plants Güssing (start-up 2002), Oberwart (start-up 2008), and Senden (start-up 2012) as well as of the GoBiGas plant for BioSNG production (start-up 2014).

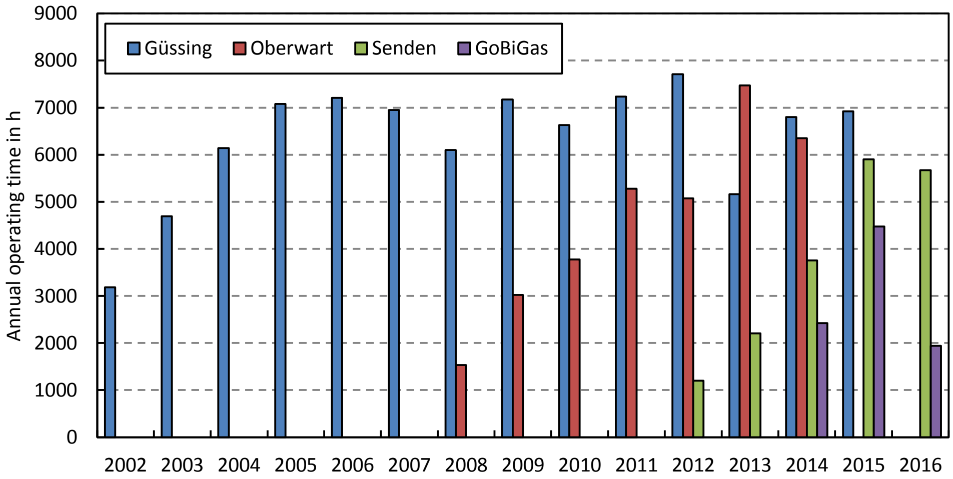

Figure 13: Annual operating hours of the CHP plants Güssing, Oberwart, and Senden as well as of the GoBiGas plant [50, 51].

The plants in Güssing and Oberwart reached more than 7000 operating hours per year. This indicates that the technology is proven and reliable. If problems occurred than in most cases either with the fuel feeding system or due to heat exchanger clogging (product gas as well as flue gas line). However, the reliability problems in Senden and at the GoBiGas BioSNG plant can be dedicated to scale effects due to larger plant capacities and greater dimensions of the gasification reactor [52]. The accumulated operating time of all four DFB plants is more than 150000 hours. Based on this information, the annual operating time for the techno-economic assessment of the investigated processes was chosen with 8000 hours.

2.1.2 Water gas shift unit

In order to increase the H_2 content and to lower the CO content of the generated product gas, a water gas shift (WGS) unit can be employed, where the WGS reaction (Equation 12) takes place.

$$CO + H_2O \rightleftharpoons H_2 + CO_2 \quad \Delta H_{298} = -41.2 \text{ kJ} \cdot \text{mol}^{-1} \tag{12}$$

It converts carbon monoxide and steam to hydrogen and carbon dioxide. At the industrial scale, a WGS unit is usually a fixed bed reactor. In order to reach economic reaction rates, different catalysts can be used. Fe-Cr-based catalysts are suitable for a high temperature WGS stage. This high temperature stage operates adiabatically with a gas inlet temperature of 350 to 550 °C and space velocities from 400 to 1200 h^{-1}. The operating pressure depends on the plant requirements [21]. Fe-Cr-based catalysts seem to be robust against sulfur poisoning at levels of about 100 to 200 ppm H_2S which are observed in the product gas of DFB biomass gasification plants [53, 54]. Catalysts for the low temperature stage (about 200 °C) are Co-Mo or Cu-Zn-based catalysts. The Co-Mo catalyst is resistant against the presence of sulfur components but the amount of H_2S in the product gas of biomass steam gasification is too low for the Co-Mo catalyst to reach a high level of activity as the Co-Mo catalyst is activated by sulfur (compare [53]). In contrast, Cu-Zn catalysts are sensitive to sulfur poisoning [21], therefore sulfur removal would be necessary. This section focuses on the Fe-Cr-based catalyst as it has proofed very suitable for the operation with the product gas from DFB biomass gasification plants and its long-term investigation is a significant part of this thesis (Section 3.1 and Paper 1 to Paper 5).

The Fe-Cr-based high temperature shift catalyst is composed of Fe_3O_4 and Cr_2O_3, basically the same catalyst as developed by BASF in 1915. The catalyst is relatively inexpensive, because of the Cr_2O_3 resistant to sintering and robust against sulfur and chlorine compounds. Zhu and Wachs [55] give an extensive review of iron-based high temperature water gas shift catalysts.

One key factor which affects the performance of the Fe-Cr-based WGS catalyst and influences the overall heat integration of a plant is the steam to dry gas ratio at the reactor inlet. Both, laboratory and commercial data, indicate that higher steam to dry gas ratios also increase the water gas shift reaction rate. As a result of the steam to dry gas ratio's effect on the thermodynamic and kinetic properties of the process, higher values give higher CO conversions and a lower CO content in the exit gas. In addition to the CO conversion, the steam to dry gas ratio can also affect the production of hydrocarbons (mainly methane) by the Fischer-Tropsch reaction. In order to minimize such undesirable reactions, a minimum steam to dry gas ratio of 0.4 should be ensured at the inlet of a WGS reactor. Depending on the feed of the WGS reactor, typical molar steam to dry gas ratios are between 0.6 and 2.2 and steam to carbon ratios between 2.8 and 4.2 [56].

2.1.3 Tar scrubber

The product gas generated by the DFB gasification system contains a significant amount of tar. In order to remove the tar and to condense the steam by lowering the gas temperature, RME has been a well proven scrubbing liquid at the commercial DFB plants in Güssing, Oberwart, and Senden [45, 52, 57]. Bardolf [49] summarizes the state of the art and latest research results regarding the RME scrubbing units employed at commercial DFB plants serving tar removal and steam condensation. Therefore, in all investigated processes the RME scrubber was employed to remove tar. It was assumed that the scrubber operating temperature is 50 °C, therefore tar is partially removed (GCMS tar content decreased from $5\ \mathrm{g} \cdot \mathrm{m}^{-3}$ to $1.5\ \mathrm{g} \cdot \mathrm{m}^{-3}$) and steam condensed.

2.1.4 Amine scrubber

Amine scrubbing has been used to separate carbon dioxide from gaseous streams since 1930 [58]. The CO_2-rich gas stream is contacted with an aqueous amine solution. The amine solvent reversibly reacts with CO_2 forming water-soluble salts. Amine-based solvent processes are well-suited to capture CO_2 from dilute low-pressure streams [59]. Problems during operation can occur due to the corrosive behavior of amines, formation of non-soluble salts, and foaming [60].

Due to the high affinity of especially CO_2 to the used solvents, mainly aqueous solutions of monoethanolamine (MEA), diethanolamine (DEA) and methyldiethanolamine (MDEA), the operating pressure of amine scrubbers can be kept at ambient level. The high capacity and high selectivity of the amine solution turns out to be a disadvantage during the regeneration of the scrubbing solution. Chemical scrubbing liquids require a significant amount of energy for the regeneration which has to be provided as process heat. As a small part of the scrubbing liquid is lost due to evaporation, it has to be replenished frequently. Hydrogen sulfide could also be chemically absorbed but higher temperatures during regeneration would be needed [61].

Amine systems have taken a great step forward in the market of biogas upgrading plants. In 2009, amine scrubbers were still only used at demonstration plants in the biogas sector, whereas the systems are commercially used now. Today MDEA is the most commonly used solvent in amine scrubbing systems [62].

The loading capacity for chemical solvents like amines is primarily dependent on the concentration of the active components and the achievable loading according to the thermodynamic equilibrium. For the range of alkanolamines, the primary amines (MEA) will be more favorable in terms of reaction rates compared to secondary (DEA), or tertiary (MDEA) amines. However, achievable loadings and heat requirement for regeneration will be also higher for primary amines [63]. Today, the most common industrially used amine system is a mixture of MDEA and piperazine (PZ), often termed activated MDEA (aMDEA). Activated MDEA uses piperazine as a catalyst to increase the speed of the reaction with CO_2. This system is today supplied by several major suppliers of chemicals such as BASF, DOW chemicals, Shell, and Taminco [62, 64, 65]. In general, different solvents show the following CO_2 removal efficiency: water $<$ MDEA $<$ DEA $<$ MEA. With PZ activated MDEA has the same CO_2 removal efficiency as MEA, but is less corrosive. Furthermore, the energy requirements of MDEA are usually lower compared to MEA and DEA [66].

Figure 14 shows the principle of an amine scrubbing unit with amine regeneration.

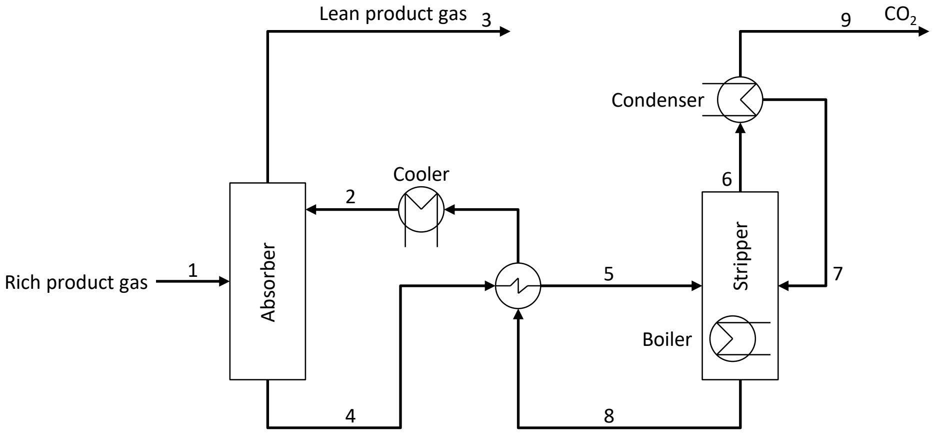

Figure 14: Simplified flowchart of an amine scrubbing process (based on [62]).

The CO_2 rich gas stream (1) is fed into the absorber where the CO_2 reacts with the amine solution resulting in the lean gas stream (3). The liquid amine solution (8, referred to as lean amine with a low CO_2 content) enters from the top of the absorber (2) and leaves at the bottom (4, rich amine). The rich amine is then preheated and enters the stripper (5). In the stripper, the rich amine solution flows in counter-current flow down to the bottom. At the bottom, the aqueous amine solution is heated up in order to desorb CO_2. The steam and the desorbed CO_2 leave the stripper at the top (6). Subsequently, the steam and a small part of evaporated amine is condensed and fed back to the stripper (7), whereas the CO_2 leaves the stripper (9). The regenerated amine solution (8) is cooled and used again in the absorber (2).

According to Bauer et al. [62], amine scrubbers can reach CO_2 removal efficiencies of up to 99.8 % with biogas with a volumetric fraction of 40 % CO_2 in the feed. Ryckebosch et al. [67] report CO_2 removal efficiencies up to 99.5%. Further CO_2 purification would bring the CO_2 quality up to food-grade standard [63].

In the following, typical operating parameters of amine scrubbers are given. The operating conditions depend on the CO_2 concentration in the feed and the used amine solvent.

- Stripper temperature: 100 to 160 °C [58, 61, 62, 68, 69]
- Absorber temperature: 40 to 65 °C [62, 68, 69]
- Electricity demand: 300 to 700 $\mathrm{kJ \cdot kg^{-1}}$ of absorbed CO_2 [62, 70, 71, 72, 73]
- Heat demand for regeneration: 1400 to 4000 $\mathrm{kJ \cdot kg^{-1}}$ of absorbed CO_2 [62, 70, 71, 73, 74, 75]
- Solvent consumption: 0.35 to 2 $\mathrm{kg \cdot t^{-1}}$ of absorbed CO_2 [63, 72, 74]

In order to calculate the mass and energy balances of the different investigated processes, the assumptions for the amine scrubbing units were taken based on the presented literature. According to Bauer et al. [62] and Privalova [76], aMDEA is the most common amine for CO_2 removal today. Therefore, it was selected as solvent for the amine scrubbers. A CO_2 removal efficiency of 99 % was chosen (compare Bauer et al. [62] and Ryckebosch et al. [67]). According to Bauer et al. [62] and Tobiesen et al. [77], about 2.4 MJ thermal energy per kg of absorbed CO_2 are necessary to regenerate the aqueous amine solution. If H_2S is included in the removal, about 10 % extra energy consumption would be necessary. In contrast, the application of MEA would lead to a significant higher energy demand of about 4.0 MJ per kg of absorbed CO_2 [78]. Furthermore, based on Bauer et al. [62] an electricity consumption of 0.4 MJ per kg absorbed CO_2 was assumed. The stripper temperature for regeneration of the amine solution was 110 to 120 °C according to Aaron and Tsouris [79] and Dugas [80]. The absorber temperature was chosen with 50 °C according to Aaron and Tsouris [79].

2.1.5 Methanation and prior gas cleaning

The oil crisis in the 1970s intensified the development of lignite and coal gasification processes with SNG production. One commercial SNG plant was erected. The Great Plains Synfuels Plant by the Dakota Gasification Company (North Dakota, United States) was commissioned in 1984 and has been producing 4.8 Mio m^3 SNG per day [28, 81]. Schildhauer [82] gives a detailed overview about SNG production via gasification.

Fixed bed methanation reactors are state of the art as gas cleaning units in, for example ammonia plants. They are used to eliminate small concentrations of CO by methanation in hydrogen-rich streams before the ammonia synthesis to avoid catalyst deactivation [54, 83]. The removal of the reaction heat is not a problem in these applications because of the high heat capacity of the large gas volumes and the low CO content. However, for the production of SNG, the heat of reaction has to be considered due to the high amount of CO in the product gas. In this case, several methanation reactors are connected in series with intermediate gas cooling or recycling of product gas. Fixed bed methanation processes are commercially available from different companies [84]. For example, the Haldor Topsoe TREMP process was employed at the GoBiGas project for the production of SNG from biomass [30, 85].

Fluidized bed reactors are known to be suitable for large scale operation of heterogeneously catalyzed reactions with highly exothermic behavior. The excellent mixing of the fluidized solids leads to almost isothermal conditions in the reactor, which allows simple and easy control of the operation. However, special attention should be paid to attrition and the entrainment of the catalyst particles. Several research projects regarding fluidized bed methanation were carried out. One example is the successful demo operation at the DFB plant in Güssing which is well described in Rehling [31] and Rehling et al. [32]. However, although there are certain advantages, fluidized bed methanation processes are not commercially available. Therefore, in this thesis, the focus lies on the commercially available fixed bed methanation processes because of the higher technology readiness level (TRL) of 9 [84].

Equations 13 to 17 are the main reactions which take place during methanation processes.

$$
\begin{aligned}
3H_2 + CO &\rightleftharpoons CH_4 + H_2O & \Delta H_{298} &= -206.2\ \mathrm{kJ \cdot mol^{-1}} \qquad (13)\\
CO + H_2O &\rightleftharpoons H_2 + CO_2 & \Delta H_{298} &= -41.2\ \mathrm{kJ \cdot mol^{-1}} \qquad (14)\\
2H_2 + 2CO &\rightleftharpoons CH_4 + CO_2 & \Delta H_{298} &= -247.3\ \mathrm{kJ \cdot mol^{-1}} \qquad (15)\\
4H_2 + CO_2 &\rightleftharpoons CH_4 + 2H_2O & \Delta H_{298} &= -165.0\ \mathrm{kJ \cdot mol^{-1}} \qquad (16)\\
2CO &\rightleftharpoons C + CO_2 & \Delta H_{298} &= -172.4\ \mathrm{kJ \cdot mol^{-1}} \qquad (17)
\end{aligned}
$$

Low temperatures and high pressures are thermodynamically preferred. The reaction of CO via the Sabatier process [1] is preferred and can even inhibit the CO_2 methanation because of the far stronger adsorption strength of CO on catalyst surfaces [86]. It is still unclear if CO_2 methanation needs CO as intermediate product or not. However, even for CO methanation, there is still no consensus about the kinetics and the mechanism [87]. According to Twigg [54], the methanation of CO_2 is inhibited until CO levels are lower than 200 to 300 ppm. Furthermore, the methanation reactions are accompanied by the WGS reaction (Equation 14), which can be suppressed by proper choice of the feed gas mixture, the catalyst, and the operating conditions [82].

Basically, all metals located in groups 8 to 10 of the periodic table are suited for catalyzing the methanation reaction. Due to a good combination of price, activity, and selectivity, nickel catalysts are predominantly applied in commercial methanation plants [84, 88].

In particular for CO methanation, prevention of fouling caused by carbon deposition is one of the major challenges [89]. In contrast, carbon deposition seems to cause no problems in CO_2 methanation processes [90]. If coking and carbon deposition is thermodynamically favored can be checked with C-H-O ternary diagrams. The equilibrium calculations show that a higher steam to carbon ratio or a higher O_2 to carbon ratio is generally needed to prevent carbon deposition with decreasing temperature. Furthermore, the addition of CO_2 suppresses the deposition at higher temperatures around 1000 °C [91, 92]. However, these temperature levels are usually not reached in methanation processes. Carbon deposition and coke formation occur at relatively low rates under favorable reaction conditions. However, under unfavorable conditions, high rates can lead to catastrophic failure of the catalyst and plugging of reactor voids leading to shut down within hours. The order of reactivity for coke formation is structure dependent: polynuclear aromatics > aromatics > olefins > branched alkanes > normal alkanes [93]. Key factors to prevent carbon deposition and coke formation include:

---

[1] The Sabatier reaction or Sabatier process was discovered by the French chemist Paul Sabatier in the 1910s. It involves the reaction of hydrogen with carbon dioxide at elevated temperatures (optimally 300 to 400 °C) and pressures in the presence of a nickel catalyst to produce methane and water.

(a) operating under conditions that minimize formation,

(b) optimizing catalyst design, for example in the case of zeolites optimizing acidity to minimize coke formation, and

(c) purifying the feed to remove precursors that accelerate carbon or coke formation [90, 93]

Carbon deposits are formed by the Boudouard reaction (compare Equation 17). In this reaction, carbon monoxide is converted into carbon dioxide and solid carbon, which deposits on the active nickel surface [89]. Moreover, the presence of olefins like ethylene enhances the risk for carbon deposition [93, 94]. Therefore, gas conditioning is needed upstream of fixed bed methanation processes [95].

Gas cleaning prior methanation Catalysts for alkene hydrogenation include a wide variety of nickel metals, noble metals, and sulfided (Ni-Mo/Al_2O_3 and Co-Mo/Al_2O_3) materials. The less expensive nickel catalysts can be used for hydrogenation of relatively pure feeds, for example with low concentrations of sulfur compounds and other poisons. Noble metal catalysts are preferred for hydrogenation involving molecules containing impurities, such as halides or sulfur (at low levels), that would poison nickel. Ni-Mo and Co-Mo sulfides are used for processes in which sulfur removal to low levels is impractical. Hence, they can be used for sulfur containing feeds [83].

According to Haro et al., Deithorn, Marsh and Rodriguez-Reinoso, and Yang [85, 96, 97, 98] activated carbon (AC) is well suited and commercially widely used for the removal of organic compounds from gas streams. Furthermore, according to a report from TU Wien [61] impregnated activated carbon is well suitable for removal of H_2S contents of up to 150 ppm which is about the same H_2S content of the product gas of DFB gasifiers operated with wood chips (Paper 1 to Paper 4). For desorption and regeneration of the loaded activated carbon, Woods [99] gives a value of 3 to 5 kg of steam per kg of adsorbed organic. In addition, the regeneration temperature has to be high enough to heat the adsorbent about 50 °C above the boiling temperature of the highest boiling organic.

The removal of COS with state of the art adsorbents at low temperature is difficult since COS is rather inactive compared to H_2S probably due to its neutrality and similarity to CO_2 [21, 100]. Therefore, hydrodesulfurization (HDS) with a subsequent ZnO adsorber is often used to remove COS from gaseous streams [21]. In this process, the feed gas is, if necessary, mixed with a small quantity of hydrogen and passes over a catalyst bed. The typical HDS catalyst is either a Co-Mo/Al_2O_3 or a Ni-Mo/Al_2O_3 catalyst. The organic sulfur is reduced to H_2S and hydrocarbon. Subsequently, the H_2S can be removed by adsorption on a bed of ZnO sorbent at temperatures between 300 to 400 °C. ZnO sorption capacity for H_2S is much higher than that of other sorbents, which leads to lower inventories of sorbent and decreasing sorbent replacement frequency [21].

In this work, the VESTA process developed by Amec Foster Wheeler and Clariant was chosen as methanation process because it is commercially available and avoids expensive gas recycling in order to restrict the temperature increase over the fixed bed methanation reactors. Therefore, its investment costs should be also suitable for small-scale plants which use biomass as feedstock [101, 102, 103].

2.1.6 Pressure swing adsorption

The pressure swing adsorption (PSA) process is based on the physical binding of gas molecules to a solid adsorbent material. The interaction between the gas and the adsorbent depends mainly on the gas component, its partial pressure, the type of adsorbent, and the temperature. It is a state of the art process for gas separation and widely used at commercial scale for different applications, for example air separation, hydrogen production, and biogas upgrading [23, 61, 104]. Figure 15 shows a simplified flowchart of a PSA process.

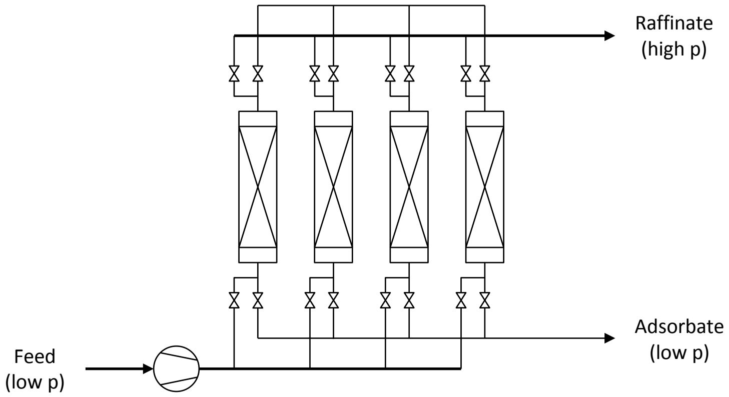

Figure 15: Simplified flowchart of a PSA process.

The feed is compressed and successively fed into the different adsorber vessels. Those vessels, which are not in contact with the feed, are regenerated by lowering the pressure and flushing with high-pressure product (raffinate). The low-pressure product (adsorbate) which contains the contaminants of the feed can be reused within upstream or downstream processes.

Considering the main gas components of the processed gas, the adsorption strength on activated carbon can be described by the following relation: $CO_2 > CH_4 > CO > H_2$ [21]. This means that CO_2 is preferably adsorbed on the activated carbon and, hence better removed from the feed gas stream than, for example H_2. Consequently, activated carbon is a suitable adsorbent for the production of pure H_2. In contrast, carbon molecular sieve (CMS) is often used for biogas upgrading in order to separate CO_2 from CH_4 [105]. In Paper 7, the authors observed the following adsorption strength of the main product gas components at CMS: $CO_2 > CO > H_2 > CH_4$.

In the last years, several approaches aiming to reach the fuel cell grade H_2 production via PSA from product gas derived from DFB biomass steam gasification plants were carried out at the sites of the DFB plants in Güssing and Oberwart. During these experiments with a lab-scale PSA unit employing activated carbon as adsorbents, H_2 recoveries up to 80 % were reached [106, 107]. With additional CO_2 separation before the PSA unit and further optimization measures, 90 % H_2 recovery (also used in this work) can be achieved [21]. However, there is always a trade-off between H_2 recovery and purity. Therefore, if high grade H_2 (purity higher than 99.999 %) should be generated, the recovery could be significantly lower.

In addition, the production of a gas mixture consisting mainly of H_2 and CH_4, sometimes referred to as hythane and BioHNG in this work, was also carried out with the lab-scale PSA unit. In contrast to the experiments aiming at pure H_2 production, in these test runs, CMS was used as adsorbent (compare Paper 7).

2.1.7 Gas engines

Today, gas engines are widely operated for generation of heat and power [108]. They can be operated with a variety of gaseous fuels, for example natural gas, biogas, and even hydrogen rich syngases from biomass gasifiers [109, 110]. Operated with natural gas, an electrical efficiency up to 49 % can be achieved. Gas engines have been successfully operated with the hydrogen rich product gas from DFB gasification plants for several thousand hours for CHP [45, 111]. Operated with the product gas from DFB plants, the gas engines can reach the following key figures [46, 48, 112, 113]:

- Electrical efficiency based on product gas input: 38.8 %
- Heat losses of the gas engine without considering flue gas losses: 7.4 %

- Thermal efficiency without flue gas cooling: 21.8 % at a district heat feed flow of 90 °C and a return flow of 70 °C [114]
- Air to product gas ratio: 8.2 $\text{kg} \cdot \text{kg}^{-1}$

In addition, the flue gas leaves the gas engines with a temperature between 430 and 500 °C. The flue gas can be cooled and the heat can be used for different applications, for example generation of additional district heat. The high air to product gas ratio is necessary to reduce knocking tendency caused by the high hydrogen content of the product gas from the DFB plants [110].

2.2 Calculation of the mass and energy balances

Mass and energy balances of the investigated processes were carried out using the process simulation tools IPSEpro and COCO. IPSEpro is a software system for calculating heat balances and simulating processes. It comprises a set of software modules for creating process models for a wide range of applications and for utilizing these models throughout the lifecycle of process plants [115]. It is possible to implement an actual process from a small scale experimental setup into a formal scheme to predict specific behavior of a system and to scale up this process into industrial-scale. The Biomass Gasification Library (compare Pröll [46]) implemented in the IPSEpro software is used for the presented work. COCO (CAPE-OPEN to CAPE-OPEN) is a free-of-charge CAPE-OPEN[2] compliant steady-state simulation environment [116].

A 10 MW reference plant for CHP based on state of the art DFB plants and corresponding literature data was simulated in IPSEpro [48]. Input data for the gasifier was mainly provided by operating data from the commercial DFB plants in Güssing and Oberwart. Therefore, this data can be seen as very reliable and robust. Based on this data, the mass and energy balances of the investigated process for CHP, BioH_2, BioSNG, and BioHNG production were calculated with the COCO simulator. As equation of state, the Peng-Robinson approach was chosen [117]. Tar and sulfur components were not considered in the COCO simulation, but in the IPSEpro simulation. Compressors were calculated with an isentropic efficiency of 75 % (according to manufacturer data in Müller [118]). Water gas shift, hydrogenation, and methanation reactors were simulated as equilibrium reactors minimizing the Gibbs enthalpy without kinetic data. For the simulation of the water gas shift reactors, only CO, H_2O, H_2, and CO_2 were considered as reactive components. This behavior was also observed during experiments with a lab-scale water gas shift unit with real product gas from the commercial DFB plant in Oberwart, Austria (compare Paper 1 to 5). Heat losses were only considered of the DFB gasifier as commercial plant data was available as source [44, 45, 46, 48]. These are based on operational experience. Pressure losses where not considered in the calculation of the mass and energy balance. The reference conditions for the enthalpy calculation were 25 °C (298.15 K) and 101325 Pa.

---

[2] The CAPE-OPEN Interface Standard consists of a series of specifications to expand the range of application of process simulation technologies.

The steam to dry gas ratio (Equation 18) is the ratio of the molar steam flow rate to the molar dry gas flow rate in the feed:

$$\mathrm{StG} = \frac{\dot{n}_{\mathrm{Steam}}}{\dot{n}_{\mathrm{G}}} \tag{18}$$

The steam to carbon ratio (Equation 19) is the ratio of the molar steam flow rate to the molar carbon flow rate in the feed:

$$\mathrm{StC} = \frac{\dot{n}_{\mathrm{Steam}}}{\dot{n}_{\mathrm{G}} \cdot (\varphi_{CO} + \varphi_{CO_2} + \varphi_{CH_4} + 2 \cdot \varphi_{C_2H_4} + 2 \cdot \varphi_{C_2H_6} + 3 \cdot \varphi_{C_3H_8})} \tag{19}$$

Two efficiencies were calculated based on the mass and energy balances of the investigated processes. The wet fuel-based main product efficiency (Equation 20)

$$\eta_{\mathrm{MP}} = \frac{P_{\mathrm{El,g}} + \dot{m}_{H_2} \cdot \mathrm{LHV}_{H_2} + \dot{m}_{\mathrm{SNG}} \cdot \mathrm{LHV}_{\mathrm{SNG}} + \dot{m}_{\mathrm{HNG}} \cdot \mathrm{LHV}_{\mathrm{HNG}}}{\dot{m}_{\mathrm{BM}} \cdot \mathrm{LHV}_{\mathrm{BM}}} \tag{20}$$

is the ratio of the main products (district heat is not included) of each process to the wet biomass-based energy input.

The overall efficiency

$$\eta_{\mathrm{O}} = \frac{P_{\mathrm{El,g}} + P_{\mathrm{DH}} + \dot{m}_{H_2} \cdot \mathrm{LHV}_{H_2} + \dot{m}_{\mathrm{SNG}} \cdot \mathrm{LHV}_{\mathrm{SNG}} + \dot{m}_{\mathrm{HNG}} \cdot \mathrm{LHV}_{\mathrm{HNG}}}{\dot{m}_{\mathrm{BM}} \cdot \mathrm{LHV}_{\mathrm{BM}} + \dot{m}_{\mathrm{RME}} \cdot \mathrm{LHV}_{\mathrm{RME}} + P_{\mathrm{El,c}}} \tag{21}$$

is the ratio of the energy streams of all generated products (district heat is included) of each process to the wet biomass-based energy input, the RME input, and the electricity consumption.

In addition, the carbon conversion efficiency was calculated as follows.

$$\eta_{\mathrm{C}} = \frac{\dot{m}_{\mathrm{C,Product}}}{\dot{m}_{\mathrm{C,BM}} + \dot{m}_{\mathrm{C,RME}}} \tag{22}$$

This key figure is the ratio of the carbon in the generated product to the carbon fed into the system. For calculation of this key figure, electricity and district heat were not considered.

2.3 Pinch analysis and heat integration

After the calculation of the mass and energy balances, pinch analysis of the investigated processes was carried out in order to find a suitable heat exchanger layout which minimizes external heating and cooling utilities. In general, pinch analysis is a methodology for minimizing energy consumption of chemical processes by calculating thermodynamically feasible energy targets (or minimum energy consumption) and achieving them by optimizing heat recovery systems, energy supply methods, and process operating conditions. It is also referred to as process integration, heat integration, energy integration, or pinch technology. The methodology is well described in Kemp [119] and Brunner and Krummenacher [120].

In this work, the pinch analysis was carried out using Microsoft Excel and under the assumption of a constant specific isobaric heat capacity over the whole temperature range. Heat losses of the heat exchangers were neglected and ΔT_{min} was set to 20 °C as this value seems to be a good compromise between technical and economic feasibility [120]. Subsequently, the composite curves (CC) and the grand composite curve (GCC) were drawn and the necessary cold and hot utilities were determined. District heat was considered with a feed flow temperature of 90 °C and a return flow temperature of 70 °C.

2.4 Techno-economic assessment

The techno-economic assessment is based on previously developed approaches [121]. First, the overall investment and production costs were estimated. Subsequently, the selling price of the main product for a net present value (NPV) equally zero was calculated. The base year for the calculations was 2017. In addition, it was assumed that 2016 prices are equal to 2017 prices where applicable.

2.4.1 Investment costs

Capital expenditures (CAPEX) were estimated based on a literature study as well as on budget quotes from different plant manufacturers. CAPEX from years different than 2017 were adjusted using the chemical engineering plant cost index (CEPI) and converted to actual prices considering the respective currency exchange rates.

$$\frac{\text{CAPEX 1}}{\text{CAPEX 2}} = \frac{\text{CEPI 1}}{\text{CEPI 2}} \tag{23}$$

The CAPEX of plants and units of different sizes were adjusted using order-of-magnitude estimates and capacity rationing was accounted for with Equation 24.

$$\frac{\text{CAPEX 1}}{\text{CAPEX 2}} = \left(\frac{\text{Capacity 1}}{\text{Capacity 2}}\right)^{m} \tag{24}$$

An exponent m of 0.67 was used as scale factor in this work as it seems to be a reasonable value for scaling whole plants [121]. In addition, the plant start-up expenses (SUEX) were considered to be 10 % of the calculated CAPEX. Therefore, the overall investment costs (INV) of a plant were calculated as follows.

$$\mathrm{INV} = \mathrm{CAPEX} + \mathrm{SUEX} = \mathrm{CAPEX} \cdot (1 + 10\%) \tag{25}$$

Nevertheless, according to Brown [121], in this early stage of process development, if few design details are known, the CAPEX estimation has an uncertainty from –30 % to +50 %. Furthermore, Weber [122] gives an uncertainty between 20 % and 30 % (positive and negative) at the beginning of the engineering phase of a process. Therefore, the sensitivity analysis of the CAPEX in this thesis is carried out with an uncertainty between –25 % to +25 %.

2.4.2 Production costs

The production costs or operating expenditures (OPEX) of a certain plant were split into detailed and factored estimates. The detailed estimates were calculated based on actual prices of the year 2017 of materials and energy streams according to the amounts calculated in the process simulations. Factored estimates were either considered as a percentage of the operating labor or as a percentage of the capital investment. Table 6 gives an overview of how the production costs were calculated.

Table 6: Overview of estimated OPEX.

Production costs	Detailed estimates	Factored estimates
Raw materials	Process simulation	
Operating labor	Plant data	
Utilities	Process simulation	
Employee benefits		30 % of operating labor
Supervision		10 % of operating labor
Laboratory		10 % of operating labor
Maintenance		6 % of CAPEX
Insurance and taxes		3 % of CAPEX
Operating supplies		3 % of CAPEX
Plant overhead		1 % of CAPEX
Depreciation	Equation 26	

Raw materials consider the wood chips and operating labor the wage of a plant operator before taxes. Utilities consider all other material and energy streams which need to be bought in order to operate the plant. Employee benefits consider the non-wage labor costs. Supervision considers the plant management and laboratory covers labor and equipment for analysis. Maintenance considers labor, replacement, and maintenance parts, and contract maintenance. Insurance and taxes covers non-income taxes and insurances. Operating supplies covers lubricants, filters, and custodial supplies. Plant overhead considers clerical stuff and groundskeeping. The depreciation was assumed linear and calculated according to Equation 26.

$$\text{Depreciation} = \frac{\text{CAPEX}}{n} \tag{26}$$

The raw material costs, utility costs, and revenues were calculated with the specific prices in Table 7.

Table 7: Specific prices for calculation of the production costs (OPEX).

	Values	Units	Sources
Input streams			
Wood chips (dry)	0.088	$\text{EUR} \cdot \text{kg}^{-1}$	[6]
Electricity (consumption)	0.080	$\text{EUR} \cdot \text{kWh}^{-1}$	[123] [124]
N_2	0.090	$\text{EUR} \cdot \text{m}^{-3}$	DFB plant Oberwart
RME	1.100	$\text{EUR} \cdot \text{kg}^{-1}$	DFB plant Güssing
CaO	0.150	$\text{EUR} \cdot \text{kg}^{-1}$	DFB plant Oberwart
Olivine	0.156	$\text{EUR} \cdot \text{kg}^{-1}$	DFB plant Oberwart
Makeup water	0.002	$\text{EUR} \cdot \text{kg}^{-1}$	DFB plant Güssing
Output streams			
Ash disposal	0.090	$\text{EUR} \cdot \text{kg}^{-1}$	DFB plant Güssing
District heat (generation)	0.050	$\text{EUR} \cdot \text{kWh}^{-1}$	DFB plant Oberwart

According to expert talks and experiences, the makeup amine (aMDEA) of the employed amine scrubbers does not have to be considered in the production costs as its consumption is not significant.

2.4.3 Assessment

In order to carry out the economic assessment, the assumptions in Table 8 were made for all investigated processes.

It was assumed that six employees are needed to ensure a safe, twenty-four-seven operation of the plants. The annual operating time (t) was set to

Table 8: Assumptions for the techno-economic assessment.

	Values	Units
Number of employees	6	-
Wage per employees	50 000	$\mathrm{EUR} \cdot \mathrm{a}^{-1}$
Annual operating hours (t)	8000	$\mathrm{h} \cdot \mathrm{a}^{-1}$
Plant lifetime (n)	20	a
Tax rate	25 %	-
Discount rate or ROI (i)	10 %	-

8000 hours and the expected plant lifetime (n) was set to 20 years. Furthermore, a tax rate of 25 %, which is the standard tax rate on profits in Austria, was assumed. Finally, a discount rate or a return of investment (ROI[3], i) of 10 % was chosen for the NPV calculation. The before tax (BT) cash flow was calculated based on the OPEX estimation in Table 6. It was calculated according to Equation 27 as the difference of revenues (REV) and OPEX.

$$\text{BT cash flow} = \text{REV} - \text{OPEX} \tag{27}$$

The after tax (AT) cash flow was calculated according to Equation 28, which takes the BT cash flow, the tax rate and depreciation into account.

$$\text{AT cash flow} = \text{BT cash flow} \cdot (1 - \text{Tax rate}) + \text{Depreciation} \tag{28}$$

The techno-economic assessments were based on the NPV, which was calculated with the AT cash flow, the discount rate, the plant lifetime, and the investment costs according to Equation 29.

$$\text{NPV} = \text{AT cash flow} \cdot \left(\frac{(1+i)^n - 1}{i \cdot (1+i)^n} \right) - \text{INV} \tag{29}$$

Based on the assumption of NPV = 0, the specific selling prices of the electricity, BioH_2, BioSNG, and BioHNG were calculated.

---

[3] Sometimes referred to as internal rate of return (IRR).

The specific investment costs (INV_s) were calculated according to Equation 30 and considered the overall investment costs and the generated amount of the main product (electricity, $\mathrm{BioH_2}$, BioSNG, or BioHNG).

$$\mathrm{INV}_s = \frac{\mathrm{INV}}{n \cdot t \cdot \dot{m}_i \cdot LHV_i} \tag{30}$$

The specific operating expenditures (OPEX_s) were calculated according to Equation 31 and considered the production costs (expenses, compare Table 6) and the generated main product.

$$\mathrm{OPEX}_s = \frac{\mathrm{OPEX}}{t \cdot \dot{m}_i \cdot LHV_i} \tag{31}$$

The specific total expenditures (TOTEX_s) are simply the sum of INV_s and OPEX_s according to Equation 32.

$$\mathrm{TOTEX}_s = \mathrm{INV}_s + \mathrm{OPEX}_s \tag{32}$$

Furthermore, a sensitivity analysis showing the influence of different parameters on the main product selling price was carried out for all three investigated plant capacities. The varied parameters were the annual operating hours, the CAPEX, the wood chip prices, the number of employees, the main product production efficiency, and the district heat production efficiency.

3 Results and discussion

This section presents the results of experimental investigations with a WGS unit (Section 3.1 and Papers 1 to 5) as well as of the techno-economic assessment of the four investigated processes (Section 3.2). The results in Section 3.1 were a fundamental basis for Section 3.2.

3.1 Experimental investigation of a water gas shift unit

The described experiments in this section were carried out at the site of the commercial DFB plant in Oberwart using real product gas. Several experiments were carried out with a WGS unit, which employed a commercial Fe-Cr-based catalyst (Shiftmax 120 from the company Clariant). The same catalyst batch was operated for more than 3000 hours, therefrom more than 2200 hours with tar-rich product gas extracted after the product gas filter of the plant. Figure 16 shows a simplified flowchart of the investigated WGS unit.

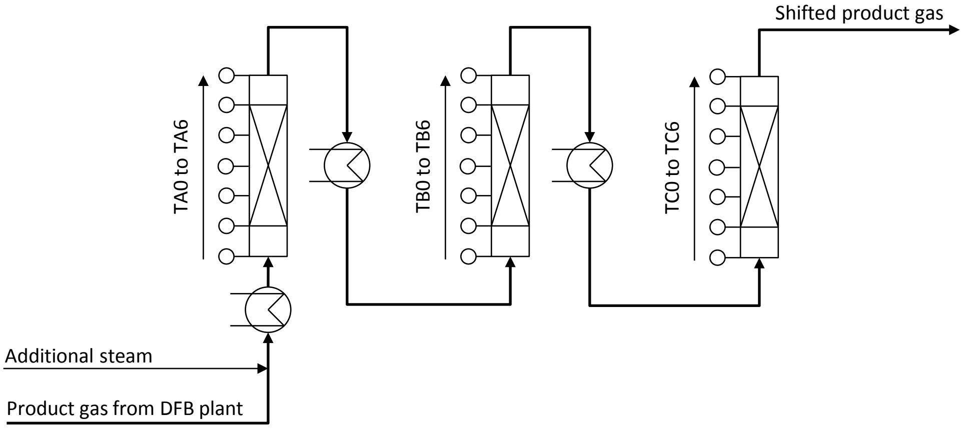

Figure 16: Simplified flowchart of the WGS unit located at the site of the DFB plant Oberwart.

The WGS unit consisted of three fixed bed reactors (A, B, and C) in series filled with a commercial Fe-Cr-based catalyst. Each catalyst bed had a diameter of about 9 cm and a bed height of about 40 cm, resulting in an catalyst volume of about 2.5 dm^3 for each reactor. Along the reactor height of each reactor, seven type J thermocouples (TA0 to TA6, TB0 to TB6, and TC0 to TC6) recorded the temperature profile along the reactors. At the inlet and outlet of reactors A and B, the gas stream could be heated or cooled in order to achieve the desired gas inlet temperatures. At the inlet of the first reactor, the product gas was mixed with additional steam to ensure a sufficient steam to carbon ratio. The WGS unit was operated at ambient pressure. During the investigations, the gas hourly space velocity (GHSV) of the first reactor was between 326 and 495 h^{-1} (dry gas based).

Paper 1 compared the operation of the WGS unit with product gas extracted before and after the RME scrubber respectively before and after tar removal. No significant performance differences could be observed. In both cases, a CO conversion of at least 91 % was achieved and the CO content could be lowered from more than 20 % to below 2 %. Those results indicated, that a WGS unit can be operated with filtered but tar-rich product gas extracted after the filter and before the RME scrubber of a DFB plant.

In Paper 2, the WGS unit was operated for more than 2250 hours with tar-rich product gas extracted before the RME scrubber of the DFB plant in Oberwart. Figures 17 and 18 show the ternary C-H-O-diagram for 1 bar and 10 bar indicating if coking and carbon deposition is thermodynamically favored.

The steam to dry gas ratio was 1.6, the steam to carbon ratio 2.7. It can be seen that during the long-term operation, the steam to dry gas ratio was sufficient in order to avoid coking and carbon deposition on the catalyst surface.

Figure 19 shows the temperature profile of the first reactor of the WGS unit.

No catalyst deactivation could be observed during the long-term operation. The concentration of COS significantly decreased along the WGS unit. The H_2S and C_4H_4S concentration did not decrease although both should have been decreased due to a higher volumetric dry gas flow rate after a WGS reactor. Consequently, it can be assumed that COS reacted to H_2S and C_4H_4S or other non-detected sulfur components. This statement is sup-

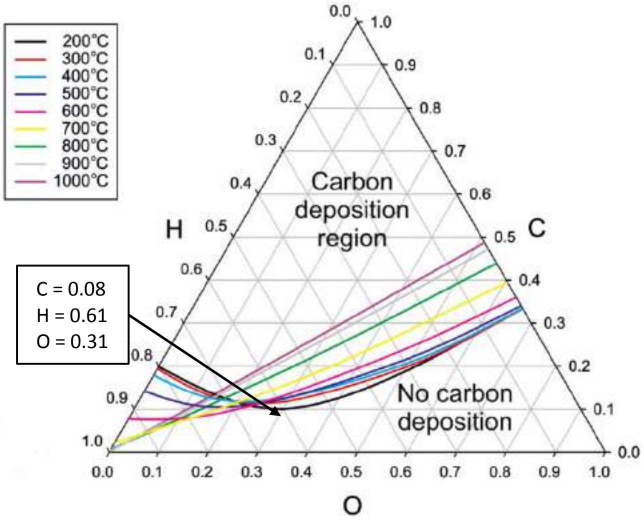

Figure 17: C-H-O ternary diagram for p = 1 bar indicating the C-H-O-ratio of the feed. The figure shows if coke formation and carbon deposition is thermodynamically favored. Based on [91], all carbon allotropes.

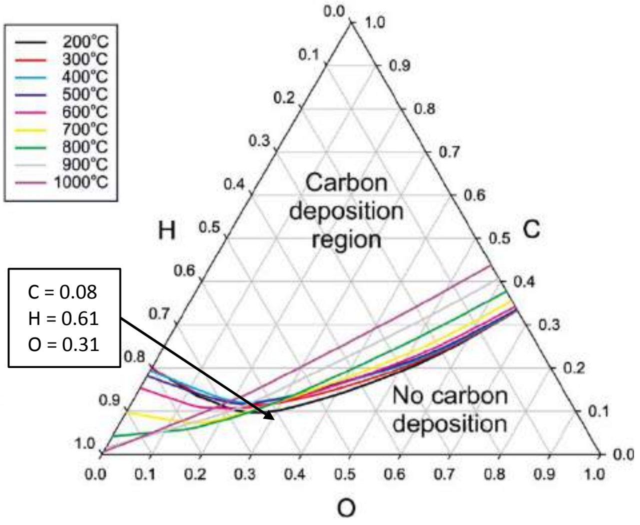

Figure 18: C-H-O ternary diagram for p = 10 bar indicating the C-H-O-ratio of the feed. The figure shows if coke formation and carbon deposition is thermodynamically favored. Based on [91], all carbon allotropes.

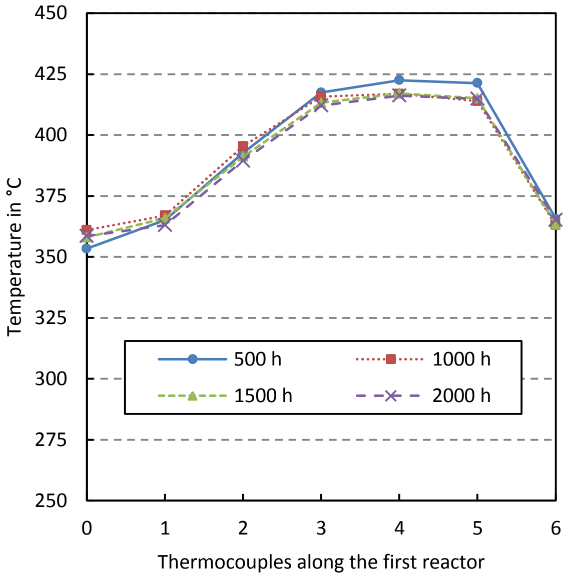

Figure 19: Temperature profile along the first reactor of the WGS unit during the long-term operation (based on Paper 2).

ported by Twigg [54] who reports that Fe-Cr-based catalysts also catalyze the conversion of COS to H_2S. The results also show that the NH_3 concentration along the WGS unit decreased due to a higher volumetric dry gas flow rate. No chemical conversion of NH_3 could be observed.

Figure 20, which is based on the results in Paper 3, shows the GCMS tar concentration at the inlet and outlet of the WGS unit in dependence of the operating time. It is also an indicator for the running time of the commercial DFB gasifier. The product gas was extracted after the filter and before the RME scrubber of the plant.

The DFB gasification plant in Oberwart was started up with fresh olivine and the first GCMS tar measurement was carried out after 430 hours of operation. The GCMS tar concentration decreased with increasing plant operating time, which can be dedicated to the formation of a catalytic layer on the used bed material. Between the third measurement after 1710 operating hours and the fourth measurement after 2050 operating hours, the plant was stopped for a few days [125]. The start-up was carried out with the same batch of bed material. Nevertheless, this interruption of the operation could

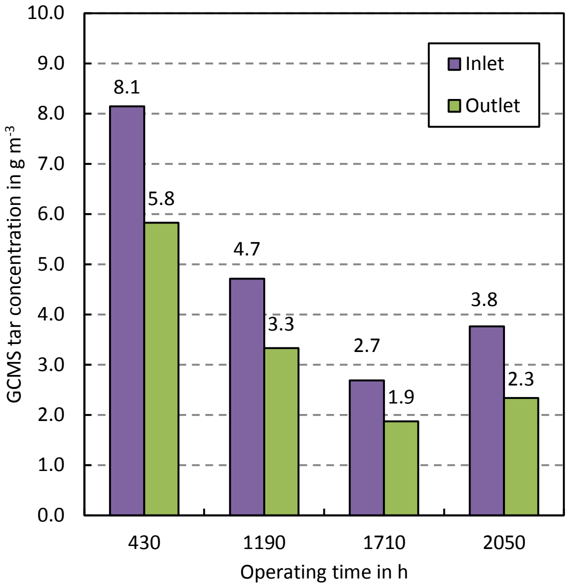

Figure 20: GCMS tar concentration of the dry product gas along the WGS unit. The product gas was extracted after the filter and before the RME scrubber of the DFB plant Oberwart.

explain the higher tar concentration at the fourth measurement. In addition, the results show that along the WGS unit, no significant GCMS tar reduction occurred. The GCMS tar concentration mainly decreased due to a higher volumetric dry gas flow rate after the WGS unit. The decrease was between –28 and – 38 % depending on the measurement. The results also indicate that some tar components were converted into tar components with lower molecular weight.

Paper 4 investigated the partial load behavior of the WGS unit during the operation with tar-rich product gas. The partial load operation did not have a negative influence on the performance, the catalyst lifetime, or the CO conversion of the WGS unit.

Based on the results in Paper 1 to 4 and based on previous work from Fail [53], an improved kinetic model (see Equation 33) for a WGS unit employing a Fe-Cr-based catalyst was developed and validated in Paper 5. The results qualify the kinetic model for basic design and engineering of a WGS unit which processes tar-rich product gas from DFB biomass gasification plants.

$$\begin{aligned} r(\varphi_x, T) =& 117.8 \, \frac{\mathrm{mol}}{\mathrm{g} \cdot \mathrm{Pa}^{1\ 71} \cdot \mathrm{s}} \cdot \exp\left(\frac{-126.6 \, \frac{\mathrm{kJ}}{\mathrm{mol}}}{R \cdot T}\right) \cdot \\ & \cdot p_{CO}^{1.77} \cdot p_{H_2O}^{0.23} \cdot p_{CO_2}^{-0.17} \cdot p_{H_2}^{-0.12} \cdot \left(1 - \frac{K_{MAL}}{K_g}\right) \end{aligned} \tag{33}$$

Overall, the experimental results showed that a WGS unit employing a commercial Fe-Cr-based catalyst can be operated with filtered but tar-rich product gas extracted before the RME scrubber of a commercial DFB gasification plant if a certain steam to carbon ratio is adjusted in the feed of the reactor. Using tar-rich product gas also enhances the energy efficiency of the process as steam, which is already contained in the product gas can also be used in the feed of the WGS unit. Therefore, steam addition can be significant lower compared to an operation with product gas extracted after the RME scrubber.

For the calculation of the mass and energy balances of the investigated processes, the same steam to dry gas and steam to carbon ratios were assumed as during the WGS unit long-term operation (compare Figures 17 and 18). The inlet gas temperature was set between 300 and 350 °C depending on the investigated process.

3.2 Techno-economic assessment

This section presents the results of the techno-economic assessment of the four investigated processes. The CHP process, the process aiming at the production of $\mathrm{BioH_2}$ and district heat, the BioSNG and district heat generation process, and the process aiming at the generation of BioHNG are presented. The technical assessment was carried out for 10 MW gasifier fuel power as most data are available from industrial plants for this size. Subsequently, the economic assessment was carried out considering three different plant capacities with 10, 50, and 100 MW gasifier fuel power. It is assumed that the efficiencies and technical coherencies do not change with increasing plant capacity.

3.2.1 Process A: Combined heat and power

In this section the technical and economic assessment of the DFB-based CHP plant is presented.

Technical assessment The technical assessment was carried out by means of mass and energy balance and heat integration of the plant with 10 MW gasifier fuel power.

Figure 21 shows a simplified flowchart of the CHP process. Wood chips with a water content of 40 % are fed into the dryer, where the water content is reduced to 20 %. Subsequently, the wood chips enter the gasifier, where they react with steam to product gas. The product gas is cooled to 150 °C before it passes through a filter, where dust particles and fly ash are removed. Furthermore, the product gas enters a RME scrubber where the majority of tar is removed, steam is condensed, and the product gas is cooled to 50 °C before it enters the gas engine to generate electricity and district heat. Tar saturated RME is recycled to the combustion reactor where it serves as additional fuel. The flue gas of the gas engine is cooled for district heat generation. The flue gas of the combustion reactor of the DFB gasification system is used for air preheating as well as for the generation of steam which serves as gasification agent. Excess heat of the process is used to operate a biomass dryer in order to enable steady conditions in the gasifier. The whole process operates at ambient pressure.

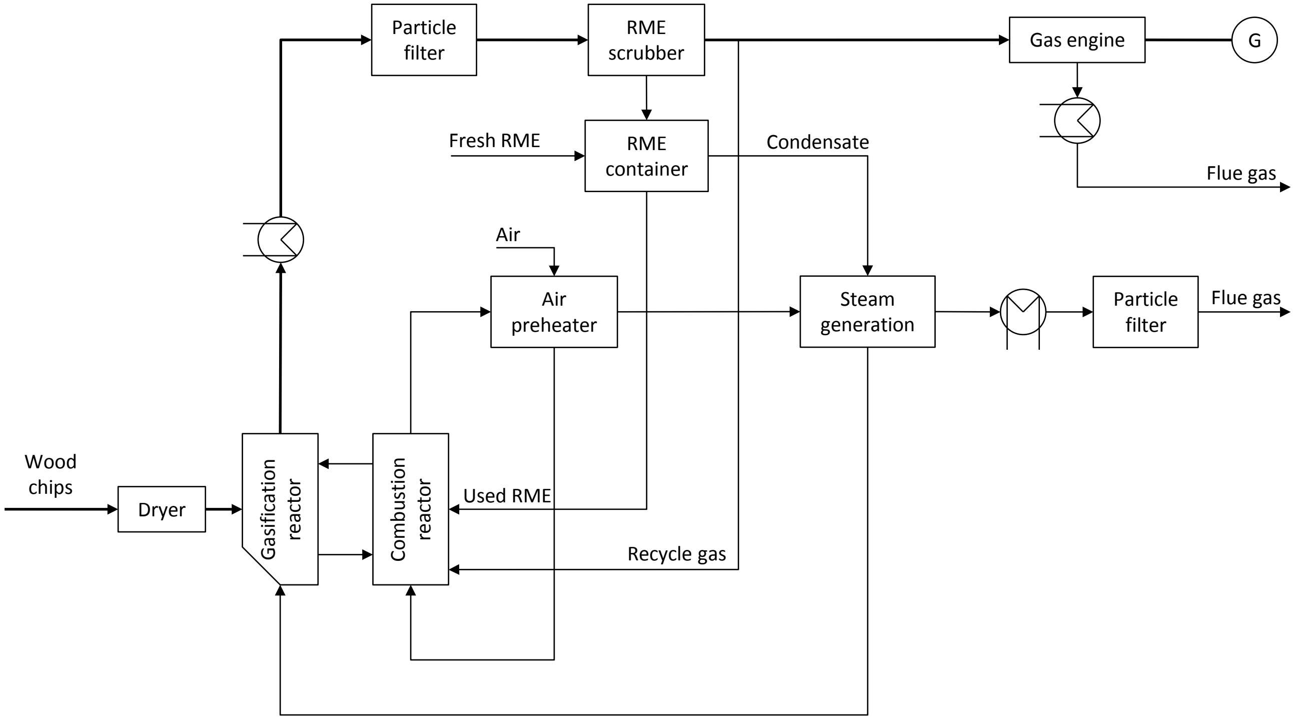
Particle filter
RME scrubber
Gas engine
G
Fresh RME
RME container
Condensate
Flue gas
Air
Air preheater
Steam generation
Particle filter
Flue gas
Wood chips
Dryer
Gasification reactor
Combustion reactor
Used RME
Recycle gas

Figure 21: Simplified flowchart of the investigated CHP process.

Figure 22 shows the composite curves (CC, left) and the grand composite curve (GCC, right) of the CHP process.

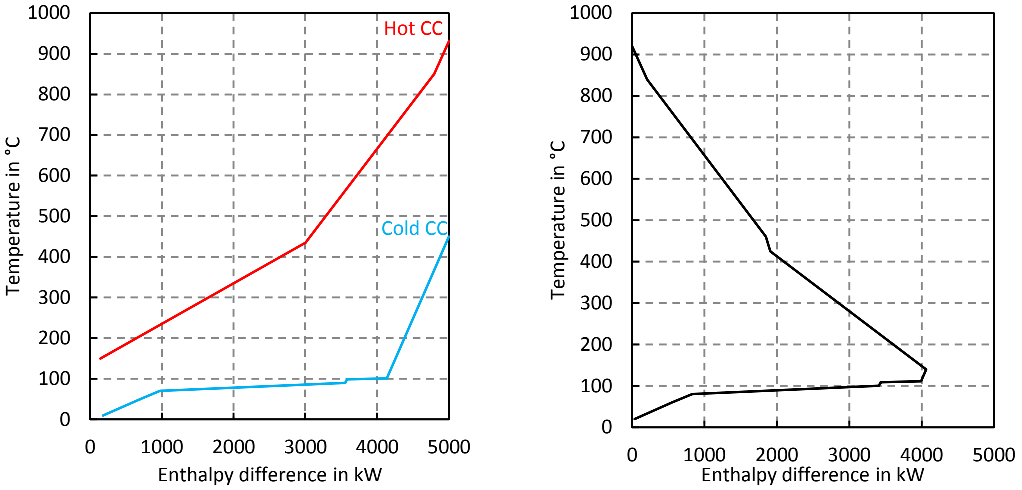

Figure 22: Composite curves (CC, left) and grand composite curve (GCC, right) for $\Delta T_{min} = 20$ °C of the investigated 10 MW CHP plant.

One can see that there is no heat exchanger network design limitation regarding temperature differences resulting in no clear pinch point. This makes the heat exchanger network design relatively straight forward (compare Figure 23). However, because of the high temperature level of the hot composite curve, there would be more potential for usage of high temperature heat.

Figure 24 shows the Sankey diagram of the investigated CHP process.

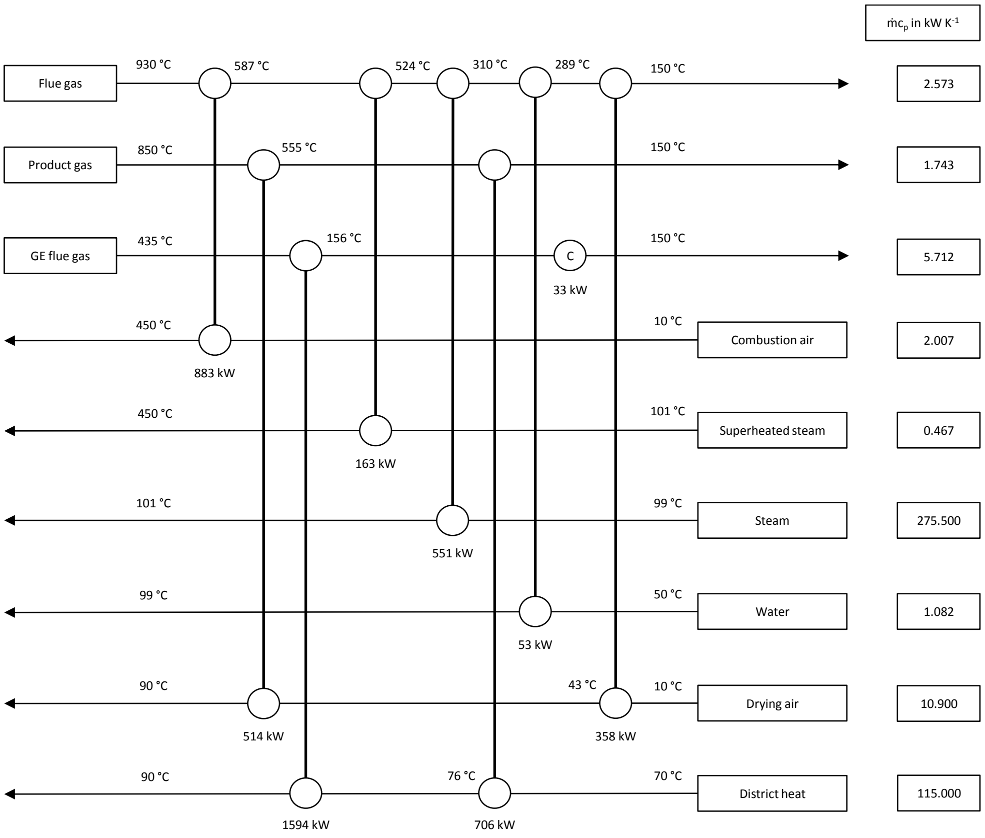
ṁc$_p$ in kW K^{-1}
Flue gas
930 °C
587 °C
524 °C
310 °C
289 °C
150 °C
2.573
Product gas
850 °C
555 °C
150 °C
1.743
GE flue gas
435 °C
156 °C
C
33 kW
150 °C
5.712
450 °C
883 kW
10 °C
Combustion air
2.007
450 °C
163 kW
101 °C
Superheated steam
0.467
101 °C
551 kW
99 °C
Steam
275.500
99 °C
53 kW
50 °C
Water
1.082
90 °C
514 kW
43 °C
358 kW
10 °C
Drying air
10.900
90 °C
1594 kW
76 °C
706 kW
70 °C
District heat
115.000

Figure 23: Heat exchanger network of the investigated 10 MW CHP plant.

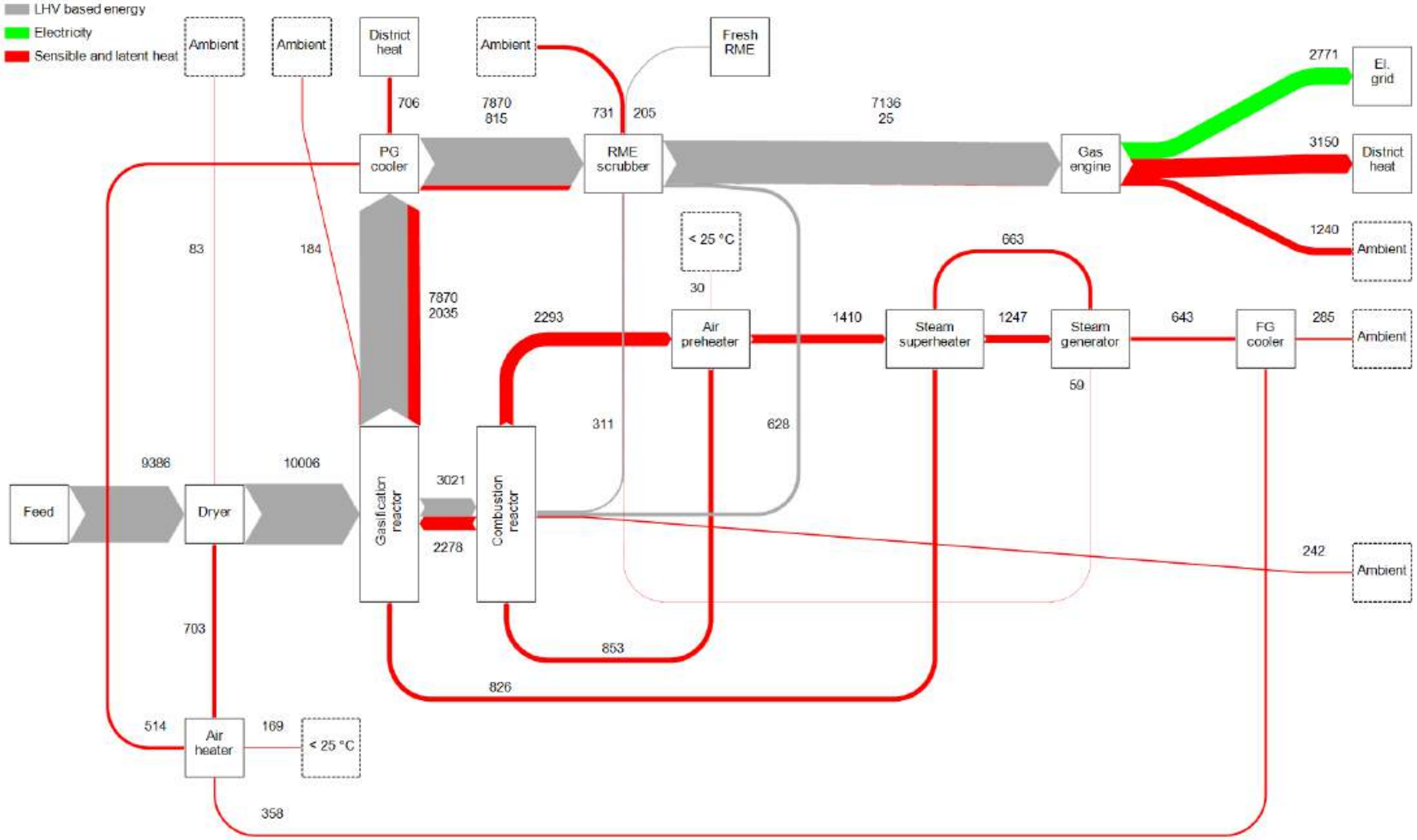
LHV based energy
Electricity
Sensible and latent heat
Ambient
Ambient
District heat
Ambient
Fresh RME
El. grid
2771
706
7870
815
731
205
7136
25
PG cooler
RME scrubber
Gas engine
3150
District heat
1240
Ambient
83
184
< 25 °C
30
663
7870
2035
2293
Air preheater
1410
Steam superheater
1247
Steam generator
643
FG cooler
285
Ambient
59
311
628
9386
10006
3021
Feed
Dryer
Gasification reactor
Combustion reactor
2278
242
Ambient
703
853
826
514
Air heater
169
< 25 °C
358

Figure 24: Sankey diagram of the investigated 10 MW CHP plant. All streams are given in kW.

The CHP process reaches an electrical efficiency of 29.5 % (main product efficiency, Equation 20) based on the lower heating value of the wood chip before the biomass dryer. In addition, it is shown that the biomass dryer has a heat demand of 872 kW low temperature heat, which could have been used for district heat generation as well. However, operation without a biomass dryer would lead to higher product gas consumption for the combustion reactor. Hence, less electricity could be produced. The overall efficiency according to Equation 21 of the process is 66.7 % (compare Figure 25). In contrast, according to Koppejan [126], conventional biomass combustion CHP plants employing a steam cycle and back pressure turbines reach electrical efficiencies between 8 and 12 %. At operation with condensation turbines and without co-generation of district heat, the electrical efficiency is between 20 to 25 % [127]. In comparison, natural gas powered combined cycle plants can reach electrical efficiencies of about 59 % [128].

These results show the advantage of the DFB gasification CHP plant, the high electrical efficiency in co-generation (electricity and district heat) operation. However, the overall fuel-based efficiency considering electricity and district heat generation seems to be similar or slightly lower compared to biomass combustion steam cycle CHP plants [127].

Table 9 shows the material and energy streams which were considered for the calculation of the production costs for the techno-economic assessment.

Table 9: Material and energy streams of the investigated CHP plants. Volumetric flow rates are given at STP.

Plant capacity	10	50	100	MW
Input streams				
Wood chips (dry)	2050	10250	20500	$kg \cdot h^{-1}$
Electricity (consumption)	350	1750	3500	kW
N_2	40	200	400	$m^3 \cdot h^{-1}$
RME	20	100	200	$kg \cdot h^{-1}$
CaO	15	75	150	$kg \cdot h^{-1}$
Olivine	20	100	200	$kg \cdot h^{-1}$
Output streams				
Ash disposal	45	225	450	$kg \cdot h^{-1}$
Electricity (generation)	2771	13855	27710	kW
District heat (generation)	3856	19280	38560	kW

It can be seen that the plants have a remarkable electricity consumption, even without compressor, which is caused by pumps, blowers, the fuel feeding system, and other consumers. The N_2 consumption can be dedicated to fuel feeding overlay and bag house filter cleaning. In addition, beside the olivine, the plants also use additional CaO in order to enhance the catalytic activity of the bed material [42, 43].

Figure 25 shows the energy distribution of the investigated CHP process.

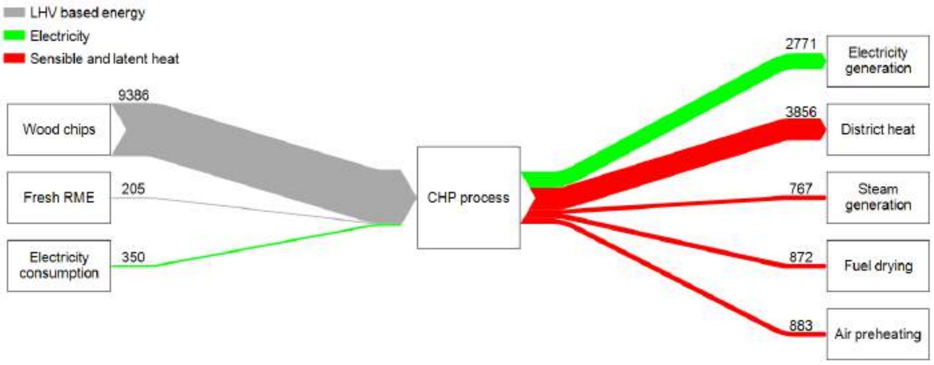
LHV based energy
Electricity
Sensible and latent heat
9386
Wood chips
205
Fresh RME
350
Electricity consumption
CHP process
2771
Electricity generation
3856
District heat
767
Steam generation
872
Fuel drying
883
Air preheating

Figure 25: Energy distribution of the investigated 10 MW CHP plant. All streams are given in kW.

It can be seen that most of the energy input is converted into district heat followed by electricity. On the one hand, without biomass drying a higher district heat output would be possible. On the other hand, more product gas has to be recycled into the combustion reactor of the gasifier in order to evaporate the moisture. This would lead to a lower electricity generation as less product gas would be available for the gas engine to generate power.

Economic assessment In this section, the results of the economic assessment of the CHP process for a gasifier fuel power of 10, 50, and 100 MW are presented.

Figure 26 shows the learning curve of the commercial DFB gasification plants.

The figure does not consider gas engines (Güssing, Oberwart, Villach, and Senden) or the methanation sections (GoBiGas) but does consider fuel

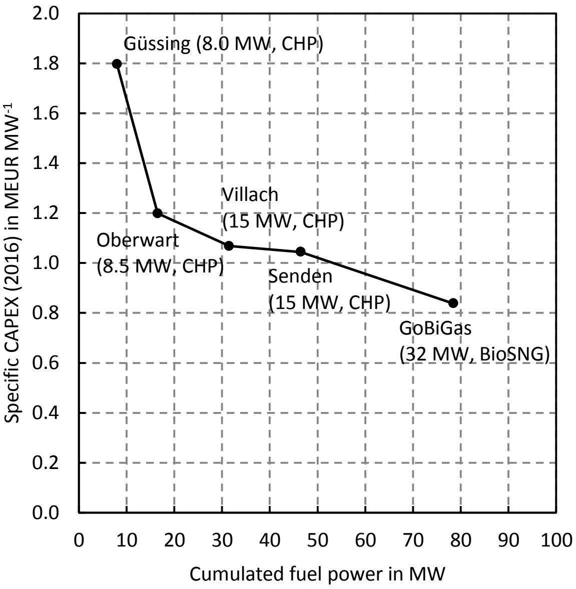

Figure 26: DFB gasification plant learning curve considering ISBL CAPEX based on experiences and [30, 118].

feeding and drying (when applicable), the gasification section, the product gas line, the flue gas line, and other equipment parts which are needed for the DFB gasification process. In addition, the specific CAPEX are based on inside battery limit (ISBL) considerations. According to expert talks and experience, the CAPEX of gas engines are about 1 million EUR per MW electrical power. The specific CAPEX of years other than 2016 were converted with the respective annual average exchange rate into US dollar as the CEPI is an US index and then converted into 2016 CAPEX using the CEPI. Subsequently, the 2016 US dollar CAPEX were converted back into EUR CAPEX. It is assumed that the 2016 costs are the same as the 2017 costs.

Table 10 shows the capital costs of the investigated CHP plants.

Table 10: Investment costs of the investigated CHP plants.

Plant capacity	10	50	100	MW
CAPEX	12 000 000	35 000 000	56 000 000	EUR
SUEX	1 200 000	3 500 000	5 600 000	EUR
INV	13 200 000	38 500 000	61 600 000	EUR

The capital costs of the 10 MW CHP plant are based on Figure 26 considering ISBL costs. A specific CAPEX of 1 million EUR per MW gasifier fuel power was chosen. The gas engine was considered with 2 million EUR. The capital costs of the other plant capacities were calculated using capacity rationing (see Equation 24).

Table 11 shows the results of the techno-economic assessment.

Table 11: Results of the techno-economic assessment of the investigated CHP plants.

Plant capacity	10	50	100	MW
OPEX	4 557 360	16 486 800	30 003 600	$\mathrm{EUR} \cdot \mathrm{a}^{-1}$
REV	5 824 649	20 183 061	35 917 617	$\mathrm{EUR} \cdot \mathrm{a}^{-1}$
BT cash flow	1 267 289	3 696 261	5 914 017	$\mathrm{EUR} \cdot \mathrm{a}^{-1}$
AT cash flow	1 550 467	4 522 196	7 235 513	$\mathrm{EUR} \cdot \mathrm{a}^{-1}$
El. selling price for NPV = 0	193	113	92	$\mathrm{EUR} \cdot \mathrm{MWh}^{-1}$

The BT cash flow is lower than the AT cash flow. This can be explained by the fact that depreciation is added back to the AT cash flow. The electricity selling price of the 10 MW plant is significantly higher than the current (2017) feed-in tariff of 133 $\mathrm{EUR} \cdot \mathrm{MWh}^{-1}$ for biomass-based plants between 5 and 10 MW [17]. In contrast, the feed-in tariff for plants over 10 MW is currently at 105 $\mathrm{EUR} \cdot \mathrm{MWh}^{-1}$ [17]. This value is lower than the electricity selling price of the 50 MW plant but higher than the electricity selling price of the 100 MW plant. Therefore, from this point of view, the CHP plant with 100 MW gasifier fuel capacity would be economically feasible.

Figure 27 compares different electricity generation processes. The values for DFB gasification are based on the electricity selling prices calculated in this thesis for the 10 and 100 MW plant (see Table 11). The values of the other processes are based on German data from 2013 in Kost et al. [129].

It can be seen that the 10 MW CHP plant has similar production costs as existing biogas plants (no heat generation considered) and the upper limit of offshore wind turbines. The 100 MW CHP plant has similar performance as gas combined cycle plants. However, the production costs of lignite and black coal power plants are significantly lower.

Figure 28 shows the specific cost distribution of the investigated plant capacities.

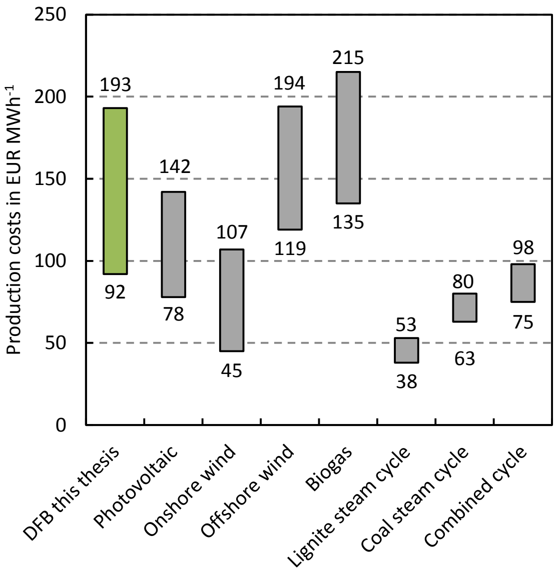

Figure 27: Typical production costs of different electricity generation routes. Only the DFB process considers CHP.

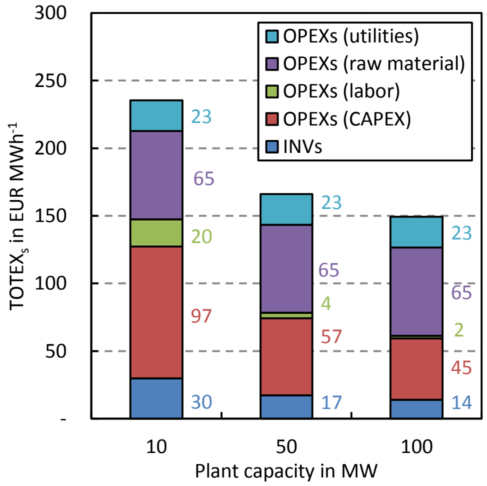

Figure 28: Specific cost distribution based on the generated electricity.

In case of the 10 MW plant capacity, the CAPEX related costs have the highest share followed by the raw material (wood chips) related costs. In addition, the share of the labor related costs is the lowest. With increasing plant capacity, the CAPEX and labor related costs decrease which can be dedicated to economy of scale effects. In contrast, at the higher plant capacities, the raw material and utility related costs become more significant.

Figure 29 shows the distribution of the raw material and utility costs for the 10 MW CHP plant.

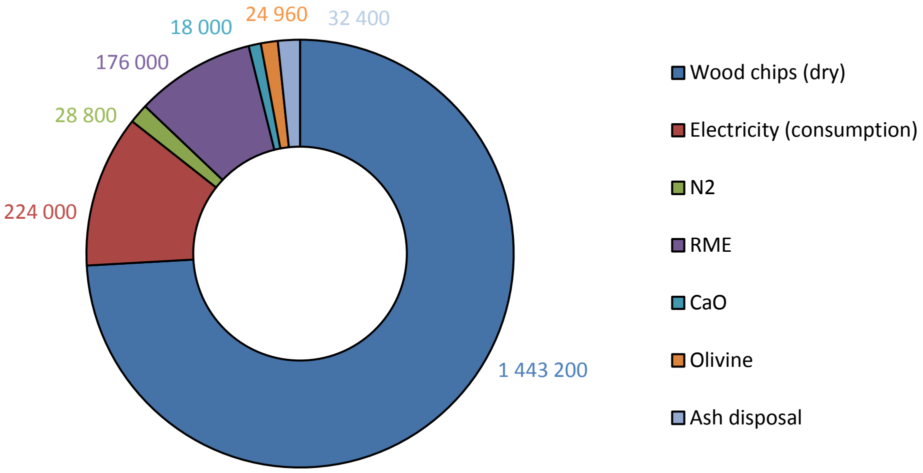

Figure 29: Distribution of annual raw material and utility costs based on the 10 MW plant in EUR $\cdot$ a^{-1}.

It can be seen that the costs for the wood chips account for about 74 % of the specific material and energy costs. In addition, the electricity costs account for 12 %. Moreover, the RME consumption accounts for about 9 % of the annual material and energy costs. Therefore, the wood chips, the electricity, and the RME account for about 95 % of the annual raw material and utility costs.

Figures 30 to 32 show the influence of different process variables on the specific electricity selling price for the 10, 50, and 100 MW CHP plant. From the slope of the lines one can see how significant the influence of single variables is.

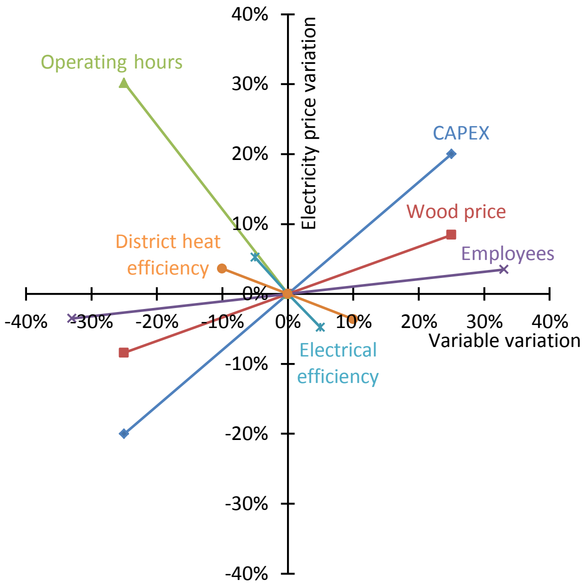

Figure 30: Sensitivity analysis of the 10 MW CHP plant.

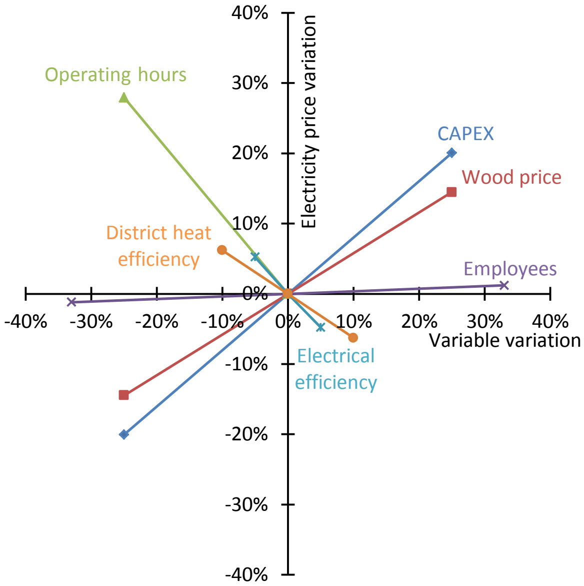

Figure 31: Sensitivity analysis of the 50 MW CHP plant.

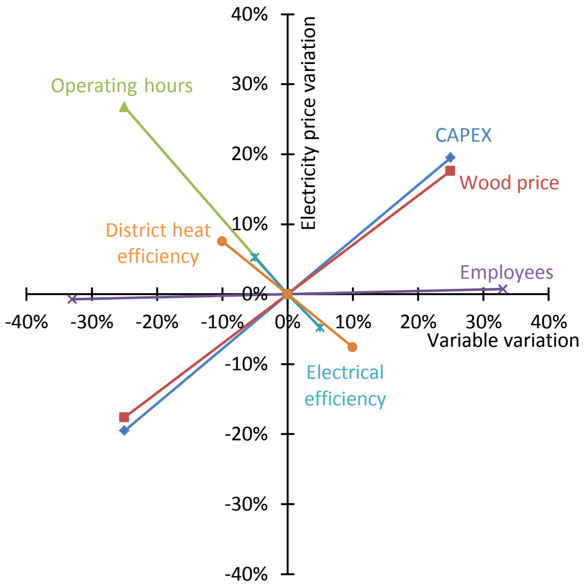

Figure 32: Sensitivity analysis of the 100 MW CHP plant.

In case of the 10 MW plant it can be seen that a change of the operating hours and the electrical efficiency would have the most significant influence on the economic feasibility of the CHP process. Furthermore, a variation of the CAPEX and the wood chip prices would also have a high influence. In contrast, the influence of the number of employees and the district heat power is relatively low. It can also be seen that with increasing plant capacity to 50 or 100 MW the influence of the wood price and the district heat increases whereas the influence of the number of employees decreases even more.

3.2.2 Process B: Hydrogen and district heat

In this section the technical and economical assessment of the DFB-based plant for $BioH_2$ and district heat is presented.

Technical assessment The technical assessment was carried out by means of mass and energy balance calculations and heat integration of the plant with 10 MW gasifier fuel power.

Figure 33 shows a simplified flowchart of the investigated process. Wood chips are dried and subsequently enter the gasifier where they are converted into the H_2-rich product gas. The product gas is cooled, filtered, and enters an adiabatic fixed bed WGS reactor employing a Fe-Cr-based catalyst. Before the WGS reactor, the product gas is mixed with additional steam in order to avoid coking and carbon deposition on the catalyst (compare Section 3.1). In the WGS reactor, CO and H_2O are converted into additional H_2 and CO_2 according to Equation 14. Because of the exothermic WGS reaction, the gas has to be cooled and is subsequently fed into the RME scrubber where steam is condensed and tar removed. The condensate is used for steam generation for the DFB gasifier and the WGS reactor. The cleaned product gas enters an amine scrubbing unit where 99 % of the CO_2 is removed via chemisorption with aMDEA (1847 $\mathrm{kg \cdot h^{-1}}$). A partial flow of the CO_2 (79.2 $\mathrm{kg \cdot h^{-1}}$) is used as overlaying and inertization agent for the fuel feeding system and blowers along the process. Therefore, it replaces N_2 which is used as inertization fluid for the CHP process. Subsequently, the product gas is dried and compressed to an absolute pressure of 10 bar before it is fed into a PSA unit where H_2 with a purity of 99.9 % is separated from the other gaseous components at a recovery of 90 %. A partial flow of the adsorbate of the PSA unit is recycled into the combustion reactor of the DFB gasification system as fuel whereas the main fraction of the adsorbate is burnt in order to provide heat for the steam generation and other units along the process. The flue gas of the process is mainly used for air preheating. Subsequently, it is filtered and led into the ambient. The gasification process operates at ambient pressure.

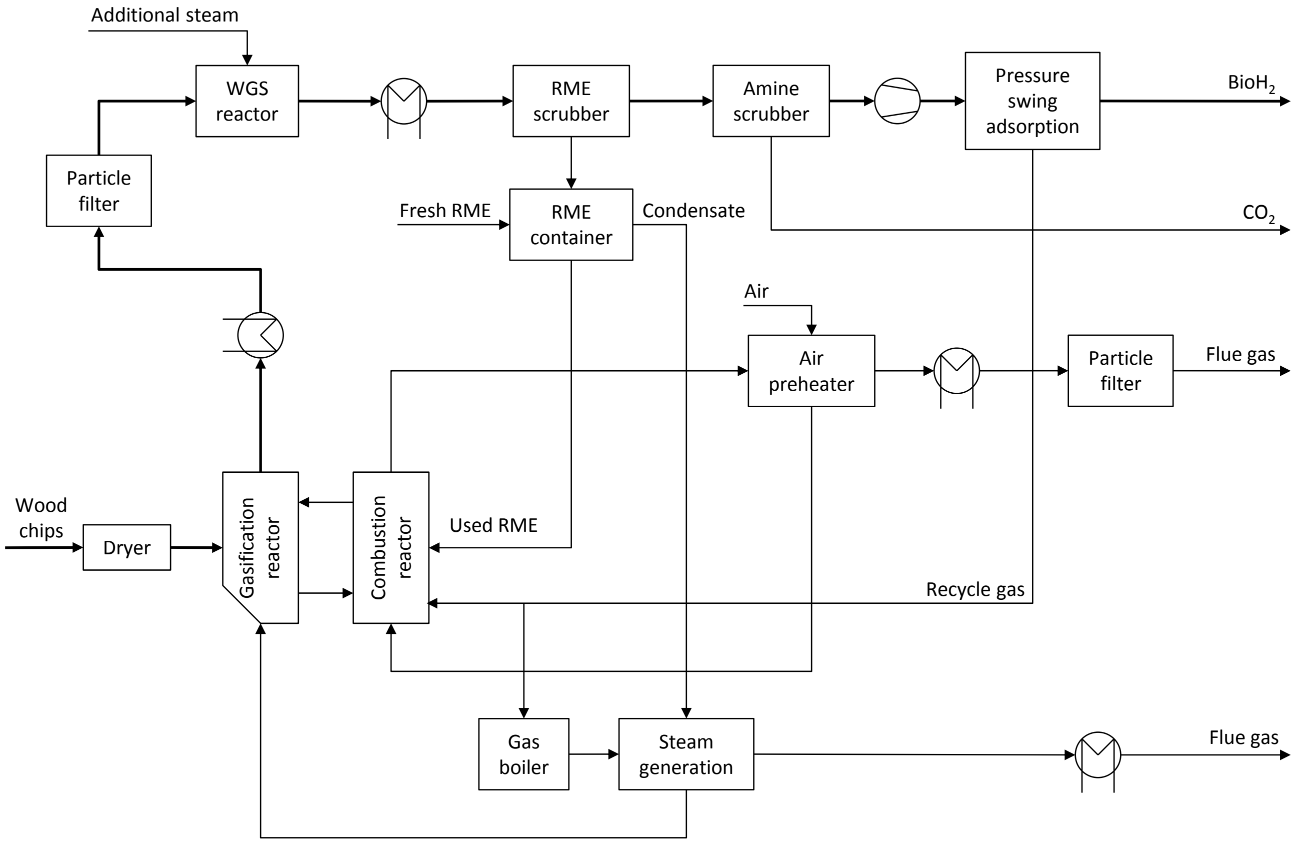
Additional steam
WGS reactor
RME scrubber
Amine scrubber
Pressure swing adsorption
BioH$_2$
Particle filter
Fresh RME
RME container
Condensate
CO$_2$
Air
Air preheater
Particle filter
Flue gas
Wood chips
Dryer
Gasification reactor
Combustion reactor
Used RME
Recycle gas
Gas boiler
Steam generation
Flue gas

Figure 33: Simplified flowchart of the plant for BioH$_2$ and district heat generation.

Figure 34 shows the composite curves and the grand composite curve of the investigated process.

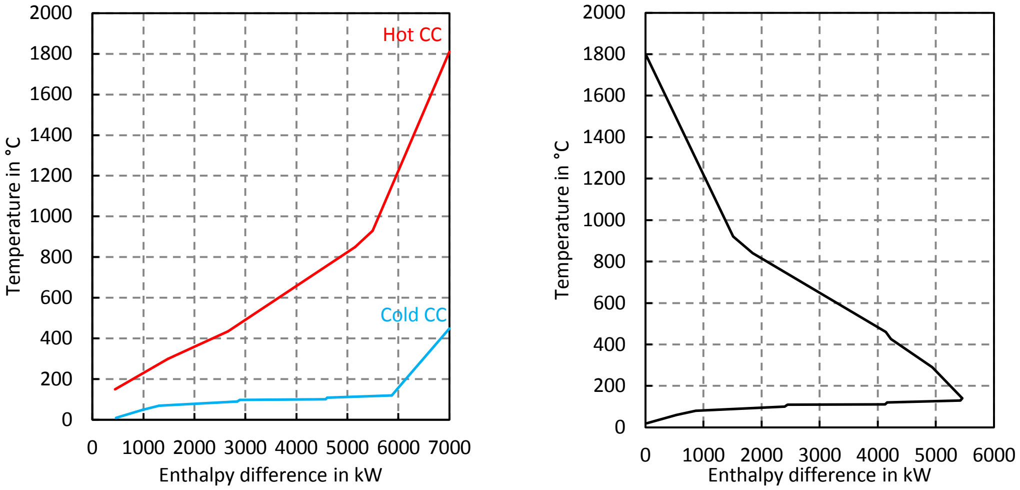

Figure 34: Composite curves (left) and grand composite curve (right) for $\Delta T_{min} = 20$ °C of the investigated plant for BioH_2 and district heat generation with 10 MW fuel power.

It can be seen that there is a sufficient high temperature difference at all temperature levels to realize an economic heat exchanger network (see Figure 35). The most significant cold streams which need to be heated up are the water for steam generation and the CO_2 rich amine stream for regeneration.

Figure 35 shows the heat exchanger network of the investigated process.

Along the overall process 20 kW of cooling utility is necessary. In addition, 1200 kW of district heat at a feed flow temperature of 90 °C and a return flow temperature of 70 °C can be generated.

Figure 36 shows a Sankey diagram of the investigated process for BioH_2 and district heat production.

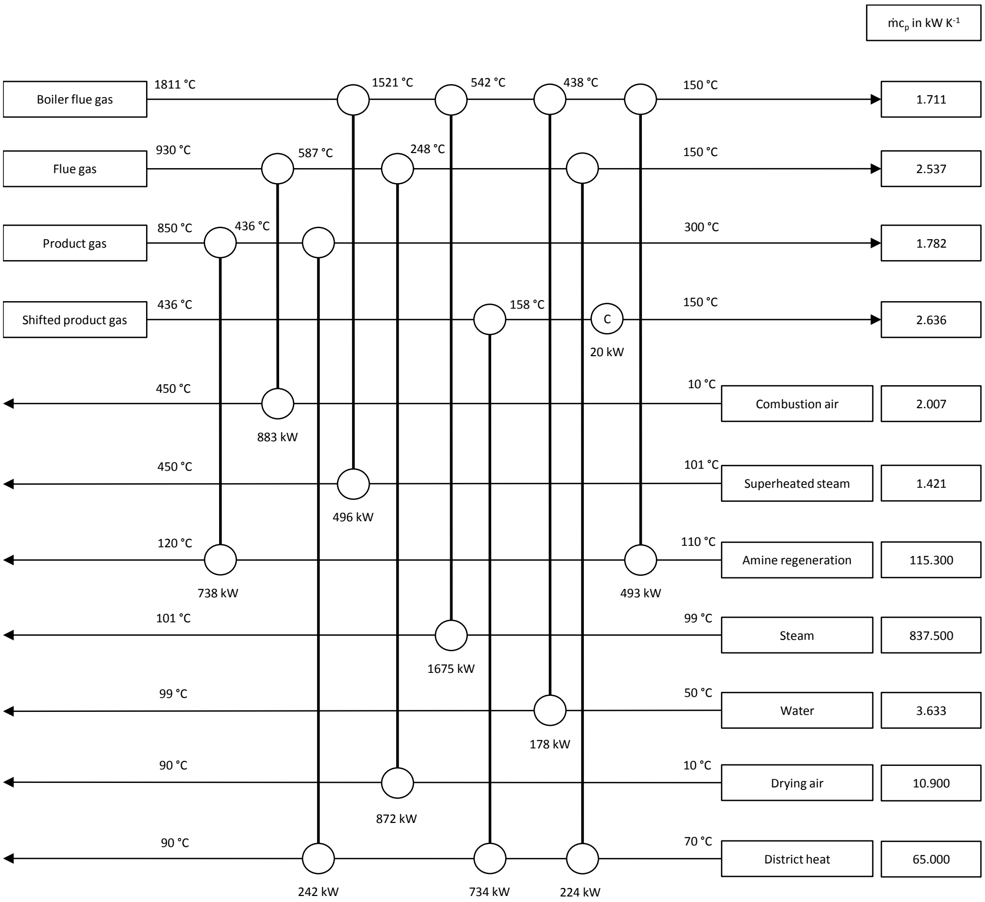
ṁcp in kW K-1
Boiler flue gas
1811 °C
1521 °C
542 °C
438 °C
150 °C
1.711
Flue gas
930 °C
587 °C
248 °C
150 °C
2.537
Product gas
850 °C
436 °C
300 °C
1.782
Shifted product gas
436 °C
158 °C
C
150 °C
2.636
20 kW
450 °C
10 °C
Combustion air
2.007
883 kW
450 °C
101 °C
Superheated steam
1.421
496 kW
120 °C
110 °C
Amine regeneration
115.300
738 kW
493 kW
101 °C
99 °C
Steam
837.500
1675 kW
99 °C
50 °C
Water
3.633
178 kW
90 °C
10 °C
Drying air
10.900
872 kW
90 °C
70 °C
District heat
65.000
242 kW
734 kW
224 kW

Figure 35: Heat exchanger network of the investigated plant for BioH$_2$ and district heat generation with 10 MW fuel power.

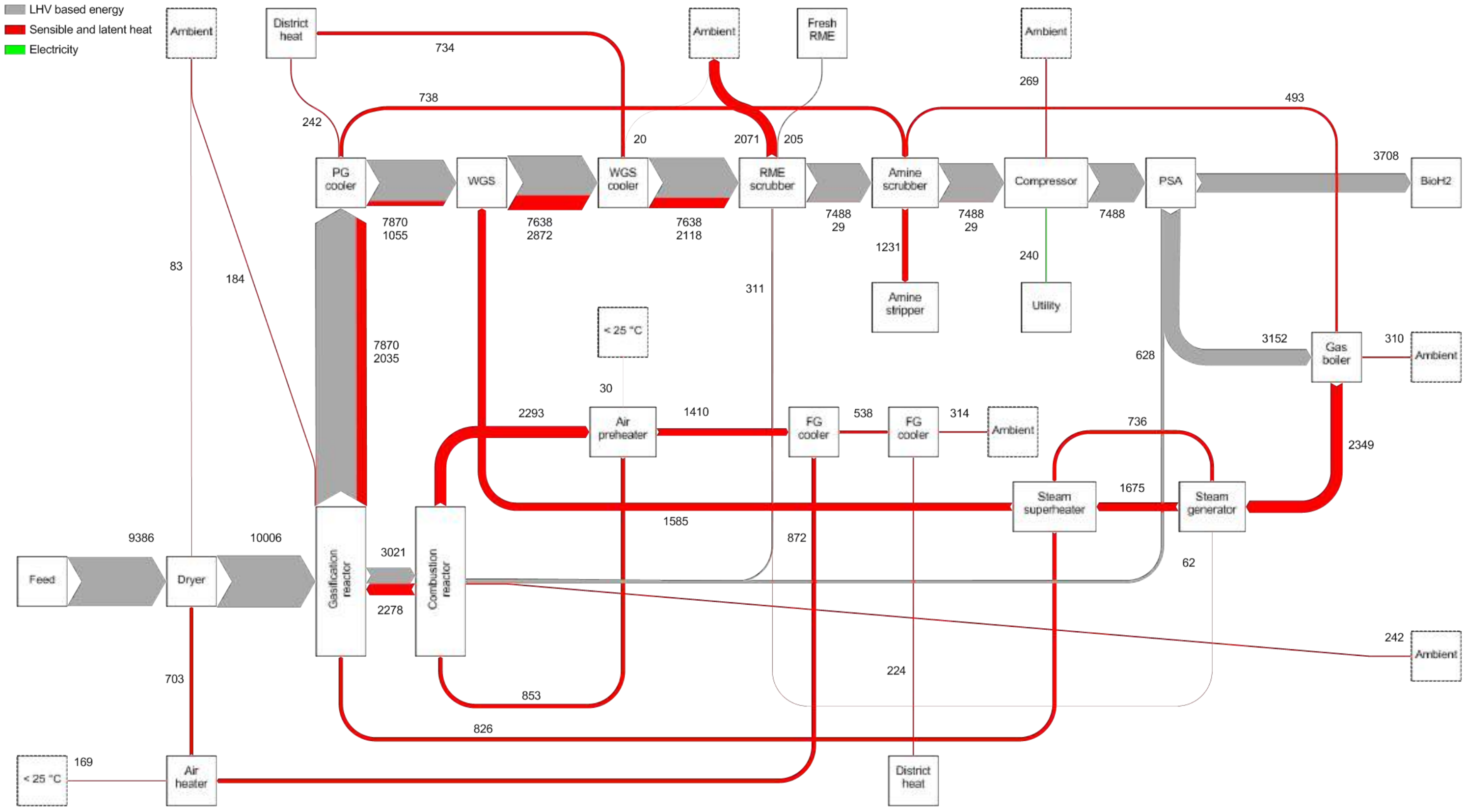
LHV based energy
Sensible and latent heat
Electricity
Ambient
District heat
734
Ambient
Fresh RME
Ambient
738
242
269
493
20
2071
205
3708
PG cooler
WGS
WGS cooler
RME scrubber
Amine scrubber
Compressor
PSA
BioH2
7870
1055
7638
2872
7638
2118
7488
29
7488
29
7488
1231
240
83
184
311
Amine stripper
Utility
7870
2035
< 25 °C
628
3152
Gas boiler
310
Ambient
30
2293
Air preheater
1410
FG cooler
538
FG cooler
314
Ambient
736
2349
1675
Steam superheater
Steam generator
1585
9386
10006
872
62
Feed
Dryer
Gasification reactor
3021
Combustion reactor
2278
242
Ambient
703
224
853
826
< 25 °C
169
Air heater
District heat

Figure 36: Sankey diagram of the investigated plant for BioH$_2$ and district heat generation with 10 MW gasifier fuel power. All streams are given in kW.

A fuel-based BioH_2 production efficiency of about 39.5 % can be reached with the suggested process layout (main product efficiency, Equation 20). The overall efficiency (Equation 21) is about 47.3 %. The diagram also indicates that the amine scrubber and the steam generation units are the most significant heat consumers. Furthermore, even though the BioH_2 recovery in the PSA unit was set to 90 %, only about 49.5 % of the energy content of the feed gas can be found in the raffinate (high pressure BioH_2) fraction of the PSA, which can be mainly dedicated to the high CH_4 content in the adsorbate (low pressure product).

These results are in agreement with the results in Paper 8 and similar to published literature [130]. However, the efficiency of 61 % reported in Müller et al. [131] is higher which can be dedicated to an additional steam reforming unit which converts hydrocarbons into additional H_2. Other ways for renewable H_2 production can be based on biogas steam reforming or water electrolysis. According to Paper 8 and Miltner et al. [130], biogas steam reforming plants achieve a fuel-based H_2 production efficiency between 40 % and slightly more than 50 %. Alkaline water electrolyzers reach H_2 production efficiencies up to 70 % and PEM electrolyzers efficiencies up to 82 % (compare Paper 8, Zeng and Zhang [27], and Miltner et al. [130]). In contrast, according to Mueller-Langer et al. [132], fossil natural gas steam reforming plants reach H_2 production efficiencies between 70 and 80 %. The carbon conversion efficiency of the BioH_2 production process is zero as no carbon containing products are generated.

Figure 37 shows a Sankey diagram indicating the H flow in BioH_2, CH_4, C_xH_y, and H_2O streams.

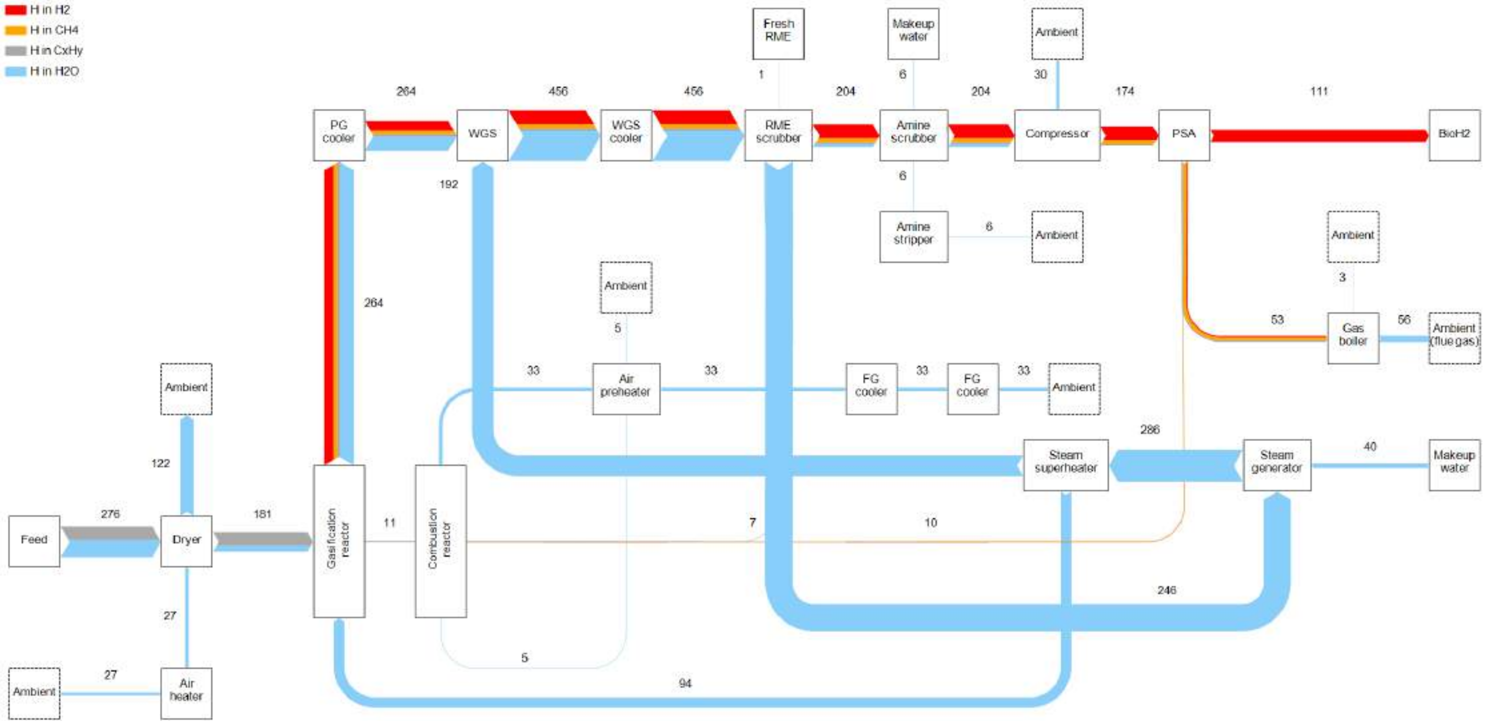
H in H2
H in CH4
H in CxHy
H in H2O
Fresh RME
Makeup water
Ambient
1
6
30
264
456
456
204
204
174
111
PG cooler
WGS
WGS cooler
RME scrubber
Amine scrubber
Compressor
PSA
BioH2
192
6
Amine stripper
6
Ambient
Ambient
3
264
Ambient
5
53
Gas boiler
56
Ambient (flue gas)
33
Air preheater
33
FG cooler
33
FG cooler
33
Ambient
Ambient
122
286
Steam superheater
Steam generator
40
Makeup water
Feed
276
Dryer
181
Gasification reactor
11
Combustion reactor
7
10
27
246
5
Ambient
27
Air heater
94

Figure 37: Sankey diagram of the investigated plant for $BioH_2$ and district heat generation with 10 MW gasifier fuel power showing the H flows in H_2, CH_4, C_xH_y, and H_2O streams in $kg \cdot h^{-1}$.

It can be seen that 40.2 % of the H_2 which is contained in the biomass feedstock is recovered as pure BioH_2 at the end of the process. This equals a specific H_2 production rate of 54 g H_2 per kg dry biomass. The specific production rate is in agreement with the results in Paper 8 and higher than in Fail et al. [106] which can be dedicated to the assumption of a higher H_2 recovery of the PSA unit. This assumption is applicable because of the CO_2 separation with the amine scrubber upstream of the PSA unit. Therefore, the PSA has to separate significantly less CO_2.

Table 12 shows the material and energy streams of the investigated process for BioH_2 and district heat generation.

Table 12: Material and energy streams of the investigated process for BioH_2 and district heat generation.

Plant capacity	10	50	100	MW
Input streams				
Wood chips (dry)	2050	10250	20500	$kg \cdot h^{-1}$
Electricity (consumption)	795	3975	7950	kW
RME	20	100	200	$kg \cdot h^{-1}$
CaO	15	75	150	$kg \cdot h^{-1}$
Olivine	20	100	200	$kg \cdot h^{-1}$
Makeup water	360	1800	3600	$kg \cdot h^{-1}$
Output streams				
Ash disposal	45	225	450	$kg \cdot h^{-1}$
BioH_2 (generation)	111.3	556.5	1113	$kg \cdot h^{-1}$
BioH_2 (generation)	3708	18540	37080	kW
District heat (generation)	1200	6000	12000	kW

The electricity consumption is split up into the consumption of the compressor (240 kW), the amine scrubber (205 kW), and other electricity consumers (350 kW[4]). The values are given for the 10 MW plant. For the other plant sizes the values are a multiple of five respectively ten. The amount of generated district heat results from the pinch analysis and the heat exchanger network with a feed flow temperature of 90 °C and a return flow temperature of 70 °C.

Figure 38 shows the energy distribution of the investigated BioH_2 process.

---

[4] The same value as for the CHP plant was used.

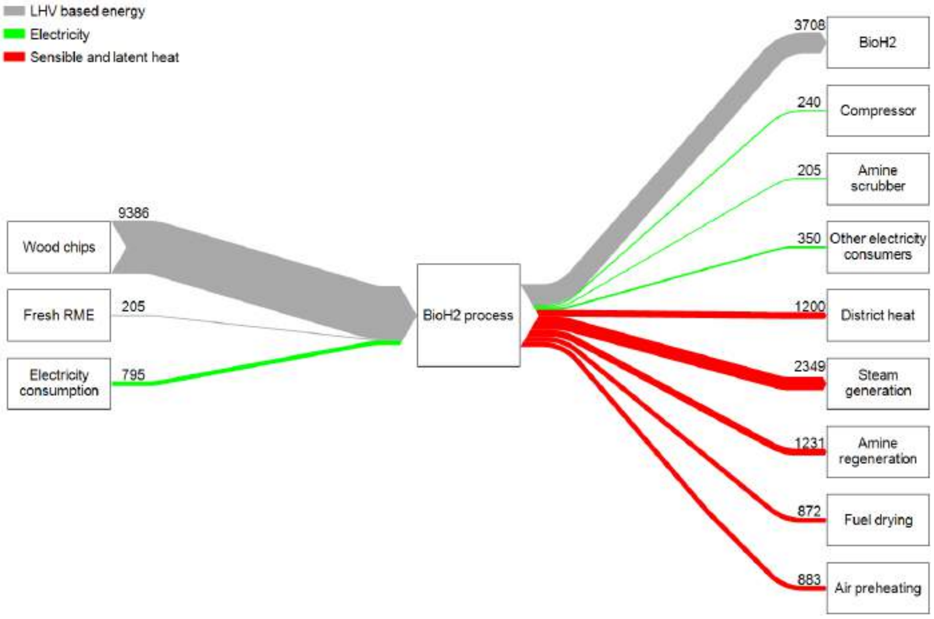
LHV based energy
Electricity
Sensible and latent heat
Wood chips
9386
Fresh RME
205
Electricity consumption
795
BioH2 process
3708
BioH2
240
Compressor
205
Amine scrubber
350
Other electricity consumers
1200
District heat
2349
Steam generation
1231
Amine regeneration
872
Fuel drying
883
Air preheating

Figure 38: Energy distribution of the investigated 10 MW BioH_2 plant. All streams are given in kW.

It can be seen that most of the energy input is converted into BioH_2. In addition, a significant amount of heat is used for steam generation for the gasifier and the WGS reactor in order to ensure a sufficient steam to carbon ratio to avoid coking and carbon deposition. Therefore, in order to reduce the heat demand for steam generation, catalyst development aiming at lower steam to carbon ratios would be desirable. Hence, more heat could be used for district heat generation. The amine regeneration also requires a high amount of heat. Without biomass drying, a higher district heat output would be possible. On the other hand, more product gas had to be recycled into the combustion reactor of the gasifier in order to evaporate the moisture. This would lead to a lower BioH_2 generation.

Economic assessment In this section, the results of the economic assessment of the process for BioH_2 and district heat production for a gasifier fuel power of 10, 50, and 100 MW are presented.

Table 13 shows the investment costs for the plants with 10, 50, and 100 MW.

Table 13: Investment costs of the investigated process for $BioH_2$ and district heat generation.

Plant capacity	10	50	100	MW
CAPEX	15 000 000	44 000 000	70 000 000	EUR
SUEX	1 500 000	4 400 000	7 000 000	EUR
INV	16 500 000	48 400 000	77 000 000	EUR

The capital costs of the 10 MW plant are based on Figure 26 and on expert talks as well as on data from single unit operations. The capital costs for the 50 and 100 MW plant are calculated based on the capital cost estimation of the 10 MW plant by using capacity rationing (Equation 24).

Table 14 shows the results of the techno-economic assessment.

Table 14: Results of the techno-economic assessment of the investigated process for $BioH_2$ and district heat generation.

Plant capacity	10	50	100	MW
OPEX	5 359 120	19 415 600	35 141 200	$EUR \cdot a^{-1}$
REV	6 943 232	24 062 328	42 533 722	$EUR \cdot a^{-1}$
BT cash flow	1 584 112	4 646 728	7 392 522	$EUR \cdot a^{-1}$
AT cash flow	1 938 084	5 685 046	9 044 391	$EUR \cdot a^{-1}$
$BioH_2$ selling price for NPV = 0	7.3	4.9	4.2	$EUR \cdot kg^{-1}$
$BioH_2$ selling price for NPV = 0	218	146	127	$EUR \cdot MWh^{-1}$

It can be seen that the BT cash flows are lower than the AT cash flows which can be explained by the high depreciation which is added back to the AT cash flows.

Figure 39 shows the specific cost distribution of the investigated plant capacities.

In case of the 10 MW plant capacity, the CAPEX-related costs have the highest share followed by the raw material-related costs. In addition, the share of the labor related costs is the lowest. With increasing plant capacity, the CAPEX and labor-related costs decrease which can be dedicated to economy of scale effects. In contrast, at the higher plant capacities, the raw material and utility-related costs become more significant.

The specific production costs are in the same order of magnitude as the results presented in Paper 8 and in Zech et al. [133]. However, the reported values in Zech et al. [133] are slightly smaller than the values reported in

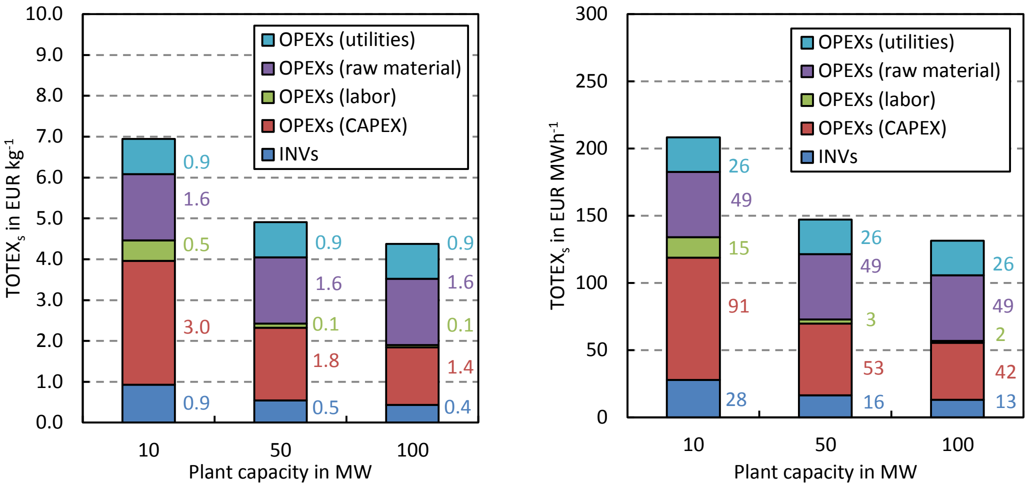

Figure 39: Specific cost distribution based on the generated $BioH_2$.

this work which can be dedicated to different assumptions and a different base year (2011). Müller et al. [131] reports specific H_2 production costs of 54 $EUR \cdot MWh^{-1}$ for a 100 MW fuel input plant which is significantly lower than the results presented in this work. However, this can be dedicated to the higher process efficiency of the also biomass-based process. In contrast, Müller-Langer [132] reports production costs of natural gas steam reforming plants between 1.03 $EUR \cdot kg^{-1}$ (large scale) and 2.60 $EUR \cdot kg^{-1}$ (small scale). Those comparably low production costs can be, on the one hand, dedicated to the low natural gas prices and, on the other hand, to the high generation efficiency of natural gas steam reforming plants.

Figure 40 shows the cost distribution of the annual material and energy streams of the 10 MW plant.

The wood chip costs have the most significant share with about 65 % followed by the electricity consumption with 23 % and the RME consumption with 8 %. The distribution for the 50 MW and 100 MW plants is equal.

Figures 41 to 43 show the influence of different process variables on the specific $BioH_2$ selling price for the 10, 50, and 100 MW $BioH_2$ plant. From the slope of the lines one can see how significant the influence of single variables is.

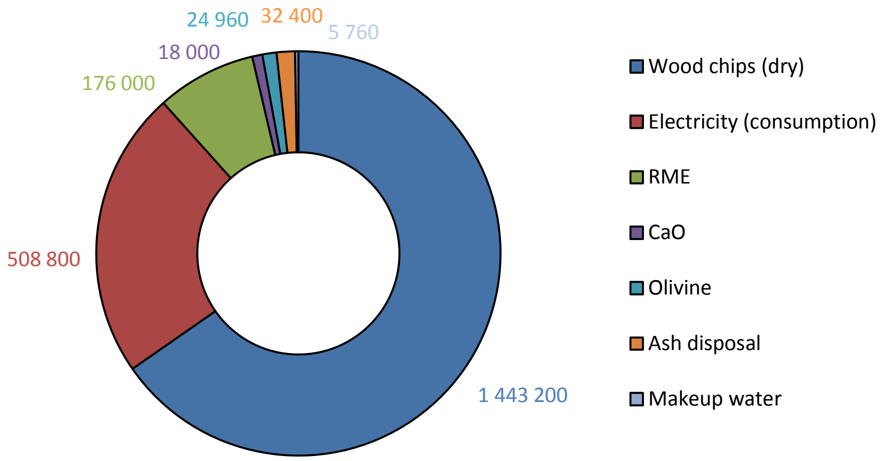

Figure 40: Distribution of annual raw material and utility costs. Based on the 10 MW plant in EUR $\cdot$ a^{-1}.

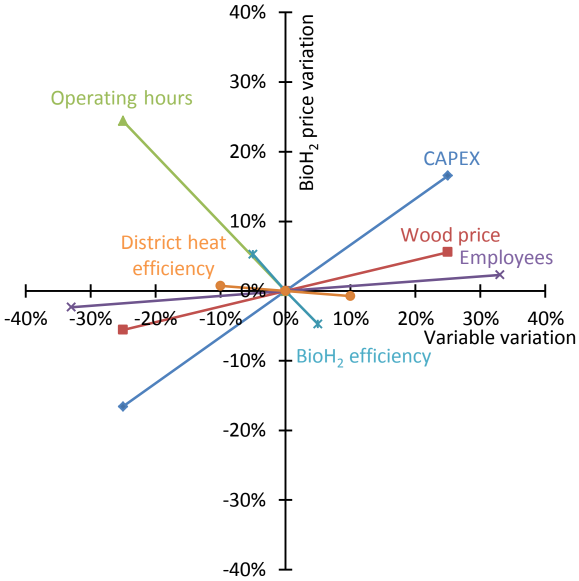

Figure 41: Sensitivity analysis of the 10 MW $BioH_2$ plant.

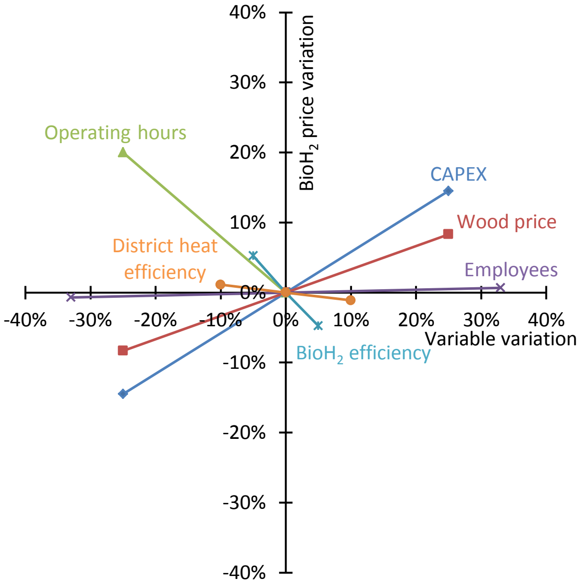

Figure 42: Sensitivity analysis of the 50 MW BioH$_2$ plant.

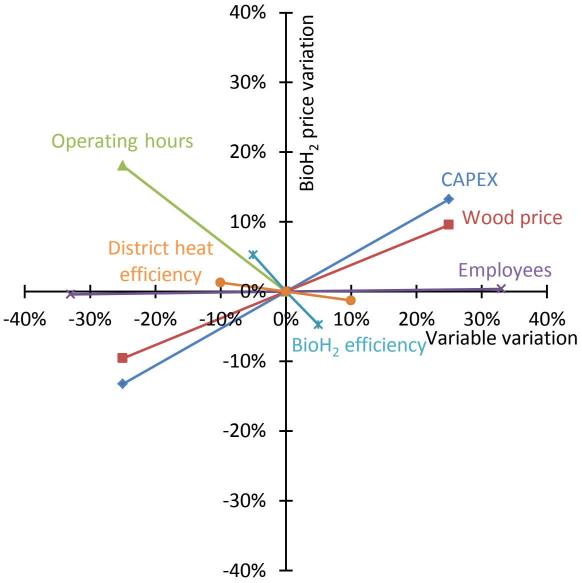

Figure 43: Sensitivity analysis of the 100 MW BioH$_2$ plant.

Those results are analogous to the results of the CHP process. It can be seen that a change of the operating hours and the $BioH_2$ production efficiency has the most significant impact on economic feasibility followed by the capital costs, and the wood chips price. The influence of the number of employees and the district heat production rate is relatively low. Furthermore, the influence of the $BioH_2$ efficiency increases compared to the influence of the operating hours with increasing plant capacity.

3.2.3 Process C: Synthetic natural gas and district heat

In this section, the technical and economical assessment of the DFB-based plant for BioSNG and district heat production is presented. The SNG synthesis part is based on the VESTA process from Amec Foster Wheeler and Clariant.

Technical assessment The technical assessment is carried out by means of mass and energy balance and heat integration of the plant with 10 MW gasifier fuel power. Figure 44 shows a simplified flowchart of the process for BioSNG production. Basically, it consists of the DFB part which covers the gasification, a part of the gas cleaning, and compression and the VESTA part which covers the final gas cleaning, methanation, CO_2 removal, and BioSNG upgrading in order to reach the gas grid specifications. Wood chips are fed into the dryer where the water content is reduced from 40 % to 20 %. Subsequently, the wood chips are fed into the gasifier, where they are converted with steam into product gas. The product gas is cooled, filtered, and subsequently fed into the RME scrubber where most of the tar, except BTEX, is removed and steam condensed. The condensate is reused for steam fluidization in the gasifier. After the RME scrubber, a partial flow of the product gas is extracted and used as fuel for the combustion reactor of the DFB system. Subsequently, the remaining product gas is led into fixed bed adsorbers filled with activated carbon for removal of sulfur, especially H_2S, and BTEX. The adsorbers are in batch operation and are regenerated with steam. Then, the product gas is compressed to 10 bar (278 kW) and fed into the VESTA part of the process. In the first step the product gas is led into the fixed bed hydrogenation reactor employing a Co-Mo catalyst with a temperature of 300 °C, where ethene is hydrogenated to ethane and COS to H_2S. The H_2S is subsequently removed by a ZnO adsorber bed. Then the gas is mixed with additional steam in order to avoid coking and carbon deposition in the downstream fixed bed reactors. Subsequently, the gas is fed into a WGS reactor at a temperature of 330 °C where CO and H_2O react to H_2 and CO_2. Then the gas is cooled and led into the first methanation reactor at an inlet temperature of 350 °C. In this first reactor CO and H_2 are converted into CH_4 and H_2O. In addition, higher hydrocarbons are also reformed and decomposed. After the first methanation reactor, the gas enters the second methanation reactor at an inlet temperature of 300 °C where methanation continues before the gas enters the third methanation reactor. The inlet temperature of the third methanation reactor is 250 °C. This seems to be the lower temperature limit due to low methanation rate of commercial catalysts below 250 °C [84]. After the third methanation reactor, the gas is cooled to about 50 °C which leads to condensation of steam. Subsequently the gas enters the amine scrubber where CO_2 is removed with a removal efficiency of 99 % (1228 $kg \cdot h^{-1}$). A partial flow of the removed CO_2 (79.2 $kg \cdot h^{-1}$) is used for inertization and overlaying of the fuel feeding systems and gas blowers. Then, the gas enters the final methanation reactor with 250 °C in order to reach the gas grid specifications before it is released into the gas grid as BioSNG. The flue gas of the DFB system is cooled and mainly used for air preheating and steam generation which is needed for fluidization of the gasifier and for steam addition before the WGS reactor. The gasification process operates at ambient pressure.

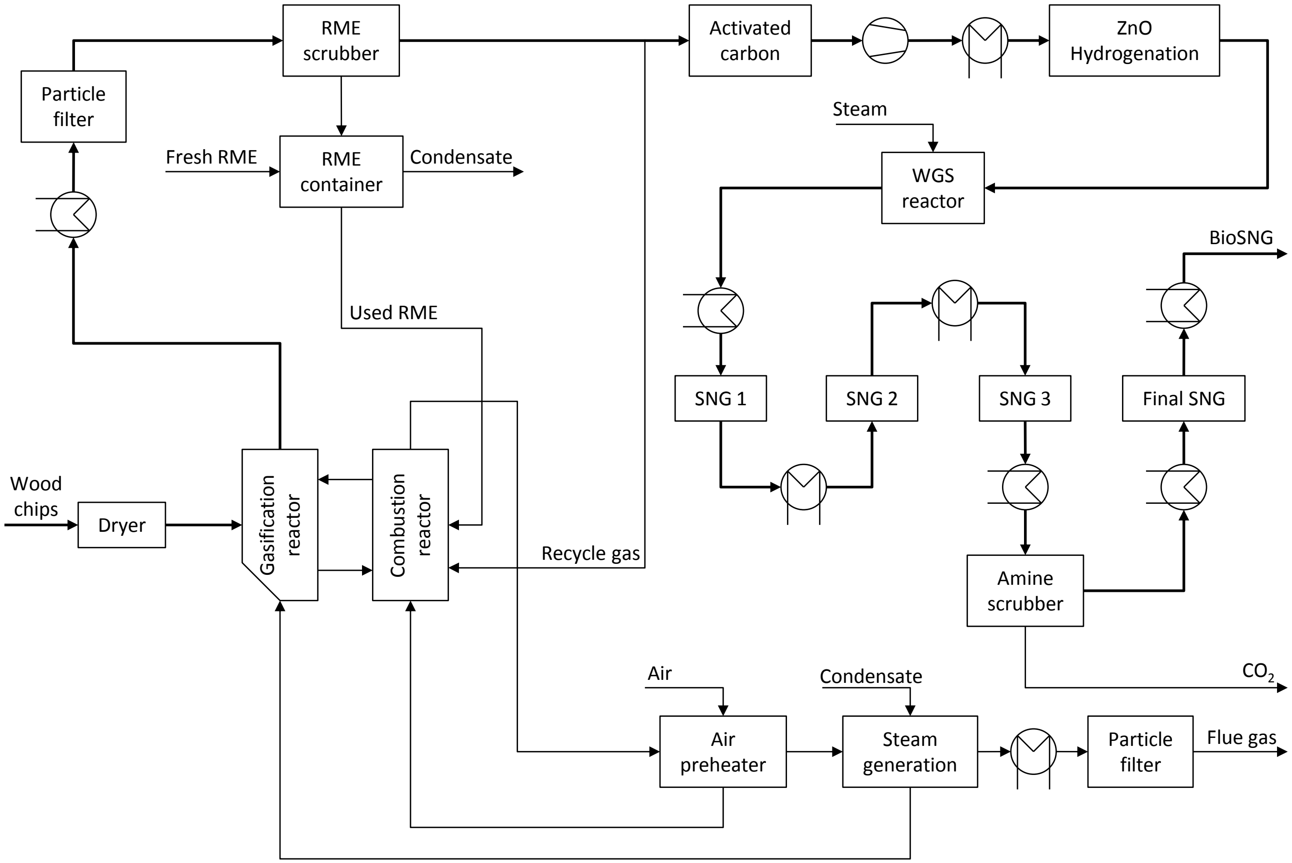
RME scrubber
Activated carbon
ZnO Hydrogenation
Particle filter
Steam
Fresh RME
RME container
Condensate
WGS reactor
BioSNG
Used RME
SNG 1
SNG 2
SNG 3
Final SNG
Wood chips
Dryer
Gasification reactor
Combustion reactor
Recycle gas
Amine scrubber
Air
Condensate
CO_2
Air preheater
Steam generation
Particle filter
Flue gas

Figure 44: Simplified flowchart of the plant for BioSNG and district heat generation.

Figure 45 shows the composite curves and the grand composite curve of the investigated process.

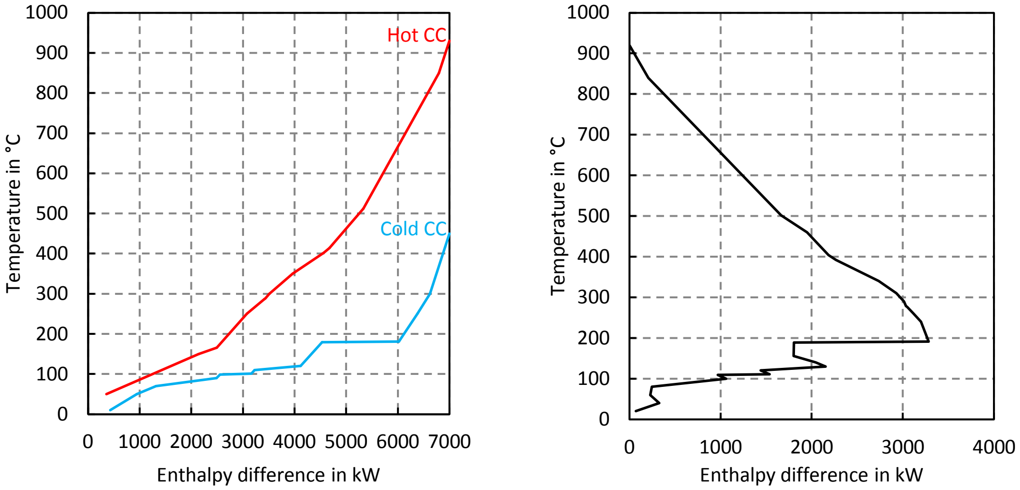

Figure 45: Composite curves (CC, left) and grand composite curve (GCC, right) for $\Delta T_{min} = 20\,°\mathrm{C}$ of the DFB plant for BioSNG and district heat production.

It can be seen that all heat demand of the process can be covered by the process itself. Therefore, no additional heating utility is required. In addition, in the investigated configuration for the 10 MW plant, 800 kW of district heat are generated.

Figure 46 shows the heat exchanger network of the investigated process for BioSNG production.

Figures 47 and 48 show energy Sankey diagrams of the DFB and VESTA part of the investigated process for BioSNG and district heat production.

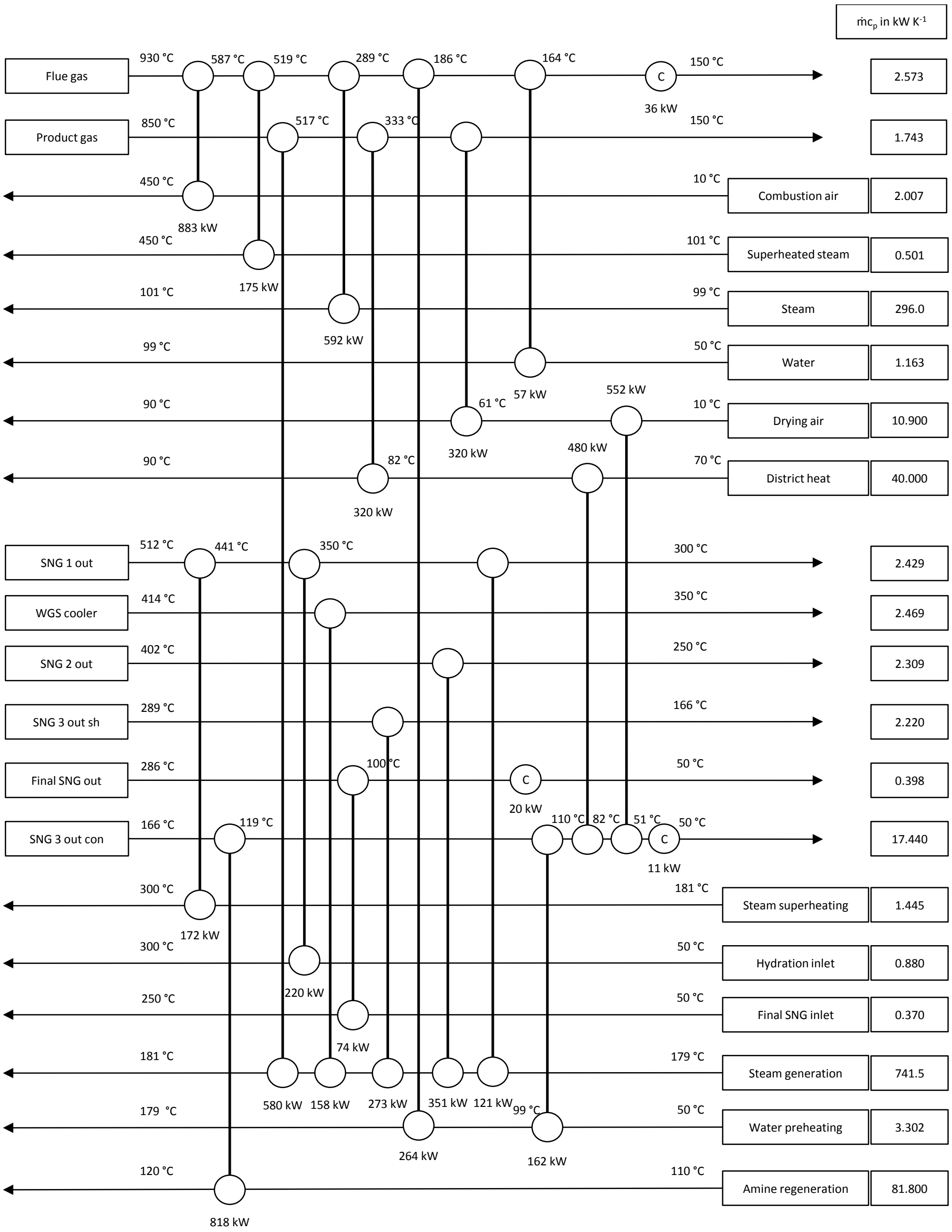
ṁc$_p$ in kW K^{-1}
Flue gas
930 °C
587 °C
519 °C
289 °C
186 °C
164 °C
C
150 °C
36 kW
2.573
Product gas
850 °C
517 °C
333 °C
150 °C
1.743
450 °C
10 °C
Combustion air
2.007
883 kW
450 °C
101 °C
Superheated steam
0.501
175 kW
101 °C
99 °C
Steam
296.0
592 kW
99 °C
50 °C
Water
1.163
57 kW
552 kW
90 °C
61 °C
10 °C
Drying air
10.900
320 kW
480 kW
90 °C
82 °C
70 °C
District heat
40.000
320 kW
SNG 1 out
512 °C
441 °C
350 °C
300 °C
2.429
WGS cooler
414 °C
350 °C
2.469
SNG 2 out
402 °C
250 °C
2.309
SNG 3 out sh
289 °C
166 °C
2.220
Final SNG out
286 °C
100 °C
C
50 °C
0.398
20 kW
SNG 3 out con
166 °C
119 °C
110 °C
82 °C
51 °C
C
50 °C
17.440
11 kW
300 °C
181 °C
Steam superheating
1.445
172 kW
300 °C
50 °C
Hydration inlet
0.880
220 kW
250 °C
50 °C
Final SNG inlet
0.370
74 kW
181 °C
179 °C
Steam generation
741.5
580 kW
158 kW
273 kW
351 kW
121 kW
99 °C
179 °C
50 °C
Water preheating
3.302
264 kW
162 kW
120 °C
110 °C
Amine regeneration
81.800
818 kW

Figure 46: Heat exchanger network of the 10 MW plant for BioSNG and district heat production. The upper part of the figure shows the DFB part of the process and the lower part shows the VESTA part of the process.

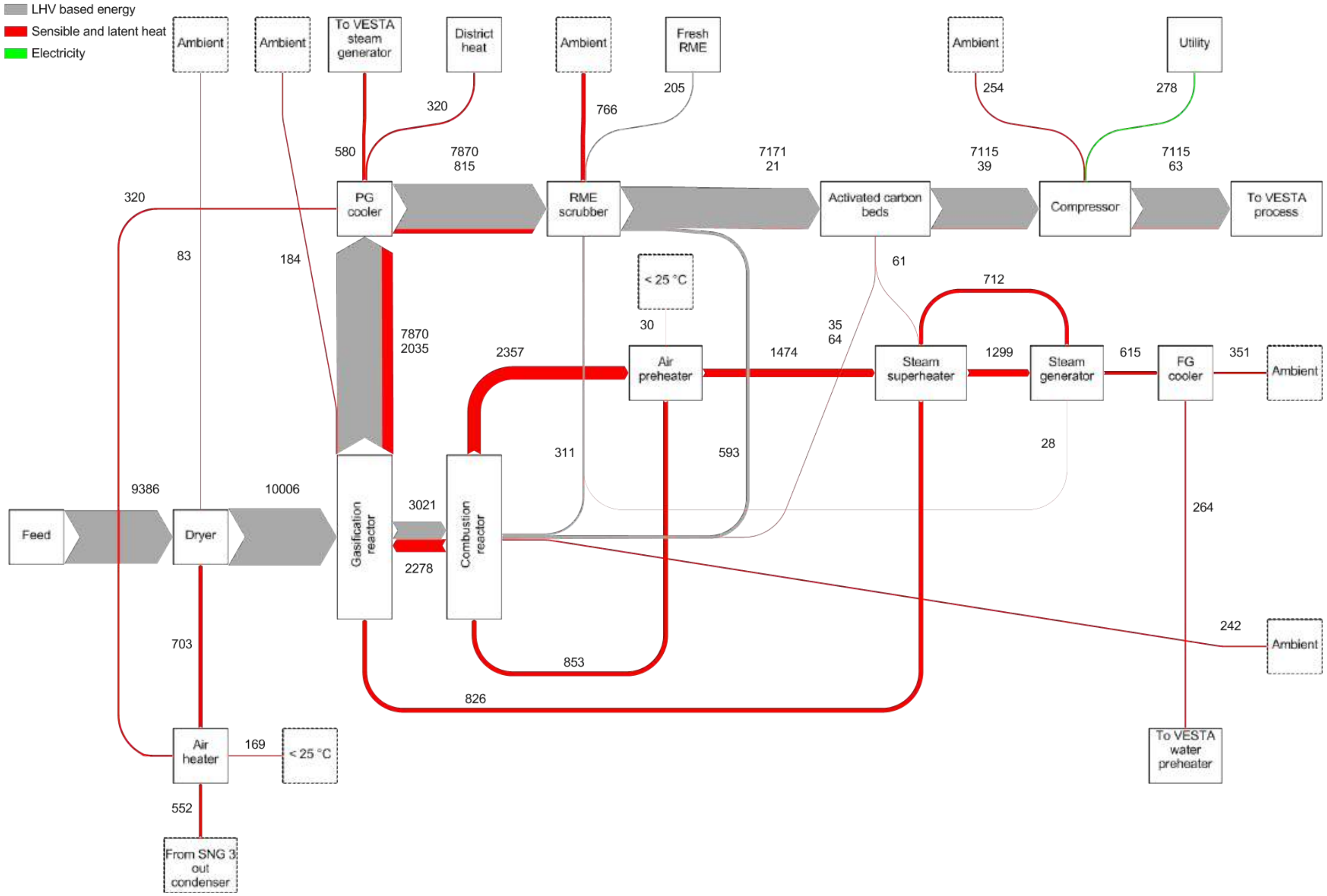
LHV based energy
Sensible and latent heat
Electricity
Ambient
Ambient
To VESTA steam generator
District heat
Ambient
Fresh RME
Ambient
Utility
320
580
766
205
254
278
7870
815
7171
21
7115
39
7115
63
320
PG cooler
RME scrubber
Activated carbon beds
Compressor
To VESTA process
83
184
61
< 25 °C
712
7870
2035
2357
30
35
64
Air preheater
1474
Steam superheater
1299
Steam generator
615
FG cooler
351
Ambient
311
593
28
9386
10006
264
Feed
Dryer
Gasification reactor
3021
2278
Combustion reactor
242
Ambient
703
853
826
Air heater
169
< 25 °C
To VESTA water preheater
552
From SNG 3 out condenser

Figure 47: Energy Sankey diagram of the DFB part of the plant for BioSNG and district heat production for 10 MW gasifier fuel power. All streams are given in kW.

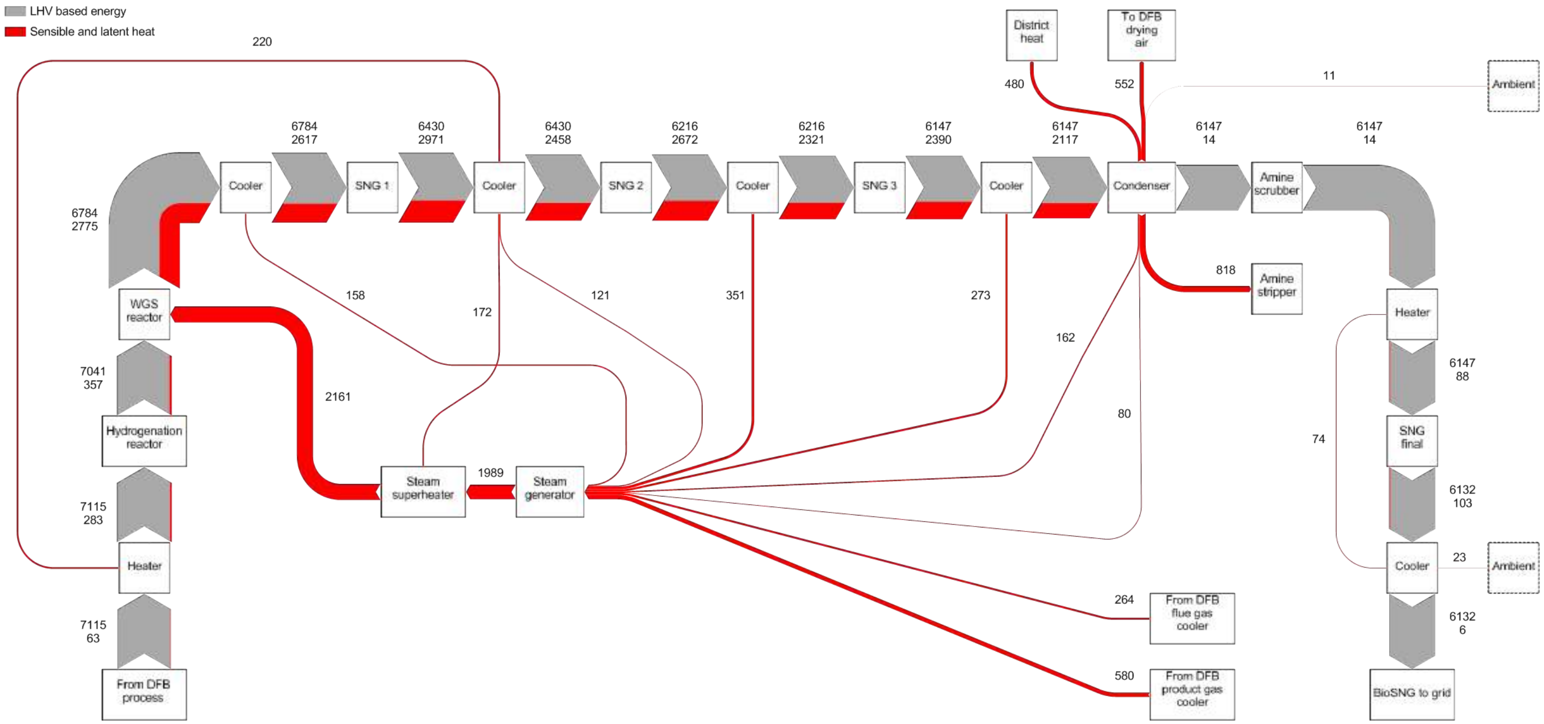

▨ LHV based energy
🟥 Sensible and latent heat
220
From DFB process
7115
63
Heater
7115
283
Hydrogenation reactor
7041
357
WGS reactor
6784
2775
Cooler
6784
2617
SNG 1
6430
2971
Cooler
6430
2458
SNG 2
6216
2672
Cooler
6216
2321
SNG 3
6147
2390
Cooler
6147
2117
Condenser
6147
14
Amine scrubber
6147
14
District heat
480
To DFB drying air
552
11
Ambient
818
Amine stripper
158
172
121
351
273
162
80
2161
Steam superheater
1989
Steam generator
264
From DFB flue gas cooler
580
From DFB product gas cooler
Heater
6147
88
74
SNG final
6132
103
Cooler
23
Ambient
6132
6
BioSNG to grid

Figure 48: Energy Sankey diagram of the VESTA part of the plant for BioSNG and district heat production for 10 MW gasifier fuel power. All streams are given in kW.

It can be seen that an overall biomass-based BioSNG production efficiency of 65.3 % is reached (main product efficiency, Equation 20). The overall efficiency (Equation 21) is 66.9 % considering biomass, electricity, RME input, and district heat. Furthermore, most of the heat released is used for steam generation, either for the gasification reactor or the steam addition before the WGS reactor. In addition, the amine scrubber also needs a significant share of the heat released.

In contrast to this work, Rehling et al. [32] simulated a DFB gasification-based SNG process using an isothermal SNG reactor and achieved a production efficiency of 66.0 %. Furthermore, Hemetsberger [134] simulated a combination of a DFB-based SNG process with addition of H_2 from a power to gas PEM electrolyzer where an overall efficiency of 64.2 % was reached by considering the biomass input and the electricity input from the PEM electrolyzer. Moreover, at the GoBiGas plant, which employs the DFB steam gasification process and the fixed bed methanation TREMP process from Haldor Topsoe, a SNG production efficiency of 61.8 % is achieved [30]. The lower value can be explained by the lower water content of the fuel (8 % compared to 40 % in this work) and the corresponding decrease of the lower heating value of the biomass feed. Bunten [135] reports a SNG production efficiency of 62 % converting municipal solid waste into SNG by employing the VESTA SNG process. Moreover, Ruggeri [136] gives a SNG conversion efficiency of woody biomass between 60 and 67 % by using the VESTA SNG process. In conclusion, all presented results from literature are in good agreement with the results in this work. The carbon conversion efficiency of the BioSNG process is 31.9 % based on the carbon contained in the produced BioSNG, related to the carbon in the biomass feedstock, and in the fresh RME.

Table 15 shows the Austrian gas grid specifications according to ÖVGW G31 in comparison with data from the calculated BioSNG composition of the investigated process.

It can be seen that the specification for the higher Wobbe index and the higher heating value are reached by the generated SNG. However, the relative density cannot be achieved. Regarding dew points and impurities,

Table 15: Gas grid specifications according to Austrian ÖVGW G31 in comparison with the calculated BioSNG data.

	ÖVGW G31	BioSNG	Units
Higher Wobbe index	47.9 to 56.5	52.6	$MJ \cdot m^{-3}$
Higher heating value	38.5 to 46.1	38.5	$MJ \cdot m^{-3}$
Relative density	0.55 to 0.65	0.54	-
C_xH_y condensation point	0	–125	°C
H_2O condensation point at 40 bara	–8	< -8	°C
O_2	< 0.5 %	0.0	$m^3 \cdot m^{-3}$
CO_2	< 2.0 %	73 ppm	$m^3 \cdot m^{-3}$
N_2	< 5.0 %	1.60 %	$m^3 \cdot m^{-3}$
H_2	< 4.0 % (< 2.0 %)	2.35 %	$m^3 \cdot m^{-3}$

all specifications are in agreement except the one of the H_2 content, if a compressed natural gas (CNG) fueling station is nearby the grid. In this case the H_2 content should be lower than 2.0 %. The volumetric CO content of the generated BioSNG is below 100 ppm which would meet the requirements of the standard EN 16723-1:2016, which gives a maximum CO content of 0.1 % or 1000 ppm for biomethane grid injection. The standard is valid for biomethane via biogas upgrading as well as BioSNG via methanation of syngas from biogenous resources.

Table 16 shows the material and energy streams of the investigated BioSNG plant.

Table 16: Material and energy streams of the investigated process for BioSNG and district heat production.

Plant capacity	10	50	100	MW
Input streams				
Wood chips (dry)	2050	10250	20500	$kg \cdot h^{-1}$
Electricity (consumption)	764	3820	7640	kW
RME	20	100	200	$kg \cdot h^{-1}$
CaO	15	75	150	$kg \cdot h^{-1}$
Olivine	20	100	200	$kg \cdot h^{-1}$
Output streams				
Ash disposal	45	225	450	$kg \cdot h^{-1}$
BioSNG (generation)	452.93	2264.65	4529.3	$kg \cdot h^{-1}$
BioSNG (generation)	6132	30660	61320	kW
District heat (generation)	800	4000	8000	kW

For a 10 MW plant capacity, the electricity consumption considers the compression to p = 10 bara (278 kW), the amine scrubber (136 kW), and other consumers (350 kW[5]).

Figure 49 shows the energy distribution of the investigated BioSNG process.

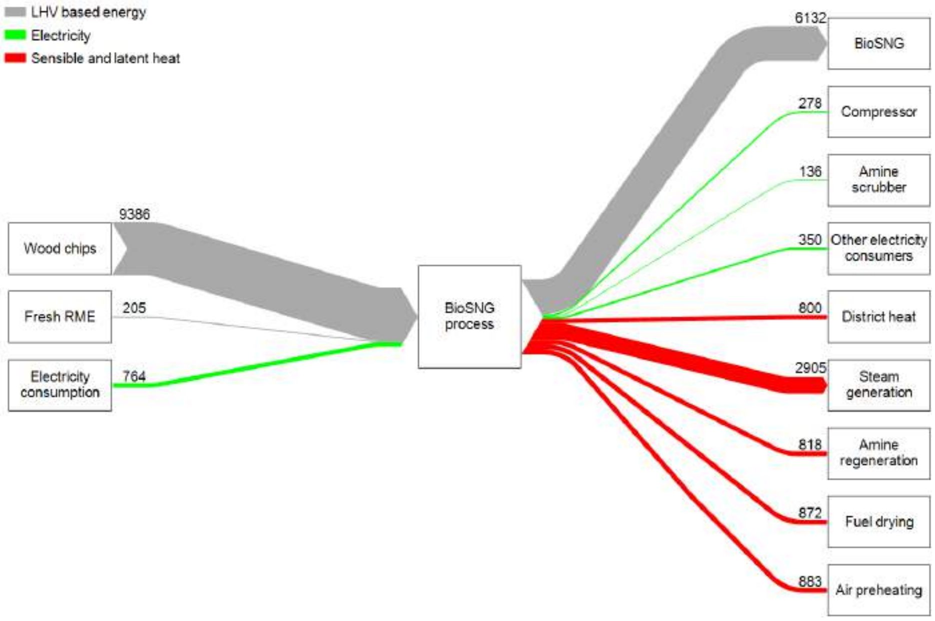
LHV based energy
Electricity
Sensible and latent heat
Wood chips
9386
Fresh RME
205
Electricity consumption
764
BioSNG process
6132
BioSNG
278
Compressor
136
Amine scrubber
350
Other electricity consumers
800
District heat
2905
Steam generation
818
Amine regeneration
872
Fuel drying
883
Air preheating

Figure 49: Energy distribution of the investigated 10 MW BioSNG plant. All streams are given in kW.

It can be seen that most of the energy input is converted into BioSNG. In addition, a significant amount of heat is used for steam generation for the gasifier and the WGS reactor in order to ensure a sufficient steam to carbon ratio to avoid coking and carbon deposition. More heat could be used for district heat generation if a lower steam to carbon ratio at the inlet of the WGS reactor were technically feasible. Furthermore, the amine regeneration also requires a high amount of heat. Additionally, without biomass drying, a higher district heat output would be also possible. However, more product gas has to be recycled into the combustion reactor of the gasifier in order to evaporate the moisture. This would lead to a lower BioSNG generation.

---

[5] The same value as for the CHP plant was used.

Economic assessment In this section, the results of the economic assessment of the process for BioSNG and district heat production for a gasifier fuel power of 10, 50, and 100 MW are presented.

Table 17 shows the estimated investment costs for the three investigated plant capacities for the production of BioSNG.

Table 17: Investment costs of the investigated process for BioSNG production.

Plant capacity	10	50	100	MW
CAPEX	17 000 000	50 000 000	80 000 000	EUR
SUEX	1 700 000	5 000 000	8 000 000	EUR
INV	18 700 000	55 000 000	88 000 000	EUR

The estimation of the gasification part was based on Figure 26 and on expert talks with a DFB plant manufacturer. The capital costs of the VESTA part were estimated based on an internal study where the costs of main process equipment (compressor, reactors, and amine scrubber) were estimated in collaboration with project partners who have experience in erection of synthesis plants.

Table 18 shows the results of the techno-economic assessment of the three investigated plant capacities.

Table 18: Results of the techno-economic assessment of the investigated process for BioSNG and district heat production.

Plant capacity	10	50	100	MW
OPEX	5 693 520	20 367 600	36 685 200	$\mathrm{EUR} \cdot \mathrm{a}^{-1}$
REV	7 488 847	25 647 973	45 133 796	$\mathrm{EUR} \cdot \mathrm{a}^{-1}$
BT cash flow	1 795 327	5 280 373	8 448 596	$\mathrm{EUR} \cdot \mathrm{a}^{-1}$
AT cash flow	2 196 495	6 460 279	10 336 447	$\mathrm{EUR} \cdot \mathrm{a}^{-1}$
BioSNG selling price for NPV = 0	146	98	85	$\mathrm{EUR} \cdot \mathrm{MWh}^{-1}$
BioSNG selling price for NPV = 0	2.0	1.3	1.2	$\mathrm{EUR} \cdot \mathrm{kg}^{-1}$

The BT cash flow is lower than the AT cash flow because of the comparable high investment costs of the plants. Therefore, the depreciation which is added back for the after tax calculation is significantly high which leads to an increase of the AT cash flow over the BT cash flow. Gassner and Marechal [137] report SNG production costs based on biomass gasification from 76 to 107 $\mathrm{EUR} \cdot \mathrm{MWh}^{-1}$ for a fuel power of 20 MW and 59 to 97 $\mathrm{EUR} \cdot \mathrm{MWh}^{-1}$

for a fuel power of 150 MW in 2009. However, they assumed higher production efficiencies between 69 and 76 %. Moreover, Billig [138] reports BioSNG production costs of biomass steam gasification plants between 68 and 182 $\mathrm{EUR} \cdot \mathrm{MWh}^{-1}$ depending on plant capacity and feedstock for the reference year 2012. In contrast, biomethane from biogas upgrading plants has production costs from 57 to 129 $\mathrm{EUR} \cdot \mathrm{MWh}^{-1}$ depending on the feedstock and the upgrading unit in the year 2012 [138]. The actual price for natural gas in Austria (November 2017) according to E-Control [139, 140] is about 44 $\mathrm{EUR} \cdot \mathrm{MWh}^{-1}$ (incl. taxes and other charges).

Figure 50 shows the specific cost distribution of the investigated plant capacities.

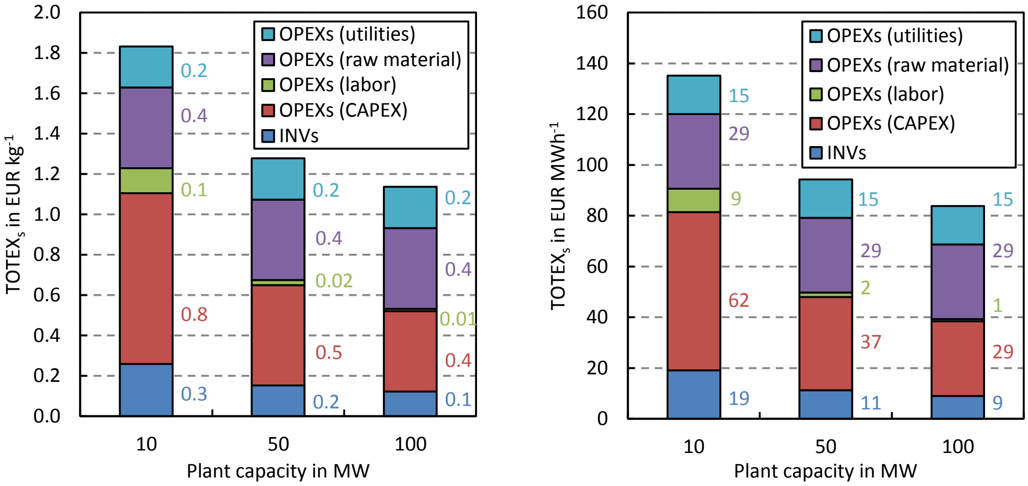

Figure 50: Specific cost distribution based on the generated BioSNG.

In case of the 10 MW plant capacity, the CAPEX related costs have the highest share followed by the raw material related costs. In addition, the share of the labor related costs is the lowest. With increasing plant capacity, the CAPEX and labor related costs decrease which can be dedicated to economy of scale effects. In contrast, at the higher plant capacities, the raw material and utility related costs become more significant.

Figure 51 shows the distribution of the raw material and utility costs of the 10 MW plant capacity. The distribution of the other plant capacities is equal.

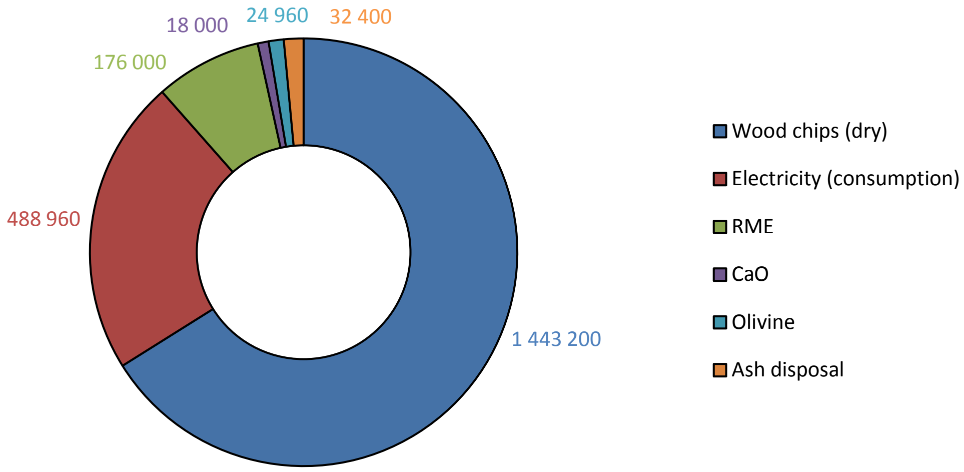

Figure 51: Distribution of annual raw material and utility costs. Based on the 10 MW plant in $\mathrm{EUR} \cdot \mathrm{a}^{-1}$.

It can be seen that the raw material costs (wood chips) have a 66 % share of the overall raw material and utility costs. The electricity consumption accounts for 22 % and the RME consumption for 8 %.

Figures 52 to 54 show the influence of different process variables on the specific BioSNG selling price for the 10, 50, and 100 MW plant.

It can be seen that a change of the operating hours and the BioSNG production efficiency has the most significant impact on economic feasibility followed by the capital costs, and the wood chips price. The influence of the number of employees and the district heat production rate is relatively low. The influence of the BioSNG production efficiency increases compared to the influence of the operating hours with increasing plant capacity. The same results were observed for the subsequent investigated CHP and $BioH_2$ processes.

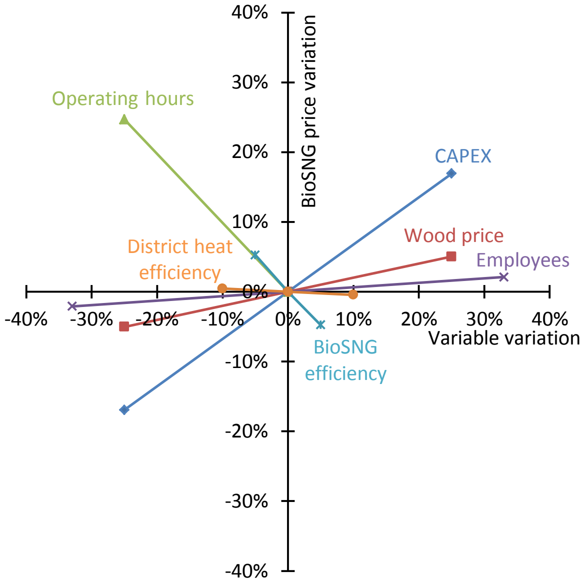

Figure 52: Sensitivity analysis of the 10 MW BioSNG plant.

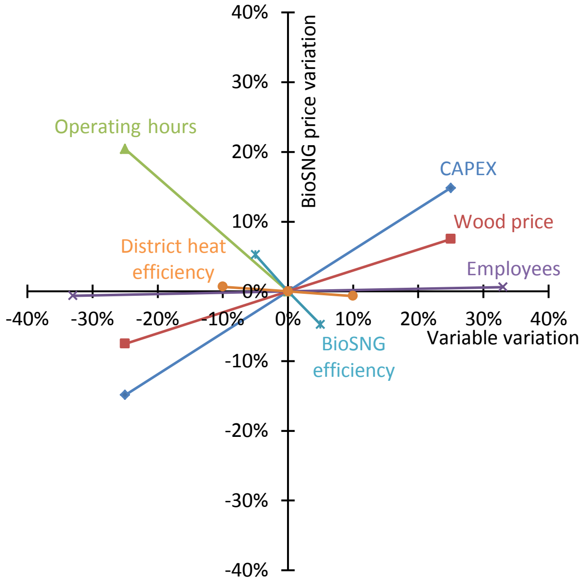

Figure 53: Sensitivity analysis of the 50 MW BioSNG plant.

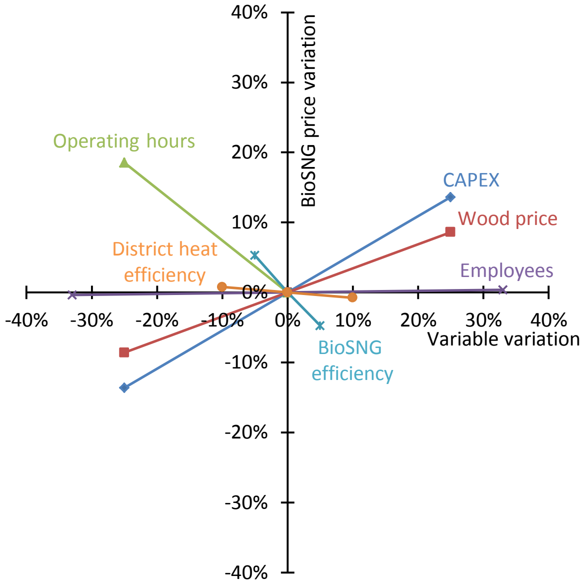

Figure 54: Sensitivity analysis of the 100 MW BioSNG plant.

3.2.4 Process D: Hydrogen and methane

In this section the technical and economic assessment of a process for the generation of BioHNG, a gas mixture composed of H_2 and CH_4, in order to replace or supplement natural gas in certain applications is presented.

Technical assessment Figure 55 shows a simplified flowchart of the investigated process.

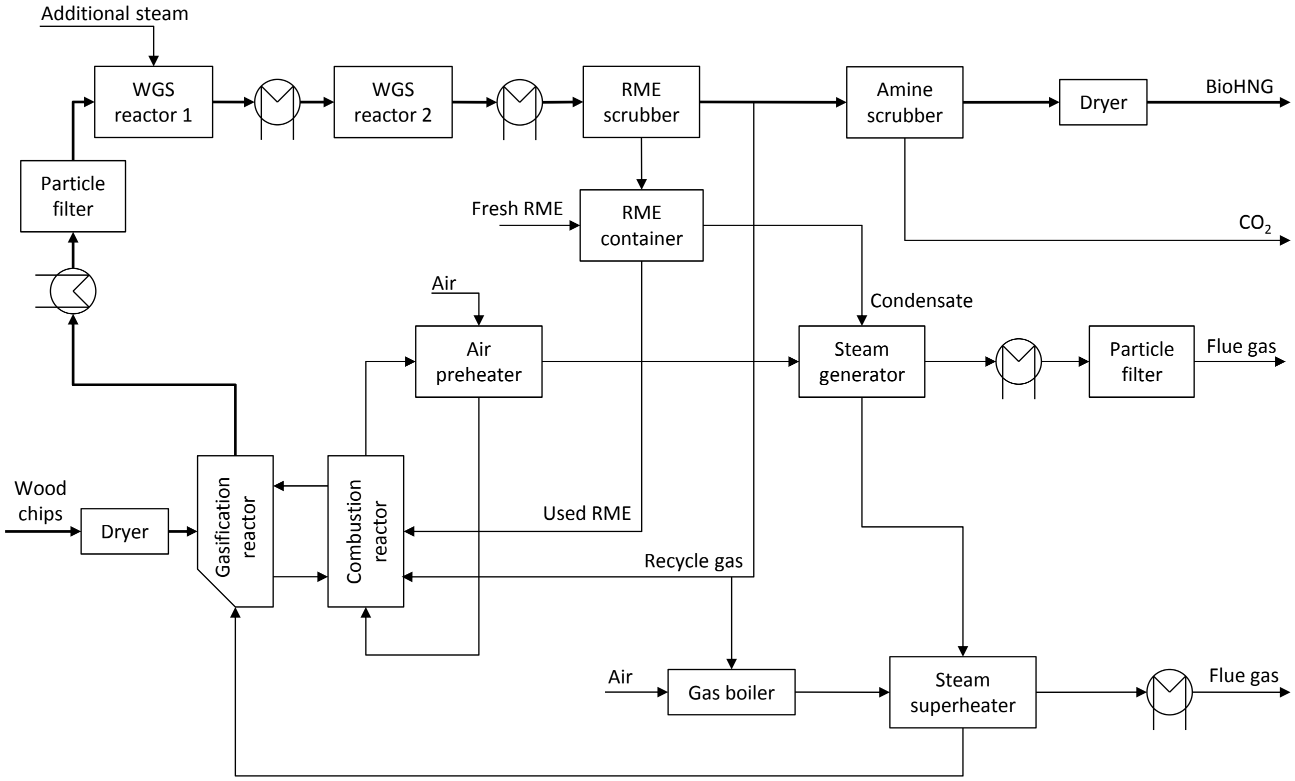
Additional steam
WGS reactor 1
WGS reactor 2
RME scrubber
Amine scrubber
Dryer
BioHNG
Particle filter
Fresh RME
RME container
CO₂
Air
Air preheater
Condensate
Steam generator
Particle filter
Flue gas
Wood chips
Dryer
Gasification reactor
Combustion reactor
Used RME
Recycle gas
Air
Gas boiler
Steam superheater
Flue gas

Figure 55: Simplified flowchart of the plant for BioHNG generation.

Wood chips are fed into the biomass dryer and subsequently into the gasifier. The product gas is cooled, filtered, and fed into the first WGS reactor. At the inlet of the first WGS reactor, addition steam is added in order to avoid coking and carbon deposition of the catalyst. The inlet temperature of the first WGS reactor is 350 °C. Before the second WGS reactor, the gas is cooled to 300 °C in order to benefit from the lower temperature regarding the equilibrium composition. Both WGS reactors employ an Fe-Cr-based catalyst. After the second WGS reactor, the gas is cooled and fed into the RME scrubber where the gas is cooled from 150 °C to 50 °C. Consequently, steam is condensed and most of the tar removed. The condensed steam is reused for steam generation. A partial flow of the product gas is fed into the combustion reactor of the DFB gasification system in order to provide heat for the endothermic gasification reactions. Subsequently, the main fraction of the gas is fed into an amine scrubbing unit where CO_2 is removed with an efficiency of 99 % ($1363\ \mathrm{kg} \cdot \mathrm{h}^{-1}$). The removed CO_2 is partially used for inertization and overlay of the fuel feeding system and the gas blowers ($79.2\ \mathrm{kg} \cdot \mathrm{h}^{-1}$). Finally, the product gas is dried and the BioHNG gas mixture is fed into a gas grid or can be used for other applications. The flue gas from the combustion reactor of the DFB system is mainly used for air preheating, steam generation, and amine regeneration before it is filtered and released into the ambient. The whole process operates at ambient pressure.

Figure 56 shows the composite curves and the grand composite curve of the investigated process for BioHNG generation.

The high temperature heat is mainly required by the steam generation system and air preheating of the combustion air of the combustion reactor of the DFB system. The low temperature heat is mainly required for amine regeneration and biomass drying.

Figure 57 shows the corresponding heat exchanger network.

74 kW of external cooling utility is required for the process. In addition to the heat recovery along the process, the heat utility is also satisfied by combustion of a partial flow of the product gas which is extracted downstream of the RME scrubber.

Figure 58 shows an energy Sankey diagram of the investigated process.

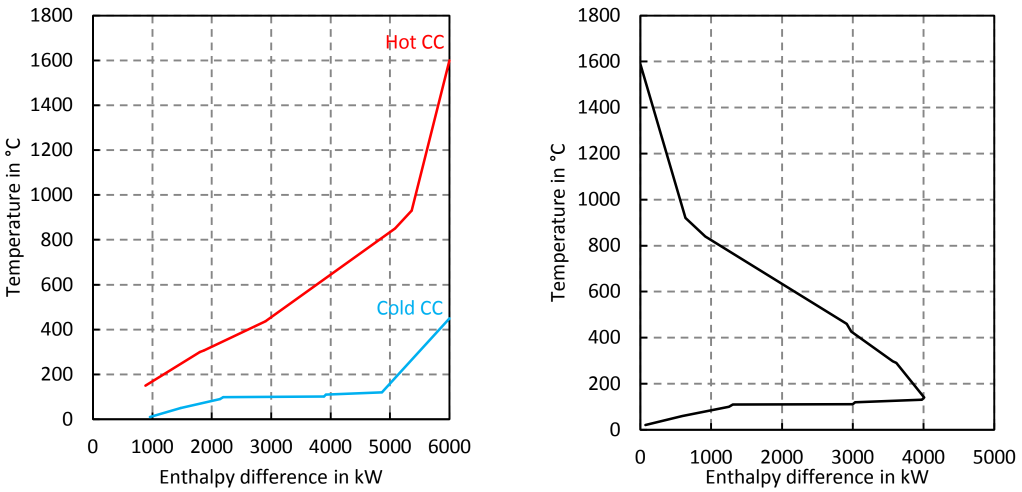

Figure 56: Composite curves (CC, left) and grand composite curve (GCC, right) of the plant for BioHNG generation for $\Delta T_{min} = 20$ °C.

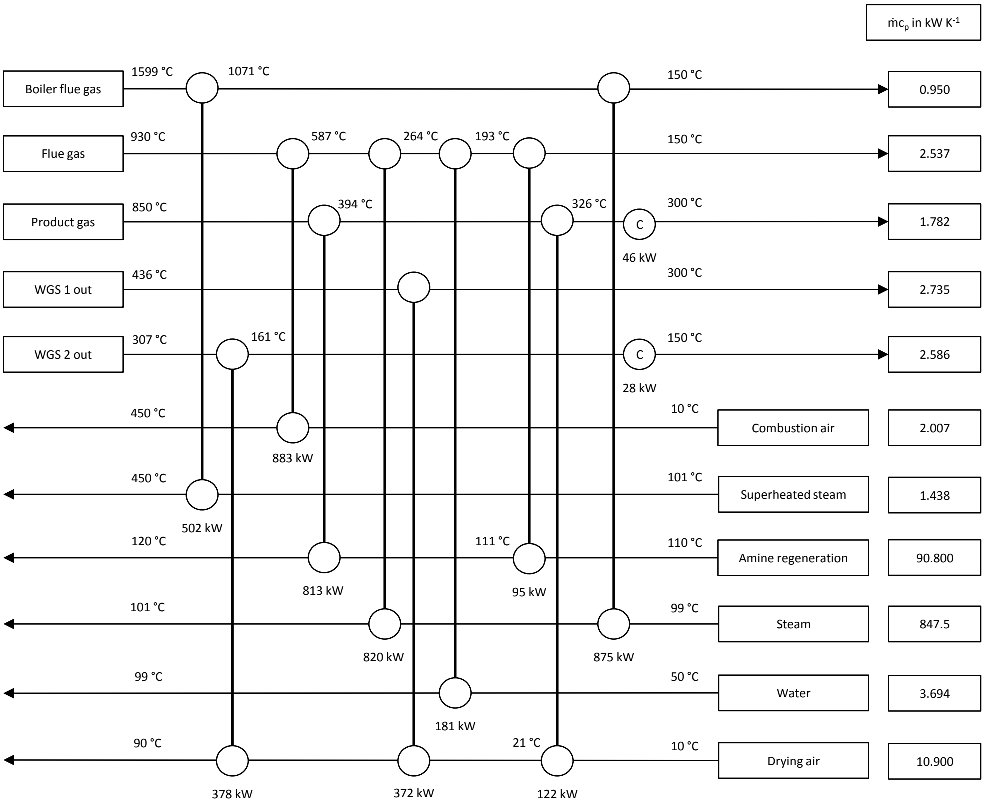
$\dot{m}c_p$ in kW K^{-1}
Boiler flue gas
1599 °C
1071 °C
150 °C
0.950
Flue gas
930 °C
587 °C
264 °C
193 °C
150 °C
2.537
Product gas
850 °C
394 °C
326 °C
C
300 °C
1.782
46 kW
WGS 1 out
436 °C
300 °C
2.735
WGS 2 out
307 °C
161 °C
C
150 °C
2.586
28 kW
450 °C
10 °C
Combustion air
2.007
883 kW
450 °C
101 °C
Superheated steam
1.438
502 kW
120 °C
111 °C
110 °C
Amine regeneration
90.800
813 kW
95 kW
101 °C
99 °C
Steam
847.5
820 kW
875 kW
99 °C
50 °C
Water
3.694
181 kW
90 °C
21 °C
10 °C
Drying air
10.900
378 kW
372 kW
122 kW

Figure 57: Heat exchanger network of the process for BioHNG generation.

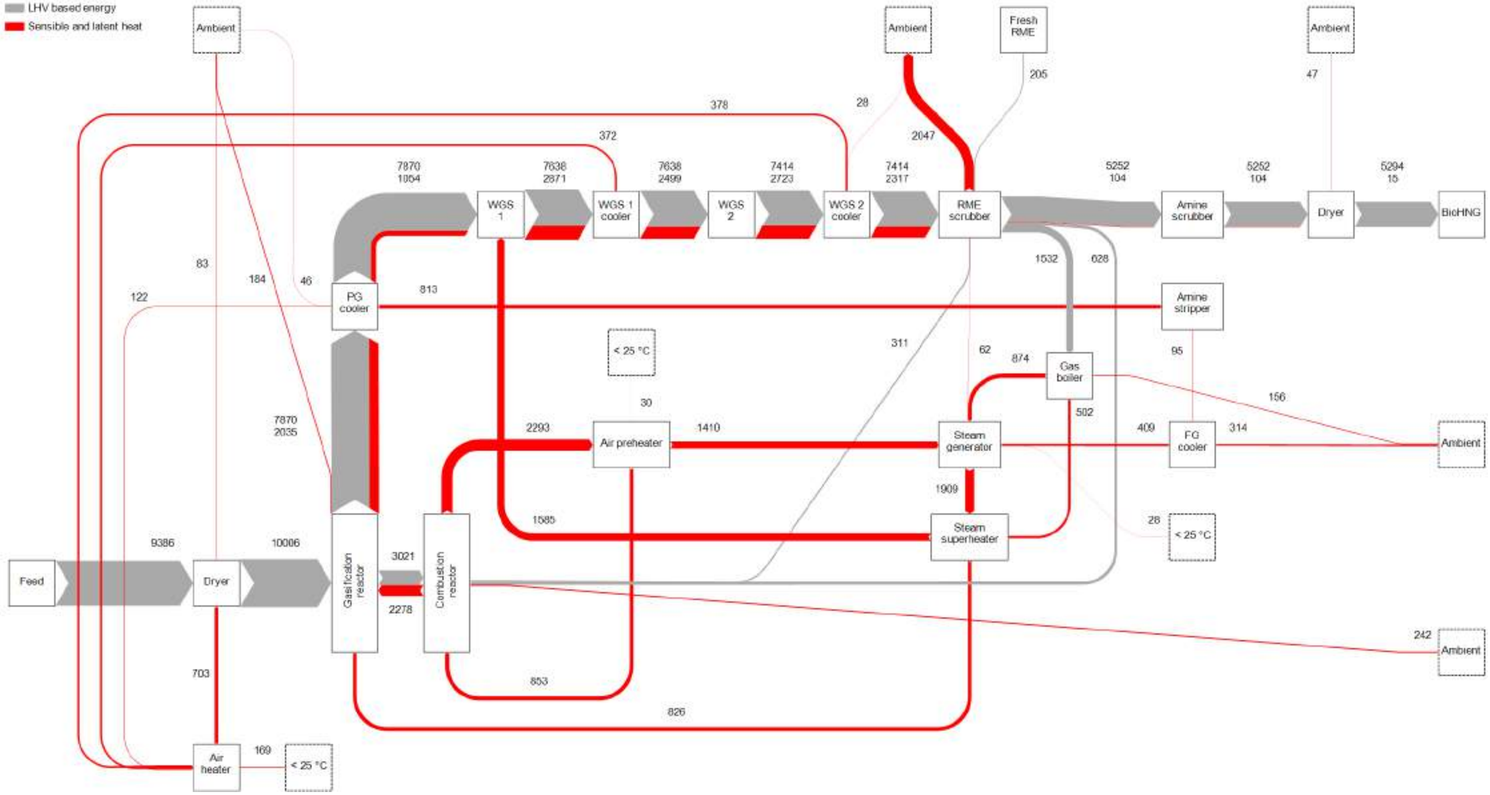
LHV based energy
Sensible and latent heat
Ambient
Ambient
Fresh RME
Ambient
378
372
28
2047
205
47
7870
1054
7638
2871
7638
2499
7414
2723
7414
2317
5252
104
5252
104
5294
15
WGS 1
WGS 1 cooler
WGS 2
WGS 2 cooler
RME scrubber
Amine scrubber
Dryer
BioHNG
83
184
46
122
PG cooler
813
1532
628
Amine stripper
311
62
874
Gas boiler
95
156
< 25 °C
30
7870
2035
2293
Air preheater
1410
502
409
Steam generator
FG cooler
314
Ambient
1909
1585
28
Steam superheater
< 25 °C
9386
10006
3021
Feed
Dryer
Gasification reactor
Combustion reactor
2278
242
Ambient
703
853
826
Air heater
169
< 25 °C

Figure 58: Sankey diagram of the process for BioHNG generation. All streams are given in kW.

The main product efficiency (Equation 20) is 56.4 % based on the LHV of the biomass fed into the dryer and the LHV of the generated BioHNG. This efficiency is significantly higher than the value reported in Paper 7 because of significant gas losses to the adsorbate of the employed PSA. However, no external heat source was necessary with this process configuration. Moreover, in Kraussler et al. [141] the BioHNG production efficiency was 44.4 % which can also be dedicated to losses along the employed PSA unit. However, it can be seen that 1532 kW of product gas are needed in order to cover the heat utility. Hence, an overall efficiency (Equation 21) of 52.2 % is reached. The carbon conversion efficiency of the BioHNG process is 13.5 % based on the carbon contained in the produced BioHNG, in the biomass feedstock, and in the additional RME.

Table 19 shows the Austrian natural gas grid specifications in comparison with the data of the generated BioHNG.

Table 19: Gas grid specifications according to Austrian ÖVGW G31 in comparison with the calculated BioHNG data.

	ÖVGW G31	BioHNG	Units
Higher Wobbe index	47.9 to 56.5	42.5	$MJ \cdot m^{-3}$
Higher heating value	38.5 to 46.1	18.0	$MJ \cdot m^{-3}$
Relative density	0.55 to 0.65	0.18	-
C_xH_y condensation point	0	–116	°C
H_2O condensation point at 40 bara	–8	< –8	°C
O_2	< 0.5 %	0.0	$m^3 \cdot m^{-3}$
CO_2	< 2.0 %	0.57 %	$m^3 \cdot m^{-3}$
N_2	< 5.0 %	0.64 %	$m^3 \cdot m^{-3}$
H_2	< 4.0 % (< 2.0 %)	82.4 %	$m^3 \cdot m^{-3}$

It can be seen that the higher Wobbe index is slightly lower than the grid specifications. However, the higher heating value and the relative density of the generated BioHNG is significantly lower than the gas grid specifications. In contrast, all other given specifications except the H_2 level are reached. In addition, the volumetric CO content of the generated BioHNG is about 0.7 % which would not meet the requirements of the standard EN 16723-1:2016, which gives a maximum volumetric or molar CO content of 0.1 % or 1000 ppm for biomethane or BioSNG grid injection. The standard includes biomethane via biogas upgrading as well as biomethane via methanation of syngas from biogenous resources.

Table 20 shows the material and energy streams which were considered for the techno-economic assessment.

Table 20: Material and energy streams of the investigated process for BioHNG generation.

Plant capacity	10	50	100	MW
Input streams				
Wood chips (dry)	2050	10250	20500	$\mathrm{kg \cdot h^{-1}}$
Electricity (consumption)	500	2500	5000	kW
RME	20	100	200	$\mathrm{kg \cdot h^{-1}}$
CaO	15	75	150	$\mathrm{kg \cdot h^{-1}}$
Olivine	20	100	200	$\mathrm{kg \cdot h^{-1}}$
Makeup water	440	2200	4400	$\mathrm{kg \cdot h^{-1}}$
Output streams				
Ash disposal	45	225	450	$\mathrm{kg \cdot h^{-1}}$
BioHNG	290.9	1454.5	2909.0	$\mathrm{kg \cdot h^{-1}}$
BioHNG	5294	26470	52940	kW

The electricity consumption considers the plant consumption (350 kW[6]) and the consumption of the amine scrubber (150 kW). The makeup water is needed for steam generation and for the amine scrubber.

Figure 59 shows the energy distribution of the investigated BioHNG process.

It can be seen that most of the energy input is converted into BioHNG. In addition, a significant amount of heat is used for steam generation for the gasifier and the WGS reactors in order to ensure a sufficient steam to carbon ratio to avoid coking and carbon deposition. Therefore, in order to reduce the heat demand for steam generation, catalyst development aiming at lower steam to carbon ratios would be sufficient. Hence, more heat could be used for district heat generation. The amine regeneration also requires a high amount of heat. Without biomass drying, a higher district heat output would be possible. On the other hand, more product gas had to be recycled into the combustion reactor of the gasifier in order to evaporate the moisture. This would lead to a lower BioHNG generation.

---

[6] The same value as for the CHP plant was used.

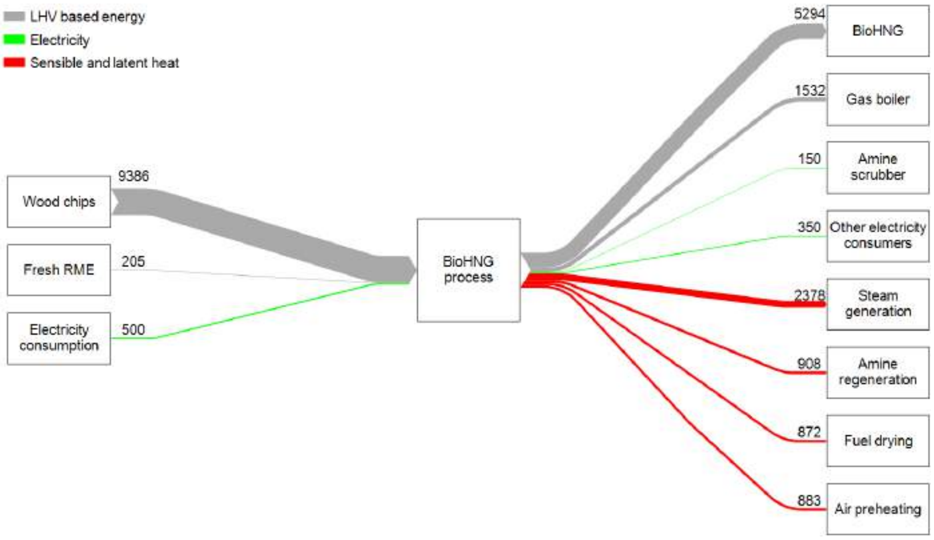
LHV based energy
Electricity
Sensible and latent heat
Wood chips
9386
Fresh RME
205
Electricity consumption
500
BioHNG process
5294
BioHNG
1532
Gas boiler
150
Amine scrubber
350
Other electricty consumers
2378
Steam generation
908
Amine regeneration
872
Fuel drying
883
Air preheating

Figure 59: Energy distribution of the investigated 10 MW BioHNG plant. All streams are given in kW.

Economic assessment In this section, the results of the economic assessment of the process for BioHNG production for a gasifier fuel power of 10, 50, and 100 MW are presented.

Table 21 shows the investment costs of the three investigated plant capacities.

Table 21: Investment costs of the investigated process for BioHNG production.

Plant capacity	10	50	100	MW
CAPEX	14 000 000	41 000 000	65 000 000	EUR
SUEX	1 400 000	4 100 000	6 500 000	EUR
INV	15 400 000	45 100 000	71 500 000	EUR

The CAPEX are based on manufacturer data as well as on a detailed literature study and Figure 26.

Table 22 shows the results of the techno-economic assessment.

Similar to the other processes, it can be seen that the AT cash flow is higher than the BT cash flow for all three plant capacities. This can again be dedicated to the depreciation which is added back for AT cash flow calculation (compare Equation 28).

Table 22: Results of the techno-economic assessment of the investigated process for BioHNG production.

Plant capacity	10	50	100	MW
OPEX	4 991 600	17 938 000	32 366 000	$\mathrm{EUR \cdot a^{-1}}$
REV	6 470 104	22 267 905	39 230 484	$\mathrm{EUR \cdot a^{-1}}$
BT cash flow	1 478 504	4 329 905	6 864 484	$\mathrm{EUR \cdot a^{-1}}$
AT cash flow	1 808 878	5 297 429	8 398 363	$\mathrm{EUR \cdot a^{-1}}$
BioHNG selling price for NPV = 0	153	105	93	$\mathrm{EUR \cdot MWh^{-1}}$
BioHNG selling price for NPV = 0	2.8	1.9	1.7	$\mathrm{EUR \cdot kg^{-1}}$

Figure 60 shows the specific cost distribution of the investigated plant capacities.

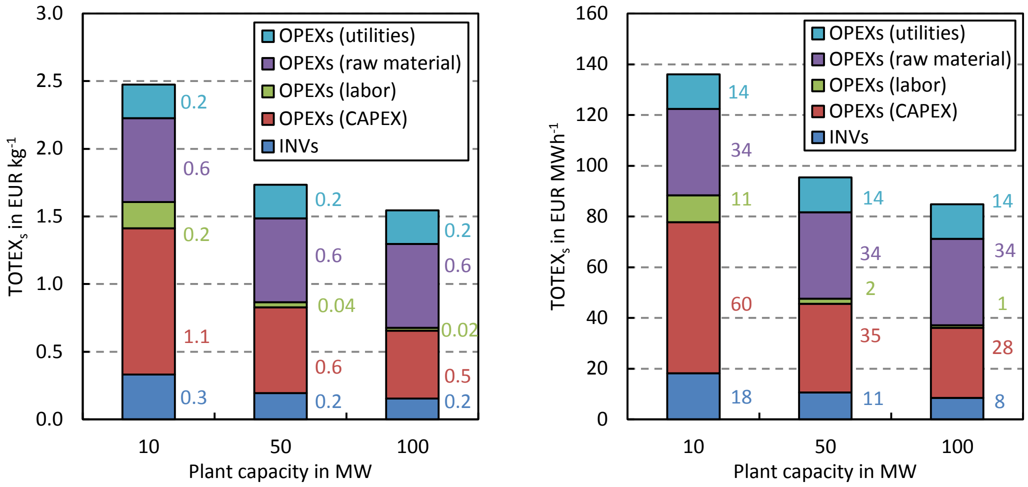

Figure 60: Specific cost distribution based on the generated BioHNG.

As observed for the other investigated processes, in case of the 10 MW plant capacity, the CAPEX related costs have the highest share followed by the raw material related costs and the share of the labor related costs is the lowest. With increasing plant capacity, the CAPEX and labor related costs decrease which can be dedicated to economy of scale effects. In contrast, at the higher plant capacities, the raw material and utility related costs become more significant.

Figure 61 shows the annual cost distribution of the material and energy streams for the 10 MW plant.

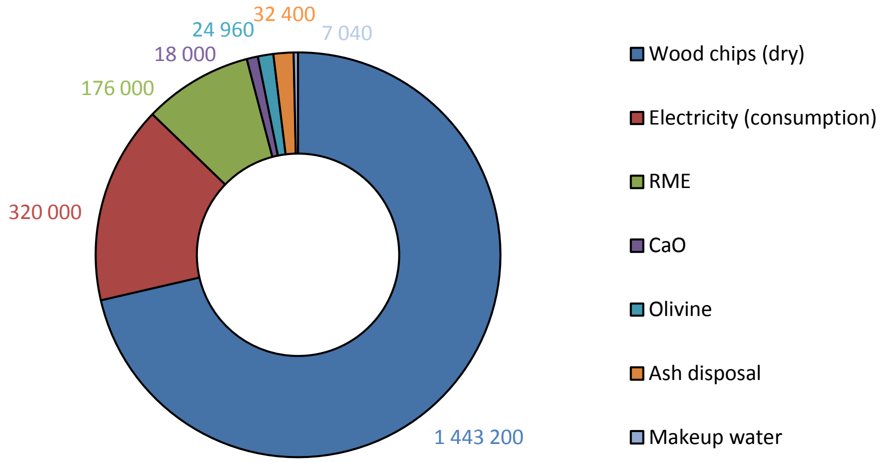

Figure 61: Distribution of the annual raw material and utility costs. Based on the 10 MW plant in EUR $\cdot$ a^{-1}.

It can be seen that the wood chips have the highest share (71 %) followed by the electricity consumption (16 %) and the RME consumption (9 %). The share of the other material streams is negligible.

Figures 62 to 64 show the influence of different process variables on the specific BioHNG selling price for the 10, 50, and 100 MW BioHNG plant.

In agreement with the other processes, it can be seen that a change of the operating hours and the BioHNG production efficiency has the most significant impact on economic feasibility followed by the capital costs, and the wood chips price. The influence of the number of employees is relatively low. It is remarkable that the influence of the BioHNG production efficiency increases compared to the influence of the operating hours with increasing plant capacity.

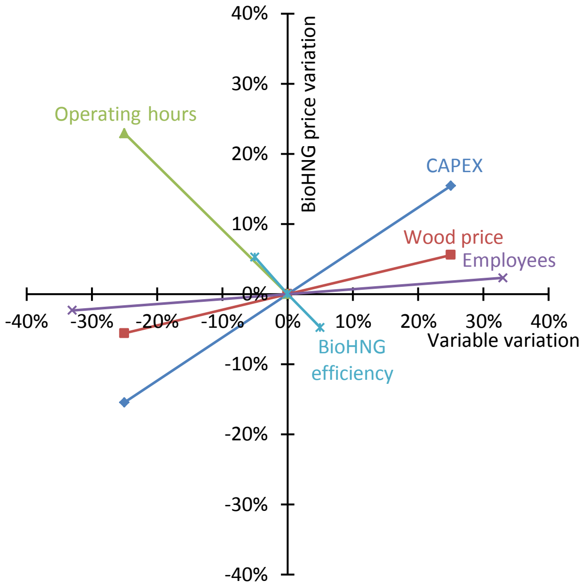

Figure 62: Sensitivity analysis of the 10 MW BioHNG plant.

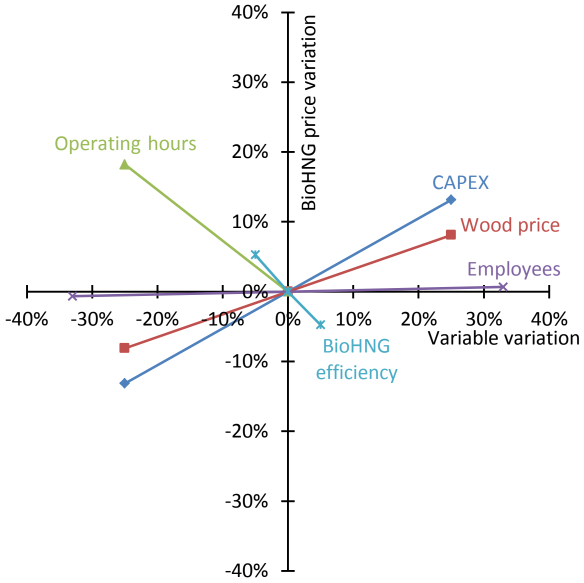

Figure 63: Sensitivity analysis of the 50 MW BioHNG plant.

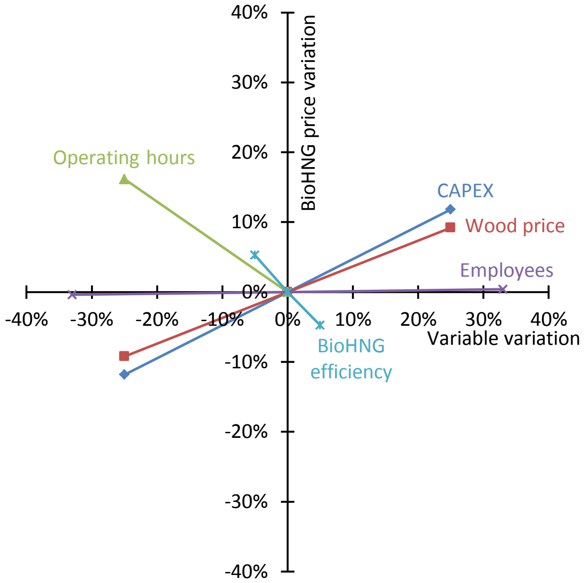

Figure 64: Sensitivity analysis of the 100 MW BioHNG plant.

4 Comparison of the investigated processes

This section compares and summarizes the results of the assessment of the four investigated processes with the three different plant capacities (10, 50, and 100 MW). Figure 65 compares the main product and the overall efficiencies of the four investigated processes.

The process for the generation of BioSNG and district heat has the highest main product efficiency and the CHP process the lowest. This can be dedicated to the comparable low electrical efficiency of the gas engine. In addition, the BioSNG process has also the highest overall efficiency. In contrast, the BioH_2 process has the lowest overall efficiency which can be dedicated to the PSA unit, where the CH_4, with its high heating value, is separated as well as to the heat demand for steam generation and amine regeneration.

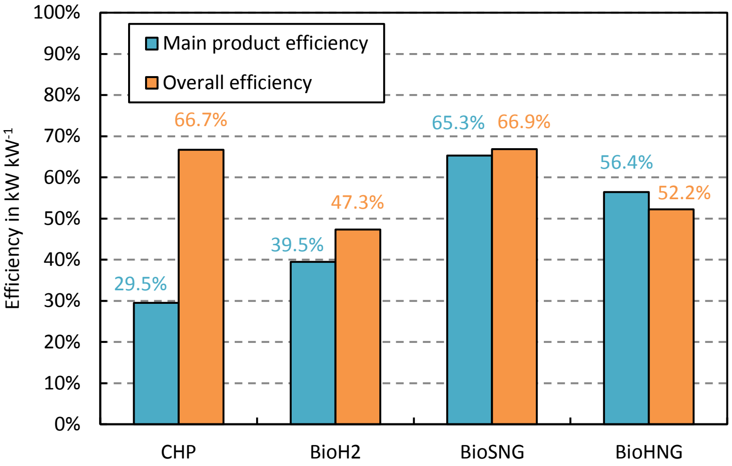

Figure 65: Efficiency comparison of the four investigated processes with 10 MW gasifier fuel power. The efficiency of the other plant capacities is assumed to be the same value.

4.1 10 MW plants

Figure 66 shows the comparison of the investment costs, the TOTEX_s, and the selling price at $\text{NPV} = 0$ (Equation 29) of the investigated 10 MW plants.

The BioSNG process has the highest investment costs which can be explained by the complex BioSNG process with the gas cleaning steps. The CHP process has the lowest investment costs because of its simple process layout and low number of unit operations. Moreover, the CHP process has the highest TOTEX_s which can be dedicated to the lowest main product efficiency. The BioSNG process has the lowest TOTEX_s because of the high efficiency. In case of the CHP process, the TOTEX_s are higher than main product selling price. This can be explained by the fact that the calculation of the TOTEX_s does not consider the generated district heat. However, for the calculation of the main product selling price, the revenues gained from the district heat were considered. The other processes show the expected case where the main product selling price is higher than the TOTEX_s because of the discounted cash flows over the plant life time.

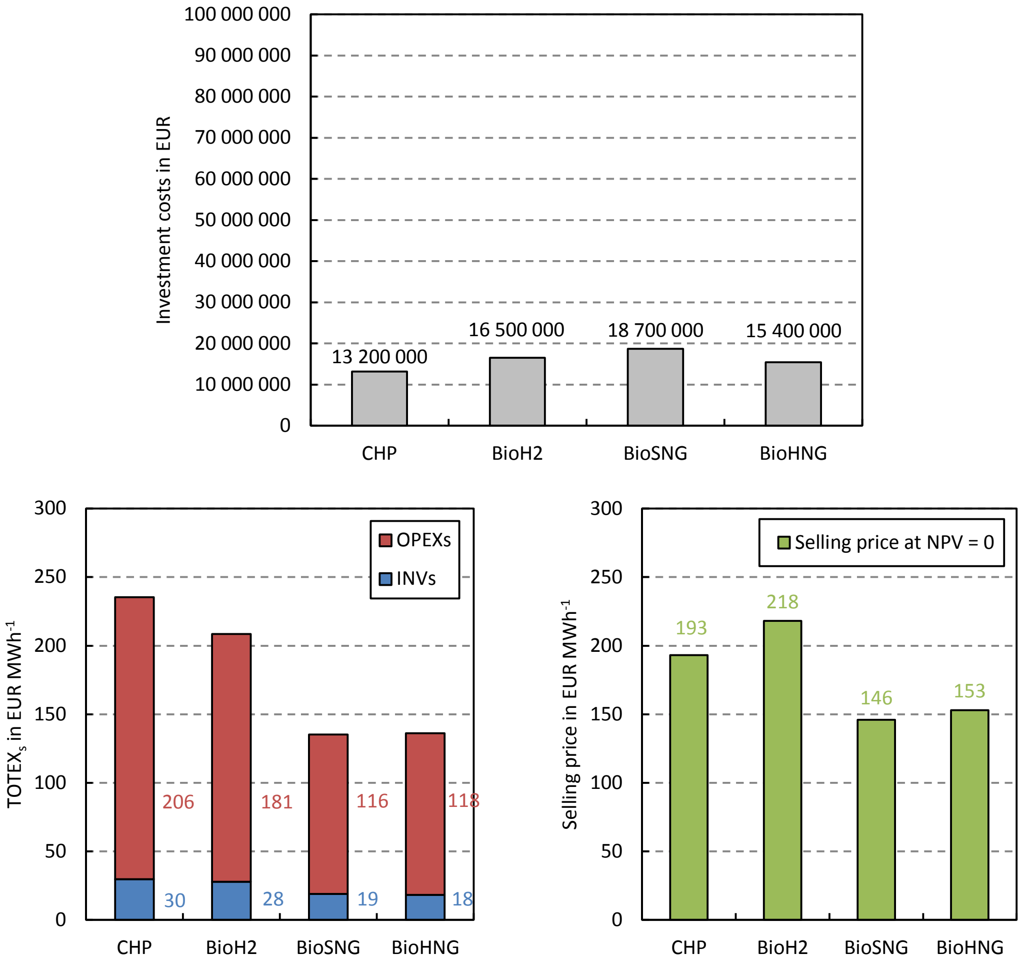

Figure 66: Investment costs (top) and TOTEX$_s$ (left), and the selling prices for NPV = 0 (right) of the investigated 10 MW plants.

4.2 50 MW plants

Figure 67 shows the comparison of the investment costs, the TOTEX$_s$, and the selling price at NPV = 0 of the investigated 50 MW plants.

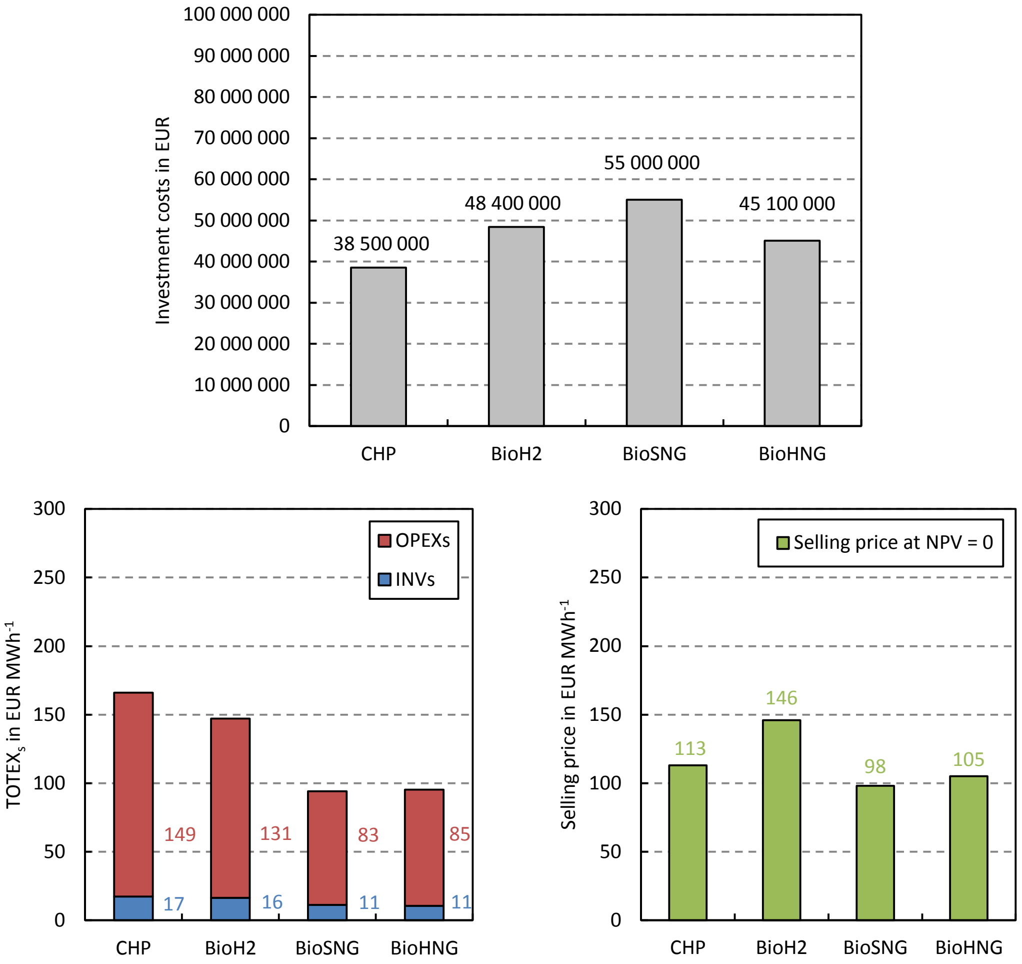

Figure 67: Investment costs (top) and TOTEX$_s$ (left), and the selling prices for NPV = 0 (right) of the investigated 50 MW plants.

The comparison of the investment costs shows the same correlation as the comparison of the 10 MW plants. However, at 50 MW plant capacity, also the BioH$_2$ process has higher TOTEX$_s$ than the main product selling price. This is caused by two effects, the district heat generation and revenues, which are, again, only considered for the calculation of the main product selling price and economy of scale effects which lead to decreased CAPEX and labor related costs. Moreover, it can be seen, that the TOTEX_s and the main product selling prices come closer to each other in case of the BioSNG and the BioHNG process compared to the 10 MW plants. This can also be dedicated to economy of scale effects.

4.3 100 MW plants

Figure 68 shows the comparison of the investment costs, the TOTEX_s, and the selling price at NPV = 0 of the investigated 100 MW plants.

The investment costs comparison and the TOTEX_s comparison shows the same correlations as for the 10 MW and 50 MW plant The TOTEX_s of the CHP and BioH_2 process are higher than the respective main product selling prices. Again, this can be dedicated to the fact that the generation and the revenues of district heat are only considered for the calculation of the main product selling price. However, the usual behavior can be seen in case of the BioSNG and the BioHNG process with a higher main product selling price compared to the TOTEX_s.

4.4 Sensitivity comparison

In this section, the influence of the annual operating hours, the CAPEX, and the wood price on the main product selling prices is shown for all investigated processes and plant capacities as those parameters have a significant influence on the economic feasibility beside the production efficiency. The field height in the figures is directly proportional to the respective sensitivity.

Figure 69 shows the sensitivity of the selling price depending on a variation of the annual operating hours.

It can be seen that with increasing plant capacities the sensitivity regarding the operating hours decreases. The CHP process has the highest sensitivity followed by the BioH_2 process, the BioHNG, and the BioSNG process which can be dedicated to the respective main product efficiencies.

Figure 70 shows the sensitivity of the selling price depending on the variation of the CAPEX.

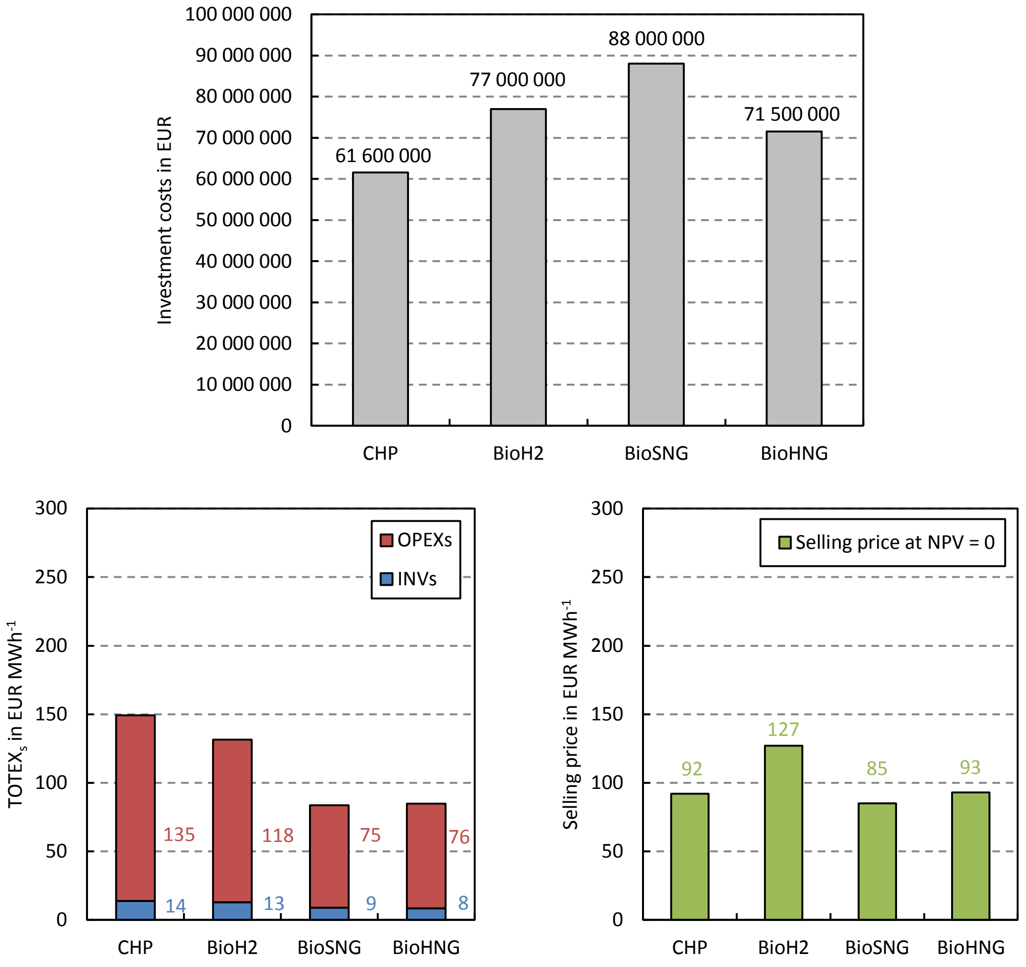

Figure 68: Investment costs (top) and TOTEX$_s$ (left), and the selling prices for NPV = 0 (right) of the investigated 100 MW plants.

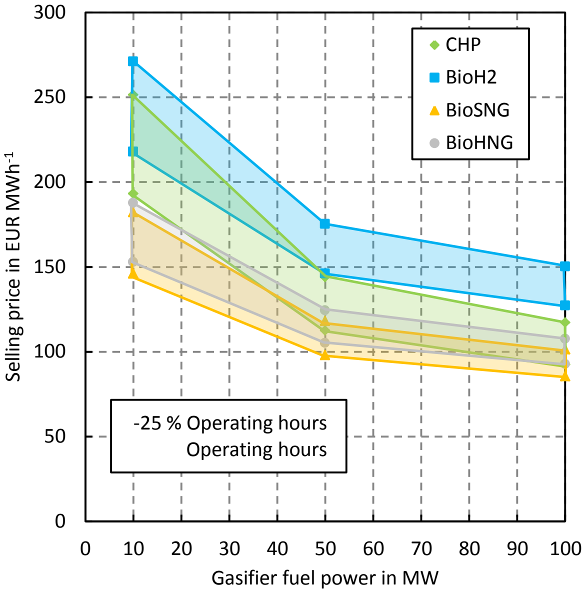

Figure 69: Selling price comparison of the investigated processes. The lower limit indicates the reference operating hours of 8000 $\mathrm{h \cdot a^{-1}}$. The upper limit indicates an operating hours variation of –25 %.

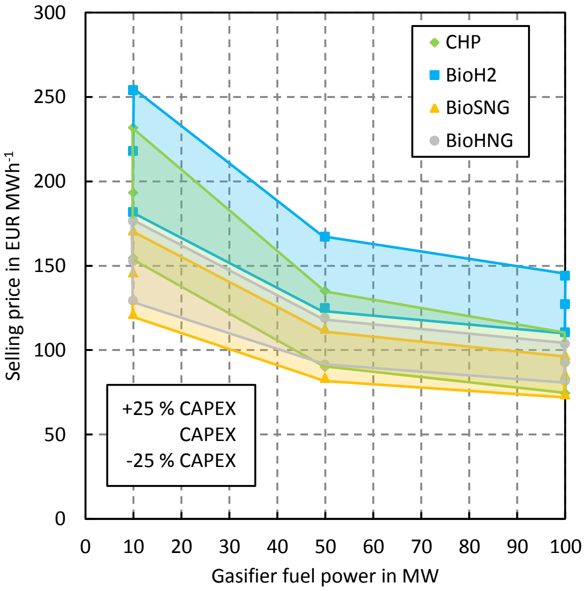

Figure 70: Selling price comparison of the investigated processes. The upper limit indicates a CAPEX variation of +25 % and the lower limit indicates a CAPEX variation of –25 %. The center point indicates the reference.

Again, it can be seen that the CHP process has the highest sensitivity followed by the $BioH_2$ process, the BioHNG, and the BioSNG process. Also the sensitivity depending on the CAPEX decreases with increasing plant capacity.

Figure 71 shows the sensitivity of the selling price depending on the variation of the wood price.

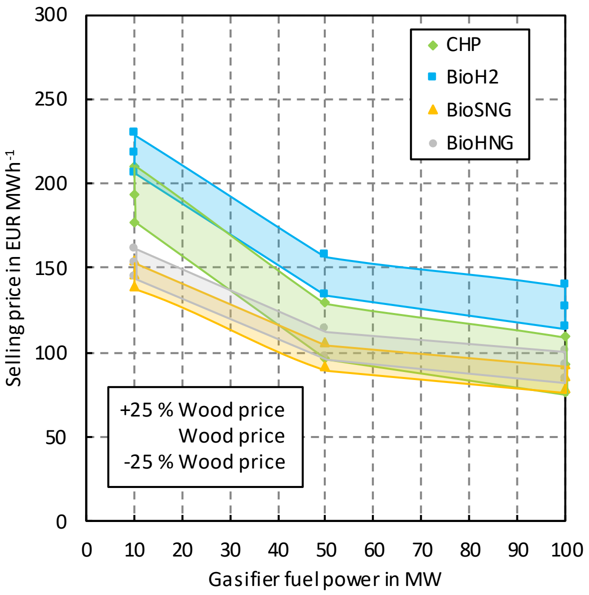

Figure 71: Selling price comparison of the investigated processes. The upper limit indicates a wood price variation of +25 % and the lower limit indicates a wood price variation of –25 %. The center point indicates the reference.

It can be seen, that in contrast to the figures before, the sensitivity increases with increasing plant capacity. Nevertheless, the CHP process has the highest sensitivity followed by the $BioH_2$, the BioHNG, and the BioSNG process.

5 Conclusion and outlook

At the beginning of this thesis, the following questions were raised:

- What are technically feasible operating conditions for a WGS unit processing product gas from biomass steam gasification plants?
- What are economically feasible selling prices for electricity, BioH_2, BioSNG, BioHNG for different plant capacities in Austria in 2017 and
- which parameters and variables have the most significant influence on the techno-economic feasibility of the investigated processes?
- Furthermore, how can those parameters be influenced and improved?

Based on the results, the following answers can be given:

The long-term operation of the WGS unit at the site of the DFB plant in Oberwart was demonstrated. No catalyst deactivation could be observed with the experimental layout and equipment which was used during the experiments. The results show that the application of a commercial Fe-Cr-based catalyst in a WGS unit is possible, even if tar-rich product gas from biomass steam gasification plants is processed if certain operating conditions (steam to carbon ratio, operating temperature) are ensured. However, future research should focus on further observations on possible catalyst deactivation during additional long-term experiments. In addition, process simplification by means of a lower steam to carbon ratio should be a goal for future research activities.

The CHP process could be economically feasible between 50 and 100 MW gasifier fuel power with the current (2017) feed-in tariffs for renewable electricity in Austria. However, realization of a biomass plant of this size is unlikely to happen in Austria. The largest biomass CHP plant in Austria is the biomass CHP in Wien Simmering, operated by Wien Energie GmbH with a fuel power of 66 MW [127]. Furthermore, biomass-based electricity generation seems not to be competitive compared to other renewable electricity sources like wind and photovoltaic. Nevertheless, there is some potential for optimization, especially for plants with smaller capacity; reducing the

RME consumption or using a cheaper fuel as feedstock, for example logging residues. In addition, further adaption of the gas engine to the requirements of the generated product gas could increase the electrical efficiency. Future work should also focus on the replacement of the gas engines with fuel cells in order to increase the electrical efficiency.

The BioH_2 process is not competitive in comparison with H_2 from natural gas steam reformers but in comparison with H_2 from other renewable sources. Compared to the other renewable H_2 generation technologies, biogas steam reforming or water electrolysis, the biomass steam gasification route can cover a wide range of scale. In order to improve the process, an additional steam reforming unit could be employed. However, this would increase the gas cleaning demand because of the Ni-based catalysts in commercial steam reformers. Furthermore, it would significantly influence the heat integration of the process.

The selling price of BioSNG is not competitive with the price of fossil natural gas. Nevertheless, based on the calculated results the generated BioSNG could be used in natural gas grids with the regulations today. BioSNG would have the advantage that it has the highest production efficiency of the investigated processes and could be distributed and stored via the existing natural gas infrastructure. Therefore, it could be used as fuel for the transportation sector, as fuel for steam reformer plants for H_2 production, and for electricity generation in combined cycle plants, where a combined electrical efficiency of over 35 % could be achieved based on the results in this work and typical electrical efficiency of gas combined cycle plants.

The BioHNG process could be an economically feasible alternative because of lower investment costs and a comparable high production efficiency. However, so far, there are no regulations, which support the injection of pure H_2 or HNG into the natural gas grids. Nevertheless, HNG could be used in industrial applications as natural gas replacement or substitute because the Wobbe index is similar to the Wobbe index of natural gas. Depending on the electricity price, other processes to separate the CO_2 could be applicable and should be investigated, for example membrane-based processes.

In all investigated processes, the production efficiency has a significant influence on the economic feasibility. In addition, the production efficiency is directly depending on the cold gas efficiency of the gasification process. Consequently, measures to increase the cold gas efficiency of the gasification process should be investigated.

Beside the product generation efficiency, the annual operating hours have the most significant influence on an economically feasible operation of the investigated plants. At the commercial DFB CHP plants in Güssing and Oberwart, annual operating times of up to 7500 hours were reached. The limiting factors were in most cases the reliability of the fuel feeding system and heat exchanger clogging. Both factors need certain attention, especially if a different, respectively low-quality fuel is used as feedstock. Therefore, experimental test runs regarding the fuel feeding should be carried out before utilizing alternative fuels. In order to reduce the clogging tendency of heat exchangers, the gas cleaning should be adopted and checked for reliability in experimental test runs as well (tar condensation). In addition, redundancy of certain equipment parts would also contribute to an increase of the annual operating time. However, most of these measures go hand in hand with an increase of the investment costs.

In general, the investment costs and the wood chip prices also have a significant influence on the economic feasibility of the investigated processes. In addition, also the electricity consumption of the processes is a factor which should be considered. Nevertheless, plant operators have nearly no influence on those parameters.

Labor related costs are of lower significance. Therefore, the number of employees and operators should be sufficient enough to enable a reliable plant operation to achieve high annual operating times.

The district heat generation has only significant influence in case of the CHP process. For example, fuel drying needs a significant amount of energy which could be used for district heat generation. However, without fuel drying, more product gas needs to be recycled into the combustion reactor of the DFB gasification system which would reduce the electrical efficiency of the CHP process. Also, the steam generation has a significant influence on the energy balance of the processes, especially of the BioH_2, the BioSNG, and the BioHNG process. This is mainly caused by the required steam to achieve a certain steam to carbon ratio at the inlet of fixed bed reactors in order to avoid coking and carbon deposition. Therefore, different catalysts should be investigated which are able to handle a lower steam to carbon ratio of the product gas.

CO_2 from the amine stripping units could also be used as product which would generate additional revenues and increase the economic feasibility of the investigated processes for BioH_2, BioSNG, and BioHNG generation. However, CO_2 pretreatment demand should be investigated before utilization, for example in the food industry.

In conclusion, without proper boundary conditions by means of governmental economic support and subsidies, an economic feasible operation of the investigated processes seems not possible if the processes have to compete with fossil energy carriers or renewable electricity sources like wind turbines or photovoltaic. Different measures to increase the annual operating time and to lower the fuel price should be realized in order to increase the economic feasibility of the processes. Therefore, extensive research regarding the utilization of different low-quality fuels should be carried out, especially the fuel feeding and gas cleaning has to be investigated in order to achieve high process reliabilities and to ensure a sufficient product gas quality for downstream unit operations.

Abbreviations and acronyms

AC	Activated carbon
AEL	Alkaline electrolysis
aMDEA	Activated methyldiethanolamine
AT	After taxes
BASF	Badische Anilin und Soda-Fabrik
$BioH_2$	Biomass derived H_2
BioHNG	Biomass derived gas mixture mainly composed of H_2 and CH_4
BioSNG	Biomass derived synthetic natural gas
BM	Biomass
BT	Before taxes
BTEX	Benzene, toluene, ethylbenzene, xylene
CC	Composite curve
CHP	Combined heat and power
CMS	Carbon molecular sieve
CNG	Compressed natural gas
COCO	Cape-open to cape-open
con	Condensation
CR	Combustion reactor
DEA	Diethanolamine
DFB	Dual fluidized bed
DH	District heat
El.	Electricity
FG	Flue gas
GCC	Grand composite curve
GCMS	Gas chromatography mass spectroscopy
GE	Gas engine
GR	Gasification reactor

HNG	Gas mixture composed of H_2 and CH_4
HDS	Hydrodesulfurization
IRR	Internal rate of return
ISBL	Inside battery limit
MDEA	Methyldiethanolamine
MEA	Monoethanolamine
NG	Natural gas
OSBL	Outside battery limit
ÖVGW	Österreichischer Verein für das Gas- und Wasserfach
PEM	Proton exchange membrane or polymer electrolyte membrane
PG	Product gas
PSA	Pressure swing adsorption
PV	Photovoltaic
PZ	Piperazine
RME	Rapeseed methyl ester
sh	Superheated
SNG	Synthetic natural gas
STP	Standard temperature and pressure (273.15 K and 101325 Pa)
TRL	Technology readiness level
UNFCCC	United Nations Framework Convention on Climate Change
US	United States
WGS	Water gas shift

Latin symbols

AT cash flow	Cash flow after taxes in $\mathrm{EUR} \cdot \mathrm{a}^{-1}$
BT cash flow	Cash flow before taxes in $\mathrm{EUR} \cdot \mathrm{a}^{-1}$
CAPEX	Capital expenditures in EUR
CAPEX_s	Specific capital expenditures in $\mathrm{EUR} \cdot \mathrm{MWh}^{-1}$ or $\mathrm{EUR} \cdot \mathrm{kg}^{-1}$
Capacity	Fuel or product capacities of different plants or unit operations in MW or $\mathrm{kg} \cdot \mathrm{h}^{-1}$
CEPI	Chemical engineering plant index in -
Depreciation	Plant depreciation in $\mathrm{EUR} \cdot \mathrm{a}^{-1}$
GHSV_i	Gas hourly space velocity in h^{-1}
HHV_i	Higher heating value of component i in $\mathrm{MJ} \cdot \mathrm{m}^{-3}$ or $\mathrm{MJ} \cdot \mathrm{kg}^{-1}$
HWO_i	Higher Wobbe index of component i in $\mathrm{MJ} \cdot \mathrm{m}^{-3}$ or $\mathrm{MJ} \cdot \mathrm{kg}^{-1}$
i	Discount rate in -
INV	Investment costs in EUR
INV_s	Specific investment costs in $\mathrm{EUR} \cdot \mathrm{MWh}^{-1}$ or $\mathrm{EUR} \cdot \mathrm{kg}^{-1}$
K_g	Equilibrium constant calculated by thermo-physical properties in -
K_{MAL}	Equilibrium constant calculated by the mass action law in -
LHV_i	Lower heating value of component i in $\mathrm{MJ} \cdot \mathrm{m}^{-3}$ or $\mathrm{MJ} \cdot \mathrm{kg}^{-1}$
LWO_i	Lower Wobbe index in $\mathrm{MJ} \cdot \mathrm{m}^{-3}$ or $\mathrm{MJ} \cdot \mathrm{kg}^{-1}$
m	Capacity rationing factor in -
$\dot{m}_i$	Mass flow rate of component i in $\mathrm{kg} \cdot \mathrm{h}^{-1}$
$\dot{m}c_p$	Heat capacity flow rate in $\mathrm{kW} \cdot \mathrm{K}^{-1}$

n	Plant lifetime in a
$\dot{n}_{\mathrm{G}}$	Molar dry gas flow rate in $\mathrm{kmol} \cdot \mathrm{h}^{-1}$
$\dot{n}_{\mathrm{Steam}}$	Molar steam flow rate in $\mathrm{kmol} \cdot \mathrm{h}^{-1}$
NPV	Net present value in EUR
OPEX	Operational expenditures or production costs in $\mathrm{EUR} \cdot \mathrm{a}^{-1}$
OPEX_s	Specific operating expenditures in $\mathrm{EUR} \cdot \mathrm{MWh}^{-1}$ or $\mathrm{EUR} \cdot \mathrm{kg}^{-1}$
ROI	Return on investment in -. The ROI is the discount rate i at which the NPV equals zero.
Tax rate	Tax rate in -
$\mathrm{P}_{\mathrm{El,c}}$	Consumed electrical power in kW
$\mathrm{P}_{\mathrm{El,g}}$	Generated electrical power in kW
p	Absolute pressure in Pa or bar
p_x	Partial pressure of component x in Pa or bar
R	General gas constant in $\mathrm{J} \cdot \mathrm{mol}^{-1} \cdot \mathrm{K}^{-1}$
r	Reaction rate in in $\mathrm{mol} \cdot \mathrm{g}^{-1} \cdot \mathrm{s}^{-1}$
REV	Plant revenues in $\mathrm{EUR} \cdot \mathrm{a}^{-1}$
SUEX	Start-up expenses in $\mathrm{EUR} \cdot \mathrm{a}^{-1}$
T	Temperature in K or °C
t	Annual plant operating hours in $\mathrm{h} \cdot \mathrm{a}^{-1}$
TOTEX_s	Specific total expenditures in $\mathrm{EUR} \cdot \mathrm{MWh}^{-1}$ or $\mathrm{EUR} \cdot \mathrm{kg}^{-1}$

Greek symbols

η_{C}	Carbon efficiency in $\mathrm{kg} \cdot \mathrm{kg}^{-1}$
η_{MP}	Main product efficiency in $\mathrm{kW} \cdot \mathrm{kW}^{-1}$
η_{O}	Overall efficiency in $\mathrm{kW} \cdot \mathrm{kW}^{-1}$
ΔH_{298}	Enthalpy of formation at 25 °C (298.15 K) and 101325 Pa in $\mathrm{kJ} \cdot \mathrm{mol}^{-1}$
ΔT_{min}	Minimum temperature difference for the pinch analysis in °C
φ_x	Volumetric fraction of component x in $\mathrm{m}^3 \cdot \mathrm{m}^{-3}$
ω_x	Mass fraction of component x in $\mathrm{kg} \cdot \mathrm{kg}^{-1}$

List of figures

1 Distribution of the total primary energy production (left) and the primary energy production of renewables (right) in Austria in 2015 [4]. 9

2 Distribution of the electricity generation (left) and district heat generation (right) in Austria in 2015 [4]. 10

3 Gross domestic consumption (left) and energetic end use (right) in Austria in 2015 [4]. 11

4 Consumer price index of different energy carriers in Austria from 2000 to 2015 [4]. 12

5 Development of industry prices for electricity and natural gas in Austria from 2005 to 2015 (excl. taxes and other charges) [11, 12]. 13

6 End-user prices of electricity, natural gas, and wood chips for the private sector in Austria from 2011 to 2017 [13]. 14

7 Overview of Austrian electricity feed-in tariffs for CHP plants using solid biomass as feedstock in $\mathrm{EUR} \cdot \mathrm{kWh}^{-1}$ from 2003 to 2017 [15, 16, 17]. 15

8 Simplfied flowchart of a natural gas steam reforming process for H_2 production based on [25]. 16

9 Graphical overview about the investigated processes. 20

10 Approach for the evaluation of the investigated processes. . . . 22

11 Principle of the DFB gasification process. 25

12 10 MW reference DFB gasifier Sankey diagram. All streams are given in kW. 28

13 Annual operating hours of the CHP plants Güssing, Oberwart, and Senden as well as of the GoBiGas plant [50, 51]. 29

14 Simplified flowchart of an amine scrubbing process (based on [62]). 33

15 Simplified flowchart of a PSA process. 39

16 Simplified flowchart of the WGS unit located at the site of the DFB plant Oberwart. 49

17 C-H-O ternary diagram for p = 1 bar indicating the C-H-O-ratio of the feed. The figure shows if coke formation and carbon deposition is thermodynamically favored. Based on [91], all carbon allotropes. 51
18 C-H-O ternary diagram for p = 10 bar indicating the C-H-O-ratio of the feed. The figure shows if coke formation and carbon deposition is thermodynamically favored. Based on [91], all carbon allotropes. 51
19 Temperature profile along the first reactor of the WGS unit during the long-term operation (based on Paper 2). 52
20 GCMS tar concentration of the dry product gas along the WGS unit. The product gas was extracted after the filter and before the RME scrubber of the DFB plant Oberwart. 53
21 Simplified flowchart of the investigated CHP process. 56
22 Composite curves (CC, left) and grand composite curve (GCC, right) for $\Delta T_{min} = 20$ °C of the investigated 10 MW CHP plant. 57
23 Heat exchanger network of the investigated 10 MW CHP plant. 58
24 Sankey diagram of the investigated 10 MW CHP plant. All streams are given in kW. 59
25 Energy distribution of the investigated 10 MW CHP plant. All streams are given in kW. 61
26 DFB gasification plant learning curve considering ISBL CAPEX based on experiences and [30, 118]. 62
27 Typical production costs of different electricity generation routes. Only the DFB process considers CHP. 64
28 Specific cost distribution based on the generated electricity. . . 64
29 Distribution of annual raw material and utility costs based on the 10 MW plant in $\mathrm{EUR} \cdot \mathrm{a}^{-1}$. 65
30 Sensitivity analysis of the 10 MW CHP plant. 66
31 Sensitivity analysis of the 50 MW CHP plant. 66
32 Sensitivity analysis of the 100 MW CHP plant. 67
33 Simplified flowchart of the plant for $\mathrm{BioH_2}$ and district heat generation. 69

34 Composite curves (left) and grand composite curve (right) for $\Delta T_{min} = 20$ °C of the investigated plant for $BioH_2$ and district heat generation with 10 MW fuel power. 70
35 Heat exchanger network of the investigated plant for $BioH_2$ and district heat generation with 10 MW fuel power. 71
36 Sankey diagram of the investigated plant for $BioH_2$ and district heat generation with 10 MW gasifier fuel power. All streams are given in kW. 72
37 Sankey diagram of the investigated plant for $BioH_2$ and district heat generation with 10 MW gasifier fuel power showing the H flows in H_2, CH_4, C_xH_y, and H_2O streams in $kg \cdot h^{-1}$. . 74
38 Energy distribution of the investigated 10 MW $BioH_2$ plant. All streams are given in kW. 76
39 Specific cost distribution based on the generated $BioH_2$. 78
40 Distribution of annual raw material and utility costs. Based on the 10 MW plant in $EUR \cdot a^{-1}$. 79
41 Sensitivity analysis of the 10 MW $BioH_2$ plant. 79
42 Sensitivity analysis of the 50 MW $BioH_2$ plant. 80
43 Sensitivity analysis of the 100 MW $BioH_2$ plant. 80
44 Simplified flowchart of the plant for BioSNG and district heat generation. 84
45 Composite curves (CC, left) and grand composite curve (GCC, right) for $\Delta T_{min} = 20$ °C of the DFB plant for BioSNG and district heat production. 85
46 Heat exchanger network of the 10 MW plant for BioSNG and district heat production. The upper part of the figure shows the DFB part of the process and the lower part shows the VESTA part of the process. 86
47 Energy Sankey diagram of the DFB part of the plant for BioSNG and district heat production for 10 MW gasifier fuel power. All streams are given in kW. 87

48 Energy Sankey diagram of the VESTA part of the plant for BioSNG and district heat production for 10 MW gasifier fuel power. All streams are given in kW. 88
49 Energy distribution of the investigated 10 MW BioSNG plant. All streams are given in kW. 91
50 Specific cost distribution based on the generated BioSNG. . . 93
51 Distribution of annual raw material and utility costs. Based on the 10 MW plant in EUR $\cdot$ a^{-1}. 94
52 Sensitivity analysis of the 10 MW BioSNG plant. 95
53 Sensitivity analysis of the 50 MW BioSNG plant. 95
54 Sensitivity analysis of the 100 MW BioSNG plant. 96
55 Simplified flowchart of the plant for BioHNG generation. . . . 97
56 Composite curves (CC, left) and grand composite curve (GCC, right) of the plant for BioHNG generation for $\Delta T_{min} = 20$ °C. 99
57 Heat exchanger network of the process for BioHNG generation. 99
58 Sankey diagram of the process for BioHNG generation. All streams are given in kW. 100
59 Energy distribution of the investigated 10 MW BioHNG plant. All streams are given in kW. 103
60 Specific cost distribution based on the generated BioHNG. . . 104
61 Distribution of the annual raw material and utility costs. Based on the 10 MW plant in EUR $\cdot$ a^{-1}. 105
62 Sensitivity analysis of the 10 MW BioHNG plant. 106
63 Sensitivity analysis of the 50 MW BioHNG plant. 106
64 Sensitivity analysis of the 100 MW BioHNG plant. 107
65 Efficiency comparison of the four investigated processes with 10 MW gasifier fuel power. The efficiency of the other plant capacities is assumed to be the same value. 108
66 Investment costs (top) and TOTEX_s (left), and the selling prices for NPV = 0 (right) of the investigated 10 MW plants. . 109
67 Investment costs (top) and TOTEX_s (left), and the selling prices for NPV = 0 (right) of the investigated 50 MW plants. . 110

68 Investment costs (top) and TOTEX_s (left), and the selling prices for NPV = 0 (right) of the investigated 100 MW plants. 112
69 Selling price comparison of the investigated processes. The lower limit indicates the reference operating hours of 8000 $\mathrm{h} \cdot \mathrm{a}^{-1}$. The upper limit indicates an operating hours variation of –25 %. 113
70 Selling price comparison of the investigated processes. The upper limit indicates a CAPEX variation of +25 % and the lower limit indicates a CAPEX variation of –25 %. The center point indicates the reference. 113
71 Selling price comparison of the investigated processes. The upper limit indicates a wood price variation of +25 % and the lower limit indicates a wood price variation of –25 %. The center point indicates the reference. 114

List of tables

1 Overview about the investigated processes. 19

2 Input streams of commercial DFB CHP plants. 26

3 Typical dry product gas composition of the DFB gasification process with olivine as bed material [41]. 26

4 Analysis of the wood chips, fresh RME, tar, and char used for the simulation of the DFB gasifier. All values on water-free basis [48]. 27

5 Key data of the reference DFB gasification plant [48]. N_2 was used as inertization fluid for the CHP process whereas CO_2 was used for the other processes. The volumetric flow rate is given at STP. 28

6 Overview of estimated OPEX. 45

7 Specific prices for calculation of the production costs (OPEX). 46

8 Assumptions for the techno-economic assessment. 47

9 Material and energy streams of the investigated CHP plants. Volumetric flow rates are given at STP. 60

10 Investment costs of the investigated CHP plants. 62

11 Results of the techno-economic assessment of the investigated CHP plants. 63

12 Material and energy streams of the investigated process for BioH_2 and district heat generation. 75

13 Investment costs of the investigated process for BioH_2 and district heat generation. 77

14 Results of the techno-economic assessment of the investigated process for BioH_2 and district heat generation. 77

15 Gas grid specifications according to Austrian ÖVGW G31 in comparison with the calculated BioSNG data. 90

16 Material and energy streams of the investigated process for BioSNG and district heat production. 90

17 Investment costs of the investigated process for BioSNG production. 92

18 Results of the techno-economic assessment of the investigated process for BioSNG and district heat production. 92
19 Gas grid specifications according to Austrian ÖVGW G31 in comparison with the calculated BioHNG data. 101
20 Material and energy streams of the investigated process for BioHNG generation. 102
21 Investment costs of the investigated process for BioHNG production. 103
22 Results of the techno-economic assessment of the investigated process for BioHNG production. 104

References

[1] UNFCCC. Adoption of the Paris agreement. Technical Report FCCC/CP/2015/L.9/Rev.1, United Nations, Paris, December 2015. URL: `https://unfccc.int/resource/docs/2015/cop21/eng/l09r01.pdf`.

[2] UNTC. Status of the Paris Agreement, February 2017. URL: `https://treaties.un.org/pages/ViewDetails.aspx?src=TREATY&mtdsg_no=XXVII-7-d&chapter=27&clang=_en`.

[3] BMWFW. Energiestatus Österreich 2015 - Entwicklung bis 2013. Technical report, Bundesministerium für Wissenschaft, Forschung und Wirtschaft, Wien, 2015. URL: `http://www.bmwfw.gv.at/EnergieUndBergbau/Energieeffizienz/Documents/Energiestatus%20%C3%96sterreich%202015.pdf`.

[4] Manfred Gollner. Energiedaten Österreich 2015. Technical report, Statistik Austria, Wien, December 2016.

[5] BASIS. European Wood Chips Plants - Country analysis. Technical Report 2, Biomass Availability and Sustainability Information System, July 2015. URL: `http://www.basisbioenergy.eu/fileadmin/BASIS/D3.6_Global_Country__analysis_version2.pdf`.

[6] Peter Biermayr, Christa Dißauer, Manuela Eberl, Monika Enigl, Hubert Fechner, Kurt Leonhartsberger, Florian Maringer, Stefan Moidl, Christoph Schmidl, Christoph Strasser, Werner Weiss, Patrik Wonisch, and Elisabeth Wopienka. Innovative Energietechnologien in Österreich Marktentwicklung 2016. Technical report, Bundesministerium für Verkehr, Innovation und Technologie, 2017. URL: `https://nachhaltigwirtschaften.at/resources/nw_pdf/201713-marktentwicklung-2016.pdf`.

[7] Gerald Kalt, Lukas Kranzl, and Reinhard Haas. Long-term strategies for an efficient use of domestic biomass resources in Austria. *Biomass*

and Bioenergy, 34(4):449–466, April 2010. URL: `http://linkinghub.elsevier.com/retrieve/pii/S0961953409002566`, `doi:10.1016/j.biombioe.2009.12.009`.

[8] Josef Lichtscheidl, Reinhard Rauch, Stefan Müller, Christian Aichernig, Manfred Wörgetter, and Rita Ehrig. Erzeugung von Wasserstoff für Raffinierien über Biomassevergasung. Technical report, Österreichische Forschungsförderungsgesellschaft mbH (FFG), Wien, December 2011. URL: `https://www.klimafonds.gv.at/assets/Uploads/Blue-Globe-Reports/Erneuerbare-Energien/2008-2011/BGR0292011EE.Erzeugung-von-Wasserstoff.pdf`.

[9] Rita Ehrig, Manfred Wörgetter, Christa Kristöfel, Nikolaus Ludwigczek, Christian Pointner, Christoph Strasser, and Josef Lichtscheidl. Biomasseverfügbarkeit zur Versorgung einer Biowasserstoffanlage am Standort Wien. Technical Report 002 TR IK-1-1-17, Bioenergy 2020+ GmbH, Wieselburg, February 2010.

[10] Bernhard Lang. Marktanalyse Energieholz Teil 3: Preisentwicklung der Energieholzsortimente. Technical report, Austrian Energy Agency, Wien, August 2013.

[11] E-Control. Entwicklung Industriepreise Gas. Online resource, accessed 30.10.2017. URL: `https://www.e-control.at/industrie/gas/gaspreis/industriegaspreise/industriepreise`.

[12] E-Control. Entwicklung Industriepreise Strom. Online resource, accessed 30.10.2017. URL: `https://www.e-control.at/industrie/strom/strompreis/industriestrompreise/entwicklung-industriepreise`.

[13] Österreichischer Biomasseverband. Energieträgervergleich. Online resource, accessed 05.08.2017, January 2017. URL: `http://www.biomasseverband.at/service/energietraegervergleich/`.

[14] D.W. Wu and R. Z. Wang. Combined cooling, heating and power: A review. *Progress in Energy and Combustion Science*, 32(5-6):459–495, 2006. `doi:10.1016/j.pecs.2006.02.001`.

[15] E-Control. Einspeisetarife für neue Ökostromanlagen 2003 und 2006 bis 2009. Technical report, Energie-Control GmbH, Wien, February 2010. URL: `https://www.e-control.at/industrie/oeko-energie/einspeisetarife/einspeisetarife-archiv`.

[16] E-Control. Einspeisetarife für neue Ökostromanlagen 2010 und 2011. Technical report, Energie-Control GmbH, Wien, January 2011. URL: `https://www.e-control.at/industrie/oeko-energie/einspeisetarife/einspeisetarife-archiv`.

[17] Marina Luggauer, Martin Höher, and Lorenz Strimitzer. Ökostrom Einspeisetarifverordnung 2016. Technical report, Klimaaktiv Energieholz, Wien, March 2016.

[18] Austrian Power Grid. Installierte Kraftwerksleistung. Online resource, accessed 13.11.2017. URL: `https://www.apg.at/de/markt/Markttransparenz/erzeugung/installierte-leistung`.

[19] H. Hofbauer, S. Fürnsinn, G. Bauer, C. Heilig, and C. Aichernig. Technische, ökonomische und ökologische Bewertung verschiedener Wege der energetischen und stofflichen Verwertung von Synthesegas aus der Biomassevergasung. Technical report, BMVIT, 2009.

[20] Reinhard Rauch. The FICFB-gasification system. Online resource, accessed 06.11.2017. URL: `http://www.ficfb.at/`.

[21] Ke Liu, Chunshan Song, and Velu Subramani. *Hydrogen and Syngas Production and Purification Technologies*. Wiley, 2010.

[22] Havva Balat and Elif Kirtay. Hydrogen from biomass - Present scenario and future prospects. *International Journal of Hydrogen Energy*, 35(14):7416–7426, 2010. `doi:10.1016/j.ijhydene.2010.04.137`.

[23] Angela Miltner. *Techno-ökonomische Analyse der regenerativen Produktion von Wasserstoff für den Einsatz in Fahrzeugen.* PhD thesis, TU Wien, 2010.

[24] Christopher Yang and Joan Ogden. Determining the lowest-cost hydrogen delivery mode. *International Journal of Hydrogen Energy*, 32(2):268–286, 2007. `doi:10.1016/j.ijhydene.2006.05.009`.

[25] James A. Ritter and Armin D. Ebner. State-of-the-Art Adsorption and Membrane Separation Processes for Hydrogen Production in the Chemical and Petrochemical Industries. *Separation Science and Technology*, 42(6):1123–1193, 2007. `doi:10.1080/01496390701242194`.

[26] Marcelo Carmo, David L. Fritz, Jürgen Mergel, and Detlef Stolten. A comrehensive review on PEM water electrolysis. *International Journal of Hydrogen Energy*, 38(12):4901–4934, 2013. `doi:10.1016/j.ijhydene.2013.01.151`.

[27] Kai Zeng and Dongke Zhang. Recent progress in alkaline water electrolysis for hydrogen production and applications. *Progress in Energy and Combustion Science*, 36(3):307–326, 2010. `doi:10.1016/j.pecs.2009.11.002`.

[28] U.S. Department of Energy Office of Fossil Energy. Practical Experience Gained During the First Twenty Years of Operation of the Great Plains Gasification Plant and Implications for Future Projects. Technical report, U.S. Department of Energy Office of Fossil Energy, 2006.

[29] Chi-Jen Yang and Robert B. Jackson. China's synthetic natural gas revolution. *Nature Climate Change*, 3:852–854, 2013. `doi:10.1038/nclimate1988`.

[30] Alberto Alamia, Anton Larsson, Claes Breitholtz, and Henrik Thunman. Performance of large-scale biomass gasifiers in a biorefinery, a state-of-the-art reference. *International Journal of Energy Research*, 41(14):2001–2019, 2017. `doi:10.1002/er.3758`.

[31] Barbara Rehling. *Development of the 1MW Bio-SNG plant, evaluation on technological and economical aspects and upscaling considerations.* PhD thesis, TU Wien, 2012.

[32] Barbara Rehling, Hermann Hofbauer, Reinhard Rauch, and Christian Aichernig. BioSNG - process simulation and comparison with first results from a 1-MW demonstration plant. *Biomass Conversion and Biorefineries*, 1:111–119, 2011. `doi:10.1007/s13399-011-0013-3`.

[33] Jakub Niesner, David Jecha, and Petr Stehlik. Biogas Upgrading Technologies: State of Art Review in European Region. *Chemical Engineering Transactions*, 35:517–522, 2013. `doi:10.3303/CET1335086`.

[34] C. Nelsson, C. Hulteberg, J. Saint-Just, and M. Kaiadi. HCNG - A Dead End or a Bridge to the Future. In *Proceedings of the 18th World Hydrogen Energy Conference (WHEC)*, pages 195–201, 2010.

[35] J. F. Larsen and J. S. Wallace. Comparison of Emissions and Efficiency of a Turbocharged Lean-Burn Natural Gas and Hythane-Fueled Engine. *Journal of Engineering for Gas Turbines and Power*, 119:218–226, 1997.

[36] Fernando Ortenzi, Maria Chiesa, Riccardo Scarcelli, and Giovanni Pede. Experimental tests of blends of hydrogen and natural gas in light-duty vehicles. *International Journal of Hydrogen Energy*, 33(12):3225–3229, 2008. `doi:10.1016/j.ijhydene.2008.01.050`.

[37] R. Sierens and E. Rosseel. Variable Composition Hydrogen/Natural Gas Mixtures for Increased Engine Efficiency and Decreased Emissions. *Journal for Engineering for Gas Turbines and Power*, 122(1):135–140, 1999. `doi:10.1115/1.483191`.

[38] Sebastian Verhelst and Thomas Wallner. Hydrogen-fueled internal combustion engines. *Progress in Energy and Combustion Science*, 35(6):490–527, 2009. `doi:10.1016/j.pecs.2009.08.001`.

[39] Manfred Klell, Helmut Eichlseder, and Markus Sartory. Mixtures of hydrogen and methane in the internal combustion engine - Synergies, potential and regulations. *International Journal of Hydrogen Energy*, 37(15):11531–11540, 2012.

[40] A.D. Dekate, S.H. Nikam, S.D. Rairikar, M. Sreenivasulu, S.S. Thipse, A.V. Mannikar, and T.V. Singh. A Study on Material Compatibility with Various Blends of HCNG on Existing CNG Fuel Kit. In *Proceedings of the Symposium on International Automotive Technology*, 2013. `doi:10.4271/2013-26-0079`.

[41] Martin Kaltschmitt, Hans Hartmann, and Hermann Hofbauer. *Energie aus Biomasse*. Springer Vieweg, 3rd edition, 2016.

[42] Friedrich Kirnbauer and Hermann Hofbauer. The mechanism of bed material coating in dual fluidized bed biomass steam gasification plants and its impact on plant optimization. *Powder Technology*, 245:94–104, 2013. `doi:10.1016/j.powtec.2013.04.022`.

[43] Matthias Kuba, Fabian Havlik, Friedrich Kirnbauer, and Hermann Hofbauer. Influence of bed material coatings on the water-gas-shift reaction and steam reforming of toluene as tar model compound of biomass gasification. *Biomass and Bioenergy*, 89:40–49, 2016. `doi:10.1016/j.biombioe.2015.11.029`.

[44] Martin Stidl. *Ersatz fossiler Brennstoffe durch die Zweibett-Wirbelschicht-Dampfvergasung fester Biomasse*. PhD thesis, TU Wien, 2012.

[45] Veronika Wilk and Hermann Hofbauer. Analysis of optimization potential in commercial biomass gasification plants using process simulation. *Fuel Processing Technology*, 141(1):138–147, 2016. `doi:10.1016/j.fuproc.2015.07.035`.

[46] Tobias Pröll. *Potenziale der Wirbelschichtdampfvergasung fester Biomasse - Modellierung und Simulation auf Basis der Betriebserfahrungen am Biomassekraftwerk Güssing*. PhD thesis, TU Wien, 2004.

[47] Reinhard Rauch, Jitka Hrbek, and Hermann Hofbauer. Biomass gasification for synthesis gas production and applications of the syngas. *WIREs Energy Environ*, 3:343–362, 2014. `doi:10.1002/wene.97`.

[48] Florian Benedikt. IPSEpro simulation - Reference plant 10 MW fuel input. Technical report, TU Wien, 2017.

[49] Robert Bardolf. *Optimierung eines Produktgaswäschers bei der Biomassedampfvergasung im Zweibettwirbelschichtverfahren.* PhD thesis, TU Wien, 2017.

[50] Klaus Bosch. Biomass Power Plant Oberwart. Scheduled presentation at the Central European Biomass Conference and Exhibition 2017 in Graz, Austria.

[51] Markus Luisser. SNG aus Biomasse am Beispiel Göteburg. Presentation at the Austrian Biomass Day at November 2017.

[52] Matthias Kuba, Stephan Kraft, Friedrich Kirnbauer, Frank Maierhans, and Hermann Hofbauer. Influence of controlled handling of solid inorganic materials and design changes on the product gas quality in dual fluid bed gasification of woody biomass. *Applied Energy*, 210:230–240, 2018. `doi:10.1016/j.apenergy.2017.11.028`.

[53] Silvester Fail. *Biohydrogen Production Based on the Catalyzed Water Gas Shift Reaction in Wood Gas.* PhD thesis, TU Wien, 2014.

[54] M.V. Twigg. *Catalyst Handbook.* Manson Publishing, 1989.

[55] Minghui Zhu and Isreal E. Wachs. Iron-Based Catalysts for the High-Temperature Water-Gas Shift (HT-WGS) Reaction: A Review. *ACS Catalysis*, 6:722–732, 2016. `doi:10.1021/acscatal.5b02594`.

[56] Chandra Ratnasamy and Jon P. Wagner. Water Gas Shift Catalysis. *Catalysis Reviews*, 51(3):325–440, 2009. `doi:10.1080/01614940903048661`.

[57] Tobias Pröll, Reinhard Rauch, Christian Aichernig, and Hermann Hofbauer. Fluidized Bed Steam Gasification of Solid Biomass - Performance Characteristics of an 8 MWth Combined Heat and Power Plant. *International Journal of Chemical Reactor Engineering*, 5(1), 2007. `doi:doi:10.2202/1542-6580.1398`.

[58] Gary T. Rochelle. Amine Scrubbing for CO_2 Capture. *Science*, 2009. `doi:10.1126/science.1176731`.

[59] Niall MacDowell, Nick Florin, Antoine Buchard, Jason Hallett, Amparo Galindo, George Jackson, Claire S. Adjiman, Charlotte K. Williams, Nilay Shah, and Paul Fennell. An overview of CO_2 capture technologies. *Energy & Environmental Science*, 3:1645–1669, 2010. `doi:10.1039/c004106h`.

[60] Stefan Klinski. Einspeisung von Biogas in das Erdgasnetz. Technical report, nachwachsende-rohstoffe.de, 2006. URL: `http://www.biogaspartner.de/fileadmin/biogas/Downloads/Studien/Einspeisestudie.pdf`.

[61] Research Division Thermal Process Engineering TU Wien, Instutite of Chemical Engineering and Simulation. Biogas to Biomethane Technology Review. Technical report, Bio-Methane Regions, 2012. URL: `http://bio.methan.at/sites/default/files/BiogasUpgradingTechnologyReview_ENGLISH.pdf`.

[62] Fredric Bauer, Christian Hulteberg, Tobias Persson, and Daniel Tamm. Biogas upgrading - Review of commercial technologies. Technical report, Swedish Gas Technology Center (SGC), 2013.

[63] D.W. Bailey and P.H.M. Feron. Post-combustion Decarbonisation Processes. *Oil & Gas Science and Technology*, 60(3):461–474, 2005.

[64] J.C. Meerman, E.S. Hamborg, T. van Keulen, A. Ramírez, W.C. Turkenburg, and A.P.C. Faaij. Techno-economic assessment of CO_2

capture at steam methane reforming facilities using commercially available technology, International Journal of Greenhouse Gas Control. *International Journal of Greenhouse Gas Control*, 9:160–171, 2012. `doi:10.1016/j.ijggc.2012.02.018`.

[65] Shell Global Solutions. For cost-effective, enhanced removal of carbon dioxide (CO_2). Online resource, accessed 07.10.2017, 2011. URL: `http://www.shell.com/business-customers/global-solutions/gas-processing-licensing/licensed-technologies/acid-gas-removal/adip-process/_jcr_content/par/textimage.stream/1487623032063/e1036bff9415d92b3c102ab4c57dee386e45468064fca3a58585d8d894ecab48/adip-x.pdf`.

[66] E. Privalova, S. Rasi, P Mäki-Arvela, K. Eränen, J. Rintala, D. Yu. Murzin, and J.P. Mikkola. CO_2 capure from biogas: absorbent selection. *RSC Advances*, 3:2979, 2013. `doi:10.1039/c2ra23013e`.

[67] E. Ryckebosch, M. Drouillon, and H. Vervaeren. Techniques for transformation of biogas to biomethane. *Biomass and Bioenergy*, 35:1633–1645, 2011. `doi:10.1016/j.biombioe.2011.02.033`.

[68] Wolfgang Urban, Kai Girod, and Heiko Lohmann. Technologien und Kosten der Biogasaufbereitung und Einspeisung in das Erdgasnetz. Ergebnisse der Markterhebung 2007-2008. Technical report, Fraunhofer Institut Umwelt-, Sicherheits, Energietechnik UMSICHT, 2009.

[69] M. Wang, A. Lawal, P. Stephenson, J. Sidders, and C. Ramshaw. Post-combustion CO_2 capture with chemical absorption: A state-of-the-art review. *Chemical Engineering Research and Design*, 89:1609–1624, 2011. `doi:10.1016/j.cherd.2010.11.005`.

[70] Luis M. Romeo, Irene Bolea, and Jesus M. Escosa. Integration of power plant and amine scrubbing to reduce CO_2 capture costs. *Applied Thermal Engineering*, 28:1039–1046, 2008. `doi:10.1016/j.applthermaleng.2007.06.036`.

[71] Marco Scholz, Thomas Melin, and Matthias Wessling. Transforming biogas into biomethane using membrane technology. *Renewable and Sustainable Energy Reviews*, 17:199–212, 2013. `doi:10.1016/j.rser.2012.08.009`.

[72] Katherine Starr, Xavier Gabarrell, Gara Villalba, Laura Talens, and Lidia Lombardi. Life cycle assessment of biogas upgrading technologies. *Waste Management*, 32:991–999, 2012. `doi:doi:10.1016/j.wasman.2011.12.016`.

[73] Daniela Thrän, Eric Billig, Tobias Persson, Mattias Svensson, Jaqueline Daniel-Gromke, Jens Ponitka, Michael Seiffert, John Baldwin, Lukas Kranzl, Fabian Schipfer, Julian Matzenberger, Nathalie Devriendt, Mathieu Dumont, Jonas Dahl, and Günther Bochmann. Biomethane - status and factors affecting market development and trade. Technical report, IEA Bioenergy Task 40 and Task 37, 2014.

[74] Jacob N. Knudsen, Jørgen N. Jensen, Poul-Jacob Vilhelmsen, and Ole Biede. Experience with CO_2 capture from coal flue gas in pilot-scale: Testing of different amine solvents. *Energy Procedia*, 1:783–790, 2009.

[75] Tobias Persson. Biogas up-grading: a technical review. Presentation Svenskt Gastekniskt Center AB, 2013.

[76] Elena Privalova. *Towards novel biogas upgrading processes*. PhD thesis, Abo Akademi University, 2013.

[77] Finn Andrew Tobiesen, Hallvard F. Svendsen, and Thor Mejdell. Modeling of Blast Furnance CO_2 Capture Using Amine Absorbents. *Industrial and Engineering Chemistry Research*, 46:7811–7819, 2007. `doi:10.1021/ie061556j`.

[78] Lars Erik Oi. Aspen HYSIS Simulation of CO_2 Removal by Amine Absorption from a Gas Based Power Plant. In *SIMS2007 Conference, Gothenburg*, 2007.

[79] Douglas Aaron and Costas Tsouris. Separation of CO_2 from Flue Gas: A Review. *Separation Science and Technology*, 40(1-3):321–348, 2005. `doi:10.1081/SS-200042244`.

[80] Ross E. Dugas. *Carbon Dioxide Absorption, Desorption, and Diffusion in Aqueous Piperazine and Monoethanolamine*. PhD thesis, The University of Texas at Austin, 2009.

[81] Jan Kopyscinski, Tilman J. Schildhauer, and Serge M. A. Biollaz. Production of synthetic natural gas (SNG) from coal and dry biomass - A technology review from 1950 to 2009. *Fuel*, 89(8):1763–1783, 2010. `doi:10.1016/j.fuel.2010.01.027`.

[82] Tilman J. Schildhauer. *Synthetic natural gas from coal, dry biomass, and power-to-gas applications*. Wiley, 2016.

[83] Calvin H. Bartholomew and Robert J. Farrauto. *Fundamentals of industrial catalytic processes*. Wiley Interscience, 2006.

[84] Stefan Rönsch, Jens Schneider, Steffi Matthischke, Michael Schlüter, Manuel Götz, Konathan Lefebvre, Praseeth Prabhakaran, and Siegfried Bajohr. Review on methanation - from fundamentals to current projects. *Fuel*, 166:276–296, 2016. `doi:10.1016/j.fuel.2015.10.111`.

[85] Pedro Haro, Filip Johnsson, and Henrik Thunman. Improved syngas processing for enhanced Bio-SNG production: A techno-economic assessment. *Energy*, 101:380–389, 2016. `doi:10.1016/j.energy.2016.02.037`.

[86] Tomoyuki Inui, Masaki Funabiki, and Yoshinobu Takegami. Simultaneous Methanation of CO and CO_2 on Supported Ni-Based Composite Catalysts. *Ind. Eng. Chem. Prod. Res. Dev.*, 19:385–388, 1980.

[87] Wang Wei and Gong Jinlong. Methanation of carbon dioxide: an overview. *Frontiers of Chemical Science and Engineering*, 5(1):2–10, 2011. `doi:10.1007/s11705-010-0528-3`.

[88] G. Alex Mills and Fred W. Steffgen. Catalytic Methanation. *Catalysis Reviews: Science and Engineering*, 8(1):159–210, 1974. `doi:10.1080/01614947408071860`.

[89] Seemann M. *Methanation of biosyngas in a fluidized bed reactor – development of a one-step synthesis process, featuring simultaneous methanation, watergas shift and low temperature tar reforming*. PhD thesis, ETH Zürich, 2006.

[90] Götz M. *Methanisierung im Dreiphasen-Reaktor*. PhD thesis, Karlsruher Institut für Technologie, 2014.

[91] Jaworski Z., Zakrzewska B., and Pianko-Oprych P. On thermodynamic equilibrium of carbon deposition from gaseous C-H-O mixtures: updating for nanotubes. *Reviews in Chemical Engineering*, 33(3):217–235, 2017. `doi:doi:10.1515/revce-2016-0022`.

[92] K. Sasaki and Y. Teraoka. Equilibria in Fuel Cell Gases II. The C-H-O Ternary Diagrams. *Journal of The Electrochemical Society*, 150(7):A885–A888, 2003. `doi:10.1149/1.1577338`.

[93] Calvin H. Bartholomew. Mechanism of catalyst deactivation. *Applied Catalysis A. General*, 212(1-2):17–60, 2001. `doi:10.1016/S0926-860X(00)00843-7`.

[94] Izabela Czekaj, Francois Loviat, Fabio Raimondi, Jörg Wambach, Serge Biollaz, and Alexander Wokaun. Characterization of surface processes at the Ni-based catalyst during the methanation of biomass-derived synthesis gas: X-ray photoelectron spectroscopy (XPS). *Applied Catalysis A: General*, 329:68–78, October 2007. `doi:10.1016/j.apcata.2007.06.027`.

[95] Martin C. Seemann, Tilman J. Schildhauer, and Serge M. A. Biollaz. Fluidzed Bed Methanation of Wood-Derived Producer Gas for the Production of Synthetic Natural Gas. *Industrial & Engineering Chemistry Research*, 49(15):7034–7038, 2010. `doi:10.1021/ie100510m`.

[96] Robert Deithorn. Carbon adsorption & reactivation. CalgonCarbon, 2012.

[97] Harry Marsh and Francisco Rodriguez-Reinoso. *Activated Carbon*. Elsevier Science & Technology Books, 2006.

[98] Ralph T. Yang. *Adsorbents: Fundamentals and Applications*. Wiley-Interscience, 2003.

[99] Donald R. Woods. *Rules of Thumb in Engineering Pratice*. Wiley-VCH, 2007.

[100] Kinya Sakanishi, Zhiheng Wu, Akimitsu Matsumura, Ikuo Saito, Toshiaki Hanaoka, Tomoaki Minowa, Mitsuhiro Tada, and Toshihiko Iwasaki. Simultaneous removal of H_2S and COS using activated carbons and their supported catalysts. *Catalysis Today*, 104(1):94–100, 2005. `doi:10.1016/j.cattod.2005.03.060`.

[101] Luigi Bressan. VESTA - a Noval SNG Technology. Presentation at Defining the Future V, Bejing, China, 2011.

[102] Letizia Romano, Fabio Ruggeri, and Robert Marx. SNG Producion from Coal: A Possible Solution to Energy Demand. *Energy Procedia*, 45:1330–1336, 2014. `doi:10.1016/j.egypro.2014.01.139`.

[103] Fabio Ruggeri. The Novel VESTA Process for Substitute Natural Gas Production. Presentation at Gasification Technologies Conference, Washington, 2012. URL: `http://archive.amecfw.com/file.axd?pointerID=55a7ba2d8b0c1e0e04f11a6b&sid=635726523334250000`.

[104] Shivaji Sircar. Pressure Swing Adsorption. *Industrial & Engineering Chemistry Research*, 41(6):1389–1392, 2002. `doi:10.1021/ie0109758`.

[105] Carlos A. Grande. *Biogas Upgrading by Pressure Swing Adsorption*, chapter 3, pages –. InTech, 2011. URL: `https://www.intechopen.com/books/biofuel-s-engineering-process-technology/biogas-upgrading-by-pressure-swing-adsorption`, `doi:10.5772/18428`.

[106] Silvester Fail, Nicolas Diaz, Florian Benedikt, Michael Kraussler, Julian Hinteregger, Klaus Bosch, Marius Hackel, Reinhard Rauch, and Hermann Hofbauer. Wood Gas Processing To Generate Pure Hydrogen Suitable for PEM Fuel Cells. *Sustainable Chemistry & Engineering*, 2014. `doi:10.1021/sc500436m`.

[107] Nicolas Felipe Diaz Perez. *Hydrogen Separation from Producer Gas Generated by Biomass Steam Gasification.* PhD thesis, TU Wien, 2013.

[108] M. Grotz, R. Böwing, J. Lang, J. Thalhauser, P. Christiner, and A. Wimmer. Efficiency increase of a high performance gas engine for distributed power generation. Presentation, February 2015. URL: `http://www.cimac.com/cms/upload/events/cascades/previous_cascades/CASCADES_2015_Graz/Matthias_Grotz_GE.pdf`.

[109] Jan Brandin, Martin Tuner, and Ingemar Odenbrand. Gas Engine CHP for Biofuels. Technical report, Lund University, 2011. URL: `http://www.diva-portal.org/smash/get/diva2:445550/FULLTEXT01.pdf`.

[110] G.R. Herdin, F. Gruber, D. Plohberger, and M. Wagner. Experience with gas engines optimized for H_2-rich fuels. In *Processdings of ICES03*, 2003.

[111] H. Hofbauer, R. Rauch, K. Bosch, R. Koch, and C. Aichernig. Biomass CHP Plant Güssing: A Success Story. Online resource, accessed 10.08.2017, Augus. URL: `http://members.aon.at/biomasse/strassbourg.pdf`.

[112] IEA Bioenergy. Fact Sheet - Gas Engines. Online resource, accessed 11.08.2017. URL: `http://task33.ieabioenergy.com/app/webroot/files/file/publications/Fact_sheets/IEA_Gas_engines.pdf`.

[113] Jan Kotik. *Über den Einsatz von Kraft-Wärme-Kopplungsanlagen auf Basis der Wirbelschicht-Dampfvergasung fester Biomasse am Beispiel des Biomassekraftwerks Oberwart.* PhD thesis, TU Wien, May 2010.

[114] Klaus Payrhuber. Betriebserfahrungen, Möglichkeiten des flexiblen Einsatzes von BHKW. Presentation, June 2012.

[115] SimTech. What is IPSEpro? Online resource, accessed 06.11.2017. URL: `http://www.simtechnology.com/CMS/index.php/ipsepro`.

[116] COCO. Cape open to cape open simulation environment. Online resource, accessed 10.08.2017. URL: `http://cocosimulator.org/`.

[117] Ding-Yu Peng and Donald B. Robinson. A New Two-Constant Equation of State. *Industrial and Engineering Chemistry Fundamentals*, 15(1):59–64, 1976. URL: `http://pubs.acs.org/doi/pdf/10.1021/i160057a011`.

[118] Stefan Müller. *Hydrogen from Biomass for Industry*. PhD thesis, TU Wien, 2013.

[119] Ian C. Kemp. *Pinch Analysis and Process Integration*. Elsevier, 2007.

[120] Florian Brunner und Pierre Krummenacher. *Einführung in die Prozessintegration mit der Pinch-Methode*. Bundesamt für Energie, 2015. URL: `https://pinch-analyse.ch/downloads/Einfuehrung_in_die_Pinch-Methode_Endversion.pdf`.

[121] Thane Brown. *Engineering Economics and Economic Design for Process Engineers*. CRC Press Taylor & Francis Group, Boca Raton, 1st edition, 2007.

[122] Klaus H. Weber. *Engineering verfahrenstechnischer Anlagen*. Springer Vieweg, 2014.

[123] E-Control. Entwicklung der Großhandelspreise Strom. Online resource, accessed 09.08.2017. URL: `https://www.e-control.at/industrie/strom/strompreis/grosshandelspreise`.

[124] E-Control. Preiszusammensetzung Strom. Online resource, accessed 09.08.2017. URL: `https://www.e-control.at/industrie/strom/strompreis/grosshandelspreise`.

[125] Matthias Binder. Long Term Performance of an Fe/Cr Based Water Gas Shift Catalyst Processing Tar-Rich Wood Gas. Master's thesis, TU Wien, 2015.

[126] Jaap Koppejan. *The Handbook of Biomass Combustion and Co-firing*. Taylor and Francis, 2012.

[127] Wien Energie. Biomasskraftwerk Simmering - Technische Daten. Online resource, accessed 03.08.2017. URL: `https://www.wienenergie.at/eportal3/ep/channelView.do?channelId=-48494`.

[128] Verbund Thermal Power GmbH. Gas-Kombikraftwerk Mellach. Online resource, accessed 21.11.2017. URL: `https://www.verbund.com/de-at/ueber-verbund/kraftwerke/unsere-kraftwerke/mellach-gaskombikraftwerk`.

[129] Christoph Kost, Johannes N. Mayer, Jessica Thomsen, Niklas Hartmann, Charlotte Senkpiel, Simon Philiipps, Sebastian Nold, Simon Lude, and Thomas Schlegl. Stromgestehungskosten Erneuerbare Energien. Technical report, Fraunhofer ISE, 2013. URL: `https://www.ise.fraunhofer.de/content/dam/ise/de/documents/publications/studies/DE2013_ISE_Studie_Stromgestehungskosten_Erneuerbare_Energien.pdf`.

[130] Angela Miltner, Walter Wukovits, Tobias Pröll, and Anton Friedl. Renewable hydrogen production: a technical evaluation based on process simulation. *Journal of Cleaner Production*, 18(1):S51–S62, 2010. `doi:10.1016/j.jclepro.2010.05.024`.

[131] Stefan Müller, Martin Stidl, Tobias Pröll, Reinhard Rauch, and Hermann Hofbauer. Hydrogen from biomass: large-scale hydrogen production based on a dual fluidized bed steam gasification system. *Biomass Conversion and Biorefinery*, 2011.

[132] F. Mueller-Langer, E. Tzimas, M. Kaltschmitt, and S. Peteves. Techno-economic assessment of hydrogen production processes for the hydrogen

economy for the short and medium term. *International Journal of Hydrogen Energy*, 32(16):3797–3810, 2007. `doi:10.1016/j.ijhydene.2007.05.027`.

[133] Konstantin Zech, Katja Oehmichen, Elias Grasemann, Julia Michaelis, Simon Funke, and Michael Seiffert. Technical, economic and environmental assessment of technologies for the production of biohydrogen and its distribution - results of the hy-NOW study. *International Journal of Hydrogen Energy*, 40:5487–5495, 2015. `doi:10.1016/j.ijhydene.2015.01.177`.

[134] Stefan Hemetsberger. *Gasification in Power to Gas concepts.* PhD thesis, TU Wien, 2017.

[135] Kevin Bunten. Waste utilisation to produce green natural gas. Presentation from Amec Foster Wheeler, October 2016. URL: `http://www.gasification-syngas.org/uploads/downloads/2016%20Conference/2016-presentations/2016-11-2-Amec-Foster-Wheeler.pdf`.

[136] Fabio Ruggeri. La conversione delle biomasse in vettore energetico primario: Il gas naturale. Presentation Amec Foster Wheeler, April 2016. URL: `http://www.ati2000.it/media/docs/107-nb.5%20AMECFWI%20-%20ing.%20F.%20Ruggeri.pdf`.

[137] Martin Gassner and Francois Marechal. Thermo-economic process model for thermochemical production of Synthetic Natural Gas (SNG) from lignocellulosic biomass. *Biomass and Bioenergy*, 33(11):1587–1604, 2009. `doi:10.1016/j.biombioe.2009.08.004`.

[138] Eric Billig. *Bewertung technischer und wirtschaftlicher Entwicklungspotenziale künftiger und bestehender Biomasse-zu-Methan-Konversionsprozesse.* PhD thesis, Universität Leipzig, 2016.

[139] E-Control. Entwicklung der Großhandelspreise Erdgas. Online resource, accessed 15.11.2017. URL: `https://www.e-control.at/industrie/gas/gaspreis/grosshandelspreise`.

[140] E-Control. Preiszusammensetzung Erdgas. Online resource, accessed 15.11.2017. URL: `https://www.e-control.at/industrie/gas/gaspreis/preiszusammensetzung`.

[141] Michael Kraussler, Florian Benedikt, Juraj Priscak, and Hermann Hofbauer. Simulation of a polygeneration process for the generation of hydrogen, H_2CH_4, and district heat via sorption enhanced reforming of wood chips. In *Proceedings of the 25th European Biomass Conference and Exhibition, 12-15 June, Stockholm, Sweden*, pages 732–737, 2017.

A Simulation stream data

Data tables of the COCO simulations, which were carried out to acquire the mass and energy balances of the investigated processes for a gasifier fuel power of 10 MW. Tar, BTEX, and sulfur components were not simulated.

A.1 Process A: Combined heat and power

	PG from GR	RME scrubber inlet	RME scrubber outlet	PG to GE	Units
p	1.0	1.0	1.0	1.0	bar
T	850.0	150.0	50.0	50.0	°C
$\dot{m}$	3045.6	3045.6	2154.1	1981.8	kg · h^{-1}
φ_{H_2}	0.2572	0.2572	0.3714	0.3714	m^3 · m^{-3}
φ_{CO}	0.1420	0.1420	0.2050	0.2050	m^3 · m^{-3}
φ_{CO_2}	0.1295	0.1295	0.1869	0.1869	m^3 · m^{-3}
φ_{CH_4}	0.0581	0.0581	0.0839	0.0839	m^3 · m^{-3}
$\varphi_{C_2H_4}$	0.0133	0.0133	0.0192	0.0192	m^3 · m^{-3}
$\varphi_{C_2H_6}$	0.0009	0.0009	0.0013	0.0013	m^3 · m^{-3}
$\varphi_{C_3H_8}$	0.0031	0.0031	0.0045	0.0045	m^3 · m^{-3}
φ_{N_2}	0.0118	0.0118	0.0171	0.0171	m^3 · m^{-3}
φ_{O_2}	0.0000	0.0000	0.0000	0.0000	m^3 · m^{-3}
φ_{H_2O}	0.3840	0.3840	0.1107	0.1107	m^3 · m^{-3}
	PG to CR	GE mixture	Ambient air to GE	FG from GE	Units
p	1.0	1.0	1.0	1.0	bar
T	50.0	21.8	10.0	435.1	°C
$\dot{m}$	172.3	18284.5	16302.7	18223.4	kg · h^{-1}
φ_{H_2}	0.3714	0.0569	0.0000	0.0000	m^3 · m^{-3}
φ_{CO}	0.2050	0.0314	0.0000	0.0008	m^3 · m^{-3}
φ_{CO_2}	0.1869	0.0286	0.0000	0.0855	m^3 · m^{-3}
φ_{CH_4}	0.0839	0.0128	0.0000	0.0000	m^3 · m^{-3}
$\varphi_{C_2H_4}$	0.0192	0.0029	0.0000	0.0000	m^3 · m^{-3}
$\varphi_{C_2H_6}$	0.0013	0.0002	0.0000	0.0000	m^3 · m^{-3}
$\varphi_{C_3H_8}$	0.0045	0.0007	0.0000	0.0000	m^3 · m^{-3}
φ_{N_2}	0.0171	0.6674	0.7850	0.6987	m^3 · m^{-3}
φ_{O_2}	0.0000	0.1736	0.2050	0.0970	m^3 · m^{-3}
φ_{H_2O}	0.1107	0.0254	0.0100	0.1180	m^3 · m^{-3}

	RME scrubber condensate	Excess condensate	Steam	Superheated steam	Units
p	1.0	1.0	1.0	1.0	bar
T	50.0	50.0	101.0	450.0	°C
$\dot{m}$	891.5	44.6	846.9	846.9	$\mathrm{kg} \cdot \mathrm{h}^{-1}$
φ_{H_2}	0.0000	0.0000	0.0000	0.0000	$\mathrm{m}^3 \cdot \mathrm{m}^{-3}$
φ_{CO}	0.0000	0.0000	0.0000	0.0000	$\mathrm{m}^3 \cdot \mathrm{m}^{-3}$
φ_{CO_2}	0.0000	0.0000	0.0000	0.0000	$\mathrm{m}^3 \cdot \mathrm{m}^{-3}$
φ_{CH_4}	0.0000	0.0000	0.0000	0.0000	$\mathrm{m}^3 \cdot \mathrm{m}^{-3}$
$\varphi_{C_2H_4}$	0.0000	0.0000	0.0000	0.0000	$\mathrm{m}^3 \cdot \mathrm{m}^{-3}$
$\varphi_{C_2H_6}$	0.0000	0.0000	0.0000	0.0000	$\mathrm{m}^3 \cdot \mathrm{m}^{-3}$
$\varphi_{C_3H_8}$	0.0000	0.0000	0.0000	0.0000	$\mathrm{m}^3 \cdot \mathrm{m}^{-3}$
φ_{N_2}	0.0000	0.0000	0.0000	0.0000	$\mathrm{m}^3 \cdot \mathrm{m}^{-3}$
φ_{O_2}	0.0000	0.0000	0.0000	0.0000	$\mathrm{m}^3 \cdot \mathrm{m}^{-3}$
φ_{H_2O}	1.0000	1.0000	1.0000	1.0000	$\mathrm{m}^3 \cdot \mathrm{m}^{-3}$
	FG from CR	FG to ambient	Ambient air	Preheated air	Units
p	1.0	1.0	1.0	1.0	bar
T	930.0	150.0	10.0	450.0	°C
$\dot{m}$	7836.9	7836.9	6888.8	6888.8	$\mathrm{kg} \cdot \mathrm{h}^{-1}$
φ_{H_2}	0.0000	0.0000	0.0000	0.0000	$\mathrm{m}^3 \cdot \mathrm{m}^{-3}$
φ_{CO}	0.0000	0.0000	0.0000	0.0000	$\mathrm{m}^3 \cdot \mathrm{m}^{-3}$
φ_{CO_2}	0.1300	0.1300	0.0000	0.0000	$\mathrm{m}^3 \cdot \mathrm{m}^{-3}$
φ_{CH_4}	0.0000	0.0000	0.0000	0.0000	$\mathrm{m}^3 \cdot \mathrm{m}^{-3}$
$\varphi_{C_2H_4}$	0.0000	0.0000	0.0000	0.0000	$\mathrm{m}^3 \cdot \mathrm{m}^{-3}$
$\varphi_{C_2H_6}$	0.0000	0.0000	0.0000	0.0000	$\mathrm{m}^3 \cdot \mathrm{m}^{-3}$
$\varphi_{C_3H_8}$	0.0000	0.0000	0.0000	0.0000	$\mathrm{m}^3 \cdot \mathrm{m}^{-3}$
φ_{N_2}	0.7160	0.7160	0.7850	0.7850	$\mathrm{m}^3 \cdot \mathrm{m}^{-3}$
φ_{O_2}	0.0640	0.0640	0.2050	0.2050	$\mathrm{m}^3 \cdot \mathrm{m}^{-3}$
φ_{H_2O}	0.0900	0.0900	0.0100	0.0100	$\mathrm{m}^3 \cdot \mathrm{m}^{-3}$

	Cold drying air	Hot drying air	Units
p	1.0	1.0	bar
T	10.0	90.0	°C
$\dot{m}$	38435.0	38435.0	$\mathrm{kg} \cdot \mathrm{h}^{-1}$
φ_{H_2}	0.0000	0.0000	$\mathrm{m}^3 \cdot \mathrm{m}^{-3}$
φ_{CO}	0.0000	0.0000	$\mathrm{m}^3 \cdot \mathrm{m}^{-3}$
φ_{CO_2}	0.0000	0.0000	$\mathrm{m}^3 \cdot \mathrm{m}^{-3}$
φ_{CH_4}	0.0000	0.0000	$\mathrm{m}^3 \cdot \mathrm{m}^{-3}$
$\varphi_{C_2H_4}$	0.0000	0.0000	$\mathrm{m}^3 \cdot \mathrm{m}^{-3}$
$\varphi_{C_2H_6}$	0.0000	0.0000	$\mathrm{m}^3 \cdot \mathrm{m}^{-3}$
$\varphi_{C_3H_8}$	0.0000	0.0000	$\mathrm{m}^3 \cdot \mathrm{m}^{-3}$
φ_{N_2}	0.7850	0.7850	$\mathrm{m}^3 \cdot \mathrm{m}^{-3}$
φ_{O_2}	0.2050	0.2050	$\mathrm{m}^3 \cdot \mathrm{m}^{-3}$
φ_{H_2O}	0.0100	0.0100	$\mathrm{m}^3 \cdot \mathrm{m}^{-3}$

A.2 Process B: Hydrogen and district heat

	PG from GR	WGS in	WGS out	RME scrubber out	Units
p	1.0	1.0	1.0	1.0	bar
T	850.0	356.4	436.4	50.0	°C
$\dot{m}$	3045.6	4775.3	4775.3	2564.7	$\mathrm{kg \cdot h^{-1}}$
φ_{H_2}	0.2561	0.1600	0.2397	0.4605	$\mathrm{m^3 \cdot m^{-3}}$
φ_{CO}	0.1414	0.0883	0.0086	0.0166	$\mathrm{m^3 \cdot m^{-3}}$
φ_{CO_2}	0.1376	0.0860	0.1657	0.3183	$\mathrm{m^3 \cdot m^{-3}}$
φ_{CH_4}	0.0578	0.0361	0.0361	0.0694	$\mathrm{m^3 \cdot m^{-3}}$
$\varphi_{C_2H_4}$	0.0132	0.0083	0.0083	0.0159	$\mathrm{m^3 \cdot m^{-3}}$
$\varphi_{C_2H_6}$	0.0009	0.0006	0.0006	0.0011	$\mathrm{m^3 \cdot m^{-3}}$
$\varphi_{C_3H_8}$	0.0031	0.0020	0.0020	0.0038	$\mathrm{m^3 \cdot m^{-3}}$
φ_{N_2}	0.0031	0.0019	0.0019	0.0037	$\mathrm{m^3 \cdot m^{-3}}$
φ_{O_2}	0.0000	0.0000	0.0000	0.0000	$\mathrm{m^3 \cdot m^{-3}}$
φ_{H_2O}	0.3867	0.6168	0.5371	0.1107	$\mathrm{m^3 \cdot m^{-3}}$

	Amine scrubber out	Removed CO_2	PSA feed	PSA raffinate (BioH_2)	Units
p	1.0	1.0	10.0	10.0	bar
T	50.0	50.0	50.0	50.0	°C
$\dot{m}$	717.7	1847.0	452.1	111.3	$\mathrm{kg \cdot h^{-1}}$
φ_{H_2}	0.6724	0.0000	0.8021	> 0.9990	$\mathrm{m^3 \cdot m^{-3}}$
φ_{CO}	0.0242	0.0000	0.0289	< 0.0001	$\mathrm{m^3 \cdot m^{-3}}$
φ_{CO_2}	0.0046	1.0000	0.0055	< 0.0001	$\mathrm{m^3 \cdot m^{-3}}$
φ_{CH_4}	0.1014	0.0000	0.1209	< 0.0001	$\mathrm{m^3 \cdot m^{-3}}$
$\varphi_{C_2H_4}$	0.0232	0.0000	0.0277	< 0.0001	$\mathrm{m^3 \cdot m^{-3}}$
$\varphi_{C_2H_6}$	0.0016	0.0000	0.0019	< 0.0001	$\mathrm{m^3 \cdot m^{-3}}$
$\varphi_{C_3H_8}$	0.0055	0.0000	0.0065	< 0.0001	$\mathrm{m^3 \cdot m^{-3}}$
φ_{N_2}	0.0054	0.0000	0.0064	< 0.0001	$\mathrm{m^3 \cdot m^{-3}}$
φ_{O_2}	0.0000	0.0000	0.0000	< 0.0001	$\mathrm{m^3 \cdot m^{-3}}$
φ_{H_2O}	0.1617	0.0000	0.0000	< 0.0000	$\mathrm{m^3 \cdot m^{-3}}$

	PSA adsorbate	Adsorbate to CR	RME scrubber condensate	Makeup water	Units
p	1.0	1.0	1.0	1.0	bar
T	47.2	47.2	50.0	10.0	°C
$\dot{m}$	340.8	56.9	2210.6	366.0	$\mathrm{kg} \cdot \mathrm{h}^{-1}$
φ_{H_2}	0.2884	0.2884	0.0000	0.0000	$\mathrm{m}^3 \cdot \mathrm{m}^{-3}$
φ_{CO}	0.1038	0.1038	0.0000	0.0000	$\mathrm{m}^3 \cdot \mathrm{m}^{-3}$
φ_{CO_2}	0.0199	0.0199	0.0000	0.0000	$\mathrm{m}^3 \cdot \mathrm{m}^{-3}$
φ_{CH_4}	0.4348	0.4348	0.0000	0.0000	$\mathrm{m}^3 \cdot \mathrm{m}^{-3}$
$\varphi_{C_2H_4}$	0.0996	0.0996	0.0000	0.0000	$\mathrm{m}^3 \cdot \mathrm{m}^{-3}$
$\varphi_{C_2H_6}$	0.0069	0.0069	0.0000	0.0000	$\mathrm{m}^3 \cdot \mathrm{m}^{-3}$
$\varphi_{C_3H_8}$	0.0235	0.0235	0.0000	0.0000	$\mathrm{m}^3 \cdot \mathrm{m}^{-3}$
φ_{N_2}	0.0231	0.0231	0.0000	0.0000	$\mathrm{m}^3 \cdot \mathrm{m}^{-3}$
φ_{O_2}	0.0000	0.0000	0.0000	0.0000	$\mathrm{m}^3 \cdot \mathrm{m}^{-3}$
φ_{H_2O}	0.0000	0.0000	1.0000	1.0000	$\mathrm{m}^3 \cdot \mathrm{m}^{-3}$
	Steam	Ambient air	Preheated air	Superheated steam to GR	Units
p	1.0	1.0	1.0	1.0	bar
T	101.0	10.0	450.0	450.0	°C
$\dot{m}$	2576.6	6888.8	6888.8	846.9	$\mathrm{kg} \cdot \mathrm{h}^{-1}$
φ_{H_2}	0.0000	0.0000	0.0000	0.0000	$\mathrm{m}^3 \cdot \mathrm{m}^{-3}$
φ_{CO}	0.0000	0.0000	0.0000	0.0000	$\mathrm{m}^3 \cdot \mathrm{m}^{-3}$
φ_{CO_2}	0.0000	0.0000	0.0000	0.0000	$\mathrm{m}^3 \cdot \mathrm{m}^{-3}$
φ_{CH_4}	0.0000	0.0000	0.0000	0.0000	$\mathrm{m}^3 \cdot \mathrm{m}^{-3}$
$\varphi_{C_2H_4}$	0.0000	0.0000	0.0000	0.0000	$\mathrm{m}^3 \cdot \mathrm{m}^{-3}$
$\varphi_{C_2H_6}$	0.0000	0.0000	0.0000	0.0000	$\mathrm{m}^3 \cdot \mathrm{m}^{-3}$
$\varphi_{C_3H_8}$	0.0000	0.0000	0.0000	0.0000	$\mathrm{m}^3 \cdot \mathrm{m}^{-3}$
φ_{N_2}	0.0000	0.7850	0.7850	0.0000	$\mathrm{m}^3 \cdot \mathrm{m}^{-3}$
φ_{O_2}	0.0000	0.2050	0.2050	0.0000	$\mathrm{m}^3 \cdot \mathrm{m}^{-3}$
φ_{H_2O}	1.0000	0.0100	0.0100	1.0000	$\mathrm{m}^3 \cdot \mathrm{m}^{-3}$

	FG from CR	FG from CR out	Boiler inlet	Boiler FG	Units
p	1.0	1.0	1.0	1.0	bar
T	930.0	150.0	47.2	1810.8	°C
$\dot{m}$	7836.9	7836.9	283.9	4635.1	$kg\cdot h^{-1}$
φ_{H_2}	0.0000	0.0000	0.2884	0.0000	$m^3\cdot m^{-3}$
φ_{CO}	0.0000	0.0000	0.1038	0.0000	$m^3\cdot m^{-3}$
φ_{CO_2}	0.1300	0.1300	0.0199	0.0896	$m^3\cdot m^{-3}$
φ_{CH_4}	0.0000	0.0000	0.4348	0.0000	$m^3\cdot m^{-3}$
$\varphi_{C_2H_4}$	0.0000	0.0000	0.0996	0.0000	$m^3\cdot m^{-3}$
$\varphi_{C_2H_6}$	0.0000	0.0000	0.0069	0.0000	$m^3\cdot m^{-3}$
$\varphi_{C_3H_8}$	0.0000	0.0000	0.0235	0.0000	$m^3\cdot m^{-3}$
φ_{N_2}	0.736	0.736	0.0231	0.7273	$m^3\cdot m^{-3}$
φ_{O_2}	0.069	0.069	0.0000	0.0172	$m^3\cdot m^{-3}$
φ_{H_2O}	0.065	0.065	0.0000	0.1659	$m^3\cdot m^{-3}$
	Boiler FG out	Cold drying air	Hot drying air		Units
p	1.0	1.0	1.0		bar
T	150.0	10.0	90.0		°C
$\dot{m}$	4635.1	38435.0	38435.0		$kg\cdot h^{-1}$
φ_{H_2}	0.0000	0.0000	0.0000		$m^3\cdot m^{-3}$
φ_{CO}	0.0000	0.0000	0.0000		$m^3\cdot m^{-3}$
φ_{CO_2}	0.0896	0.0000	0.0000		$m^3\cdot m^{-3}$
φ_{CH_4}	0.0000	0.0000	0.0000		$m^3\cdot m^{-3}$
$\varphi_{C_2H_4}$	0.0000	0.0000	0.0000		$m^3\cdot m^{-3}$
$\varphi_{C_2H_6}$	0.0000	0.0000	0.0000		$m^3\cdot m^{-3}$
$\varphi_{C_3H_8}$	0.0000	0.0000	0.0000		$m^3\cdot m^{-3}$
φ_{N_2}	0.7273	0.7850	0.7850		$m^3\cdot m^{-3}$
φ_{O_2}	0.0172	0.2050	0.2050		$m^3\cdot m^{-3}$
φ_{H_2O}	0.1659	0.0100	0.0100		$m^3\cdot m^{-3}$

A.3 Process C: Synthetic natural gas and district heat

	PG from GR	RME scrubber out	RME scrubber condensate	PG to VESTA process	Units
p	1.0	1.0	1.0	1.0	bar
T	850.0	50.0	50.0	50.0	°C
$\dot{m}$	3045.6	2151.5	894.1	1985.9	$\mathrm{kg} \cdot \mathrm{h}^{-1}$
φ_{H_2}	0.2561	0.3714	0.0000	0.3714	$\mathrm{m}^3 \cdot \mathrm{m}^{-3}$
φ_{CO}	0.1414	0.2050	0.0000	0.2050	$\mathrm{m}^3 \cdot \mathrm{m}^{-3}$
φ_{CO_2}	0.1376	0.1996	0.0000	0.1996	$\mathrm{m}^3 \cdot \mathrm{m}^{-3}$
φ_{CH_4}	0.0578	0.0839	0.0000	0.0839	$\mathrm{m}^3 \cdot \mathrm{m}^{-3}$
$\varphi_{C_2H_4}$	0.0132	0.0192	0.0000	0.0192	$\mathrm{m}^3 \cdot \mathrm{m}^{-3}$
$\varphi_{C_2H_6}$	0.0009	0.0013	0.0000	0.0013	$\mathrm{m}^3 \cdot \mathrm{m}^{-3}$
$\varphi_{C_3H_8}$	0.0031	0.0045	0.0000	0.0045	$\mathrm{m}^3 \cdot \mathrm{m}^{-3}$
φ_{N_2}	0.0031	0.0044	0.0000	0.0044	$\mathrm{m}^3 \cdot \mathrm{m}^{-3}$
φ_{O_2}	0.0000	0.0000	0.0000	0.0000	$\mathrm{m}^3 \cdot \mathrm{m}^{-3}$
φ_{H_2O}	0.3867	0.1107	1.0000	0.1107	$\mathrm{m}^3 \cdot \mathrm{m}^{-3}$

	PG to CR	Hydration in	Hydration out	WGS in	Units
p	1.0	10.0	10.0	10.0	bar
T	50.0	300.0	381.2	330.9	°C
$\dot{m}$	165.7	1783.0	1783.0	4339.0	$\mathrm{kg} \cdot \mathrm{h}^{-1}$
φ_{H_2}	0.3714	0.4176	0.4047	0.1556	$\mathrm{m}^3 \cdot \mathrm{m}^{-3}$
φ_{CO}	0.2050	0.2305	0.2356	0.0906	$\mathrm{m}^3 \cdot \mathrm{m}^{-3}$
φ_{CO_2}	0.1996	0.2244	0.2293	0.0884	$\mathrm{m}^3 \cdot \mathrm{m}^{-3}$
φ_{CH_4}	0.0839	0.0943	0.0964	0.0371	$\mathrm{m}^3 \cdot \mathrm{m}^{-3}$
$\varphi_{C_2H_4}$	0.0192	0.0216	0.0000	0.0000	$\mathrm{m}^3 \cdot \mathrm{m}^{-3}$
$\varphi_{C_2H_6}$	0.0013	0.0015	0.0236	0.0091	$\mathrm{m}^3 \cdot \mathrm{m}^{-3}$
$\varphi_{C_3H_8}$	0.0045	0.0051	0.0052	0.0020	$\mathrm{m}^3 \cdot \mathrm{m}^{-3}$
φ_{N_2}	0.0044	0.0050	0.0051	0.0020	$\mathrm{m}^3 \cdot \mathrm{m}^{-3}$
φ_{O_2}	0.0000	0.0000	0.0000	0.0000	$\mathrm{m}^3 \cdot \mathrm{m}^{-3}$
φ_{H_2O}	0.1107	0.0000	0.0000	0.6154	$\mathrm{m}^3 \cdot \mathrm{m}^{-3}$

	WGS out	SNG 1 in	SNG 1 out	SNG 2 in	Units
p	10.0	10.0	10.0	10.0	bar
T	413.8	350.0	511.7	300.0	°C
$\dot{m}$	4339.0	4339.0	4339.0	4339.0	$\text{kg} \cdot \text{h}^{-1}$
φ_{H_2}	0.2387	0.2387	0.1179	0.1179	$\text{m}^3 \cdot \text{m}^{-3}$
φ_{CO}	0.0074	0.0074	0.0062	0.0062	$\text{m}^3 \cdot \text{m}^{-3}$
φ_{CO_2}	0.1716	0.1716	0.1529	0.1529	$\text{m}^3 \cdot \text{m}^{-3}$
φ_{CH_4}	0.0371	0.0371	0.0958	0.0958	$\text{m}^3 \cdot \text{m}^{-3}$
$\varphi_{C_2H_4}$	0.0000	0.0000	0.0000	0.0000	$\text{m}^3 \cdot \text{m}^{-3}$
$\varphi_{C_2H_6}$	0.0091	0.0091	0.0000	0.0000	$\text{m}^3 \cdot \text{m}^{-3}$
$\varphi_{C_3H_8}$	0.0020	0.0020	0.0000	0.0000	$\text{m}^3 \cdot \text{m}^{-3}$
φ_{N_2}	0.0020	0.0020	0.0021	0.0021	$\text{m}^3 \cdot \text{m}^{-3}$
φ_{O_2}	0.0000	0.0000	0.0000	0.0000	$\text{m}^3 \cdot \text{m}^{-3}$
φ_{H_2O}	0.5322	0.5322	0.6251	0.6251	$\text{m}^3 \cdot \text{m}^{-3}$

	SNG 2 out	SNG 3 out	SNG 3 out	Amine scrubber in	Units
p	10.0	10.0	10.0	10.0	bar
T	401.3	250.0	289.4	50.0	°C
$\dot{m}$	4339.0	4339.0	4339.0	1704.2	$\text{kg} \cdot \text{h}^{-1}$
φ_{H_2}	0.0420	0.0420	0.0089	0.0311	$\text{m}^3 \cdot \text{m}^{-3}$
φ_{CO}	0.0007	0.0007	0.0000	0.0001	$\text{m}^3 \cdot \text{m}^{-3}$
φ_{CO_2}	0.1436	0.1436	0.1382	0.4841	$\text{m}^3 \cdot \text{m}^{-3}$
φ_{CH_4}	0.1217	0.1217	0.1324	0.4647	$\text{m}^3 \cdot \text{m}^{-3}$
$\varphi_{C_2H_4}$	0.0000	0.0000	0.0000	0.0000	$\text{m}^3 \cdot \text{m}^{-3}$
$\varphi_{C_2H_6}$	0.0000	0.0000	0.0000	0.0000	$\text{m}^3 \cdot \text{m}^{-3}$
$\varphi_{C_3H_8}$	0.0000	0.0000	0.0000	0.0000	$\text{m}^3 \cdot \text{m}^{-3}$
φ_{N_2}	0.0022	0.0022	0.0022	0.0078	$\text{m}^3 \cdot \text{m}^{-3}$
φ_{O_2}	0.0000	0.0000	0.0000	0.0000	$\text{m}^3 \cdot \text{m}^{-3}$
φ_{H_2O}	0.6898	0.6898	0.7183	0.0122	$\text{m}^3 \cdot \text{m}^{-3}$

	Amine scrubber out	Final SNG in	Final SNG out	BioSNG to grid	Units
p	10.0	10.0	10.0	10.0	bar
T	50.0	250.0	285.9	50.0	°C
$\dot{m}$	475.9	475.9	475.9	452.9	$\mathrm{kg} \cdot \mathrm{h}^{-1}$
φ_{H_2}	0.0597	0.0597	0.0225	0.0235	$\mathrm{m}^3 \cdot \mathrm{m}^{-3}$
φ_{CO}	0.0003	0.0003	0.0000	0.0000	$\mathrm{m}^3 \cdot \mathrm{m}^{-3}$
φ_{CO_2}	0.0093	0.0093	0.0001	0.0001	$\mathrm{m}^3 \cdot \mathrm{m}^{-3}$
φ_{CH_4}	0.8924	0.8924	0.9193	0.9606	$\mathrm{m}^3 \cdot \mathrm{m}^{-3}$
$\varphi_{C_2H_4}$	0.0000	0.0000	0.0000	0.0000	$\mathrm{m}^3 \cdot \mathrm{m}^{-3}$
$\varphi_{C_2H_6}$	0.0000	0.0000	0.0000	0.0000	$\mathrm{m}^3 \cdot \mathrm{m}^{-3}$
$\varphi_{C_3H_8}$	0.0000	0.0000	0.0000	0.0000	$\mathrm{m}^3 \cdot \mathrm{m}^{-3}$
φ_{N_2}	0.0149	0.0149	0.0152	0.0159	$\mathrm{m}^3 \cdot \mathrm{m}^{-3}$
φ_{O_2}	0.0000	0.0000	0.0000	0.0000	$\mathrm{m}^3 \cdot \mathrm{m}^{-3}$
φ_{H_2O}	0.0234	0.0234	0.0429	0.0000	$\mathrm{m}^3 \cdot \mathrm{m}^{-3}$
	Steam	**Superheated steam**	**FG from CR**	**FG from CR out**	**Units**
p	1.0	1.0	1.0	1.0	bar
T	101.0	450.0	930.0	150.0	°C
$\dot{m}$	910.1	850.9	7836.9	7836.9	$\mathrm{kg} \cdot \mathrm{h}^{-1}$
φ_{H_2}	0.0000	0.0000	0.0000	0.0000	$\mathrm{m}^3 \cdot \mathrm{m}^{-3}$
φ_{CO}	0.0000	0.0000	0.0000	0.0000	$\mathrm{m}^3 \cdot \mathrm{m}^{-3}$
φ_{CO_2}	0.0000	0.0000	0.1300	0.1300	$\mathrm{m}^3 \cdot \mathrm{m}^{-3}$
φ_{CH_4}	0.0000	0.0000	0.0000	0.0000	$\mathrm{m}^3 \cdot \mathrm{m}^{-3}$
$\varphi_{C_2H_4}$	0.0000	0.0000	0.0000	0.0000	$\mathrm{m}^3 \cdot \mathrm{m}^{-3}$
$\varphi_{C_2H_6}$	0.0000	0.0000	0.0000	0.0000	$\mathrm{m}^3 \cdot \mathrm{m}^{-3}$
$\varphi_{C_3H_8}$	0.0000	0.0000	0.0000	0.0000	$\mathrm{m}^3 \cdot \mathrm{m}^{-3}$
φ_{N_2}	0.0000	0.0000	0.7160	0.7160	$\mathrm{m}^3 \cdot \mathrm{m}^{-3}$
φ_{O_2}	0.0000	0.0000	0.0640	0.0640	$\mathrm{m}^3 \cdot \mathrm{m}^{-3}$
φ_{H_2O}	1.0000	1.0000	0.0900	0.0900	$\mathrm{m}^3 \cdot \mathrm{m}^{-3}$

	Ambient air	Preheated air	Superheated steam to VESTA	SNG condensate	Units
p	1.0	1.0	10.0	10.0	bar
T	10.0	450.0	300.0	50.0	°C
$\dot{m}$	6888.8	6888.8	2556.0	2634.8	$\mathrm{kg \cdot h^{-1}}$
φ_{H_2}	0.0000	0.0000	0.0000	0.0000	$\mathrm{m^3 \cdot m^{-3}}$
φ_{CO}	0.0000	0.0000	0.0000	0.0000	$\mathrm{m^3 \cdot m^{-3}}$
φ_{CO_2}	0.0000	0.0000	0.0004	0.0004	$\mathrm{m^3 \cdot m^{-3}}$
φ_{CH_4}	0.0000	0.0000	0.0000	0.0000	$\mathrm{m^3 \cdot m^{-3}}$
$\varphi_{C_2H_4}$	0.0000	0.0000	0.0000	0.0000	$\mathrm{m^3 \cdot m^{-3}}$
$\varphi_{C_2H_6}$	0.0000	0.0000	0.0000	0.0000	$\mathrm{m^3 \cdot m^{-3}}$
$\varphi_{C_3H_8}$	0.0000	0.0000	0.0000	0.0000	$\mathrm{m^3 \cdot m^{-3}}$
φ_{N_2}	0.7850	0.7850	0.0000	0.0000	$\mathrm{m^3 \cdot m^{-3}}$
φ_{O_2}	0.2050	0.2050	0.0000	0.0000	$\mathrm{m^3 \cdot m^{-3}}$
φ_{H_2O}	0.0100	0.0100	0.9996	0.9996	$\mathrm{m^3 \cdot m^{-3}}$

	Removed CO_2	Cold drying air	Hot drying air	Makeup water	Units
p	10.0	1.0	1.0	1.0	bar
T	50.0	10.0	90.0	10.0	°C
$\dot{m}$	1228.2	38435.0	38435.0	16.0	$\mathrm{kg \cdot h^{-1}}$
φ_{H_2}	0.0000	0.0000	0.0000	0.0000	$\mathrm{m^3 \cdot m^{-3}}$
φ_{CO}	0.0000	0.0000	0.0000	0.0000	$\mathrm{m^3 \cdot m^{-3}}$
φ_{CO_2}	1.0000	0.0000	0.0000	0.0000	$\mathrm{m^3 \cdot m^{-3}}$
φ_{CH_4}	0.0000	0.0000	0.0000	0.0000	$\mathrm{m^3 \cdot m^{-3}}$
$\varphi_{C_2H_4}$	0.0000	0.0000	0.0000	0.0000	$\mathrm{m^3 \cdot m^{-3}}$
$\varphi_{C_2H_6}$	0.0000	0.0000	0.0000	0.0000	$\mathrm{m^3 \cdot m^{-3}}$
$\varphi_{C_3H_8}$	0.0000	0.0000	0.0000	0.0000	$\mathrm{m^3 \cdot m^{-3}}$
φ_{N_2}	0.0000	0.7850	0.7850	0.0000	$\mathrm{m^3 \cdot m^{-3}}$
φ_{O_2}	0.0000	0.2050	0.2050	0.0000	$\mathrm{m^3 \cdot m^{-3}}$
φ_{H_2O}	0.0000	0.0100	0.0100	1.0000	$\mathrm{m^3 \cdot m^{-3}}$

	SNG condensate to steam generator	Excess condensate	Steam to VESTA	AC regeneration steam	
p	10.0	10.0	10.0	1.0	bar
T	50.0	50.0	300.0	200.0	°C
$\dot{m}$	2556.0	81.2	2556.0	59.2	$\mathrm{kg \cdot h^{-1}}$
φ_{H_2}	0.0000	0.0000	0.0000	0.0000	$\mathrm{m^3 \cdot m^{-3}}$
φ_{CO}	0.0000	0.0000	0.0000	0.0000	$\mathrm{m^3 \cdot m^{-3}}$
φ_{CO_2}	0.0004	0.0004	0.0004	0.0000	$\mathrm{m^3 \cdot m^{-3}}$
φ_{CH_4}	0.0000	0.0000	0.0000	0.0000	$\mathrm{m^3 \cdot m^{-3}}$
$\varphi_{C_2H_4}$	0.0000	0.0000	0.0000	0.0000	$\mathrm{m^3 \cdot m^{-3}}$
$\varphi_{C_2H_6}$	0.0000	0.0000	0.0000	0.0000	$\mathrm{m^3 \cdot m^{-3}}$
$\varphi_{C_3H_8}$	0.0000	0.0000	0.0000	0.0000	$\mathrm{m^3 \cdot m^{-3}}$
φ_{N_2}	0.0000	0.0000	0.0000	0.0000	$\mathrm{m^3 \cdot m^{-3}}$
φ_{O_2}	0.0000	0.0000	0.0000	0.0000	$\mathrm{m^3 \cdot m^{-3}}$
φ_{H_2O}	0.9996	0.9996	0.9996	1.0000	$\mathrm{m^3 \cdot m^{-3}}$

A.4 Process D: Hydrogen and methane

	PG from GR	WGS 1 in	WGS 1 out	WGS 2 in	Units
p	1.0	1.0	1.0	1.0	bar
T	850.0	357.0	436.6	300.0	°C
$\dot{m}$	3045.6	4805.4	4805.4	4805.4	$\mathrm{kg} \cdot \mathrm{h}^{-1}$
φ_{H_2}	0.2561	0.1590	0.2382	0.2382	$\mathrm{m}^3 \cdot \mathrm{m}^{-3}$
φ_{CO}	0.1414	0.0877	0.0085	0.0085	$\mathrm{m}^3 \cdot \mathrm{m}^{-3}$
φ_{CO_2}	0.1376	0.0854	0.1647	0.1647	$\mathrm{m}^3 \cdot \mathrm{m}^{-3}$
φ_{CH_4}	0.0578	0.0359	0.0359	0.0359	$\mathrm{m}^3 \cdot \mathrm{m}^{-3}$
$\varphi_{C_2H_4}$	0.0132	0.0082	0.0082	0.0082	$\mathrm{m}^3 \cdot \mathrm{m}^{-3}$
$\varphi_{C_2H_6}$	0.0009	0.0006	0.0006	0.0006	$\mathrm{m}^3 \cdot \mathrm{m}^{-3}$
$\varphi_{C_3H_8}$	0.0031	0.0019	0.0019	0.0019	$\mathrm{m}^3 \cdot \mathrm{m}^{-3}$
φ_{N_2}	0.0031	0.0019	0.0019	0.0019	$\mathrm{m}^3 \cdot \mathrm{m}^{-3}$
φ_{O_2}	0.0000	0.0000	0.0000	0.0000	$\mathrm{m}^3 \cdot \mathrm{m}^{-3}$
φ_{H_2O}	0.3867	0.6193	0.5401	0.5401	$\mathrm{m}^3 \cdot \mathrm{m}^{-3}$

	WGS 2 out	RME scrubber out	PG to CR	Amine scrubber in	Units
p	1.0	1.0	1.0	1.0	bar
T	306.7	50.0	50.0	50.0	°C
$\dot{m}$	4805.4	2598.3	220.9	1844.3	$\mathrm{kg} \cdot \mathrm{h}^{-1}$
φ_{H_2}	0.2446	0.4665	0.4665	0.4665	$\mathrm{m}^3 \cdot \mathrm{m}^{-3}$
φ_{CO}	0.0021	0.0041	0.0041	0.0041	$\mathrm{m}^3 \cdot \mathrm{m}^{-3}$
φ_{CO_2}	0.1710	0.3262	0.3262	0.3262	$\mathrm{m}^3 \cdot \mathrm{m}^{-3}$
φ_{CH_4}	0.0359	0.0685	0.0685	0.0685	$\mathrm{m}^3 \cdot \mathrm{m}^{-3}$
$\varphi_{C_2H_4}$	0.0082	0.0157	0.0157	0.0157	$\mathrm{m}^3 \cdot \mathrm{m}^{-3}$
$\varphi_{C_2H_6}$	0.0006	0.0011	0.0011	0.0011	$\mathrm{m}^3 \cdot \mathrm{m}^{-3}$
$\varphi_{C_3H_8}$	0.0019	0.0037	0.0037	0.0037	$\mathrm{m}^3 \cdot \mathrm{m}^{-3}$
φ_{N_2}	0.0019	0.0036	0.0036	0.0036	$\mathrm{m}^3 \cdot \mathrm{m}^{-3}$
φ_{O_2}	0.0000	0.0000	0.0000	0.0000	$\mathrm{m}^3 \cdot \mathrm{m}^{-3}$
φ_{H_2O}	0.5337	0.1107	0.1107	0.1107	$\mathrm{m}^3 \cdot \mathrm{m}^{-3}$

	Amine scrubber out	BioHNG	Removed CO_2	Dryer condensate	Units
p	1.0	1.0	1.0	1.0	bar
T	50.0	50.0	50.0	50.0	°C
$\dot{m}$	482.1	290.9	1362.7	191.3	$\mathrm{kg \cdot h^{-1}}$
φ_{H_2}	0.6889	0.8236	0.0000	0.0000	$\mathrm{m^3 \cdot m^{-3}}$
φ_{CO}	0.0060	0.0072	0.0000	0.0000	$\mathrm{m^3 \cdot m^{-3}}$
φ_{CO_2}	0.0048	0.0058	1.0000	0.0000	$\mathrm{m^3 \cdot m^{-3}}$
φ_{CH_4}	0.1011	0.1209	0.0000	0.0000	$\mathrm{m^3 \cdot m^{-3}}$
$\varphi_{C_2H_4}$	0.0232	0.0277	0.0000	0.0000	$\mathrm{m^3 \cdot m^{-3}}$
$\varphi_{C_2H_6}$	0.0016	0.0019	0.0000	0.0000	$\mathrm{m^3 \cdot m^{-3}}$
$\varphi_{C_3H_8}$	0.0055	0.0065	0.0000	0.0000	$\mathrm{m^3 \cdot m^{-3}}$
φ_{N_2}	0.0054	0.0064	0.0000	0.0000	$\mathrm{m^3 \cdot m^{-3}}$
φ_{O_2}	0.0000	0.0000	0.0000	0.0000	$\mathrm{m^3 \cdot m^{-3}}$
φ_{H_2O}	0.1635	0.0000	0.0000	1.0000	$\mathrm{m^3 \cdot m^{-3}}$

	RME scrubber condensate	Makeup water	Steam	Ambient air	Units
p	1.0	1.0	1.0	1.0	bar
T	50.0	10.0	101.0	10.0	°C
$\dot{m}$	2207.1	400.0	2607.1	6888.8	$\mathrm{kg \cdot h^{-1}}$
φ_{H_2}	0.0000	0.0000	0.0000	0.0000	$\mathrm{m^3 \cdot m^{-3}}$
φ_{CO}	0.0000	0.0000	0.0000	0.0000	$\mathrm{m^3 \cdot m^{-3}}$
φ_{CO_2}	0.0000	0.0000	0.0000	0.0000	$\mathrm{m^3 \cdot m^{-3}}$
φ_{CH_4}	0.0000	0.0000	0.0000	0.0000	$\mathrm{m^3 \cdot m^{-3}}$
$\varphi_{C_2H_4}$	0.0000	0.0000	0.0000	0.0000	$\mathrm{m^3 \cdot m^{-3}}$
$\varphi_{C_2H_6}$	0.0000	0.0000	0.0000	0.0000	$\mathrm{m^3 \cdot m^{-3}}$
$\varphi_{C_3H_8}$	0.0000	0.0000	0.0000	0.0000	$\mathrm{m^3 \cdot m^{-3}}$
φ_{N_2}	0.0000	0.0000	0.0000	0.7850	$\mathrm{m^3 \cdot m^{-3}}$
φ_{O_2}	0.0000	0.0000	0.0000	0.2050	$\mathrm{m^3 \cdot m^{-3}}$
φ_{H_2O}	1.0000	1.0000	1.0000	0.0100	$\mathrm{m^3 \cdot m^{-3}}$

	Preheated air	Superheated steam to GR	FG from CR	FG from CR out	Units
p	1.0	1.0	1.0	1.0	bar
T	450.0	450.0	930.0	150.0	°C
$\dot{m}$	6888.8	847.3	7836.9	7836.9	$\mathrm{kg \cdot\ h^{-1}}$
φ_{H_2}	0.0000	0.0000	0.0000	0.0000	$\mathrm{m^3 \cdot m^{-3}}$
φ_{CO}	0.0000	0.0000	0.0000	0.0000	$\mathrm{m^3 \cdot m^{-3}}$
φ_{CO_2}	0.0000	0.0000	0.1300	0.1300	$\mathrm{m^3 \cdot m^{-3}}$
φ_{CH_4}	0.0000	0.0000	0.0000	0.0000	$\mathrm{m^3 \cdot m^{-3}}$
$\varphi_{C_2H_4}$	0.0000	0.0000	0.0000	0.0000	$\mathrm{m^3 \cdot m^{-3}}$
$\varphi_{C_2H_6}$	0.0000	0.0000	0.0000	0.0000	$\mathrm{m^3 \cdot m^{-3}}$
$\varphi_{C_3H_8}$	0.0000	0.0000	0.0000	0.0000	$\mathrm{m^3 \cdot m^{-3}}$
φ_{N_2}	0.7850	0.0000	0.736	0.736	$\mathrm{m^3 \cdot m^{-3}}$
φ_{O_2}	0.2050	0.0000	0.069	0.069	$\mathrm{m^3 \cdot m^{-3}}$
φ_{H_2O}	0.0100	1.0000	0.065	0.065	$\mathrm{m^3 \cdot m^{-3}}$
	Boiler FG	Boiler FG out	Cold drying air	Hot drying air	Units
p	1.0	1.0	1.0	1.0	bar
T	1599.0	150.0	10.0	90.0	°C
$\dot{m}$	2477.3	2477.3	38435.0	38435.0	$\mathrm{kg \cdot\ h^{-1}}$
φ_{H_2}	0.0000	0.0000	0.0000	0.0000	$\mathrm{m^3 \cdot m^{-3}}$
φ_{CO}	0.0000	0.0000	0.0000	0.0000	$\mathrm{m^3 \cdot m^{-3}}$
φ_{CO_2}	0.1380	0.1380	0.0000	0.0000	$\mathrm{m^3 \cdot m^{-3}}$
φ_{CH_4}	0.0000	0.0000	0.0000	0.0000	$\mathrm{m^3 \cdot m^{-3}}$
$\varphi_{C_2H_4}$	0.0000	0.0000	0.0000	0.0000	$\mathrm{m^3 \cdot m^{-3}}$
$\varphi_{C_2H_6}$	0.0000	0.0000	0.0000	0.0000	$\mathrm{m^3 \cdot m^{-3}}$
$\varphi_{C_3H_8}$	0.0000	0.0000	0.0000	0.0000	$\mathrm{m^3 \cdot m^{-3}}$
φ_{N_2}	0.6025	0.6025	0.7850	0.7850	$\mathrm{m^3 \cdot m^{-3}}$
φ_{O_2}	0.0143	0.0143	0.2050	0.2050	$\mathrm{m^3 \cdot m^{-3}}$
φ_{H_2O}	0.2452	0.2452	0.0100	0.0100	$\mathrm{m^3 \cdot m^{-3}}$

	Additional steam	PG to boiler	Units
p	1.0	1.0	bar
T	450.0	50.0	°C
$\dot{m}$	1759.8	532.7	$kg \cdot h^{-1}$
φ_{H_2}	0.0000	0.4665	$m^3 \cdot m^{-3}$
φ_{CO}	0.0000	0.0041	$m^3 \cdot m^{-3}$
φ_{CO_2}	0.0000	0.3262	$m^3 \cdot m^{-3}$
φ_{CH_4}	0.0000	0.0685	$m^3 \cdot m^{-3}$
$\varphi_{C_2H_4}$	0.0000	0.0157	$m^3 \cdot m^{-3}$
$\varphi_{C_2H_6}$	0.0000	0.0011	$m^3 \cdot m^{-3}$
$\varphi_{C_3H_8}$	0.0000	0.0037	$m^3 \cdot m^{-3}$
φ_{N_2}	0.0000	0.0036	$m^3 \cdot m^{-3}$
φ_{O_2}	0.0000	0.0000	$m^3 \cdot m^{-3}$
φ_{H_2O}	1.0000	0.1107	$m^3 \cdot m^{-3}$

B Publications

Overview of the peer-reviewed journal papers as well as about conference papers, posters, and presentations the author of this thesis made major contributions to. In addition to the peer-reviewed journal papers at the end of this thesis, the following contributions were published:

Conference papers

- Kraussler M., Binder M., Fail S., Plaza A., Cortes A., Hofbauer H., Validation of a kinetic model for the catalyzed water gas shift reaction applying a Fe/Cr catalyst processing product gas from biomass steam gasification, 23rd European Biomass Conference and Exhibition, 1-4 June 2015, Vienna, Austria, Pages 810-818
- Kraussler M., Binder M., Fail S., Bosch K., Hackel M., Hofbauer H., Performance of a water gas shift unit processing product gas from biomass steam gasification, 23rd European Biomass Conference and Exhibition, 1-4 June 2015, Vienna, Austria, Pages 668-678
- Benedikt F., Kraussler M., Konlechner D., Bosch K., Hackel M., Hofbauer H., Polygeneration at the biomass steam gasification plant Oberwart - Evaluation of process chains to produce hydrogen, electricity and heat, 23rd European Biomass Conference and Exhibition, 1-4 June 2015, Vienna, Austria, Pages 792-799
- Michael Kraussler, Philipp Schindler, Matthias Binder, Hermann Hofbauer, Hydrogen production within a polygeneration concept based on dual fluidized bed biomass steam gasification, 24th European Biomass Conference and Exhibition, 6-9 June 2016, Amsterdam, The Netherlands, Pages 1715-1721
- Michael Kraussler, Florian Benedikt, Juraj Priscak, Hermann Hofbauer, Simulation of a polygeneration process for the generation of hydrogen, HNG, and district heat via sorption enhanced reforming of

wood chips, 25th European Biomass Conference and Exhibition, 12-15 June 2017, Stockholm, Sweden, Pages 732-737

Conference posters

- Kraussler M., Binder M., Fail S., Plaza A., Cortes A., Hofbauer H., Validation of a kinetic model for the catalyzed water gas shift reaction applying a Fe/Cr catalyst processing product gas from biomass steam gasification, 23rd European Biomass Conference and Exhibition, 1-4 June 2015, Vienna, Austria
- Michael Kraussler, Philipp Schindler, Hermann Hofbauer, Hythane from biomass steam gasification as natural gas substitute in industrial applications, 1st International Conference Bioresource Technology for Bioenergy, Bioproducts & Environmental Sustainability, 23-26 October 2016, Sitges, Spain
- Michael Kraussler, Florian Benedikt, Juraj Priscak, Hermann Hofbauer, Simulation of a polygeneration process for the generation of hydrogen, H_2CH_4, and district heat via sorption enhanced reforming of wood chips, 25th European Biomass Conference and Exhibition, 12-15 June 2017, Stockholm, Sweden

Conference presentations

- Michael Kraussler, Performance of a Water Gas Shift Unit Processing Product Gas from Biomass Steam Gasification, 23rd European Biomass Conference and Exhibition, 1-4 June 2015, Vienna, Austria
- Kraussler M., Binder M., Hofbauer H., Performance of a water gas shift pilot plant processing tar-rich product gas from a commercial biomass steam gasification plant operating at partial load conditions, International Bioenergy Exhibition and Asian Bioenergy Conference, 21-23 October 2015, Shanghai, China

- Michael Kraussler, Operation of a PEM fuel cell with H_2 generated from biomass steam gasification, Fuel Cells Science and Technology, 13-14 April 2016, Glasgow, UK

- Michael Kraussler, H_2 production within a Polygeneration concept based on dual fluidized bed biomass steam gasification, 24th European Biomass Conference and Exhibition, 6-9 June 2015, Amsterdam, The Netherlands

- Michael Kraussler, Hydrogen from biomass - Status and perspective, Mitteleuropäische Biomassekonferenz, 18-20 January 2017, Graz, Austria

- Michael Kraussler, Hythane production from biomass steam gasification, Mitteleuropäische Biomassekonferenz, 18-20 January 2017, Graz, Austria

In the following, the peer-reviewed journal papers are presented:

Paper 1

M. Kraussler, M. Binder, S. Fail, K. Bosch, M. Hackel, H. Hofbauer, Performance of a water gas shift pilot plant processing product gas from an industrial scale biomass steam gasification plant, Biomass and Bioenergy, Volume 89, 2016, Pages 50-57, `http://dx.doi.org/10.1016/j.biombioe.2015.12.001`.

Contribution: Experimental work, data treatment, writing

Biomass and Bioenergy 89 (2016) 50–57

Contents lists available at ScienceDirect

Biomass and Bioenergy

journal homepage: http://www.elsevier.com/locate/biombioe

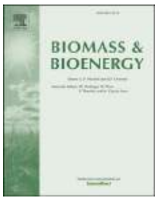

Research paper

Performance of a water gas shift pilot plant processing product gas from an industrial scale biomass steam gasification plant

M. Kraussler [a, *], M. Binder [b], S. Fail [b], K. Bosch [c], M. Hackel [d], H. Hofbauer [a, b]

[a] Bioenergy 2020+ GmbH, Wienerstrasse 49, 7540 Guessing, Austria
[b] Vienna University of Technology, Institute of Chemical Engineering, Getreidemarkt 9, 1060 Vienna, Austria
[c] Energie Burgenland AG, Kasernenstrasse 9, 7000 Eisenstadt, Austria
[d] Air Liquide, Forschung und Entwicklung GmbH, Frankfurt Research and Technology Center (FRTC), Gwinnerstrasse 27-33, 60388 Frankfurt am Main, Germany

ARTICLE INFO

Article history:
Received 4 August 2015
Received in revised form
27 November 2015
Accepted 1 December 2015
Available online 23 December 2015

Keywords:
Biomass
Gasification
Hydrogen
Product gas
Dual fluidized bed
Water gas shift

ABSTRACT

In this paper, the performance of a commercial Fe/Cr based catalyst for the water gas shift reaction was investigated. The catalyst was used in a water gas shift pilot plant which processed real product gas from a commercial biomass steam gasification plant with two different qualities: extracted before and extracted after scrubbing with a rapeseed methyl ester gas scrubber. The performance of the WGS pilot plant regarding these two different gas qualities was investigated. For this reason, extensive chemical analyses were carried out. CO, CO_2, CH_4, N_2, O_2, C_2H_6, C_2H_4, and C_2H_2 and H_2S, COS, and C_4H_4 S were measured. In addition, GCMS tar and NH_3 analyses were performed. Furthermore, the catalyst's activity was observed by measuring the temperature profiles along the reactors of the water gas shift pilot plant. During the 200 h of operation with both product gas qualities, no catalyst deactivation could be observed. A CO conversion up to 93% as well as a GCMS tar reduction (about 28%) along the water gas shift pilot plant was obtained. Furthermore, a specific H_2 production of 63 g H_2 per kg biomass (dry and ash free) was reached with both product gas qualities. No significant performance difference could be observed.

© 2015 Elsevier Ltd. All rights reserved.

1. Introduction

Today, hydrogen is an important resource for a wide range of applications in the chemical industry [1]. Steam reforming of natural gas and other processes with fossil fuels as feedstock produce more than 95% of the hydrogen which is needed in industry. Against a background of climate change, a CO_2 neutral method for hydrogen production should be established [2]. Biomass steam gasification is a proven technology and a CO_2 neutral alternative to steam reforming of natural gas [3].

A promising technology for biomass steam gasification is the dual fluidized bed (DFB) process [4,5]. The commercial biomass steam gasification plants in Guessing and Oberwart have been using this technology for several years. Both plants generate a product gas from woodchips with an high H_2 content ($\varphi_{H_2} \approx 40\,\%$,d.b.). The other main components are CO ($\varphi_{CO} \approx 25\,\%$,d.b.), CO_2 ($\varphi_{CO_2} \approx 20\,\%$,d.b.), and CH_4 ($\varphi_{CH_4} \approx 10\,\%$,d.b.). In addition, it contains small amounts of N_2, O_2, higher hydrocarbons, and H_2S ($\varphi_{H_2S} \approx 100\,cm^3 \cdot m^{-3}$,d.b.) and minor amounts of other sulfur components. The high H_2 content makes this product gas a promising CO_2 neutral H_2 source [6]. A process which can further increase the hydrogen content in the product gas is the water gas shift (WGS) reaction (see Equation (1)).

$$CO + H_2O \rightleftharpoons H_2 + CO_2 \quad \Delta H = -41.1\,\frac{kJ}{mol} \tag{1}$$

It converts carbon monoxide and steam to hydrogen and carbon dioxide. At the industrial scale, a WGS unit consits of a high temerature stage and a low temperature stage. In order to reach economic reaction rates, catalysts are necessary. A suitable catalyst for the high temperature stage is an Fe/Cr based catalyst. The high temperature stage operates adiabatically with a gas inlet temperature of 350–550 °C and space velocities from 400–1200 h^{-1}. The operating pressure depends on the plant requirements [1].

---

* Corresponding author.
E-mail address: michael.kraussler@bioenergy2020.eu (M. Kraussler).

http://dx.doi.org/10.1016/j.biombioe.2015.12.001
0961-9534/© 2015 Elsevier Ltd. All rights reserved.

Fe/Cr based catalysts seem to be robust against sulfur poisoning at the amounts of H_2S which are contained in the product gas of biomass steam gasification [7,8]. Catalysts for the low temperature stage (about 200 °C) are Co/Mo or Cu/Zn based catalysts. The Co/Mo catalyst is resistant to the presence of sulfur components but the amount of H_2S in the product gas of biomass steam gasification is too low for the Co/Mo catalyst (see Ref. [9]) to reach a high activity [8]. In contrast, Cu/Zn catalysts are sensitive to sulfur poisoning [1].

Several studies have been carried out regarding the H_2 production from biomass (see Ref. [10]). In Refs. [11] and [12], a high temperature and low temperature WGS unit was operated after a H_2O—O_2 gasifier and a steam reformer. In Ref. [13], synthetic gas mixtures which simulated the gas composition of pressurized oxygen gasification were used together with a high temperature WGS catalyst in order to achieve high H_2 yields. In Ref. [14], sawdust was gasified with mixtures of O_2, N_2, and H_2O in a fluidized bed gasifier. In Ref. [15], a model biogas was used with a steam reformer and a two-stage WGS reactor for increasing the H_2 yield. In addition, a lot of research in the field of gasification of biomass with supercritical water has been carried out (see Ref. [16]). For example, in Ref. [17], biomass was gasified in a heated batch reactor with supercritical water.

For this work, a WGS pilot plant applying a commercial Fe/Cr based catalyst was operated with product gas from the commercial biomass steam gasification plant in Oberwart, Austria. The WGS pilot plant was operated with product gas extracted before a rapeseed methyl ester (RME) gas scrubber for more than 100 h as well as with product gas extracted after a RME gas scrubber, again, for more than 100 h. Refs. [12] and [18] showed that an operation with product gas extracted after a RME gas scrubber with a low tar content is possible. The performance of the WGS pilot plant which processed the product gas extracted before the RME gas scrubber with a high content of tar is compared with the performance of the WGS pilot plant which processed the product gas extracted after the RME gas scrubber with a low content of tar. The shifted product gas could be the basis for a simple polygeneration process which can generate valuable gases (H_2 and CH_4), electricity, and heat.

2. Materials and methods

The experimental work was carried out at the plant site of the biomass steam gasification plant in Oberwart, Austria, where the WGS pilot plant is located. The pilot plant consisted of three reactors in series which applied an Fe/Cr based catalyst. The gas composition and the steam content were measured before and after each reactor. GCMS tar and NH_3 analyses were performed by the Test Laboratory for Combustion Systems at the Vienna University of Technology. The temperature profile along each reactor was recorded. This allowed judging the activity of the applied Fe/Cr based catalyst.

2.1. The biomass gasification plant

The WGS pilot plant processed product gas from the combined heat and power (CHP) plant in Oberwart. Fig. 1 shows a simplified flowchart of the CHP plant.

The plant is based on the DFB steam gasification technology described in detail in Refs. [4] and [5]. The CHP plant generates district heat and electricity with biomass (woodchips) as feedstock. Table 1 shows the main operating parameters of the CHP plant.

Biomass is fed into the biomass dryer. The dried biomass is transported into the gasifier by a screw conveyor. In the gasifier, the biomass reacts with steam and is in contact with the bed material (olivine) at about 850 °C at ambient pressure. The result is a product gas with a high hydrogen content ($\varphi_{H_2} \approx 40\,\%$, d.b.). Then, the product gas is cooled and cleaned in a bag house filter and in an RME gas scrubber. In the RME gas scrubber, tar, NH_3, and other

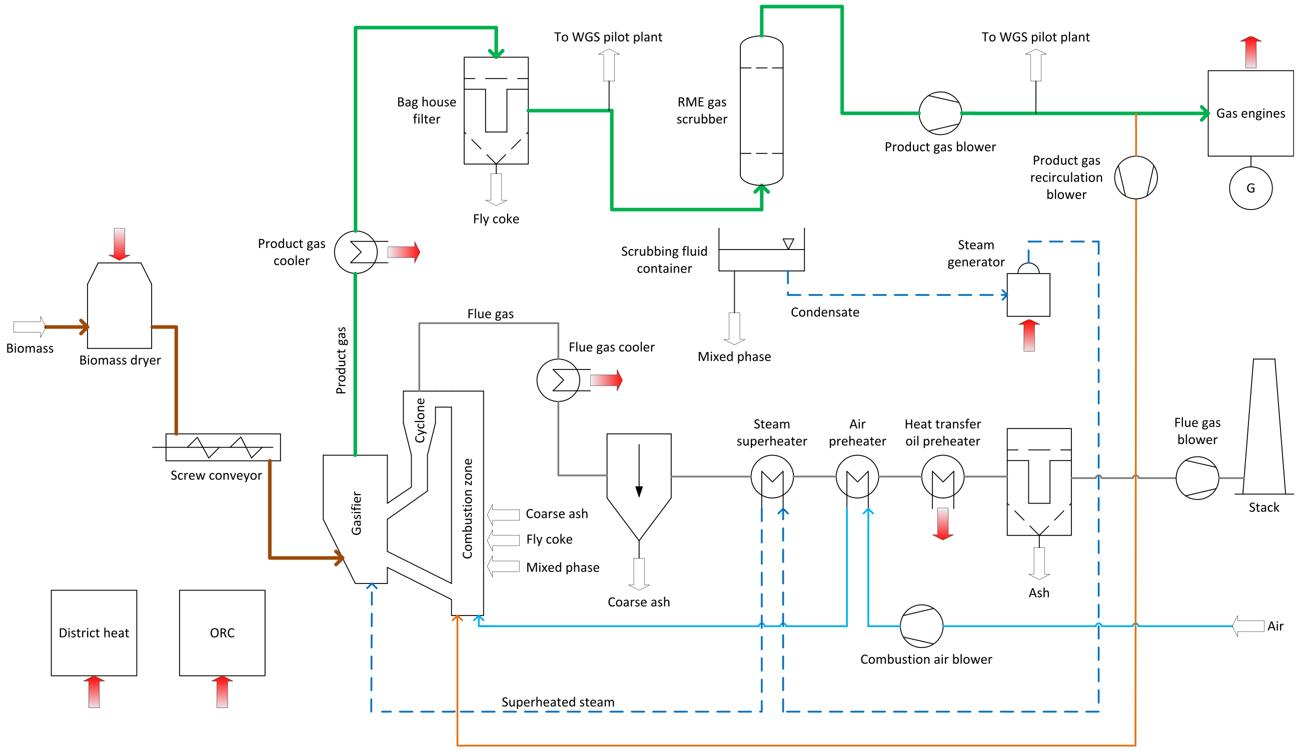
To WGS pilot plant
Bag house filter
RME gas scrubber
To WGS pilot plant
Gas engines
Product gas blower
Product gas recirculation blower
G
Fly coke
Product gas cooler
Scrubbing fluid container
Steam generator
Condensate
Biomass
Biomass dryer
Product gas
Flue gas
Flue gas cooler
Mixed phase
Cyclone
Screw conveyor
Combustion zone
Gasifier
Steam superheater
Air preheater
Heat transfer oil preheater
Flue gas blower
Stack
Coarse ash
Fly coke
Mixed phase
Coarse ash
Ash
District heat
ORC
Air
Combustion air blower
Superheated steam

Fig. 1. Simplified flowchart of the CHP plant in Oberwart, Austria. Heat sources and heat sinks of the process are indicated by arrows. The flowchart also shows the extraction points for experimental work before and after the RME gas scrubber of the CHP plant.

condensable fractions of the product gas are removed before the product gas is fed into the gas engines for electricity generation. Heat from the flue gas line is mainly recovered for the process and for district heating. Fly ash is removed before the flue gas is released into the atmosphere.

For experimental work, it is possible to take a partial flow of the product gas from two different extraction points along the product gas line (see Fig. 1). The first extraction point is before the RME gas scrubber and the second extraction point is after the RME gas scrubber. Table 2 shows the conditions at the two extraction points.

During the investigations, the product gas was taken from each extraction point for about 100 h. The water content, the tar content, and the temperature of the product gas at the extraction point before the RME gas scrubber is significantly higher than at the extraction point after the RME gas scrubber. Therefore, from an energy efficiency point of view, it is useful to take the product gas from the extraction point before the RME gas scrubber as the temperature and the water content is more suitable for a WGS reaction compared to the extraction point after the RME gas scrubber. In contrast, the higher tar content of the product gas extracted before the RME gas scrubber could be a challenge for a reliable operation of the WGS pilot plant. The higher tar content could lead to coking and carbon deposition on the catalyst's surface if the steam content in the processed gas is too low. A detailed description of the process and the CHP plant can be found in Refs. [4,6,8].

2.2. The WGS pilot plant

The experimental work was carried out with a WGS pilot plant located at the plant site of the CHP plant in Oberwart. Fig. 2 shows a simplified flowchart of the WGS pilot plant.

The WGS pilot plant consisted of three fixed bed reactors (A, B, and C) in series filled with a commercial Fe/Cr based catalyst (ShiftMax® 120, [19]). Each catalyst bed had a diameter of about 9 cm and a bed height of about 40 cm, resulting in an Fe/Cr based catalyst volume of about 2.5 dm^3 for each reactor.

Along the reactor height of each reactor, seven type J thermocouples (TA0 to TA6, TB0 to TB6, and TC0 to TC6) were installed in order to record the temperature profile along the reactors. At the inlet and outlet of reactors A and B, the gas stream could be heated or cooled in order to achieve the desired gas inlet temperatures.

Before and after each reactor, a partial flow of the processed gas was sent to the analytic devices where the gas composition measurements, water measurements, tar samplings, and NH_3 samplings were done.

At the inlet of the first reactor, the product gas was mixed with additional steam in order to avoid coking and carbon deposition.

The WGS pilot plant was operated at ambient pressure.

Table 1
Main operating parameters of the CHP plant in Oberwart, Austria [6].

Parameter	Value	Units
Fuel power	8.7	MW
District heat power	4.0	MW
Electrical power	2.8	MW

Table 2
Operating conditions at the extraction points (see Fig. 1) along the CHP plant in Oberwart, Austria, at full load operation of the CHP plant [18].

Parameter	Before RME scrubber	After RME scrubber	Units
Temperature	≈150	≈40	°C
$\varphi_{H_2O(g)}$	≈35	≈7	%
GCMS tar content	≈8200	≈1100	$mg \cdot m^{-3}$

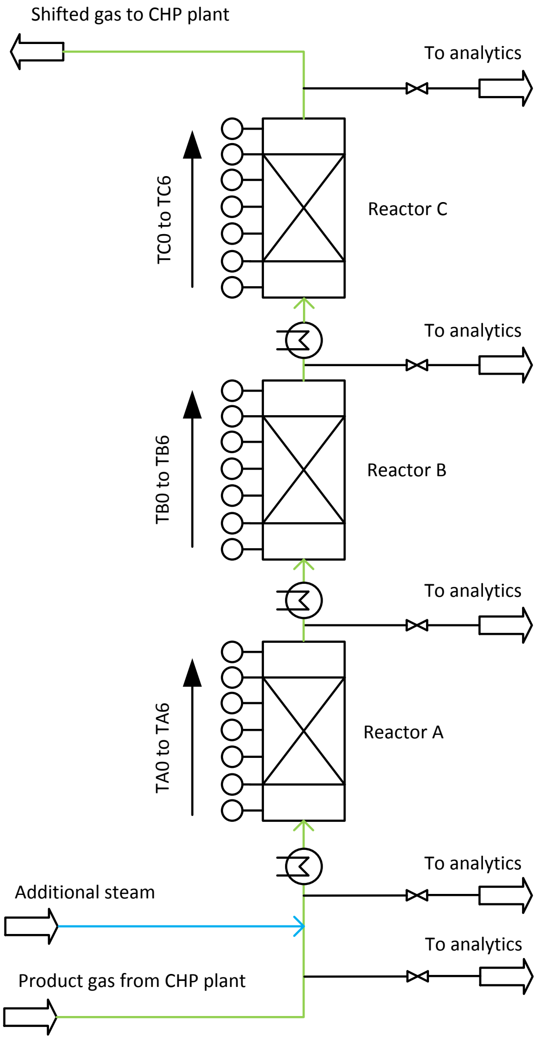

Fig. 2. Simplified flowchart of the WGS pilot plant located at the plant site of the CHP plant in Oberwart.

2.3. Temperature measurement along the WGS reactors

Fig. 2 shows the positions of the thermocouples (type J) along the studied WGS reactors. Thermocouple T0 was positioned before the fixed bed Fe/Cr based catalyst. Therefore, it was not in the reactive zone. T1 to T5 were positioned along the catalyst bed at a distance of 10 cm from each other. T1 was positioned directly at the beginning of the catalyst bed and T5 was positioned directly at the end of the catalyst bed. T6 was outside the catalyst bed. This arrangement was the same in each of the three reactors. A LabVIEW™ program recorded the temperature profiles.

2.4. Measurement of the gas composition

A gas chromatograph (GC, Clarus 500™ from Perkin Elmer) measured the gas composition before and after each WGS reactor. Fig. 3 shows the setup of the gas conditioning for the GC.

The sample gas stream was led through two gas washing bottles filled with glycol at a temperature of about −5 °C in order to condense the steam. Therefore, a dry gas stream could be assumed

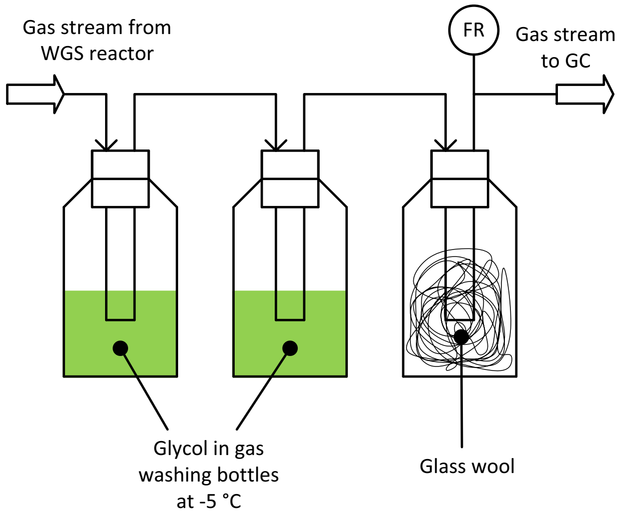

Fig. 3. Sampling line for the gas composition analytics before the GC and the water measurement.

after the two gas washing bottles. The dry gas stream passed another gas washing bottle filled with glass wool in order to prevent aerosols from entering the GC. After the glass wool, a gas meter recorded the volumetric dry gas flow.

In the GC, a thermal conductivity detector (TCD) enabled the quantification of the CO, CO_2, CH_4, N_2, O_2, C_2H_6, C_2H_4, and C_2H_2. The C_2 species were summarized and are referred to as C_2H_y. A flame photometric detector (FPD) was used to detect H_2S, COS, and C_4H_4S.

2.5. Measurement of the steam content and the volumetric flow rates of the gas

Fig. 3 also shows the flowchart and the principle of the gravimetric determination of the steam content. The gas passed through the glycol gas washing bottles at −5 °C for a certain time. Subsequently, the volumetric dry gas flow was recorded with a gas meter.

By weighing the gas washing bottles, the water content before the steam addition, at the inlet, and at the outlet of each WGS reactor was determined. The volumetric flow rates were calculated based on the water balance.

In this work, the volumetric gas flow rates and the gas volumes are always given at standard temperature and pressure (STP, 273.15 K and 101325 Pa).

2.6. Tar sampling method

During the experimental runs, tar measurements at the inlet (reactor A) and outlet (reactor C) of the WGS pilot plant were performed. Additional information about the method is available in Ref. [20]. Fig. 4 shows the principle of the tar sampling.

For the GCMS tar analyses, toluene was used as a solvent because tar has a good solubility in it [20]. Toluene also allows the determination of the tar and water content at the same time.

A sample flow of the product gas passed five gas washing bottles filled with 0.5 dm^3 toluene in all, and one gas washing bottle filled with glass wool in order to prevent aerosols from entering the analytic gas pump.

The first three gas washing bottles were cooled to about 0 °C. Consequently, the tar was dissolved and the steam condensed. The next two gas washing bottles were cooled to −8 °C in order to make sure that all other remaining tar components were finally dissolved in the toluene.

The gas was sampled for about 3 h. In addition, the volumetric dry gas flow was recorded by a gas meter. The dry gas sampling flow rate was set to 2.0 to 2.5 $dm^3 \cdot min^{-1}$.

After the sampling, the content of the five gas washing bottles filled with toluene was mixed. The samples were handed over to the Test Laboratory for Combustion Systems at the Vienna University of Technology. The test laboratory determined the amount of GCMS tar components.

2.7. NH_3 sampling method

The NH_3 sampling was carried out according to the instructions of the Test Laboratory for Combustion Systems at the Vienna University of Technology. Fig. 5 shows the principle.

A sample flow of the processed gas at the inlet and outlet of the WGS pilot plant was led through the NH_3 sampling line. The gas passed through two gas washing bottles, each filled with about 0.1 dm^3 of 0.05 $mol \cdot dm^{-3}$ sulfuric acid. The sampling time was about 15 min. The volumetric dry gas flow was recorded by a gas meter. The volumetric dry gas sampling flow rate was set to about 0.6 $dm^3 \cdot min^{-1}$.

After the sampling, the contents of the two gas washing bottles were mixed and the sample volume was filled up to a certain

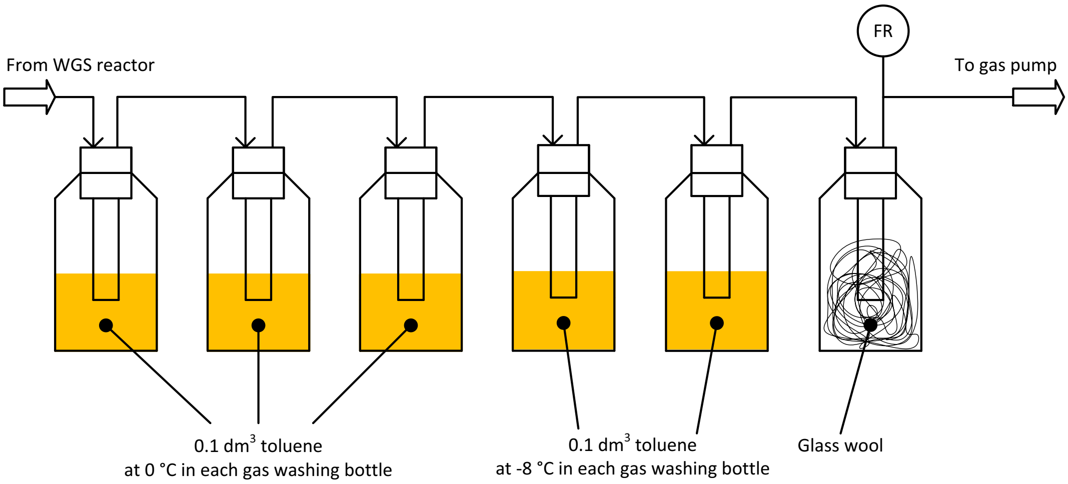
FR
From WGS reactor
To gas pump
0.1 dm³ toluene
at 0 °C in each gas washing bottle
0.1 dm³ toluene
at -8 °C in each gas washing bottle
Glass wool

Fig. 4. Flowchart of the tar sampling.

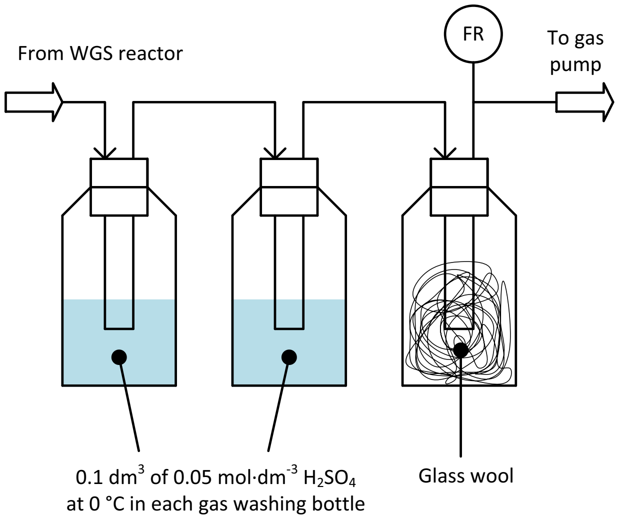
From WGS reactor
FR
To gas pump
0.1 dm³ of 0.05 mol·dm⁻³ H₂SO₄ at 0 °C in each gas washing bottle
Glass wool

Fig. 5. Flowchart of the NH_3 sampling.

volume with sulfuric acid in order to obtain the volumetric NH_3 content of the product gas.

The analyses were carried out using column chromatography by the Test Laboratory for Combustion Systems at the Vienna University of Technology.

2.8. *Characteristic figures describing the performance of the WGS pilot plant*

The WGS pilot plant was described by characteristic figures. The first figure (Equation (2)) was the gas hourly space velocity (GHSV). It was calculated as the ratio of the volumetric dry gas flow rate at the inlet of the reactor to the catalyst volume of the reactor. It indicates the stress of the catalyst.

$$GHSV = \frac{\dot{V}_{Dry}}{V_{Catalyst}} \quad (2)$$

The second figure (Equation (3)) was the steam to dry gas ratio (STDGR). This figure was calculated as the ratio of the volumetric steam flow rate to the volumetric dry gas flow rate in the feed of the WGS pilot plant.

$$STDGR = \frac{\dot{V}_{H_2O}}{\dot{V}_{Dry,In}} \quad (3)$$

The third figure (Equation (4)) was the steam to carbon ratio (STCR). This figure was calculated as the ratio of the volumetric steam flow rate to the volumetric flow rate of all gas components which included at least one carbon atom. The value of the STCR must not be too low, in order to avoid coking and carbon deposition on the surface of the catalyst.

$$STCR = \frac{\dot{V}_{H_2O}}{\dot{V}_{Dry,In} \cdot \left(\varphi_{CO} + \varphi_{CO_2} + \varphi_{CH_4} + \varphi_{C_2H_y}\right)} \quad (4)$$

Another typical figure of the WGS pilot plant was the CO conversion in Equation (5).

$$X_{CO} = \frac{\varphi_{CO,In} \cdot \dot{V}_{Dry,In} - \varphi_{CO,Out} \cdot \dot{V}_{Dry,Out}}{\varphi_{CO,In} \cdot \dot{V}_{Dry,In}} \quad (5)$$

It was calculated with the CO concentrations and the volumetric dry gas flow rate at the inlet and the outlet of the WGS pilot plant and the reactors.

All four figures described the conditions along the WGS pilot plant. In addition, those figures make different WGS units and WGS reactors comparable.

3. Results and discussion

This chapter presents the results of the WGS pilot plant operation with product gas extracted before and extracted after the RME gas scrubber. The results were determined during two successive 100 h runs of the WGS pilot plant with each gas quality. The real and unconditioned product gas from the CHP plant was directly fed into the WGS pilot plant for both test runs.

The Fe/Cr based catalyst was activated in previous experiments. The activation procedure and results of these previous experiments can be found in Refs. [8] and [18].

3.1. *Operation with product gas extracted before the RME gas scrubber*

Table 3 shows the WGS pilot plant operating parameters and the corresponding figures during the operation with product gas extracted before the RME gas scrubber.

The STDGR and STCR were chosen in order to protect the Fe/Cr based catalyst from coking and carbon deposition. During this 100 h of operation, an overall CO conversion of 93% was achieved.

Fig. 6 shows the average temperature profiles along reactors A, B, and C during the 100 h of operation.

It indicates that the WGS reaction mainly took place in reactor A. The temperature increased along reactor A because of the exothermic WGS reaction. After the maximum temperature was reached, the temperature along reactor A decreased. This was the result of two effects. First, a gas composition near the equilibrium composition of the reactive species of the WGS reaction was reached. Therefore, the reaction and, consequently, the temperature increase stopped. Second, heat losses occurred, which finally caused a slight temperature decrease.

The product gas was cooled before it entered reactors B and C. The aim was to achieve about the same reactor inlet temperature at the inlet of all three WGS reactors.

In reactor B, significantly less WGS reaction occurred because the gas composition was near the equilibrium composition, at a temperature of about 350 °C. Consequently, the heat losses exceeded the temperature increase caused by the exothermic reaction. Therefore, the temperature decreased. In reactor C, the same effects as in reactor B occurred.

Table 4 shows the volumetric concentrations of the main gas components at the inlet and outlet of all three reactors during the 100 h of operation with product gas extracted before the RME gas scrubber. The CHP plant in Oberwart provided product gas with a steady composition during the 100 h of operation of the WGS pilot plant (see WGS inlet).

In addition, Table 4 indicates that an volumetric H_2

Table 3
Operating data of the WGS pilot plant with product gas extracted before the RME gas scrubber. The GHSV is given for the first reactor (reactor A). The STDGR and the STCR are given for the inlet of reactor A. X_{CO} is given for reactor A and the whole WGS pilot plant.

GHSV	STDGR	STCR	X_{CO}(reactor A)	X_{CO}(overall)
h^{-1}	-	-	%	%
478	1.6	2.6	84	93

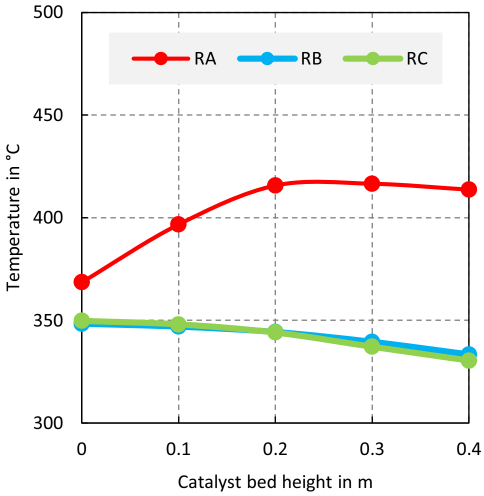

Fig. 6. Average temperature profiles of reactors A, B, and C during the operation with product gas extracted before the RME gas scrubber.

Table 4
Concentrations (d.b.) of the main gas components during the 100 h of operation with product gas extracted before the RME gas scrubber (DL = 2 $cm^3 \cdot m^{-3}$).

	φ_{H_2} %	φ_{CO} %	φ_{CO_2} %	φ_{CH_4} %
WGS inlet	37.9 ± 1.5	24.8 ± 1.1	22.7 ± 0.8	10.5 ± 0.5
Outlet A	48.7 ± 1.0	3.4 ± 0.3	35.7 ± 0.7	8.9 ± 0.4
Outlet B	49.3 ± 0.8	2.1 ± 0.2	36.8 ± 0.5	8.8 ± 0.3
Outlet C	49.7 ± 0.9	1.5 ± 0.1	37.0 ± 0.5	8.6 ± 0.3
	$\varphi_{C_2H_y}$ %	φ_{N_2} %	φ_{O_2} %	
WGS inlet	2.8 ± 0.3	1.3 ± 0.2	0.08 ± 0.03	
Outlet A	2.2 ± 0.2	1.1 ± 0.2	0.03 ± 0.01	
Outlet B	2.1 ± 0.3	1.0 ± 0.2	0.03 ± 0.01	
Outlet C	2.0 ± 0.2	1.0 ± 0.2	0.03 ± 0.01	

concentration of about 50% was reached at the outlet of the WGS pilot plant. Along the WGS pilot plant, the volumetric dry gas flow rate increased by a factor of 1.2. With a product gas output of about 1.18 $m^3 \cdot h^{-1}$ (d.b.) per kg biomass (see Ref. [21]), a specific H_2 production of about 63 g H_2 per kg biomass was obtained on a d.a.f. (dry and ash free) biomass basis.

Table 5 shows the volumetric concentrations of the sulfur components during the 100 h of operation with product gas extracted before the RME gas scrubber. It can be seen that the concentrations of all sulfur components except COS remained nearly constant.

During the 100 h of operation with product gas extracted before the RME gas scrubber, GCMS tar and NH_3 analyses were carried out at the inlet (reactor A) and outlet (reactor C) of the WGS pilot plant. Table 6 shows the results for these samples.

Table 5
Concentrations (d.b.) of the sulfur components during the 100 h of operation with product gas extracted before the RME gas scrubber (DL = 0.3 $cm^3 \cdot m^{-3}$).

	φ_{H_2S} $cm^3 \cdot m^{-3}$	φ_{COS} $cm^3 \cdot m^{-3}$	$\varphi_{C_4H_4S}$ $cm^3 \cdot m^{-3}$
WGS inlet	104 ± 10	3.1 ± 0.5	5.6 ± 1.7
Outlet A	107 ± 8	BDL	5.1 ± 1.4
Outlet B	108 ± 14	BDL	5.4 ± 0.8
Outlet C	110 ± 12	BDL	5.3 ± 1.0

Table 6
GCMS tar and NH_3 concentration (d.b.) at the inlet (reactor A) and outlet (reactor C) of the WGS pilot plant during the 100 h of operation with product gas extracted before the RME gas scrubber. The measurements were single sample measurements. Therefore, no standard deviation could be calculated.

	GCMS tar $mg \cdot m^{-3}$	φ_{NH_3} $cm^3 \cdot m^{-3}$
WGS inlet	8145	3395
WGS outlet	5829	2840

It shows that the GCMS tar content decreased along the WGS pilot plant because the pilot plant offered a reactive environment and, consequently, a certain residence time for tar reduction. The NH_3 content decreased because of the higher volumetric dry gas flow rate after the WGS pilot plant. No NH_3 reaction occurred according to these results.

Table 7 shows the detailed results of the GCMS tar analyses where all detected GCMS tar components are listed.

The amount of naphthalene, the main tar component, mainly decreased because of the dilution effect caused by the fact that the volumetric dry gas flow rate after the WGS pilot plant was higher. Styrene, indene, and phenylacetylene were probably hydrogenated to species which were not detected by this GCMS tar analysis. Acenaphthylene was most probably hydrogenated to acenaphthene. Beside acenaphthene, the amount of anthracene, flouranthene, pyrene, phenanthrene, and 4,5-methylphenanthrene also increased along the WGS pilot plant. Further information regarding tar reduction mechanism can be found in Refs. [22–24].

3.2. Operation with product gas extracted after the RME gas scrubber

The results of the operation with product gas extracted after the RME scrubber are quite similar compared to the results which were achieved during the operation with product gas extracted before

Table 7
Detailed GCMS tar analyses in $mg \cdot m^{-3}$ (d.b.) at the inlet (reactor A) and outlet (reactor C) of the WGS pilot plant during the operation with product gas extracted before the RME gas scrubber. The measurement was a single sample measurements. Therefore, no standard deviation could be calculated (DL = 1 $mg \cdot m^{-3}$).

GCMS tar component	WGS inlet	WGS outlet
Naphthalene	5804	4291
Styrene	272	32
Indene	376	109
Phenylacetylene	47	BDL
Mesitylene	BDL	BDL
Benzofuran	2	BDL
Dibenzofuran	48	36
1-Benzothiophene	7	5
2-Methylnaphthalene	57	38
1-Methylnaphthalene	34	25
Biphenyl	57	44
Acenaphthylene	835	47
Acenaphthene	24	506
Anthracene	375	467
Flouranthene	38	56
Pyrene	29	44
Flourene	71	56
Quinoline	6	4
Phenol	2	BDL
Isoquinoline	1	BDL
Cresol	BDL	BDL
Phenanthrene	49	55
4,5-Methylphenanthrene	11	14
Indole	BDL	BDL
Total GCMS tar	8145	5829

Table 8
Operating data of the WGS pilot plant with product gas extracted after the RME gas scrubber. The GHSV is given for one reactor (reactor A). The STDGR and the STCR are given for reactor A. X_{CO} is given for reactor A and the whole WGS pilot plant.

GHSV	STDGR	STCR	X_{CO}(reactor A)	X_{CO}(overall)
h^{-1}	–	–	%	%
394	1.2	2.0	83	91

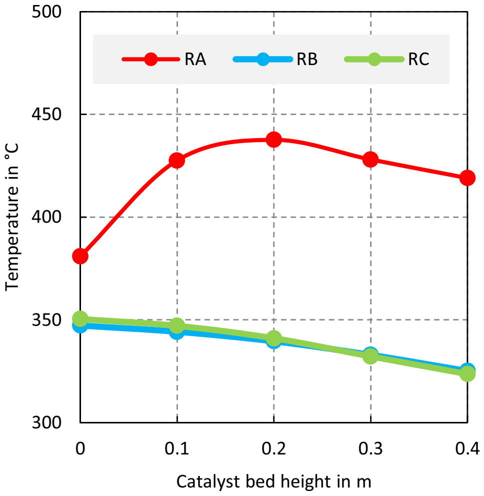

Fig. 7. Average temperature profiles of reactors A, B, and C during the operation with product gas extracted after the RME gas scrubber.

the RME scrubber. Nevertheless, the operating parameters were not exactly the same as during the operation with product gas extracted before the RME scrubber (see Table 3).

The reason for the different operating conditions was the low steam content in the product gas which was extracted after the RME scrubber. Due to this low steam content, the steam addition system of the WGS pilot plant already worked at its maximum load and no higher STDGR and STCR could be achieved (see Table 8).

During these 100 h of operation, an overall CO conversion of 91% was achieved.

Fig. 7 shows the average temperature profiles along reactors A, B, and C during the operation with product gas extracted after the RME gas scrubber.

It shows nearly the same result as already observed during the test with product gas extracted before the RME gas scrubber.

Table 9 shows the volumetric concentrations of the main gas components at the inlet and outlet of all three reactors during the 100 h of operation with product gas extracted after the RME gas scrubber. Again, it can be seen that the CHP plant in Oberwart provided product gas with a steady composition during these 100 h of operation of the WGS pilot plant and that the CO content in the product gas decreased significantly.

In addition, Table 9, again, indicates that an volumetric H_2 concentration of about 50% was reached at the outlet of the WGS pilot plant. Also the same specific H_2 production of about 63 g H_2 per kg biomass was obtained on a d.a.f. biomass basis with product gas extracted after the RME scrubber.

Table 10 shows the volumetric concentrations of the sulfur components during the operation with product gas extracted after the RME gas scrubber.

In contrast to the operation with product gas extracted before the RME gas scrubber, the H_2S content decreased. Before the operation with product gas extracted after the RME gas scrubber, the WGS pilot plant was flushed with steam and nitrogen. As soon as the operation with the product gas started, FeS could have been formed from Fe_3O_4 which could be the reason for the H_2S decrease (compare [8]).

During the 100 h of operation with product gas extracted after the RME gas scrubber, no tar and NH_3 samples were taken. Refs. [8]. and [18] provide the data of the tar and NH_3 samples which were taken during a previous operation of the WGS pilot plant with product gas extracted after the RME gas scrubber.

According to the achieved results with the relatively low GHSV, future work should test the long term stability of the Fe/Cr based catalyst during operation with tar-rich product gas extracted before the RME gas scrubber. Therefore, a long operating time (preferable more than 1000 h) should be chosen in order to compensate for the relatively low GHSV.

4. Conclusion

During both 100 h of operation, one with product gas extracted before and the other with product gas extracted after the RME gas scrubber, no significant differences regarding the performance of the WGS pilot plant could be observed.

In both cases, an overall CO conversion of more than 91% and a specific H_2 production of 63 g H_2 per kg biomass (d.a.f.) was achieved. According to Ref. [14], this equals about 38% of the theoretical maximum of 165 g H_2 per kg biomass (d.a.f.). Consequently, the volumetric CO concentration of the product gas could be lowered to less than 2% (d.b.) at the outlet of the WGS pilot plant which is also in the same range of industrial high temperature WGS units (compare [1]).

In contrast to these results, [11] and [12] achieved a specific H_2 production of 140 g H_2 per kg biomass (d.a.f.) which can be dedicated to the additional steam reformer and the low temperature WGS reactor. In Ref. [14], 62–128 g H_2 per kg biomass (d.a.f.) were achieved in a bench scale fluidized bed gasifier at varying operating conditions and without a WGS unit. In Ref. [13], a volumetric CO concentration of less than 2.5% (d.b.) and a CO conversion of 93% were reached, using synthetic gas mixtures, simulating synthesis

Table 9
Concentrations (d.b.) of the main gas components during the operation with product gas extracted after the RME gas scrubber (DL = 2 $ccm^3 \cdot m^{-3}$).

	φ_{H_2}	φ_{CO}	φ_{CO_2}	φ_{CH_4}
	%	%	%	%
WGS inlet	38.2 ± 0.8	23.3 ± 0.9	22.7 ± 0.7	10.0 ± 0.4
Outlet A	48.5 ± 0.9	3.4 ± 0.3	35.1 ± 0.4	8.6 ± 0.3
Outlet B	48.9 ± 0.9	2.2 ± 0.1	36.0 ± 0.3	8.5 ± 0.3
Outlet C	49.2 ± 0.9	1.8 ± 0.1	36.3 ± 0.3	8.4 ± 0.3

	$\varphi_{C_2H_y}$	φ_{N_2}	φ_{O_2}
	%	%	%
WGS inlet	2.8 ± 0.3	2.7 ± 0.3	0.30 ± 0.04
Outlet A	2.2 ± 0.3	2.2 ± 0.2	0.03 ± 0.01
Outlet B	2.2 ± 0.2	2.1 ± 0.2	0.03 ± 0.01
Outlet C	2.2 ± 0.2	2.1 ± 0.2	0.03 ± 0.01

Table 10
Concentrations (d.b.) of the sulfur components during the 100 h of operation with product gas extracted after the RME gas scrubber (DL = 0.3 $cm^3 \cdot m^{-3}$).

	φ_{H_2S}	φ_{COS}	$\varphi_{C_4H_4S}$
	$cm^3 \cdot m^{-3}$	$cm^3 \cdot m^{-3}$	$cm^3 \cdot m^{-3}$
WGS inlet	91 ± 13	3.8 ± 0.9	5.6 ± 1.6
Outlet A	79 ± 12	BDL	5.1 ± 1.0
Outlet B	59 ± 13	BDL	5.6 ± 0.9
Outlet C	44 ± 9	BDL	5.7 ± 1.0

gas from pressurized oxygen gasification, and a high temperature WGS unit. In Ref. [15], with model biogas, a steam reformer, and a two-stage WGS reactor, a volumetric H_2 concentration of 68% and CO conversion of 99% were achieved. In Ref. [17], a H_2 conversion of 38% was reached with supercritical water gasification of biomass.

During the 100 h of operation with product gas extracted before the RME gas scrubber, the WGS pilot plant operated flawlessly. With the presented experimental layout and the operating conditions of the WGS pilot plant which were significantly influenced by the CHP plant operating conditions, the Fe/Cr based catalyst (ShiftMax® 120) showed no performance decrease caused by the higher tar and NH_3 content in the product gas extracted before the RME gas scrubber. This is an important as well as encouraging result for future applications.

The two different product gas qualities (extracted before and after the RME gas scrubber) showed no difference regarding the performance of the WGS pilot plant.

Acknowledgments

The authors want to thank Energie Burgenland AG and Air Liquide for making this work possible. Especially the plant operators of the CHP plant in Oberwart are gratefully acknowledged.

The authors also thank Binder Industrieanlagenbau for constructing the WGS pilot plant as well as the company Clariant for providing the Fe/Cr based catalyst (ShiftMax® 120).

This work was carried out in the frame of the Bioenergy2020+ GmbH project “C-II-1-16 Polygeneration II”. Bioenergy2020+ GmbH is funded by the states Burgenland, Niederoesterreich, Steiermark, and within the Austrian COMET program which is managed by the Austria Research Promoting Agency (FFG).

Abbreviations and acronyms

BDL	Below detection limit
CHP	Combined heat and power
d.a.f.	Dry and ash free
d.b.	Dry basis
DFB	Dual fluidized bed
DL	Detection limit
FPD	Flame photometric detector
FR	Flow record
g	Gaseous state
GC	Gas chromatograph
GCMS	Gas chromatography mass spectroscopy
ORC	Organic Rankine cycle
RME	Rapeseed methyl ester
STP	Standard temperature and pressure (273.15 K and 101325 Pa)
TCD	Thermal conductivity detector
WGS	Water gas shift

Symbols

φ_i	Volumetric fraction of component i in -
GHSV	Gas hourly space velocity in h^{-1}
ΔH	Enthalpy of formation (at 298.15 K and 101325 Pa) in $kJ \cdot mol^{-1}$
STDGR	Steam to dry gas ratio in -
STCR	Steam to carbon ratio in -
$V_{Catalyst}$	Catalyst volume in m^3
$\dot{V}_{Dry}$	Volumetric dry gas flow rate at STP in $m^3 \cdot h^{-1}$
$\dot{V}_{H_2O}$	Volumetric steam flow rate at STP in $m^3 \cdot h^{-1}$
X_{CO}	CO conversion in -

References

[1] K. Liu, C. Song, V. Subramani, Hydrogen and Syngas Production and Purification Technologies, first ed., Wiley VCH, 2010 http://dx.doi.org/10.1002/9780470561256.fmatter.

[2] H. Balat, E. Kirtay, Hydrogen from biomass – Present scenario and future prospects, Int. J. Hydrogen Energy 35 (14) (2010) 7416–7426, http://dx.doi.org/10.1016/j.ijhydene.2010.04.137.

[3] S. Mueller, Hydrogen from Biomass for Industry - Industrial Application of Hydrogen Production Based on Dual Fluid Gasification, Ph.D. thesis, Vienna University of Technology, 2013.

[4] T. Proell, R. Rauch, C. Aichernig, H. Hofbauer, Fluidized Bed Steam Gasification of Solid Biomass - Performance Characteristics of an 8 MWth Combined Heat and Power Plant, Int. J. Chem. React. Eng. 5 (1) (2007) 1542–6580, http://dx.doi.org/10.2202/1542-6580.1398.

[5] M. Kaltschmitt, H. Hartmann, H. Hofbauer, Energie aus Biomasse, second ed., Springer-Verlag Berlin Heidelberg, 2009 http://dx.doi.org/10.1007/978-3-8348-9327-7_9.

[6] N. Diaz, Hydrogen Separation from Producer Gas Generated by Biomass Steam Gasification, Ph.D. thesis, Vienna University of Technology, 2013.

[7] M.V. Twigg, Catalyst Handbook, second ed., Oxford University Press, 1997.

[8] S. Fail, Biohydrogen Production Based on the Catalyzed Water Gas Shift Reaction in Wood Gas, Ph.D. thesis, Vienna University of Technology, 2014.

[9] Sour Gas Shift, 20th of November 2015. URL: http://www.catalysts.clariant.com/bu/catalysis/internet.nsf/023cfbb98594ad5bc12564e400555162/0998cec035acb257c1257ad0002d259b?OpenDocument.

[10] M. Ni, D.Y. Leung, M.K. Leung, K. Sumathy, An overview of hydrogen production from biomass, Fuel Process Technol. 87 (5) (2006) 461–472, http://dx.doi.org/10.1016/j.fuproc.2005.11.003.

[11] M.P. Aznar, M.A. Caballero, J. Corella, G. Molina, J.M. Toledo, Hydrogen Production by Biomass Gasification with Steam-O_2 Mixtures Followed by a Catalytic Steam Reformer and a CO-Shift System, Energ Fuels 20 (3) (2006) 1305–1309, http://dx.doi.org/10.1021/ef050428p.

[12] J. Corella, M.P. Aznar, M.A. Caballero, G. Molina, J.M. Toledo, 140 g H_2 /kg biomass d.a.f. by a CO-shift reactor downstream from a FB biomass gasifier and a catalytic steam reformer, Int. J. Hydrogen Energy 33 (7) (2008) 1820–1826, http://dx.doi.org/10.1016/j.ijhydene.2008.02.003.

[13] M. Maroo, J. Snchez, E. Ruiz, Hydrogen-rich gas production from oxygen pressurized gasification of biomass using a Fe-Cr Water Gas Shift catalyst, Int. J. Hydrogen Energy 35 (1) (2010) 37–45, http://dx.doi.org/10.1016/j.ijhydene.2009.10.078.

[14] S. Turn, C. Kinoshita, Z. Zhang, D. Ishimura, J. Zhou, An experimental investigation of hydrogen production from biomass gasification, Int. J. Hydrogen Energy 23 (8) (1998) 641–648, http://dx.doi.org/10.1016/S0360-3199(97)00118-3.

[15] A. Effendi, K. Hellgardt, Z.G. Zhang, T. Yoshida, Optimising H_2 production from model biogas via combined steam reforming and co shift reactions, Fuel 84 (7–8) (2005) 869–874, http://dx.doi.org/10.1016/j.fuel.2004.12.011.

[16] Y. Guo, S. Wang, D. Xu, Y. Gong, H. Ma, X. Tang, Review of catalytic supercritical water gasification for hydrogen production from biomass, Renew. Sust. Energ Rev. 14 (1) (2010) 334–343, http://dx.doi.org/10.1016/j.rser.2009.08.012.

[17] P.T. Williams, J. Onwudili, Subcritical and Supercritical Water Gasification of Cellulose, Starch, Glucose, and Biomass waste, Energ Fuels 20 (3) (2006) 1259–1265, http://dx.doi.org/10.1021/ef0503055.

[18] S. Fail, N. Diaz, F. Bendikt, M. Kraussler, J. Hinteregger, K. Bosch, et al., Wood gas processing to generate pure hydrogen suitable for PEM fuel cells, ACS Sustain Chem. Eng. 2 (12) (2014) 2690–2698, http://dx.doi.org/10.1021/sc500436m.

[19] Water Gas Shift Reactions, 20th of November 2015. URL: http://www.catalysts.clariant.com/bu/Catalysis/internet.nsf/023cfbb98594ad5bc12564e400555162/ada6e191f2e1f9e8c1257ad0002d2c03?OpenDocument.

[20] U. Wolfesberger, I. Aigner, H. Hofbauer, Tar content and composition in producer gas of fluidized bed gasification of wood - Influence of temperature and pressure, Environ. Prog. Sustain Energ 28 (3) (2009) 372–379, http://dx.doi.org/10.1002/ep.10387.

[21] F. Kirnbauer, V. Wilk, H. Hofbauer, Performance improvement of dual fluidized bed gasifiers by temperature reduction: The behavior of tar species in the product gas, Fuel 108 (2013) 534–542, http://dx.doi.org/10.1016/j.fuel.2012.11.065.

[22] M.A. Uddin, H. Tsuda, S. Wu, E. Sasaoka, Catalytic decomposition of biomass tars with iron oxide catalysts, Fuel 87 (4–5) (2008) 451–459, http://dx.doi.org/10.1016/j.fuel.2007.06.021.

[23] Y. Shen, K. Yoshikawa, Recent progresses in catalytic tar elimination during biomass gasification or pyrolysis - A review, Renew. Sust. Energ Rev. 21 (2013) 371–392, http://dx.doi.org/10.1016/j.rser.2012.12.062.

[24] L. Devi, K.J. Ptasinski, F.J.J.G. Janssen, Decomposition of Naphthalene as a Biomass Tar over Pretreated Olivine: Effect of Gas Composition, Kinetic Approach, and Reaction Scheme, Ind. Eng. Chem. Res. 44 (24) (2005) 9096–9104, http://dx.doi.org/10.1021/ie050801g.

Paper 2

Michael Kraussler, Matthias Binder, Hermann Hofbauer, 2250-h long term operation of a water gas shift pilot plant processing tar-rich product gas from an industrial scale dual fluidized bed biomass steam gasification plant, International Journal of Hydrogen Energy, Volume 41, Issue 15, 2016, Pages 6247-6258, `http://dx.doi.org/10.1016/j.ijhydene.2016.02.137`.

Contribution: Experimental work, data treatment, writing

INTERNATIONAL JOURNAL OF HYDROGEN ENERGY 41 (2016) 6247–6258

Available online at www.sciencedirect.com

ScienceDirect

journal homepage: www.elsevier.com/locate/he

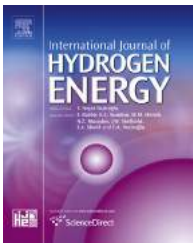

2250-h long term operation of a water gas shift pilot plant processing tar-rich product gas from an industrial scale dual fluidized bed biomass steam gasification plant

Michael Kraussler [a,*], Matthias Binder [b], Hermann Hofbauer [a,b]

[a] Bioenergy 2020+ GmbH, Wienerstrasse 49, 7540 Guessing, Austria
[b] TU Wien, Institute of Chemical Engineering, Getreidemarkt 9, 1060 Vienna, Austria

ARTICLE INFO

Article history:
Received 23 September 2015
Received in revised form
23 February 2016
Accepted 29 February 2016
Available online 23 March 2016

Keywords:
Biomass
Dual fluidized bed
Steam gasification
Water gas shift
Hydrogen

ABSTRACT

In this paper, the performance of a water gas shift (WGS) pilot plant which processed tar-rich product gas for about 2250 h is investigated. The WGS pilot plant employed a commercial Fe/Cr based catalyst (ShiftMax® 120). The product gas was generated by the industrial scale and commercial dual fluidized bed (DFB) biomass steam gasification plant in Oberwart, Austria. A partial flow of tar-rich product gas was extracted for the WGS pilot plant before the tar scrubber of the gasification plant. The extracted product gas had a temperature of about 150 °C and a GCMS tar content between 2.7 and 8.2 g m^{-3} (d.b.). In order to investigate the stability of the catalyst and to observe the performance of the WGS pilot plant, extensive chemical analyses were carried out: CO, CO_2, CH_4, N_2, O_2, C_2H_6, C_2H_4, C_2H_2, H_2S, COS, and C_4H_4S were measured. In addition, GCMS tar and NH_3 analyses were performed. Furthermore, the catalyst's activity was observed by measuring the temperature profiles along the reactors of the three stage WGS pilot plant. During the about 2250 h of operation, no significant catalyst deactivation could be observed. A CO conversion of up to 92% as well as a GCMS tar reduction along the WGS pilot plant was obtained. The results showed that the application of a commercial Fe/Cr based catalyst in a WGS unit seems to be a suitable way for increasing the hydrogen content in a product gas generated by dual fluidized bed biomass steam gasification. Furthermore, with such a technique, it is possible to optimally adjust the required CO/H_2 ratio for several synthesis reactions, for example, methanation and Fischer-Tropsch synthesis.

Copyright © 2016, Hydrogen Energy Publications, LLC. Published by Elsevier Ltd. All rights reserved.

Introduction

Biomass is one of the most promising renewable resources. Besides its use as solid fuel for heating and combustion applications, it can be converted to gaseous and liquid fuels via gasification. Therefore, biomass is seen as a promising resource for the renewable production of different energy carriers and chemical products. One of these products, which is mostly needed by the chemical industry, is hydrogen [1–3].

A promising technology for biomass gasification is steam gasification, especially, the dual fluidized bed (DFB) process [4,5].

---

* Corresponding author.
E-mail address: michael.kraussler@bioenergy2020.eu (M. Kraussler).

http://dx.doi.org/10.1016/j.ijhydene.2016.02.137
0360-3199/Copyright © 2016, Hydrogen Energy Publications, LLC. Published by Elsevier Ltd. All rights reserved.

The commercial biomass steam gasification plants in Guessing and Oberwart have been using this technology for several years. Both plants generate a product gas from wood chips with an volumetric H_2 content of about 40%. The volumetric concentrations of the other main gas components are about 25% CO, 20% CO_2, and 10% CH_4 (all d.b.). In addition, the product gas contains small amounts of N_2, O_2, higher hydrocarbons, and a volumetric concentration of about 100 $cm^3\,m^{-3}$ H_2S and minor amounts of other sulfur components. The typical volumetric H_2O content of the product gas is between 30 and 40%.

The high volumetric H_2 content makes this product gas a promising CO_2 neutral H_2 source. A process which can further increase the hydrogen content in the product gas is the water gas shift (WGS) reaction (see Equation (1)).

$$CO + H_2O \rightleftharpoons H_2 + CO_2 \quad \Delta H = -41.1\ \mathrm{kJ \cdot mol^{-1}} \tag{1}$$

It converts carbon monoxide and steam to hydrogen and carbon dioxide. At the industrial scale, a WGS unit usually consists of a high temperature stage and a low temperature stage. In order to reach economic reaction rates, catalysts are necessary. A suitable catalyst for the high temperature stage is an Fe/Cr based catalyst. The high temperature stage operates adiabatically with a gas inlet temperature of 350–550 °C and space velocities from 400 to 1200 h^{-1}. The operating pressure depends on the plant requirements [6]. Fe/Cr based catalysts seem to be robust against sulfur poisoning at the amounts of H_2S which are observed in the product gas of biomass steam gasification [7,8]. Catalysts for the low temperature stage (about 200 °C) are Co/Mo or Cu/Zn based catalysts. The Co/Mo catalyst is resistant to the presence of sulfur components but the amount of H_2S in the product gas of biomass steam gasification is too low for the Co/Mo catalyst to reach a high level of activity. In contrast, Cu/Zn catalysts are sensitive to sulfur poisoning [6].

For this research, a WGS pilot plant employing a commercial Fe/Cr based catalyst was operated with tar-rich product gas from the industrial scale and commercial biomass steam gasification plant in Oberwart, Austria. The WGS pilot plant was continuously operated for about 2250 h. Some authors ([8–10]) showed that an operation with product gas with a low tar content is possible. In addition, Kraussler et al. ([11]) showed that a short term operation with tar-rich product gas for about 100 h is possible. This paper investigates the long term performance of the WGS pilot plant which processed tar-rich product gas extracted before a rapeseed methyl ester (RME) gas scrubber.

Materials and methods

The experimental work was carried out at the site of the biomass steam gasification plant in Oberwart, Austria, where the WGS pilot plant is located. The pilot plant consists of three reactors in series which employ an Fe/Cr based catalyst. The gas compositions and the steam contents were measured before and after each reactor. GCMS tar and NH_3 analyses were performed by the Test Laboratory for Combustion Systems at the TU Wien. The temperature profile along each reactor was recorded. This allowed judging the activity of the Fe/Cr based catalyst.

The biomass steam gasification plant in Oberwart

The WGS pilot plant processed product gas from the combined heat and power (CHP) plant in Oberwart. Fig. 1 shows a simplified flowchart of the process employed.

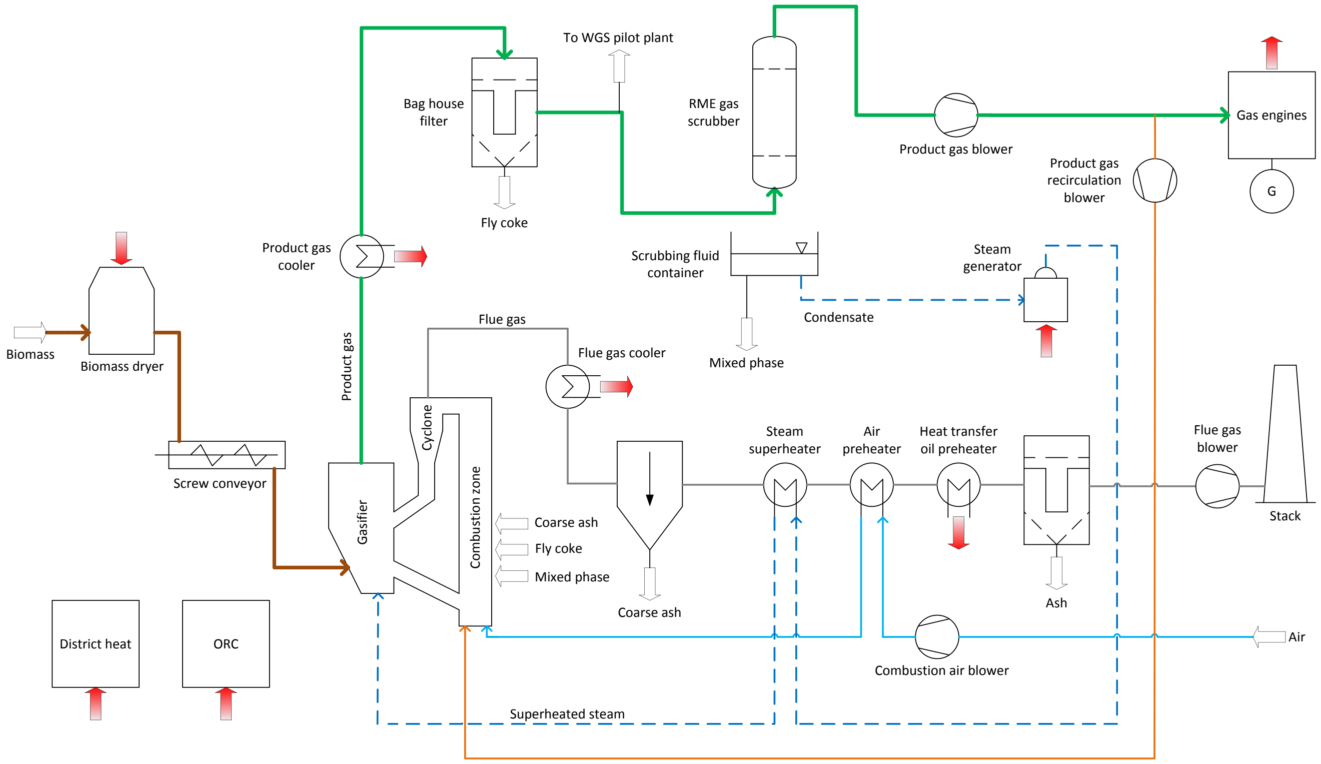
To WGS pilot plant
Bag house filter
RME gas scrubber
Gas engines
Product gas blower
Product gas recirculation blower
G
Fly coke
Product gas cooler
Scrubbing fluid container
Steam generator
Condensate
Biomass
Biomass dryer
Flue gas
Flue gas cooler
Mixed phase
Product gas
Cyclone
Screw conveyor
Steam superheater
Air preheater
Heat transfer oil preheater
Flue gas blower
Stack
Gasifier
Combustion zone
Coarse ash
Fly coke
Mixed phase
Coarse ash
Ash
Air
Combustion air blower
District heat
ORC
Superheated steam

Fig. 1 – Simplified flowchart of the CHP plant in Oberwart, Austria, showing the extraction point of the product gas for the operation of the WGS pilot plant.

The plant is based on the dual fluidized bed (DFB) steam gasification technology described in detail in [4,5]. The CHP plant generates district heat and electricity with biomass (woodchips) as feedstock. Table 1 shows the main operating parameters of the CHP plant.

Biomass is fed into the biomass dryer. Afterwards, a screw conveyor transports the biomass into the gasifier. In the gasifier, the biomass is in contact with steam (steam to fuel ratio, d.a.f., of about 0.5) and the bed material (olivine) at about 850 °C. The resulting product gas has a high volumetric hydrogen content (about 40%, d.b.), a lower heating value of about 14 MJ m^{-3} [12], and a dust content of about 50 g m^{-3}. In the following process steps, the product gas is cooled and passes through a bag house filter. The bag house filter shows a particle separation efficiency of more than 99%. Therefore, a dust free product gas can be assumed after the filter [13]. Furthermore, in the following RME gas scrubber, tar, NH_3, and other condensible fractions of the product gas are removed before the product gas is fed into the gas engines for electricity generation. Heat from the flue gas line is mainly recovered for the process and for district heating. Fly ash is removed before the flue gas is released into the atmosphere.

It is possible to extract a partial flow of the product gas for experimental work from the extraction point located before the RME gas scrubber (see Fig. 1). Table 2 shows the conditions at this extraction point.

The tar content of the gas before the RME gas scrubber is much higher than after the RME gas scrubber, which is a challenge for the reliable operation of the WGS pilot plant. A detailed description of the process and the CHP plant can be found in [4,8,12,14].

The water gas shift pilot plant

The experimental work was carried out at a WGS pilot plant located at the site of the CHP plant in Oberwart. Fig. 2 shows a simplified flowchart of the WGS pilot plant.

The WGS pilot plant consists of three fixed bed reactors (A, B, and C) in series filled with a commercial Fe/Cr based catalyst (ShiftMax® 120). Each catalyst bed had a diameter of about 9 cm and a bed height of about 40 cm resulting in an Fe/Cr based catalyst volume of about 2.5 dm^3 for each reactor. The catalyst was used in its original size. Discs with a diameter of about 6 mm and a height of about 3 mm. The bulk density was 1.24 kg dm^{-3}.

Along the reactor height of each reactor, seven type J thermocouples (TA0 to TA6, TB0 to TB6, and TC0 to TC6) were installed in order to record the temperature profile along the reactors. At the inlet and outlet of the reactors A and B, the gas stream could be heated or cooled in order to achieve the desired gas inlet temperature.

Before and after each reactor, a partial flow of the processed gas was sent to the analytical line where the gas composition measurements, water measurements, GCMS tar samplings, and NH_3 samplings were done.

At the inlet of the first reactor, the product gas was mixed with steam to assure a high steam content in the processed gas along the WGS pilot plant. Due to the lack of experience with the tar-rich product gas, the maximum load for the steam addition was chosen aiming the protection of the Fe/Cr based catalyst from coking and carbon deposition.

The WGS pilot plant was operated at ambient pressure.

Table 1 – Main operating parameters of the CHP plant in Oberwart, Austria [8].

Parameter	Value	Units
Fuel power	8.7	MW
District heat power	4.0	MW
Electrical power	2.8	MW

Table 2 – Operating conditions at the extraction point (see Fig. 1) at the CHP plant in Oberwart, Austria, at full load operation of the CHP plant.

Parameter	Value	Units
Temperature	≈150	°C
Volumetric H_2O content	30–40	%
GCMS tar content	2.7–8.2	g m^{-3}

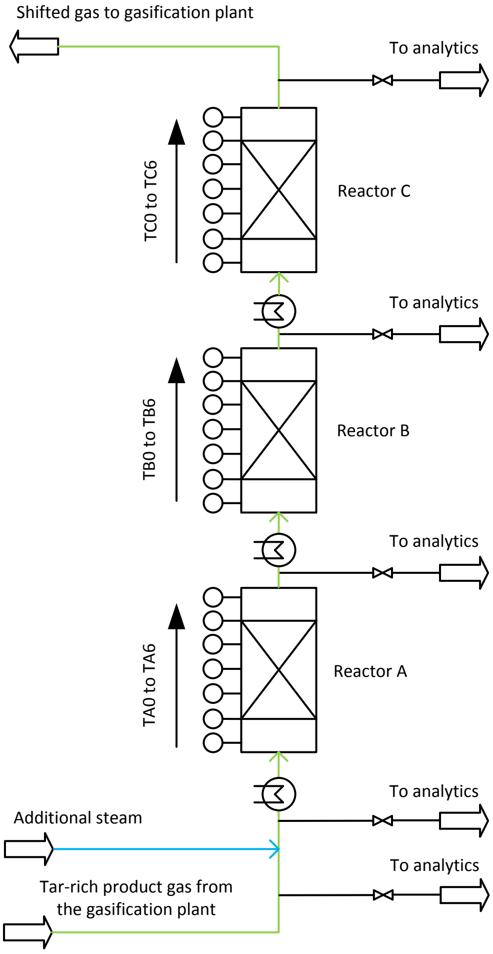

Fig. 2 – Simplified flowchart of the WGS pilot plant located at the site of the CHP plant in Oberwart.

Temperature measurement along the water gas shift reactors

Fig. 2 also shows the positions of the thermocouples (type J) along the studied WGS reactors. Thermocouple T0 was positioned before the catalyst bed. Therefore, it was not in the reactive zone. T1 to T5 were positioned along the catalyst bed at a distance of 10 cm from each other. T1 was positioned directly at the beginning of the catalyst bed and T5 was positioned directly at the end of the catalyst bed. T6 was outside the catalyst bed. This arrangement was the same in each of the three reactors. A LabVIEW™ program recorded the temperature profiles during the about 2250 h of operation.

Measurement of the volumetric gas composition

A gas chromatograph (GC, Clarus 500™ from Perkin Elmer) measured the volumetric gas composition before and after each WGS reactor. Fig. 3 shows the setup of the gas conditioning for the gas chromatograph.

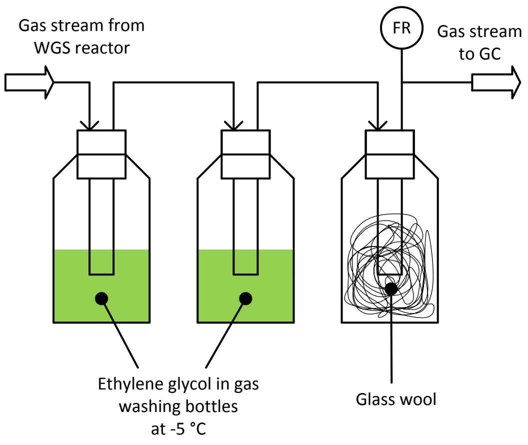

Fig. 3 – Sampling line for the gas composition analytics before the gas chromatograph (GC).

The sample gas stream was led through two gas washing bottles filled with ethylene glycol at a temperature of about −5 °C in order to condense the steam. Therefore, a dry gas stream could be assumed after having passed through the two gas washing bottles. The dry gas stream passed through another gas washing bottle filled with glass wool in order to prevent aerosols from entering the GC. After passing through the glass wool, a gas meter (FR) recorded the volumetric dry gas flow.

In the GC, a thermal conductivity detector (TCD) enabled the quantification of the CO, CO_2, CH_4, N_2, O_2, C_2H_6, C_2H_4, and C_2H_2. The C_2 species were summarized and are referred to as C_2H_y. The H_2 content was determined via calculation. A flame photometric detector (FPD) was used to detect the H_2S, COS, and C_4H_4S.

Measurement of the volumetric steam content in the gas

Fig. 3 also shows the flowchart for the gravimetric steam content determination. The gas passed through the ethylene glycol gas washing bottles at −5 °C for a certain time where the steam was condensed. Subsequently, the volumetric dry gas flow was recorded with a gas meter (FR). By weighing the gas washing bottles and calculations, the volumetric steam content before the steam addition, at the inlet, and at the outlet of each reactor was determined.

Tar sampling method for the determination of the GCMS tar concentration

During the experimental runs, GCMS tar measurements at the inlet and outlet of the WGS pilot plant were performed. Additional information about the method is available in [15]. Fig. 4 shows the principle of the tar sampling.

A sample flow of the product gas passed through five gas washing bottles filled with 0.5 dm^3 toluene in all, and one gas washing bottle filled with glass wool in order to prevent aerosols from entering the analytical gas pump. Tar has a good solubility in toluene [15]. However, toluene as a solvent did not allow the determination of the concentration of

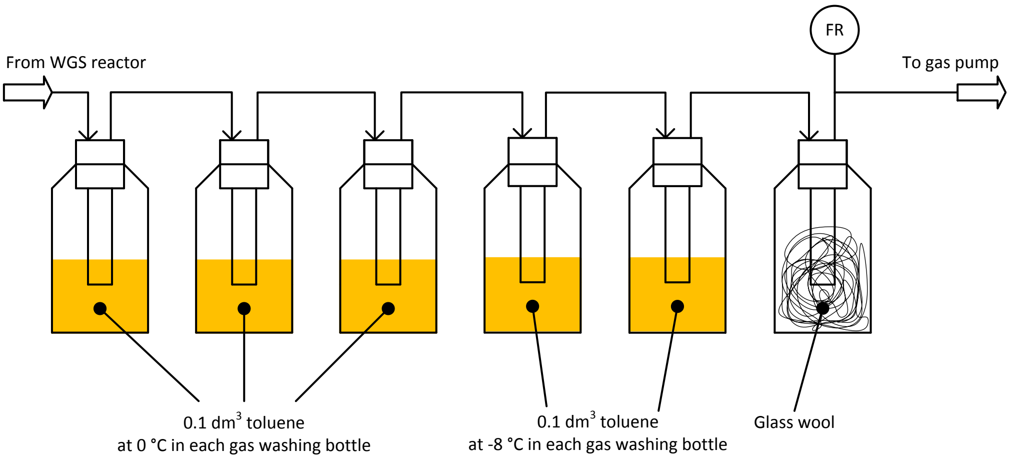
FR
From WGS reactor
To gas pump
0.1 dm³ toluene
at 0 °C in each gas washing bottle
0.1 dm³ toluene
at -8 °C in each gas washing bottle
Glass wool

Fig. 4 – Flowchart of the tar sampling line.

benzene, toluene, ethylbenzene, and xylenes (BTEX). The first three gas washing bottles were cooled to about 0 °C. Consequently, the tar was dissolved and the steam condensed. The next two gas washing bottles were cooled to −8 °C in order to make sure that all other remaining tar components were finally dissolved in the toluene. The gas passed the sampling line for about 3 h. In addition, the volumetric dry gas flow was recorded by a gas meter (FR). The dry gas sampling flow rate was set between 2.0 and 2.5 $dm^3\ min^{-1}$.

After the sampling, the content of the five gas washing bottles filled with toluene was mixed. The samples were handed over to the Test Laboratory for Combustion Systems at the TU Wien. The test laboratory determined the amount of the GCMS tar components.

NH_3 sampling method

The NH_3 sampling was carried out according to the instructions of the Test Laboratory for Combustion Systems at the TU Wien. Fig. 5 shows the principle.

A sample flow of the processed gas at the inlet and outlet of the WGS pilot plant was led through the NH_3 sampling line. The gas passed through two gas washing bottles filled with overall 0.2 dm^3 of 0.05 mol dm^{-3} sulfuric acid. The sampling time for one sample was about 15 min. The volumetric dry gas flow was recorded by a gas meter (FR). The dry gas sampling flow rate was set to about 0.6 $dm^3\ min^{-1}$.

After the sampling, the content of the two gas washing bottles was mixed and the sample volume was filled up to a certain volume with sulfuric acid. The sample was handed over to the Test Laboratory for Combustion Systems at the TU Wien where the volumetric NH_3 concentration was determined with column chromatography.

Determination of the volumetric flow rates along the water gas shift pilot plant

The volumetric flow rates along the WGS pilot plant were determined by the water balance before the first WGS reactor according to Fig. 6.

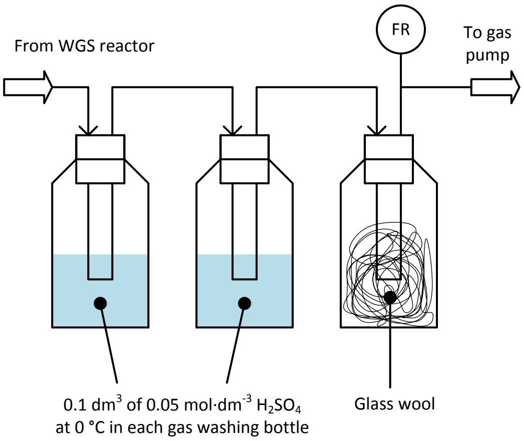
From WGS reactor
FR
To gas pump
0.1 dm³ of 0.05 mol·dm⁻³ H₂SO₄ at 0 °C in each gas washing bottle
Glass wool

Fig. 5 – Flowchart of the NH_3 sampling line.

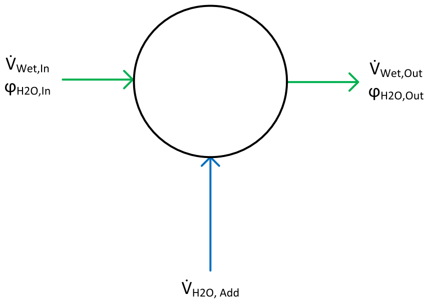

Fig. 6 – Balance for the determination of the volumetric flow rates along the WGS pilot plant before the first WGS reactor.

The overall volumetric balance and the water balance can be seen in Equations (2) and (3).

$$\dot{V}_{Wet,Out} = \dot{V}_{Wet,In} + \dot{V}_{H_2O,\ Add} \tag{2}$$

$$\underbrace{\dot{V}_{Wet,Out} \cdot \varphi_{H_2O,Out}}_{\dot{V}_{H_2O}} = \dot{V}_{Wet,In} \cdot \varphi_{H_2O,In} + \dot{V}_{H_2O,\ Add} \tag{3}$$

The steam contents ($\varphi_{H_2O,In}$ and $\varphi_{H_2O,Out}$) as well as the steam addition ($\dot{V}_{H_2O,\ Add}$) were determined. Consequently, the overall volumetric flow rate before the steam addition ($\dot{V}_{Wet,In}$) was calculated according to Equation (4) where $\dot{V}_{H_2O,\ Add}$ was the controlled and, therefore, known amount of steam which was added to the processed gas, $\varphi_{H_2O,In}$ the steam content before the steam addition, and $\varphi_{H_2O,Out}$ the steam content after the steam addition.

$$\dot{V}_{Wet,In} = \frac{\dot{V}_{H_2O,Add} \cdot \varphi_{H_2O,Out} - \dot{V}_{H_2O,Add}}{\left(\varphi_{H_2O,In} - \varphi_{H_2O,Out}\right)} \tag{4}$$

In general, the volumetric dry gas flow rate along before the first WGS reactor was calculated using Equation (5).

$$\dot{V}_{Dry,In} = \dot{V}_{Wet,In} \cdot \left(1 - \varphi_{H_2O,In}\right) \tag{5}$$

All gas volumes and volumetric flow rates in this work are given at standard temperature and pressure (STP, 273.15 K and 101325 Pa).

Characteristic figures of the water gas shift pilot plant

The WGS pilot plant and its reactors were described by characteristic figures. The first figure (Equation (6)) is the gas hourly space velocity (GHSV). It was calculated as the ratio of the volumetric dry gas flow rate at the inlet of the first reactor to the catalyst volume of the first reactor. It indicates the stress of the catalyst.

$$GHSV = \frac{\dot{V}_{Dry,In}}{V_{Catalyst}} \tag{6}$$

The second figure (Equation (7)) is the steam to dry gas ratio (STDGR). This figure was calculated as the ratio of the volumetric steam flow rate after the steam addition to the volumetric dry gas flow rate of the feed of the WGS pilot plant.

$$\mathrm{STDGR} = \frac{\dot{V}_{H_2O}}{\dot{V}_{Dry,In}} \tag{7}$$

The third figure (Equation (8)) is the steam to carbon ratio (STCR). This figure was calculated as the ratio of the volumetric steam flow rate after the steam addition to the volumetric flow rate of all gas components which included at least one carbon atom. The value of the STCR must not be too low in order to avoid coking and carbon deposition on the surface of the catalyst.

$$\mathrm{STCR} = \frac{\dot{V}_{H_2O}}{\dot{V}_{Dry,In} \cdot \left(\varphi_{CO} + \varphi_{CO_2} + \varphi_{CH_4} + 2 \cdot \varphi_{C_2H_y}\right)} \tag{8}$$

Another typical figure of the WGS pilot plant is the CO conversion in Equation (9).

$$X_{CO} = \frac{\dot{V}_{Dry,In} \cdot \varphi_{CO,In} - \dot{V}_{Dry,Out} \cdot \varphi_{CO,Out}}{\dot{V}_{Dry,In} \cdot \varphi_{CO,In}} \tag{9}$$

It was calculated with the CO concentrations and the volumetric dry gas flow rates at the inlet and the outlet of the reactors of the WGS pilot plant.

All four figures describe the conditions along the WGS pilot plant. The GHSV, the STDGR, and the STCR were calculated before the first reactor of the WGS pilot plant. The CO conversion was calculated for the whole pilot plant as well as for every single reactor. In addition, those figures make different WGS units, respectively, WGS reactors comparable.

Results and discussion

This section presents the results which were gathered during the about 2250 h of operation of the WGS pilot plant with tar-rich product gas from the biomass steam gasification plant in Oberwart.

Operating conditions of the water gas shift pilot plant

Table 3 shows the operating conditions during the about 2250 h of operation of the WGS pilot plant with tar-rich product gas extracted before the RME gas scrubber of the CHP plant in Oberwart.

The GHSV is given for the first reactor as well as the STDGR and the STCR which were chosen in order to protect the catalyst from coking and carbon deposits. During the whole operating time, an average CO conversion of 92% was reached for the whole WGS pilot plant. The WGS pilot plant was operated at ambient pressure.

Table 3 – Operating parameters of the WGS pilot plant during the about 2250 h of operation with tar-rich product gas. The parameters are given for the first reactor of the WGS pilot plant.

GHSV h^{-1}	STDGR –	STCR –	Overall X_{CO} %
479	1.6	2.6	92

Concentration profiles along the water gas shift pilot plant

Fig. 7 shows the concentration profiles of the main components during the whole operating time at the inlet of the WGS pilot plant, respectively, at the inlet of reactor A, after reactor A, after reactor B, and after reactor C which is the outlet of the WGS pilot plant.

It can be seen (Fig. 7-I) that the gasification process of the CHP plant provided a constant product gas quality during the whole operating time. Between the operating hours 1150 and 1450, the CHP plant operated at partial load with only one of the two gas engines due to a technical problem. The partial load operation of the CHP plant resulted in a higher steam to fuel ratio in the gasifier and, therefore, in a higher CO_2 and lower CO content in the product gas (see Fig. 7-I and compare [16]). The CH_4 concentration decreased due to the higher volumetric dry gas flow rate after reactor A. Along the whole WGS pilot plant, the volumetric dry gas flow rate increased by a factor of about 1.2. The CO mostly reacted in the first of the three reactors (reactor A) of the WGS pilot plant. The volumetric CO content could be lowered to below 5% after reactor A and below 2% after reactor C.

Fig. 8 shows the concentration profiles of the sulfur components during the whole operation time at the inlet of the WGS pilot plant, respectively, at the inlet of reactor A, after reactor A, after reactor B, and after reactor C which is the outlet of the WGS pilot plant.

The concentration profiles of the sulfur components at the inlet of the WGS pilot plant was also very stable (see Fig. 8-I). The relatively low sulfur content makes the product gas of the DFB biomass steam gasification suitable for the Fe/Cr based catalyst. Fig. 8 also shows that the COS content decreased to below the detection limit in reactor A. The H_2S and C_4H_4S concentrations remained constant after reactor A.

Table 4 shows the concentrations of all the measured main components along the WGS pilot plant during the about 2250 h of operation. It shows that the concentration of the reactive components (CO, CO_2, and H_2) changed significantly along the WGS pilot plant. The non-reactive components (CH_4, C_2H_y, N_2, and O_2) were lowered due to the dilution effect caused by the higher volumetric dry gas flow rate after a WGS reactor.

With a product gas output of about 1.18 $m^3\,h^{-1}$ (d.b.) per kg biomass (dry and ash free, see [17]) and the higher volumetric dry gas flow rate (by a factor of 1.2), a specific H_2 production of about 64 g H_2 per kg biomass was achieved.

Table 5 shows the concentrations of all measured sulfur components along the WGS pilot plant during the about 2250 h of operation.

The concentration of COS significantly decreased along the WGS pilot plant. H_2S and C_4H_4S were not affected by the dilution effect due to the higher volumetric dry gas flow rate. Consequently, it can be assumed that COS reacted to H_2S and C_4H_4S or other non-detected sulfur components. Twigg reports (see [7]) that Fe/Cr based catalysts also catalyze the conversion of COS to H_2S according to Equation (10).

$$COS + H_2O \rightleftharpoons H_2S + CO_2 \quad \Delta H = -34.6\ \mathrm{kJ \cdot mol^{-1}} \tag{10}$$

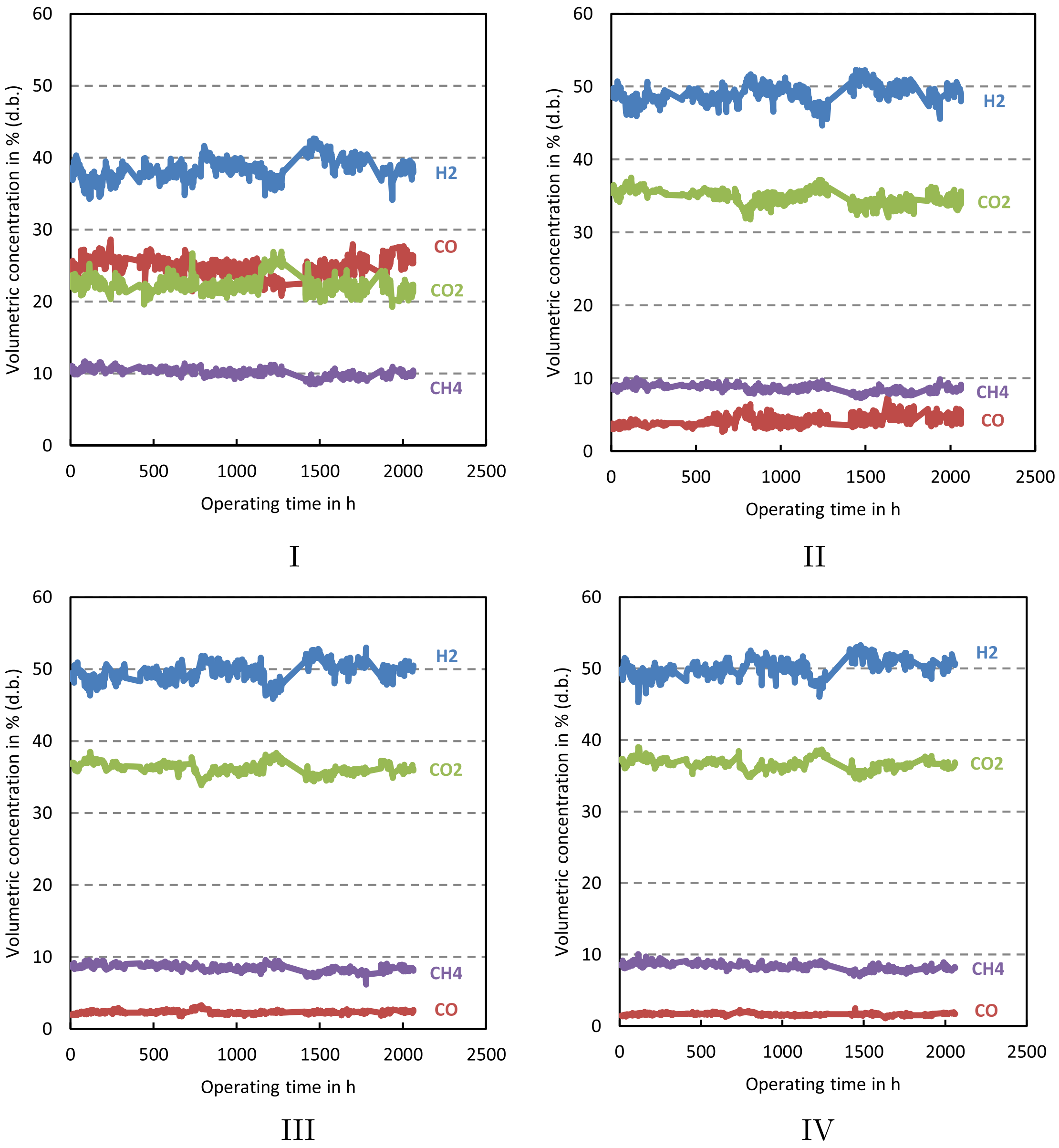

I

II

III

IV

Fig. 7 – **Concentration profiles of the main gas components of the product gas during the about 2250 h of operation at the inlet of the WGS pilot plant (I), after reactor A (II), after reactor B (III), and after reactor C (IV) (DL = 2 cm^3 m^{-3}).**

Steam content of the processed gas during the about 2250 h of operation

Fig. 9 shows the steam content of the product gas along the WGS pilot plant. The steam content was determined with the method described in Section 2.5.

Over the whole operating time, the steam content could be kept at a nearly constant level. This was very important in order to protect the commercial Fe/Cr based catalyst from coking and carbon deposition (compare [8]).

CO conversion during the about 2250 h of operation

Fig. 10 shows the concentration of the reactive WGS species along the WGS pilot plant over the whole operating time. It shows that the CO content significantly decreased in reactor A. In reactors B and C, less WGS reaction occurred because of the unfavorable temperature for the equilibrium composition.

Therefore, reactor A showed the highest CO conversion of about 81% and reactors B and C a relatively low CO conversion of about 43%, respectively, 29% (see Fig. 11). The overall CO conversion was 92% (see Table 3).

Temperature profiles along the water gas shift reactors

The inlet temperature of each of the three WGS reactors was set to about 350 °C because earlier research showed that this temperature is a good compromise between the reaction rate and the equilibrium composition (see [8,10,11]).

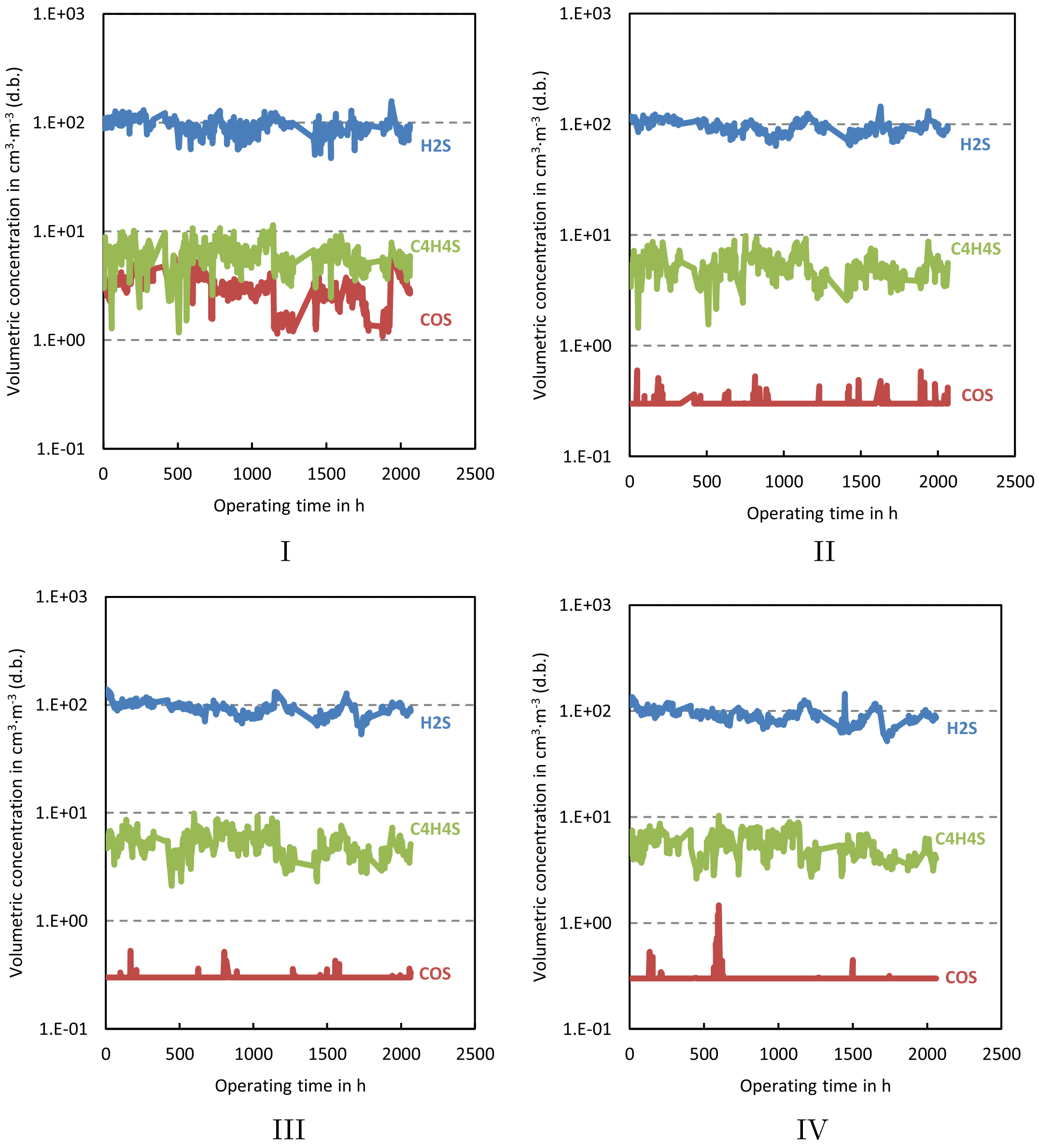

Fig. 8 – **Concentration profiles of the sulfur components of the product gas during the about 2250 h of operation at the inlet of the WGS pilot plant (I), after reactor A (II), after reactor B (III), and after reactor C (IV) (DL = 0.3 cm^3 m^{-3}).**

Fig. 12 shows the temperature profiles along reactors A, B, and C.

The temperature in reactor A increased significantly due to the exothermic WGS reaction. After the maximum temperature was reached and nearly no further reaction could take place, the temperature decreased because the equilibrium composition was reached. In addition, after thermocouple TA5, the temperature decreased because of heat losses.

Table 4 – **Concentrations (d.b.) of the main gas components of the processed gas along the WGS pilot plant during the about 2250 h of operation (DL = 2 cm^3 m^{-3}).**

	φ_{H_2} %	φ_{CO} %	φ_{CO_2} %	φ_{CH_4} %	$\varphi_{C_2H_y}$ %	φ_{N_2} %	φ_{O_2} %
Inlet	38.6 ± 1.5	24.9 ± 1.3	22.3 ± 1.2	10.1 ± 0.6	2.7 ± 0.3	1.4 ± 0.6	0.08 ± 0.04
Outlet A	49.1 ± 1.3	4.1 ± 0.7	34.9 ± 1.0	8.6 ± 0.5	2.1 ± 0.2	1.1 ± 0.4	0.03 ± 0.02
Outlet B	49.7 ± 1.3	2.3 ± 0.2	36.3 ± 0.8	8.4 ± 0.5	2.1 ± 0.2	1.1 ± 0.6	0.03 ± 0.01
Outlet C	50.2 ± 1.3	1.6 ± 0.2	36.6 ± 0.8	8.3 ± 0.5	2.1 ± 0.2	1.1 ± 0.5	0.03 ± 0.02

Table 5 – Concentrations (d.b.) of the sulfur gas components of the processed gas along the WGS pilot plant during the about 2250 h of operation (DL = 0.3 $cm^3 m^{-3}$).

	φ_{H_2S} $cm^3 m^{-3}$	φ_{COS} $cm^3 m^{-3}$	$\varphi_{C_4H_4S}$ $cm^3 m^{-3}$
Inlet	93.5 ± 16.9	3.2 ± 1.2	5.8 ± 1.9
Outlet A	94.6 ± 16.0	BDL	5.1 ± 1.6
Outlet B	93.0 ± 15.6	BDL	5.1 ± 1.6
Outlet C	90.9 ± 16.5	BDL	5.2 ± 1.7

The temperature profile had a high standard deviation. This was caused by the oscillating operating conditions of the CHP plant, especially the differing amounts of steam content in the processed gas caused by the differing fractions of biomass wood chips with varying water content.

Fig. 12 also indicates that the inlet temperature of about 350 °C at the inlet of reactors B and C was unfavorable for the equilibrium composition. Consequently, nearly no WGS reaction occurred. Therefore, the heat losses were higher than the temperature increase caused by the exothermic WGS reaction.

Furthermore, the temperature profile in Fig. 13 indicates that no significant deactivation of the commercial Fe/Cr based catalyst occurred during the about 2250 h of operation of the WGS pilot plant with tar-rich product gas.

GCMS *tar measurements*

During the about 2250 h of operation of the WGS pilot plant with product gas extracted before the RME gas scrubber, four GCMS tar measurements were performed (I to IV). Table 6 shows the results of all four GCMS tar measurements.

The table shows that the amount of GCMS tar significantly decreased along the WGS pilot plant because the pilot plant offered a reactive environment and additional residence time for tar reduction.

It can be seen that the GCMS tar concentrations significantly decreased with increasing operating time. This could be explained by advancing formation of inorganic layer at the surface of the bed material in the gasifier. Furthermore, this layer formation advances with advancing residence time of the bed material in the gasifier. These inorganic layers show significant catalytic activity regarding tar reduction [17–20]. Further information regarding this matter can be found in [21,22].

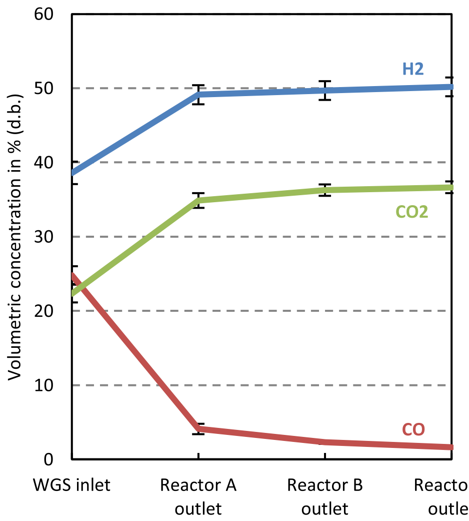

Fig. 10 – Mean volumetric concentration profile of the reactive species during the about 2250 h of operation along the WGS pilot plant.

NH_3 *measurements*

During the about 2250 h of operation of the WGS pilot plant with product gas extracted before the RME gas scrubber, three NH_3 measurements were performed (I to III). Table 7 shows the results of all three NH_3 measurements.

The table shows that the NH_3 content only decreased due to the dilution effect caused by the higher volumetric dry gas flow rate (by a factor of about 1.2) after the WGS pilot plant.

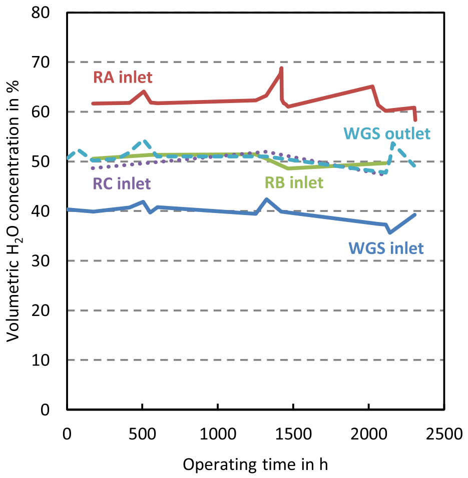

Fig. 9 – Steam content of the processed product gas during the about 2250 h of operation along the WGS pilot plant.

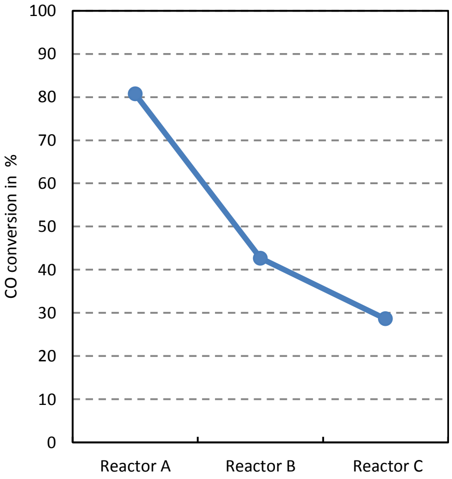

Fig. 11 – CO conversion during the about 2250 h of operation in every single reactor of the WGS pilot plant.

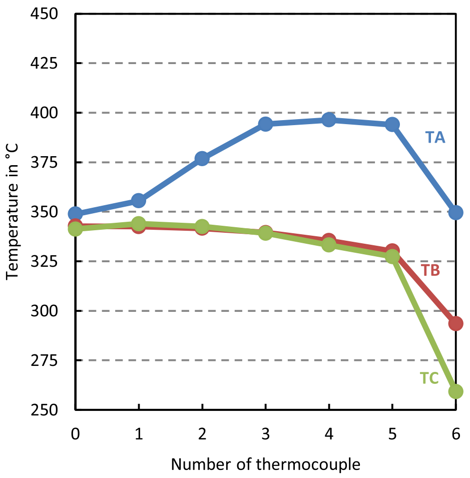

Fig. 12 – Average temperature profiles along reactors A, B, and C during the about 2250 h of operation of the WGS pilot plant.

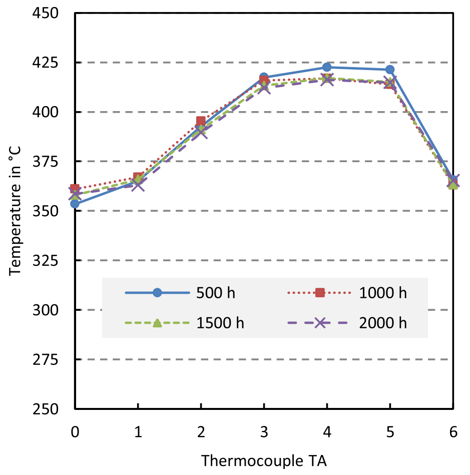

Fig. 13 – Temperature profile along reactor A after 500, 1000, 1500, and 2000 h of operation with the tar-rich product gas.

Table 6 – GCMS tar concentration (d.b.) at the inlet (reactor A) and outlet (reactor C) of the WGS pilot plant during the about 2250 h of operation with tar-rich product gas extracted before the RME gas scrubber. The measurements were single sample measurements. Therefore, no standard deviation could be calculated.

No. –	In/out –	GCMS tar mg m^{-3}	Operating time h
I	In	8145	≈430
I	Out	5829	≈433
II	In	4710	≈1190
II	Out	3331	≈1193
III	In	2697	≈1710
III	Out	1873	≈1713
IV	In	3762	≈2050
IV	Out	2335	≈2053

Table 7 – Results of the NH_3 measurements during the about 2250 h of operation of the WGS pilot plant with tar-rich product gas extracted before the RME gas scrubber (d.b.). The measurements were single sample measurements. Therefore, no standard deviation could be calculated.

No. –	WGS inlet cm^3 m^{-3}	WGS outlet cm^3 m^{-3}	Operating time h
I	3395	2840	≈1200
II	1924	1460	≈1700
III	2383	1869	≈2045

Conclusion and outlook

In this paper, a long term operation performance of a WGS pilot plant processing product gas from an industrial scale DFB biomass steam gasification plant is investigated. The pilot plant employed a commercial Fe/Cr based catalyst (ShiftMax® 120) and was operated for about 2250 h with tar-rich product gas from the gasification plant.

During these 2250 h, a flawless operation of the WGS pilot plant was demonstrated. The volumetric CO content in the product gas was decreased to below 2%. Furthermore, a CO conversion of 92% was obtained. In addition, a significant GCMS tar reduction along the WGS pilot plant occurred. No catalyst deactivation could be observed with the experimental layout and equipment which was used during the experiments.

The results show that the application of a commercial Fe/Cr based catalyst in a WGS unit is possible, even if tar-rich product gas is processed.

Future research should focus on further observations on possible catalyst deactivation during additional long term experiments. In addition, process simplification by means of a lower STDGR and STCR should be a goal for future research activities.

Acknowledgments

This work was carried out within the framework of the Bioenergy2020+GmbH project “C20005016 Polygeneration III”. Bioenergy2020+ GmbH is funded by the states Burgenland, Niederoesterreich, Steiermark, and within the Austrian COMET program which is managed by the Austria Research Promoting Agency (FFG).

The authors want to thank the project partners Air Liquide, Guessing Renewable Energy GmbH, and ISG Energy GmbH. In addition, the plant operators of the CHP plant in Oberwart are gratefully acknowledged.

The authors also thank Binder Industrieanlagenbau for constructing the WGS pilot plant as well as the Clariant company for providing the commercial Fe/Cr based catalyst (ShiftMax®' 120).

Silvester Fail is thanked for the buildup, the startup, and the optimization of the WGS pilot plant as well as for performing the first experimental runs.

The Test Laboratory for Combustion Systems at the TU Wien is acknowledged for carrying out the GCMS tar and NH_3 analyses.

Abbreviations and acronyms

BDL	below detection limit
BTEX	benzene, toluene, ethylbenzene, and xylenes
CHP	combined heat and power
d.a.f.	dry and ash free
d.b.	dry basis
DFB	dual fluidized bed
DL	detection limit
FPD	flame photometric detector
FR	flow record
GC	gas chromatograph
GCMS	gas chromatography mass spectroscopy
ORC	organic Rankine cycle
RA	reactor A
RB	reactor B
RC	reactor C
RME	rapeseed methyl ester
STP	standard temperature and pressure (273.15 K and 101325 Pa)
TA	thermocouple number along reactor A
TB	thermocouple number along reactor B
TC	thermocouple number along reactor C
TCD	thermal conductivity detector
WGS	water gas shift

Symbols

$\varphi_{CO,In}$	volumetric CO fraction before a reactor in –
$\varphi_{CO,Out}$	volumetric CO fraction after a reactor in –
$\varphi_{H_2O,In}$	volumetric steam fraction before steam addition in –
$\varphi_{H_2O,Out}$	volumetric steam fraction after steam addition in –
φ_i	volumetric fraction of component *i* in –
GHSV	gas hourly space velocity before reactor A in h^{-1}
ΔH	enthalpy of formation (at 298.15 K and 101325 Pa) in $kJ\ mol^{-1}$
STDGR	steam to dry gas ratio before reactor A in –
STCR	steam to carbon ratio before reactor A in –
$V_{Catalyst}$	catalyst volume in m^3
$\dot{V}_{Dry,In}$	volumetric dry gas flow rate before a reactor at STP in $m^3\ h^{-1}$
$\dot{V}_{Dry,Out}$	volumetric dry gas flow rate after a reactor at STP in $m^3\ h^{-1}$
$\dot{V}_{H_2O,Add}$	steam addition at STP addition in $m^3\ h^{-1}$
$\dot{V}_{H_2O}$	volumetric steam flow rate at STP after the steam addition in $m^3\ h^{-1}$
$\dot{V}_{Wet,In}$	overall volumetric flow rate before steam addition at STP in $m^3\ h^{-1}$
$\dot{V}_{Wet,Out}$	overall volumetric flow rate after steam addition at STP in $m^3\ h^{-1}$
X_{CO}	CO conversion in –

REFERENCES

[1] Holladay J, Hu J, King D, Wang Y. An overview of hydrogen production technologies. Catal Today 2009;139:244–60. http://dx.doi.org/10.1016/j.cattod.2008.08.039.

[2] Saxena R, Seal D, Kumar S, Goyal HB. Thermo-chemical routes for hydrogen rich gas from biomass: a review. Renew Sust Energ Rev 2008;12:1909–27. http://dx.doi.org/10.1016/j.rser.2007.03.005.

[3] Ni M, Leung DYC, Leung MKH, Sumathy K. An overview of hydrogen production from biomass. Fuel Process Technol 2006;87:461–72. http://dx.doi.org/10.1016/j.fuproc.2005.11.003.

[4] Hofbauer H. Biomass CHP plant guessing - a success story. CPL Press; 2003.

[5] Kaltschmitt M, Hartmann H, Hofbauer H. Energie aus Biomasse. Springer-Verlag; 2009. http://dx.doi.org/10.1007/978-3-8348-9327-7_9.

[6] Liu K, Song C, Subramani V. Hydrogen and syngas production and purification technologies. Wiley; 2010. http://dx.doi.org/10.1002/9780470561256.fmatter.

[7] Twigg MV. Catalyst handbook. Manson Publishing; 1989.

[8] Fail S. Biohydrogen production based on the catalyzed water gas shift reaction in wood gas. Ph.D. thesis. TU Wien; 2014.

[9] Corella J, Aznar MP, Caballero MA, Molina G, Toledo JM. 140 g H_2/kg biomass d.a.f. by a CO-shift reactor downstream from a FB biomass gasifier and a catalytic steam reformer. Int J Hydrogen Energ 2008;33:1820–6. http://dx.doi.org/10.1016/j.ijhydene.2008.02.003.

[10] Fail S, Diaz N, Bendikt F, Kraussler M, Hinteregger J, Bosch K, et al. Wood gas processing to generate pure hydrogen suitable for PEM fuel cells. ACS Sustain Chem Eng 2014;2(12):2690–8. http://dx.doi.org/10.1021/sc500436m.

[11] Kraussler M, Binder M, Fail S, Bosch K, Hackel M, Hofbauer H. Performance of a water gas shift unit processing product gas from biomass steam gasification. In: Proceedings of the 23rd European Biomass Conference and Exhibition, Vienna, Austria; 2015. p. 668–78.

[12] Wilk V, Hofbauer H. Analysis of optimization potential in commercial biomass gasification plants using process simulation. Fuel Process Technol 2016;141:138–47. http://dx.doi.org/10.1016/j.fuproc.2015.07.035.

[13] Kotik J. Ueber den Einsatz von Kraft-Waerme-Kopplungsanlagen auf Basis der Wirbelschicht-Dampfvergasung fester Biomasse am Beispiel des Biomassekraftwerks Oberwart. Ph.D. thesis. TU Wien; 2010.

[14] Kirnbauer F, Koch M, Koch R, Aichernig C, Hofbauer H. Behavior of inorganic matter in a dual fluidized steam gasification plant. Energ Fuels 2013;27(6):3316–31. http://dx.doi.org/10.1021/ef400598h.

[15] Wolfesberger U, Aigner I, Hofbauer H. Tar content and composition in producer gas of fluidized bed gasification of wood - influence of temperature and pressure. Environ Prog Sustain Energ 2009;28(3):372–9. http://dx.doi.org/10.1002/ep.10387.

[16] Koppatz S, Pfeifer C, Hofbauer H. Comparison of the performance behaviour of silica and olivine in a dual fluidised bed reactor system for steam gasification of biomass at pilot plant scale. Chem Eng J 2011;175:468–83. http://dx.doi.org/10.1016/j.cej.2011.09.071.

[17] Kirnbauer F, Wilk V, Hofbauer H. Performance improvement of dual fluidized bed gasifiers by temperature reduction: the behavior of tar species in the product gas. Fuel 2013;108:534–42. http://dx.doi.org/10.1016/j.fuel.2012.11.065.

[18] Kirnbauer F, Wilk V, Kitzler H, Kern S, Hofbauer H. The positive effects of bed material coating on tar reduction in a dual fluidized bed gasifier. Fuel 2012;95:553–62. http://dx.doi.org/10.1016/j.fuel.2011.10.066.

[19] Kirnbauer F, Hofbauer H. Investigations on bed material changes in a dual fluidized bed steam gasification plant in Guessing, Austria. Energ Fuels 2011;25(8):3793–8. http://dx.doi.org/10.1021/ef200746c.

[20] Kirnbauer F, Hofbauer H. The mechanism of bed material coating in dual fluidized bed biomass steam gasification plants and its impact on plant optimization. Powder Technol

2013;245:94–104. http://dx.doi.org/10.1016/j.powtec.2013.04.022.

[21] Kuba M, He H, Kirnbauer F, Biström D, Öman M, Hofbauer H. Deposit build-up and ash behavior in dual fluid bed steam gasification of logging residues in an industrial power plant. Fuel Process Technol 2015;139:33–41. http://dx.doi.org/10.1016/j.fuproc.2015.08.017.

[22] Kuba M, Havlik F, Kirnbauer F, Hofbauer H. Influence of bed material coatings on the water-gas-shift reaction and steam reforming of toluene as tar model compound of biomass gasification. Biomass Bioenerg Available online 17 December 2015. http://dx.doi.org/10.1016/j.biombioe.2015.11.029.

Paper 3

Michael Kraussler, Matthias Binder, Hermann Hofbauer, Behavior of GCMS tar components in a water gas shift unit operated with tar-rich product gas from an industrial scale dual fluidized bed biomass steam gasification plant, Biomass Conversion and Biorefinery, Volume 7, Issue 1, 2017, Pages 69-79, `http://dx.doi.org/10.1007/s13399-016-0205-y`.

Contribution: Experimental work, data treatment, writing

Biomass Conv. Bioref. (2017) 7:69–79
DOI 10.1007/s13399-016-0205-y

ORIGINAL ARTICLE

Behavior of GCMS tar components in a water gas shift unit operated with tar-rich product gas from an industrial scale dual fluidized bed biomass steam gasification plant

Michael Kraussler[1,2] · Matthias Binder[2] · Hermann Hofbauer[1,2]

Received: 4 February 2016 / Revised: 13 March 2016 / Accepted: 15 March 2016 / Published online: 15 April 2016
© The Author(s) 2016. This article is published with open access at Springerlink.com

Abstract In this paper, the behavior of gas chromatography mass spectroscopy (GCMS) tar components in a three-stage water gas shift (WGS) unit is discussed. The GCMS tar measurements were carried out during the long-term operation (2250 h) of a WGS unit with tar-rich product gas from the commercial biomass steam gasification plant in Oberwart, Austria. In order to investigate the behavior of the GCMS tar components, four tar measurements were performed during the long-term operation of the WGS unit which employed a commercial Fe/Cr-based catalyst. The tar-rich product gas was extracted before reaching the scrubbing unit of the biomass steam gasification plant, therefore, the extracted gas contained a high amount of tar. In order to investigate the behavior of the GCMS tar in the WGS unit, the GCMS tar concentrations were determined at the inlet and the outlet of the WGS unit. The samples were taken during full load operation and during partial load operation of the WGS unit, respectively, the biomass steam gasification plant. In addition to the increase of the volumetric hydrogen content from about 40 % (d.b.) to 50 % (d.b.), the amount of GCMS tar was reduced (up to 38 %) as the gas passed through the WGS unit. No catalyst deactivation was observed. Furthermore, the efficiency of the hydrogen increase or the GCMS tar reduction did not depend on whether the operation of the WGS unit, respectively, the gasification plant was at partial load or full load.

Keywords Biomass steam gasification · Dual fluidized bed · Hydrogen · Product gas · Water gas shift · GCMS tar

Abbreviations

AC	Aromatic components
ANC	Aromatic nitrogen components
BDL	Below detection limit
BTEX	Benzene, toluene, ethylbenzene, and xylene
CHP	Combined heat and power
d.b.	Dry basis
DFB	Dual fluidized bed
DL	Detection limit
FPD	Flame photometric detector
FR	Flow record
GC	Gas chromatograph
GCMS	Gas chromatography mass spectroscopy
ORC	Organic Rankine cycle
PAH	Polycyclic aromatic hydrocarbons
RME	Rapeseed methyl ester
STP	Standard temperature and pressure (273.15 K and 101325 Pa)
TA	Thermocouples along reactor A
TB	Thermocouples along reactor B
TC	Thermocouples along reactor C
TCD	Thermal conductivity detector
WGS	Water gas shift

Symbols

ϕ_i	Volumetric fraction of component i in -
$c_{i,\ Inlet}$	GCMS tar concentration of component i at the inlet of the WGS unit in mg m^{-3}

✉ Michael Kraussler
michael.kraussler@bioenergy2020.eu

[1] Bioenergy2020+ GmbH, Wienerstraße 49, 7540 Guessing, Austria

[2] Institute of Chemical Engineering, TU Wien, Getreidemarkt 9, 1060 Vienna, Austria

$c_{i,\ Outlet}$	GCMS tar concentration of component i at the outlet of the WGS unit in mg m^{-3}
Δ	Absolute change of the GCMS tar concentration in mg m^{-3}
δ	Relative change of the GCMS tar concentration in %
ΔH	Enthalpy of formation (at 298.15 K and 101325 Pa) in kJ mol^{-1}
STDGR	Steam to dry gas ratio in –
STCR	Steam to carbon ratio in –
$V_{Catalyst}$	Catalyst volume in m^3
$\dot{V}_{Dry}$	Volumetric dry gas flow rate in $m^3\ h^{-1}$
$\dot{V}_{H2O}$	Volumetric dry gas flow rate in $m^3\ h^{-1}$
X_{CO}	CO conversion in –

1 Introduction

The increasing CO_2 emissions caused by increasing energy consumption are one reason for global warming. In order to stop this climate change, CO_2 neutral alternatives for the energy supply need to be established. Beside wind, water, and solar energy, biomass is a promising CO_2 neutral energy source which has been used for centuries and which is available all over the world.

Biomass gasification offers the possibility of the renewable production of a wide range of products for chemical industry and energy supply. Especially biomass steam gasification, employing the dual fluidized bed (DFB) technology is a proven process. Various products from the biomass, for example, electricity, heat, hydrogen, synthetic natural gas, Fischer-Tropsch products, and alcohols (see [6, 20, 21, 23]) can be produced.

The water gas shift (WGS) reaction (see Eq. 1) can be used to adjust the H_2/CO ratio in the generated product gas for several of the above-mentioned synthesis reactions.

$$CO + H_2O \rightleftharpoons H_2 + CO_2 \quad \Delta H = -41.1\,kJmol^{-1} \tag{1}$$

An unwanted side product of the gasification process is tar. According to [4], tar is a hydrocarbon-containing mixture which can form deposits (ranging from liquid to highly viscous to solid) by a cooling of the gaseous phase down to the ambient temperature.

The tar formation and reduction related to biomass gasification was extensively discussed by different authors, for example in [2, 3, 10, 12, 26].

During a long-term operation of a WGS unit (see [15]), gas chromatography mass spectroscopy (GCMS) tar measurements were performed. The WGS unit employed a commercial Fe/Cr-based catalyst and was operated with tar-rich product gas that was extracted before reaching the scrubbing unit of the commercial DFB biomass steam gasification plant in Oberwart, Austria.

This paper discusses the effects of the WGS unit on the GCMS tar components which were measured in the tar-rich product gas from the commercial DFB biomass steam gasification plant. However, it should be pointed out that the WGS unit was rather operated to increase the hydrogen content of the product gas than to reduce the tar content. Consequently, the observed tar reduction was a positive side effect.

2 Materials and methods

The experimental work was carried out at the site of the DFB biomass steam gasification plant in Oberwart, Austria, where the WGS unit is located. The WGS unit consisted of three reactors in series which employed a commercial Fe/Cr-based catalyst. The GCMS tar samples were taken at the inlet and the outlet of the WGS unit. The GCMS tar analyses were performed by the Test Laboratory for Combustion Systems at the TU Wien. In addition, during the tar sampling, the temperature profile along each reactor was recorded and the gas composition was determined.

2.1 The biomass steam gasification plant

The WGS unit processed product gas from the DFB biomass steam gasification plant in Oberwart, Austria. This plant is a combined heat and power (CHP) plant. Figure 1 shows a simplified flowchart of the overall process.

The gasification plant is based on the DFB steam gasification technology described in detail in [7, 9]. The plant generates heat for the district and electricity with biomass (woodchips) as feedstock. [5, 14] give a short overview of the working principle of the process.

Biomass is fed into the biomass dryer and, subsequently, transported into the gasifier by a screw conveyor. In the gasifier which operates at ambient pressure, the biomass reacts with steam and is in contact with the catalytically active bed material (olivine) at about 850 °C resulting in a product gas with a high hydrogen content ($\phi_{H2} \approx 40$ % (d.b.)). Then, the product gas is cooled and cleaned in a bag house filter and in an Rapeseed methyl ester (RME) gas scrubber. In the RME gas scrubber, tar, NH_3, and other condensable fractions of the product gas are removed before the product gas is fed into the gas engines for electricity generation.

Heat from the flue gas line is mainly recovered for the process and for district heating. Fly ash is removed before the flue gas is released into the atmosphere.

For the operation of the WGS unit, a partial flow of the product gas was extracted before reaching the RME gas scrubber of the gasification plant (see Fig. 1). Table 1 shows the conditions at this extraction point.

The overall tar content in the product gas which is extracted before the RME gas scrubber is much higher compared to a point after the RME gas scrubber. This is a challenge for a reliable operation of the WGS unit. The product gas composition at the extraction point can be seen in Sect. 3.

2.2 The water gas shift unit

The experimental work was carried out with a WGS unit located at the site of the gasification plant in Oberwart. The WGS unit employed a commercial Fe/Cr-based catalyst (ShiftMax 120). Figure 2 shows a simplified flowchart of the WGS unit.

The WGS unit consisted of three fixed bed reactors (A, B, and C) in series filled with the Fe/Cr-based catalyst. Each catalyst bed had a diameter of about 9 cm and a bed height of about 40 cm, resulting in an Fe/Cr-based catalyst volume of about 2.5 dm^3 for each reactor.

Table 1 Operating conditions at the extraction point (see Fig. 1) of the CHP plant in Oberwart, Austria, at full load operation [6]

Parameter	Before RME scrubber	Units
Temperature	≈ 150	°C
Volumetric H_2O content	≈ 35	%
GCMS tar content	≈ 2700–8200	mg m^{-3}

Along the height of each reactor, seven type J thermocouples (TA0 to TA6, TB0 to TB6, and TC0 to TC6) were installed in order to record the temperature profiles. At the inlet and outlet of reactors A and B, the gas stream could be heated or cooled in order to achieve the desired gas inlet temperatures of about 350 °C.

In addition to the steam which was already contained in the product gas, more steam was added to the product gas before the inlet of the WGS unit in order to avoid coking and carbon deposition on the surface of the catalyst.

The WGS unit was operated at ambient pressure.

[14, 15] give a detailed description of the WGS unit.

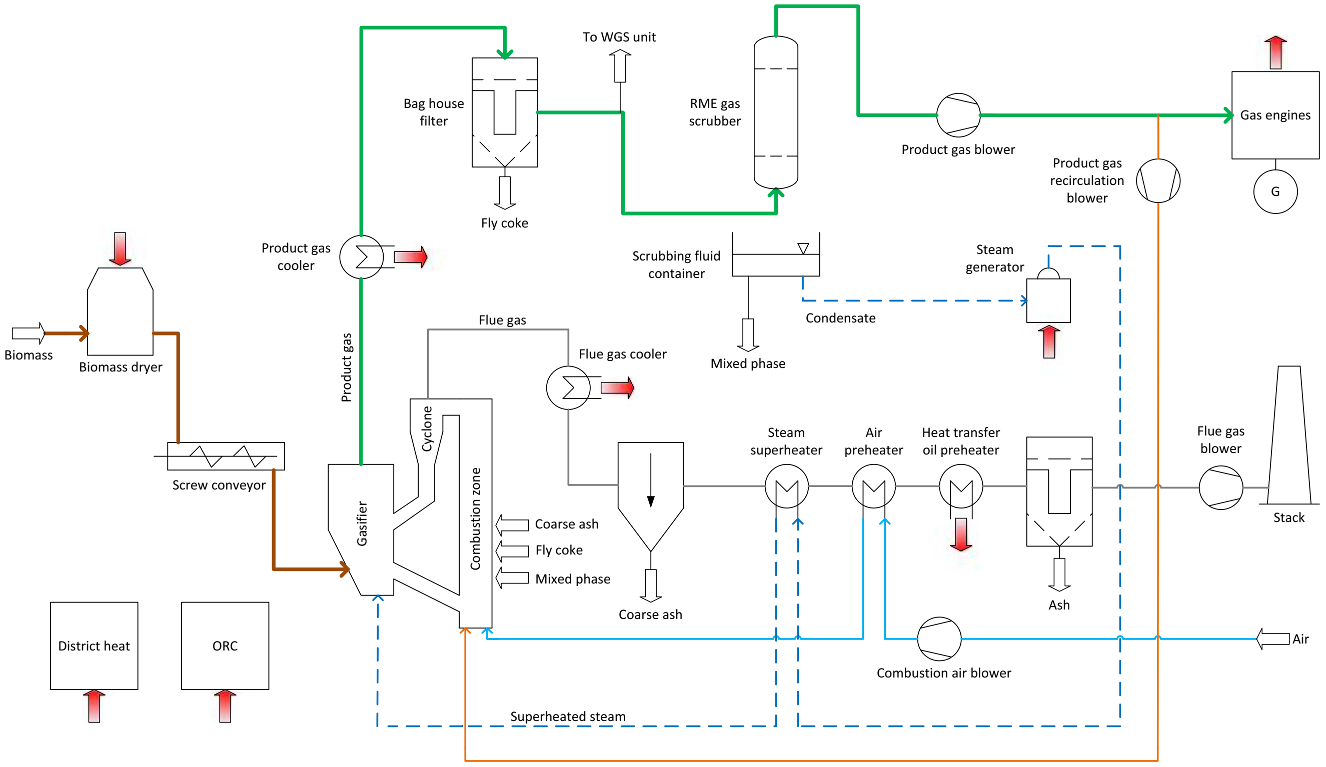
To WGS unit
Bag house filter
RME gas scrubber
Gas engines
Product gas blower
Product gas recirculation blower
G
Fly coke
Product gas cooler
Scrubbing fluid container
Steam generator
Condensate
Flue gas
Biomass
Biomass dryer
Product gas
Flue gas cooler
Mixed phase
Cyclone
Steam superheater
Air preheater
Heat transfer oil preheater
Flue gas blower
Screw conveyor
Combustion zone
Gasifier
Coarse ash
Fly coke
Mixed phase
Coarse ash
Ash
Stack
District heat
ORC
Air
Combustion air blower
Superheated steam

Fig. 1 Simplified flowchart of the gasification plant in Oberwart, Austria

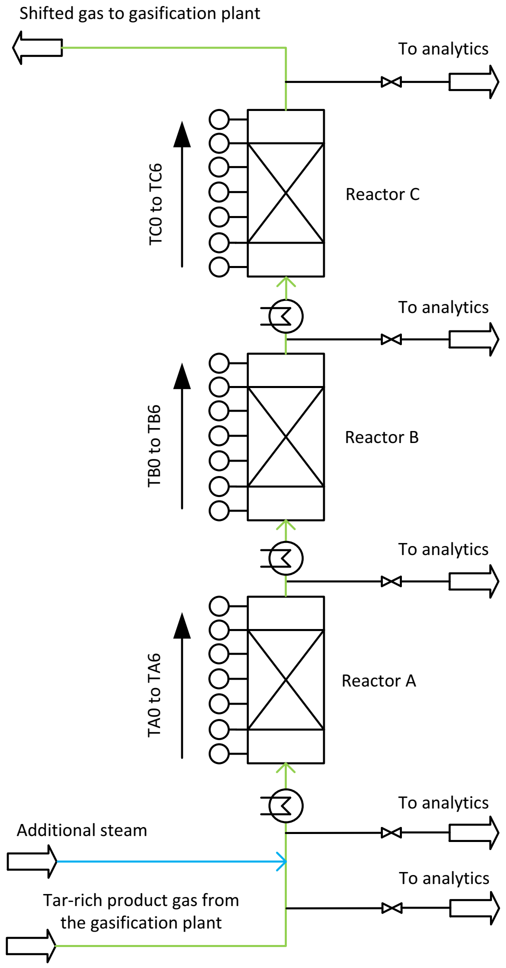
Shifted gas to gasification plant
To analytics
TC0 to TC6
Reactor C
To analytics
TB0 to TB6
Reactor B
To analytics
TA0 to TA6
Reactor A
To analytics
Additional steam
To analytics
Tar-rich product gas from the gasification plant

Fig. 2 Simplified flowchart of the WGS unit located at the site of the gasification plant in Oberwart, Austria

2.3 Measurement of the gas composition and the steam content

A gas chromatograph (GC, Clarus 500 from Perkin Elmer) measured the gas composition before and after the WGS unit. In the GC, a thermal conductivity detector (TCD) enabled the quantification of CO, CO_2, CH_4, N_2, O_2, C_2H_6, C_2H_4, and C_2H_2. The C_2 species were summarized and are referred to as C_2H_y. The H_2 content was determined via calculation. A flame photometric detector (FPD) was used to detect the H_2S, COS, and C_4H_4S content in the product gas.

The steam content of the processed gas was determined via the water balance along the whole of its passage through the WGS unit.

In addition, all gas volumes and volumetric gas flow rates are given at standard temperature and pressure (STP, 273.15 K and 101325 Pa).

2.4 Tar sampling and classification

During the experimental run of the WGS unit, tar samples from the inlet (reactor A) and outlet (reactor C) of the WGS unit were taken. Additional information about the method is available in [24, 25]. Figure 3 shows the principle of the tar sampling, which is described in detail in [15].

Toluene as solvent allowed the determination of the GCMS tar concentration and the water content of the extracted product gas at the same time. However, it did not allow the detection of benzene, toluene, ethylbenzene, and xylenes (BTEX).

The samples were handed over to the Test Laboratory for Combustion Systems at the TU Wien. The Test Laboratory determined the concentrations of the GCMS tar components.

Overall, according to the tar guideline (see [1]), tar can be classified into gravimetric tar and GCMS tar. In addition, several additional classifications for biomass tar exists in literature ([16, 18, 19]). For example, the classification in primary, secondary, and tertiary tar (see [18]). Another approach was chosen by [8, 17]. These authors classified the tar based on the molecular weight.

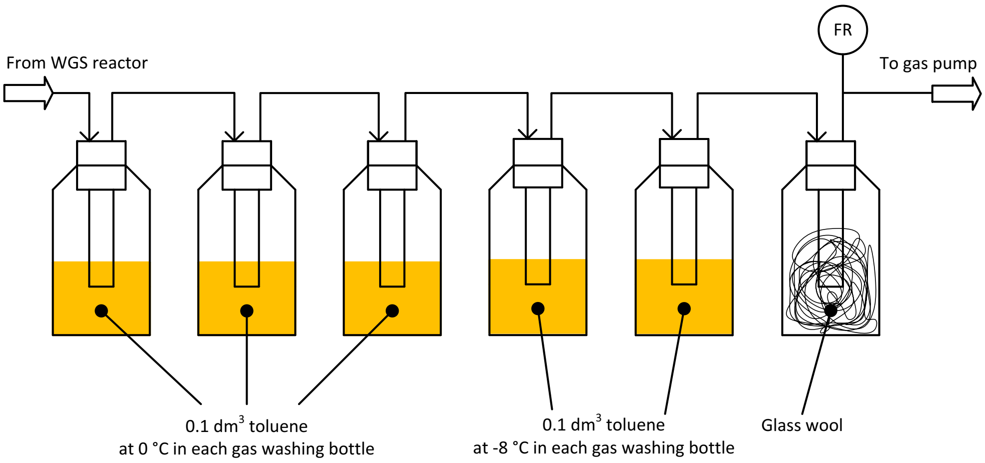
FR
From WGS reactor
To gas pump
0.1 dm^3 toluene
at 0 °C in each gas washing bottle
0.1 dm^3 toluene
at -8 °C in each gas washing bottle
Glass wool

Fig. 3 Flowchart of the tar sampling principle

In this work, the tar is classified according to the molecular weight and the chemical properties which strongly depend on the functional groups of the components (compare [25]). However, this work only considers GCMS tar components which were categorized into groups as described in Table 2.

2.5 Characteristic figures

The operating conditions of the WGS unit were described by the following three characteristic figures (see Eqs. 2, 3, and 4). These figures were the gas hourly space velocity (GHSV), the steam to dry gas ratio (STDGR), and the steam to carbon ratio (STCR).

$$GHSV = \frac{\dot{V}_{Dry}}{V_{Catalyst}} \tag{2}$$

$$STDGR = \frac{\dot{V}_{H2O}}{\dot{V}_{Dry}} \tag{3}$$

$$STCR = \frac{\dot{V}_{H2O}}{\dot{V}_{Dry} \cdot \left(\phi_{CO} + \phi_{CO2} + \phi_{CH4} + \phi_{C2Hy}\right)} \tag{4}$$

The values of the GHSV, the STDGR, and the STCR were calculated for the first reactor of the WGS unit and do not consider the other two reactors.

Two figures were used in order to describe the behavior of the GCMS tar components. They were calculated according to Eqs. 5 and 6.

$$\Delta = c_{i,\mathrm{Outlet}} - c_{i,\mathrm{Inlet}} \tag{5}$$

$$\delta = \left(1 - \frac{c_{i,\mathrm{Outlet}}}{c_{i,\mathrm{Inlet}}}\right) \cdot (-1) \cdot 100\% \tag{6}$$

A negative value of Δ or δ means a decrease of GCMS tar, and a positive value means an increase of GCMS tar along the WGS unit.

In addition, the dilution effect caused by the higher volumetric dry gas flow rate after the WGS unit has to be taken into account. The volumetric dry gas flow rate after the WGS unit is about 20 % higher than the volumetric dry gas flow rate before the WGS unit for all performed GCMS tar measurements. The results show the measured concentrations of the GCMS tar components at the inlet and outlet of the WGS unit.

Table 2 Categorization of all detected GCMS tar components

Phenols	Phenol
Furans	Benzofuran; dibenzofuran
AC	Phenylacetylene; styrene; mesitylene; 1H-indene
ANC	Isoquinoline; indole; quinoline
Naphthalenes	Naphthalene; 2-methylnaphthalene; 1-methylnaphthalene
PAH	Biphenyl; acenaphthylene; acenaphthene; fluorene; anthracene; phenanthrene; 4,5-methylphenanthrene; fluoranthene; pyrene
Thiophenes	1-benzothiophene

Based on [10, 11, 17, 24]

Table 3 Overview of the GCMS tar samplings

Number	Hours of operation	Load conditions gasification plant	Load conditions WGS unit
1st	≈ 430 h	Full	Full
2nd	≈ 1190 h	Partial	Full
3rd	≈ 1710 h	Full	Partial
4th	≈ 2050 h	Full	Full

3 Results and discussion

This section presents the results of four GCMS tar measurements which were carried out during a long-term operation (2250 h) of the WGS unit with tar-rich product gas (see [15]).

For all four GCMS tar measurements, the GCMS tar content was within the typical order of magnitude for DFB biomass steam gasification systems (compare [25]).

3.1 Load conditions of the water gas shift unit and the gasification plant during the GCMS tar samplings

Table 3 gives an overview of the load conditions of the gasification plant and the WGS unit during the four GCMS tar samplings.

It can be seen that during the first and the fourth GCMS tar sampling, both, the WGS and the gasification plant, operated at full load. However, during the second sampling, the gasification plant operated at partial load due to maintenance work which resulted in a higher steam to fuel ratio in the gasifier of the gasification plant. During the third sampling, the WGS unit operated at partial load due to a problem with the membrane gas pump which extracted the product gas from the gasification plant.

Table 4 Operating parameters of the WGS unit during the GCMS tar samplings

Number	GHSV	STDGR	STCR
–	h^{-1}	–	–
1st	495	1.6	2.7
2nd	445	1.9	3.2
3rd	326	1.6	2.7
4th	495	1.6	2.7

All parameters are given for the inlet, respectively, the first reactor of the WGS unit

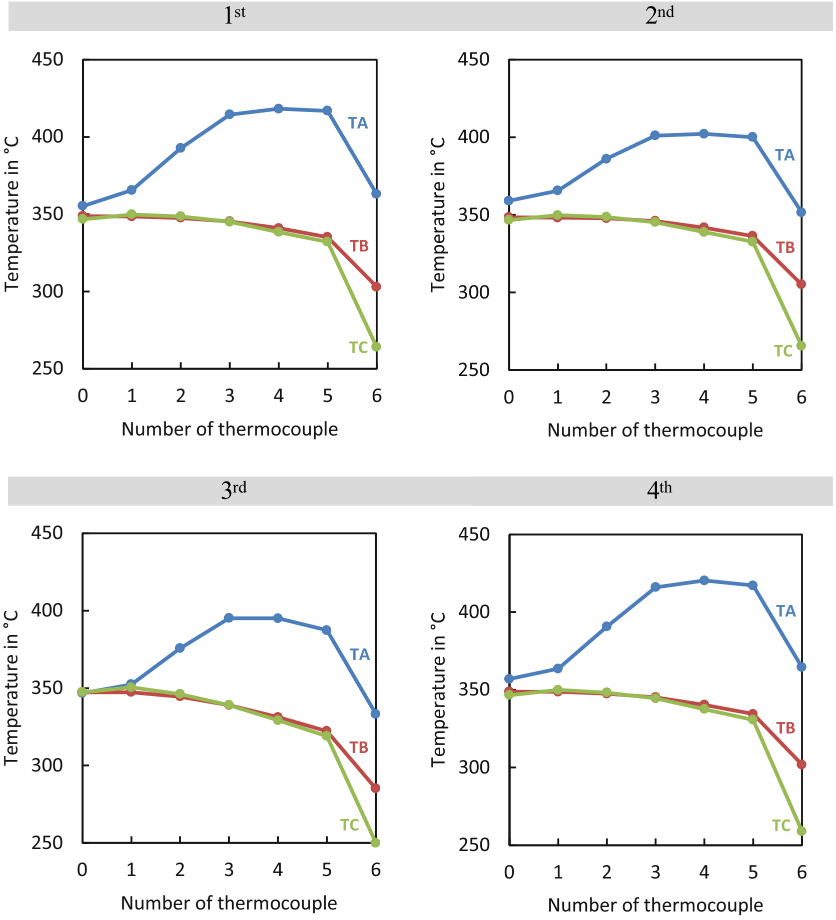

Fig. 4 Temperature profiles along reactors A, B, and C during the first, second, third, and fourth GCMS tar sampling

Table 5 Volumetric concentrations (d.b.) of the main gas components of the processed gas along the WGS unit (DL = 2 cm^3 m^{-3})

	ϕ_{H2} %	ϕ_{CO} %	ϕ_{CO2} %	ϕ_{CH4} %
1st Inlet	38.9	25.4	20.7	10.5
1st Outlet	50.0	1.7	36.5	8.7
2nd Inlet	37.3	23.0	24.1	10.4
2nd Outlet	46.0	1.5	37.7	8.7
3rd Inlet	39.8	25.3	21.1	9.5
3rd Outlet	51.4	1.5	36.2	7.8
4th Inlet	38.6	25.9	21.1	9.9
4th Outlet	51.2	1.8	36.3	8.0

	ϕ_{C2Hy} %	ϕ_{N2} %	ϕ_{O2} %
1st Inlet	2.8	1.5	0.2
1st Outlet	1.9	1.1	0.1
2nd Inlet	2.4	2.0	0.2
2nd Outlet	1.9	2.0	0.2
3rd Inlet	2.5	1.7	0.1
3rd Outlet	1.9	1.1	0.1
4th Inlet	2.6	1.8	0.1
4th Outlet	1.9	0.7	0.03

The measurement was a single sample measurement. Therefore, no standard deviation can be given

3.2 Operating conditions of the water gas shift unit during the GCMS tar samplings

Table 4 shows the operating parameters of the WGS unit during the GCMS tar samplings.

During the first GCMS tar sampling, both the WGS unit and the gasification plant operated at full load. It

Table 6 Volumetric concentrations (d.b.) of the sulfur gas components of the processed gas in the WGS unit (DL = 0.3 cm^3·m^{-3}). The measurement was a single sample measurement. Therefore, no standard deviation can be given

	ϕ_{H2S} cm^3 m^{-3}	ϕ_{COS} cm^3 m^{-3}	ϕ_{C4H4S} cm^3 m^{-3}
1st inlet	93.7	3.1	4.3
1st outlet	89.3	BDL	2.4
2nd inlet	94.5	4.5	5.1
2nd outlet	84.9	BDL	BDL
3rd inlet	88.6	2.7	4.3
3rd outlet	55.2	BDL	1.5
4th inlet	83.6	2.9	3.9
4th outlet	84.3	BDL	3.7

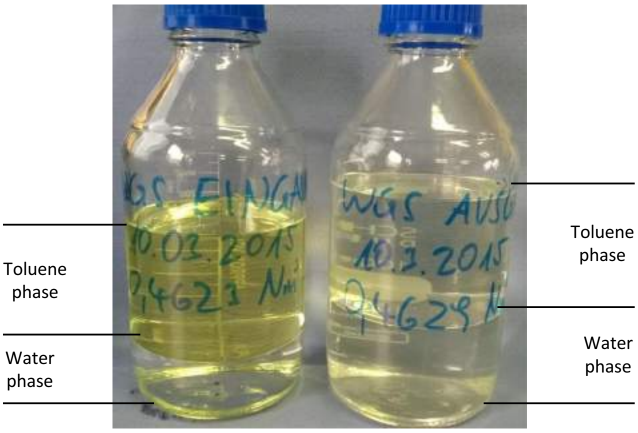

Fig. 5 Picture of a typical tar sample. *Left* before reaching the WGS unit. *Right* after leaving the WGS unit. The *upper phase* is the toluene phase with dissolved tar and the *lower phase* is the water phase

can be seen that the STDGR and the STCR are higher during the second GCMS tar sampling because the gasification plant operated at partial load. During the third tar sampling, the gasification plant operated at full load and the WGS unit at partial load which is indicated by the lower GHSV. During the fourth GCMS tar sampling, the GHSV, STDGR, and STCR were at the same level as for the first GCMS tar sampling.

3.3 Temperature profiles along the water gas shift reactors

Figure 4 shows the temperature profiles along all three WGS reactors during the GCMS tar samplings.

The temperature profiles indicate that most of the exothermic WGS reaction occurred in the first reactor (reactor A). In reactors B and C, nearly no reaction occurred, therefore, the temperature profile decreased along these two reactors due to heat losses exceeding the temperature increase caused by the exothermic reaction.

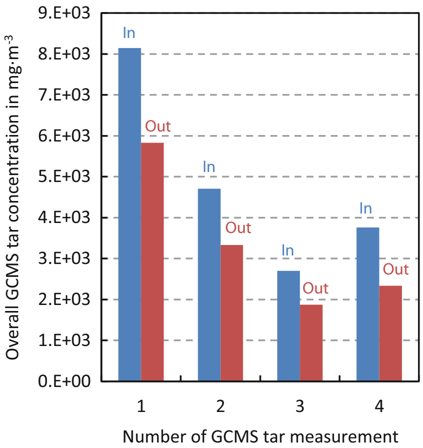

Fig. 6 Overall GCMS tar concentration of all four GCMS tar measurements during the operation of the WGS unit with tar-rich product gas from the gasification plant in Oberwart

During the second GCMS tar sampling, the temperature maximum in reactor A was slightly lower which can be attributed to the lower CO content in the product gas because of the partial load operation of the gasification plant.

During the third sampling, the temperature maximum in reactor A was also lower and the temperature profiles in reactors B and C decreased even more compared to the other GCMS tar samplings. This effect can be attributed to the overall lower volumetric product gas flow rate through the WGS unit caused by the defect membrane gas pump.

3.4 Gas concentrations along the water gas shift unit

Table 5 shows the volumetric concentrations of the measured main gas components during the GCMS tar samplings.

Typical for the partial load operation of the gasification plant was the higher CO_2 content at the inlet of the WGS unit compared to the full load operation of the gasification plant. In this case, it was even higher than the CO content. This can be

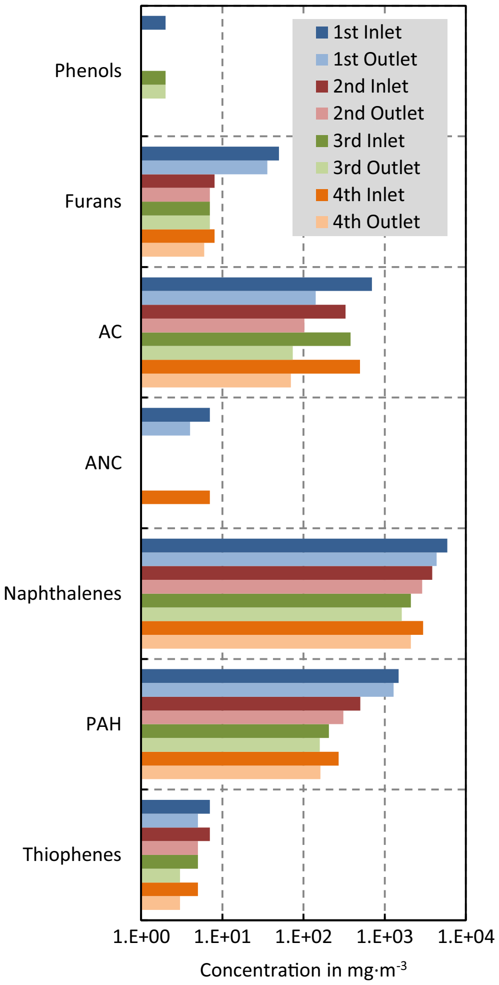

Fig. 7 Concentrations of the tar groups at the inlet and outlet of the WGS unit. Results printed on logarithmic scale

explained by the higher steam to fuel ratio in the gasifier (compare [13]).

Table 6 shows the volumetric concentrations of the measured sulfur components.

It can be seen that the sulfur concentrations were within the same order of magnitude during all GCMS tar samplings. In addition, COS was most likely converted to H_2S along the WGS unit (compare [22]).

3.5 GCMS tar measurements

Figure 5 shows typical GCMS tar samples taken before reaching and after leaving the WGS unit.

The sample which was taken before reaching the WGS unit can be seen on the left, and the sample which was taken after leaving the WGS unit can be seen on the right. The upper phase of a sample is the toluene phase with the dissolved tar and the lower phase is the water phase. In the following, detailed results of all four GCMS tar measurements will be presented.

Figure 6 summarizes the results of all four GCMS tar measurements.

It can be seen that the overall amount of GCMS tar was reduced while passing through the WGS unit because the unit offered a reactive environment with additional residence time. Depending on the measurement, the overall amount of GCMS tar was reduced by 28 to 38 %.

However, the figure also shows that the overall amount of GCMS tar is different for every single measurement. During the first GCMS tar sampling, fresh olivine was used as bed material in the gasifier. With increasing residence time of the olivine in the gasifier, it came to advancing layer formation on the surface of the olivine. These layers improved the catalytic activity of the olivine and, therefore, led to a lower overall tar content in the product gas which was processed in the WGS unit (compare [11]).

Figure 7 shows the amount of the different tar groups according to Table 2.

Based on these results, aromatic components (AC), naphthalenes, and polyaromatic hydrocarbons (PAH) were considered as the significant GCMS tar groups because they were present in a much higher amount than the other tar groups. This could be explained by

Table 7 First GCMS tar measurement in mg m^{-3}

Group	Component	Inlet	Outlet	Δ	δ
Phenols	Phenol	2	BDL	−2	−100 %
Furans	Benzofuran	2	BDL	−2	−100 %
	Dibenzofuran	48	36	−12	−25 %
AC	Phenylacetylene	47	BDL	−47	−100 %
	Styrene	272	32	−240	−88 %
	Mesitylene	BDL	BDL		
	1H-indene	376	109	−267	−71 %
ANC	Isoquinoline	1	BDL	−1	−100 %
	Indole	BDL	BDL		
	Quinoline	6	4	−2	−33 %
Naphthalenes	Naphthalene	5804	4291	−1513	−26 %
	2-Methylnaphthalene	57	38	−19	−33 %
	1-Methylnaphthalene	34	25	−9	−26 %
PAH	Biphenyl	57	44	−13	−23 %
	Acenaphthylene	835	47	−788	−94 %
	Acenaphthene	24	506	+482	+2008 %
	Fluorene	71	56	−15	−21 %
	Anthracene	375	467	+92	+25 %
	Phenanthrene	49	55	+6	+12 %
	4,5-Methylphenanthrene	11	14	+3	+27 %
	Fluoranthene	38	56	+18	+47 %
	Pyrene	29	44	+15	+52 %
Thiophenes	1-Benzothiophene	7	5	−2	−29 %
All	∑	8145	5829	−2316	−28 %

The measurement was a single sample measurement. Therefore, no standard deviation can be given (DL = 1 mg m^{-3})

Table 8 Second GCMS tar measurement in mg m^{-3}

Group	Component	Inlet	Outlet	Δ	δ
Phenols	Phenol	BDL	BDL		
Furans	Benzofuran	BDL	BDL		
	Dibenzofuran	8	7	−1	−13 %
AC	Phenylacetylene	25	BDL	−25	−100 %
	Styrene	166	38	−128	−77 %
	Mesitylene	BDL	BDL		
	1H-indene	138	65	−73	−53 %
ANC	Isoquinoline	BDL	BDL		
	Indole	BDL	BDL		
	Quinoline	1	BDL	−1	−100 %
Naphthalenes	Naphthalene	3822	2870	−952	−25 %
	2-Methylnaphthalene	26	21	−5	−19 %
	1-Methylnaphthalene	18	15	−3	−17 %
PAH	Biphenyl	24	21	−3	−13 %
	Acenaphthylene	233	6	−228	−97 %
	Acenaphthene	37	190	+153	+414 %
	Fluorene	9	6	−3	−33 %
	Anthracene	118	46	−73	−61 %
	Phenanthrene	11	4	−7	−64 %
	4,5-Methylphenanthrene	4	2	−2	−50 %
	Fluoranthene	33	18	−15	−45 %
	Pyrene	30	17	−13	−43 %
Thiophenes	1-Benzothiophene	7	5	−2	−29 %
All	$\sum$	4710	3331	−1379	−29 %

The measurement was a single sample measurement. Therefore, no standard deviation can be given (DL = 1 mg m^{-3})

Table 9 Third GCMS tar measurement in mg m^{-3}

Group	Component	Inlet	Outlet	Δ	δ
Phenols	Phenol	2	2		
Furans	Benzofuran	2	2		
	Dibenzofuran	5	5		
AC	Phenylacetylene	24	BDL	−24	−100 %
	Styrene	190	20	−170	−89 %
	Mesitylene	1	7	+6	+600 %
	1H-indene	165	47	−118	−72 %
ANC	Isoquinoline	BDL	BDL		
	Indole	BDL	BDL		
	Quinoline	1	1		
Naphthalenes	Naphthalene	2060	1595	−465	−23 %
	2-Methylnaphthalene	22	19	−3	−14 %
	1-Methylnaphthalene	15	13	−2	−13 %
PAH	Biphenyl	15	12	−3	−20 %
	Acenaphthylene	128	7	−121	−95 %
	Acenaphthene	17	103	+86	+506 %
	Fluorene	5	5		
	Anthracene	19	15	−4	−21 %
	Phenanthrene	4	3	−1	−25 %
	4,5-Methylphenanthrene	2	2		
	Fluoranthene	8	6	−2	−25 %
	Pyrene	7	6	−1	−14 %
Thiophenes	1-Benzothiophene	5	3	−2	−40 %
All	$\sum$	2697	1873	−824	−31 %

The measurement was a single sample measurement. Therefore, no standard deviation can be given (DL = 1 mg m^{-3})

the fact that the furans (O), ANC (N), and thiophenes (S) contained a heteroatom in the aromatic ring which made them more reactive. In addition, the OH group of the phenols enhances the reactivity. However, each single tar group decreased along the WGS unit. The decrease was based on two effects. First, the WGS reaction which lead to a higher volumetric dry gas flow rate after the WGS unit. Therefore, the dry gas concentrations of all measured components, except hydrogen and carbon dioxide, decreased. Second, the hydrogenation and decomposition reactions involving tar components. The content of the furans, naphthalenes, PAH, and thiophenes was most probably not significantly decreased by chemical reaction. The decrease mainly occurred because of the about 20 % higher volumetric dry gas flow rate after the WGS unit. The results regarding naphthalene were in agreement with the results gathered by Devi et al. [4] who reported that an increasing amount of H_2 in the product gas leads to a decrease in naphthalene conversion.

In contrast, the concentration of the phenols, AC, and ANC was most probably decreased by hydrogenation and decomposition reactions. The decrease caused by hydrogenation and decomposition reactions significantly exceeded the decrease caused by the higher volumetric dry gas flow rate after the WGS unit.

Based on the detailed results (see Tables 7, 8, 9, and 10), it can be seen that phenylacetylene, styrene, 1H-indene, naphthalene, and acenaphthylene were contained in a much higher amount at the inlet of the WGS unit in all four GCMS tar measurements.

4 Conclusion and outlook

The varying GCMS tar compositions at the inlet of the WGS unit could be explained by the bed material used, which was olivine. Fresh olivine has significantly less catalytic activity. Therefore, the tar content with fresh olivine is much higher. In contrast, used olivine has significantly higher catalytic activity and, therefore, the tar content is significantly lower [11].

Table 10 Fourth GCMS tar measurement in mg m^{-3}

Group	Component	Inlet	Outlet	Δ	δ
Phenols	Phenol	BDL	BDL		
Furans	Benzofuran	2	2		
	Dibenzofuran	6	4	−2	−33 %
AC	Phenylacetylene	25	BDL	−25	−100 %
	Styrene	253	31	−222	−88 %
	Mesitylene	BDL	BDL		
	1H-indene	220	39	−181	−82 %
ANC	Isoquinoline	BDL	BDL		
	Indole	4	BDL	−4	−100 %
	Quinoline	3	BDL	−3	−100 %
Naphthalenes	Naphthalene	2925	2069	−856	−29 %
	2-Methylnaphthalene	28	15	−13	−46 %
	1-Methylnaphthalene	19	10	−9	−47 %
PAH	Biphenyl	25	17	−8	−32 %
	Acenaphthylene	196	3	−193	−98 %
	Acenaphthene	26	122	+96	+369 %
	Fluorene	5	2	−3	−60 %
	Anthracene	13	9	−4	−31 %
	Phenanthrene	1	1		
	4,5-Methylphenanthrene	BDL	BDL		
	Fluoranthene	3	4	+1	+33 %
	Pyrene	3	4	+1	+33 %
Thiophenes	1-Benzothiophene	5	3	−2	−40 %
All	∑	3762	2335	−1427	−38 %

The measurement was a single sample measurement. Therefore, no standard deviation can be given (DL = 1 mg m^{-3})

According to the operators of the gasification plant, the bed material had been recently changed before the first GCMS tar measurement. This could explain the significantly higher GCMS tar content at the inlet and the outlet of the WGS unit during the first GCMS tar measurement.

However, the operating conditions of the gasification plant and the WGS unit did not affect the efficiency of the GCMS tar reduction.

The significant GCMS tar components were the AC, the naphthalenes, and the PAH. In passing through the WGS unit, the decrease of the AC was significantly higher than that of the naphthalenes and the PAH. However, beside the increase of the hydrogen content, the WGS unit was able to decrease the GCMS tar content by about 28 to 38 %.

Consequently, the presented results could lead to a simpler tar cleaning process step in the gasification plant process by means of a different and more economical scrubbing agent being used for the gas scrubber when a WGS unit is employed in the process in order to increase the hydrogen content of the product gas.

Acknowledgments Open access funding provided by TU Wien (TUW). The authors want to thank Air Liquide, Guessing Renewable Energy GmbH, and ISG Energy GmbH for making this research possible. In addition, the plant operators of the CHP plant in Oberwart are gratefully acknowledged.

The authors also thank Binder-Industrieanlagenbau for constructing the WGS unit as well as the company Clariant for providing the Fe/Cr-based catalyst (ShiftMax 120).

Robert Bardolf and Matthias Kuba are gratefully acknowledged for the lively discussions regarding the behavior of the GCMS tar components.

Finally, Silvester Fail is thanked for designing, building, and optimizing the WGS unit in Oberwart, Austria.

This work was carried out within the framework of the Bioenergy2020+ GmbH project "C20005 Polygeneration III." Bioenergy2020+ GmbH is funded by the states Burgenland, Niederoesterreich, and Steiermark and within the Austrian COMET program which is managed by the Austria Research Promoting Agency (FFG).

Open Access This article is distributed under the terms of the Creative Commons Attribution 4.0 International License (http://creativecommons.org/licenses/by/4.0/), which permits unrestricted use, distribution, and reproduction in any medium, provided you give appropriate credit to the original author(s) and the source, provide a link to the Creative Commons license, and indicate if changes were made.

References

1. CEN (2006) Biomass Gasification. Tar and Particles in Product Gases. Sampling and Analysis, CEN/TS 15439:2006; European Committee for Standardization (CEN): Brussels, Belgium
2. D. Dayton. A review of the literature on catalytic biomass tar destruction. Technical Report NREL/TP-510-32815, National Renewable Energy Laboratory (NREL), 2002.
3. Devi L, Ptasinski KJ, Janssen FJ (2003) A review of the primary measures for tar elimination in biomass gasification processes. Biomass Bioenerg 24:125–140. doi:10.1016/S0961-9534(02)00102-2
4. Devi L, Ptasinski KJ, Janssen FJ, van Paasen SV, Bergman PC, Kiel JH (2005) Catalytic decomposition of biomass tars: use of dolomite and untreated olivine. Renew Energ 30(4):565–587. doi:10.1016/j.renene.2004.07.014
5. N Diaz. *Hydrogen Separation from Producer Gas Generated by Biomass Steam Gasification*. PhD thesis, Vienna University of Technology, 2013.
6. Fail S, Diaz N, Benedikt F, Kraussler M, Hinteregger J, Bosch K, Hackel M, Rauch R, Hofbauer H (2014) Wood gas processing to generate pure hydrogen suitable for PEM fuel cells. *ACS Sustain Chem Eng* 2(12):2690–2698. doi:10.1021/sc500436m
7. Hofbauer H, Rauch R, Bosch K, Koch R, Aichernig C (2002) Biomass CHP plant guessing—a success story. In: Expert meeting on pyrolysis and gasification of biomass and waste, Strasbourg, France
8. H. Huettler, R. Rauch, and H. Hofbauer. Tar formation in a dual fluidised bed biomass steam gasification plant: quantification and influencing parameters. In BioEuro Success and Visions for Bioenergy, Salzburg, Austria, 2007.
9. Kaltschmitt M, Hartmann H, Hofbauer H (2009) Energie aus biomasse. Springer-Verlag
10. Kiel J (2004) Primary measures to reduce tar formation in fluidised-bed biomass gasifiers. Technical report, ECN Biomass

11. Kirnbauer F, Wilk V, Kitzler H, Kern S, Hofbauer H (2012) The positive effects of bed material coating on tar reduction in a dual fluidized bed gasifier. Fuel 95:553–562. doi:10.1016/j.fuel.2011.10.066
12. Kirnbauer F, Wilk V, Hofbauer H (2013) Performance improvement of dual fluidized bed gasifiers by temperature reduction: the behavior of tar species in the product gas. Fuel 108:534–542. doi:10.1016/j.fuel.2012.11.065
13. Koppatz S, Pfeifer C, Hofbauer H (2011) Comparison of the performance behaviour of silica and olivine in a dual fluidised bed reactor system for steam gasification of biomass at pilot plant scale. Chem Eng J 175:468–483. doi:10.1016/j.cej.2011.09.071
14. M. Kraussler, M. Binder, S. Fail, K. Bosch, M. Hackel, and H. Hofbauer. Performance of a water gas shift unit processing product gas from biomass steam gasification. In *Proceedings of the 23rd European Biomass Conference and Exhibition*, Vienna, Austria, pages 668–678, 2015.
15. Kraussler M, et al (2016) 2250-h long term operation of a water gas shift pilot plant processing tar-rich product gas from an industrial scale dual fluidized bed biomass steam gasification plant. Int J Hydrog Energy. doi:10.1016/j.ijhydene.2016.02.137
16. M Kuebel. *Teerbildung und Teerkonversion bei der Biomassevergasung*. PhD thesis, University of Stuttgart, Germany, 2007.
17. Li C, Suzuki K (2009) Tar property, analysis, reforming mechanism and model for biomass gasification—an overview. Renew Sustain Energ Rev 13(3):594–604. doi:10.1016/j.rser.2008.01.009
18. Milne T, Abatzoglou N, Evans R (1998.) Biomass gasifier "tars": their nature, formation and conversion. Technical Report Report No. NREL/TP-570-25357. National Renewable Energy Laboratory (NREL), Golden, Colorado
19. Rabou L, Zwart R, Vreugdenhil B, Bos L (2009) Tar in biomass producer gas; the Energy Research Centre of The Netherlands (ECN) experience: an enduring challenge. Energ Fuels 23:6189–6198. doi:10.1021/ef9007032
20. Rehling B, Hofbauer H, Rauch R, Aichernig C (2011) BioSNG—process simulation and comparison with first results from a 1-MW demonstration plant. Biomass Conv Bioref 1:111–119. doi:10.1007/s13399-011-0013-3
21. Sauciuc A, Abosteif Z, Weber G, Potetz A, Rauch R, Hofbauer H, Schaub G, Dumitrescu L (2012) Influence of operating conditions on the performance of biomass-based Fischer-Tropsch synthesis. Biomass Conv Bioref 2(3):253–263. doi:10.1007/s13399-012-0060-4
22. Twigg MV (1989) Catalyst handbook. CRC Press, Boca Raton, Florida
23. Weber G, Rauch R, Hofbauer H (2015) Influence of ethylene on the formation of mixed alcohols over a MoS_2 catalyst using biomass-derived synthesis gas. Biomass Conv Bioref 5(1):85–94. doi:10.1007/s13399-014-0140-8
24. Wolfesberger U, Aigner I, Hofbauer H (2009) Tar content and composition in producer gas of fluidized bed gasification of wood—influence of temperature and pressure. Environ Prog Sustain Energ 28(3):372–379. doi:10.1002/ep.10387
25. Wolfesberger-Schwabl U, Aigner I, Hofbauer H (2012) Mechanism of tar generation during fluidized bed gasification. Ind Eng Chem Res 51:13001–13007. doi:10.1021/ie300827d
26. Zhang R, Brown RC, Suby A, Cummer K (2005) Catalytic destruction of tar in biomass derived producer gas. Energ Conv Manag 45:995–1014. doi:10.1016/j.enconman.2003.08.016

Paper 4

Michael Kraussler, Matthias Binder, Hermann Hofbauer, Performance of a water gas shift unit processing tar-rich product gas from a commercial biomass steam gasification plant operating at partial load, International Journal of Oil, Gas and Coal Technology, Volume 14, Issue 1-2, 2017, Pages 32-48, `http://dx.doi.org/10.1504/IJOGCT.2017.081098`.

Contribution: Experimental work, data treatment, writing

Performance of a water gas shift unit processing tar-rich product gas from a commercial biomass steam gasification plant operating at partial load

Michael Kraussler* and Matthias Binder

Bioenergy2020+ GmbH,
Wienerstrasse 49, 7540 Guessing, Austria
Email: michael.kraussler@bioenergy2020.eu
Email: matthias.binder@bioenergy2020.eu
*Corresponding author

Hermann Hofbauer

Institute of Chemical Engineering,
TU Wien,
Getreidemarkt 9, 1060 Wien, Austria
Email: hermann.hofbauer@tuwien.ac.at

Abstract: In this paper, the performance of a water gas shift unit processing product gas from a commercial dual fluidised bed biomass steam gasification plant is studied. The experiments were carried out during a partial load operation of the gasification plant. In order to investigate a water gas shift process, a water gas shift unit, located at the site of the gasification plant in Oberwart, Austria, was used. The water gas shift unit consisted of three reactors in series filled with a commercial Fe/Cr-based catalyst and was operated with tar-rich product gas. No performance decrease of the water gas shift unit was observed during the partial load operation of the gasification plant. Furthermore, a CO conversion of 92% and a GCMS tar reduction of about 30% were reached. In addition, it was found that partial load operation of the gasification plant did not negatively affect the performance of the water gas shift unit. [Received: December 23, 2015; Accepted: April 24, 2016]

Keywords: biomass; steam gasification; dual fluidised bed; DFB; hydrogen; product gas; water gas shift; WGS; partial load operation; tar-rich product gas; commercial Fe/Cr-based catalyst.

Reference to this paper should be made as follows: Kraussler, M., Binder, M. and Hofbauer, H. (2017) 'Performance of a water gas shift unit processing tar-rich product gas from a commercial biomass steam gasification plant operating at partial load', *Int. J. Oil, Gas and Coal Technology*, Vol. 14, Nos. 1/2, pp.32–48.

Biographical notes: Michael Kraussler studied Chemical Engineering at the TU Wien. After his graduation in August 2014, he started his PhD at the Bioenergy 2020+ GmbH and the TU Wien in the field of gasification and product gas conditioning.

Matthias Binder is currently working as a Junior Researcher at Bioenergy 2020+ GmbH in the field of gasification and synthesis of mixed alcohols. He is also pursuing his PhD in Chemical Engineering at the TU Wien.

Copyright © 2017 Inderscience Enterprises Ltd.

Hermann Hofbauer is a Full Professor at the TU Wien, Institute of Chemical Engineering and he is leading the research group Future Energy Technology. He holds a Masters in Mechanical Engineering, a PhD in Energy Technology and is Docent in Chemical Engineering. For more than 20 years he has been the Austrian representative in IEA-Bioenergy in several tasks (e.g., combustion, gasification) as well in the executive committee. In 2012 he received the prestigious Linneborn Award for the life time scientific work in the field of biomass utilisation at the European Biomass Conference in Milano 2012.

This paper is a revised and expanded version of a paper entitled 'Performance of a water gas shift pilot plant processing tar-rich product gas from a commercial biomass steam gasification plant operating at partial load conditions' presented at IBSCE 2015, Shanghai, 21–23 October 2015.

1 Introduction

Today, hydrogen is an important resource for a lot of applications in industry (Liu et al., 2010). The production is mainly based on fossil feedstock. Against a background of climate change, a CO_2 neutral method for hydrogen production should be established (Balat and Kirtay, 2010). Biomass steam gasification is a proven technology and a promising CO_2 neutral alternative to state of the art steam reforming processes which are mainly used for hydrogen production (Mueller, 2013).

A well-established technology for biomass steam gasification is the dual fluidised bed (DFB) process (Kaltschmitt et al., 2009; Proell et al., 2007). The commercial DFB biomass steam gasification plants in Guessing and Oberwart have been using this technology for several years. Both gasification plants generate a product gas with a volumetric hydrogen content of about 38 % which makes this product gas a promising CO_2 neutral hydrogen source (Diaz, 2013). A process which can further increase the H_2 content in the product gas is the exothermic water gas shift (WGS) reaction [see equation (1)].

$$CO + H_2O \leftrightarrow CO_2 + H_2 \quad \Delta H = -41.1\,\text{kJ}\cdot\text{mol}^{-1} \tag{1}$$

It converts carbon monoxide and steam to hydrogen and carbon dioxide. In order to reach economic reaction rates, catalysts are necessary. A suitable catalyst is a Fe/Cr-based catalyst. Fe/Cr-based catalysts seem to be robust against sulphur poisoning at H_2S amounts which are contained in the product gas of the DFB biomass steam gasification plants (Fail, 2014; Twigg, 1997).

The Fe/Cr-based catalyst is used since the beginning of the twentieth century as a high temperature catalyst for the WGS reaction (Rhodes et al., 1995). It was developed by the company BASF in order to improve the hydrogen yield for the ammonia production (Boon et al., 1992; Chinchen et al., 1984; Gottschalk et al., 1988; Shchibrya et al., 1965). Today, volumetric CO concentrations of about 1% can be reached with commercial Fe/Cr-based catalysts (Twigg, 1997).

By adding a low temperature copper-containing catalyst, volumetric CO concentrations of about 0.1 % can be reached (Twigg, 1997). However, these catalysts are highly sensitive to sulphur poisoning at sulphur levels higher than 100 $mm^3 \cdot m^{-3}$ (Rhodes et al., 1995). Therefore, the copper-containing catalysts cannot be used with the product gas of DFB biomass steam gasification plants because the product gas contains about 100 $cm^3 \cdot m^{-3}$ H_2S.

For this work, a WGS unit, employing a commercial Fe/Cr-based catalyst, was operated with real, tar-rich product gas from the commercial gasification plant in Oberwart, Austria. The WGS unit was operated with product gas which was extracted before a rapeseed methyl ester (RME) gas scrubber for more than 2,000 hours while the gasification plant operated at full load and for more than 100 hours while the gasification plant operated at partial load. The latter is the main topic of this paper. The performance of the WGS unit regarding the partial load operation of the gasification plant is investigated.

This work was carried out within the framework of the Bioenergy2020+ GmbH project ‘C20005 Polygeneration III’. Bioenergy2020+ GmbH is funded by the states Burgenland, Niederoesterreich, Steiermark, and within the Austrian COMET program which is managed by the Austrian Research Promoting Agency (FFG). In addition, the project partners Air Liquide, Guessing Renewable Energy GmbH, and ISG Energy GmbH are acknowledged.

2 Materials and methods

The experimental work was carried out at the site of the DFB biomass steam gasification plant in Oberwart, Austria, where the WGS unit is located. The WGS unit consisted of three fixed bed reactors in series which employed a commercial Fe/Cr-based catalyst. The gas composition and the steam content were measured before and after each reactor. The temperature profile along each reactor was recorded. This allowed judging the activity of the commercial Fe/Cr-based catalyst. In addition, ammonia and GCMS tar concentrations were determined at the inlet and the outlet of the WGS unit.

2.1 The DFB biomass steam gasification plant

The WGS unit processed tar-rich product gas which was extracted from the DFB biomass steam gasification plant in Oberwart which works as a combined heat and power (CHP) plant.

Figure 1 shows a simplified flowchart of the applied process which is described in detail in Kaltschmitt et al. (2009) and Proell et al. (2007). The gasification plant generates district heat and electricity from a high calorific, hydrogen rich and nitrogen free product gas with biomass (woodchips) as feedstock. The basic working principle of the gasification plant can be reviewed in Kraussler et al. (2015).

Figure 1 Simplified flowchart of the gasification plant in Oberwart, Austria (see online version for colours)

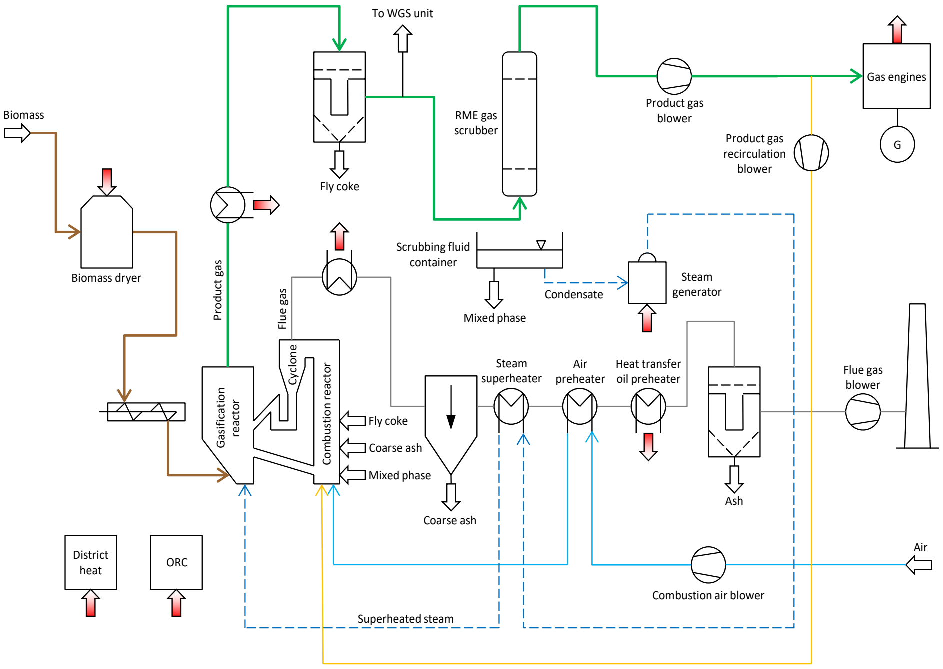
To WGS unit
Biomass
Fly coke
RME gas scrubber
Product gas blower
Gas engines
Product gas recirculation blower
G
Biomass dryer
Product gas
Flue gas
Scrubbing fluid container
Mixed phase
Condensate
Steam generator
Cyclone
Gasification reactor
Combustion reactor
Fly coke
Coarse ash
Mixed phase
Steam superheater
Air preheater
Heat transfer oil preheater
Flue gas blower
Coarse ash
Ash
District heat
ORC
Air
Combustion air blower
Superheated steam

Note: Also showing the experimental extraction point for tar-rich product gas.

Table 1 Volumetric product gas compositions (d.b.) of the main gas components of the gasification plant in Oberwart, Austria, at full load (Diaz, 2013) and partial load operation

Component	*Full load*	*Partial load*	*Units*
φ_{H2}	~38	~38	%
φ_{CO}	~24	~23	%
φ_{CO2}	~22	~26	%
φ_{CH4}	~10	~10	%
φ_{Others}	~6	~3	%

The average product gas compositions at full and partial load operation can be seen in Table 1. It is possible to take a partial flow of the tar-rich product gas for experimental work from an extraction point along the product gas line (see Figure 1). The extraction point is located before the RME gas scrubber. Therefore, the extracted product gas contains a higher amount of tar which is a challenge for a reliable operation of the WGS unit. However, at this extraction point, the product gas has already a higher water content as well as a higher temperature which is more favourable for the WGS reaction compared to the conditions at an extraction point, for example, after the RME gas scrubber.

Table 2 shows the conditions at the extraction point during the full and the partial load operation of the gasification plant. During the investigation regarding the partial load behaviour of the WGS unit, the product gas was taken from the extraction point for about 100 hours while the gasification plant operated at partial load. At full load operation of the gasification plant, the results of the performance of the WGS unit operation can be reviewed in Kraussler et al. (2015).

Table 2 Operating conditions at the extraction point (see Figure 1) at the gasification plant in Oberwart, Austria, at full load operation (Kraussler et al., 2015) and partial load operation

Parameter	*Full load*	*Partial load*	*Units*
Temperature	~150	~150	°C
φ_{H2O}	~35	~46	%
GCMS tar content	~8.2	~4.7	$g \bullet m^{-3}$

2.2 The WGS unit

The experimental work was carried out at a WGS unit located at the site of the gasification plant in Oberwart. Figure 2 shows a simplified flowchart of the WGS unit. The unit employed a commercial Fe/Cr-based high temperature WGS catalyst in all three reactors. The catalyst had a bulk density of 1.24 $kg \bullet dm^{-3}$ and the catalyst discs had a diameter of 6 mm and a height of 3 mm.

Figure 2 Simplified flowchart of the WGS unit located at the site of the gasification plant in Oberwart (see online version for colours)

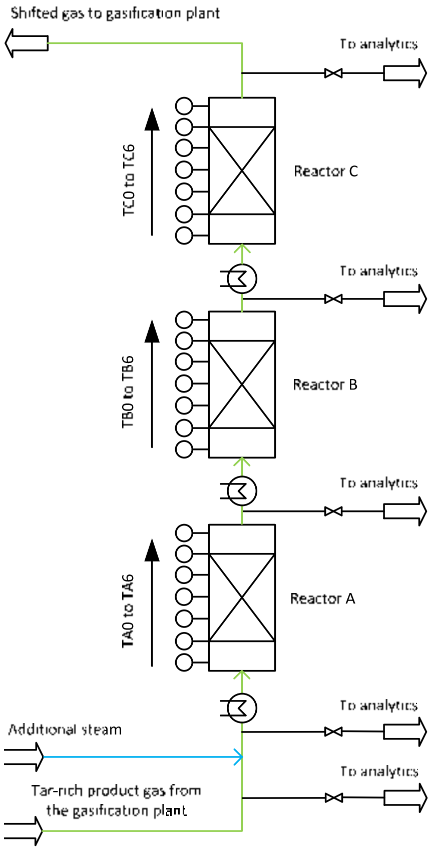
Shifted gas to gasification plant
To analytics
TC0 to TC6
Reactor C
To analytics
TB0 to TB6
Reactor B
To analytics
TA0 to TA6
Reactor A
To analytics
Additional steam
To analytics
Tar-rich product gas from the gasification plant

The same WGS unit was used for the experimental work in Kraussler et al. (2015) where the design of the unit can be reviewed (also see Fail, 2014).

A partial flow of the processed gas was successively sent to the analytical devices from four positions along the WGS unit.

Seven type J thermocouples along each reactor were used in order to observe and record the temperature profiles. This allowed judging the activity of the used catalyst. Thermocouples 0 and 6were not in the reactive zone of the catalyst bed of the reactors.

2.3 Measurement of the gas composition and the steam content of the processed product gas

A gas chromatograph (GC) measured the dry gas composition before and after each WGS reactor. Before the analyses in the GC, the sample gas stream was led through two gas washing bottles filled with ethylene glycol cooled to about −5°C in order to condense the steam. Therefore, a dry gas stream could be assumed after the two gas washing bottles. The dry gas stream passed another gas washing bottle filled with glass wool in order to prevent aerosols from entering the GC. After the glass wool, a gas meter recorded the volumetric dry gas flow. In addition, the GC was calibrated for all detected components with the expected concentrations.

In the GC, a thermal conductivity detector (TCD) enabled the quantification of the CO, CO_2, CH_4, N_2, O_2, C_2H_6, C_2H_4 and C_2H_2. The C_2 species were summarised and are referred to as C_2H_y. A flame photometric detector (FPD) was used to detect the H_2S, COS and C_4H_4S. The H_2 content was determined by calculation. Because helium was used as carrier gas, the H_2 could not be quantified by the GC.

The steam content in the processed gas was gravimetrically determined and the volumetric dry gas flow rate was determined by closing the water balance along the WGS unit.

The gas volumes and the volumetric gas flow rates in this work are always given at standard temperature and pressure (STP, 273.15 K and 101,325 Pa).

2.4 Ammonia and GCMS tar measurements

Both, the ammonia and the GCMS tar samplings were carried out according to the instructions of the Test Laboratory for Combustion System at the TU Wien.

Figure 3 Principle of the ammonia sampling (see online version for colours)

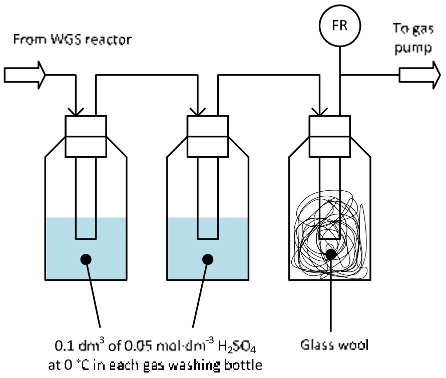
From WGS reactor
FR
To gas pump
0.1 dm³ of 0.05 mol·dm⁻³ H₂SO₄ at 0 °C in each gas washing bottle
Glass wool

For the ammonia sampling, a partial flow of the processed gas was successively extracted from the inlet (before reactor A) and the outlet (after reactor C) of the WGS unit. The extracted gas stream was led through two cooled gas washing bottles filled with 0.05 mol•dm^{-3} H_2SO_4 which was used as solvent for the ammonia. Figure 3 shows the principle of the ammonia sampling. For the determination of the ammonia content, the samples were handed over to the Test Laboratory for Combustion System at the TU Wien.

For the tar sampling, again, a partial flow of the processed gas was successively extracted from the inlet (before reactor A) and the outlet (after reactor C) of the WGS unit. A sample stream of the product gas passed five gas washing bottles filled with 0.5 dm^3 toluene in all and one gas washing bottle filled with glass wool in order to prevent aerosols from entering the analytic gas pump. The first three gas washing bottles were cooled to about 0°C. Consequently, the tar was dissolved and the steam condensed. The next two gas washing bottles were cooled to –8°C in order to make sure that all other remaining tar components were finally dissolved in the toluene. The gas was sampled for about 3 h. In addition, the volumetric dry gas flow was recorded by a gas meter. The dry gas sampling flow rate was set to 2.0 to 2.5 dm^3•min^{-1} (compare Figure 4).

Figure 4 Principle of the tar sampling (see online version for colours)

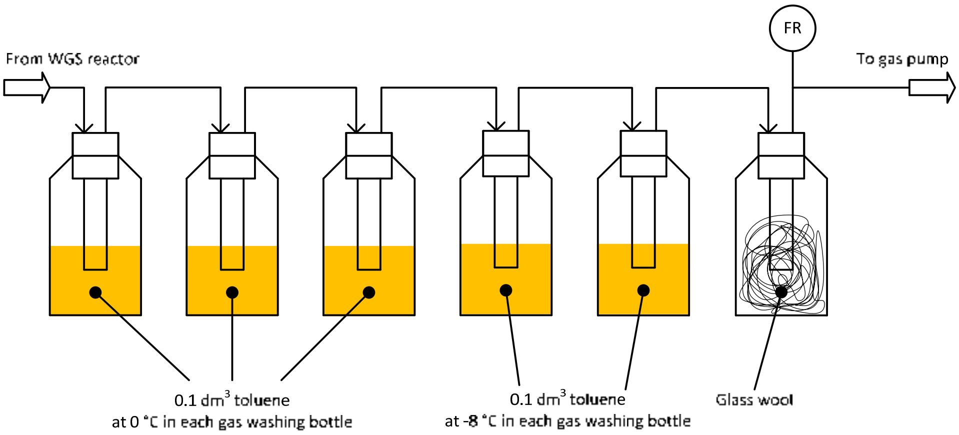

Toluene as tar solvent has the advantage that it allows the simultaneous determination of the tar and the water content. However, it does not allow the determination of benzene, toluene, ethylbenzene and xylenes (BTEX).

After the sampling, the content of all gas washing bottles was mixed and the sample was handed over to the Test Laboratory for Combustion System at the TU Wien in order to determine the detailed GCMS tar concentrations.

2.5 *Characteristic figures of the WGS unit*

The operating conditions of the WGS unit were described by the following four figures:

$$\text{GHSV} = \frac{\dot{V}_{Dry}}{V_{Catalyst}} \tag{2}$$

$$\text{STDGR} = \frac{\dot{V}_{H2O}}{\dot{V}_{Dry}} \tag{3}$$

$$\text{STCR} = \frac{\dot{V}_{H2O}}{\dot{V}_{Dry} \cdot \left(\varphi_{CO} + \varphi_{CO2} + \varphi_{CH4} + \varphi_{C2Hy}\right)} \tag{4}$$

$$X_{CO} = \frac{\dot{V}_{Dry,IN}\varphi_{CO,IN} - \dot{V}_{Dry,OUT}\varphi_{CO,OUT}}{\dot{V}_{Dry,IN}\varphi_{CO,IN}} \tag{5}$$

The gas hourly space velocity [GHSV, equation (2)] describes the stress of the catalyst. The steam to dry gas ratio [STDGR, equation (3)] and the steam to carbon ratio [STCR, equation (4)] are an indicator if coking effects and carbon deposition could be a problem during the operation of the WGS unit. The CO conversion [X_{CO}, equation (5)] describes how much carbon monoxide was converted along the overall WGS unit.

The GHSV, the STDGR and the STCR were calculated for the inlet of the first reactor of the WGS unit.

3 Results and discussion

This chapter presents the results of the experiments which were carried out during a partial load operation of the gasification plant. First, the operating data of the WGS unit are presented. Second, the concentrations of the product gas components along the WGS unit are shown. Third, the CO conversions and the temperature profiles along the reactors of the WGS unit are discussed. Finally, the results of the ammonia and GCMS tar measurements are shown.

3.1 Operating data of the WGS unit during the partial load operation of the gasification plant

Table 3 shows the operating data of the WGS unit during the partial load operation of the gasification plant which lasted about 100 hours. The amount of additional steam was set to maximum, resulting in an overall volumetric steam flow rate of 2.2 $m^3 \cdot h^{-1}$ in order to protect to Fe/Cr-based catalyst from coking and carbon deposition. In addition, the gas pump of the WGS unit, which extracted the product gas from the gasification plant, operated at full load.

Table 3 Operating data of the WGS unit

Load	*GHSV* h^{-1}	*STDGR*	*STCR*	X_{CO} *%*
Partial	465	1.9	3.2	92
Full	478	1.6	2.6	94

Note: The GHSV, the STDGR and the STCR are given for inlet of the first reactor. The X_{CO} is given for the whole WGS unit.

The resulting STDGR and the STCR show that the steam content of the product gas was higher during the partial load operation of the gasification plant than during a full load operation. The steam fluidisation of the gasifier was kept at the same level during the partial load operation as during a full load operation. In addition, less biomass was fed into the system which resulted in the higher steam content of the product gas.

Nevertheless, despite the fact that the gasification plant worked at partial load, an overall CO conversion of 92 % was reached which was in the same order of magnitude as during a full load gasification plant operation (compare Kraussler et al., 2015). In general, a higher STDGR and STCR enhance the WGS reaction according to the principle of least constraints.

3.2 Gas composition along the WGS unit

Table 4 shows the concentrations of the measured non-sulphur gas components of the processed gas at the inlet and the outlet of all three WGS reactors.

Table 4 Volumetric concentrations (d.b.) of the measured non-sulphur gas components during the 100 hours of partial load operation (DL = 2 $cm^3 \cdot m^{-3}$)

	φ_{H2} %	φ_{CO} %	φ_{CO2} %	φ_{CH4} %
Inlet	37.1 ± 0.9	22.7 ± 0.6	25.2 ± 0.7	10.4 ± 0.4
Outlet A	47.1 ± 1.0	4.3 ± 0.5	36.2 ± 0.6	8.9 ± 0.3
Outlet B	47.9 ± 1.0	2.3 ± 0.1	37.5 ± 0.7	8.7 ± 0.3
Outlet C	48.1 ± 0.8	1.5 ± 0.1	38.1 ± 0.4	8.7 ± 0.3
	φ_{C2Hy} %	φ_{N2} %	φ_{O2} %	
Inlet	2.5 ± 0.3	2.0 ± 0.7	0.08 ± 0.02	
Outlet A	2.0 ± 0.2	1.5 ± 0.5	0.03 ± 0.01	
Outlet B	2.0 ± 0.2	1.6 ± 0.7	0.03 ± 0.01	
Outlet C	1.9 ± 0.2	1.6 ± 0.5	0.03 ± 0.01	

It can be seen that most of the WGS reaction occurred in reactor A. In reactors B and C, less WGS reaction occurred because of the unfavourable temperature level for the equilibrium composition. The H_2 content was significantly increased along the overall WGS unit (up to a volumetric fraction of 48.1%).

In addition, Table 4 shows that the CO_2 content at the inlet of the WGS unit was higher than the CO content. This effect was caused by the partial load operation of the gasification plant. Typically, the CO content in the product gas is slightly higher than the CO_2 content if the gasification plant operates at full load (see Table 1). The higher steam content caused an increase of the WGS reaction according to the principle of least constraint.

The concentrations of the other components decreased because of the dilution effect which was caused by the higher volumetric dry gas flow rate after a WGS reactor. According to these results, no other reactions occurred. In addition, the standard deviations in Table 4 indicate steady operating conditions during the 100 hours of partial load operation.

Table 5 Volumetric concentrations (d.b.) of the measured sulphur components during the 100 hours of partial load operation (DL = 0.3 $cm^3•m^{-3}$)

	$\varphi_{H2S}\ cm^3•m^{-3}$	$\varphi_{COS}\ cm^3•m^{-3}$	$\varphi_{C4H4S}\ cm^3•m^{-3}$
Inlet	101 ± 9	1.5 ± 0.5	4.7 ± 0.8
Outlet A	104 ± 11	BDL	4.0 ± 0.7
Outlet B	101 ± 18	BDL	3.8 ± 1.2
Outlet C	106 ± 10	BDL	3.9 ± 0.7

Table5 shows the concentrations of the sulphur components of the processed gas at the inlet and after all three reactors of the WGS unit.

It can be seen that the C_4H_4S content remained at about the same level along all three reactors. In contrast, the COS content of the product gas decreased below the detection limit (BDL).

Table 5 also indicates that the COS was most probably partially converted to H_2S along the WGS unit because the COS concentration decreased BDL and the H_2S concentration slightly increased.

These results could also be observed during a full load operation of the gasification plant (see Kraussler et al., 2015).

3.3 Behaviour of the reactive species and the carbon monoxide conversion along the WGS unit

Figure 5 shows the profile of the reactive species (CO, CO_2 and H_2) along the WGS unit. It also indicates that most of the WGS reaction occurred in reactor A. This was also observed during full load operation of the gasification plant.

Figure 5 Concentration profiles of the reactive species along all three reactors of the WGS unit during the partial load operation of the gasification plant (see online version for colours)

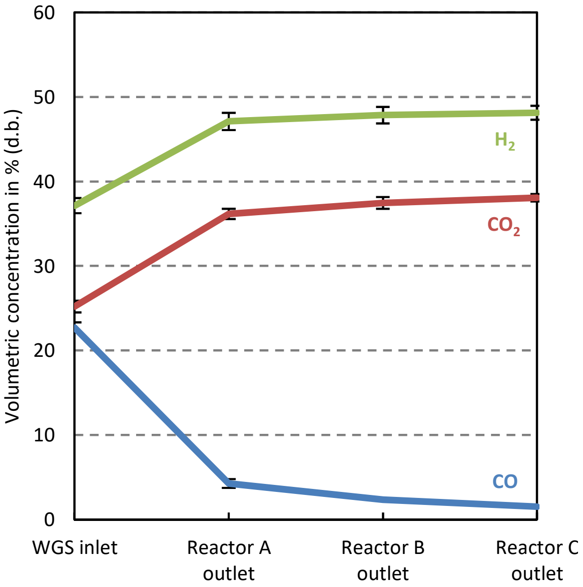

Figure 6 CO conversion of all three reactors of the WGS unit based on the inlet concentration of every single reactor during the partial load operation of the gasification plant (see online version for colours)

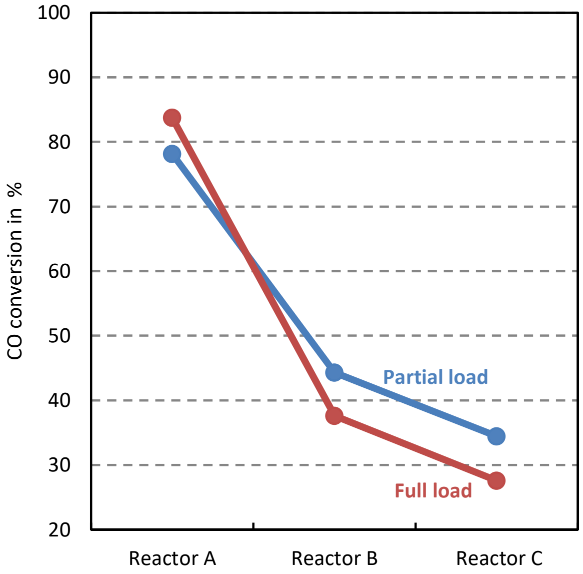

Figure 7 CO conversion of all three reactors of the WGS unit based on the inlet concentration of reactor a during the partial load operation of the gasification plant (see online version for colours)

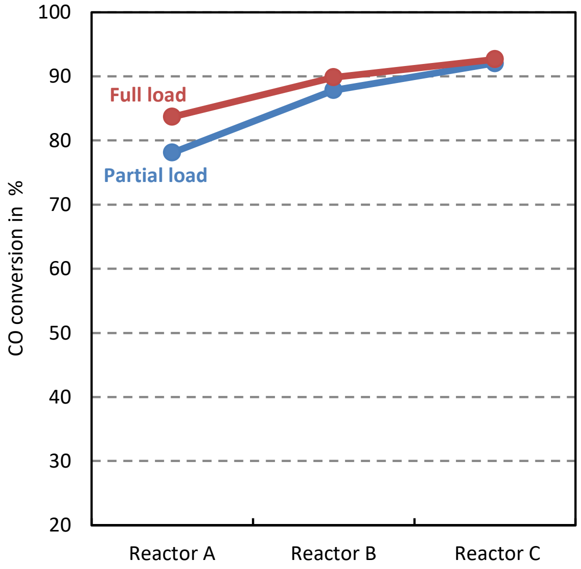

Figures 6 and 7 show the CO conversions of all three reactors of the WGS unit based on the inlet concentration of every single reactor and based on the inlet concentration of reactor A. It can be seen that a CO conversion of nearly 80% was reached in reactor A during the partial load operation of the gasification plant. In reactor B, respectively, reactor C, a CO conversion of about 45%, respectively, 35% was reached. Consequently, an overall CO conversion of 92% could be achieved at partial load operation. At full load operation of the gasification plant, an overall CO conversion of 94% could be achieved along the WGS unit.

3.4 Temperature profiles along the reactors of the WGS unit

Figure 8 shows the temperature profiles along all three reactors of the WGS unit. The gas inlet temperature before all three reactors was set to about 350°C.

Figure 8 Average temperature profiles along the WGS reactors A, B, and C during the 100 hours of partial load operation of the gasification plant (see online version for colours)

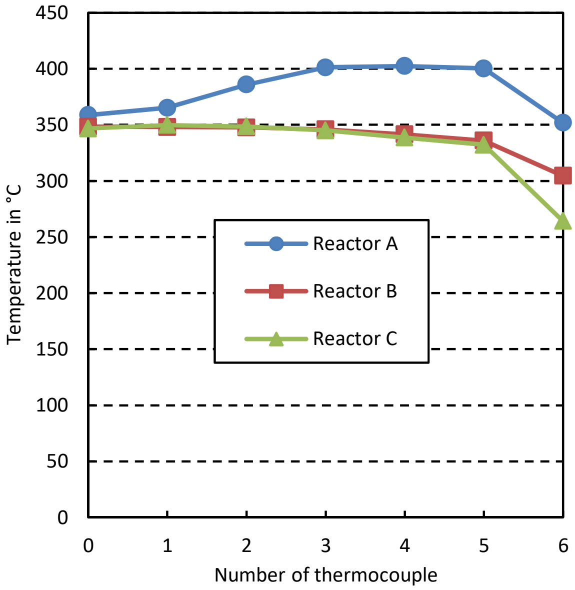

In reactor A, the temperature increased at the beginning of the catalyst bed until the temperature maximum was reached. At this point, a gas composition close to the equilibrium composition was reached. Therefore, from this point, heat losses exceeded the temperature increase and, consequently, the temperature along reactor A decreased.

In reactors B and C, nearly no WGS reaction occurred. Therefore, in those two reactors, the heat losses exceeded the temperature increase caused by the exothermic WGS reaction.

3.5 Ammonia and GCMS tar measurements

Table 6 shows the results of the ammonia measurements which were carried out at the inlet (before reactor A) and the outlet (after reactor C) of the WGS unit. According to these measurements, no chemical reaction with ammonia occurred. The concentration of ammonia decreased because of the dilution effect which was caused by the higher volumetric dry gas flow rate after the WGS unit.

Table 6 Volumetric ammonia concentrations (d.b.) at the inlet and the outlet of the WGS unit

	φ_{NH3} $cm^3 \bullet m^{-3}$
Inlet	3,350
Outlet	2,840

Notes: The measurement was a single sample measurement. Therefore, no standard deviation can be given.

Table 7 GCMS tar concentrations at the inlet and outlet of the WGS unit

GCMS tar components	*Units*	*Inlet*	*Outlet*
Phenylacetylene	$mg \bullet m^{-3}$	25	BDL
Styrene	$mg \bullet m^{-3}$	166	38
Mesitylene	$mg \bullet m^{-3}$	BDL	BDL
Phenol	$mg \bullet m^{-3}$	BDL	BDL
Benzofuran	$mg \bullet m^{-3}$	BDL	BDL
1H-Inden	$mg \bullet m^{-3}$	138	65
2-methylphenol	$mg \bullet m^{-3}$	BDL	BDL
4-methylphenol	$mg \bullet m^{-3}$	BDL	BDL
2-methylbenzofuran	$mg \bullet m^{-3}$	BDL	BDL
2,6-dimethylphenol	$mg \bullet m^{-3}$	BDL	BDL
2,5 u. 2,4-dimethylphenol	$mg \bullet m^{-3}$	BDL	BDL
3,5-dimethylphenol	$mg \bullet m^{-3}$	BDL	BDL
2,3-dimethylphenol	$mg \bullet m^{-3}$	BDL	BDL
3,4-dimethylphenol	$mg \bullet m^{-3}$	BDL	BDL
2-methoxy-4-methylphenol	$mg \bullet m^{-3}$	BDL	BDL
naphthalene	$mg \bullet m^{-3}$	3822	2870
1-benzothiophen	$mg \bullet m^{-3}$	7	5
Quinoline	$mg \bullet m^{-3}$	1	BDL
2-methylnaphthalene	$mg \bullet m^{-3}$	26	21
Isoquinoline	$mg \bullet m^{-3}$	BDL	BDL
1-methylnaphthalene	$mg \bullet m^{-3}$	18	15
1-indanon	$mg \bullet m^{-3}$	BDL	BDL
Eugenol	$mg \bullet m^{-3}$	BDL	BDL
Indole	$mg \bullet m^{-3}$	BDL	BDL
Biphenyl	$mg \bullet m^{-3}$	24	21
Isoeugenol	$mg \bullet m^{-3}$	BDL	BDL
Acenaphthylene	$mg \bullet m^{-3}$	233	6
Acenaphtene	$mg \bullet m^{-3}$	37	190
Dibenzofuran	$mg \bullet m^{-3}$	8	7
Fluorene	$mg \bullet m^{-3}$	9	6

Note: The measurement was a single sample measurement. Therefore, no standard deviation can be given (DL = 1 $mg \bullet m^{-3}$).

Table 7 GCMS tar concentrations at the inlet and outlet of the WGS unit (continued)

GCMS tar components	*Units*	*Inlet*	*Outlet*
Dibenzothiophene	mg•m^{-3}	BDL	BDL
Anthracene	mg•m^{-3}	118	46
Phenanthrene	mg•m^{-3}	11	4
Carbazole	mg•m^{-3}	BDL	BDL
4,5-methylphenanthren	mg•m^{-3}	4	2
9-methylanthracen	mg•m^{-3}	BDL	BDL
Fluoranthene	mg•m^{-3}	33	18
Pyrene	mg•m^{-3}	30	17
Benzo[a]anthracene	mg•m^{-3}	BDL	BDL
Chrysene	mg•m^{-3}	BDL	BDL
Benzo[b]fluoranthene	mg•m^{-3}	BDL	BDL
Benzo[k]fluoranthene	mg•m^{-3}	BDL	BDL
Benzo[a]pyrene	mg•m^{-3}	BDL	BDL
Benzo[g,h,i]perylene	mg•m^{-3}	BDL	BDL
Dibenz[a,h]anthracene	mg•m^{-3}	BDL	BDL
Indeno[1,2,3-cd]pyrene	mg•m^{-3}	BDL	BDL
Total GCMS amount	mg•m^{-3}	4,710	3,331

Note: The measurement was a single sample measurement. Therefore, no standard deviation can be given (DL = 1 mg•m^{-3}).

Table 7 shows the detailed GCMS tar measurements which were carried out at the inlet and the outlet of the WGS unit. The total amount of GCMS tar was reduced by 30% along the WGS unit. Naphthalene, the main GCMS tar component, was reduced by about 25 % along the WGS unit. Devi et al. (2005) shows a possible decomposition mechanism scheme of naphthalene.

However, the concentration of acenaphthene even increased by about 400% along the WGS unit. It was, most probably, partially formed from acenaphthylene by hydrogenation. Further information regarding the tar content of the product gas generated by DFB biomass steam gasification can be reviewed in Kirnbauer et al. (2012, 2013), Wolfesberger et al. (2009) and Wolfesberger-Schwabl et al. (2012).

4 Conclusions and outlook

A WGS unit processed real product gas from the commercial DFB biomass steam gasification plant in Oberwart, Austria. The WGS unit processed this tar-rich product gas for about 100 hours while the gasification plant operated at partial load. The WGS unit employed a commercial Fe/Cr-based catalyst which showed no deactivation or performance decrease during the operation with the tar-rich product gas.

Comparing the full load and the partial load operation of the gasification plant, no significant differences in the performance of the WGS unit could be observed. The volumetric CO content in the product gas could be lowered from 22.7 to 1.5 % (d.b.). Consequently, an overall CO conversion of 92 % could be achieved along the WGS unit.

In addition, a reduction of GCMS tar (about 30 %) could be achieved. Nearly the same results were obtained in the case of a full load operation of the gasification plant (Kraussler et al., 2015). All these results are within the same order of magnitude as achieved at industrial scale WGS units (Liu et al., 2010; Rhodes et al., 1995).

Recently, a lot of research regarding the hydrogen production from biomass was carried out where different processes and process chains with different unit operations were investigated (Aznar et al., 2006; Corella et al., 2008; Maroo et al., 2010; Ni et al., 2006). These results are also in agreement with the results which were achieved in this work. However, in none of these approaches, a commercial DFB biomass steam gasifier was combined with a WGS unit which, in addition, processed tar-rich product gas.

Consequently, these results show that it is possible to operate a WGS unit with the tar-rich product gas from DFB biomass steam gasification even if the gasification plant operates at partial load. This is an encouraging result for future applications regarding a process chain for hydrogen production from biomass which consists of DFB biomass steam gasification and a WGS unit.

Future research should focus on lower steam content at the inlet of the WGS unit as well as further observations regarding the performance of the commercial Fe/Cr-based catalyst during the operation with tar-rich product gas.

References

Aznar, M.P., Caballero, M.A., Molina, G. and Toledo, J.M. (2006) 'Hydrogen production by biomass gasification with steam-O_2 mixtures followed by a catalytic steam reformer and a CO-shift system', *Energy & Fuels*, Vol. 20 No. 3, pp.1305–1309.

Balat, H. and Kirtay, E. (2010) 'Hydrogen from biomass – present scenario and future prospects', *International Journal of Hydrogen Energy*, Vol. 35, No. 14, pp.7416–7426.

Boon, A.Q.M., van Looij, F. and Geus, J.W. (1992) 'Influence of surface oxygen vacancies on the catalytic activity of copper oxide: part 1. Oxidation of carbon monoxide', *Journal of Molecular Catalysis*, Vol. 75, No. 3, pp.277–291.

Chinchen, G.C., Logan, R.H. and Spencer, M.S. (1984) 'Water-gas shift reaction over an iron oxide/chromium oxide catalyst: II: stability of activity', *Applied Catalysis*, Vol. 12, No. 1, pp.89–96.

Corella, J., Aznar, M.P., Caballero, M.A., Molina, G. and Toledo, J.M. (2008) '140 g H_2/kg biomass d.a.f. by a CO-shift reactor downstream from a FB biomass gasifier and a catalytic steam reformer', *International Journal of Hydrogen Energy*, Vol. 33, No. 7, pp.1820–1826.

Devi, L., Ptasinski, K.J. and Janssen, F.J.J.G. (2005) 'Decomposition of naphthalene as a biomass tar over pretreated olivine: effect of gas composition, kinetic approach, and reaction scheme', *Industrial & Engineering Chemistry Research*, Vol. 44, No. 24, pp.9096–9104.

Diaz, N. (2013) *Hydrogen Separation from Producer Gas Generated by Biomass Steam Gasification*, Unpublished PhD Thesis, TU Wien, Vienna, Austria.

Fail, S. (2014) *Biohydrogen Production Based on the Catalyzed Water Gas Shift Reaction in Wood Gas*, Unpublished PhD Thesis, TU Wien, Vienna, Austria.

Gottschalk, F.M., Copperthwaite, R.G., van der Riet, M. and Hutchings, G.J. (1988) 'Cobalt/manganese oxide water gas shift catalysts: I. Competition between carbon monoxide hydrogenation and water gas shift activity', *Applied Catalysis*, Vol. 38, No. 1, pp.103–108.

Kaltschmitt, M., Hartmann, H. and Hofbauer, H. (2009) *Energie aus Biomasse*, 2nd ed., Springer-Verlag, Berlin, Heidelberg.

Kirnbauer, F., Wilk, V. and Hofbauer, H. (2013) 'Performance improvement of dual fluidized bed gasifiers by temperature reduction: the behaviour of tar species in the product gas', *Fuel*, Vol. 108, pp.534–542.

Kirnbauer, F., Wilk, V., Kitzler, H., Kern, S. and Hofbauer, H. (2012) 'The positive effects of bed material coating on tar reduction in a dual fluidized bed gasifier', *Fuel*, Vol. 95, pp.553–562.

Kraussler, M., Binder, M., Fail, S., Bosch, K., Hackel, M. and Hofbauer, H. (2015) 'Performance of a water gas shift unit processing product gas from biomass steam gasification', *Proceedings of the 23rd European Biomass Conference and Exhibition*, Vienna, Austria, pp.668–678.

Liu, K., Song, C. and Subramani, V. (2010) *Hydrogen and Syngas Production and Purification Technologies*, 1st ed., Wiley, VCH, New Jersey.

Maroo, M., Sanchez, J. and Ruiz, E. (2010) 'Hydrogen-rich gas production from oxygen pressurized gasification of biomass using a Fe-Cr water gas shift catalyst', *International Journal of Hydrogen Energy*, Vol. 35, No. 1, pp.37–45.

Mueller, S. (2013) *Hydrogen from Biomass for Industry – Industrial Application of Hydrogen Production Based on Dual Fluid Gasification*, Unpublished PhD Thesis, TU Wien, Vienna, Austria.

Ni, M., Leung, D.Y., Leung, M.K. and Sumathy, K. (2007) 'An overview of hydrogen production from biomass', *Fuel Processing Technology*, Vol. 87, No. 5, pp.461–472.

Proell, T., Rauch, R., Aichernig, C. and Hofbauer, H. (2007) 'Fluidized bed steam gasification of solid biomass – performance characteristics of an 8 MWth combined heat and power plant', *International Journal of Chemical Reactor Engineering*, Vol. 5, No. 1, pp.1542–6580.

Rhodes, C., Hutchings, G.J. and Ward. A.M. (1995) 'Water-gas shift reaction: finding the mechanistic boundary', *Catalysis Today*, Vol. 23, No. 1, pp.43–58.

Shchibrya, G.G., Morozov, N.M. and Temkin, M.I. (1965) 'Kinetics and mechanism of the water shift catalytic reaction', *Kinet. Katal.*, Vol. 6, No. 6, pp.1057–1068.

Twigg, M.V. (1997) *Catalyst Handbook*, 2nd ed., Oxford University Press, Oxford.

Wolfesberger, U., Aigner, I. and Hofbauer, H. (2009) 'Tar content and composition in producer gas of fluidized bed gasification of wood – influence of temperature and pressure', *Environmental Progress & Sustainable Energy*, Vol. 28, No. 3, pp.372–379.

Wolfesberger-Schwabl, U., Aigner, I. and Hofbauer, H. (2009) 'Mechanism of tar generation during fluidized bed gasification and low temperature pyrolysis', *Industrial & Engineering Chemistry Research*, Vol. 51, No. 40, pp.13001–13007.

Abbreviations and acronyms

BDL	below detection limit
BTEX	benzene, toluene, ethylbenzene, xylene
CHP	combined heat and power
d.b.	dry basis
DFB	dual fluidised bed
DL	detection limit
FPD	flame photometric detector
FR	flow record
GC	gas chromatograph

GCMS	gas chromatography mass spectroscopy
RME	rapeseed methyl ester
STP	standard temperature and pressure (273.15 K and 101,325 Pa)
TCD	thermal conductivity detector
WGS	water gas shift

Symbols

φ_i	volumetric fraction of component *i*
GHSV	gas hourly space velocity in h^{-1}
ΔH	enthalpy of formation at 298.15 K and 101,325 Pa in $kJ \cdot mol^{-1}$
STDGR	steam to dry gas ratio
STCR	steam to carbon ratio
$V_{Catalyst}$	catalyst volume in m^3
$\dot{V}_{Dry}$	dry gas flow rate at STP in $m^3 \cdot h^{-1}$
$\dot{V}_{H2O}$	steam flow rate at STP in $m^3 \cdot h^{-1}$
X_{CO}	CO conversion

Paper 5

Michael Kraussler, Hermann Hofbauer, Development and experimental validation of a water gas shift kinetic model for Fe-/Cr-based catalysts processing product gas from biomass steam gasification, Biomass Conversion and Biorefinery, Volume 7, Issue 2, 2016, Pages 153-165, `http://dx.doi.org/10.1007/s13399-016-0215-9`.

Contribution: Experimental work, data treatment, model generation, writing

Biomass Conv. Bioref.
DOI 10.1007/s13399-016-0215-9

ORIGINAL ARTICLE

Development and experimental validation of a water gas shift kinetic model for Fe-/Cr-based catalysts processing product gas from biomass steam gasification

Michael Kraussler[1,2] · **Hermann Hofbauer**[2]

Received: 27 April 2016 / Revised: 10 July 2016 / Accepted: 16 July 2016
© The Author(s) 2016. This article is published with open access at Springerlink.com

Abstract This paper introduces an improved kinetic model for the water gas shift reaction catalyzed by an Fe-/Cr-based catalyst. The improved model is based on a former model which was developed previously in order to consider the composition and the catalyst poisons (H_2S) of product gas derived from dual fluidized bed biomass steam gasification.

$$r(\varphi_i, T) = 117.8 \frac{\mathrm{mol}}{g\,Pa^{1.71}\,s} .exp\left(\frac{-126.6\frac{\mathrm{kJ}}{\mathrm{mol}}}{R.T}\right) .p_{\mathrm{CO}}^{1.77} .p_{\mathrm{H2O}}^{0.23} .p_{\mathrm{CO2}}^{-0.17} .p_{\mathrm{H2}}^{-0.12} . \left(1 - \frac{K_{MAL}}{K_g}\right)$$

Furthermore, this improved model has been validated with experimental data. The data was generated by a WGS reactor which employed a commercial Fe-/Cr-based catalyst and which processed real product gas from the dual fluidized bed biomass steam gasification plant in Oberwart, Austria. Basically, the validation showed good agreement of the measured and the calculated values for the gas composition (absolute errors of the volumetric fractions of up to 1.5 %) and the temperature profile (absolute errors of up to 21 °C) of the WGS reactor. Of all considered gas components, the CO concentration showed the highest error.

The results qualify the improved kinetic model for basic design and engineering of a WGS reactor employing a commercial Fe-/Cr-based catalyst which processes product gas from an industrial scale biomass steam gasification plant.

✉ Michael Kraussler
michael.kraussler@bioenergy2020.eu

[1] Bioenergy2020+ GmbH, Wienerstraße 49, 7540 Güssing, Austria

[2] Institute of Chemical Engineering, TU Wien, Getreidemarkt 9, 1060 Wien, Austria

Keywords Kinetic model · Water gas shift · Biomass · Steam gasification · Dual fluidized bed · Product gas

1 Introduction

The water gas shift (WGS) reaction (see Eq. 1) is a proven method for increasing the hydrogen content in a product gas generated by gasification. Recent research has extensively investigated a WGS unit, employing a commercial Fe-/Cr-based catalyst, which processed product gas from dual fluidized bed (DFB) biomass steam gasification [8, 16, 17].

$$CO + \mathrm{H_2O} \leftrightarrow \mathrm{H_2} + \mathrm{CO_2} \quad \Delta H = -41.1\ \mathrm{kJ}\ mol^{-1} \tag{1}$$

Since the first applications of the WGS reaction catalyzed by an Fe-/Cr-based catalyst (compare [23]), several kinetic models, based on power laws, have been proposed by different authors, for example, in [2, 3, 9, 13, 20] and [22]. However, most of the investigations of Fe-/Cr-based WGS catalysts were carried out for product gas derived from coal gasification [10, 11]. Zhu and Wachs [28] give a comprehensive summary about kinetic models of the WGS reaction catalyzed by Fe-/Cr-based catalysts.

In addition, Fail [7] proposed a kinetic model for the WGS reaction catalyzed by an Fe-/Cr-based catalyst. This kinetic model specifically takes the product gas from DFB biomass steam gasification into account. In the present paper, this model is referred to as the former kinetic model.

The main gas components of the product gas are H_2, CO, CO_2, and CH_4 which makes the product gas a suitable source for different synthesis reactions, for example, see [19, 21] and [24]. In addition, it contains about 100 $cm^3\ m^{-3}$ H_2S. This H_2S

Published online: 11 August 2016

content was considered within the former model because H_2S could lead to a performance decrease of the catalyst [26].

In [15], the former model was validated with experimental data from a WGS reactor which employed commercial Fe-/Cr-based catalyst disks (diameter about 6 mm and height about 3 mm, original size) and which processed real product gas from the industrial scale DFB biomass steam gasification plant in Oberwart, Austria. The validation showed significant inaccuracies of the temperature profile along the WGS reactor, which could be attributed to the fact that the former model was established with a milled Fe-/Cr-based catalyst, which did not have the original disk size. Therefore, a higher catalyst surface was available during the establishment of the former kinetic model compared to the validation experiments where the catalyst was used in its original size. However, the WGS reactor, which is located at the site of the gasification plant in Oberwart employed the catalyst in its original pellet size. Consequently, the differences between the measured and calculated temperature profile occurred.

The present paper improves the former kinetic model in order to obtain a better agreement between the experimental data and the model. Consequently, the improved kinetic model should be accurate enough to be used for basic design and engineering of WGS reactors employing Fe/Cr based catalysts which process product gas from DFB biomass steam gasification.

2 Materials and methods

First, this section presents the former kinetic model, which is based on the previous work carried out by Fail (see [7]) and which is improved in the present paper. Second, the experimental setup which generated the data material which was used to improve the former and to validate the improved kinetic model is presented. Third, the derivation of the numerical mass and energy balances of the WGS reactor is introduced, which enables the comparison of the measured data with the results of the model.

2.1 The former kinetic model

This paper is based on a kinetic model which was derived at the TU Wien from results obtained with a laboratory scale chemical kinetics test rig (see [7]). For that kinetic model, the Fe-/Cr-based catalyst was milled before the kinetic parameters were determined. Consequently, the model shows inaccuracies regarding the reaction rate and, therefore, the temperature profile (compare [15]) if the catalyst is used in its original size.

In this paper, the former kinetic model has been improved in order to meet the requirements for using this model for the basic design and engineering of a WGS reactor which processes product gas from DFB biomass steam gasification.

The starting point for both the former and the improved kinetic model was the power law in Eq. 2 which is based on [7] and [15]:

$$r(\varphi_i, T) = k_0.exp\left(\frac{-E_a}{R.T}\right).p_{\mathrm{CO}}^{a}.p_{\mathrm{H2O}}^{b}.p_{\mathrm{CO2}}^{c}.p_{\mathrm{H2}}^{d}.\left(1-\frac{K_{\mathrm{MAL}}}{K_{\mathrm{g}}}\right) \tag{2}$$

The reaction rate $r(\varphi_i, T)$ is a function of the reactive species (CO, H_2O, CO_2, and H_2) and the temperature. Other gas components which are usually contained in small amounts in the product gas of the DFB biomass steam gasification are considered as inert.

The parameters which describe the reaction rate are the rate constant k_0, the activation energy E_a, and the reaction exponents (a, b, c, and d) of each component i which is a reactant of the WGS reaction (see Eq. 1). p_i is the partial pressure, R is the general gas constant, and T is the temperature along the reactor. K_{MAL} is the mass action law and K_{g} the equilibrium constant calculated from thermo-physical properties.

$$K_{\mathrm{MAL}} = \frac{\varphi_{\mathrm{H2}}.\varphi_{\mathrm{CO2}}}{\varphi_{\mathrm{CO}}.\varphi_{\mathrm{H2O}}} \tag{3}$$

$$K_{\mathrm{g}} = exp\left(\frac{-\Delta G(T)}{R.T}\right) \tag{4}$$

The partial pressure of each component p_i can be expressed by the overall absolute pressure p and the volumetric fraction φ_i.

$$p_i = \varphi_i.p \tag{5}$$

The work in [7] led to the following parameters for Eq. 2, resulting in the former model (see Table 1).

2.2 Setup for the generation of the experimental data

This section provides information about the plants and the measurement principles which were used for the data

Table 1 Parameters of the former kinetic model (see [7] and [15])

Parameters	Values	Units
k_0	117.8	$\mathrm{mol\ g^{-1}\ Pa^{-(a+b+c+d)}\ s^{-1}}$
E_a	101.9	$\mathrm{kJ\ mol^{-1}}$
a	1.77	–
b	0.23	–
c	−0.17	–
d	−0.12	–

generation in order to improve the former and to validate the improved kinetic model.

2.2.1 The dual fluidized bed steam gasification plant

The product gas for the WGS reactor was extracted from the commercial DFB biomass steam gasification plant in Oberwart, Austria. The gasification plant is operated as combined heat and power (CHP) plant and generates electricity and heat for the district. Figure 1 shows a simplified flowchart of the gasification plant.

For the improvement of the former and the validation of the improved kinetic model, the product gas was extracted from two extraction points (see also Fig. 1). The first extraction point was located before the rapeseed methyl ester (RME) gas scrubber, and the second extraction point was located after the RME gas scrubber. The product gas which was extracted before the RME gas scrubber showed a significantly higher amount of tar (about 10 $g\ m^{-3}$) and steam (about 35 %) compared to the product gas which was extracted after the RME gas scrubber (about 2 $g\ m^{-3}$ tar and about 7 % steam).

Further details of the plant can be found in [6, 15–17].

2.2.2 The water gas shift reactor

Figure 2 shows a simplified flowchart of the cylindrical WGS reactor located at the site of the gasification plant in Oberwart which was used for the generation of the experimental data.

The WGS reactor successively processed a partial flow of the product gas of the gasification plant from the two extraction points (see Fig. 1). The product gas was mixed with additional steam which was provided by a steam generator. The gas inlet temperature was adjusted with a heating section to about 350 °C. At the bottom of the reactor, a screen plate was used for carrying the commercial Fe-/Cr-based catalyst which had been in operation for more than 2000 h at the time this research was conducted. The catalyst bed was a fixed bed with a diameter of 9 cm and a height of about 40 cm resulting in a catalyst bed volume of about 2.5 dm^3. The bulk density of the catalyst bed was 1.24 kg dm^{-3}. The wall thickness of the reactor was 3 mm and the insulation consisted of stone wool with a thickness of 10 cm and a thin layer of Al around the outer surface.

Seven thermocouples were used to measure and to record the temperature profile along the WGS reactor. The temperature profile allowed reaching some conclusion about the

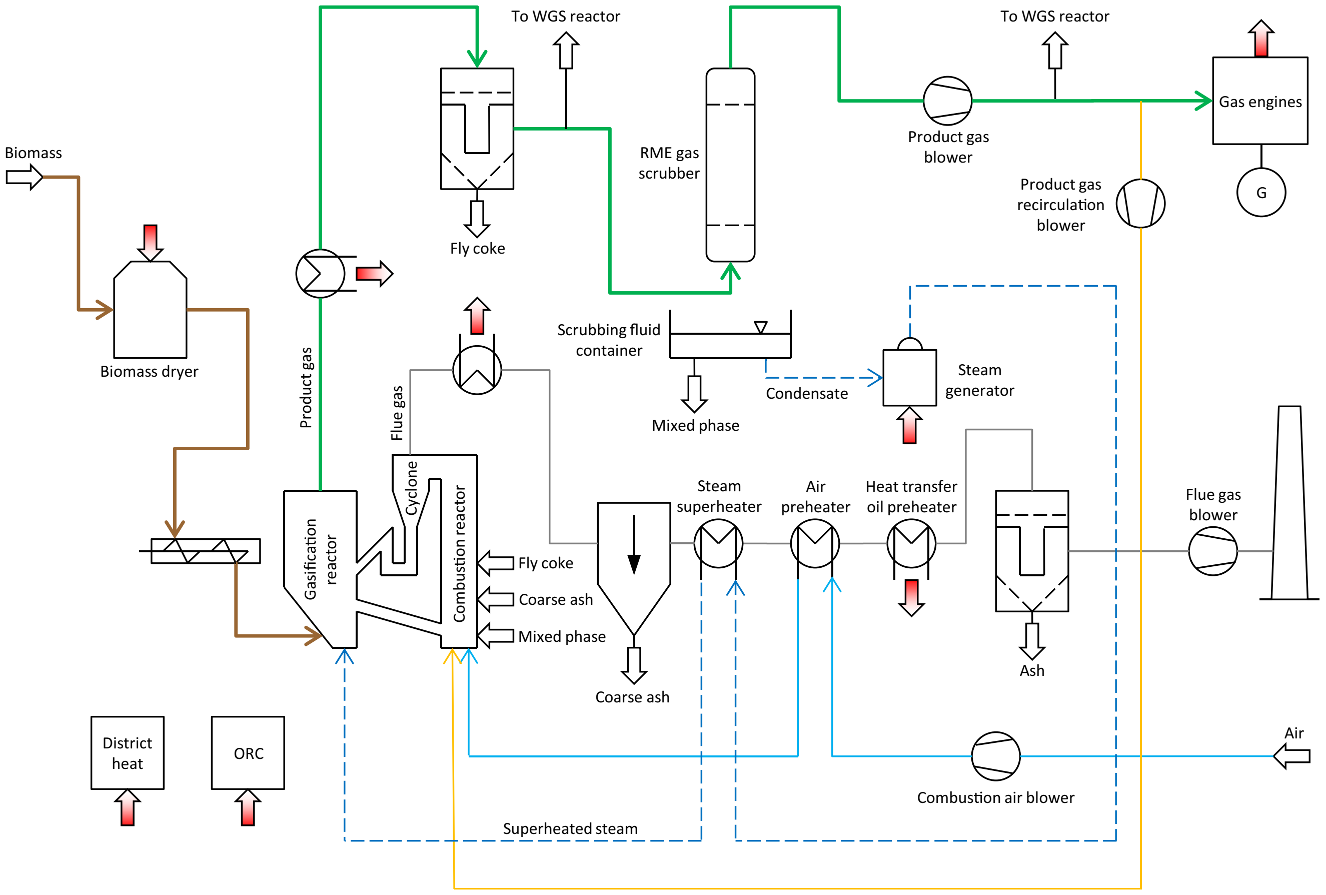
To WGS reactor
To WGS reactor
Gas engines
Biomass
RME gas scrubber
Product gas blower
Product gas recirculation blower
G
Fly coke
Biomass dryer
Scrubbing fluid container
Condensate
Steam generator
Mixed phase
Product gas
Flue gas
Cyclone
Gasification reactor
Combustion reactor
Steam superheater
Air preheater
Heat transfer oil preheater
Flue gas blower
Fly coke
Coarse ash
Mixed phase
Coarse ash
Ash
Air
District heat
ORC
Combustion air blower
Superheated steam

Fig. 1 Simplified flowchart of the gasification plant in Oberwart, Austria

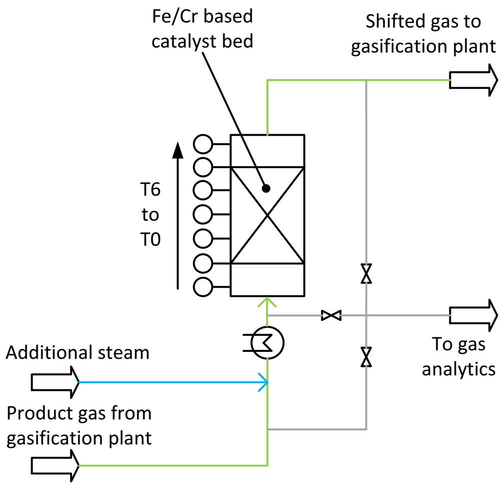

Fig. 2 Simplified flowchart of the WGS reactor which was used for the generation of the experimental data

activity of the commercial Fe-/Cr-based catalyst due to the exothermic nature of the WGS reaction.

After the product gas was processed in the reactor, it was recycled back to the gasification plant. A sample flow of the processed gas extracted before the steam addition, before the inlet, and after the outlet of the WGS reactor was sent to the analytical line and, subsequently, to a gas chromatograph (GC) in order to measure the dry gas composition of the processed gas.

The WGS reactor operated at ambient pressure and the pressure drop along the catalyst bed was between 500 and 1000 Pa during the whole operating time.

2.2.3 Measurement of the temperature profile along the water gas shift reactor

Figure 2 shows the positions of the thermocouples (type J) along the WGS reactor. Thermocouple T0 was positioned before the fixed bed Fe-/Cr-based catalyst. Therefore, it was not in the reactive zone. T1 to T5 were positioned along the catalyst bed at a distance of 10 cm from each other. T1 was positioned right at the beginning of the catalyst bed, and T5 was positioned right at the end of the catalyst bed. T6 was outside the catalyst bed. T1 to T5 enabled the measurement and recording of the temperature profile along the fixed bed WGS catalyst.

2.2.4 Measurement of the gas composition at the inlet and the outlet of the water gas shift reactor

Figure 3 shows the setup of the gas conditioning before the gas chromatograph (GC) that was used for the determination of the gas composition.

Before entering the GC, the gas stream passed through two gas washing bottles filled with glycol at a temperature of about −5 °C in order to condense and separate the steam. Therefore, a dry gas stream could be assumed after the gas washing bottles. The dry gas stream passed through another gas washing bottle filled with glass wool in order to prevent aerosols from entering the GC. After the glass wool bottle, a gas meter recorded the volumetric dry gas flow.

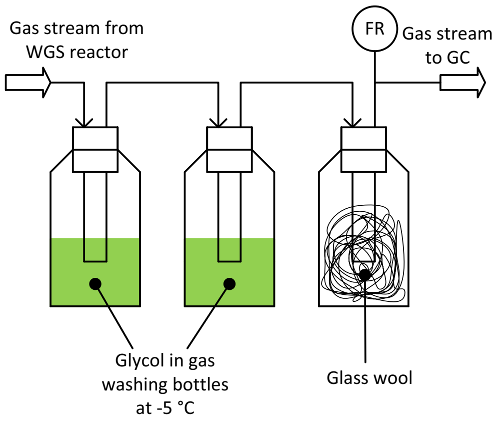

Fig. 3 Setup of the gas conditioning before the GC and the water content determination

The steam content in the product gas before the addition of steam, before the inlet of the reactor, and after the outlet of the reactor was determined with a gravimetrical method. The wet gas stream passed through the gas washing bottles for a certain time, where the steam was condensed. Subsequently, the volumetric dry gas flow was recorded and the gas washing bottles were weighed. Consequently, the steam content before the steam addition, before the inlet, and before the outlet of the reactor could be determined.

The volumetric dry gas flow rate at the inlet of the WGS reactor was calculated by the water balance of the steam generator according to the following equation and the known volumetric flow rate of the steam addition:

$$\begin{aligned}\dot{V}_{\mathrm{Dry}} &= \dot{V}_{\mathrm{Wet,In}}\cdot\left(1-\varphi_{\mathrm{H2O,In}}\right)\\ &= \frac{\left(\dot{V}_{\mathrm{H2O,Add}}\cdot\varphi_{\mathrm{H2O,Out}}-\dot{V}_{\mathrm{H2O,Add}}\right)}{\left(\varphi_{\mathrm{H2O,In}}-\varphi_{\mathrm{H2O,Out}}\right)}\cdot\left(1-\varphi_{\mathrm{H2O,In.}}\right)\end{aligned}$$

In this paper, all volumetric gas flow rates and gas volumes are given at standard temperature and pressure (STP, 273.15 K and 101325 Pa).

A GC (Clarus 500™ from Perkin Elmer) was used to measure the gas composition at the inlet and at the outlet of the WGS reactor. A thermal conductivity detector (TCD) enabled the quantification of the CO, CO_2, CH_4, N_2, and higher hydrocarbons in the gas stream with two different columns (7' HayeSep N, 60/80 1/8" SF and 9' molecular sieve 13× 45/60, 1/8" SF). The higher hydrocarbons were considered inert and, therefore, their amount was added to the N_2 concentration. The GC was not able to measure the H_2 concentration.

Consequently, the H_2 concentration was calculated by closing the overall mass balance. Furthermore, CH_4 was also considered inert for the modeling process.

In addition, the measurements were validated by applying the least squares method on the elemental balances of C, H, O, and N describing the WGS reactor.

2.3 Balances and consideration of the heat losses of the water gas shift reactor

This section describes the derivation of the numerical molar and energy balances of the WGS reactor which was used for gathering the experimental data. Furthermore, the approach for the consideration of the heat losses along the reactor is shown.

For the derivation of the balances, the assumption of an ideal plug flow reactor was made.

2.3.1 Molar balance of the water gas shift reactor

Figure 4 shows the derivation of the molar balance of the WGS reactor.

The molar balance of each reactive component *i* leads to

$$\dot{n}_i(z+\Delta z) - \dot{n}_i(z) = \pm r(\varphi_i, T).\rho_s.\Delta z.A. \tag{6}$$

$\dot{n}_i$ is the molar flow of component *i* and *A* is the cross section of the catalyst bed. ρ_s is the bulk density of the Fe-/Cr-based catalyst and Δ*z* is the grid step, which was chosen with 1 mm. ±indicates whether component *i* is an educt or a product of the WGS reaction.

The limiting process$\lim \Delta z \to 0$ leads to the following differential equation:

$$\frac{d\dot{n}_i}{dz} = \pm r(\varphi_i, T).\rho_s.A. \tag{7}$$

Replacing the molar flow rate $\dot{n}_i$ of each component *i* with the overall molar flow rate $\dot{n}$ and the volumetric fractions of each component *i* leads to

$$\frac{d\varphi_i}{dz} = \pm r(\varphi_i, T).\rho_s.A.\frac{1}{\dot{n}}. \tag{8}$$

This step is valid because of the equimolar character of the WGS reaction and the assumption of ideal gas behavior.

Using the finite difference approach (see [25]) leads to

$$\varphi_i^{K+1} = \pm r\left(\varphi_i^K, T^K\right).\rho_s.A.\frac{1}{\dot{n}}.\Delta z + \varphi_i^K. \tag{9}$$

Equation 9 enables the calculation of the concentration profiles of CO, H_2O, CO_2, and H_2 along the catalyst bed height of the WGS reactor.

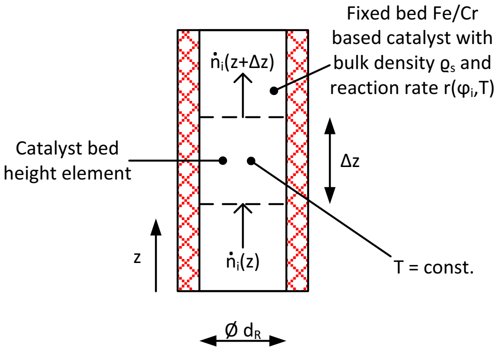
Fixed bed Fe/Cr based catalyst with bulk density ρ_s and reaction rate $r(\varphi_i, T)$
$\dot{n}_i(z+\Delta z)$
Catalyst bed height element
Δz
z
$\dot{n}_i(z)$
T = const.
Ø d_R

Fig. 4 Illustration for the calculation of the molar balance for the WGS reactor

2.3.2 Energy balance of the water gas shift reactor

Figure 5 shows a drawing for the derivation of the energy balance of the WGS reactor.

The energy balance of the differential height element leads to

$$\begin{aligned} &\dot{h}(z+\Delta z) - \dot{h}(z) \\ &\quad = \pm \Delta h_R(\varphi_i, T)\cdot r(\varphi_i, T)\cdot \rho_s \cdot A \cdot \Delta z - \Delta \dot{Q}(z). \end{aligned} \tag{10}$$

Here, $\Delta h_R(\varphi_i, T)$ is the formation enthalpy of the WGS reaction, $\dot{h}$ is the overall enthalpy flow, and $\Delta \dot{Q}(z)$ is the term which describes the heat losses along each height element Δ*z*. The limiting process $\lim \Delta z \to 0$ and the overall molar heat capacity $c_P(\varphi_i, T)$ of the gas stream lead to

$$\frac{dT}{dz} = \pm\ \Delta h_R(\varphi_i, T)\cdot r(\varphi_i, T)\cdot \frac{\rho_s \cdot A}{c_P(\varphi_i, T)\cdot \dot{n}} - \frac{d\dot{Q}(z)}{c_P(\varphi_i, T)\cdot \dot{n}\cdot dz}. \tag{11}$$

Applying the finite difference approach to Eq. 11 leads to

$$T^{K+1} = \pm\ \Delta h_R\left(\varphi_i^K, T^K\right)\cdot r\left(\varphi_i^K, T^K\right)\cdot \frac{\rho_s \cdot A}{c_P(\varphi_i, T)\cdot \dot{n}}\cdot \Delta z - \frac{\Delta \dot{Q}^K}{c_P\left(\varphi_i^K, T^K\right)\cdot \dot{n}} + T^K. \tag{12}$$

Equation 12 enables the calculation of the temperature profile along the catalyst bed height of the WGS reactor. It also considers the heat losses which occur along the WGS reactor.

Equations 9 and 12 form a system of equations which describes the concentration and temperature profiles along the WGS reactor. This system of equations was solved using an algorithm which was written with the numerical software Scilab™ [27].

The thermo-physical properties of the product gas components were calculated by NASA polynomials [18].

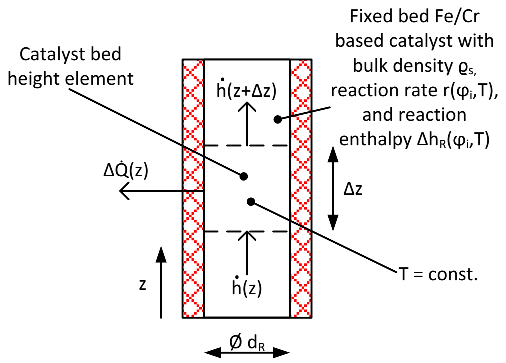
Catalyst bed height element
Fixed bed Fe/Cr based catalyst with bulk density ϱ_S, reaction rate r(φ_i,T), and reaction enthalpy Δh_R(φ_i,T)
ḣ(z+Δz)
ΔQ̇(z)
Δz
z
ḣ(z)
T = const.
Ø d_R

Fig. 5 Illustration for the calculation of the energy balance for the WGS reactor

The input values for the numerical solution are the volumetric steam flow rate $\dot{V}_{\mathrm{H2O}}$, the volumetric dry gas flow rate $\dot{V}_{\mathrm{Dry}}$, the kinetic model coefficients, the reactor geometry, the gas composition at the reactor inlet φ_i^0, the reactor inlet temperature T^0, and the ambient temperature T_0.

With the numerical calculation of the mass and energy balance of the WGS reactor, the former kinetic model (see Table 1) was improved and the resulting improved kinetic model (see Table 3) was validated with experimental data. To acquire the experimental data, the WGS reactor was operated with real product gas from the gasification plant.

2.3.3 Consideration of the heat losses along the water gas shift reactor

The heat losses along the WGS reactor were considered because they have a significant influence on the energy balance of the WGS reactor.

The heat losses $\Delta\dot{Q}(z)$ are calculated for each Δz along the WGS reactor according to

$$\Delta\dot{Q}(z) = (T(z) - T_0).R_Q(z). \tag{13}$$

Using the finite difference approach leads to

$$\Delta\dot{Q}^K = \left(T^K - T_0\right)\cdot R_Q^K. \tag{14}$$

Here, $T(z)$ is the actual reactor temperature for each z, T_0 is the ambient temperature, and $R_Q(z)$ is the overall heat transfer conductivity for each z; it can be described by four different single heat transfer conductivity coefficients (ambient, insulation, reactor wall, and inner reactor) according to Eq. 15.

$$\frac{1}{R_{\mathrm{Q}}} = \frac{1}{\alpha_0\cdot A_0} + \frac{\delta_I}{\lambda_{\mathrm{I}}\cdot A_{\mathrm{I}}} + \frac{\delta_S}{\lambda_{\mathrm{S}}\cdot A_{\mathrm{S}}} + \frac{1}{\alpha_{\mathrm{R}}\cdot A_{\mathrm{R}}}$$
$$= \frac{1}{\pi\cdot\Delta z}\cdot\left(\frac{1}{\alpha_0\cdot d_0} + \frac{\delta_{\mathrm{I}}}{\lambda_I\cdot\frac{d_{\mathrm{I}}-d_{\mathrm{S}}}{ln\left(\frac{d_{\mathrm{I}}}{d_{\mathrm{S}}}\right)}} + \frac{\delta_{\mathrm{S}}}{\lambda_S\cdot\frac{d_{\mathrm{S}}-d_{\mathrm{R}}}{ln\left(\frac{d_{\mathrm{S}}}{d_{\mathrm{R}}}\right)}} + \frac{1}{\alpha_{\mathrm{R}}\cdot d_{\mathrm{R}}}\right) \tag{15}$$

These four terms describe the heat transfer conductivity of the shell of the reactor (compare Fig. 6). The heat losses of the bottom surface and the top surface of the reactor are neglected because the surfaces are significantly smaller than the shell surface.

In the following, the derivation of the four heat transfer conductivity terms (ambient, insulation, reactor wall, and inner reactor) is shown.

Ambient This term consists of the heat transfer coefficients α_0 and the outer surface of the reactor A_0.

α_0 can be calculated with the heat transfer coefficient caused by the radiation emitted by the insulation surface (α_{Rad}, thin Al layer) and the heat transfer coefficient caused by natural convection (α_{Conv}):

$$\alpha_0 = \alpha_{\mathrm{Rad}} + \alpha_{\mathrm{Conv}} \tag{16}$$

According to [1], α_{Rad} can be calculated with Eq. 17.

$$\alpha_{\mathrm{Rad}} = \epsilon_0\cdot\sigma\cdot\frac{T_{\mathrm{S}}^4 - T_0^4}{T_{\mathrm{S}} - T_0} =$$
$$= 0.09\cdot 5.67\cdot 10^8\,\frac{W}{\mathrm{m}^2\cdot K^4}\cdot\frac{((50+273.15)K)^4 - ((25+273.15)K)^4}{(50+273.15)K - (25+273.15)K}$$
$$= 0.61\,\frac{W}{\mathrm{m}^2\cdot K} \tag{17}$$

The convective heat transfer coefficient α_{Conv} can be calculated by the Nusselt number Nu with the correlation in Eq. 18 (see [5]).

$$Nu = \frac{\alpha_{\mathrm{Conv}}\cdot d_0}{\lambda}$$
$$= \left\{0.6 + \frac{0.387\cdot(Gr\cdot Pr)^{\frac{1}{6}}}{\left[1 + \left(0.559\cdot Pr^{-1}\right)^{\frac{9}{16}}\right]^{\frac{8}{27}}}\right\}^2 \tag{18}$$

In this equation, d_0 is the outer diameter of the reactor and λ is the heat conductivity of air.

The Grashof number Gr with the gravitational constant g, the thermal expansion coefficient of air β, the

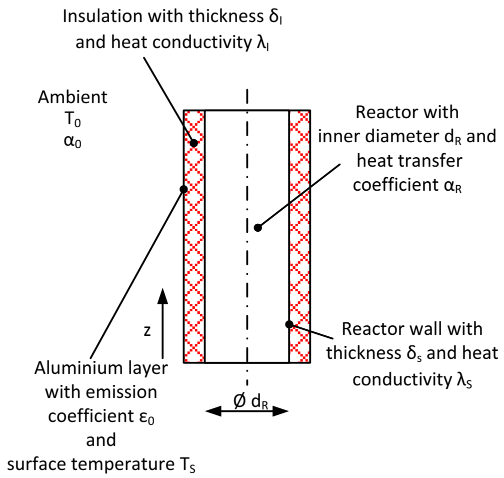
Insulation with thickness δ_I and heat conductivity λ_I
Ambient
T_0
α_0
Reactor with inner diameter d_R and heat transfer coefficient α_R
z
Reactor wall with thickness δ_s and heat conductivity λ_S
Aluminium layer with emission coefficient ε_0 and surface temperature T_S
Ø d_R

Fig. 6 Drawing for the consideration of the heat losses along the reactor shell

outer reactor diameter d_0, and the kinematic viscosity of air ν

$$Gr = \frac{g \cdot \beta \cdot (T_S - T_0) \cdot d_0^3}{\nu^2} = \frac{9.81 \frac{m}{s^2} \cdot \frac{1}{(25 + 273.15)} \frac{1}{K} \cdot (25\ K) \cdot 0.296^3\ \mathrm{m}^3}{\left(1.6 \cdot 10^{-5}\right)^2 \left(\frac{\mathrm{m}^2}{s}\right)^2} = 8.33 \cdot 10^7 \tag{19}$$

and the Prandtl number of air
$\mathrm{Pr} = 0.7$
lead to
$\mathrm{Nu} = 47.89$
and, consequently, to

$$\alpha_{\mathrm{Conv}} = \frac{Nu \cdot \lambda}{d_0} = \frac{47.89 \cdot 2.6 \cdot 10^{-2}\ \frac{W}{m \cdot K}}{0.296\ \mathrm{m}} = 4.21\ \frac{W}{\mathrm{m}^2 \cdot K}. \tag{20}$$

With Eqs. 17 and 20, the overall heat transfer coefficient for the ambient can be calculated with

$$\alpha_0 = \alpha_{\mathrm{Rad}} + \alpha_{\mathrm{Conv}} = 0.61\ \frac{W}{\mathrm{m}^2 \cdot K} + 4.21\ \frac{W}{\mathrm{m}^2 \cdot K} = 4.82\ \frac{W}{\mathrm{m}^2 \cdot K} \tag{21}$$

It can be seen that the heat transfer coefficient which is caused by the natural convection is about seven times higher than the heat transfer coefficient of the radiation at this low ambient temperature.

Furthermore, the outer surface of the reactor can be calculated with

$$A_0 = d_0 \cdot \pi \cdot \Delta z \tag{22}$$

Insulation This term consists of the thickness of the insulation δ_I, the heat conductivity of the insulation, λ_I and the mean logarithmic surface of the insulation A_I. In general, the mean logarithmic surface (A_m) can be calculated using the outer (A_o) and inner (A_i) surface of a cylindrical object according to Eq. 23.

$$A_m = \frac{A_o - A_i}{ln \frac{A_o}{A_i}} \tag{23}$$

Reactor wall This term consists of the thickness of the reactor wall δ_S, the heat conductivity of steel λ_S, and the mean logarithmic surface of the inner reactor A_R and the outer surface of the reactor wall A_S.

Inner reactor The inner reactor is considered as an ideal pipe reactor with the inner surface area A_R. Therefore, [1] (page 418) gives a Nusselt number of $\mathrm{Nu} = 3.657$. With Nu, the inner reactor diameter d_R, and the estimated heat conductivity of the product gas λ_R, the heat transfer coefficient α_R can be calculated.

Hence, the overall heat transfer conductivity R_Q for each Δz is $2.46 \cdot 10^{-4}\ W \cdot K^{-1}$ with the chosen parameters. With this information, the heat losses along the reactor can be calculated according to Eqs. 13 and 14, respectively.

3 Result and discussion

First, this section presents the determination of the parameters for the improved kinetic model. Second, the validation results of the improved kinetic model are discussed.

Table 2 gives an overview of the four different operating points of the WGS reactor (OP1 to OP4). OP1 was used to improve the former kinetic model, and OP2 to OP4 were used for the validation of the improved kinetic model with experimental data from the WGS reactor.

Table 2 Overview of the operating points for the improvement of the kinetic model and its subsequent validation

OP	GHSV	STDGR	$\dot{V}_{\mathrm{Dry}}$	Usage
-	h^{-1}	–	$\mathrm{m}^3 \cdot \mathrm{h}^{-1}$	–
1	495	1.6	1.24	Improvement
2	445	1.9	1.11	Validation
3	326	1.6	0.82	Validation
4	414	1.2	1.04	Validation

The operating conditions of the WGS reactor were described by the gas hourly space velocity (GHSV) and the steam to dry gas ratio (STDGR) in Eqs. 24 and 25.

$$\mathrm{GHSV} = \frac{\dot{V}_{\mathrm{Dry}}}{V_{\mathrm{Cat}}} \tag{24}$$

$$\mathrm{STDGR} = \frac{\dot{V}_{\mathrm{H2O}}}{\dot{V}_{\mathrm{Dry}}} \tag{25}$$

OP1, OP2, and OP3 processed product gas which was extracted before the RME gas scrubber of the gasification plant and OP4 processed gas which was extracted after the RME gas scrubber.

3.1 The improved kinetic model

In order to improve the former kinetic model, a new parameter for the activation energy E_a was sought, one that should consider the fact that the catalyst was used in its original pellet size during this experimental approach, which was in contrast to the determination of the former kinetic model, where the catalyst was milled and, therefore showed a higher specific surface. E_a was chosen as the parameter to improve because it significantly affects the temperature profile (compare Eq. 2). To do so, a variation of E_a with subsequent error calculation regarding the temperature profile was done.

For each E_a, the temperature profile along the WGS reactor (thermocouples 1 to 5) was calculated and compared with the measured values of OP1. Subsequently, the overall error for each E_a was calculated according to Eq. 26.

$$\mathrm{Err} = \sum_{i=1}^{5} \sqrt{\left(T_{c,i} - T_{m,i}\right)^2} \tag{26}$$

The result can be seen in Fig. 7.

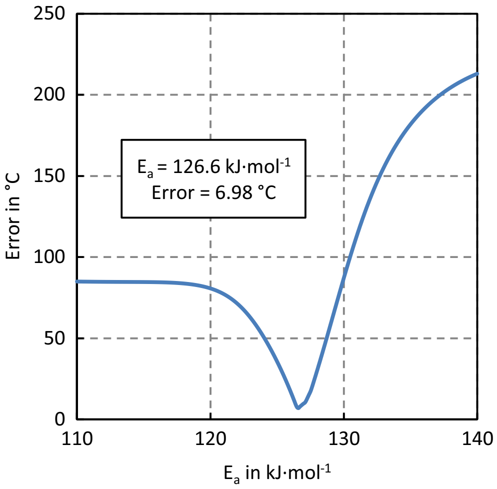

Fig. 7 Variation of E_a with corresponding error for OP1

The new value for $E_{a,j}$ was chosen to be that for which the error Err was a minimum.

The new value of E_a and, consequently, the other parameters for Eq. 2 which were not changed can be seen in Table 3.

Compared to the models in [2, 7, 13, 15] and [22], the activation energy E_a is higher. In these approaches, the activation energy values varied between 95 and 118 kJ mol^{-1}. However, Chinchen et al. [4] give a value of 129.4 kJ mol^{-1} for the activation energy for WGS catalysts used at industrial scale and at pressures of up to 3.0 MPa, which is in good agreement with the value found in this work.

In addition, the presented value of factor a shows that the influence of the CO partial pressure is also higher (1.77 in this work versus about 1.0 in [2, 13], and [22]). This could be explained by the low operating pressure in this work and, therefore, an even lower adsorption of CO on the catalyst surface.

In contrast, the reaction exponents b, c, and d are in the same order of magnitude, which also indicates that the supply of H_2O, CO_2, and H_2 to the catalyst surface is not limiting the reaction.

3.2 Validation of the improved kinetic model with experimental data

The improved kinetic model was validated with temperature measurements and concentration measurements of all four operating points where real product gas from the gasification plant was processed in the WGS reactor.

Figure 8 shows the validation of the kinetic model with the measured temperature profiles along the WGS reactor from all four operating points (OP1 to OP4). The temperatures at T1 were the boundary conditions; therefore, the measurements and the calculations have the same value.

It can be seen that the calculated and measured temperature profiles have nearly no difference at OP1 because the improved model is based on this operating point.

The temperature profiles of OP2 also have a higher difference. However, the calculated profile was slightly lower than the measured profile. Consequently, the chosen activation energy of $E_a = 126.6$ kJ mol^{-1} seems to be too high for OP2.

Table 3 Parameters of the improved kinetic model

Parameters	Values	Units
k_0	117.8	mol g^{-1} $Pa^{-(a+b+c+d)}$ s^{-1}
E_a	126.6	kJ mol^{-1}
a	1.77	–
b	0.23	–
c	−0.17	–
d	−0.12	–

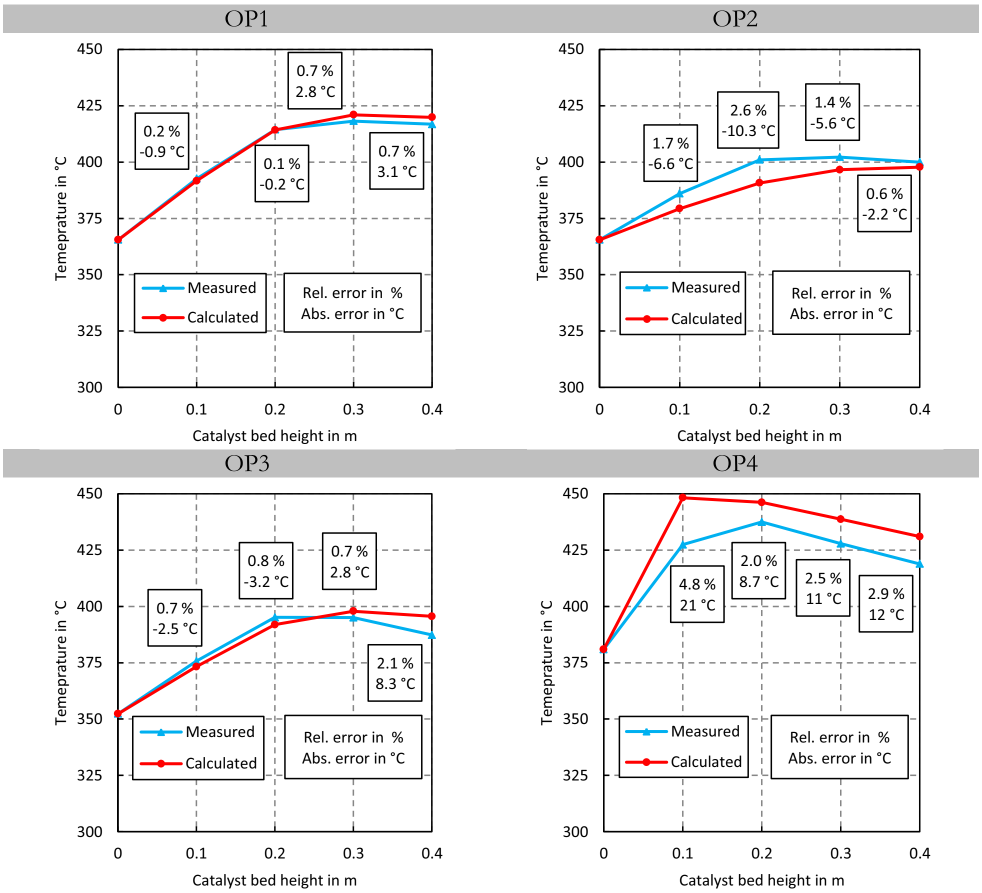

Fig. 8 Temperature profiles along the water gas shift reactor for all four operating points

For OP3, the temperature profiles show good agreement for the first three measurement points. However, it seems that the calculated heat losses in the improved model are too low compared to the measured values, which explains the higher calculated temperature profile at measurement points 4 and 5. Consequently, the highest error occurred at the last measurement point.

OP4 shows the highest gap regarding the calculated and the measured temperature profile which could be explained by the fact, that this operating point processed product gas with a lower STDGR of 1.2 compared to the other operating points. For this operating point, the chosen value of E_a was too low, which indicates that a lower STDGR ratio has a negative effect on the kinetics. This is in agreement with Hla et al. [12], where the authors observed that higher steam content increased the reaction rate of the WGS reaction. However, the measurement points 3 to 5 indicate good agreement between the calculated and measured heat losses.

Table 4 shows the calculated and measured values of the gas compositions at the inlet and outlet of the WGS reactor. The measured inlet concentrations were the boundary conditions for the calculation.

Overall, it can be seen that the error of the CO concentration is the highest of all measured and calculated components. However, the absolute error is quite low, which indicates a good agreement of the measured and calculated values.

Taking a look at OP1, it can be seen that the measured and calculated values show good agreement regarding the concentrations of H_2, CO_2, CH_4, and N_2. The relative error of CO is higher than the relative errors of the other gas components. However, the absolute error is about 1 %.

Looking at OP2, it can be seen that the absolute and relative errors of the CO concentration are slightly higher than for OP1. In addition, OP2 has a higher CO_2 concentration than the CO concentration at the inlet of the WGS reactor which can be attributed to a partial load operation of the gasification plant during this measurement. At partial load operation, a higher steam to fuel ratio leads to higher CO_2 concentrations and, consequently, to lower CO concentrations (compare [14]).

OP3 shows similar results as for OP1. However, the overall errors are higher; especially, the CO concentration shows a higher relative error and a higher absolute error compared to OP1.

OP4 shows, again, good agreement of the measured and calculated concentrations at the outlet of the WGS reactor. It shows again the highest relative error for the CO concentrations. The absolute error of 0.9 % is also in the same order of magnitude as for the other operating points.

Table 4 Concentrations at the inlet and outlet of the WGS reactor for all operating points. The measured reactor inlet concentrations as well as the measured and calculated reactor outlet concentrations are shown. The H_2 concentration of the measurements was calculated by closing the mass balance as H_2 could not be detected by the GC. The measurements were single sample measurements; therefore, no standard deviation can be given

	φ_{H2} %	φ_{CO} %	φ_{CO2} %	φ_{CH4} %	φ_{N2} %
OP1					
Inlet	38.9	25.4	20.7	10.5	4.5
Outlet measured	48.9	3.4	35.0	9.0	3.7
Outlet calculated	49.9	2.9	34.9	8.6	3.7
Rel. error	1.9 %	14.1 %	0.3 %	3.7 %	0.3 %
OP2					
Inlet	37.3	23.0	24.1	10.4	5.2
Outlet measured	46.7	4.4	36.0	9.0	3.9
Outlet calculated	46.4	5.1	35.2	8.9	4.4
Rel. error	0.6 %	17.2 %	2.4 %	1.0 %	12.7 %
OP3					
Inlet	39.8	25.3	21.1	9.5	4.3
Outlet measured	49.8	5.1	33.3	8.4	3.4
Outlet calculated	50.3	3.6	34.8	7.9	3.6
Rel. error	0.8 %	30.0 %	4.5 %	6.6 %	4.7 %
OP4					
Inlet	38.2	23.3	22.7	10.0	5.8
Outlet measured	48.4	3.4	35.2	8.7	4.5
Outlet calculated	48.7	2.5	35.8	8.3	4.8
Rel. error	0.6 %	27.5 %	1.7 %	3.9 %	8.1 %

3.3 Comparison of the improved with the former model

In this section, the improved and the former kinetic model are compared by using the experimental data from OP1. Figure 9 shows the comparison of the temperature profile between the measured data, the improved kinetic model, and the former kinetic model.

It can be seen that the temperature profile, which was calculated with the former kinetic model, shows significant deviation compared with the measured data and, therefore, also with the improved kinetic model.

Table 5 shows the comparison of the volumetric fractions of the gas components between the measured data, the improved kinetic model, and the former model.

It can be seen that the former kinetic model shows a higher H_2 and CO_2 concentration and, consequently, a lower CO content. This could be explained by the higher reaction rate of the former kinetic model. In addition, the volumetric fractions of the former kinetic model are very close to the equilibrium composition at the given parameters.

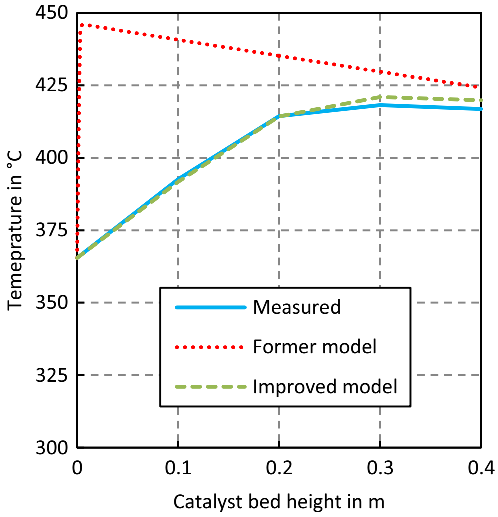

Fig. 9 Comparison of the temperature profile along the WGS reactor between the measured data, the improved kinetic model, and the former kinetic model using data from OP1

In contrast, the CH_4 and N_2 concentrations of the former and improved are at the same level, which indicates, that CH_4 and N_2 did not take part in a reaction and the error between the measured and calculated values was caused by a measurement error. The small deviation can be explained by the slightly higher volumetric dry gas flow rate if the former kinetic model is employed for the calculation.

4 Conclusion and outlook

In this paper, a former kinetic model for the water gas shift reaction was improved with experimental data from a water gas shift reactor which processed real product gas from dual fluidized bed biomass steam gasification and which employed a commercial Fe-/Cr-based catalyst. Both kinetic models, the former one and the improved one, considered a H_2S amount of about 100 $cm^3\ m^{-3}$ which is usually contained in the product

Table 5 Comparison of the volumetric fractions of the gas components between the measured data, the improved kinetic model, and the former model using data from OP1

	φ_{H2} (%)	φ_{CO} (%)	φ_{CO2} (%)	φ_{CH4} (%)	φ_{N2} (%)
Inlet	38.9	25.4	20.7	10.5	4.5
Outlet measured	48.9	3.4	35.0	9.0	3.7
Outlet improved	49.9	2.9	34.9	8.6	3.7
Outlet former	50.5	1.7	35.7	8.5	3.6

gas generated from dual fluidized bed biomass steam gasification.

$$r(\varphi_i, T) = 117.8\,\frac{\mathrm{mol}}{g\ \ Pa^{1.71}s}\cdot exp\left(\frac{-126.6\,\frac{\mathrm{kJ}}{\mathrm{mol}}}{R\cdot T}\right)\cdot p_{\mathrm{CO}}^{1.77}\cdot p_{\mathrm{H2O}}^{0.23}\cdot p_{\mathrm{CO2}}^{-0.17}\cdot p_{\mathrm{H2}}^{-0.12}\cdot\left(1-\frac{K_{\mathrm{MAL}}}{K_g}\right)$$

Furthermore, this improved kinetic model was validated with the experimental data from four different operating points of the water gas shift reactor.

In order to enhance the accuracy of the validation, the heat losses of the water gas shift reactor, which play a significant part in the energy balance, were also considered.

For the improvement of the former kinetic model and the validation of the improved kinetic model, the gas composition at the inlet and the outlet of the water gas shift reactor was measured. In addition, the temperature profile along the catalyst bed of the reactor was recorded.

Overall, the validation showed good agreement of the measured and calculated values for the gas compositions and the temperature profiles of the water gas shift reactor. Of all considered gas components, the CO concentration showed the highest error. However, the highest absolute error was about 1.5 % (relative error of 30.0 %). The highest absolute error of the temperature profile was 21 °C (relative error of 4.8 %). In addition, a low steam to dry gas ratio at the reactor inlet (from 1.2 and below), reduced the accuracy of the model.

Hence, these results qualify the presented improved kinetic model for basic design and engineering of a water gas shift reactor which employs a commercial Fe-/Cr-based catalyst and which processes product gas derived from dual fluidized biomass steam gasification if the steam to dry gas ratio at the reactor inlet is set to about 1.5.

Furthermore, future work should focus on an additional kinetic model which considers a product gas which is derived from the gasification of alternative fuels like waste or, for example, plastic residues.

Abs, absolute; BDL, below detection limit; Cat, catalyst; CHP, combined heat and power; d.b., dry basis; DFB, dual fluidized bed; DL, detection limit; FR, flow record; GC, gas chromatograph; OP, operating point; ORC, organic Rankine cycle; Rel, relative; RME, rapeseed methyl ester; STP, standard temperature and pressure (273.15 K and 101325 Pa); TX, thermocouple X along the WGS reactor; TCD, thermal conductivity detector; WGS, water gas shift.

Greek Symbols α_0 Heat transfer coefficient of the outer reactor wall to the ambient in W m^{-2} K^{-1}

α_{Conv} Heat transfer coefficient of the outer reactor wall caused by natural convection in W m^{-2} K^{-1}

α_{R} Heat transfer coefficient of the inner reactor wall in W m^{-2} K^{-1}

α_{Rad} Heat transfer coefficient of the outer reactor wall caused by radiation in W m^{-2} K^{-1}

β Thermal expansion coefficient of air in K^{-1}

φ_i Volumetric fraction of component *i* in −

δ_{I} Insulation thickness in m

δ_{S} Reactor wall thickness in m

$\in_0$ Emission coefficient of the thin aluminum layer in −

$\Delta G(T)$ Gibbs enthalpy as function of temperature in kJ mol^{-1}

Δh_{R} Enthalpy of formation for a certain temperature in kJ mol^{-1}

ΔH Enthalpy of formation at 298.15 K and 101,325 Pa in kJ mol^{-1}

$\Delta\,\dot{Q}\,(z)$ Heat losses along the reactor in W

λ Heat conductivity of air in W m^{-1} K^{-1}

λ_{I} Heat conductivity of the insulation in W m^{-1} K^{-1}

λ_{S} Heat conductivity of the reactor wall in W m^{-1} K^{-1}

v Kinematic viscosity of air in m^2 s^{-1}

ρ_{S} Catalyst bulk density

σ Stefan-Boltzmann constant in W m^{-2} K^{-4}

Δz Differential height element of the reactor in m

Latin Symbols *a* Reaction exponent for CO in -

A Cross section of the reactor in m^2

A_0 Outer reactor surface in m^2

A_i General inner cylindrical surface in m^2

A_{I} Mean logarithmic surface of the insulation in m^2

A_{m} General mean logarithmic surface in m^2

A_o General outer cylindrical surface in m^2

A_{R} Inner reactor surface in m^2

A_{S} Mean logarithmic surface of the reactor in m^2

b Reaction exponent for H_2O in −

c Reaction exponent for CO_2 in −

d Reaction exponent for H_2 in −

d_0 Outer reactor diameter in m

d_{I} Inner reactor diameter including reactor wall and insulation in m

d_{R} Inner reactor diameter in m

d_{S} Inner reactor diameter including reactor wall in m

E_{a} Activation energy in kJ mol^{-1}

Err Error in K

g Gravitational constant in m^2 s^{-1}

GHSV Gas hourly space velocity in h^{-1}

Gr Grashof number in −

k_0 Rate constant in mol g^{-1} $Pa^{-(a+b+c+d)}$ s^{-1}

K Control variable for the finite difference approach in −

K_{g} Equilibrium constant calculated by thermo-physical properties in −

K_{MAL} Equilibrium constant calculated by the mass action law in −

$\dot{n}_i$ Molar flow rate of component *i* in mol s^{-1}

Nu Nusselt number in −

p Absolute pressure in Pa
p_i Partial pressure of component i in Pa
Pr Prandtl number in −
r Reaction rate in mol g^{-1} s^{-1}
R General gas constant in J mol^{-1} K^{-1}
R_Q Overall heat transfer conductivity in W K^{-1}
STDGR Steam to dry gas ratio in −
T Temperature in K
T_0 Ambient temperature in K
T_S Surface temperature of the thin Al layer of the insulation in K
$T_{c,i}$ Calculated temperature at thermocouple i in K
$T_{m,i}$ Measured temperature at thermocouple i in K
V_Cat Catalyst bulk volume in m^3
$\dot{V}_\mathrm{Dry}$ Volumetric dry gas flow rate at STP in m^3 h^{-1}
$\dot{V}_\mathrm{H2O}$ Volumetric steam flow rate at STP in m^3 h^{-1}
X_CO CO conversion in −

Acknowledgments Open access funding provided by TU Wien. The authors want to thank Air Liquide, Guessing Renewable Energy GmbH, and ISG Energy for making this research possible. In addition, the plant operators of the gasification plant in Oberwart are gratefully acknowledged.

The company Clariant is thanked for providing the commercial Fe-/Cr-based catalyst.

Stephan Kraft is acknowledged for lively discussions regarding the Scilab™ source code and Matthias Binder is acknowledged for help with the experimental work and Silvester Fail is thanked for the buildup and construction of the water gas shift reactor.

This work was carried out within the framework of the Bioenergy2020+ GmbH project “C20005 Polygeneration III”. Bioenergy2020+ GmbH is funded by the states Burgenland, Niederösterreich, Steiermark, and within the Austrian COMET program which is managed by the Austria Research Promoting Agency (FFG).

Open Access This article is distributed under the terms of the Creative Commons Attribution 4.0 International License (http://creativecommons.org/licenses/by/4.0/), which permits unrestricted use, distribution, and reproduction in any medium, provided you give appropriate credit to the original author(s) and the source, provide a link to the Creative Commons license, and indicate if changes were made.

References

1. H. D. Baehr. Waerme- und Stoffuebertragung. Springer, 2013. doi: 10.1007/978-3-642-36558-4
2. Bohlbro H, Jorgensen M (1970) Catalysts for conversion of carbon monoxide. Chem Eng World 46:5–8
3. H. Bohlbro and E. Mogensen. An Investigation on the Kinetics of the Conversion of Carbon Monoxide with Water Vapour Over Iron Oxide Based Catalysts, 1969
4. Chinchen G, Logan R, Spencer M (1984) Water-gas shift reaction over an iron oxide/chromium oxide catalyst.: III: kinetics of reaction. Applied Catal 12(1):97–103. doi:10.1016/S0166-9834(00)81507-9
5. Churchill S, Chu H (1975) Correlating equations for laminar and turbulent free convection from a horizontal cylinder. Int J Heat Mass Transf 18:1049–1053. doi:10.1016/0017-9310(75)90222-7
6. N. Diaz. Hydrogen Separation from Producer Gas Generated by Biomass Steam Gasification. PhD thesis, TU Wien, 2013
7. S. Fail. Biohydrogen Production Based on the Catalyzed Water Gas Shift Reaction in Wood Gas. PhD thesis, TU Wien, 2014
8. S. Fail, N. Diaz, F. Benedikt, M. Kraussler, J. Hinteregger, K. Bosch, M. Hackel, R. Rauch, and H. Hofbauer. Wood gas processing to generate pure hydrogen suitable for PEM fuel cells. ACS Sustain Chem Eng, 2 (12): 2690–2698, 2014. doi: 10.1021/sc500436m.
9. Glavachek V, Morek M, Korzhinkova M (1968) Kinet Katal 9: 1107–1110
10. S. Hla, G. Duffy, L. Morpeth, A. Cousins, D. Roberts, and J. Edwards. Investigation of the effect of total pressure on performance of the catalytic water gas shift reaction using simulated coal-derived syngases. Catal Comm, 11 (4): 272–275, 2009. doi: 10.1016/j.catcom.2009.10.013.
11. S. Hla, D. Park, G. Duffy, J. Edwards, D. Roberts, A. Ilyushechkin, L. Morpeth, and T. Nguyen. Investigation into the performance of a Co-Mo based sour shift catalyst using simulated coal-derived syngases. Chem Eng J, 146 (1): 148–154, 2009. doi: 10.1016/j.cej.2008.09.023.
12. S. S. Hla, D. Park, G. Duffy, J. Edwards, D. Roberts, A. Ilyushechkin, L. Morpeth, and T. Nguyen. Kinetics of high-temperature water-gas shift reaction over two iron-based commercial catalysts using simulated coal-derived syngases. Chem Eng J, 146 (1): 148–154, 2009. doi: 10.1016/j.cej.2008.09.023.
13. Keiski RL, Salmi T, Niemisto P, Ainassaari J, Pohjola VJ (1995) Stationary and transient kinetics of the high temperature water-gas shift reaction. Applied Catal A: General 137(2):349–370. doi:10.1016/0926-860X(95)00315-0
14. Koppatz S, Pfeifer C, Hofbauer H (2011) Comparison of the performance behaviour of silica and olivine in a dual fluidised bed reactor system for steam gasification of biomass at pilot plant scale. Chem Eng J 175:468–483. doi:10.1016/j.cej.2011.09.071
15. M. Kraussler, M. Binder, S. Fail, A. Plaza, A. Cortes, and H. Hofbauer. Validation of a kinetic model for the catalyzed water gas shift reaction applying a Fe/Cr catalyst processing product gas from biomass steam gasification. In Proceedings of the 23rd European Biomass Conference and Exhibition, 2015
16. Kraussler M, Binder M, Fail S, Bosch K, Hackel M, Hofbauer H (2016) Performance of a water gas shift pilot plant processing product gas from an industrial scale biomass steam gasification plant. Biomass Bioenerg 89:50–57. doi:10.1016/j.biombioe.2015.12.001
17. Kraussler M, Binder M, Hofbauer H (2016) 2250-h long term operation of a water gas shift pilot plant processing tar-rich product gas from an industrial scale biomass steam gasification plant. Int J Hydorgen Energ 41(15):6247–6258. doi:10.1016/j.ijhydene.2016.02.137
18. B. J. McBride, S. Gordon, and M. A. Reno. Coefficients for Calculating Thermodynamic and Transport Properties of Individual Species. Technical report, NASA Lewis Research Center, 1993
19. Mueller S, Stidl M, Proell T, Hofbauer H (2011) Hydrogen from biomass: large-scale hydrogen production based on a dual fluidized bed steam gasification system. Biomass Conv Bioref 1(1):55–61. doi:10.1007/s13399-011-0004-4
20. Podolski WF, Kim YG (1974) Modeling the water-gas shift reaction. Ind Eng Chem Process Des Dev 13(4):415–421. doi:10.1021/i260052a021
21. Rehling B, Hofbauer H, Rauch R, Aichernig C (2011) BioSNG-process simulation and comparison with first results from a 1-MW demonstration plant. Biomass Conv Bioref 1(2):111–119. doi:10.1007/s13399-011-0013-3
22. Rhodes C, Hutchings GJ (2003) Studies of the role of the copper promoter in the iron oxide/chromia high temperature water gas shift catalyst. Phys Chem Chem Phys 5:2719–2723. doi:10.1039/B303236C

23. Rhodes C, Hutchings G, Ward A (1995) Water-gas shift reaction: finding the mechanistic boundary. Catal Today 23(1):43–58. doi:10.1016/0920-5861(94)00135-O
24. Sauciuc A, Abosteif Z, Weber G, Potetz A, Rauch R, Hofbauer H, Schaub G, Dumitrescu L (2012) Influence of operating conditions on the performance of biomass-based Fischer-Tropsch synthesis. Biomass Conv Bioref 2(3):253–263. doi:10.1007/s13399-012-0060-4
25. G. Smith. Numerical Solution of Partial Differential Equations: Finite Difference Methods. Oxford University Press, 3rd edition, 1985
26. M. V. Twigg. Catalyst Handbook. Manson Publishing, 1989.
27. www.scilab.org. Open source software for numerical computation, November 2015. URL www.scilab.org.
28. Zhu M, Wachs IE (2015) Iron-based catalysts for the high-temperature water-gas shift (HT-WGS) reaction: a review. ACS Catal 6(2):722–732. doi:10.1021/acscatal.5b02594

Paper 6

Michael Kraussler, Matthias Binder, Philipp Schindler, Hermann Hofbauer, Hydrogen production within a polygeneration concept based on dual fluidized bed biomass steam gasification, Biomass and Bioenergy, Available online 24. December 2016, `http://dx.doi.org/10.1016/j.biombioe.2016.12.008`.

Contribution: Experimental work, data treatment, writing

ARTICLE IN PRESS

Biomass and Bioenergy xxx (2016) 1–10

Contents lists available at ScienceDirect

Biomass and Bioenergy

journal homepage: http://www.elsevier.com/locate/biombioe

Research paper

Hydrogen production within a polygeneration concept based on dual fluidized bed biomass steam gasification

Michael Kraussler [a, b, *], Matthias Binder [a, b], Philipp Schindler [b], Hermann Hofbauer [b]

[a] Bioenergy2020+ GmbH, Wienerstrasse 49, 7540 Güssing, Austria
[b] TU Wien, Institute of Chemical Engineering, Getreidemarkt 9, 1060 Wien, Austria

ARTICLE INFO

Article history:
Received 12 August 2016
Received in revised form
24 November 2016
Accepted 12 December 2016
Available online xxx

Keywords:
Polygeneration
Biomass
Dual fluidized bed
Steam gasification
Water gas shift
Hydrogen

ABSTRACT

Dual fluidized bed biomass steam gasification generates a high calorific, practically nitrogen-free product gas with a volumetric H_2 content of about 40%. Therefore, this could be a promising route for a polygeneration concept aiming at the production of valuable gases (for example H_2), electricity, and heat. In this paper, a lab-scale process chain, based on state of the art unit operations, which processed a tar-rich product gas from a commercial dual fluidized bed biomass steam gasification plant, is investigated regarding H_2 production within a polygeneration concept. The lab-scale process chain employed a water gas shift step, two gas scrubbing steps, and a pressure swing adsorption step. During the investigations, a volumetric H_2 concentration of 99.9% with a specific H_2 production of 30 g kg^{-1} biomass was reached. In addition, a valuable off-gas stream with a lower heating value of 7.9 MJ m^{-3} was produced. Moreover, a techno-economic assessment shows the economic feasibility of such a polygeneration concept, if certain feed in tariffs for renewable electricity and H_2 exist. Consequently, these results show, that the dual fluidized bed biomass steam gasification technology is a promising route for a polygeneration concept, which aims at the production of H_2, electricity, and district heat.

© 2016 Elsevier Ltd. All rights reserved.

1. Introduction

Today, the steam reforming of fossil fuels, mainly of natural gas, is the state of the art technology for H_2 production. After steam reforming, the generated gas passes through a water gas shift (WGS) unit and is finally fed into a pressure swing adsorption (PSA) unit, where H_2 with a purity higher than 99.999% can be produced [1]. H_2 from biomass within a polygeneration concept could be a CO_2 neutral alternative offering a high fuel utilization ratio considering all products.

The dual fluidized bed (DFB) biomass steam gasification generates a product gas with a volumetric H_2 content of about 40% using biomass (wood chips) as feed stock. Therefore, this product gas could be used for CO_2 neutral H_2 production as well as for electricity generation if it is burned in gas engines. Moreover, the process heat can be used for district heating. In addition, in previous experimental investigations, it was also shown that DFB biomass steam gasification is a suitable process for the production of Fischer-Tropsch fuels as well as synthetic natural gas (SNG) [2,3]. Consequently, DFB biomass steam gasification offers a route for the simultaneous production of valuable gases (e.g. H_2 or CH_4), liquids, electricity, and district heat. This concept is referred to as polygeneration.

Several polygeneration processes have been comprehensively investigated by different authors. For example, Gassner et al. extensively investigated the polygeneration of SNG, power, and district heat [4]–[6]. Moreover, Gale et al. [7] investigated Fischer-Tropsch polygeneration concepts and Gao et al. [8], Li et al. [9], and Liu et al. [10] investigated polygeneration concepts aiming mainly at methanol production. In contrast, Tock and Marchal [11] investigated a polygeneration concept for H_2 production based on biomass and Kyriakarakos et al. [12] investigated a process aiming the production of H_2, potable water, and power based on wind energy and solar energy.

Former experiments carried out by this research group have investigated different process chains, which aimed at H_2 production from the product gas generated by DFB biomass steam gasification technology. The investigations were conducted at the site of the commercial DFB biomass steam gasification plant in Oberwart, Austria, which is a plant for heat and power generation. However, in

---

* Corresponding author. Bioenergy2020+ GmbH, Wienerstrasse 49, 7540 Güssing, Austria.
E-mail address: michael.kraussler@bioenergy2020.eu (M. Kraussler).

http://dx.doi.org/10.1016/j.biombioe.2016.12.008
0961-9534/© 2016 Elsevier Ltd. All rights reserved.

Please cite this article in press as: M. Kraussler, et al., Hydrogen production within a polygeneration concept based on dual fluidized bed biomass steam gasification, Biomass and Bioenergy (2016), http://dx.doi.org/10.1016/j.biombioe.2016.12.008

these investigations, the product gas was extracted after the tar scrubber of the gasification plant [13,14].

In contrast, recent research activities have shown that it is even possible to operate a lab-scale WGS unit with tar-rich product gas from the gasification plant without experiencing catalyst deactivation [15]–[17]. Processing the tar-rich product gas gives advantages regarding the energy efficiency because it can be extracted at a higher temperature (about 150°C) and with a higher volumetric steam content (about 35%). Therefore, less heating and steam addition is required before feeding the gas into a WGS unit.

This paper presents the investigations of a lab-scale process chain for the simultaneous production of pure H_2 and a valuable off-gas, which can be used for heat and power generation. The process chain was operated with tar-rich product gas extracted from the commercial DFB biomass steam gasification plant in Oberwart and employed a WGS step, two gas scrubbing steps, and a PSA step. Furthermore, a techno-economic assessment of the presented polygeneration process based on real gasification plant data and the experimental results was carried out.

2. Materials and methods

This section describes the process chain which was used for the experimental investigations. It covers the gasification plant and the lab-scale process chain with a WGS step, gas scrubbing steps, and a PSA step. A parameter study of the lab-scale process chain was conducted prior to this investigation in order to find suitable operating parameters for the different units. In addition, the methodology, which was used for the techno-economic assessment, is described.

2.1. The gasification plant

The lab-scale process chain processed tar-rich product gas from the industrial scale combined heat and power (CHP) gasification plant in Oberwart (fuel power 8 MW). Fig. 1 shows a simplified flowchart of the employed process.

The plant is based on the dual fluidized bed (DFB) steam gasification technology described in detail in Ref. [18]. The CHP plant generates district heat and electricity with biomass (wood chips) as feed stock. Information about the average feed stock composition can be reviewed in Ref. [19].

Biomass is fed into the biomass dryer and, subsequently, into a screw conveyor which transports the biomass into the gasifier. In the gasifier, the biomass is in contact with steam (steam to fuel ratio, d.a.f., of about 0.5) and the bed material (olivine) at about 850°C. The resulting product gas has a volumetric composition of about 40% H_2, 25% CO, 22% CO_2, 10% CH_4, as well as minor amounts of C_xH_y, N_2, and sulfur components. Furthermore, the product gas has a lower heating value (LHV) of up to 14 MJ m^{-3} (d.b.) and a dust content of about 26 g m^{-3} [19].

In the subsequent process steps, the product gas is cooled and passes through a bag house filter. The bag house filter has a particle separation efficiency of more than 99%. Therefore, a practically dust free product gas can be assumed after the filter [20]. In addition, in the following rapeseed methyl ester (RME) gas scrubber, the product gas is cooled from about 150 to 40°C, therefore, tar, steam, and other condensable fractions of the product gas are removed before the product gas is fed into the gas engines for electricity generation. Heat from the flue gas line is mainly recovered for the process and for district heating. Fly ash is removed before the flue gas is released into the atmosphere.

It is possible to extract a partial flow of the product gas for experimental work from an extraction point located before the RME gas scrubber (see Fig. 1). The tar content of the gas extracted before the RME gas scrubber is significantly higher (about 9 g m^{-3} GCMS tar [19]) than after the RME gas scrubber (about 3 g m^{-3} GCMS tar [19]), which is a challenge for the reliable operation of the subsequent process chain. However, the tar-rich product gas has a higher temperature and a higher volumetric steam content (about 150°C and 35%) compared to the gas extracted after the RME scrubber (temperature about 40°C and volumetric steam content of about 7%). Therefore, the tar-rich product gas shows advantages regarding the energy efficiency because the gas needs less heating and less additional steam before processing in a WGS reactor. A detailed description of the process and the CHP plant can be found in Refs. [13,20,21].

2.2. The lab-scale process chain

This section describes the lab-scale process chain which processed the tar-rich product gas extracted from the gasification plant in order to generate H_2 and a valuable off-gas stream. Fig. 2 shows a simplified flowchart of the process chain where I to V indicate the gas sampling points. The process chain employed a WGS unit, an RME scrubber, a glycol scrubber, and a PSA unit for the final gas separation. These different units are discussed below.

2.2.1. The water gas shift unit

The aim of the water gas shift unit was the conversion of CO to H_2 according to Equation (1).

$$CO + H_2O \rightleftharpoons H_2 + CO_2 \quad \Delta H = -41.1 \mathrm{kJ \cdot mol^{-1}} \tag{1}$$

The WGS unit consisted of three fixed bed reactors (A, B, and C) in series filled with a commercially available Fe/Cr based catalyst. Each catalyst bed had a diameter of about 9 cm and a bed height of about 40 cm resulting in a catalyst volume of approximately 2.5 dm^3 in each reactor. The activation procedure of the catalyst before the operation is described in detail in Ref. [21].

Along the height of each reactor, seven type J thermocouples were installed in order to record the temperature profile along the reactors. At the inlet and outlet of each reactor, the gas stream could be heated or cooled in order to achieve the desired gas inlet, respectively, outlet temperatures.

Before the inlet (I, Fig. 2) of the first reactor, steam was added to assure a high steam content in the processed gas in order to avoid coking and carbon deposition on the catalyst surface. The WGS unit was operated at ambient pressure and the gas inlet temperature was set to about 350°C (I, Fig. 2).

In previous experiments, the WGS unit was operated with a tar-rich product gas for more than 2250 h in order to prove the stability of the catalyst under the conditions of a tar-rich product gas. During that investigation, no catalyst deactivation could be observed [16].

2.2.2. The gas scrubbing units

Two gas scrubbing units were employed after the WGS unit in order to remove tar and NH_3 from the processed gas. In addition, steam should be condensed.

The first scrubbing device, which is referred to as the RME scrubber, used RME as the scrubbing fluid. In past investigations, it turned out that RME is a good solvent for tar [22]. The RME scrubber was operated at ambient pressure and at a temperature of about 15°C. Therefore, the tar-rich gas stream was cooled and, consequently, tar was condensed and dissolved in the RME. Furthermore, steam contained in the gas stream was condensed and most of the NH_3 was dissolved in the condensed steam. Some RME in the scrubber was continually removed and replaced with fresh RME in order to avoid saturation with tar.

After the RME scrubber, the processed gas passed through a

Please cite this article in press as: M. Kraussler, et al., Hydrogen production within a polygeneration concept based on dual fluidized bed biomass steam gasification, Biomass and Bioenergy (2016), http://dx.doi.org/10.1016/j.biombioe.2016.12.008

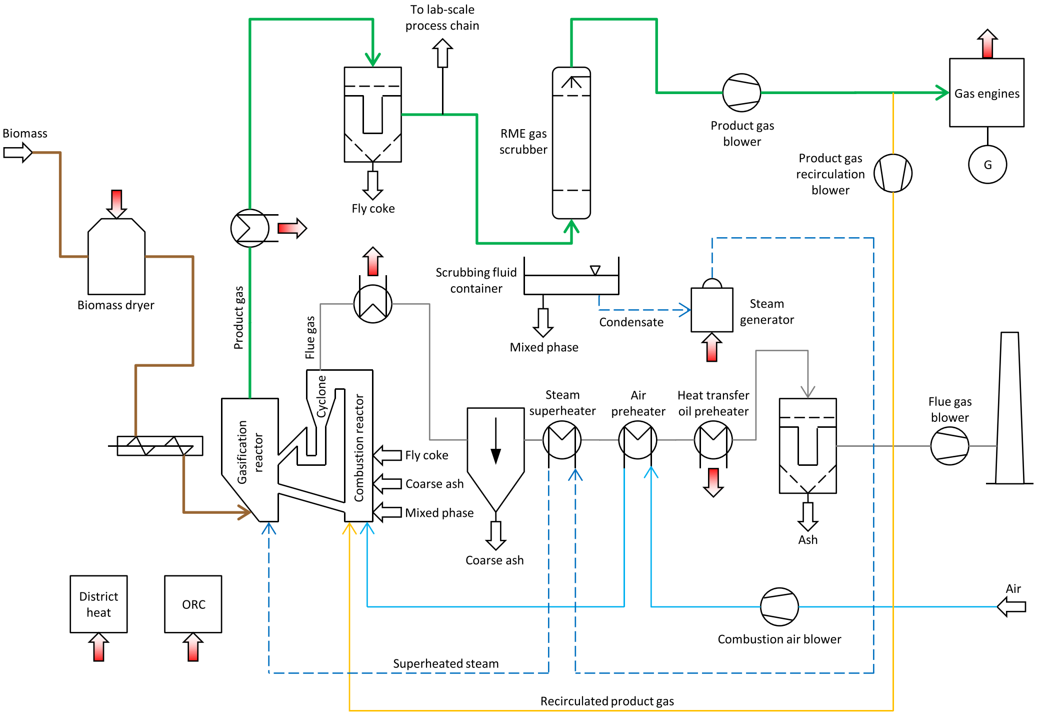
To lab-scale process chain
Biomass
Biomass dryer
Product gas
Flue gas
Fly coke
RME gas scrubber
Product gas blower
Gas engines
G
Product gas recirculation blower
Scrubbing fluid container
Mixed phase
Condensate
Steam generator
Gasification reactor
Cyclone
Combustion reactor
Fly coke
Coarse ash
Mixed phase
Coarse ash
Steam superheater
Air preheater
Heat transfer oil preheater
Ash
Flue gas blower
Air
Combustion air blower
District heat
ORC
Superheated steam
Recirculated product gas

Fig. 1. Simplified flowchart of the gasification plant in Oberwart, Austria.

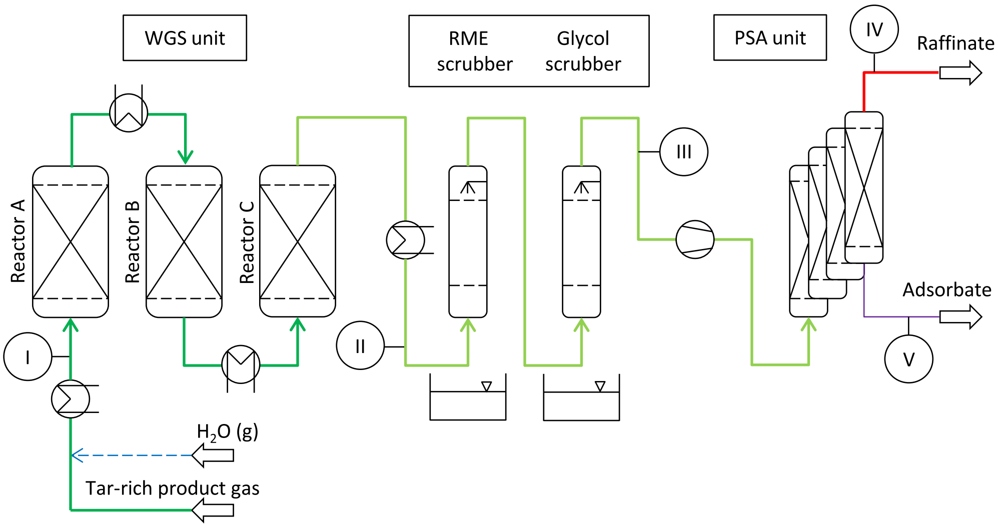
WGS unit
RME scrubber
Glycol scrubber
PSA unit
IV
Raffinate
III
Reactor A
Reactor B
Reactor C
I
II
Adsorbate
V
H₂O (g)
Tar-rich product gas

Fig. 2. Simplified flowchart of the investigated lab-scale process chain. I, II, III, IV, and V indicate sampling points for measurements.

glycol scrubber which was also operated at ambient pressure but at a lower temperature of about -5°C, in order to condense the remaining steam and other remaining minor condensable impurities. The glycol in the scrubber was also continually removed and replaced with fresh glycol in order to avoid saturation as well. Therefore, after the glycol scrubber, a dry gas stream could be assumed which was, subsequently, led to the compressor of the PSA unit.

2.2.3. *The pressure swing adsorption unit*

The first part of the PSA unit was a compression of the dry gas stream (feed) to an absolute pressure of 0.4 MPa. The compressed gas stream was subsequently led to the second part of the PSA.

This second part consisted of four pressure vessels, each one filled with about 4.7 dm^3 of activated carbon (Norit RB 2). The four pressure vessels were interconnected with automated valves in order to enable a continuous operation of the PSA unit. When the activated carbon in one of the pressure vessels reached saturation, it was regenerated by removing the adsorbed gas components via lowering the pressure to about 0.02 MPa. These gas components were extracted from the bottom of the pressure vessel and are referred to as adsorbate (off-gas). The high pressure product is referred to as raffinate and was, during this investigation, pure H_2.

The different gas components have different adsorbing behaviors with the activated carbon. Looking at the main gas components of the processed gas, the adsorption strength can be described by

Please cite this article in press as: M. Kraussler, et al., Hydrogen production within a polygeneration concept based on dual fluidized bed biomass steam gasification, Biomass and Bioenergy (2016), http://dx.doi.org/10.1016/j.biombioe.2016.12.008

the following relation: $CO_2 > CH_4 > CO > H_2$ [1]. This means that CO_2 is preferably adsorbed on the activated carbon and, therefore, better removed from the feed gas stream than, for example, H_2. Hence, activated carbon is a suitable adsorbent for the production of pure H_2.

In order to find suitable operating parameters for the PSA unit, a parameter study was carried out before the test run of the whole process chain. During the study, the adsorption pressure and the adsorption time was varied.

2.3. Gas analytics

A gas chromatograph (GC, Clarus 500™ from Perkin Elmer) was used to measure the gas composition at the sampling points I to V (Fig. 2). A small analytical gas stream was led through two gas washing bottles filled with glycol at a temperature of about −5°C in order to condense the steam. Therefore, a dry gas stream could be assumed after the two gas washing bottles. The dry gas stream passed another gas washing bottle filled with glass wool in order to prevent aerosols from entering the GC. After the glass wool filter, a gas meter recorded the volumetric dry gas flow.

In the GC, a thermal conductivity detector (TCD) enabled the quantification of CO, CO_2, CH_4, N_2, O_2, C_2H_6, C_2H_4, and C_2H_2 with two different columns (7′ HayeSep N, 60/80 1/8″ SF and 9′ molecular sieve 13x 45/60, 1/8″ SF). The C_2 species were summarized and are referred to as C_2H_y. The H_2 content was calculated by closing the mass balance. Furthermore, H_2, CO, CO_2, and CH_4 are referred to as the main gas components.

In order to measure the steam content, the gas was sent through the glycol gas washing bottles at −5°C for a certain time. Subsequently, the volumetric dry gas flow was recorded with a gas meter. By weighing the gas washing bottles before and after a certain time, the water content was determined. Subsequently, the volumetric flow rates were calculated with the water balance.

In this paper, all gas volumes and volumetric gas flow rates are given at standard temperature and pressure (STP, 273.15 K and 101325 Pa).

In addition, the least squares method, using the numerical software package Scilab™, was applied to the WGS and PSA unit in order to find a balanced solution for the composition of all gas streams and for the volumetric flow rates. This approach of data reconciliation includes the standard deviation of every single measured value (compare [23]).

2.4. Key figures

The following key figures (Equations (2)–(4)) describe the operating conditions as well as results along the process chain.

The gas hourly space velocity (GHSV, see Equation (2)) indicates the stress of the catalyst in a chemical reactor. The GHSV was calculated for the first reactor of the WGS unit.

$$GHSV = \frac{\dot{V}_I}{V_{Cat}} \tag{2}$$

The steam to dry gas ratio (STDGR, see Equation (3)) describes the relative amount of steam along the WGS unit, which is very important for an adequate operation of the catalyst. It must not be too low in order to avoid coking and carbon deposition on the surface of the catalyst employed in the WGS unit.

$$STDGR = \frac{\dot{V}_{H_2O,I}}{\dot{V}_I} \tag{3}$$

The recovery of a component i (see Equation (4)) is the ratio of the amount of that component in two different streams. It is an indicator of a unit's efficiency at separating; in this paper, especially of the PSA unit.

$$\Omega_i = \frac{\varphi_{i,IV} \cdot \dot{V}_{IV}}{\varphi_{i,III} \cdot \dot{V}_{III}} \tag{4}$$

2.5. Techno-economic assessment

Based on real gasification plant data and the experimental results, a techno-economic assessment for the production of H_2, electricity, and district heat was carried out. Fig. 3 shows the process concept for the techno-economic assessment. Wood chips (fuel power of 8 MW) are converted in the DFB gasfication unit into the product gas. The product gas is fed into a WGS unit, where CO is converted with steam into additional H_2 and CO_2. Then, the product gas is fed into the RME scrubber, where tar is removed and the remaining steam is condensed. Furthermore, the gas is fed into a PSA unit were H_2 is separated. The adsorbate of the PSA unit is fed into a gas engine for electricity and district heat generation. In addition, heat, which is not needed for the process is also used for district heat generation. Moreover, a partial flow of the product gas is used as fuel for the combustion reactor of the DFB gasification system.

The techno-economic assessment is based on the approach described in Brown [24]. Data for the DFB gasification unit are based on Wilk and Hofbauer [19] and on data from the operators of the gasification plant Oberwart. Data for the other unit operations are based on the experiments described in this work.

The investment costs were estimated based on the information of a plant manufacturer and on expert talks. Investment costs from a different year than 2016 were adjusted using the chemical engineering plant cost index (CEPI). Additionally, the plant start-up expenses were considered with 10% of the calculated capital costs.

The production costs were split into detailed estimates and factored estimates. The detailed estimates were calculated on actual 2016 prices of material and energy streams based on the information of the plant operators of the gasification plant Oberwart. Table 1 gives an overview about the considered production costs.

In addition, it was assumed, that the renewable electricity feed-in tariff is higher than the electricity costs for the plant. Therefore, all electricity, which is needed for plant operation, is extracted from the grid.

Further assumptions were a staff of five employees in order to maintain a twenty-four-seven operation of the plant. In addition, the plant should operate for 8000 h per year in a 20 years lifetime. The techno-economic assessment was based on the net present value (NPV).

3. Results and discussion

This section discusses the results that were gathered with the lab-scale process chain during the investigations at the CHP plant Oberwart. A parameter study with the PSA unit was carried out prior to the investigation in order to determine the optimum process chain parameters for the production of H_2 and a valuable off-gas within a polygeneration concept based on DFB biomass steam gasification. Furthermore, the results of the techno-economic assessment are discussed.

Please cite this article in press as: M. Kraussler, et al., Hydrogen production within a polygeneration concept based on dual fluidized bed biomass steam gasification, Biomass and Bioenergy (2016), http://dx.doi.org/10.1016/j.biombioe.2016.12.008

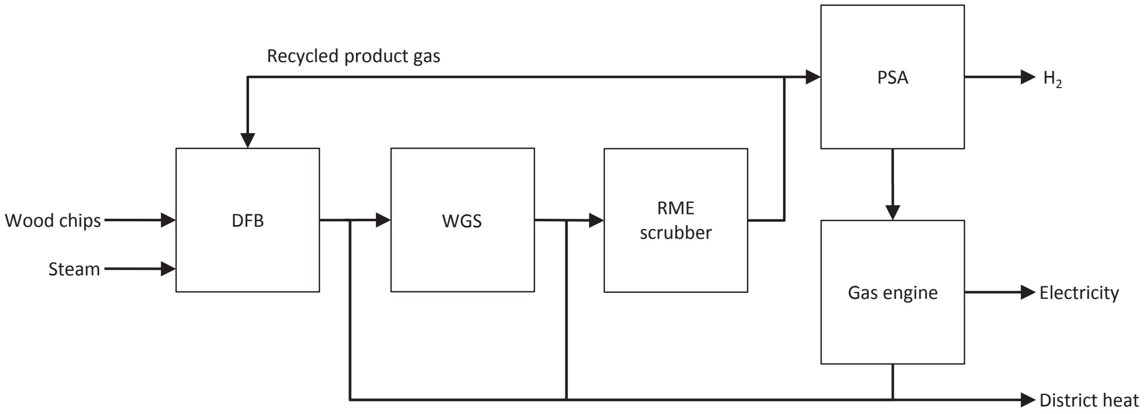

Fig. 3. Polygeneration concept for the techno-economic assessment.

Table 1
Production cost estimates (based on Ref. [24]).

	Detailed estimates	Factored estimates
Raw materials	Based on plant data	
Operating labor	Based on plant data	
Utilities	Based on plant data	
Employee benefits		22% of operating labor
Supervision		10% of operating labor
Laboratory		10% of operating labor
Maintenance		6% of investment costs
Insurance and taxes		3% of investment costs
Operating supplies		3% of investment costs
Plant overhead		1% of investment costs
Depreciation	$\frac{\text{Investmentcosts}}{\text{Plantlifetime}}$	

3.1. Parameter study of the pressure swing adsorption unit

Based on previous experiences (see Refs. [13] and [14]), this section shows the results of the parameter study, which was carried out with the PSA unit prior to the test run of the whole process chain. Fig. 4 shows the profile of the raffinate H_2 fraction over the adsorption time. It can be seen that with increasing adsorption time the H_2 purity decreased. In addition, at the same adsorption time, a higher adsorption pressure increased the H_2 purity.

Fig. 5 shows the profile of the raffinate H_2 recovery over the adsorption time.

A higher adsorption time led to an increased H_2 recovery. Furthermore, a higher adsorption pressure lowered the H_2 recovery.

Fig. 6 shows the profile of the raffinate H_2 fraction over the raffinate H_2 recovery. It summarizes the results of Figs. 4 and 5. It shows that there was a trade-off between H_2 purity and H_2 recovery. However, it also shows that a higher overall adsorption pressure increased the purity of the H_2 at constant H_2 recovery. Therefore, the operating point with an adsorption pressure of 0.4 MPa and an adsorption time of 300 s was chosen for the operation.

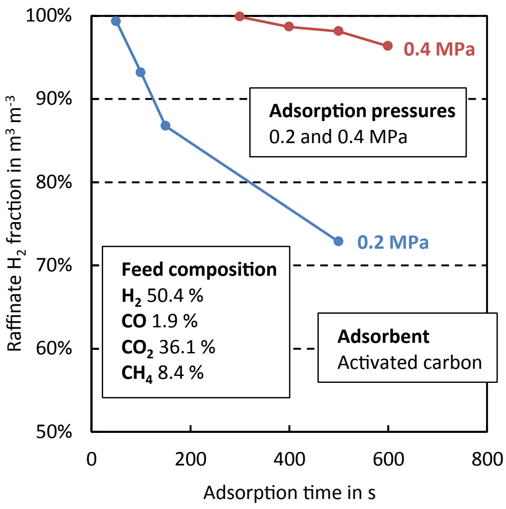

Fig. 4. Raffinate H_2 fraction over the adsorption time.

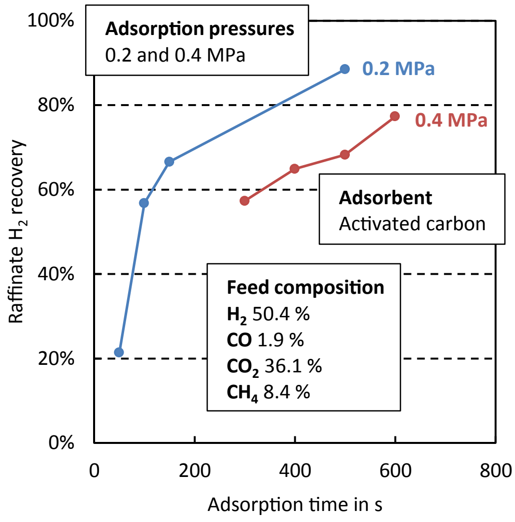

Fig. 5. Raffinate H_2 recovery over the adsorption time.

3.2. Operation of the whole process chain

Table 2 shows the main operating parameters of the process chain that were chosen for the investigation. The GHSV and the STDGR of the first reactor of the WGS unit were on the same order of magnitude as in previous experiments (see Refs. [14], [15], [16], and [17]). The adsorption pressure p_{Ads} and the adsorption time t_{Ads} were chosen in order to obtain a good compromise between H_2 purity and H_2 recovery as discussed in the previous section. In addition, as further requirement for the process, the adsorbate should also be suitable for combustion in a gas engine.

Please cite this article in press as: M. Kraussler, et al., Hydrogen production within a polygeneration concept based on dual fluidized bed biomass steam gasification, Biomass and Bioenergy (2016), http://dx.doi.org/10.1016/j.biombioe.2016.12.008

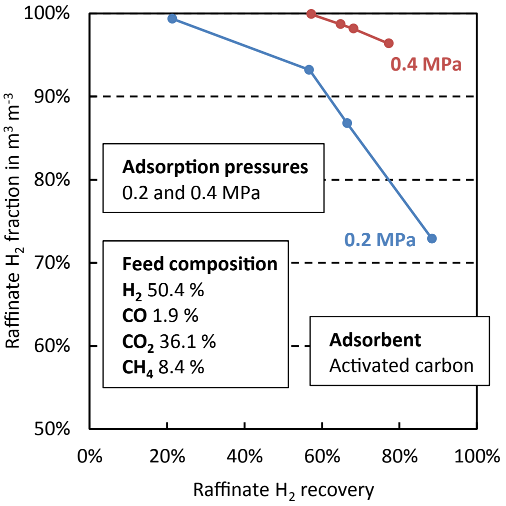

Fig. 6. Raffinate H_2 fraction over the raffinate H_2 recovery.

Table 3 shows the temperatures, pressures, and volumetric dry gas flow rates along the process chain at the sampling points I to V (compare Fig. 2). The product gas which was extracted from the gasification plant had a temperature of about 150°C with a steam content of about 35%. Before being processed in the WGS unit, steam was added to the gas stream and the resulting gas stream was subsequently heated up to the reactor inlet temperature of about 350°C (I, Table 3).

Along the first reactor of the WGS unit (reactor A), the temperature increased up to 420°C because of the exothermic nature of the WGS reaction. The gas inlet temperature of reactors B and C was also set to about 350°C. However, because of the unfavorable temperature level for the equilibrium composition of the gas stream before reactors B and C, nearly no WGS reaction occurred. Consequently, the heat losses along reactors B and C exceeded the temperature increase and the gas stream left reactor C at about 320°C. Along the WGS unit, there came about an increase of the volumetric dry gas flow rate by a factor of 1.15 due to the WGS reaction.

Before entering the RME scrubber, the gas stream was cooled to about 150°C (II, Table 3). In the RME scrubber, the gas stream was cooled to about 15°C. Therefore, tar and steam condensed and NH_3 was dissolved in the condensate. After the RME scrubber, the gas stream entered the glycol scrubber, which cooled the gas to about −5°C. Consequently, the remaining steam and minor impurities were condensed and separated from the gas stream (III, Table 3).

Based on a more than 2250 h lasting operation of the WGS unit employing the same Fe/Cr based catalyst wand processing tar-rich product gas (compare [16]), it can be assumed, that the higher tar content does not cause deactivation of the catalyst, if a certain steam to dry gas ratio is adhered. In addition, the results in Refs. [14,16,17] indicate, that no problems related to the higher tar or NH_3 content can be expected if the process chain is operated with tar-rich product gas. Subsequently, the gas stream was compressed to 0.4 MPa before entering the PSA unit, where the gas stream was split into the raffinate (IV, Table 3) and the adsorbate (V, Table 3).

Table 2
Main operating conditions of the lab-scale process chain. GHSV and STDGR are given for the inlet of the first WGS reactor.

GHSV h^{-1}	STDGR	p_{Ads} MPa	t_{Ads} s
483	1.5	0.4	300

Table 3
Temperatures, pressures, and volumetric dry gas flow rates along the lab-scale process chain.

	I	II	III	IV	V	Units
T	350	150	−5	20	20	°C
p	0.1	0.1	0.1	0.4	0.1	MPa
$\dot{V}_x$	1.2	1.4	1.4	0.4	1.0	$m^3\ h^{-1}$

Table 4 shows the measured dry gas compositions along the process chain. It can be seen that the extracted tar-rich product gas contained about 38.7% H_2 (I, Table 4). Along the WGS unit, the H_2 concentration was increased to 50.4% (II, Table 4). Along the scrubbing devices (RME and glycol), no change in the main gas composition could be observed. Furthermore, in the raffinate of the PSA unit, (IV, Table 4) an H_2 concentration of 99.9% was measured.

The CO content in the extracted product gas could be lowered from 26.0% to 1.9% along the WGS unit (I and II, Table 4). In reactor A, the CO content was decreased from 26.0% to about 4.0%, which was close to the equilibrium composition. In reactors B and C, the CO content was lowered to 1.9%. The reason for the low CO conversion in reactors B and C was the unfavorable temperature level for the equilibrium composition.

The CO_2 concentration increased from 21.5% to 36.1% along the WGS unit due to the WGS reaction (I and II, Table 4).

The CH_4 in the extracted product gas was lowered from 9.8% to 8.4% (I and II, Table 4) which can be attributed to the higher volumetric dry gas flow rate after the WGS unit (factor 1.15). Based on these results and other investigations (see Refs. [14–17,21]), it can be assumed that there were no reactions with CH_4 within the WGS unit.

Table 5 shows the raffinate recoveries of the main gas components within the PSA unit. It can be seen that activated carbon is a suitable adsorbent for H_2 production based on the product gas from biomass steam gasification with the chosen operating conditions. More than the half of the H_2 which was contained in the product gas after the WGS unit was found as a high pressure and high purity product in the raffinate stream of the PSA unit. In addition, CO, CO_2, and CH_4, were effectively separated and could be found in the adsorbate stream of the PSA unit.

Fig. 7 shows a Sankey diagram of the main gas components' volumetric flow rates along the investigated process chain. It indicates, that the raffinate stream (IV, Fig. 7) effectively contained practically only H_2 and the adsorbate stream (V, Fig. 7) contained H_2 as well as all the CO, CH_4, and CO_2. Moreover, based on a specific overall product gas production in the gasification plant of about $1\ m^3\ kg^{-1}$ biomass on a dry and ash free basis (Kirnbauer [25] gives a factor of 1.18 and Wilk [19] gives a factor of 0.9), a specific production of pure H_2 of about $30\ g\ kg^{-1}$ biomass (d.a.f.) (or

Table 4
Volumetric dry gas compositions along the process chain (DL = 2 $cm^3\ m^{-3}$). The measurements were validated with the least squares method in order to find the balanced solution.

	φ_{H_2} $m^3\ m^{-3}$	φ_{CO} $m^3\ m^{-3}$	φ_{CO_2} $m^3\ m^{-3}$	φ_{CH_4} $m^3\ m^{-3}$	$\varphi_{C_2H_y}$ $m^3\ m^{-3}$	φ_{N_2} $m^3\ m^{-3}$	φ_{O_2} $m^3\ m^{-3}$
I	38.7%	26.0%	21.5%	9.8%	2.5%	1.4%	0.07%
II	50.4%	1.9%	36.1%	8.4%	2.0%	1.2%	0.02%
III	50.4%	1.9%	36.1%	8.4%	2.0%	1.2%	0.02%
IV	99.9%	0.002%	0.04%	0.015%	0.01%	0.04%	0.015%
V	30.2%	2.7%	50.8%	11.9%	2.8%	1.6%	0.015%

Please cite this article in press as: M. Kraussler, et al., Hydrogen production within a polygeneration concept based on dual fluidized bed biomass steam gasification, Biomass and Bioenergy (2016), http://dx.doi.org/10.1016/j.biombioe.2016.12.008

Table 5
Recovery of the main gas components within the raffinate of the PSA unit.

Ω_{H_2} –	Ω_{CO} –	Ω_{CO_2} –	Ω_{CH_4} –
57.31%	0.030%	0.032%	0.052%

$0.33\ m^3\ kg^{-1}$) was reached after passing through the whole process chain. However, based on the given product gas composition in this paper, an ideal CO conversion in the WGS unit, and an ideal separation in the PSA unit, a specific production of pure H_2 of about 46 g kg^{-1} biomass (d.a.f.) would be possible. Therefore, the investigated process chain achieved an H_2 production efficiency of about 65%.

In contrast, Fig. 8 shows the sankey diagram of the mass flows of the main gas components. It shows, that the PSA unit has to separate a significant amount of CO_2. Hence, for a scale-up of the process chain, an additional CO_2 separation unit could be considered.

Fig. 9 shows a Sankey diagram of the energy streams of the main gas components based on their LHV.

It can be seen that the CH_4 accounted for about one-third of the energy content of the extracted product gas (I, Fig. 9). The CO_2 is not shown because it does not contribute to the LHV but dilutes and, therefore, lowers the LHV of the gas streams. Along the WGS unit, the overall energy content of the gas stream decreased because of the exothermic WGS reaction and the conversion of CO to H_2 and CO_2 leading to an overall feed energy stream of 3.4 kW (II and III, Fig. 9). Furthermore, the chosen PSA parameters led to an energy distribution of 35% to the raffinate (IV, Fig. 9) and 65% to the adsorbate (V, Fig. 9). Hence the raffinate stream had a LHV of 10.8 MJ m^{-3} and the adsorbate stream had a LHV of 7.9 MJ m^{-3}. Therefore, based on the fuel data of the gasification plant (see Ref. [19]) - LHV of 18.3 MJ m^{-3} and H_2O mass fraction of 32% - a fuel based raffinate efficiency of 20.8% and a fuel based adsorbate efficiency of 37.3% was reached. Consequently, the adsorbate stream could be used as fuel for the combustion reactor of the DFB process and/or as fuel for a gas engine for electricity and heat generation as one option within a polygeneration concept. Additionally, the lower H_2 content in the adsorbate, compared to the product gas, would reduce any knocking tendency in a gas engine.

3.3. Techno-economic assessment

In this section, the results of the techno-economic assessment are presented. Table 6 shows the main energy streams of the polygeneration plant. It can be seen, that the polygeneration process reaches an overall efficiency of about 70%, which is about the same order of magnitude as the commercial gasification plant for CHP in Güssing [26]. The H_2 efficiency is about 21%, the electrical efficiency is about 12.5%, and the district heat efficiency is about 36%.

Table 7 shows the results of the assessment of key figures which were the basis for the NPV calculation.

Fig. 10 shows the necessary H_2 price for a NPV equal zero at given electricity and district heat prices. It indicates, that, in order to reach a NPV equal zero, a H_2 price between 0.200 and 0.300 EUR kWh^{-1} (6.65 and 9.98 EUR kg^{-1}) is necessary at typical prices for renewable electricity (0.150 EUR kWh^{-1}) and district heat (0.040 EUR kWh^{-1}). However, the results show, that certain feed in tariffs are needed in order for economic feasibility of the presented polygeneration concept.

4. Conclusion and outlook

The investigations showed that dual fluidized bed biomass steam gasification technology is a suitable route for a polygeneration process which can produce valuable gases (for example H_2), electricity, and district heat. Tar-rich product gas was extracted from a commercial dual fluidized bed biomass steam gasification plant and processed in a lab-scale process chain which employed state of the art unit operations. Those unit operations were a water gas shift unit, a rapeseed methyl ester scrubber, a glycol scrubber, and a pressure swing adsorption unit. The gasification plant and the process chain enabled a flawless production of H_2 and a valuable off-gas which could be used as fuel for gas engines in order to generate electricity and heat.

During the investigations, an H_2 purity of 99.9% as well as an H_2 recovery of more than 57.3% was obtained with the PSA unit. Consequently, a specific H_2 production of 30 g kg^{-1} biomass was reached. This value is lower than the value described in Ref. [14], where a specific H_2 production of 46 g kg^{-1} was reached. However, in Ref. [14], the pressure swing adsorption unit was operated with a higher adsorption pressure (0.6 MPa), which allowed a higher H_2 recovery at nearly the same H_2 purity. Moreover, in Ref. [27], the

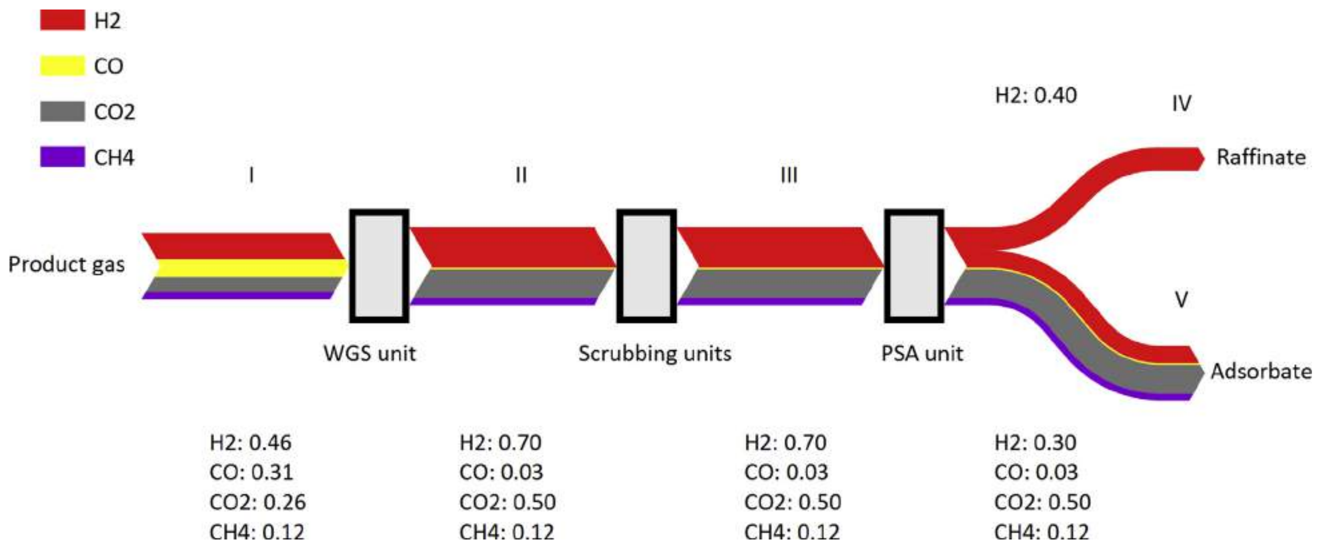

Fig. 7. Sankey diagram of the main gas components volumetric flow rates (H_2, CO, CO_2, and CH_4) along the lab-scale process chain. Volumetric flow rates are given in $m^3\ h^{-1}$ at STP.

Please cite this article in press as: M. Kraussler, et al., Hydrogen production within a polygeneration concept based on dual fluidized bed biomass steam gasification, Biomass and Bioenergy (2016), http://dx.doi.org/10.1016/j.biombioe.2016.12.008

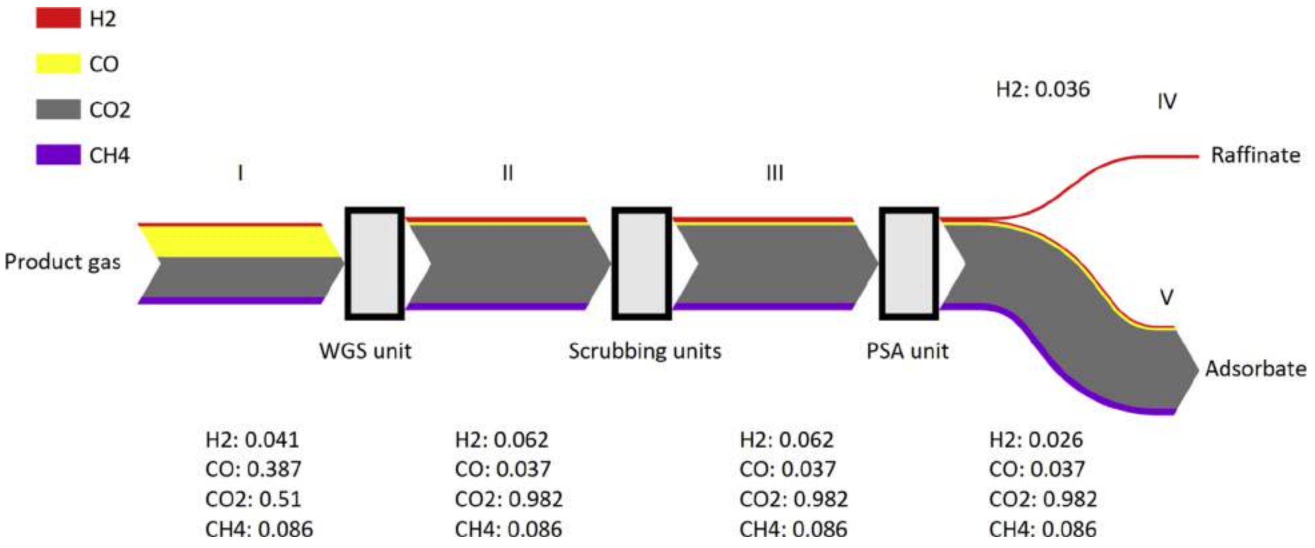
H2
CO
CO2
CH4
I
II
III
IV
V
H2: 0.036
Raffinate
Product gas
WGS unit
Scrubbing units
PSA unit
Adsorbate
H2: 0.041
CO: 0.387
CO2: 0.51
CH4: 0.086
H2: 0.062
CO: 0.037
CO2: 0.982
CH4: 0.086
H2: 0.062
CO: 0.037
CO2: 0.982
CH4: 0.086
H2: 0.026
CO: 0.037
CO2: 0.982
CH4: 0.086

Fig. 8. Sankey diagram of the main gas components mass flow rates (H_2, CO, CO_2, and CH_4) along the lab-scale process chain. Mass flow rates are given in kg h^{-1}.

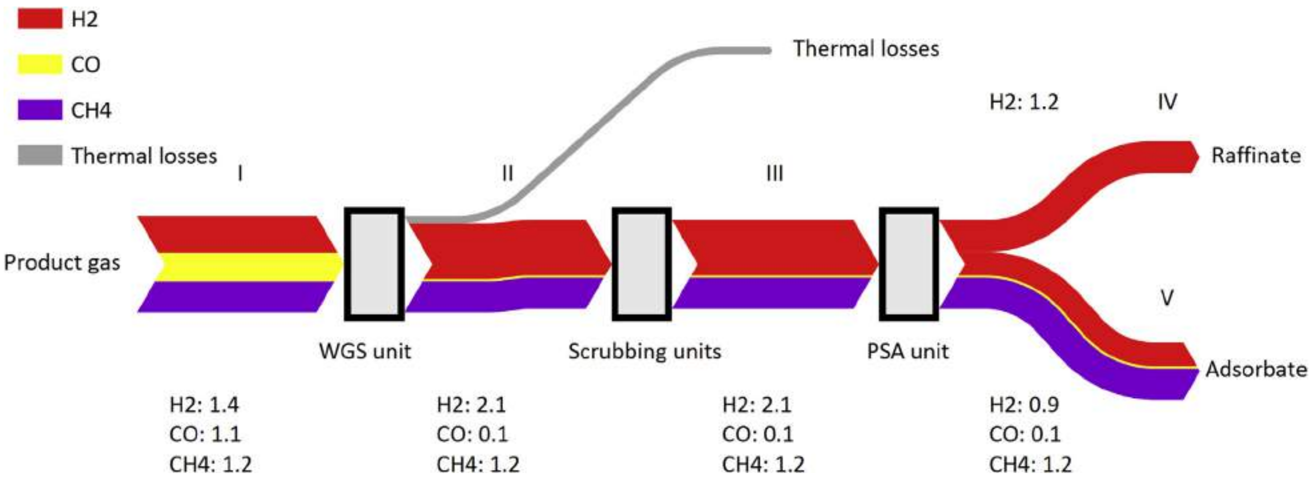
H2
CO
CH4
Thermal losses
Thermal losses
I
II
III
IV
V
H2: 1.2
Raffinate
Product gas
WGS unit
Scrubbing units
PSA unit
Adsorbate
H2: 1.4
CO: 1.1
CH4: 1.2
H2: 2.1
CO: 0.1
CH4: 1.2
H2: 2.1
CO: 0.1
CH4: 1.2
H2: 0.9
CO: 0.1
CH4: 1.2

Fig. 9. Sankey diagram of the energy streams of the main gas components (H_2, CO, and CH_4) along the lab-scale process chain based on their LHV. All energy streams are given in kW.

Table 6
Assumptions for the techno-economic assessment.

	Values	Units
Fuel power	8.0	MW
H_2 power	1.7	MW
Electricity power	1.0	MW
District heat	2.9	MW

Table 7
Techno-economic key figures for the 8 MW fuel power polygeneration concept based on DFB biomass steam gasification for a plant in Austria in 2016.

	Values	Units
Investment costs	13 200 000	EUR
Plant lifetime	20	a
Expenses	4 680 643.94	EUR a^{-1}
Tax rate	25%	–
Depreciation	660 000.00	EUR a^{-1}
Discount rate	10%	–

authors give a maximum specific biomass based H_2 yield of 165 g kg^{-1} considering ideal steam reforming and water gas shift reaction. In addition, the generated adsorbate stream had a lower heating value of 7.9 MJ m^{-3}.

In order to optimize the H_2 production, future work could focus on the steam reforming and subsequent recycling of the adsorbate stream in order to further increase the H_2 yield of the process. However, if polygeneration (simultaneous production of H_2, electricity, and district heat) is employed, the adsorbate stream should be used as fuel for the combustion reactor of the dual fluidized bed gasification system and/or as fuel for the combustion in gas engines for the generation of electricity and heat.

The techno-economic assessment showed, that a profitable operation of the plant would be possible if certain feed in tariffs for renewable electricity and renewable H_2 exist.

In order to improve the process, the CO_2 after the water gas shift unit could be removed in order to increase the H_2 recovery as well as increase the lower heating value of the adsorbate of the pressure swing adsorption unit. Therefore, different CO_2 separation technologies should be evaluated for their suitability for the tar-rich product gas generated by the dual fluidized bed biomass steam

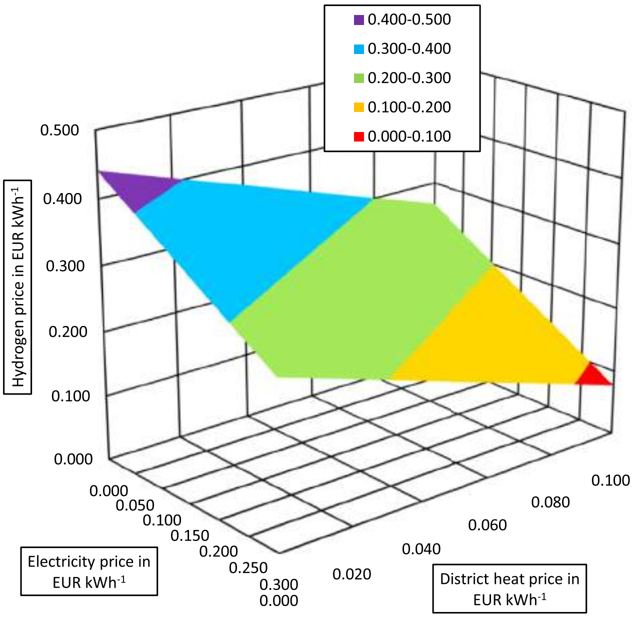

Fig. 10. H_2 price in dependence of the electricity price and district heat price for a NPV equal zero.

gasification plants. Furthermore, the process chain should be simplified by using only one water gas shift reactor as most of the CO conversion takes place there.

Acknowledgements

This work was carried out within the framework of the Bioenergy2020+ GmbH project “C20005 Polygeneration III”. Bioenergy2020+ GmbH is funded by the states Burgenland, Niederösterreich, Steiermark, and within the Austrian COMET program, which is managed by the Austria Research Promoting Agency (FFG).

The authors want to thank the project partners Air Liquide, Güssing Renewable Energy, and ISG Energy. In addition, the plant operators of the gasification plant in Oberwart are gratefully acknowledged.

Moreover, Silvester Fail and Nicolas Diaz are gratefully acknowledged for designing and constructing the water gas shift and the pressure swing adsorption unit.

Abbreviations and acronyms

I, II, III, IV, V	Sampling point positions along the lab-scale process chain
BDL	Below detection limit
CEPI	Chemical engineering plant cost index
CHP	Combined heat and power
d.a.f.	Dry and ash free
d.b.	Dry basis
DFB	Dual fluidized bed
DL	Detection limit
GC	Gas chromatograph
GCMS	Gas chromatography mass spectroscopy
NPV	Net present value
ORC	Organic Rankine cycle
PSA	Pressure swing adsorption
RME	Rapeseed methyl ester
STP	Standard temperature and pressure (273.15 K and 101325 Pa)
TCD	Thermal conductivity detector
WGS	Water gas shift

Symbols

φ_i	Volumetric fraction of component i in $m^3\ m^{-3}$
Ω_i	Recovery of component i in %
GHSV	Gas hourly space velocity in h^{-1}
ΔH	Enthalpy of formation at 298.15 K and 101325 Pa in $kJ\ mol^{-1}$
LHV	Lower heating value in $MJ\ m^{-3}$
$\boldsymbol{V_{Cat}}$	Catalyst volume in m^3
$\dot{V}_x$	Overall volumetric dry gas flow rate at position x at STP in $m^3\ h^{-1}$
$\dot{V}_{H_2O,x}$	Volumetric steam flow rate at position x at STP in $m^3\ h^{-1}$
p	Absolute pressure in MPa
p_{Ads}	Adsorption pressure in MPa
STDGR	Steam to dry gas ratio in -
T	Temperature in °C
t_{Ads}	Adsorption time in s

References

[1] K. Liu, C. Song, V. Subramani, Hydrogen and Syngas Production and Purification Technologies, Wiley, 2010, http://dx.doi.org/10.1002/9780470561256.fmatter.

[2] B. Rehling, H. Hofbauer, R. Rauch, C. Aichernig, BioSNG-process simulation and comparison with first results from a 1-MW demonstration plant, Biomass Conv. Bioref 1 (2011) 111–119, http://dx.doi.org/10.1007/s13399-011-0013-3.

[3] A. Sauciuc, Z. Abosteif, G. Weber, A. Potetz, R. Rauch, H. Hofbauer, G. Schaub, L. Dumitrescu, Influence of operating conditions on the performance of biomass-based Fischer-Tropsch synthesis, Biomass Conv. Bioref 2 (3) (2012) 253–263, http://dx.doi.org/10.1007/s13399-012-0060-4.

[4] M. Gassner, F. Marechal, Methodology for the optimal thermo-economic, multi-objective design of thermochemical fuel production from biomass, Comp. Chem. Eng. 33 (3) (2009) 769–781, http://dx.doi.org/10.1016/j.compchemeng.2008.09.017.

[5] M. Gassner, F. Vogel, G. Heyen, F. Marechal, Optimal process design for the polygeneration of SNG, power and heat by hydrothermal gasification of waste biomass: thermo-economic process modelling and integration, Energ Environ. Sci. 4 (2011) 1726–1741, http://dx.doi.org/10.1039/C0EE00629G.

[6] M. Gassner, F. Marechal, Thermo-economic optimisation of the polygeneration of synthetic natural gas (SNG), power and heat from lignocellulosic biomass by gasification and methanation, Energ Environ. Sci. 5 (2012) 5768–5789, http://dx.doi.org/10.1039/C1EE02867G.

[7] J. Gale, H. Herzog, J. Braitsch, R.H. Williams, E.D. Larson, G. Liu, T.G. Kreutz, Fischetropsch fuels from coal and biomass: strategic advantages of once-through (polygeneration) configurations, Energ Proc. 1 (1) (2009) 4379–4386, http://dx.doi.org/10.1016/j.egypro.2009.02.252.

[8] L. Gao, H. Li, B. Chen, H. Jin, R. Lin, H. Hong, Proposal of a natural gas-based polygeneration system for power and methanol production, in: 19th International Conference on Efficiency, Cost, Optimization, Simulation and Environmental Impact of Energy Systems ECOS 2006, Vol. 33, 2008, pp. 206–212. http://dx:doi.org/10.1016/j.energy.2007.10.011.

[9] H. Li, H. Hong, H. Jin, R. Cai, Analysis of a feasible polygeneration system for power and methanol production taking natural gas and biomass as materials, Appl. Energ 87 (9) (2010) 2846–2853, http://dx.doi.org/10.1016/j.apenergy.2009.07.001.

[10] G. jian Liu, Z. Li, M. hua Wang, W. dou Ni, Energy savings by co-production: a methanol/electricity case study, Appl. Energ 87 (9) (2010) 2854–2859, http://dx.doi.org/10.1016/j.apenergy.2009.08.036.

[11] L. Tock, F. Marechal, Co-production of hydrogen and electricity from lignocellulosic biomass: process design and thermo-economic optimization, Energ 45 (1) (2012) 339–349, http://dx.doi.org/10.1016/j.energy.2012.01.056.

[12] G. Kyriakarakos, A.I. Dounis, S. Rozakis, K.G. Arvanitis, G. Papadakis, Polygeneration microgrids: a viable solution in remote areas for supplying power, potable water and hydrogen as transportation fuel, Appl. Energ 88 (12) (2011) 4517–4526, http://dx.doi.org/10.1016/j.apenergy.2011.05.038.

[13] N. Diaz, Hydrogen Separation from Producer Gas Generated by Biomass Steam Gasification, Ph.D. thesis, TU Wien, 2013.

[14] S. Fail, N. Diaz, F. Benedikt, M. Kraussler, J. Hinteregger, K. Bosch, M. Hackel, R. Rauch, H. Hofbauer, Wood gas processing to generate pure hydrogen suitable for PEM fuel cells, ACS Sustain Chem. Eng. 2 (12) (2014) 2690–2698, http://dx.doi.org/10.1021/sc500436m.

[15] M. Kraussler, M. Binder, S. Fail, K. Bosch, M. Hackel, H. Hofbauer, Performance

Please cite this article in press as: M. Kraussler, et al., Hydrogen production within a polygeneration concept based on dual fluidized bed biomass steam gasification, Biomass and Bioenergy (2016), http://dx.doi.org/10.1016/j.biombioe.2016.12.008

of a water gas shift pilot plant processing product gas from an industrial scale biomass steam gasification plant, Biomass Bioenerg. 89 (2015) 50–57, http://dx.doi.org/10.1016/j.biombioe.2015.12.001.

[16] M. Kraussler, M. Binder, H. Hofbauer, 2250-hour long term operation of a water gas shift pilot plant processing tar-rich product gas from an industrial scale biomass steam gasification plant, Int. J. Hydorgen Energ 41 (15) (2016) 6247–6258, http://dx.doi.org/10.1016/j.ijhydene.2016.02.137.

[17] M. Kraussler, M. Binder, H. Hofbauer, Behavior of GCMS tar components in a water gas shift unit operated with tar-rich product gas from an industrial scale dual fluidized bed biomass steam gasification plant, Biomass Conv. Bioref Open access (2016) 1–11, http://dx.doi.org/10.1007/s13399-016-0205-y.

[18] M. Kaltschmitt, H. Hartmann, H. Hofbauer, Energie aus Biomasse, third ed., Springer-Verlag, 2016 http://dx.doi.org/10.1007/978-3-662-47438-9.

[19] V. Wilk, H. Hofbauer, Analysis of optimization potential in commercial biomass gasification plants using process simulation, Fuel Process Techn 141 (2016) 138–147, http://dx.doi.org/10.1016/j.fuproc.2015.07.035.

[20] J. Kotik, Über den Einsatz von Kraft-Wärme-Kopplungsanlagen auf Basis der Wirbelschicht-Dampfvergasung fester Biomasse am Beispiel des Biomassekraftwerks Oberwart, Ph.D. thesis, TU Wien, 2010.

[21] S. Fail, Biohydrogen Production Based on the Catalyzed Water Gas Shift Reaction in Wood Gas, Ph.D. thesis, TU Wien, 2014.

[22] K. Jörg, Abwasserfreie Abscheidung von Partikeln und Teeren aus Holzgas, Ph.D. thesis, TU Wien, 2003.

[23] S. Narasimhan, C. Jordache, Data Reconciliation and Gross Error Detection, first ed., Gulf Professional Publishing, Burlington, 1999.

[24] T. Brown, Engineering Economics and Economic Design for Process Engineers, first ed., CRC Press Taylor & Francis Group, 2007.

[25] F. Kirnbauer, V. Wilk, H. Hofbauer, Performance improvement of dual fluidized bed gasifiers by temperature reduction: the behavior of tar species in the product gas, Fuel 108 (2013) 534–542, http://dx.doi.org/10.1016/j.fuel.2012.11.065.

[26] T. Pröll, R. Rauch, C. Aichernig, H. Hofbauer, Fluidized bed steam gasification of solid biomass - performance characteristics of an 8 MWth combined heat and power plant, Int. J. React. Eng. 5 (1) (2007) 6542–6580, http://dx.doi.org/10.2202/1542-6580.1398.

[27] S. Turn, C. Kinoshita, Z. Zhang, D. Ishimura, J. Zhou, An experimental investigation of hydrogen production from biomass gasification, Int. J. Hydrogen Energ 23 (8) (1998) 641–648, http://dx.doi.org/10.1016/S0360-3199(97)00118-3.

Please cite this article in press as: M. Kraussler, et al., Hydrogen production within a polygeneration concept based on dual fluidized bed biomass steam gasification, Biomass and Bioenergy (2016), http://dx.doi.org/10.1016/j.biombioe.2016.12.008

Paper 7

Michael Kraussler, Philipp Schindler, Hermann Hofbauer, An experimental approach aiming the production of a gas mixture composed of hydrogen and methane from biomass as natural gas substitute in industrial applications, Bioresource Technology, Volume 237, 2017, Pages 39-46, `http://dx.doi.org/10.1016/j.biortech.2017.03.040`.

Contribution: Experimental work, data treatment, writing

Bioresource Technology 237 (2017) 39–46

Contents lists available at ScienceDirect

Bioresource Technology

journal homepage: www.elsevier.com/locate/biortech

An experimental approach aiming the production of a gas mixture composed of hydrogen and methane from biomass as natural gas substitute in industrial applications

Michael Kraussler [a,b,*], Philipp Schindler [b], Hermann Hofbauer [b]

[a] BIOENERGY 2020+ GmbH, Wienerstrasse 49, 7540 Güssing, Austria
[b] TU Wien, Institute of Chemical, Environmental and Biological Engineering, Getreidemarkt 9, 1060 Wien, Austria

HIGHLIGHTS

- A process chain was operated with product gas from a biomass gasification plant.
- A WGS unit, scrubbing units, and a PSA unit were employed.
- A parameter study was carried out in order to find optimum operating parameters.
- A H_2CH_4 gas mixture with a Wobbe index close to the Wobbe index of CH_4 was produced.

ARTICLE INFO

Article history:
Received 31 January 2017
Received in revised form 6 March 2017
Accepted 8 March 2017
Available online 11 March 2017

Keywords:
H_2CH_4
Hythane
Biomass steam gasification
Dual fluidized bed
Carbon molecular sieve

ABSTRACT

This work presents an experimental approach aiming the production of a gas mixture composed of H_2 and CH_4, which should serve as natural gas substitute in industrial applications. Therefore, a lab-scale process chain employing a water gas shift unit, scrubbing units, and a pressure swing adsorption unit was operated with tar-rich product gas extracted from a commercial dual fluidized bed biomass steam gasification plant. A gas mixture with a volumetric fraction of about 80% H_2 and 19% CH_4 and with minor fractions of CO and CO_2 was produced by employing carbon molecular sieve as adsorbent. Moreover, the produced gas mixture had a lower heating value of about 15.5 $MJ{\cdot}m^{-3}$ and a lower Wobbe index of about 43.4 $MJ{\cdot}m^{-3}$, which is similar to the typical Wobbe index of natural gas.

© 2017 Elsevier Ltd. All rights reserved.

1. Introduction

Today, natural gas is a very important energy carrier for different industries. In Austria, its demand contributed to about 20% of the overall annual energy consumption in 2015 (compare E-Control (2017), Austria (2017)). Nevertheless, its consumption also leads to significant CO_2 emissions due to its fossil origin.

Gas mixtures composed of H_2 and CH_4 (sometimes referred to as hythane) were extensively investigated for usage in internal combustion engines in order to supplement compressed natural gas as car fuel, for example in Larsen and Wallace (1997), Ortenzi et al. (2008) and Sierens and Rosseel (2000). Some authors, for Nelsson et al. (2010), refer to hythane as blend with a maximum volumetric H_2 content of 20% in CH_4. In this work, the authors refer to H_2CH_4 as gas mixture consisting of any H_2 to CH_4 ratio. Verhelst and Wallner (2009) report that, due to the similarity of the Wobbe index of H_2 and CH_4, a gas mixture composed of those components could be used as fuel, for example, for cars, for gas boilers, or for industrial applications and, therefore can supplement fossil CH_4 in natural gas grids. The Wobbe index (according to DIN 51857) describes the flow of energy through a given throttle at a given pressure Klell et al. (2012). However, another important factor, which has to be considered according to Dekate et al. (2013), is material compatibility because of the higher H_2 content.

Several authors investigated different pathways for CO_2 neutral production of a H_2CH_4 gas mixture. For example, Cavinato et al. (2012) investigated a production route based on dark fermentation of food waste and Elreedy et al. (2015) investigated a production route from petrochemical waste water. Additionally, Roy and Das (2016) give an overview about the present state of biohythane production from organic waste. In contrast, in this work, the authors carried out an experimental approach in order to generate a

---

[*] Corresponding author at: BIOENERGY 2020+ GmbH, Wienerstrasse 49, 7540 Güssing, Austria and TU Wien, Institute of Chemical, Environmental and Biological Engineering, Getreidemarkt 9, 1060 Wien, Austria

http://dx.doi.org/10.1016/j.biortech.2017.03.040
0960-8524/© 2017 Elsevier Ltd. All rights reserved.

Abbreviations and acronyms

A, B, C	sampling points along the lab-scale process chain
CHP	combined heat and power
CMS	carbon molecular sieve
d.b.	dry basis
DFB	dual fluidized bed
GC	gas chromatograph
GCMS	gas chromatography mass spectroscopy
H_2CH_4	gas mixture composed of H_2 and CH_4 (sometimes referred to as hythane)
ORC	organic Rankine cycle
PSA	pressure swing adsorption
RME	rapeseed methyl ester
SNG	synthetic natural gas
STP	standard temperature and pressure (273.15 K and 101325 Pa)
TCD	thermal conductivity detector
WGS	water gas shift

Symbols

φ_i	volumetric fraction of component *i* in $m^3 \cdot m^{-3}$
Ω_i	recovery of component *i* in %
ω_i	mass fraction of component *i* in $kg \cdot kg^{-1}$
GHSV	gas hourly space velocity in h^{-1}
ΔH	enthalpy of formation at 298.15 K and 101325 Pa in $kJ \cdot mol^{-1}$
LHV	lower heating value in $MJ \cdot m^{-3}$
LWO	lower Wobbe index in $MJ \cdot m^{-3}$
V_{Cat}	catalyst volume in m^3
$\dot{V}_x$	overall volumetric dry gas flow rate at position *x* at STP in $m^3 \cdot h^{-1}$
$\dot{V}_{H_2O,x}$	volumetric steam flow rate at position x at STP in $m^3 \cdot h^{-1}$
p_{Ads}	adsorption pressure in MPa
STDGR	steam to dry gas ratio in –
T	temperature in °C
t_{Ads}	adsorption time in s

H_2CH_4 gas mixture from real product gas from a commercial biomass steam gasification plant using a simple lab-scale process chain.

The dual fluidized bed (DFB) biomass steam gasification technology is a well established process in order to convert biomass into a product gas mainly consisting of H_2, CO, CO_2, and CH_4, where H_2 and CH_4 account for about 72% of the lower heating value (LHV). At commercial scale, the product gas is burnt in gas engines for combined heat and power (CHP) (compare Pröll et al. (2007), Wilk and Hofbauer (2016)). Furthermore, the product gas has been extensively used for experimental investigations in the past. For example, for H_2 production (see Fail (2014), Fail et al. (2014), Diaz (2013), Kraussler et al. (2015), Kraussler et al. (2016a), Kraussler et al. (2016b)), for production of synthetic natural gas (SNG) according to Rehling et al. (2011), for Fischer–Tropsch synthesis in Sauciuc et al. (2012), and for production of mixed alcohols according to Weber et al. (2015). In addition, a polygeneration concept, aiming the production of H_2, electricity, and district heat was experimentally investigated by Kraussler et al. (2016c).

This work presents an experimental approach to produce a H_2CH_4 gas mixture from biomass (wood chips) for substitution of natural gas in industrial applications. Therefore, a lab-scale process chain was operated with tar-rich product gas which was extracted from a commercial and industrial scale 8 MW (fuel power) DFB biomass steam gasification plant. About 0.8 $m^3 \cdot h^{-1}$ of real product gas were extracted and processed in the lab-scale process chain, which employed a water gas shift (WGS) unit, scrubbing units, and a pressure swing adsorption (PSA) unit, which operated at an absolute pressure of 0.6 MPa. A parameter study was conducted in order to reach suitable fuel parameters, especially, a suitable Wobbe index of the produced H_2CH_4 gas mixture.

2. Materials and methods

2.1. The gasification plant

The investigated lab-scale process chain was operated with tar-rich product gas from the industrial scale CHP gasification plant in Oberwart, Austria. Fig. 1 shows a simplified flowchart of the process. The plant employs the DFB steam gasification technology described in detail in Pröll et al. (2007) and Wilk and Hofbauer (2016). The CHP plant uses biomass (wood chips) as feed stock. Information about the average feed stock composition is given in Wilk and Hofbauer (2016).

Wood chips are fed into the biomass dryer, where the mass fraction of water is reduced to about 16%. After drying, the wood chips are fed into a screw conveyor which transports the wood chips into the gasifier. In the gasifier, the wood chips devolatilize and react with steam at the presence of the bed material (olivine) at about 850 °C. The steam to fuel ratio (dry and ash free basis) is about 0.5. The resulting dry product gas has a volumetric composition of about 40% H_2, 25% CO, 22% CO_2, 10% CH_4, as well as minor traces of C_xH_y, N_2, and sulfur components. Moreover, the product gas shows a lower heating value (LHV) of up to 14 $MJ \cdot m^{-3}$ (d.b.) (compare Wilk and Hofbauer (2016)).

In the subsequent process steps, the product gas is cooled and passes through a bag house filter with a particle separation efficiency of more than 99%. Consequently, a practically dust free product gas can be assumed after the filter. In the following rapeseed methyl ester (RME) gas scrubber, the product gas is cooled from about 150 to 40 °C. Hence, tar, steam, and other condensable fractions of the product gas are removed before the product gas is fed into the gas engines for CHP generation. Heat from the flue gas line is mainly recovered for the steam generation and for district heating as well.

It is possible to use a partial flow of the product gas for experimental work from an extraction point located before the RME gas scrubber (see Fig. 1). The tar content of the gas extracted before the RME gas scrubber is significantly higher (7.6 $g \cdot m^{-3}$ GCMS tar and 1.8 $g \cdot m^{-3}$ gravimetric tar according to Wilk and Hofbauer (2016)) than after the RME gas scrubber (2.7 $g \cdot m^{-3}$ GCMS tar and 0.1 $g \cdot m^{-3}$ gravimetric tar according to Wilk and Hofbauer (2016)). However, the tar-rich product gas has a higher temperature (about 150 °C) and a higher volumetric steam content (about 35%) compared to the gas extracted after the RME scrubber (temperature about 40 °C and steam content of about 7%). Consequently, the tar-rich product gas extracted before the RME scrubber shows advantages regarding the energy efficiency because the gas needs less heating and less additional steam before processing in a subsequent WGS reactor. A more detailed description of the CHP plant can be found in literature given by Diaz (2013) and Fail (2014).

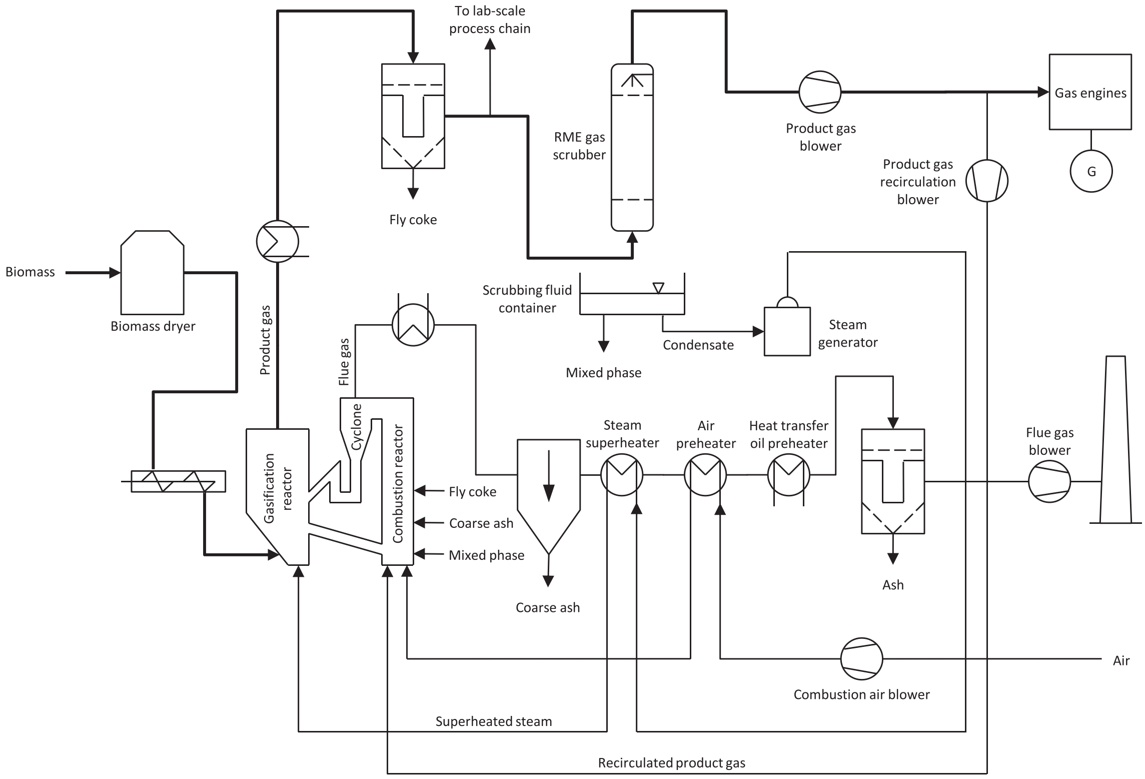
To lab-scale process chain
RME gas scrubber
Product gas blower
Gas engines
G
Product gas recirculation blower
Fly coke
Biomass
Biomass dryer
Product gas
Flue gas
Scrubbing fluid container
Mixed phase
Condensate
Steam generator
Cyclone
Gasification reactor
Combustion reactor
Steam superheater
Air preheater
Heat transfer oil preheater
Flue gas blower
Fly coke
Coarse ash
Mixed phase
Coarse ash
Ash
Air
Combustion air blower
Superheated steam
Recirculated product gas

Fig. 1. Simplified flowchart of the commercial DFB gasification plant in Oberwart, Austria.

2.2. The lab-scale process chain

This section describes the lab-scale process chain which processed the tar-rich product gas from the gasification plant to produce the H_2CH_4 gas mixture.

Fig. 2 shows a simplified flowchart of the process chain where A, B, and C indicate gas sampling points. The process chain consisted of a WGS unit, an RME scrubber, a glycol scrubber, and a PSA unit.

2.2.1. The water gas shift unit

The WGS unit converted CO to H_2 according to Eq. (1).

$$CO + H_2O \rightleftharpoons H_2 + CO_2 \quad \Delta H = -41.1\,kJ \cdot mol^{-1} \tag{1}$$

It consisted of three fixed bed reactors in series filled with a commercial Fe/Cr based catalyst. Each catalyst bed had a diameter of about 9 cm and a bed height of about 40 cm resulting in a catalyst volume of about 2.5 dm^3. The activation procedure of the cat-

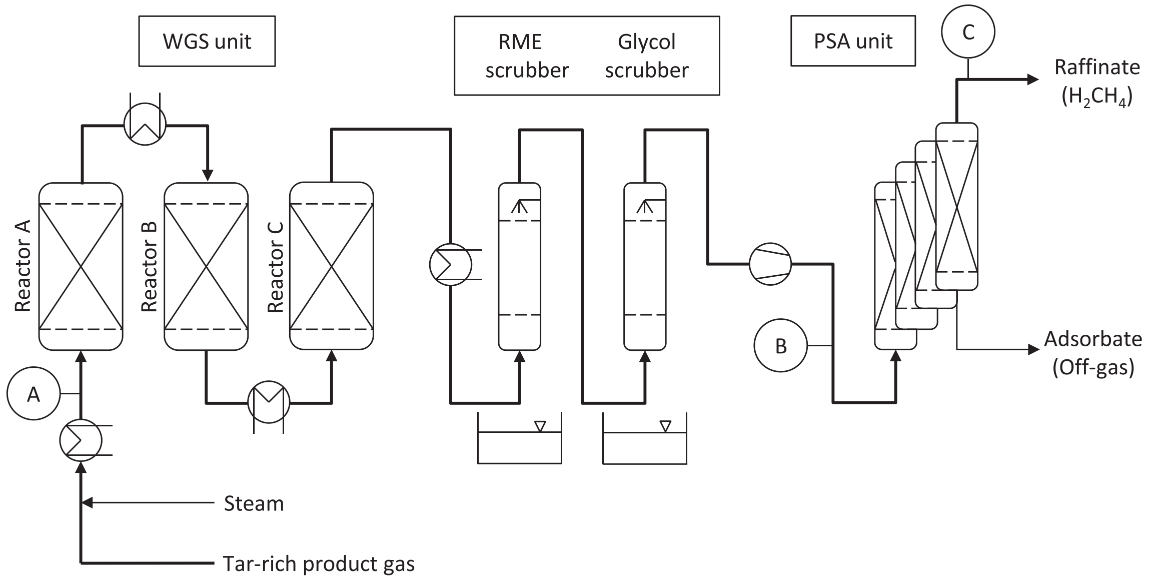
WGS unit
RME scrubber
Glycol scrubber
PSA unit
C
Raffinate (H_2CH_4)
Reactor A
Reactor B
Reactor C
B
Adsorbate (Off-gas)
A
Steam
Tar-rich product gas

Fig. 2. Simplified flowchart of the investigated lab-scale process chain. A, B, and C indicate sampling points for measurements.

alyst is described in Fail (2014). At the inlet and outlet of each reactor, the gas stream could be heated or cooled in order to achieve the desired gas inlet and outlet temperatures. These temperatures were measured with type J thermocouples. Before the inlet of the first reactor, steam was added to assure a high steam content in the processed gas in order to avoid coking and carbon deposition on the catalyst surface. The WGS unit was operated at ambient pressure and the gas inlet temperature was set to about 350 °C and the gas outlet temperature after reactor C was set to about 150 °C.

Overall, the WGS unit was operated with the same catalyst batch for more than 3000 h. During all investigations, no catalyst deactivation could be observed (compare with Fail (2014), Fail et al. (2014), Kraussler et al. (2016a)).

2.2.2. The gas scrubbing units

Two gas scrubbing units were employed downstream of the WGS unit in order to condense steam and to remove tar and NH_3 from the processed gas.

The first scrubber used RME as scrubbing fluid. This RME scrubber was operated at ambient pressure and at a temperature of about 15 °C. Therefore, the tar-rich gas stream was cooled and, consequently, tar was condensed and dissolved in the RME. Thus, steam contained in the gas stream was condensed and most of the NH_3 was dissolved in the condensate. The RME in the scrubber was continually removed and replaced with fresh RME in order to avoid saturation with tar.

After the RME scrubber, the gas passed through a glycol scrubber which was also operated at ambient pressure but at a lower temperature of about −5 °C, in order to condense the remaining steam and other remaining minor condensable impurities. The glycol was also continually removed and replaced with fresh glycol to avoid saturation as well. Consequently, after the glycol scrubber, a dry gas stream could be assumed which was, subsequently, led to the compressor of the downstream PSA unit.

2.2.3. The pressure swing adsorption unit

Upstream of the PSA unit, the dry gas stream (feed) was compressed to an absolute pressure of 0.6 MPa. The compressed gas was then fed into the adsorber vessels.

Each of the four employed adsorber vessels was filled with about 4.7 dm^3 of carbon molecular sieve (CMS) from Carbotech/Shirasagi (MSC–CT 350), which is often used for biogas upgrading in order to separate CO_2 from CH_4 (compare Grande (2011)). The four vessels were interconnected with automated valves in order to enable a continuous operation of the PSA unit. The adsorbed gas components were desorbed by lowering the pressure to about 0.02 MPa. These gas components were extracted from the bottom of the vessels and are referred to as adsorbate (off-gas). The high pressure product is in general referred to as raffinate or, in this work, H_2CH_4.

2.3. Gas analytics

A gas chromatograph (GC, Clarus 500™from Perkin Elmer) was used to measure the gas composition at the sampling points A, B, and C (Fig. 2). In the GC, a thermal conductivity detector (TCD) enabled the quantification of CO, CO_2, CH_4, N_2, O_2, C_2H_6, C_2H_4, and C_2H_2 with two different columns (7′ HayeSep N, 60/80 1/8″ SF and 9′ molecular sieve 13× 45/60, 1/8″ SF). The C_2 species were summarized and are referred to as C_2H_y. The H_2 content was calculated by closing the mass balance. In this work, H_2, CO, CO_2, and CH_4 are referred to as the main gas components.

In order to measure the steam content of the processed gas, the gas was sent through glycol gas washing bottles at −5 °C for a certain time. Subsequently, the volumetric dry gas flow was recorded with a gas meter. By weighing the gas washing bottles before and after a certain time, the water content was determined. Subsequently, the volumetric flow rates were calculated by the water balance.

In this paper, all gas volumes and volumetric gas flow rates are given at standard temperature and pressure (STP, 273.15 K and 101325 Pa). In addition, the least squares method, using the numerical software package Scilab™, was applied on the measured values of the WGS and PSA unit in order to find a balanced solution for the composition and volumetric flow rates of all gas streams. This approach of data reconciliation also included the standard deviation of every single measured value (compare Narasimhan and Jordache (1999)).

2.4. Key figures

The following key figures (Eqs. (2)–(4)) describe the operating conditions along the lab-scale process chain.

The gas hourly space velocity (GHSV, see Eq. (2)) indicates the stress of the catalyst in a chemical reactor. The GHSV was calculated for the first reactor of the WGS unit.

$$GHSV = \frac{\dot{V}_A}{V_{Cat}} \tag{2}$$

The steam to dry gas ratio (STDGR, see Eq. (3)) describes the relative amount of steam along the WGS unit, something which is very important for an adequate operation of the catalyst. It must not be too low in order to avoid coking and carbon deposition on the surface of the catalyst employed in the WGS unit. It was also calculated for the inlet of the first reactor.

$$STDGR = \frac{\dot{V}_{H_2O,A}}{\dot{V}_A} \tag{3}$$

The recovery of a component i (see Eq. (4)) is the ratio of the amount of that component (i) in two different streams. It is an indicator of a unit's separation efficiency.

$$\Omega_i = \frac{\varphi_{i,C} \cdot \dot{V}_C}{\varphi_{i,B} \cdot \dot{V}_B} \tag{4}$$

Additionally, the LHV and the lower Wobbe index (LWO) are important key figures in order to describe the interchangeability of gaseous fuels in terms of energy content and power.

3. Results and discussion

In this section, the results from the experiments for the production of the H_2CH_4 gas mixture are presented. About 0.83 $m^3 \cdot h^{-1}$ of the product gas were extracted from the commercial gasification plant, which resulted in a GHSV of 483 h^{-1} at the inlet of the first WGS reactor. In addition, a STDGR of 1.5 was chosen in order to avoid coking and carbon deposition on the surface of the commercial Fe/Cr based catalyst. Along the WGS unit, the volumetric dry gas flow rate increased to about 1.0 $m^3 \cdot h^{-1}$ due to the reaction of CO and H_2O to H_2 and CO_2. After the scrubbing units, the gas was fed into the PSA unit (adsorption pressure 0.6 MPa), where the adsorption time (t_{Ads}) was varied between 200 s and 700 s in order to find a H_2CH_4 composition aiming a LWO similar to pure CH_4.

3.1. Gas composition and recovery

Table 1 shows the gas composition of the extracted product gas (A) and the gas composition downstream of the WGS unit (B) considering only the main components H_2, CO, CO_2, and CH_4. The product gas was extracted with a typical composition for DFB gasification plants (compare Wilk and Hofbauer (2016)). Along the WGS unit, the volumetric H_2 fraction could be increased from 40.8% to 53.3%, which is in agreement with WGS units operated with the product gas from DFB biomass steam gasification (compare Chianese et al. (2015, 2016)). The volumetric CO content could be lowered from 25.4% to 1.9%. The volumetric CH_4 content was lowered due to the higher volumetric dry gas flow rate after the WGS unit. Higher hydrocarbons and sulfur components were also in the same order of magnitude as in previous published literature (see Fail (2014), Kraussler et al. (2015, 2016a,b)).

Fig. 3 shows the volumetric raffinate composition over different adsorption times of the PSA parameter study for H_2CH_4 production. It can be seen that at low adsorption times, CO and CO_2 were effectively separated from the feed gas mixture (B). At 200 s adsorption time, the volumetric CO content could be lowered to 0.32% and the volumetric CO_2 content could be lowered to 0.04%. At higher adsorption times, first, CO started to break through the CMS adsorbent, followed by CO_2.

It could also be observed that during the whole parameter study the volumetric H_2 content was between 80 and 81%, whereas, the volumetric CH_4 content was between 16 and 19%. It seems that the CH_4 tended to a sharper decrease than H_2. This can be explained by the fact that the overall higher H_2 amount in the feed caused an overall lower decrease of the H_2 fraction in the raffinate over the investigated adsorption times. Actually, even more H_2 molecules were adsorbed than CH_4 molecules (compare recoveries in Fig. 4)).

Fig. 4 shows the recoveries of the main components over the investigated PSA adsorption times. It can be seen that with increasing adsorption time, the recovery of all main components increased. At all adsorption times, the CH_4 recovery was higher than the H_2 recovery, which is untypical for adsorption processes (compare Liu et al. (2010)) but can be explained by the fact that CMS has usually a narrow pore distribution and the pore diameter is significantly smaller (between 0.3 and 0.4 nm) compared to regular activated carbon (see Sircar et al. (1996)). Therefore, because of the steric effect (compare Yang (2003)), the smaller H_2 molecules (diameter about 0.3 nm according to Xu et al. (2003)) tended to occupy a pore at the surface of the CMS more likely than the larger CH_4 molecules (diameter about 0.4 nm according to Mao and Sinnott (2001)). Hence, CMS showed a lower adsorption capacity for CH_4 which resulted in higher recoveries. In general, the recoveries of H_2, CO, and CH_4 significantly increased with higher adsorption times. The recovery of just CO_2 slightly increased with higher adsorption times which is an indicator for strong adsorption of CO_2 on CMS.

In conclusion, Fig. 3 and Fig. 4 indicate that CMS showed a high separation efficiency for CO_2. The separation efficiency of CO was lower which can be explained by the polar character of the CO molecule and the non-polar character of the CMS (compare Yang (2003)). In contrast, the separation efficiency of H_2 and CH_4 was significantly lower. Thus, CMS seems to be a suitable adsorbent in order to separate H_2CH_4 from a CO and CO_2 containing feed gas mixture.

Table 1
Volumetric composition of the extracted product gas (A) and the PSA feed (B) considering the main components H_2, CO, CO_2, and CH_4.

Components –	A $m^3 \cdot m^{-3}$	B $m^3 \cdot m^{-3}$
φ_{H_2}	40.8%	53.3%
φ_{CO}	25.4%	1.9%
φ_{CO_2}	22.9%	35.2%
φ_{CH_4}	10.9%	9.6%

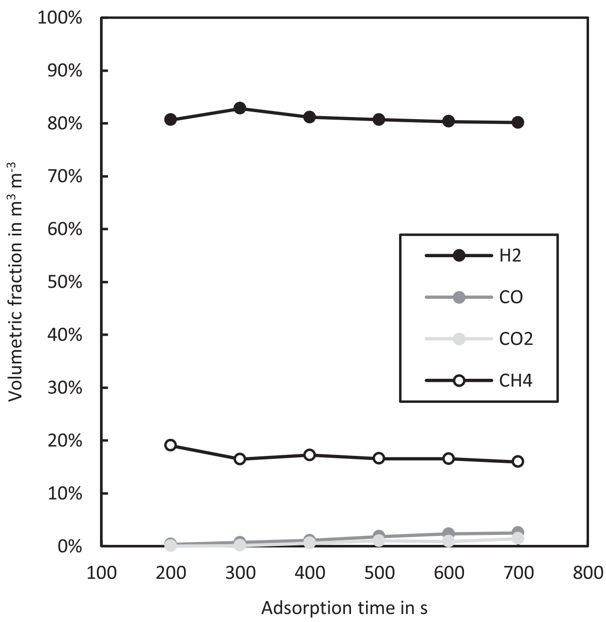

Fig. 3. Volumetric raffinate composition over different adsorptions times.

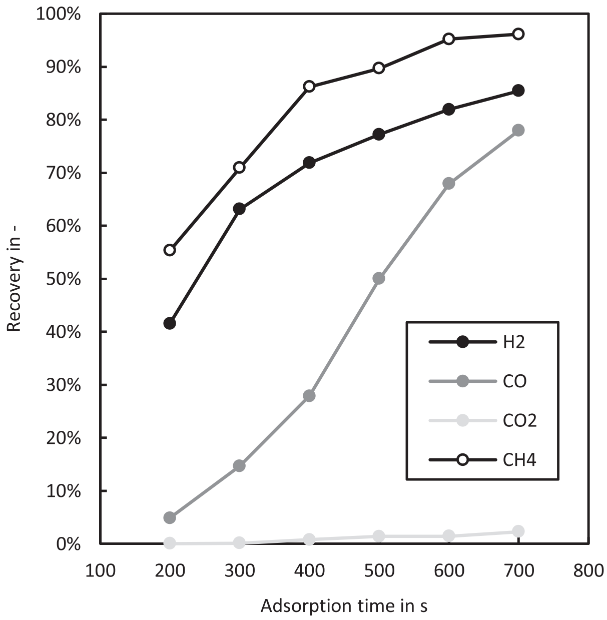

Fig. 4. Recoveries of the main components over different adsorption times.

3.2. Fuel parameters

This section presents the fuel parameters LHV and LWO achieved from the parameter study of the lab-scale process chain for H_2CH_4 production. The LHV and LWO are important key figures in order to describe the interchangeability of gaseous fuels.

Table 2 shows the LHV and LWO of the processed gas at the sampling points A, B, and C along the lab-scale process chain. The LHV after the WGS unit (B) was lower compared to the extracted product gas (A) due to the conversion of CO into H_2 and CO_2. With increasing adsorption time, the LHV of the H_2CH_4 (C) decreased from about 15.6 $MJ \cdot m^{-3}$ (200 s) to about 14.7 $MJ \cdot m^{-3}$ (700 s). However, the LHV of pure CH_4 of 35.9 $MJ \cdot m^{-3}$ is significantly higher.

Table 2
Fuel parameters (LHV and LWO) of the extracted product gas (A), the PSA feed (B), and the raffinate (C).

	A	B	C					
	–	–	200 s	300 s	400 s	500 s	600 s	700 s
	$MJ\cdot m^{-3}$	$MJ\cdot m^{-3}$	$MJ\cdot m^{-3}$	$MJ\cdot m^{-3}$	$MJ\cdot m^{-3}$	$MJ\cdot m^{-3}$	$MJ\cdot m^{-3}$	$MJ\cdot m^{-3}$
LHV	11.52	9.43	15.57	14.93	15.08	14.88	14.89	14.69
LWO	15.79	13.29	43.40	42.73	41.35	39.71	39.44	38.22

The LWO after the WGS unit (B) was also lower compared to the LWO of the extracted product gas (A), which can also be explained by the higher CO_2 content. Along the PSA unit, H_2CH_4 with a significantly higher LWO compared to sampling points A and B could be produced. Increasing adsorption time (from 200 s to 700 s) led to lower values of the LWO because of the increasing CO and CO_2 content. Nevertheless, the maximum LWO of about 43.4 $MJ\cdot m^{-3}$ is nearly the same as the LWO of pure CH_4 of about 48.1 $MJ\cdot m^{-3}$. Hence, the LWO indicates that the produced H_2CH_4 gas mixture could be used as natural gas substitute in industrial applications.

H_2 and CH_4 contributed with about 38% and 34%, respectively, to the LHV of the extracted product gas at sampling point A, whereas CO contributed to about 28%. After the WGS unit (sampling point B), H_2, CH_4, and CO contributed to the LHV with about 61, 36, and 3%, respectively. In the raffinate (H_2CH_4, sampling point C) an increasing adsorption time (200–700 s) led to an increase of the H_2 contribution from 56 to 59%, whereas the contribution of CH_4 decreased from 44 to 39%. Moreover, the contribution of CO increased to 0.3% with increasing adsorption time. A CO contribution of 0.3% is higher than the contribution in the PSA feed (sampling point B) which can be explained by the significantly lower CO_2 content in the raffinate (H_2CH_4).

3.3. H_2CH_4 process assessment

In this section, a possible process for H_2CH_4 production based on DFB biomass steam gasification is presented. The process is based on the experimental results from this paper (PSA adsorption time of 200 s) and on gasification plant data described in Pröll et al. (2007) and Wilk and Hofbauer (2016). The layout is based on a simple process which consists of a minimized number of state of the art unit operations.

Fig. 5 shows the process design for H_2CH_4 production. Wood chips (water mass fraction of about 32% according to Wilk and Hofbauer (2016)) are fed into a dryer and subsequently into the DFB gasifier where they are converted with steam into the product gas (compare sampling point A). Subsequently, the product gas is fed into the WGS unit, where CO and H_2O are converted into additional H_2 and CO_2. Then, the gas enters scrubbing units in order to condense steam and to remove tar. The condensed steam is fed back into the gasification reactor and the tar is fed back into the combustion reactor of the DFB gasifcation system. The heat from the product gas and flue gas lines is mainly used for steam generation. Subsequently, the gas is compressed and fed into a PSA unit employing CMS as adsorbent in order to separate H_2CH_4 from the feed gas stream. The off gas, a low calorific gas with a LHV of about 7.1 $MJ\cdot m^{-3}$, is split. On the one hand, a part of the off gas is recycled into the DFB gasifier and burnt in order to supply the heat for the endothermic gasification reactions. On the other hand, the excess flow of the off gas could be burnt in a gas boiler or burnt in gas engines in order to cover a certain amount of the electricity demand of the process.

Fig. 6 shows the sankey diagram of the LHV based energy streams of the possible process for H_2CH_4 production. The wet wood chips with a fuel power of 10 MW are fed into a biomass dryer and subsequently into the DFB gasifier where they are converted into product gas with an efficiency of 70%. Along the WGS unit, conversion losses of about 1% occur. 8.8 MW of the shifted product gas are fed into the PSA unit. The result is 4.0 MW of H_2CH_4 and 4.8 MW of the low calorific off gas, where 2.7 MW are recycled into the DFB gasifier and 2.1 MW could be used for additional heat and electricity generation. The sensible heat of the process (about 3.0 MW) is mainly used for steam generation and combustion air preheating. Excess heat, which cannot be utilized further, is used for the biomass dryer upstream of the gasifier. Based on these results, a wet fuel based H_2CH_4 production efficiency of 40% could be achieved.

In comparison, Roy and Das (2016) found a gaseous energy recovery of 53.6% with a two stage dark fermentation process using starchy wastewater as feedstock for production of biohythane. Fur-

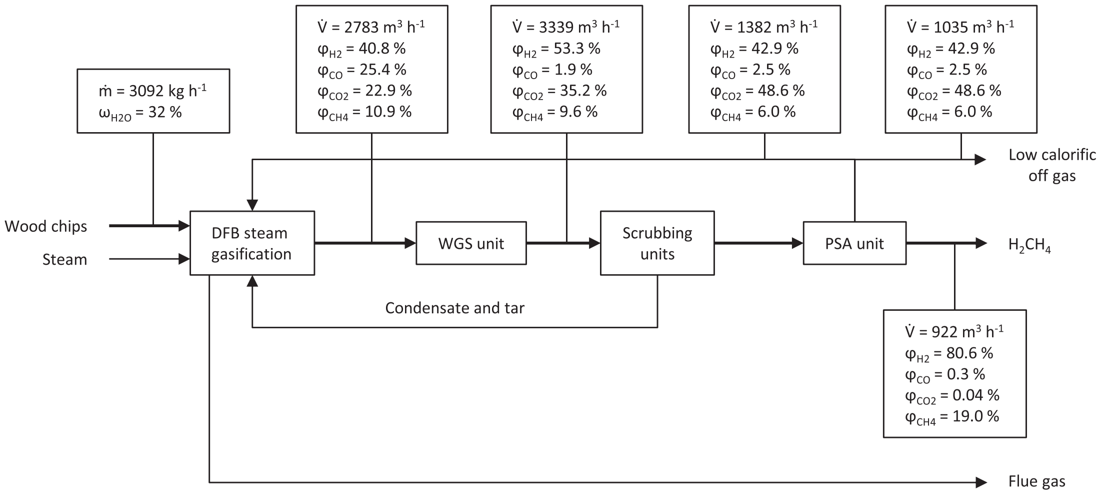

Fig. 5. Process configuration for H_2CH_4 production based on DFB biomass steam gasification (compare Figs. 1 and 2) also indicating the mass and volumetric flow rates of the wood chips and main gas components. The volumetric flow rates are given on d.b. and at STP.

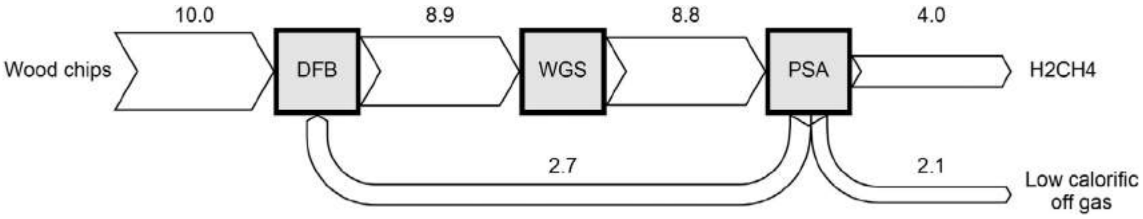

Fig. 6. LHV based sankey diagram of a possible process for H_2CH_4 production. All streams are given in MW. No sensible heat is considered.

thermore, Rehling et al. (2011) investigated a BioSNG process based on the DFB gasification technology which used wood chips with a water mass fraction of 20% as feedstock. In that study, an energy efficiency of 66% was reported. The energy efficiency based on the results in this work (40%) is lower but the process configuration is simpler compared to typical methanation processes (compare Kopyscinski et al. (2010)).

4. Conclusion

Carbon molecular sieve is a suitable adsorbent for separating CO_2 from a H_2 and CH_4 containing gas mixture. However, separation of CO turned out to be more difficult. Nevertheless, based on the Wobbe index, the generated H_2CH_4 gas mixture could be used as substitute of natural gas in industrial applications. The H_2CH_4 output of the presented process could be improved by methanation of remaining CO downstream of the CO_2 removal. This approach would increase the lower heating value as well as the lower Wobbe index of the H_2CH_4, as a result of the conversion of some H_2 into additional CH_4.

Acknowledgments

The research leading to these results has received funding from the COMET program managed by the Austrian Research Promotion Agency under grant number 844605. The program is co-financed by the Republic of Austria and the Federal Provinces of Burgenland, Lower Austria and Styria. Co-funding from the industry partners Air Liquide, Güssing Renewable Energy, and ISG Energy shall be highly acknowledged.

In addition, Silvester Fail and Nicolas Diaz is thanked for designing and building the lab-scale WGS and PSA unit. Moreover, the plant operators of the gasification plant in Oberwart are gratefully acknowledged.

References

Austria, S., 2017. Energiebilanzen. URL http://www.statistik.at/webde/statistiken/energieumweltinnovationmobilitaet/energieundumwelt/energie/energiebilanzen/index.html.

Cavinato, C., Giuliano, A., Bolzonella, D., Pavan, P., Cecchi, F., 2012. Bio-hythane production from food waste by dark fermentation coupled with anaerobic digestion process: a long-term pilot scale experience. Int. J. Hydrogen Energy 37, 11549–11555. http://dx.doi.org/10.1016/j.ijhydene.2012.03.065.

Chianese, S., Fail, S., Binder, M., Rauch, R., Hofbauer, H., Molino, A., Blasi, A., Musmarra, D., 2016. Experimental investigations of hydrogen production from CO catalytic conversion of tar rich syngas by biomass gasification. Catal. Today 277, 182–191. http://dx.doi.org/10.1016/j.cattod.2016.04.005.

Chianese, S., Loipersböck, J., Malits, M., Rauch, R., Hofbauer, H., Molino, A., Musmarra, D., 2015. Hydrogen from the high temperature water gas shift reaction with an industrial Fe/Cr catalyst using biomass gasification tar rich synthesis gas. Fuel Process. Technol. 132, 39–48. http://dx.doi.org/10.1016/j.fuproc.2014.12.034.

Dekate, A.D., Nikam, S.H., Rairikar, S.D., Sreenivasulu, M., Thipse, S.S., Mannikar, A.V., Singh, T.V., 2013. A study on material compatibility with various blends of HCNG on existing CNG fuel kit. In: SAE Technical Paper, The Automotive Research Association of India. http://dx.doi.org/10.4271/2013-26-0079.

Diaz, N., 2013. Hydrogen Separation from Producer Gas Generated by Biomass Steam Gasification (Ph.D. thesis). TU Wien.

E-Control, 2017. Jahresreihen - E-Control. URL https://www.e-control.at/statistik/gas/betriebsstatistik/jahresreihen.

Elreedy, A., Tawfik, A., Kubota, K., Shimada, Y., Harada, H., 2015. Hythane ($H_2 + CH_4$) production from petrochemical wastewater containing mono-ethylene glycol via stepped anaerobic baffled reactor. Int. Biodeterior. Biodegrad. 105, 252–261. http://dx.doi.org/10.1016/j.ibiod.2015.09.015.

Fail, S., 2014. Biohydrogen Production Based on the Catalyzed Water Gas Shift Reaction in Wood Gas (Ph.D. thesis). TU Wien.

Fail, S., Diaz, N., Benedikt, F., Kraussler, M., Hinteregger, J., Bosch, K., et al., 2014. Wood gas processing to generate pure hydrogen suitable for PEM fuel cells. ACS Sustain. Chem. Eng. 2, 2690–2698. http://dx.doi.org/10.1021/sc500436m.

Grande, C.A., 2011. Biogas Upgrading by Pressure Swing Adsorption. InTech. URL http://www.intechopen.com/books/biofuel-s-engineering-process-technology/biogas-upgrading-by-pressure-swing-adsorption, doi: http://dx.doi.org/10.5772/18428.

Klell, M., Eichlseder, H., Sartory, M., 2012. Mixtures of hydrogen and methane in the internal combustion engine? Synergies, potential and regulations. Int. J. Hydrogen Energy 37, 11531–11540. http://dx.doi.org/10.1016/j.ijhydene.2012.03.067.

Kopyscinski, J., Schildhauer, T.J., Biollaz, S.M., 2010. Production of synthetic natural gas (SNG) from coal and dry biomass – a technology review from 1950 to 2009. Fuel 89, 1763–1783. http://dx.doi.org/10.1016/j.fuel.2010.01.027.

Kraussler, M., Binder, M., Fail, S., Bosch, K., Hackel, M., Hofbauer, H., 2015. Performance of a water gas shift pilot plant processing product gas from an industrial scale biomass steam gasification plant. Biomass Bioenergy 89, 50–57. http://dx.doi.org/10.1016/j.biombioe.2015.12.001.

Kraussler, M., Binder, M., Hofbauer, H., 2016a. 2250-hour long term operation of a water gas shift pilot plant processing tar-rich product gas from an industrial scale biomass steam gasification plant. Int. J. Hydorgen Energy 41, 6247–6258. http://dx.doi.org/10.1016/j.ijhydene.2016.02.137.

Kraussler, M., Binder, M., Hofbauer, H., 2016b. Behavior of GCMS tar components in a water gas shift unit operated with tar-rich product gas from an industrial scale dual fluidized bed biomass steam gasification plant. Biomass Convers. Biorefin. Open Access, 1–11. http://dx.doi.org/10.1007/s13399-016-0205-y.

Kraussler, M., Binder, M., Schindler, P., Hofbauer, H., 2016c. Hydrogen production within a polygeneration concept based on dual fluidized bed biomass steam gasification. Biomass Bioenergy. http://dx.doi.org/10.1016/j.biombioe.2016.12.008.

Larsen, J.F., Wallace, J.S., 1997. Comparison of Emissions and Efficiency of a Turbocharged Lean-Burn Natural Gas and Hythane-Fueled Engine. J. Eng. Gas Turbines Power 119, 218. http://dx.doi.org/10.1115/1.2815553.

Liu, K., Song, C., Subramani, V., 2010. Hydrogen and Syngas Production and Purification Technologies. Wiley. http://dx.doi.org/10.1002/9780470561256.fmatter.

Mao, Z., Sinnott, S.B., 2001. Separation of organic molecular mixtures in carbon nanotubes and bundle: molecular dynamics simulation. J. Phys. Chem. B 105, 6916–6924. http://dx.doi.org/10.1021/jp0103272.

Narasimhan, S., Jordache, C., 1999. Data Reconciliation and Gross Error Detection. Gulf Professional Publishing, Burlington.

Nelsson, C., Hulteberg, C., Saint-Just, J., Kaiadi, M., 2010. HCNG – a dead end or a bridge to the future. In: Proceedings WHEC2010.

Ortenzi, F., Chiesa, M., Scarcelli, R., Pede, G., 2008. Experimental tests of blends of hydrogen and natural gas in light-duty vehicles. Int. J. Hydorgen Energy 33, 3225–3229. http://dx.doi.org/10.1016/j.ijhydene.2008.01.050.

Pröll, T., Rauch, R., Aichernig, C., Hofbauer, H., 2007. Fluidized bed steam gasification of solid biomass – performance characteristics of an 8 MW_{th} combined heat and power plant. Int. J. React. Eng. 5, 6542–6580. http://dx.doi.org/10.2202/1542-6580.1398.

Rehling, B., Hofbauer, H., Rauch, R., Aichernig, C., 2011. BioSNG-process simulation and comparison with first results from a 1-MW demonstration plant. Biomass Convers Biorefin. 1, 111–119. http://dx.doi.org/10.1007/s13399-011-0013-3.

Roy, S., Das, D., 2016. Biohythane production from organic wastes: present state of art. Environ. Sci. Pollut. Res. 23, 9391–9410. http://dx.doi.org/10.1007/s11356-015-5469-4. URL http://dx.doi.org/10.1007/s11356-015-5469-4.

Sircar, S., Golden M.R., T.C., 1996. Activated carbon for gas separation and storage. Carbon 34, 1–12. http://dx.doi.org/10.1016/0008-6223(95)00128-X.

Sauciuc, A., Abosteif, Z., Weber, G., Potetz, A., Rauch, R., Hofbauer, H., Schaub, G., Dumitrescu, L., 2012. Influence of oeprating conditions on the performance of biomass-based Fischer-Tropsch synthesis. Biomass Convers. Biorefin. 2, 253–263. http://dx.doi.org/10.1007/s13399-012-0060-4.

Sierens, R., Rosseel, E., 2000. Variable composition hydrogen/natural gas mixtures for increased engine efficiency and decreased emissions. J. Eng. Gas Turbines Power 122, 135. http://dx.doi.org/10.1115/1.483191.

Verhelst, S., Wallner, T., 2009. Hydrogen-fueled internal combustion engines. Prog. Energy Combust. Sci. 35, 490–527. http://dx.doi.org/10.1016/j.pecs.2009.08.001.

Weber, G., Rauch, R., Hofbauer, H., 2015. Influence of ethylene on the formation of mixed alcohols over a MoS_2 catalyst using biomass-derived synthesis gas. Biomass Convers. Biorefin. 5, 85–94. http://dx.doi.org/10.1007/s13399-014-0140-8.

Wilk, V., Hofbauer, H., 2016. Analysis of optimization potential in commercial biomass gasification plants using process simulation. Fuel Process. Technol. 141, 138–147. http://dx.doi.org/10.1016/j.fuproc.2015.07.035.

Xu, X., Yang, W., Song, C., Liu, J., Lin, L., 2003. Hydrogen separation by zeolite membranes. Fuel Chem. Div. Prepr. 48, 284.

Yang, R.T., 2003. Adsorbents: Fundamentals and Applications. Wiley-Interscience.

Paper 8

Jingang Yao, Michael Kraussler, Florian Benedikt, Hermann Hofbauer, Techno-economic assessment of hydrogen production based on dual fluidized bed biomass steam gasification, biogas steam reforming, and alkaline water electrolysis processes, Energy Conversion and Management, Volume 145, 2017, Pages 278-292, `https://doi.org/10.1016/j.enconman.2017.04.084`.

Contribution: Techno-economic assessment, writing

Energy Conversion and Management 145 (2017) 278–292

Contents lists available at ScienceDirect

Energy Conversion and Management

journal homepage: www.elsevier.com/locate/enconman

Techno-economic assessment of hydrogen production based on dual fluidized bed biomass steam gasification, biogas steam reforming, and alkaline water electrolysis processes

Jingang Yao [a], Michael Kraussler [b,c,*], Florian Benedikt [c], Hermann Hofbauer [c]

[a] School of Environmental Science and Engineering, Tianjin University, 92 Weijin Road, Nankai District, Tianjin 3000072, China
[b] Bioenergy 2020+ GmbH, Wienerstraβe 49, 7540 Güssing, Austria
[c] TU Wien, Institute of Chemical Engineering, Getreidemarkt 9, 1060 Wien, Austria

A R T I C L E I N F O

Article history:
Received 8 February 2017
Received in revised form 25 April 2017
Accepted 26 April 2017

Keywords:
Techno-economic assessment
CO_2-neutral H_2 production
Dual fluidized bed biomass steam gasification
Biogas steam reforming
Alkaline electrolysis

A B S T R A C T

In this paper, three CO_2-neutral H_2 production processes were investigated. The three employed technologies were dual fluidized bed (DFB) biomass steam gasification, biogas steam reforming (BSR), and alkaline electrolysis (AEL) powered by renewable electricity with their necessary downstream separation and purification process steps. Aspen Plus process simulations were carried out in order to calculate the mass and energy balances of the three processes. In addition, a techno-economic assessment was carried out for a fictitious business producing H_2 at a rate of 90 kg h^{-1} in Austria in 2016. This assumption was used so that the economic feasibility of these investigated processes could be directly compared.

The simulation results show that the DFB biomass steam gasification process has a higher H_2 conversion rate (51.4%) but a lower fuel based H_2 production efficiency (38.9%) than the BSR process (27.2% and 47.0%, respectively). Moreover, the alkaline electrolysis process shows the highest energy based H_2 conversion efficiency at about 66%.

The results of the economic assessment show that the DFB biomass steam gasification process has investment costs of 12.1 MEUR followed by the biogas steam reforming process with investment costs of 9.9 MEUR. The alkaline electrolysis process has investment costs of 4.4 MEUR. However, the after tax H_2 break-even price of the DFB process is the lowest with 0.148 EUR kWh^{-1}. The BSR process has an after tax H_2 break-even price of 0.152 EUR kWh^{-1} and the AEL process has an after tax H_2 break-even price of 0.191 EUR kWh^{-1}. The net present value (NPV) calculations reveal that the BSR process has the highest NPV, followed by the AEL process and the DFB biomass steam gasification process. However, the NPV of all three processes are very similar. In general, all three H_2 production processes perform at the same level based on the results of the process simulation and the chosen economic assumptions.

© 2017 Elsevier Ltd. All rights reserved.

1. Introduction

Today most H_2 used in industry is produced by steam reforming of natural gas or other hydrocarbons [1]. These large scale steam reformer plants mainly cover the H_2 demand of refineries and ammonia plants. However, other industries, like the glass, food, metal, and petrochemicals also need H_2 but in significantly smaller amounts. Consequently, small-scale natural gas steam reformer plants have been established throughout these markets because in most cases on-site supply of H_2 offers greater economy when compared to delivery by truck [2].

In light of climate change, small scale CO_2-neutral H_2 production processes should be established. Hence, this work investigates the following three CO_2-neutral H_2 production routes: biomass steam gasification, steam reforming of biogas, and alkaline electrolysis powered by renewable electricity together with its necessary downstream separation and purification steps.

In the case of biomass steam gasification, the dual fluidized bed (DFB) steam gasification technology was chosen because it has proven its feasibility for several years in multiple commercial plants. In addition, the product gas generated is practically free of N_2 and already contains a high volumetric H_2 fraction of about 40% [3,4]. Anaerobic digestion (AD) is an established technology for

---

* Corresponding author at: Bioenergy 2020+ GmbH, Wienerstraβe 49, 7540 Güssing, Austria.

E-mail address: michael.kraussler@bioenergy2020.eu (M. Kraussler).

http://dx.doi.org/10.1016/j.enconman.2017.04.084
0196-8904/© 2017 Elsevier Ltd. All rights reserved.

Nomenclature

Abbreviations and acronyms

AD	anaerobic digestion
AEL	alkaline electrolysis
AT	after tax
BSR	biogas steam reforming
BT	before tax
CHP	combined heat and power
DFB	dual fluidized bed
PSA	pressure swing adsorption
RME	rapeseed methyl ester
SG	steam generator
SR	steam reformer
WGS	water gas shift

Symbols

φ_j	volumetric fraction of component j in $m^3\ m^{-3}$
ϱ	density in $kg\ m^{-3}$
AT cash flow	after tax cash flow in EUR a^{-1}
BEP	break-even price in EUR kg^{-1} or EUR kWh^{-1}
BT cash flow	before tax cash flow in EUR a^{-1}
Capital	required capital for the plant in EUR
CEPI	chemical engineering plant index in –
Depreciation	linear depreciation in EUR a^{-1}
Expenses	in EUR a^{-1}
i	discount/interest rate in –
LHV	lower heating value in MJ kg^{-1}
m	exponent for order of magnitude capital estimation in –
$\dot{m}_j$	mass flow of component j in kg h^{-1}
n	plant lifetime in a
NPV	net present value in EUR
Revenues	in EUR a^{-1}
Tax rate	in –
ω_j	mass fraction of component j in kg kg^{-1}

the generation of biogas, which mainly consists of CH_4 and CO_2. Furthermore, the separation of CH_4 from biogas and its injection in the natural gas grid is commercially employed at different locations. Moreover, CH_4 in the biogas can also be used as feed stock in a steam reforming process in order to generate H_2 [5]. Alkaline water electrolysis (AEL) is a well established and commercially used route for production of H_2 from electricity. It is mainly used to generate small scale H_2 supplies on-site [6,7]. If powered by renewable electricity, the generated H_2 is CO_2-neutral.

The three CO_2-neutral H_2 production routes were evaluated via process simulation in Aspen Plus in order to acquire mass and energy balances and, consequently, to deliver the data necessary for a techno-economic assessment. Based on this assessment, a decision about which kind of plant offers the greatest economic benefit can be made.

The work presented here is based on the following fictitious business case located in Austria in 2016: A company needs about 90 kg h^{-1} (1000 $m^3\ h^{-1}$) H_2 with a volumetric purity greater than 99.9% for its process. They want to erect a H_2 production plant which needs to be available for 8000 h per year. Heat is not a required product. Company policy demands that the H_2 production plant be CO_2-neutral. Based on the results of this study, a decision should be possible, which of the three investigated CO_2-neutral H_2 production routes offers the highest economy feasibility.

2. Materials and methods

This section introduces the three processes for production of CO_2-neutral H_2. Furthermore, assumptions made for the simulation of each of the three processes are shown. In addition, the approach for the techno-economic assessment is presented.

2.1. Investigated processes

This section describes the three routes for production of CO_2-neutral H_2: DFB biomass steam gasification, steam reforming of biogas, and alkaline electrolysis. The presented principles are the basis for Aspen Plus process simulations and, further on, for the techno-economic assessment. The described processes were simulated using Aspen Plus 8.6. All volumetric flow rates are given at standard temperature and pressure (273.15 K and 101,325 Pa).

Table 1 shows the technical boundary conditions and assumptions used for all three process designs.

Table 1
Assumptions for simulations of the DFB, BSR, and AEL processes.

	Values	Units
$\dot{m}_{H2}$	90	kg h^{-1}
φ_{H2}	99.9%	$m^3\ m^{-3}$
p_{H2}	1.0	MPa
T_{H2}	25	°C

Based on these assumptions, the mass and energy balances from all three processes were calculated. No district heat generation within the DFB and BSR design was considered. Therefore, all heat was used within the processes, mainly for steam generation.

2.1.1. Dual fluidized bed biomass steam gasification

Fig. 1 shows the simplified process layout for H_2 production by DFB biomass steam gasification.

Wet wood chips are fed into the biomass dryer (not depicted), which is operated with low temperature waste heat from the process. In the dryer, the H_2O mass fraction of the feedstock is reduced from about 32% to about 16%, which is a typical value for dryers within commercial DFB biomass steam gasification plants [8]. Dried wood chips are fed into the gasifier where they devolatilize and react with H_2O. According to the endothermic gasification reactions, at about 850 °C the product gas with the main gas components H_2, CO, CO_2, and CH_4 is formed. Olivine is used as bed material and heat carrier. It exhibits catalytic activity that enhances gasification reactions and, therefore, reduces the tar content of the product gas [9–12]. Subsequently, the product gas is cooled, filtered (mainly by particle separation), and fed into a fixed bed water gas shift (WGS) reactor employing a Fe/Cr-based catalyst where CO and H_2O are converted into additional H_2 and CO_2 according to the exothermic WGS reaction. The gas inlet temperature is about 350 °C, and a molar steam to dry gas ratio of 1.5 avoids coking and carbon deposition on the catalyst surface. During past investigations, the Fe/Cr-based catalyst has proven its stability in processing tar-rich product gas [13,14]. In the next steps, the product gas is cooled and fed into a rapeseed methyl ester (RME, $\varrho = 880\ kg\ m^{-3}$, $LHV = 36.9\ MJ\ kg^{-1}$) scrubber, where the gas is further cooled from about 150 °C to about 50 °C. Consequently, tar and steam are removed and condensed. The condensed steam is recycled and used to generate more steam for the process. The RME scrubber has proven to be sufficient for removing tar and steam from the product gas stream when employed at commercial

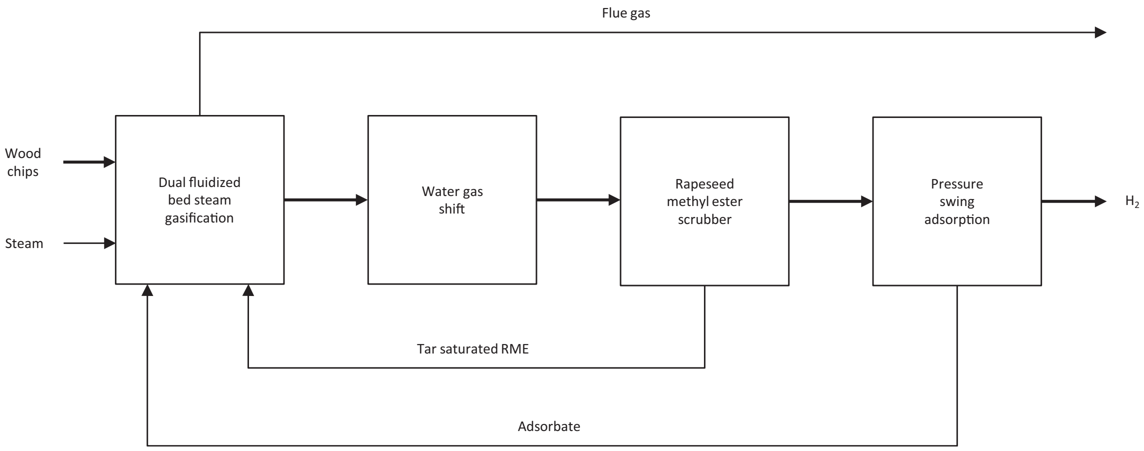
Flue gas
Wood chips
Steam
Dual fluidized bed steam gasification
Water gas shift
Rapeseed methyl ester scrubber
Pressure swing adsorption
H_2
Tar saturated RME
Adsorbate

Fig. 1. DFB biomass steam gasification process for H_2 production.

DFB biomass steam gasification plants for combined heat and power (CHP) [3,15]. In the last step, the gas is compressed to 1.0 MPa and subsequently fed into a pressure swing adsorption (PSA) unit where H_2 is separated from the other gas components. H_2 recovery in the PSA unit is assumed to be 85%, which is within the same order of magnitude reported previously [1,16–20]. Consequently, H_2 with a volumetric fraction of more than 99.9% is produced. The PSA off gas is used as fuel for the combustion reactor of the DFB gasification system and the heat from the flue gas line is recovered for use elsewhere within the process. The flue gas is filtered before it is released into the environment. A typical feed stock composition can be seen in Table 2. It is assumed that wood chips with a water mass fraction of 32% are delivered to the plant.

Table 2
Elemental analysis and LHV of wood chips (dry basis), which are typically used as fuel for DFB gasification plants [8]. Sulphur was not considered in the process simulation.

	Values	Units
C	49.4%	kg kg^{-1}
H	6.0%	kg kg^{-1}
N	0.2%	kg kg^{-1}
O[a]	43.5%	kg kg^{-1}
Ash	0.9%	kg kg^{-1}
LHV	18.3	MJ kg^{-1}

[a] By calculation.

Fig. 2 shows the simulation flowsheet for H_2 production by DFB biomass steam gasification. A RYield block is applied to model the gasifier, in which wood chips devolatilize and react with H_2O. The amount of makeup H_2O could be calculated by writing a FORTRAN statement in the calculator block and then using it before the unit operation (steam generator). Products from the gasifier enter a SSplit block (SEPERAT) which separates solid residues (Dec-char) from gaseous products into DECOMP. Gaseous products then pass through into the heat exchanger (HE1). A RYield block (DECOMP) is applied to model the decomposition of bio-char into its constituting elements (C, N, and ash). A FORTRAN statement is introduced to define the distribution of elements in term of its proximate and ultimate analysis and to determine their mass flow rate at the outlet of the block. A RStoic block is applied to model the combustor, in which the PSA off-gas combusts with air to fulfil the energy demand of the gasification process. A REquil block (WGSR) is applied to simulate the WGS reactor, in which only the WGS reaction is considered. Heater blocks are applied to simulate the steam generator and heat exchangers (HE1, HE2, and HE3). The MCompr block is applied to simulate the compressor (C1). Sep2 blocks are applied to simulate the gravitational separator and the RME scrubber. A Sep block is applied to simulate the PSA unit. FabFI blocks are applied to simulate the filtration units (Filter-1 and Filter-2). In addition, a heat stream (Q-supply) is applied to fulfil the energy demands of the gasifier. In this model, the physical properties of mixed conventional components and

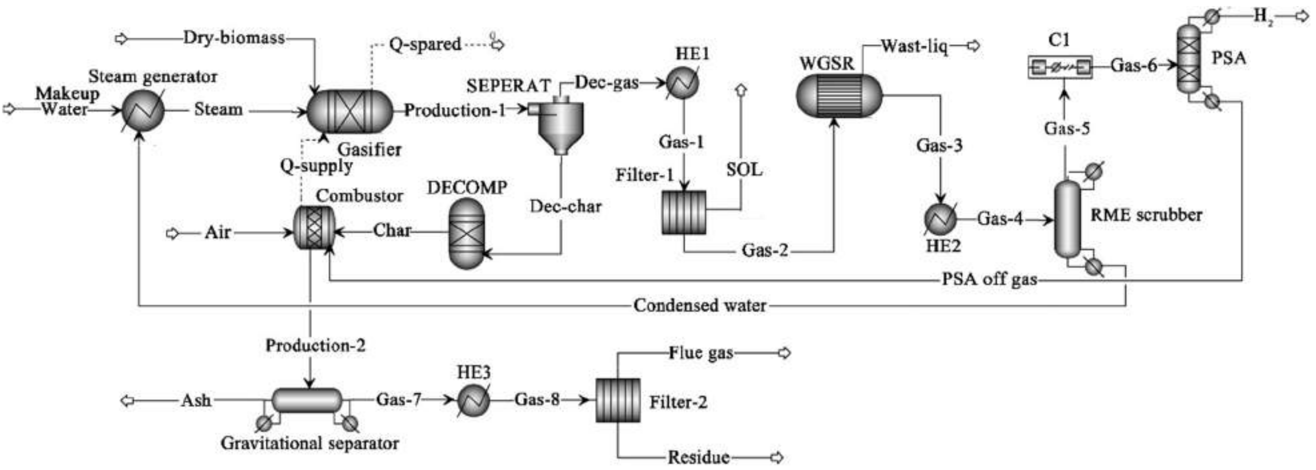
Dry-biomass
Q-spared
Steam generator
Makeup Water
Steam
Gasifier
Production-1
SEPERAT
Dec-gas
HE1
Gas-1
Filter-1
SOL
Gas-2
WGSR
Wast-liq
Gas-3
HE2
Gas-4
RME scrubber
Gas-5
C1
Gas-6
PSA
H_2
Q-supply
Combustor
DECOMP
Dec-char
Air
Char
PSA off gas
Condensed water
Production-2
Ash
Gravitational separator
Gas-7
HE3
Gas-8
Filter-2
Flue gas
Residue

Fig. 2. Aspen flowsheet of the DFB gasification process for H_2 production.

CISOLID components are calculated by the property method of IDEAL. The enthalpy and density of non-conventional components are calculated by HCOALGEN and DCOALIGT models, respectively. The reactions used in the DFB process simulation are highlighted in Table 3. The input specifications for unit operation blocks of the DFB process simulation are presented in Table 4. The component attributes used for Dec-char in gasifier block and for ash in DECOMP block are presented in Table 5.

2.1.2. Biogas steam reforming

Fig. 3 shows the process layout of the biogas steam reforming (BSR) process to generate H_2.

Wet maize silage is fed into the AD, where it is converted into biogas. Subsequently, the biogas is desulfurized via fixed bed activated carbon and ZnO beds. This step is necessary because the nickel catalyst, which is usually employed in steam reforming reactors [1], is very sensitive to sulphur poisoning. In the steam reformer, biogas, which mainly consists of CH_4 and CO_2, is converted into H_2, CO, CO_2, and minor amounts of CH_4 at a molar steam to carbon ratio of three in order to avoid coking and carbon deposition. Heating is carried out with a small amount of biogas and the off gas from the PSA. After cooling, the gas stream is fed into a WGS unit were CO and H_2O are converted into additional H_2 and CO_2. Subsequently, the remaining steam is condensed and the condensate is reused for steam generation. Further on, the gas is compressed to 1.0 MPa and, finally, fed into a PSA unit. In the PSA unit, H_2 is separated from the other gas components with an assumed H_2 recovery of 85% (compare Section 2.1.1). The PSA off gas is used to cover the heat demand of the endothermic steam reforming reactions. However, about 1.1 MW of additional heating is required. Therefore, additional maize silage is converted into biogas and burned to supply the heat required for reforming. The

Table 3
Specifications of the reactions used in the DFB process simulation.

Unit operation	Aspen block	Specification type	Stoichiometry	Fraction	Base component
Combustor	RStoic	Frac. conversion	$C + O_2 \rightarrow CO_2$	1	C
			$2H_2 + O_2 \rightarrow 2H_2O$		H_2
			$2CO + O_2 \rightarrow 2CO_2$		CO
			$CH_4 + 2O_2 \rightarrow CO_2 + 2H_2O$		CH_4
WGSR	REquil	Temp. approach	$H_2O + CO \rightarrow CO_2 + H_2$	–	–

Table 4
Specifications for unit operation blocks of the DFB process simulation.

Unit operation	Aspen block	Specifications	
Steam generator	Heater	Temperature	350 °C
		Pressure	0.1 MPa
Gasifier	RYield	Temperature	850 °C
		Pressure	0.1 MPa
		Component yields (kg kg^{-1})	H_2 = 0.016543, CO = 0.144528, CO_2 = 0.201388, CH_4 = 0.0351642, DECCHAR = 0.0580664, and H_2O = 0.5444
DECOMP	RYield	Temperature	945 °C
		Pressure	0.1 MPa
		Component yields (kg kg^{-1})	C = 0.934323, Ash = 0.055968, and N_2 = 0.009709
Combustor	RStoic	Temperature	945 °C
		Pressure	0.1 MPa
WGSR	REquil	Pressure	0.1 MPa
		Duty	0 kW
HE1, HE2, and HE3	Heater	Temperature	HE1 = 350 °C, HE2 = 150 °C, and HE3 = 25 °C
		Pressure	0.1 MPa for HE1, HE2, and HE3
C1	MCompr	Configuration	Number of stages = 1, Compressor model = Polytropic using ASME method and Specification type = Fix discharge pressure from last stage: 1 MPa
		Cooler	Stage = 1, specification = outlet Temp, Value = 25 °C, and pressure drop = 0 MPa

Table 5
Component attributes in unit operation blocks of the DFB process simulation.

			Component ID (unit operation)	
			Dec-char (Gasifier)	Ash (DECOMP)
Attribute ID	Proximate analysis (kg kg^{-1})	Moisture	0	0
		Fixed carbon	0.934323	0
		Volatile matter	0.009709	0
		Ash	0.055968	100
	Ultimate analysis (kg kg^{-1})	Ash	0.055968	100
		C	0.934323	0
		H	0	0
		N	0.009709	0
		Cl	0	0
		S	0	0
		O	0	0
	Sulfanal (kg kg^{-1})	Pyritic	0	0
		Sulfate	0	0
		Organic	0	0

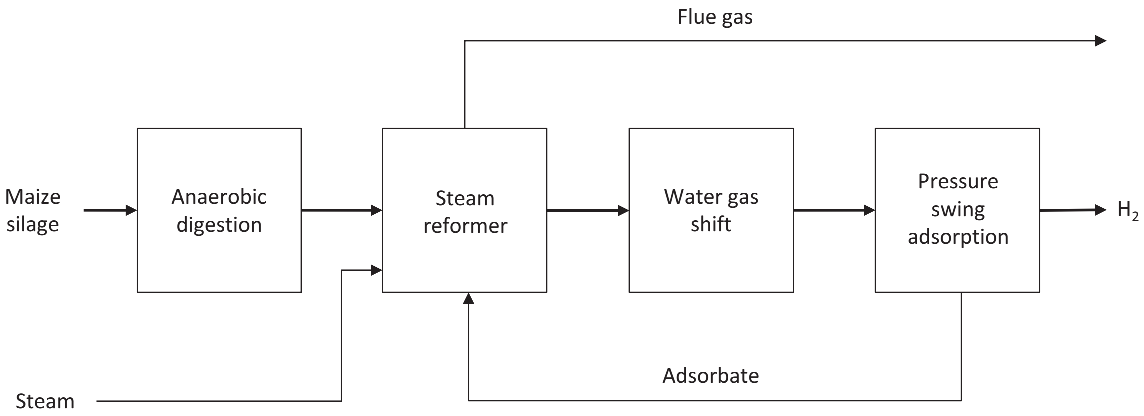
Flue gas
Maize silage
Anaerobic digestion
Steam reformer
Water gas shift
Pressure swing adsorption
H_2
Steam
Adsorbate

Fig. 3. BSR process for H_2 production.

Table 6
Elemental analysis and LHV of maize silage (wet basis) [23]. Sulphur was not considered in the process simulation.

	Values	Units
C	23.0%	kg kg^{-1}
H	1.0%	kg kg^{-1}
N	0.1%	kg kg^{-1}
O[a]	9.0%	kg kg^{-1}
Ash	1.9%	kg kg^{-1}
H_2O	65%	kg kg^{-1}
LHV	6.4	MJ kg^{-1}

[a] By calculation.

simulation data for AD have been described previously [21,22]. Table 6 shows the feedstock analysis of maize silage for the BSR process.

Fig. 4 shows the simulation flowsheet for H_2 production by the BSR process. A RYield block is applied to model the anaerobic digester. Mixtures from the anaerobic digester enter a Sep2 block (SEPERAT) which separates residues from biogas. The biogas then passes through into a heat exchanger (HE1). The amount of makeup H_2O could be calculated by writing a FORTRAN statement in the calculator block and then using it before the unit operation (steam reformer). A RGibbs block is applied to model the steam reformer. A REquil block (WGSR) is applied to simulate the WGS reactor, in which the same specifications of the reaction as that of WGSR in DFB process simulation are applied. A RGibbs block is applied to model the combustor, in which PSA off-gas and additional biogas combust with air to fulfil the energy demands of the steam reformer. Heater blocks are applied to simulate the steam generator and the heat exchangers (HE1, HE2, HE3, and HE4). A MCompr block is applied to simulate the compressor (C1). Sep2 blocks are applied to simulate the condenser. A Sep block is applied to simulate the PSA unit. In addition, heat streams (Q-supply-1 and Q-supply-2) are applied to fulfil the energy demand of the steam reformer. In this model, the physical properties of mixed conventional components and CISOLID components are calculated by the property method of RKS-BM. The enthalpy and density of non-conventional components are calculated by HCOALGEN and DCOALIGT models, respectively.

The input specifications of unit operation blocks used in the BSR process simulation are presented in Table 7. The component attributes used for the residue in anaerobic digester block are presented in Table 8.

2.1.3. Alkaline electrolysis

Fig. 5 shows the principle of H_2 generation by AEL.

Liquid water passes a scrubber, is mixed with lye (KOH) to generate a 25% aqueous solution with enhanced conductivity and is fed into the alkaline electrolyzer where the aqueous solution is split

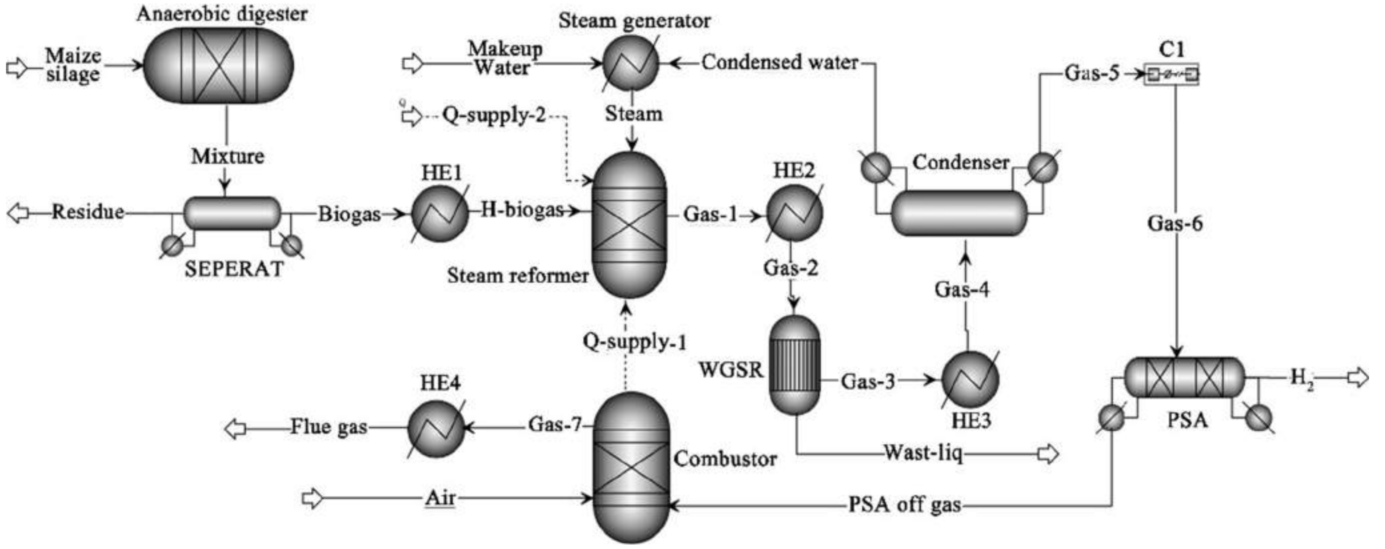
Anaerobic digester
Maize silage
Mixture
Residue
SEPERAT
Biogas
HE1
H-biogas
Steam generator
Makeup Water
Condensed water
Q-supply-2
Steam
Steam reformer
Gas-1
HE2
Gas-2
WGSR
Gas-3
HE3
Wast-liq
Gas-4
Condenser
Gas-5
C1
Gas-6
PSA
H_2
Q-supply-1
HE4
Flue gas
Gas-7
Combustor
Air
PSA off gas

Fig. 4. Aspen flowsheet of the BSR process for H_2 production.

Table 7
Specifications of unit operation blocks used in the BSR process simulation.

Unit operation	Aspen block	Specifications	
Steam generator	Heater	Temperature	400 °C
		Pressure	0.1 MPa
Anaerobic digester	RYield	Temperature	35 °C
		Pressure	0.1 MPa
		Component yields ($kg\ kg^{-1}$)	CH_4 = 0.0794029, CO_2 = 0.181416, H_2 = 0, Residue = 0.177747, and H_2O = 0.561433
Steam reformer	RGibbs	Calculation option	Restrict chemical equilibrium-specify temperature approach or reactions (900 °C)
		Products	H_2, CO, CH_4, H_2O, and CO_2
		Pressure	0.1 MPa
Combustor	RGibbs	Temperature	900 °C
		Pressure	0.1 MPa
WGSR	REquil	Pressure	0.1 MPa
		Duty	0 kW
HE1, HE2, HE3, and HE4	Heater	Temperature	HE1 = 900 °C, HE2 = 350 °C, HE3 = 25 °C, and HE4 = 50 °C
		Pressure	0.1 MPa for HE1, HE2, HE3, and HE4
C1	MCompr	Configuration	Number of stages = 1, compressor model = polytropic using ASME method and specification type = fix discharge pressure from last stage: 1 MPa
		Cooler	Stage = 1, specification = outlet Temp, value = 25 °C, and pressure drop = 0 MPa

Table 8
Component attributes used for the residue in anaerobic digester block.

			Component ID (unit operation) Residue (anaerobic digester)
Attribute ID	Proximate analysis ($kg\ kg^{-1}$)	Moisture	0
		Fixed carbon	0.270054
		Volatile matter	0.623025
		Ash	0.106921
	Ultimate analysis ($kg\ kg^{-1}$)	Ash	0.106921
		C	0.679745
		H	1.09313E-09
		N	0.00571035
		Cl	0
		S	0
		O	0.207623
	Sulfanal ($kg\ kg^{-1}$)	Pyritic	0
		Sulfate	0
		Organic	0

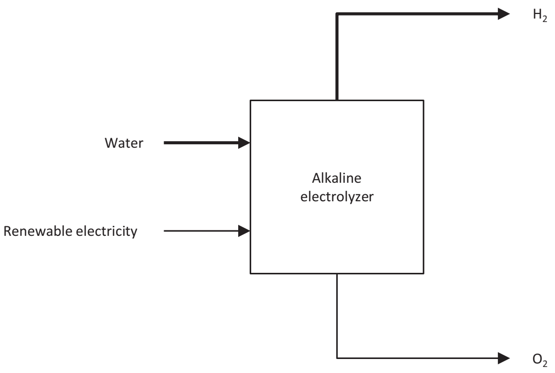

Fig. 5. AEL process for H_2 production.

into H_2 and O_2 by an electrical current. Subsequently, the H_2 produced passes the lye separator and the scrubber where it is cooled by fresh water and, finally, fed into the compressor. The O_2, which is generated during the process, is released into the ambient air after passing the lye separator.

The AEL process was simulated as black box model entirely based on manufacturer data [7,24].

2.2. Techno-economic assessment

The techno-economic assessment was based on previously developed approaches [25]. First, the investment and production costs were estimated. Then the net present value (NPV) and break-even price (BEP) were determined from the economic assessment.

2.2.1. Investment costs

Investment costs were estimated based on a literature study as well as on budget quotes from different plant manufacturers. Investment costs from years other than 2016 were adjusted using the chemical engineering plant cost index (CEPI, see Eq. (1)).

$$\frac{Capital\,1}{Capital\,2} = \frac{CEPI\,1}{CEPI\,2} \qquad (1)$$

The capital cost of plants and units of different sizes were adjusted using order-of-magnitude estimates and capacity rationing was accounted for with Eq. (2).

$$\frac{Capital\,1}{Capital\,2} = \left(\frac{Capacity\,1}{Capacity\,2}\right)^m \qquad (2)$$

An exponent m of 0.67 was used in this work to take into account the whole plant [25].

In addition, plant startup expenses were considered to be 10% of the calculated capital costs. Therefore, the overall investment costs of a plant were calculated according to Eq. (3).

$$Investment\ costs = Capital \cdot (1 + 10\%) \qquad (3)$$

Table 9
Overview of estimated production costs.

Production costs	Detailed estimates	Factored estimates
Raw materials	Based on process simulation and market prices	
Operating labor	Based on plant operator data	
Utilities	Based on process simulation and market prices	
Employee benefits		22% of operating labor
Supervision		10% of operating labor
Laboratory		10% of operating labor
Maintenance		6% of investment costs
Insurance and taxes		3% of investment costs
Operating supplies		3% of investment costs
Plant overhead		1% of investment costs
Depreciation	Based on Eq. (4)	

Table 10
Assumptions for the techno-economic assessment.

	Values	Units
Number of employees	5 (DFB)/5 (BSR)/1 (AEL)	–
Annual operating hours	8000	h
Plant lifetime (n)	20	a
Tax rate	25%	–
Discount rate (i)	10%	–

Investment costs given in US $ were converted into EUR using an exchange rate of 1.10 $ EUR^{-1} from 18th of October 2016. Investment costs given for a year other than 2016 were adjusted using Eq. (1) and costs, which were given for a different capacity, were adjusted using Eq. (2).

2.2.2. Production costs

The production costs were split into detailed and factored estimates. The detailed estimates were calculated based on actual 2016 prices of materials and energy streams according to the amounts as calculated in the process simulations. Factored estimates were either considered as a percentage of the operating labor or as a percentage of the investment costs. Table 9 gives an overview of how the production costs were calculated.

The depreciation was calculated according to Eq. (4).

$$Depreciation = \frac{Investment\,costs}{Plant\,lifetime} \tag{4}$$

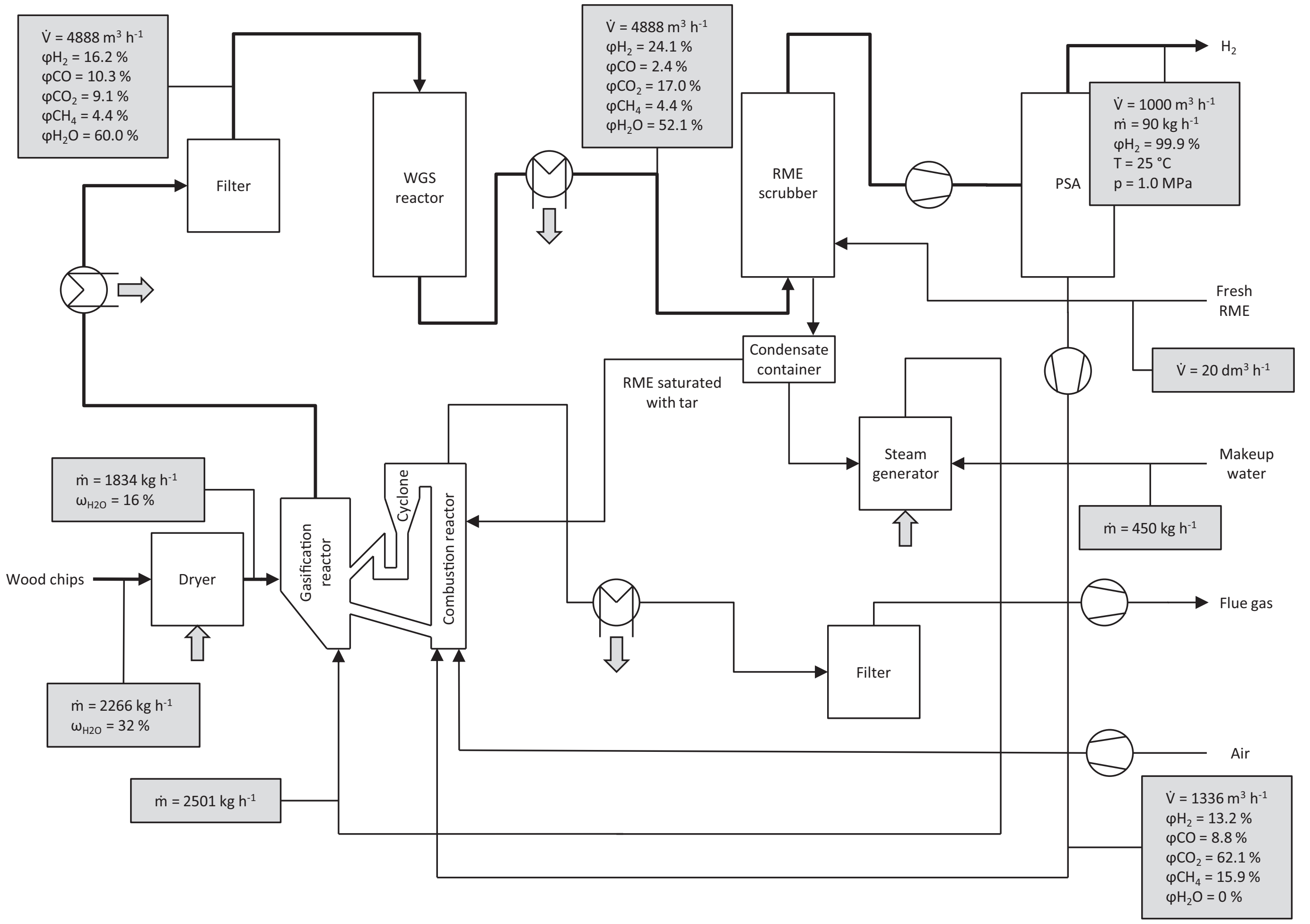
V̇ = 4888 m³ h⁻¹
φH₂ = 16.2 %
φCO = 10.3 %
φCO₂ = 9.1 %
φCH₄ = 4.4 %
φH₂O = 60.0 %
Filter
WGS reactor
V̇ = 4888 m³ h⁻¹
φH₂ = 24.1 %
φCO = 2.4 %
φCO₂ = 17.0 %
φCH₄ = 4.4 %
φH₂O = 52.1 %
RME scrubber
PSA
H₂
V̇ = 1000 m³ h⁻¹
ṁ = 90 kg h⁻¹
φH₂ = 99.9 %
T = 25 °C
p = 1.0 MPa
Fresh RME
V̇ = 20 dm³ h⁻¹
Condensate container
RME saturated with tar
Steam generator
Makeup water
ṁ = 450 kg h⁻¹
ṁ = 1834 kg h⁻¹
ω_H2O = 16 %
Wood chips
Dryer
Gasification reactor
Cyclone
Combustion reactor
Flue gas
Filter
Air
ṁ = 2266 kg h⁻¹
ω_H2O = 32 %
ṁ = 2501 kg h⁻¹
V̇ = 1336 m³ h⁻¹
φH₂ = 13.2 %
φCO = 8.8 %
φCO₂ = 62.1 %
φCH₄ = 15.9 %
φH₂O = 0 %

Fig. 6. Design of the DFB process for H_2 production including process simulation data.

2.2.3. Assessment

In order to carry out the techno-economic assessment, the assumptions in Table 10 were made for all investigated H_2 production processes. The base year for the investigation was 2016.

It was assumed that five employees are needed to ensure safe, twenty-four-seven operation of the H_2 production plants, except for the AEL plant. According to the manufacturer (personal communication Nel Hydrogen [24]), only one employee is necessary in order to watch and maintain the operation of an AEL plant. In addition, the annual operating time was set to 8000 h and the expected plant lifetime was set as 20 years. Furthermore, a tax rate of 25%, which is the standard tax rate on profits in Austria, was assumed allowing the consideration of the impact of the H_2 plant on the AT cash flow of the fictitious company. Finally, a discount rate of 10% was chosen for the NPV calculation.

The before tax (BT) cash flow was calculated according to Eq. (5). The revenue was set to zero as no H_2 was sold because all H_2 is needed for the process within the company. The expenses were based on the production costs in Table 9.

$$BT\,cashflow = Revenues - Expenses \tag{5}$$

The after tax (AT) cash flow was calculated according to Eq. (6), which takes the BT cash flow, the tax rate, and depreciation into account.

$$AT\,cashflow = BT\,cashflow \cdot (1 - Tax\,rate) + Depreciation \tag{6}$$

The techno-economic assessment was based on the NPV, which was calculated with the AT cash flow, the discount rate, the plant lifetime, and the investment costs according to Eq. (7). A higher NPV indicates a higher economic feasibility of a process over its lifetime even if it has a negative value.

$$NPV = AT\,cashflow \cdot \left[\frac{(1+i)^n - 1}{i \cdot (1+i)^n}\right] - Investment\,costs \tag{7}$$

The BEP of the produced H_2 was calculated based on before tax (BT BEP) and after tax (AT BEP) basis because tax consideration is an important factor which can significantly influence the results. Consequently, the BT BEP was calculated according to Eq. (8) and the AT BEP was calculated according to Eq. (9).

$$BT\,BEP = \frac{1}{(\dot{m}_{H2} \cdot Annual\,operating\,hours)} \cdot Expenses \tag{8}$$

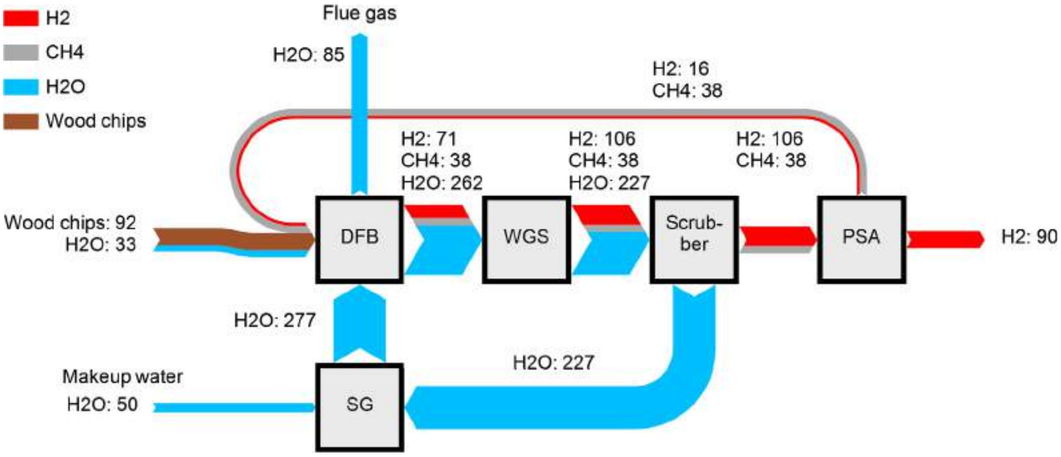
H2
CH4
H2O
Wood chips
Flue gas
H2O: 85
H2: 16
CH4: 38
H2: 71
CH4: 38
H2O: 262
H2: 106
CH4: 38
H2O: 227
H2: 106
CH4: 38
Wood chips: 92
H2O: 33
DFB
WGS
Scrub-
ber
PSA
H2: 90
H2O: 277
Makeup water
H2O: 50
SG
H2O: 227

Fig. 7. H mass flows along the DFB process. The mass flows are given in kg h^{-1}.

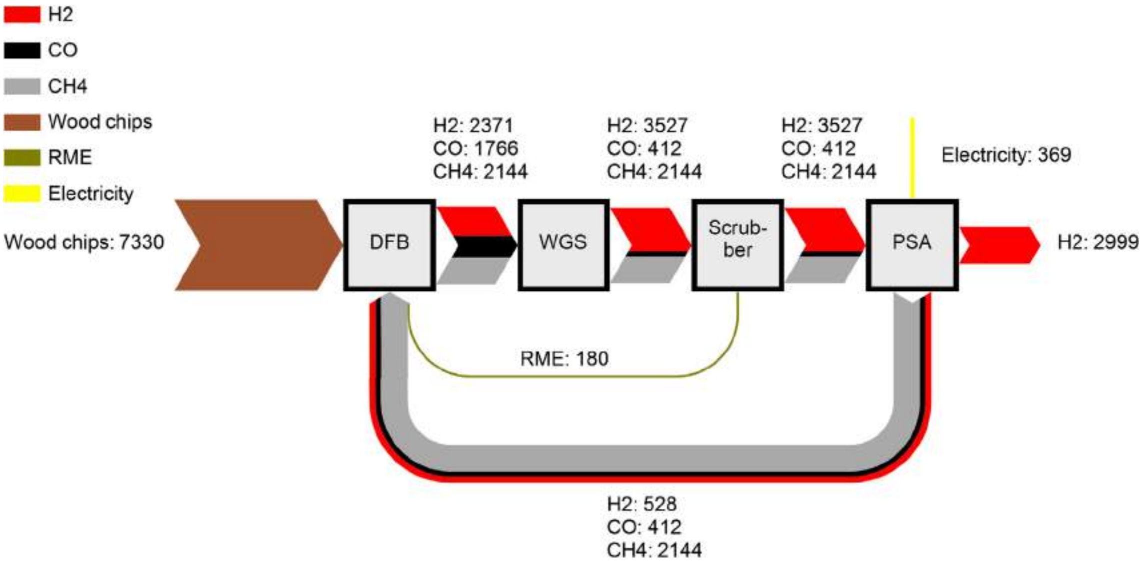
H2
CO
CH4
Wood chips
RME
Electricity
H2: 2371
CO: 1766
CH4: 2144
H2: 3527
CO: 412
CH4: 2144
H2: 3527
CO: 412
CH4: 2144
Electricity: 369
Wood chips: 7330
DFB
WGS
Scrub-
ber
PSA
H2: 2999
RME: 180
H2: 528
CO: 412
CH4: 2144

Fig. 8. DFB process energy flows. The energy flows are based on the LHV and are given in kW. Sensible heat is not depicted.

$$AT\,BEP = \frac{1}{(\dot{m}_{H2}\cdot Annual\,operating\,hours)} \cdot \left[\frac{Expenses(1-Tax\,rate)-Depreciation}{(1-Tax\,rate)}\right] \quad (9)$$

3. Results and discussion

This section shows the results of the Aspen Plus process simulations and the results of the techno-economic assessment. The results are presented in the following order: the DFB process, the BSR process, and the AEL process.

3.1. Biomass steam gasification

Fig. 6 shows a simplified flowchart of the DFB process for H_2 production and includes some of the main process parameters from the process simulation. It can be seen that 2266 kg h^{-1} wet wood chips are necessary in order to produce a H_2 output of 90 kg h^{-1}. In addition, about 450 kg h^{-1} of makeup water are needed in order to achieve the desired molar steam to dry gas ratio of 1.5 at the inlet of the WGS reactor (compare [13]). Furthermore, the product gas composition after the gasifier is in the typical order of magnitude of commercial DFB gasification plants (compare [3,8]).

Fig. 7 shows the H mass flows (in kg h^{-1}) along the DFB process considering H atoms which are derived from the wood chips as well as the H_2, CH_4, and H_2O streams.

Of the H fed into the process, 51.4% can be extracted as pure H at the end of the process. The recycle stream from the RME scrubber (227 kg h^{-1}) is composed mainly of hydrogen in the condensed steam which is used as a gasification agent in the DFB gasifier. Furthermore, about 37.5% of the H leaving the scrubber is recycled with the adsorbate of the PSA unit, which is fed into the combustion reactor of the DFB gasification system.

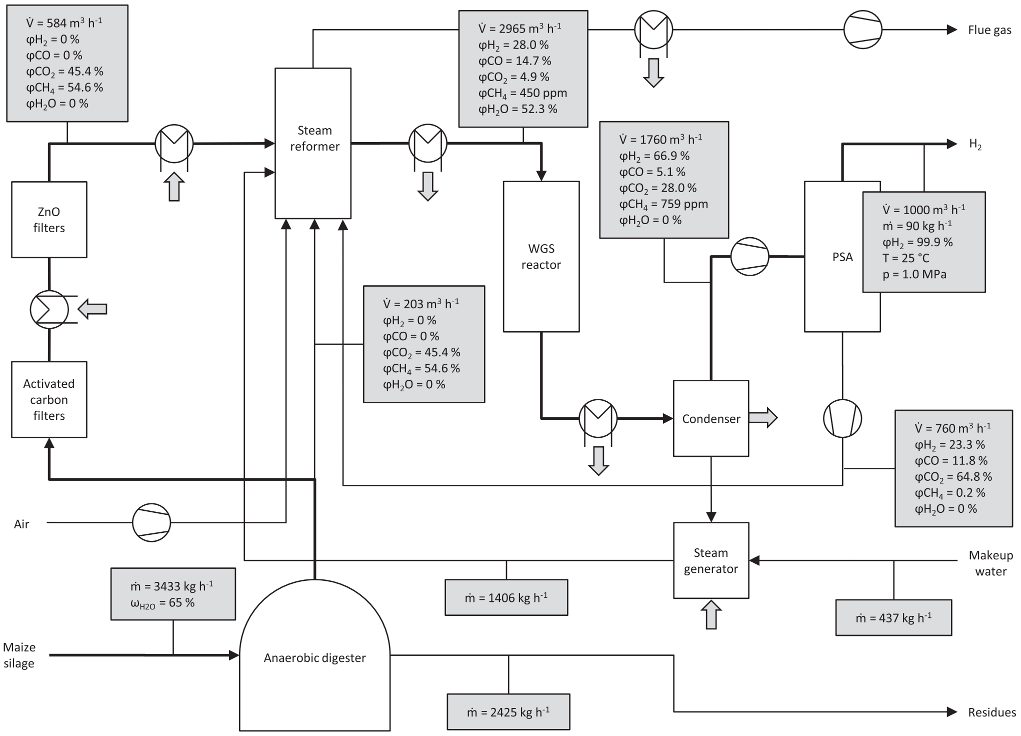
V̇ = 584 m³ h⁻¹
φH₂ = 0 %
φCO = 0 %
φCO₂ = 45.4 %
φCH₄ = 54.6 %
φH₂O = 0 %
Steam reformer
V̇ = 2965 m³ h⁻¹
φH₂ = 28.0 %
φCO = 14.7 %
φCO₂ = 4.9 %
φCH₄ = 450 ppm
φH₂O = 52.3 %
Flue gas
V̇ = 1760 m³ h⁻¹
φH₂ = 66.9 %
φCO = 5.1 %
φCO₂ = 28.0 %
φCH₄ = 759 ppm
φH₂O = 0 %
H₂
ZnO filters
WGS reactor
PSA
V̇ = 1000 m³ h⁻¹
ṁ = 90 kg h⁻¹
φH₂ = 99.9 %
T = 25 °C
p = 1.0 MPa
V̇ = 203 m³ h⁻¹
φH₂ = 0 %
φCO = 0 %
φCO₂ = 45.4 %
φCH₄ = 54.6 %
φH₂O = 0 %
Activated carbon filters
Condenser
V̇ = 760 m³ h⁻¹
φH₂ = 23.3 %
φCO = 11.8 %
φCO₂ = 64.8 %
φCH₄ = 0.2 %
φH₂O = 0 %
Air
Steam generator
Makeup water
ṁ = 3433 kg h⁻¹
ω_H2O = 65 %
ṁ = 1406 kg h⁻¹
ṁ = 437 kg h⁻¹
Maize silage
Anaerobic digester
ṁ = 2425 kg h⁻¹
Residues

Fig. 9. The BSR process for H_2 production showing the process design and process simulation data.

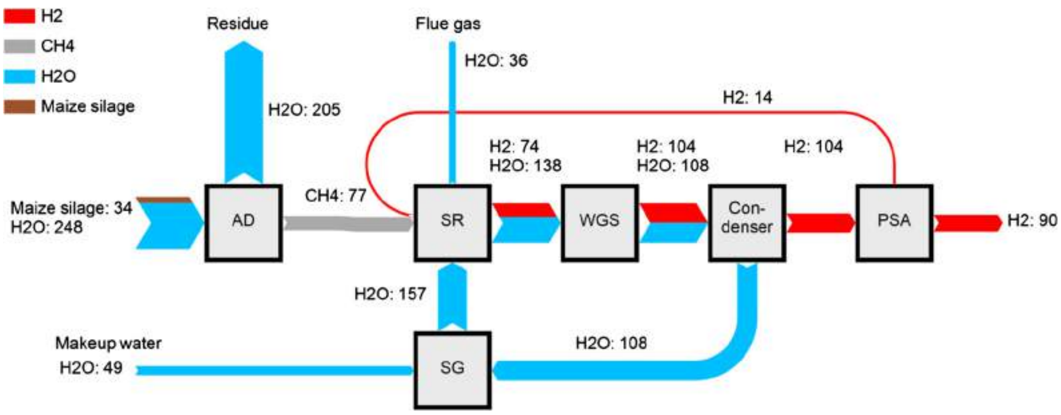
🟥 H2
▨ CH4
🟦 H2O
🟫 Maize silage
Residue
Flue gas
H2O: 36
H2O: 205
H2: 14
H2: 74
H2O: 138
H2: 104
H2O: 108
H2: 104
Maize silage: 34
H2O: 248
AD
CH4: 77
SR
WGS
Con-denser
PSA
H2: 90
H2O: 157
Makeup water
H2O: 49
SG
H2O: 108

Fig. 10. H mass flows along the BSR process. The mass flows are given in kg h^{-1}. The H contained in the CH_4 downstream of the steam reformer is negligible.

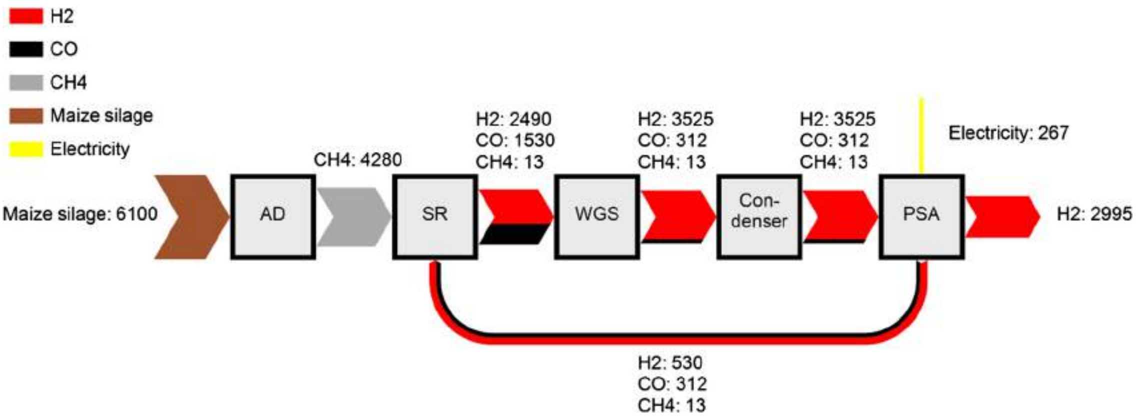
H2
CO
CH4
Maize silage
Electricity
Maize silage: 6100
AD
CH4: 4280
SR
H2: 2490
CO: 1530
CH4: 13
WGS
H2: 3525
CO: 312
CH4: 13
Con-denser
H2: 3525
CO: 312
CH4: 13
PSA
Electricity: 267
H2: 2995
H2: 530
CO: 312
CH4: 13

Fig. 11. BSR process energy flows. The energy flows are based on the LHV and given in kW. Sensible heat is not depicted.

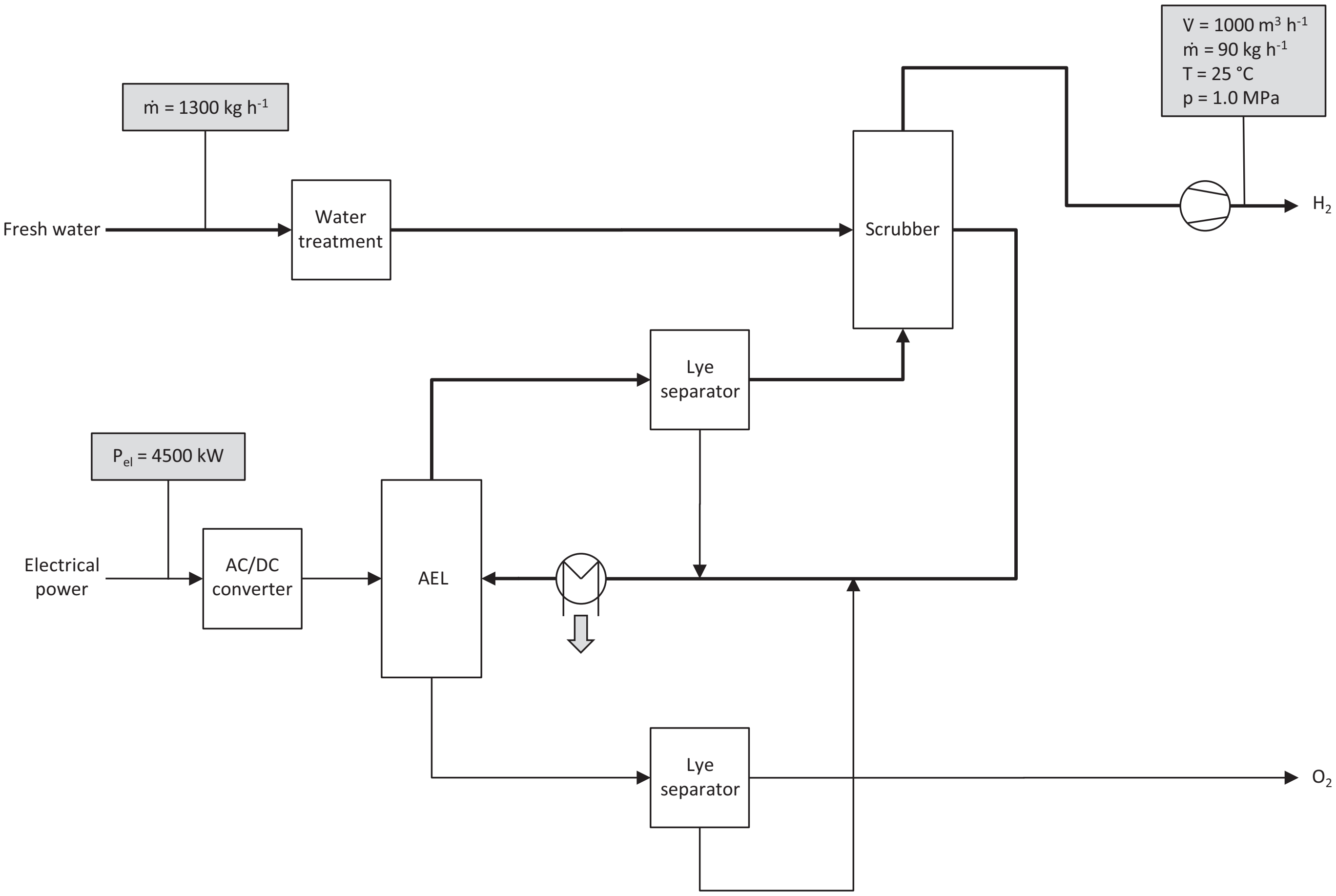
ṁ = 1300 kg h-1
Fresh water
Water treatment
Scrubber
V̇ = 1000 m3 h-1
ṁ = 90 kg h-1
T = 25 °C
p = 1.0 MPa
H2
Lye separator
Pel = 4500 kW
Electrical power
AC/DC converter
AEL
Lye separator
O2

Fig. 12. AEL process for H_2 production showing the process design and some of the process simulation data.

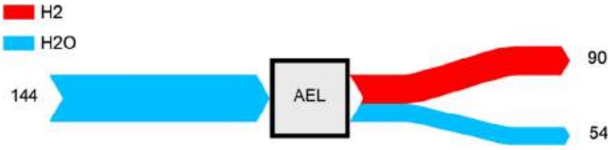
H2
H2O
144
AEL
90
54

Fig. 13. H mass flow along the AEL process. All mass flows are given in kg h^{-1}.

Fig. 8 shows the LHV based energy and electricity streams along the DFB process.

It indicates that the production efficiency is about 38.9% based on the LHV of wood chips, the electricity consumption, and H_2. Overall, within the DFB concept, a specific H_2 production rate of 39.7 g H_2 per kg wood chips (wet) and 58.4 g H_2 per kg wood chips (dry) can be achieved.

3.2. Biogas steam reforming

Fig. 9 shows a simplified flow chart of the BSR process for generating H_2 from maize silage and indicates some main process parameters.

It shows that 3433 kg h^{-1} of wet maize silage is needed in order to produce 90 kg h^{-1} H_2. Additionally, 437 kg h^{-1} of makeup water is necessary in order to achieve a molar steam to carbon ratio of 3.0 at the inlet of the steam reformer.

Fig. 10 shows the H mass flows (in kg h^{-1}) along the BSR process for H_2 production considering H atoms contained in maize silage, H_2, CH_4, and H_2O streams. About 27.2% of the H which is fed into the process can be recovered at its end as pure H_2. Most H losses occur in the AD (72.7%) in the form of water. In addition, it can be seen that the PSA losses in the BSR process are significantly lower compared to the PSA losses of the DFB process. This can be due to the higher H_2 content and, therefore, the higher partial pressure of H_2 in the PSA feed of the BSR process.

Fig. 11 shows the LHV based energy and electricity streams along the BSR process.

It indicates that the fuel and electricity based efficiency the of the H_2 generation is about 47.0%, which is in agreement with previous results [26]. In addition, according to the simulation, 267 kW of electrical power is needed for compression of the PSA feed. Overall, in the BSR concept, a specific H_2 production rate of 26.2 g H_2 per kg maize silage (wet) and 74.9 g H_2 per kg maize silage (dry) was achieved.

3.3. Alkaline electrolysis

Fig. 12 shows a simplified flowchart of the AEL process used to generate H_2 from water and renewable electricity.

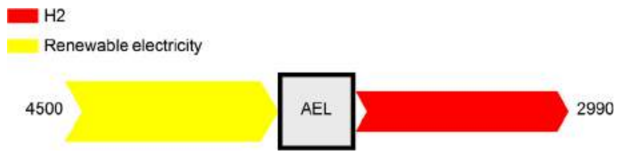

Fig. 14. AEL process energy flows. The H_2 energy flow is based on the LHV and given in kW. Sensible heat is not considered.

Table 11
Investment costs of the three investigated processes.

	DFB	BSR	AEL	Units
Capital costs	11,000,000	9,000,000	4,000,000	EUR
Startup expenses	1,100,000	900,000	400,000	EUR
Overall investment costs	12,100,000	9,900,000	4,400,000	EUR

Table 12
Material and energy streams of the three investigated processes.

	DFB	BSR	AEL	Units
Wood chips (dry)	1540			kg h^{-1}
Maize silage (wet)		3433		kg h^{-1}
Electrical energy	369	267	4500	kW
Fresh water	450	437	1300	kg h^{-1}
RME	0.020			m^3 h^{-1}
H_2	90	90	90	kg h^{-1}

Table 13
Specific costs of the considered material and energy streams.

	Value	Units	Source
Wood chips[a]	0.097	EUR kg^{-1}	Information from plant operator (July 2016)
Maize silage[b]	0.065	EUR kg^{-1}	Information from ARGE Kompost & Biogas (August 2016)
Electricity	0.11	EUR kWh^{-1}	Information from plant operator (July 2016)
Fresh water	0.002	EUR kg^{-1}	Information from plant operator (July 2016)
RME	1000	EUR m^{-3}	Information from plant operator (July 2016)

[a] Dry basis.
[b] Wet basis.

It can be seen that 1300 kg h^{-1} fresh water are necessary in order to generate 90 kg h^{-1} H_2. According to Nel Hydrogen [24], the fresh lye consumption is insignificant. Thus, it was not considered in the simulation.

Fig. 13 shows the H mass flows (in kg h^{-1}) along the AEL process following H atoms in the H_2 and H_2O streams.

It can be seen that 62.5% of the H that is contained in the feed water is recovered as product. Water is also included with the losses, as it is needed for process cooling.

Fig. 14 shows the energy streams along the AEL process for H_2 production.

It indicates a H_2 energy conversion efficiency of about 66.4%. In addition, electricity consumption also includes the electricity needed for H_2 compression.

3.4. Techno-economic assessment

This section presents the results of the techno-economic assessment based on the results of the process simulations in Sections 3.1,3.2, and 3.3.

3.4.1. Investment costs

Investment costs for the DFB process are based on experience within the research group as well as on data from a plant operator and plant manufacturer, which are comparable to the investment costs previously published [27,28]. Investment costs for the BSR process are based on information found in the literature [27–32]. Investment costs for the AEL process are based on a budget quote from the company Nel Hydrogen [24]. However, it should be mentioned that the estimation of the investment costs by order of magnitude analysis bears an uncertainty of about +50% and −30% according to [25].

Table 11 shows the investment costs of the three investigated processes for a H_2 production rate of 90 kg h^{-1} (1000 m^3 h^{-1}).

Based on these numbers, the DFB process has the highest investment cost, which is due to its complex process design. Investment costs for the AEL process are significantly lower than the investment costs of the DFB and BSR processes. This is due to the overall simplicity of the electrolysis process.

The capital cost distribution of the DFB plant is as follows: 9 MEUR for the DFB plant which also includes the biomass dryer, the WGS unit, the scrubbing unit, and the steam generation system. 1 MEUR for the compressor according to a compressor manufacturer budget quote, and 1 MEUR for the PSA unit according to the budget quote of a plant manufacturer. In comparison, the capital distribution of the BSR plant is as follows: 4.5 MEUR according to [30] for the AD unit including desulphurization and 4.5 MEUR according to a budget quote of a manufacturer for the reforming unit, which includes the steam reformer, the WGS unit, the compressor, the PSA unit, and the steam generation system. The capital costs of the AEL process are entirely based on a budget quote [24].

3.4.2. Production costs

Production costs were calculated using the material and energy streams of the process simulations (Table 12) as well as the specific cost of the feedstock materials and the electrical energy (Table 13).

Based on the information provided in Tables 9, 10, 12, and 13, production costs and expenses were calculated in Table 14.

The raw materials consist of wood chips in case of the DFB process, maize silage in case of the BSR process, and fresh water in case of the AEL process. The utilities consider additional material streams as well as electrical energy. Therefore, the utilities cause the AEL process to cost significantly more than the other processes.

Fig. 15 shows the production cost distribution of the DFB, BSR, and AEL processes.

Fig. 15 demonstrates that production costs for the DFB process are mainly determined by raw material and other costs, which include employee benefits, supervision, maintenance, insurance, taxes, operating supplies, and plant overhead. A similar picture can be observed for the BSR process. However, the raw materials have a significantly higher share of the overall production costs compared to the DFB process. Production costs for the AEL process are determined primarily by the utility costs which are mainly composed of electricity.

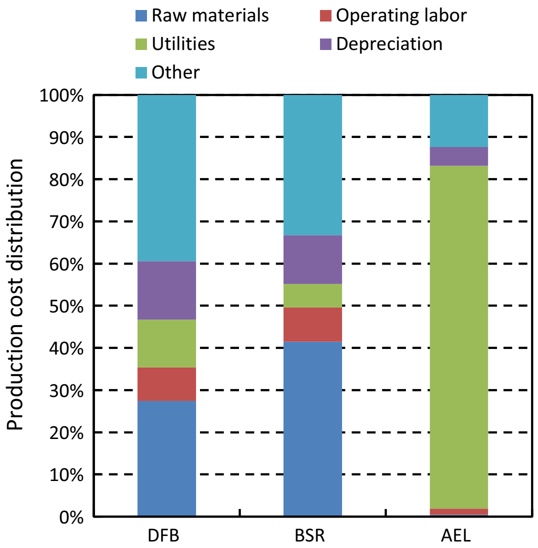

Fig. 15. Production cost distribution of the DFB, BSR, and AEL processes.

Table 14
Production costs and overall expenses of the three investigated processes.

	DFB	BSR	AEL	Units
Raw materials	1,195,040	1,785,160	20,800	EUR a^{-1}
Operating labor	350,000	350,000	70,000	EUR a^{-1}
Utilities	491,920	241,952	3,960,000	EUR a^{-1}
Employee benefits	77,000	77,000	15,400	EUR a^{-1}
Supervision	35,000	35,000	7000	EUR a^{-1}
Laboratory	35,000	35,000	7000	EUR a^{-1}
Maintenance	726,000	594,000	264,000	EUR a^{-1}
Insurances and taxes	363,000	297,000	132,000	EUR a^{-1}
Operating supplies	363,000	297,000	132,000	EUR a^{-1}
Plant overhead	121,000	99,000	44,000	EUR a^{-1}
Depreciation	605,000	495,000	220,000	EUR a^{-1}
Overall expenses	4,361,960	4,306,112	4,872,200	EUR a^{-1}

Table 15
NPV calculations for the investigated processes.

	DFB	BSR	AEL	Units
Investment costs	12,100,000	9,900,000	4,400,000	EUR
Lifetime	20	20	20	a
Expenses	4,361,960	4,306,112	4,872,200	EUR a^{-1}
BT cash flow	−4,361,960	−4,306,112	−4,872,200	EUR a^{-1}
Tax rate	25%	25%	25%	–
Depreciation	605,000	495,000	220,000	EUR a^{-1}
AT cash flow	−2,666,470	−2,734,584	−3,434,150	EUR a^{-1}
Discount rate	10%	10%	10%	–
NPV	−34,801,162	−33,181,055	−33,636,855	EUR

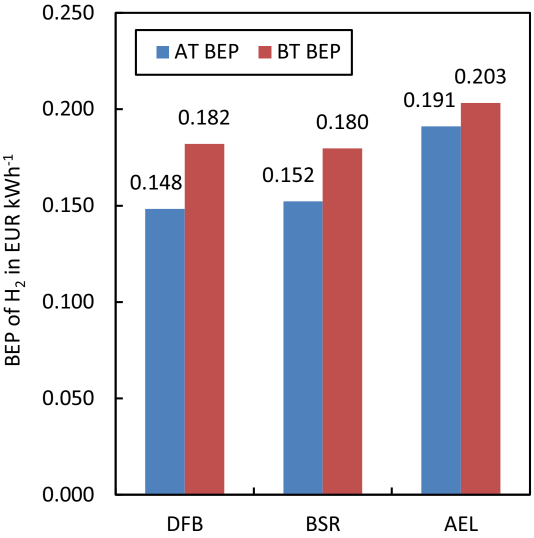

Fig. 16. BEP of H_2 on AT and BT basis.

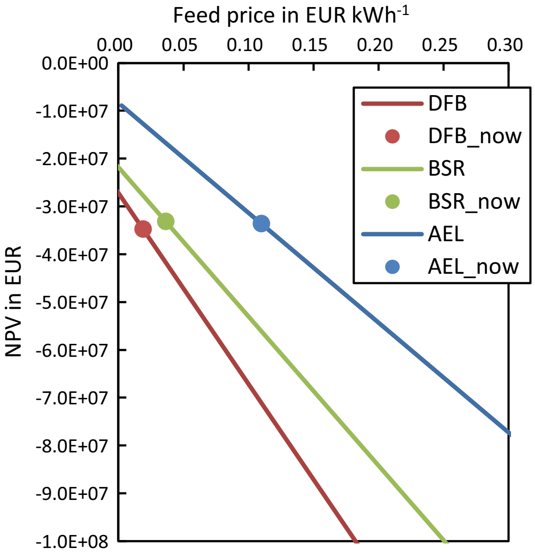

Fig. 17. NPV sensitivity analysis based on feed stock price. Dots indicate the assessment values determined in this work.

3.4.3. Net present value

Table 15 shows the NPV calculation for the three investigated processes according to Eqs. (4)–(7).

These calculations indicate that all three investigated processes have nearly the same NPV. However, based on this calculation, the BSR process would be the most profitable because it has the highest NPV. The BSR process is followed by the AEL and DFB processes in profitability.

3.4.4. Break-even price

Fig. 16 shows the BEP of H_2 on AT and BT basis which reveals the process that is the most cost efficient H_2 producer from an economic point of view.

It shows that the DFB process has the lowest AT BEP, followed by the BSR process and then the AEL process. The reason for this trend is that the specific price of dry wood chips (0.019 EUR kWh^{-1}) is lower than that for dry maize silage (0.037 EUR kWh^{-1}) and significantly lower than the price for electricity (0.110 EUR kWh^{-1}) and the tax allowance caused by the depreciation. In contrast, the BT BEP of the BSR process is lower than the BT BEP of the DFB process, followed by the AEL process. This can be explained by higher investment costs and the resulting depreciation of the DFB process and the omission of the tax allowance.

3.4.5. Sensitivity analysis

Fig. 17 shows the sensitivity analysis of the NPV depending on varying feed stock prices for the DFB and BSR processes and depending on varying electricity price for the AEL process.

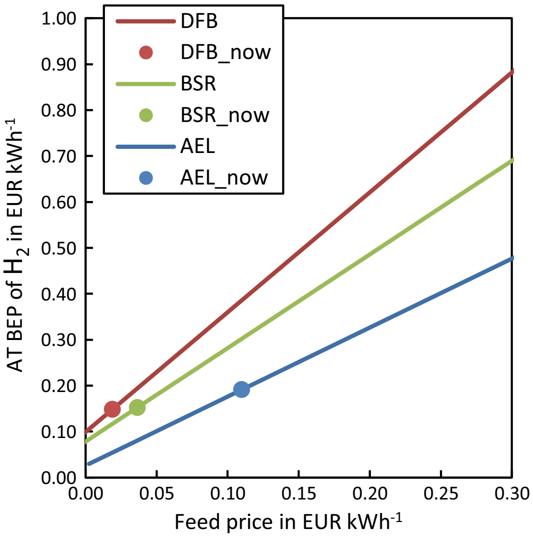

Fig. 18. AT BEP sensitivity analysis based on the feed stock price. Dots indicate the assessment values determined in this work.

From the graph, it can be seen that the DFB process has a steeper slope than the BSR and AEL processes. This indicates that the economy of the DFB process would be more sensitive to increasing (or decreasing) feed stock prices than the BSR process would be to increasing (or decreasing) maize silage prices or the AEL process would be to increasing (or decreasing) electricity prices.

Fig. 18 shows a sensitivity analysis of the AT BEP of H_2 production depending on feed stock or electricity prices.
Again, it can be seen that the DFB process has the steepest slope, which also indicates that its AT BEP is more affected by varying feed stock prices. In addition, it is of note that the actual electricity price is closer to the BEP of the AEL process than the feedstock prices for the DFB and BSR processes and their corresponding AT BEP. The BT BEP sensitivity analysis shows similar results.

4. Conclusion and outlook

In this work, three processes for CO_2-neutral H_2 production were investigated by means of process simulations and subsequent techno-economic assessment. The simulations were carried out using the software Aspen Plus. The investigated processes were based on DFB biomass steam gasification, BSR, and alkaline electrolysis powered by renewable electricity together with their necessary downstream separation and purification steps.

The technical assessment showed that the DFB biomass steam gasification process had nearly twice the H_2 conversion rate of the BSR process. Moreover, wet fuel-based H_2 production in the DFB process was significantly higher. In contrast, the BSR process had a higher dry fuel-based H_2 production efficiency compared to the DFB biomass steam gasification process. Some reports [28] have demonstrated that the biomass steam gasification process has an overall higher performance than the BSR process. However, in our study only maize silage was used as fuel for the BSR process, whereas maize silage, organic waste, and cattle manure can be used as feedstocks [28]. Organic waste and cattle manure have significantly lower biogas yields than maize silage [33]. In contrast to both biomass-based processes, the alkaline electrolysis process had the highest H_2 conversion rate and the highest fuel-based efficiency.

The techno-economic assessment for the production of $90\,\mathrm{kg\,h^{-1}}$ or $1000\,\mathrm{m^3\,h^{-1}}$ of H_2 showed that the biomass steam gasification process had the highest investment costs. The BSR process had lower investment costs and slightly lower production costs. The alkaline electrolysis process had significantly lower investment costs compared to the other two processes but had the highest production costs, which were significantly influenced by the utility costs as determined by the price of electricity. Moreover, the DFB biomass steam gasification process had the lowest AT BEP for H_2 compared to the BSR process and the AEL process. In contrast, the BSR process had the lowest BT BEP followed by the DFB and AEL process. This difference shows the importance of tax consideration in techno-economic assessments. In conclusion, all three processes have a similar NPV based on the chosen assumptions and performed calculations, which indicates that they have about the same economic feasibility for CO_2-neutral H_2 production.

Acknowledgements

This research was carried out with funding from the COMET program managed by the Austrian Research Promotion Agency under grant number 844605. The program is co-financed by the Republic of Austria and the Federal Provinces of Burgenland, Lower Austria and Styria. Co-funding and contributions from the industry partners Air Liquide, Güssing Renewable Energy, and ISG Energy shall be highly acknowledged. In addition, Eric Dabe from Nel Hydrogen and Bernhard Stürmer from ARGE Biogas are gratefully acknowledged. Jingang Yao thanks the Shanghai Tongji Gao Tingyao Environmental Science & Technology Development Foundation (STGEF).

References

[1] Liu K, Song C, Subramani V. Hydrogen and syngas production and purification technologies. Hoboken, New Jersey: Wiley; 2010.
[2] Yang C, Ogden J. Determining the lowest-cost hydrogen delivery mode. Int J Hydrog Energy 2007;32:268–86. http://dx.doi.org/10.1016/j.ijhydene.2006.05.009.
[3] Pröll T, Rauch R, Aichernig C, Hofbauer H. Fluidized bed steam gasification of solid biomass - performance characteristics of an 8 MWth combined heat and power plant. Int J Chem React Eng 2007:5. http://dx.doi.org/10.2202/1542-6580.1398.
[4] Ahrenfeldt J, Thomsen TP, Henriksen U, Clausen LR. Biomass gasification cogeneration – a review of state of the art technology and near future perspectives. Appl Therm Eng 2013;50:1407–17. http://dx.doi.org/10.1016/j.applthermaleng.2011.12.040.
[5] Petersson Anneli, Wellinger Arthur. Biogas upgrading technologies – developments and innovations. IEA Bioenergy 2009.
[6] Zeng K, Zhang D. Recent progress in alkaline water electrolysis for hydrogen production and applications. Prog Energy Combust Sci 2010;36:307–26. http://dx.doi.org/10.1016/j.pecs.2009.11.002.
[7] Nel Hydrogen. Booklet: efficient electrolysers for hydrogen production; 2014.
[8] Wilk V, Hofbauer H. Analysis of optimization potential in commercial biomass gasification plants using process simulation. Fuel Process Technol 2016;141:138–47. http://dx.doi.org/10.1016/j.fuproc.2015.07.035.
[9] Kirnbauer F, Wilk V, Kitzler H, Kern S, Hofbauer H. The positive effects of bed material coating on tar reduction in a dual fluidized bed gasifier. Fuel 2012;95:553–62. http://dx.doi.org/10.1016/j.fuel.2011.10.066.
[10] Kuba M, Havlik F, Kirnbauer F, Hofbauer H. Influence of bed material coatings on the water-gas-shift reaction and steam reforming of toluene as tar model compound of biomass gasification. Biomass Bioenergy 2016;89:40–9. http://dx.doi.org/10.1016/j.biombioe.2015.11.029.
[11] Kuba M, He H, Kirnbauer F, Skoglund N, Boström D, Öhman M, et al. Mechanism of layer formation on olivine bed particles in industrial-scale dual fluid bed gasification of wood. Energy Fuels 2016;30:7410–8. http://dx.doi.org/10.1021/acs.energyfuels.6b01522.
[12] Kuba M, Kirnbauer F, Hofbauer H. Influence of coated olivine on the conversion of intermediate products from decomposition of biomass tars during gasification. Biomass Convers Biorefin; 2016. p. 1–11. http://dx.doi.org/10.1007/s13399-016-0204-z [Open Access].
[13] Kraussler M, Binder M, Hofbauer H. 2250-h long term operation of a water gas shift pilot plant processing tar-rich product gas from an industrial scale dual fluidized bed biomass steam gasification plant. Int J Hydrog Energy 2016;41:6247–58. http://dx.doi.org/10.1016/j.ijhydene.2016.02.137.
[14] Kraussler M, Binder M, Fail S, Bosch K, Hackel M, Hofbauer H. Performance of a water gas shift pilot plant processing product gas from an industrial scale biomass steam gasification plant. Biomass Bioenergy 2016;89:50–7. http://dx.doi.org/10.1016/j.biombioe.2015.12.001.
[15] Bardolf Robert, Bosch Klaus, Rauch Reinhard, Hofbauer Hermann. The effect of packings on the separation of solvent and condensate in biomass gasification product gas scrubbers. In: Proc 24th Eur biomass conf exhib, Amsterdam; 2016.
[16] Ahn S, You Y-W, Lee D-G, Kim K-H, Oh M, Lee C-H. Layered two- and four-bed PSA processes for H_2 recovery from coal gas. Chem Eng Sci 2012;68:413–23. http://dx.doi.org/10.1016/j.ces.2011.09.053.
[17] Fail S, Diaz N, Benedikt F, Kraussler M, Hinteregger J, Bosch K, et al. Wood gas processing to generate pure hydrogen suitable for PEM fuel cells. ACS Sustain Chem Eng 2014;2:2690–8. http://dx.doi.org/10.1021/sc500436m.
[18] Lopes FVS, Grande CA, Rodrigues AE. Activated carbon for hydrogen purification by pressure swing adsorption: multicomponent breakthrough curves and PSA performance. Chem Eng Sci 2011;66:303–17. http://dx.doi.org/10.1016/j.ces.2010.10.034.
[19] Ribeiro AM, Grande CA, Lopes FVS, Loureiro JM, Rodrigues AE. A parametric study of layered bed PSA for hydrogen purification. Chem Eng Sci 2008;63:5258–73. http://dx.doi.org/10.1016/j.ces.2008.07.017.
[20] Yang J, Han S, Cho C, Lee C-H, Lee H. Bulk separation of hydrogen mixtures by a one-column PSA process. Sep Technol 1995;5:239–49. http://dx.doi.org/10.1016/0956-9618(95)00128-X.
[21] Hutnan M, Spalkova V, Bodik I, Kolesarova N, Lazor M. Biogas production from maize grains and maize silage. Pol J Env Stud 2010;19:323–9.
[22] Burgess John, Witheford Simon. Booklet: biogas in practice; 2012.
[23] Herling J. Mais-Silage-DE-2010. Mais-Silage—2010; n.d. <http://www.gemis.de/de/doc/prd/%7B0D0D5171-1933-44A6-AE1B-A35601C8EB34%7D.htm> [accessed September 19, 2016].
[24] Dabe Eric. Expert talk about Nel alkaline water electrolyzer plants; 2016.
[25] Brown T. Engineering economics and economic design for process engineers. 1st ed. Boca Raton: CRC Press Taylor & Francis Group; 2007.
[26] Miltner A, Wukovits W, Pröll T, Friedl A. Renewable hydrogen production: a technical evaluation based on process simulation. J Clean Prod 2010;18(Supplement 1):S51–62. http://dx.doi.org/10.1016/j.jclepro.2010.05.024.
[27] Mueller-Langer F, Tzimas E, Kaltschmitt M, Peteves S. Techno-economic assessment of hydrogen production processes for the hydrogen economy for

the short and medium term. Int J Hydrog Energy 2007;32:3797–810. http://dx.doi.org/10.1016/j.ijhydene.2007.05.027.

[28] Zech K, Oehmichen K, Grasemann E, Michaelis J, Funke S, Seiffert M. Technical, economic and environmental assessment of technologies for the production of biohydrogen and its distribution - results of the Hy-NOW study. Int J Hydrog Energ 2015;40:5487–95. http://dx.doi.org/10.1016/j.ijhydene.2015.01.177.

[29] European Biomass Association. Booklet: a biogas road map for Europe; 2009.

[30] Güssing Energy Technologies GmbH. Biogas Netzeinspeisung. Biogas Netzeinspeisung; n.d. <http://www.biogas-netzeinspeisung.at/technische-planung/biogasgestehung/investitionskosten.html> [accessed October 19, 2016].

[31] Melaina M, Penev M. Hydrogen station cost estimates: comparing hydrogen station cost calculator results with other recent estimates. Denver, USA: NREL; 2013.

[32] Schjølberg I, Hulteberg C, Yasuda I, Nelsson C. Small scale reformers for on-site hydrogen supply. Energy Proc 2012;29:559–66. http://dx.doi.org/10.1016/j.egypro.2012.09.065.

[33] Weiland P. Biogas production: current state and perspectives. Appl Microbiol Biotechnol 2010;85:849–60. http://dx.doi.org/10.1007/s00253-009-2246-7.

Michael Kraussler

Curriculum Vitae

Personal data

Birth	**14th of March 1988**, *Leoben*, Austria.
Citizenship	**Austria**.

Education

University

2014–today	**PhD thesis**, *Chemical and process engineering*, TU Wien, Title of the PhD thesis: Evaluation of dual fluidized bed biomass gasification plants generating electricity, valuable gases, and district heat.
2012–2014	**Master programme**, *Chemical and process engineering*, TU Wien, Title of the master thesis: PEM fuel cell operation and application using BioH_2.
2008–2012	**Bachelor programme**, *Chemical and process engineering*, TU Wien.

Military service

10/2007–04/2008	**St. Michael**, *JB 18*.

School

2002–2007	**HTBL Kapfenberg**, *Electrical engineering*, Kapfenberg.
1998–2002	**Secondary school**, *BG/BRG Leoben 1*, Leoben.
1994–1998	**Primary school**, *Franz Jonas*, Trofaiach.

Work experience

08/2014–today	**Bioenergy2020+ GmbH**, *Junior Researcher, Project manager.*

Internships

07/2013	**TECON Engineering GmbH**, *Leobersdorf.*
07/2012	**Air Liquide Austria GmbH**, *Schwechat.*
08/2011	**Air Liquide Austria GmbH**, *Schwechat.*
07/2010	**Air Liquide Austria GmbH**, *Schwechat.*
07/2009	**Air Liquide Austria GmbH**, *Schwechat.*
07/2008	**Voest Alpine Stahl Donawitz GmbH**, *Leoben.*
08/2007	**Voest Alpine Stahl Donawitz GmbH**, *Leoben.*
07/2006	**Voest AlpineStahl Donawitz GmbH**, *Leoben.*
07/2005	**RHI AG**, *Leoben.*
07/2004	**RHI AG**, *Leoben.*

Qualifications

Languages

German	**Native speaker**.
English	**Fluent in speech and writing**.

Engineering

Project management, process simulation, pinch analysis, data reconciliation and error detection, techno-economic studies.

Computers

Operating systems	**MS Windows, Linux, Apple OS X**.
Software	**MS Office, MS Project, HTML, PHP, Java, SQL, C, Matlab/Simulink, LaTeX, CAD, Labview**.

Miscellaneous

Driving licenses	**Class A and B**.
Interests	**Hiking, motorcycles, running, scuba diving, swimming**.

Vienna, January 31, 2018